

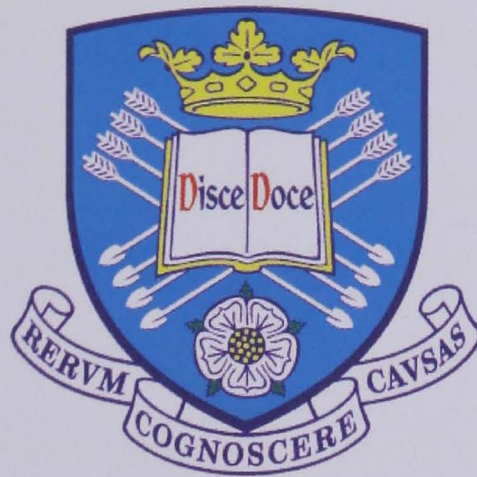
A STUDY OF SHOT PEENING EFFECTS ON FRETTING FATIGUE

THESIS SUBMITTED BY

RACHEL ELIZABETH EDWARDS

IN PARTIAL FULFILMENT OF THE REQUIREMENTS FOR THE
DEGREE OF

DOCTOR OF PHILOSOPHY



THE UNIVERSITY OF SHEFFIELD

DEPARTMENT OF MECHANICAL ENGINEERING

JULY 2008

PREFACE

This thesis is based upon the findings of research conducted in the Department of Mechanical Engineering at the University of Sheffield.

The content of this thesis is original, except where specific references are made to other work.

No part of this thesis has been submitted to any other university.

Rachel Elizabeth Edwards

ABSTRACT

The high clamping forces in lap-joints in the body and wings of an aircraft result in fretting fatigue damage at the contacting surfaces. Shot peening may provide an efficient technique to delay or eliminate fretting fatigue failures. In this study, the fretting fatigue behaviour of unpeened and peened aluminium alloy 2024 T351 in flat-on-flat contact with rectangular bridge pads of aluminium alloy 2024 T351 was investigated and compared with results from previous research where steel pads were used. Contact normal pressure was maintained at a constant value during the tests while the axial load was cyclic with a stress ratio of -1 and a sinusoidal waveform of 20 Hz. The friction force acting over the contact area was measured by strain gauges mounted on the bridges.

There was a considerable reduction in fatigue strength due to fretting, although improved performance for the peened condition. In all cases, fretting fatigue life was found to decrease with an increase in the normal pressure, up to a critical value of normal pressure. Above this critical value, a further increase in normal pressure tended to increase fretting fatigue life. This behaviour was observed at three different axial stresses and indicates a changed sensitivity to pressure for the fatigue damage mechanism. In order to distinguish and quantify the parameters that control such a phenomenon, both an experimental and an analytical methodology have been utilised.

Fretting fatigue life was investigated in terms of the contact region and the specific roles of friction, crack growth and surface modification. The test data was used to develop and assess a fracture mechanics model based on the mechanics of the fretting fatigue process, constructed to predict fretting fatigue life. Components of friction stress estimated from surface roughness profiles, axial stress and normal stress were combined to account for the biaxiality of the loading and the benefits of shot peening were modelled by incorporating the effect of a residual stress.

ACKNOWLEDGEMENTS

To my supervisors, Professor J. R. Yates and Professor M. W. Brown, I express my sincere thanks and gratitude for your patience, guidance, faith and encouragement which has enabled me to make it to the finishing line. Your advice has contributed substantially towards this work.

I would like to thank a number of other individuals and organisations without whom this work could not have been completed:

- Dr. U. Fernando for introducing me to the field of fretting fatigue;
- Dr. E. R. de los Rios for providing me with the opportunity to study the subject;
- Dr. Y.-H. Huh of the Korean Research Institute of Standards and Science for his collaboration during the initial year of the test programme, subsequent finite element analysis and partnership on a paper entitled “Fretting Fatigue Behaviour of an Aluminium Alloy In Contact With an Aluminium Alloy and a Steel”;
- Dr. S. A. Curtis for his assistance in writing the cyclic data analysis program;
- Miss S. Scorey for her work on the scar data analysis program;
- The Engineering and Physical Sciences Research Council and BAE Systems for providing funding for the project;

- Carbon Machining and the Denison Mayes Group for machining and technical support;
- The Metal Improvement Company for the shot peening;
- Simpson Associates for allowing me the time away to complete this thesis;
- The administrative and technical staff at The University of Sheffield and particularly Mrs. J. Hoskins, Mr. J. Goodliffe in the electrical workshop, Mr. B. Platt in the manufacturing workshop and Miss D. Bussey in the Sorby centre. In addition, Prof. Papken Hovsepian in The Materials and Engineering Research Institute at Sheffield Hallam University, for allowing me the use of the laser profilometer;
- Colleagues Dr. C. Rodopoulos for his enthusiasm, advice and encouragement and Dr. S.A. Curtis and Dr. D.T. Asquith for the numerous technical (and not so technical) discussions and debates;

I would like to thank my parents for their continued backing of my academic pursuits and friends and family for whom the connotation of the words fretting and fatigue have come to mean something else entirely! Special thanks go to my Sister for her unrelenting support and my Mother and Grandmother for providing such a fine proof reading service.

Finally I would like to remember Professor K. Miller with whom I had hoped to be able to share the results of this work.

...and to Alan, thank you for your patience.

CONTENTS

Preface		i
Abstract		ii
Acknowledgements		iii
Nomenclature		ix
CHAPTER 1	INTRODUCTION	1
1.1	THE PROBLEM IN CONTEXT	1
1.2	KEY SUBJECTS	2
1.2.1	Fretting fatigue	2
1.2.2	Shot peening	3
1.3	AIM	4
CHAPTER 2	LITERATURE	5
2.1	FRETTING WEAR	5
2.1.1	An introduction to fretting wear	5
2.1.2	A definition of fretting wear	6
2.1.3	The fretting wear mechanism	8
2.1.4	Fretting wear damage	9
2.1.5	Influential factors in fretting wear	10
2.1.6	Palliatives and fretting wear	13
2.2	FRETTING FATIGUE	14
2.2.1	An introduction to fretting fatigue	14
2.2.2	A definition of fretting fatigue	17
2.2.3	The fretting fatigue mechanism	17
2.2.4	Fretting fatigue damage	18
2.2.5	Influential factors in fretting fatigue	30
2.3	SHOT PEENING	45
2.3.1	An introduction to shot peening	45
2.3.2	The shot peening mechanism	46
2.3.3	Shot peening effects	46
2.3.4	Influential factors in shot peening	48

2.4	SHOT PEENING & FRETTING FATIGUE	50
2.4.1	An introduction to shot peening & fretting fatigue	50
2.4.2	The mechanism of shot peening & fretting fatigue	51
2.4.3	Influential factors in shot peening & fretting fatigue	53
2.4.4	The effects of shot peening on fretting fatigue	54
2.5	OBJECTIVES	58
CHAPTER 3	EXPERIMENTAL METHODOLOGY	60
3.1	INTRODUCTION	60
3.2	THE FRETTING FATIGUE TESTS	62
3.2.1	Test rig	62
3.2.2	Grips	63
3.2.3	Control and acquisition	65
3.3	THE SPECIMENS	67
3.3.1	Design	67
3.3.2	Materials	72
3.3.3	Shot peening parameters	73
3.4	THE TEST PROGRAMME	75
3.4.1	Test conditions	75
3.4.2	Loading	76
3.5	THE FRETTING FATIGUE SCARS	78
3.5.1	Evolutionary tests	78
3.5.2	Surface roughness measurements	79
3.5.3	Surface roughness analysis	81
3.6	THE FRACTURE SURFACES	84
3.5.1	The scanning electron microscope	84
CHAPTER 4	RESULTS	86
4.1	INTRODUCTION	86
4.2	FRETTING FATIGUE TEST RESULTS	87
4.2.1	Life	87
4.2.2	Friction	87
4.3	FRETTING SCARS	116
4.3.1	Surface roughness analysis	116
4.4	FRETTING FATIGUE CRACKS	175
4.4.1	Fretting fatigue crack initiation	175
4.4.2	Fretting fatigue crack propagation	177

4.5	FRACTURE SURFACES	182
4.5.1	Topography	182
CHAPTER 5	MODELLING	192
5.1	INTRODUCTION	192
5.2	FRETTING FATIGUE CRACKS	195
5.2.1	Finite element analyses	195
5.2.2	Results	199
5.3	FRETTING FATIGUE LIFE	204
5.3.1	Unpeened	204
5.3.2	Peened	232
CHAPTER 6	DISCUSSION	241
6.1	FRETTING FATIGUE	241
6.1.1	Experimental programme	241
6.1.2	Modelling	258
6.2	SHOT PEENING & FRETTING FATIGUE	268
6.2.1	Experimental programme	268
6.2.2	Modelling	271
CHAPTER 7	CONCLUSION	278
CHAPTER 8	RECOMMENDATIONS	283
8.1	ADDITIONAL TESTS	283
8.2	MODEL IMPROVEMENTS	285
Bibliography		289

APPENDIX A	PROGRAMME: FRETTING TESTS	312
APPENDIX B	PROGRAM: CYCLIC DATA ANALYSIS	315
APPENDIX C	PROGRAMME: EVOLUTION OF FRETTING SCARS	323
APPENDIX D	PROGRAM: SCAR DATA ANALYSIS	327
APPENDIX E	RESULTS: FRETTING FATIGUE LIFE	342
APPENDIX F	RESULTS: FRICTION DATA	345
APPENDIX G	RESULTS: EVOLUTION OF MAX FRICTION VALUES	347
APPENDIX H	RESULTS: FRICTION HYSTERESIS LOOPS	352
APPENDIX I	RESULTS: EVOLUTION OF FRICTION COEFFICIENTS	359
APPENDIX J	RESULTS: SCAR MEASUREMENTS	364
APPENDIX K	RESULTS: PEAK TO VALLEY DEPTH	383
APPENDIX L	RESULTS: SCAR WIDTH	397
APPENDIX M	RESULTS: NOTCH DEPTH PROFILES	411
APPENDIX N	RESULTS: CRACK ANGLES	430
APPENDIX O	RESULTS: FRACTURE SURFACES	434
APPENDIX P	RESULTS: SEM IMAGES FRACTURE SURFACES	443
APPENDIX Q	RESULTS: SEM IMAGES SURFACE DEGRADATION	448
APPENDIX R	RESULTS: SEM IMAGES DEGRADATION	451
APPENDIX S	RESULTS: SEM IMAGES STAGE I CRACK GROWTH	455
APPENDIX T	RESULTS: SEM IMAGES STAGE II CRACK GROWTH	457
APPENDIX U	RESULTS: SEM IMAGES STRIATIONS	459
APPENDIX V	ANALYTICAL MODEL: Y_I & Y_{II}	463
APPENDIX W	ANALYTICAL MODEL: K_I & K_{II}	467
APPENDIX X	ANALYTICAL MODEL: da/dN	474
APPENDIX Y	ANALYTICAL MODEL: ΔN	478
APPENDIX Z	ANALYTICAL MODEL: $K_{RESIDUAL}$	482

NOMENCLATURE

a	=	Crack half-length
a	=	Crack length
a_f	=	Final crack length
a_i	=	Initial crack length
A	=	Axial force
c	=	Y intercept
C	=	Material constant of the Paris law
d	=	Grain size
d	=	Scar peak to valley depth at from a baseline of 0
da/dN	=	Crack growth rate
E	=	Young's elastic modulus
E'	=	Modified modulus for plane strain
F	=	Friction force
F	=	Tangential force
G	=	Shear modulus
G	=	Strain energy release rate
G_I	=	Mode I strain energy release rate
G_{II}	=	Mode II strain energy release rate
h	=	Scar peak to valley depth
h_{avg}	=	Average scar peak to valley depth
h_{max}	=	Maximum scar peak to valley depth
h_0	=	Increase in surface roughness due to the shot peening process
K	=	Stress intensity factor
K_e	=	Equivalent stress intensity factor
K_I	=	Mode I stress intensity factor
K_{IC}	=	Fracture toughness
$K_{residual}$	=	Stress intensity due to a residual stress field

K_t	=	Stress concentration factor
K_I	=	Mode I stress intensity factor
$K_{I \text{ axial}}$	=	Mode I stress intensity factor for an applied axial stress
$K_{I \text{ friction}}$	=	Mode I stress intensity factor for a resultant friction stress
$K_{I \text{ min}}$	=	Minimum mode I stress intensity factor
$K_{I \text{ normal}}$	=	Mode I stress intensity factor for an applied normal stress
K_{II}	=	Mode II stress intensity factor
$K_{II \text{ axial}}$	=	Mode II stress intensity factor for an applied axial stress
$K_{II \text{ friction}}$	=	Mode II stress intensity factor for a resultant friction stress
$K_{II \text{ normal}}$	=	Mode II stress intensity factor for an applied normal stress
K_{III}	=	Mode III stress intensity factor
ΔK	=	Stress intensity factor range
ΔK_e	=	Equivalent stress intensity factor range
ΔK_{th}	=	Threshold stress intensity factor range
ΔK_I	=	Mode I stress intensity factor range
ΔK_{II}	=	Mode II stress intensity factor range
ΔK_{III}	=	Mode III stress intensity factor range
ΔK_e	=	Equivalent stress intensity factor range
ΔK_{th}	=	Threshold stress intensity factor range
l	=	Scar peak to peak width
m	=	Slope
n	=	Material constant of the Paris law
N	=	Number of cycles
N	=	Normal force
N_f	=	Number of cycles to failure
p	=	Pressure
P	=	Normal load
q	=	Shear stress
r	=	Depth
r, θ	=	Polar coordinates

R	=	Stress ratio
Ra	=	Centre line average
S	=	Stress
w	=	Scar peak to peak width at a baseline of 0
x	=	Scale factor for initial crack length
x	=	Horizontal profile measurement
x_i	=	Horizontal profile measurement at a point i
x_j	=	Horizontal profile measurement at a point j
y	=	Vertical profile measurement
y_E	=	Error in vertical profile measurement
y_M	=	Vertical profile measurement
y_T	=	True vertical profile
Y	=	Geometrical factor
Y_a	=	Geometrical factor for an applied axial stress
Y_f	=	Geometrical factor for a resultant friction stress
Y_n	=	Geometrical factor for an applied normal stress
Y_I	=	Mode I geometrical factor
Y_{II}	=	Mode II geometrical factor
Y_{III}	=	Mode III geometrical factor
$Y_{I \text{ axial}}$	=	Mode I geometrical factor for an applied axial stress
$Y_{I \text{ friction}}$	=	Mode I geometrical factor for a resultant friction stress
$Y_{I \text{ normal}}$	=	Mode I geometrical factor for an applied normal stress
$Y_{II \text{ axial}}$	=	Mode II geometrical factor for an applied axial stress
$Y_{II \text{ friction}}$	=	Mode II geometrical factor for a resultant friction stress
$Y_{II \text{ normal}}$	=	Mode II geometrical factor for an applied normal stress
$Y_{III \text{ axial}}$	=	Mode III geometrical factor for an applied axial stress
$Y_{III \text{ friction}}$	=	Mode III geometrical factor for a resultant friction stress
$Y_{III \text{ normal}}$	=	Mode III geometrical factor for an applied normal stress
θ	=	Crack angle
θ	=	Notch included angle

θ_0	=	Critical angle
μ	=	Coefficient of friction
$\mu\rho$	=	Friction stress
σ	=	Applied stress
σ	=	Smoothing constant
σ_a	=	Axial stress
σ_a	=	Axial stress amplitude
$\sigma_{a\ max}$	=	Maximum axial stress
σ_f	=	Friction stress
$\sigma_{f\ max}$	=	Maximum friction stress
$\sigma_{f\ min}$	=	Minimum friction stress
σ_m	=	Mean stress
σ_{max}	=	Maximum stress
σ_{min}	=	Minimum stress
σ_n	=	Normal stress
σ_n	=	Normal stress amplitude
σ_u	=	Tensile strength
σ_{xx}	=	Tangential stress
$\sigma_{\theta\theta\ max}$	=	Maximum tangential stress
$\sigma_{\theta\theta^*max}$	=	Maximum effective amplitude of tangential stress
$\Delta\sigma$	=	Applied stress range
$\Delta\sigma_f$	=	Friction stress range
$\Delta\sigma_{xx}$	=	Tangential stress range
$\Delta\sigma_{\theta\theta\ max}$	=	Maximum tangential stress range
$\Delta\tau_{r\theta\ max}$	=	Maximum shear stress range
τ_{xy}	=	Shear stress
$\Delta\tau_{xy}$	=	Shear stress range
ν	=	Poisson's ratio

CHAPTER

1

INTRODUCTION

1.1 THE PROBLEM IN CONTEXT

On the 28 April 1988, an Aloha Airlines Boeing 737 suffered a catastrophic failure and consequently the loss of the life of a flight attendant. Corrosion in and around fastening holes of the lap joints in the fuselage, combined with concentrated stresses, led to fatigue cracks which linked up, resulting in the loss of a section of the fuselage [1], see Figure 1.1.

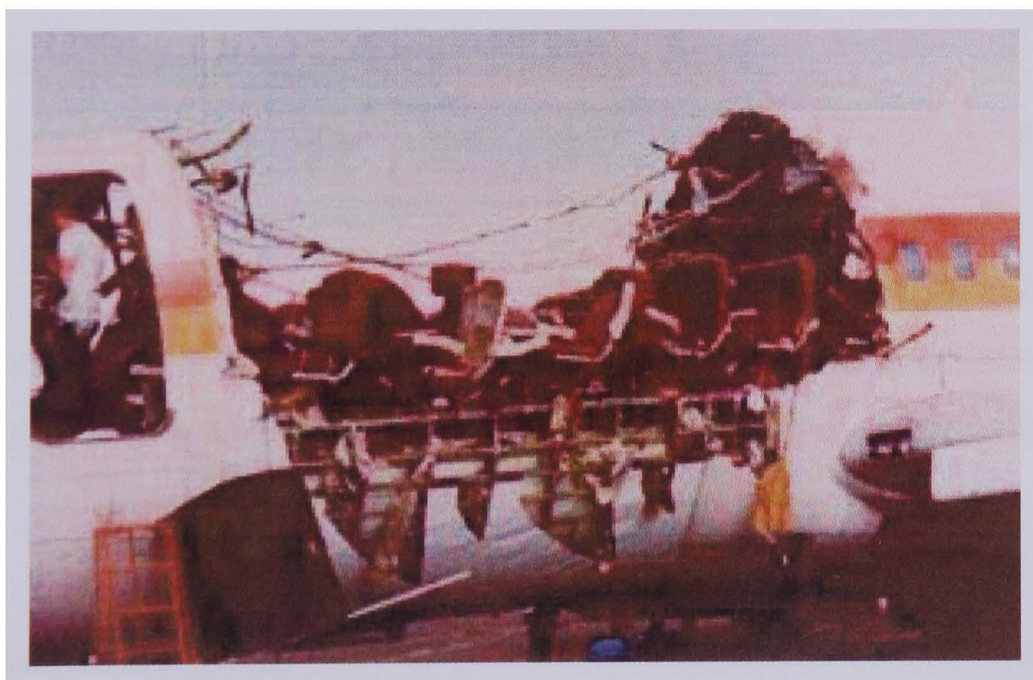


Figure 1.1: Aloha Airlines Boeing 737, flight number 243, flight from Hilo to Honolulu, at Kahului Airport on 28 April 1988 after a section of its fuselage was lost during flight [2].

Fretting fatigue was first documented by Eden et al. [3] in 1911, a specialists' meeting on fretting in aircraft was held in 1974, but despite being the focus of a great deal of research [4], [5], [6], [7], [8], [9], the fretting fatigue of bolted joints, riveted joints and other structural members subject to cyclic loading continues to be a serious issue in ageing airframes and engines.

Fretting fatigue has also been responsible for failures across a wide range of industries. Other practical examples of where fretting conditions can be observed include: in the seating of a turbine disc on a drive shaft in a steam or gas turbine [10], in railway axles/wheels [11], the dovetailed regions of turbo machinery [12], orthopaedic implants [13], and wire ropes used in the marine, mining and power industries [14]. The sites in which fretting fatigue can initiate fatigue failure really are widespread and diverse [15].

1.2 KEY SUBJECTS

1.2.1 Fretting fatigue

The American Society for Metals defines fretting as:

“...a wear phenomenon occurring between two surfaces having oscillatory relative motion of small amplitude.” [16]

Fretting fatigue is likely to occur, when a cyclic load is also applied.

A diagnosis of failure by means of fretting fatigue can be made from the observation of a fracture surface with the naked eye. The presence of debris, surface roughening and evidence of multiple cracks are all related evidence [17].

The mechanisms of fretting fatigue are extremely complex [18] and involve high stress gradients, non-proportional multi-axial loading and surface finish effects [19].

A seminal book on the subject was published by Waterhouse in 1981 [20], proceeded by a paper of the same name in 1992 [17], which has been followed by reviews periodically, including: Hoepfner [18], Mutoh [21], Hills et al. [22] and Nowell et al. [19].

From the time when fretting was first identified to the present day, a great deal of progress has been made in understanding the mechanisms of fretting fatigue, which in turn has done much to assist the science, engineering and business communities to deal with this phenomenon. However, much remains to be done [18].

Since the mechanism of fretting fatigue involves surface contact and relative movement between two components, much of the work to alleviate the problem has focussed on the properties and behaviour of the surfaces in contact.

1.2.2 Shot peening

A wide range of surface treatments, coatings and shims have been employed in attempts to mitigate fretting wear and fatigue, with varying degrees of success as reviewed and tested by researchers including Gordelier and Chivers [23], [24]. The success of a palliative is dependent upon specific application [23], [25] and should be selected with the objective of modifying the fretting process in some deliberate and controlled way [25].

Interference fitting of fasteners creates stresses that are compressive near the fastener but becomes tensile near the faying surfaces where fretting cracks are known to initiate. One surface engineering treatment that ameliorates tensile residual stresses is shot peening, which is known to extend the fretting fatigue life of engineering components [26]. Shot peening involves firing large quantities of small, hard media, or shot, at the surface of a component, which deforms the material plastically [27].

Shot peening has a significant effect on the mitigation of fretting fatigue. The resultant improvement in the fretting fatigue life of a specimen has been documented to be over 22% [28] and even up to the order of 50% [29].

1.3 AIMS

The primary aim of this work is to investigate fretting fatigue life in terms of the contact region and the specific roles of friction and surface modification. The second aim is to consider the effects of shot peening on fretting fatigue, and finally to develop a life prediction model based on the mechanics of the fretting fatigue process.

CHAPTER

2

LITERATURE

2.1 FRETTING WEAR

2.1.1 An introduction to fretting wear

The fretting phenomenon was first documented in 1911 by Eden et al. [3], on observing the formation of brown oxide debris between the steel grips and a steel specimen in a fatigue rig. In 1927, Tomlinson [30] conducted the first investigation of the process utilising specially designed machinery, which has been redesigned extensively over the years [31], [32], [33], [34]. It was not until 1950, that Godfrey [35] attempted to characterise the nature of fretting and define distinct fretting mechanisms and 1953, that sufficient progress had been made for the first American Society for Testing and Materials (ASTM) symposium on the subject of fretting to be held. Waterhouse published his paper on the subject in 1955 [36] and his seminal book in 1972 [37]. In 1983, Bill [38] published a paper on a comparison between fretting wear and fretting fatigue, followed by similar works by Berthier et al. [39].

2.1.2 A definition of fretting wear

“Fretting is the action which causes fretting damage when two contacting bodies are subject to a relative oscillatory sliding motion of small displacement amplitude.” [37]

The relative movement that has to occur for fretting wear to appear was termed ‘slip’ by Tomlinson [30]. Extremely small amplitudes of slip are sufficient to cause damage; the threshold amplitude of slip at which fretting damage becomes apparent is in the region of $0.5 \mu\text{m}$ [40].

Slip is caused by a concentration of shear stresses at a contact. For a Hertzian contact subjected to normal and tangential loads, Mindlin [41], showed theoretically that the tangential load produces shear tractions at the interface, the effect of which is to produce a region of displacement. This region propagates towards the centre from the edges of the contact, as shown in Figure 2.1. The two bodies are assumed to have identical material properties and a constant coefficient of friction is assumed at the interface.

Johnson [42] subsequently conducted experiments creating microscopic interfacial slip between two spherical surfaces, leading to energy dissipation and surface damage in the manner Mindlin predicted.

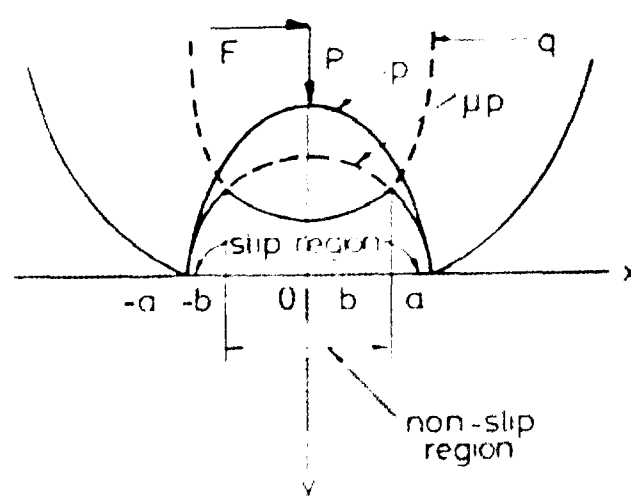


Figure 2.1: The Mindlin diagram [41], [17].

In the stick regime, see Figure 2.2 a), displacement is accommodated by the elastic deformation of asperities. This occurs at low amplitudes of oscillation, where no energy is dissipated; there is very little surface damage and an absence of cracks [43].

Partial slip, see Figure 2.2 b), occurs with an increasing amplitude of oscillation, where there is still a central region of stick and now an outer region where plastic deformation of the surfaces occurs, termed microslip, but where there is no rigid body motion between the bodies in contact. Partial slip can occur under the action of a normal load alone, when surface particles displace tangentially by different amounts, resisted by shearing tractions. This can take place if one body is very much stiffer than the other, either because it is much a greater bulk, or elastic constants differ [44]. Wear effects are small, but crack growth is accelerated compared to that in plain fatigue.

When slip occurs only over part of an interface subjected to fretting, the border between the two elastic bodies in contact may be divided into regions of slip and non-slip or stick. Boundaries develop between these regions, the position of which can move, possibly as a result of a change in the coefficient of friction present, or because of changes in the local stresses accompanying crack initiation [45]. It is at this point where fatigue cracks are expected to initiate.

Gross slip, see Figure 2.2 c), occurs when the amplitude of oscillation reaches a critical value and the coefficient of friction drops from the static level to a lower value corresponding to a kinetic coefficient of friction. The entire contact area is subject to macroslip and severe surface damage by wear; however, fretting fatigue cracks are continuously eliminated. The amplitude of slip at which significant fretting wear occurs is between 10 μm and 100 μm , above which the wear rate is characteristic of unidirectional sliding [46].

Under a gross slip regime, fretting wear is the prevalent damage mechanism, whereas under a mixed stick-slip regime, fretting fatigue becomes the dominant factor [47].

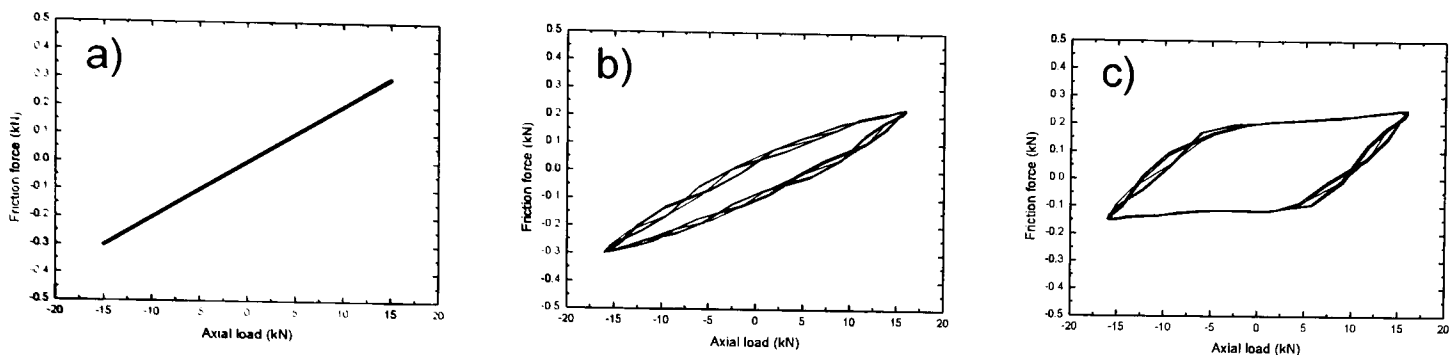


Figure 2.2: a) Stick, b) Partial slip, c) Gross slip.

2.1.3 The fretting wear mechanism

In 1970, Hurricks [48] provided an extensive review of the mechanisms of fretting, identifying the following three common stages:

1. The initial adhesion and transfer of metal;
2. The production of debris in a normally oxidised state;
3. The steady state wear condition.

This was followed by the most widely accepted theory of fretting, based on the following assumptions on the mechanical and chemical effects, as according to Waterhouse [37]:

- Mating surfaces come into contact at high asperity points;
- Oscillatory slip causes cyclic shear stresses, which together with high Hertzian stresses, induce local plastic deformation at these asperities;
- Micro welding or adhesion and fracture of the asperities results in fretting debris and material transfer;
- Under corrosion conditions, the debris produced is harder than the base metal and may cause abrasion.

Adhesion results immediately from contact in the fretting process, following which fine particles of debris break loose [35] from a tribologically transformed layer formed during the very first cycles of fretting loading [49]. Investigations have shown unusual dislocation structures in very heavily deformed surface layers [17].

Protective oxide films are continuously abraded [50], hence the term 'fretting wear' and the structure of the debris changes due to continuous oxidation of these particles [51]. The formation of oxides accelerates the development of fretting wear [52] and ultimately, the fretting action of two surfaces in contact will result in the production of a fretting scar.

The disruption of an oxide film can allow metal-to-metal contact, further metal transfer [45] and potentially local welding on a scale sufficient to produce high stresses, due to tangential displacement, in a volume of material large enough for definitive cracks to be developed [21].

2.1.4 Fretting wear damage

Depending on the conditions, fretting can result in the following forms of damage:

- Pits;
- Oxide and debris;
- Scratches;
- Material transfer;
- Surface plasticity;
- Subsurface cracking and/or voids;
- Fretting craters [18].

Fretting can modify the structure of a surface in a number of ways [53]. The fretting action of two surfaces can result in local welding, adhesion and metal transfer across the interface between the contacting bodies, involving local plastic deformation at asperity contacts with consequent surface roughening [17]. This includes pitting due to the shearing of the welds giving rise to particle detachment, and pits are known to be highly detrimental in the case of plain fatigue [45].

As well as modification by means of plastic deformation, fretting can also lead to attendant work hardening, the generation of heat and the possible over ageing of age-hardened materials [53]. For ductile materials, a competition also ensues between the formation of a tribologically transformed structure, particle detachment and the nucleation of fatigue cracks [54].

Fretting damage ultimately leads to surface and near surface degradation that produces a fretting scar and causes cracks to become nucleated at various angles to the surface, which propagate under the appropriate conditions [18]. In work by Alic et al. [55], no evidence for either delamination type processes or any role of precipitate particles in initiating cracks was found.

The degradation modes of particle detachment and cracking are generally achieved simultaneously, but depending on the fretting regime one or other becomes predominant when comparing the behaviour of different alloys [56].

2.1.5 Influential factors in fretting wear

The amount of wear debris produced and surface fretting damage created by contacting components, is a function of the contact conditions, including: the contact pressure, the frequency of the axial load, environmental issues, the contact geometry, the properties of the component materials and the amplitude of the interfacial slip [17].

2.1.5.1 Amplitude

The elimination of wear debris is greater at higher amplitudes, therefore wear should increase with amplitude [57].

2.1.5.2 Contact

Wear depends largely on how debris is trapped in a contact [58]. It has been demonstrated that there exists a critical contact size, below which, fretting has no effect on fatigue life [59]. However, this appears to be affected by the condition of the surfaces in contact, i.e. friction [60].

2.1.5.3 Cycles

Particle detachment starts at the first few strokes, but particle elimination can take much longer depending on the contact conditions [57].

2.1.5.4 Environment

It has been suggested that wearing surfaces reach temperatures locally high enough to affect properties, including the yield stress, that determine wear rate [61]. It has also been shown that fretting damage itself is affected by environmental conditions [62], [63], such as temperature and aqueous solutions, as these govern the composition and flow of wear debris. At high temperatures, protective surface oxide films develop; in aqueous electrolytes, passive films are disrupted [46].

2.1.5.5 Frequency

Fretting is observed over a wide range of frequencies; even extremely low frequencies can produce appreciable damage [40]. At low amplitudes, partial stick occurs and material damage by surface degradation and crack initiation is greatly accelerated by an increase in frequency. The volume of material removed per cycle is little affected by frequency [64].

2.1.5.6 Friction

A higher value of friction force causes higher shear stresses at the interface, which can generate delamination cracks. However, an increase in friction can also cause a decrease in slip, decreasing abrasive wear [65]. In addition, any wear debris generated may contribute towards a lowered coefficient of friction, thereby causing an increase in life.

2.1.5.7 Materials

Initial adhesion varies with the combination of the materials in contact, as can be shown by the initial coefficients of friction observed [66]. The materials in contact also govern the depth of the tribologically transformed layer and subsequently the amount of wear debris that forms [58]. With some metals, the wear debris produced oxidises rapidly and provides an abrasive that promotes the fretting wear process, this is typical with steel specimens, where fine iron particles have been found to cause surface damage [45]. However, sometimes hard debris produced during fretting can actually form a third body between the surfaces that acts like a roller bearing [17].

The severity of wear damage depends in part on the hardness of the oxides and the parent materials as well [50]. Increased hardness of a parent material causes a decrease in wear owing to the improved mechanical strength [65]. However, for any combination of components, surface damage from wear is greater in the softer material. If metal transfer occurs from one component to the other in a fretting assembly, then it is invariably from the softer to the harder material [45].

2.1.5.8 Normal Load

The conflicting beneficial or detrimental role of oxide debris on wear depends in part on the magnitude of the normal load. The removal rate of oxide debris generally increases with increasing normal load, decreasing at higher loads when the particles become compacted [67].

If debris is retained then it will often occupy a greater volume than the material it replaces and the contact pressure will also increase [45]. With a flat-on-flat contact, the distribution of the contact pressure will evolve continuously [68].

2.1.5.9 Slip

Material damage is often linked to sliding conditions; generally, wear prevails when the gross slip regime is established [69]. In the partial slip regime, metal-to-metal contact is still maintained in the non-slip region; evidence of welding and plastic deformation in this region has been established, as has proof of work hardening and in some cases work softening in the surface [37]. With a small slip range then fretting scars tend to be patchy with little fretting wear; whereas at higher values of slip range, considerable wear is encountered over the whole contact area [45].

With increasing slip amplitude, the depth of wear scars increases and wear damage becomes more severe. At slip amplitudes of 45 μm , adhesive transfer and abrasion occur [70]. Scars on specimens having undergone gross slip tend to be much deeper than those on generated in the stick-slip regime. In general, the depth of a fretting scar increases as the relative slip increases under the partial slip condition [60].

2.1.6 Palliatives and fretting wear

Methods of avoiding the detrimental effects of fretting wear are based on the following two principles:

1. Avoiding metallic contact by structural design or non-metallic layers;
2. Surface treatment to improve surface wear resistance or to introduce compressive residual stresses [71].

2.2 FRETTING FATIGUE

2.2.1 An introduction to fretting fatigue

The effect of fretting on fatigue properties was first investigated in 1941 by Warlow-Davies [72], who found a reduction in the fatigue strength of a steel of up to 18% as a result of fretting damage. However, conjoint fretting and fatigue investigations in 1953 by McDowell [73], showed that this action was much more dangerous, producing strength reduction factors of more than 5 [17].

Fenner et al. [74] were among others to first present papers on fretting fatigue at the International Conference on Fatigue in 1956. Fenner and Field [75] went on to demonstrate that fretting greatly accelerates the crack initiation process, occurring in only 5% or less of the fatigue life in total. They were among the first to use the bridge type pad in their experiments [76], later adopted by others including Edwards [77]. Milestone [78], introduced cylindrical fretting pads, whereby the elastic stress fields may be calculated analytically.

By 1964, Hoepfner was applying his knowledge on the subject to a wide range of engineering components [18] and from 1968, noticeable works were being published by Nishioka and Hirakawa [79], [80], [81], [82], [83]. They reported the existence of non-propagating fretting fatigue cracks and hence crack arrest, the initial site and direction of fretting fatigue cracks, that a higher mean stress reduces fretting fatigue life, that the amount of relative slip has an effect on fretting fatigue life, and ultimately proposing a model for predicting fretting fatigue life based on a knowledge of the slip amplitude, contact pressure and materials involved [84].

In 1971, the first International Conference on corrosion fatigue (the earlier term for fretting fatigue), was held and in the 1970's extensive research into the fretting fatigue of aluminium and titanium alloys was initiated. The effects of the environment and surface treatments were studied, and Endo and Goto [85] applied the concepts of fracture mechanics to fretting fatigue. The majority of the publications at this time were by Hoepfner and Waterhouse.

In 1981 a major book on fretting fatigue was published by Waterhouse [20] and Edwards [77] published a paper on the application of fracture mechanics to fretting fatigue. In 1982 another ASTM symposium was held, where papers on fretting fatigue appeared once again. In 1985, Johnson [86] published his book on contact mechanics and notable works were being published by Lindley and Nix [87], [88], [89] on fretting damage formation and the application of fracture mechanics to fretting fatigue. In 1986, Sato et al. published a number of papers [90], [91], [92], [93], concluding that fretting accelerates the initial growth of cracks and in 1987 works by Nowell and Hills [94], [95], were published. In 1988, Nowell [96] published his thesis on an analysis of fretting fatigue, Hattori [97] published a paper on the application of fracture mechanics to fretting fatigue, followed by Attia's [98] summary of his works on thermal aspects of fretting and testing.

In 1990 an ASTM symposium on fretting fatigue was organised by Attia and Waterhouse and at the same time, a collaborative research programme began at the University of Sheffield into the fretting fatigue fracture of artificially aged BS L65 copper aluminium alloy. A biaxial fretting fatigue test facility was developed, unique in its ability to directly control and maintain the normal contact load on fretting pads despite any wear of the bridges or any material deformation to a specimen to which a cyclic axial load was applied [99].

The importance of friction in predicting fretting fatigue life was highlighted by Faanes and Fernando [100], who also subsequently demonstrated that mode I crack growth described fretting fatigue crack growth behaviour well, but suggested that investigations of the influence of mixed mode crack growth be carried out [101]. Meanwhile, Sheikh et al. [102] developed elastic stress intensity factors for fretting fatigue using the finite element method. These works were presented at the International Symposium on Fretting Fatigue held at the University of Sheffield in 1994, organised by Waterhouse and Lindley. In the same year, a comprehensive book on the mechanics of fretting fatigue was published by Hills and Nowell.

The second ASTM symposium on fretting fatigue was organised by Hoeppepner, Vincent, Hattori, Lindley and Attia. Many analytical techniques had emerged to assist in estimating fretting fatigue life, but by that time it was and still is, necessary to conduct experiments to simulate fretting fatigue behaviour. However, experiments had become more standardised and experimental techniques had emerged that allowed the characterisation of fretting fatigue in much greater detail than before. It was recommended that more work be done in the areas of environmental factors and surface treatments [103].

In 2001, a third ASTM symposium was organised by Mutoh, Hoeppepner, Vincent, Hattori, Lindley and Attia. The process of fretting crack nucleation under fretting wear was discussed and fretting fatigue life estimations were attempted based on fracture mechanics, notch fatigue analysis and multiaxial fatigue parameters. It was stated that small crack problems, especially those related to threshold and under mixed mode remain [104]. Since then, a special issue of the Journal of Strain Analysis has been published, with an editorial by Hills [105], noting that quantification of the function of surface finish effects has yet to be found and recognising that there has been a shift away from the 'total life' approach, to one in which the two distinct phases of failure, crack nucleation and crack propagation, are recognised.

To date, the development of asymptotic methods to characterise the stress fields found in fretting fatigue has received much attention [106], [107], [108] and short crack arrest methodologies have been developed [109], which are able to predict the arrest of fretting fatigue cracks from plain fatigue data. However, in the future, the importance of microstructure should be realised and there will be a need to predict fretting fatigue performance in the presence of residual stress [19].

2.2.2 A definition of fretting fatigue

The surface damage produced by a fretting action can take the form of fretting wear. However, the more damaging aspect of fretting is fretting fatigue, where the fatigue strength of the material is also seriously degraded [45], as when one of the members in contact is subjected to a cyclic stress. A cyclic stress is required for a failure by fatigue, and a more damaging aspect of fretting is then observed, namely the early initiation of fatigue cracks [17].

In reality however, the term fretting fatigue encompasses a range of conditions from the mild contact tractions accompanying bulk stress amplitudes sufficient to cause failure in plain fatigue, to severe fretting in the presence of relatively low bulk stresses [110].

2.2.3 The fretting fatigue mechanism

In general fretting fatigue is a combination of two dynamic phenomena: wear and fatigue [37]. Wear influences fretting fatigue in a number of ways, as outlined in Section 2.1.3, not least in the alteration it produces in the contact stresses [58]. However, the simultaneous action of the two phenomena initiates micro cracks in the fretted region, whereby crack propagation is possible if supported by an external stress field and may be accelerated by the wedging action of any fretting debris [37].

According to Hoepfner [18], the main stages of fretting fatigue are as follows:

1. Cohesion of the surfaces;
2. The breaking of the cohesion;
3. Slip of the surfaces;
4. Production of fretting debris;
5. Corrosion of the fresh surfaces and/or debris;
6. Third body production;
7. Generation of surface damage such as pits, fretting scars, subsurface fractures and eventually cracks;
8. Nucleation of cracks that may propagate at various angles to the surface, depending on the loading conditions and the material, its microstructure and texture;
9. Propagation of cracks that may be influenced by either friction forces or debris or both, in their early stages of propagation, but may become independent of contact conditions as they become longer in length;
10. Fatigue crack propagation that is independent of the conditions that produce fretting;
11. Instability.

2.2.4 Fretting fatigue damage

Fretting fatigue leads to surface and near surface degradation that causes the premature initiation and propagation of fatigue cracks [18].

Actual wear damage can be quite small [45]; however, the acceleration of the formation of cracks near to the surface can decrease the fatigue strength of an assembly by more than one third [12].

Fretting fatigue can affect significantly both the crack initiation and crack propagation phases, depending on prevailing conditions. A full understanding of fretting fatigue thus requires a consideration of the effect of fretting on the both initiation and propagation phases on crack life [110].

2.2.4.1 Crack initiation

The definition of the boundary between the processes of initiation and propagation is complicated. Miller [111], defined the nucleation of damage as:

- The nucleation of a crack like defect by, for example, debonding of the matrix inclusion interface;
- The crack whose length is in the order of microstructure size;
- The so called short cracks for lengths below which elastic fracture mechanics cannot be applied.

From an experimental standpoint, initiation is often taken to encompass that period of component or specimen life from the beginning of loading until an observable flaw is detected. However, this is a function of the detection method employed and of the experience of the user [110].

Crack initiation is a continuous process rather than a discrete event, taking place over a period of time and involving the gradual accumulation of damage. There is no specific point in time at which the damage becomes a crack [110].

The initiation of fretting fatigue cracks is a highly complex process and difficult to determine. However, even visible fatigue cracks are initiated very early in the life of a component [85] and some grow to be propagating cracks [112].

Fretting greatly accelerates the crack initiation process [45], thus the initiation phase of fretting fatigue life is often, although not always, quite short [110], resulting in much shorter fatigue lives.

In 1958, Fenner and Field [75] demonstrated that in fretting fatigue, initiation could occur in 5% or less of the fatigue life, in 2006, Giummarra et al. [113] found fretting cracks in the first 1% - 5% of total life.

Other studies have demonstrated that small fretting fatigue cracks, typically of up to 0.5 mm in depth, can be initiated rapidly within 5% - 10% of fretting fatigue life [45] and at stresses considerably below the fatigue limit [114]. In plain fatigue, crack initiation may account for 90% of the fatigue life in total.

It has been said that it is important to consider contact on an asperity scale when attempting to describe fretting fatigue crack initiation [115]. This is because crack initiation occurs on a microscopic scale, taking place at asperity level in terms of surface roughness [45] within one, two or at most three, grains of a polycrystalline material [110]. A detailed understanding of crack initiation may thus only be achieved by a micro mechanics analysis, although some progress can be made by considering bulk properties of the contact [110].

Another potential crack initiation mechanism is particle or defect induced crack initiation, which is often observed in plain fatigue tests of high-strength materials. However, it has been concluded from measurements of fretted surface geometry, that grooves worn on a fretted surface are too shallow to exert a notch effect. It has also been reported that fretting corrosion pits are not stress concentration sites that initiate micro cracks in fretting fatigue [21].

It was once suggested that delamination may contribute to the surface changes that accompany crack initiation in fretting fatigue. Indeed, in 1980 Gaul and Duquette [116] concluded that fatigue strength could be reduced as a result of the fretting wear process and that surface ductility exhaustion led to micro cracks initiating beneath the surface. These micro cracks link to cause surface delamination, with some micro cracks propagating in the opposite direction into the substrate, leading to fatigue failure.

Other researchers have since reported that fretting fatigue cracking is never associated with areas of maximum fretting damage. Whilst surface delamination and associated micro cracking are sometimes seen [117], it is also possible that the martensitic transformation of the contact surface layer [118] and hardening of subsurface layers due to delamination induced by fretting [37] may influence, to some degree, crack initiation behaviour under fretting conditions [21].

Indeed, as fretting fatigue cracks generally initiate and propagate in specimens where surface wear damage is minimal, it has been concluded that crack initiation and growth in fretting fatigue is a process controlled by high alternating shear stresses along persistent slip bands, on a contact surface [114], promoted by combining tangential forces along the contact surface and alternating bulk stresses. Shear stress amplitude appears to be a good parameter for predicting the initiation of fretting fatigue cracks, although not of ultimate failure [119]. Test evidence indicates that the stress concentration due to tangential force in fretting fatigue is significantly higher compared to those due to particles or defects [21].

Fretting fatigue damage is thus significant when combining fretting motion and alternating bulk stresses, whilst a reduction of fatigue strength due only to fretting wear is negligible [21]. In that respect, the dependence of crack initiation on the surface or near surface stress state mirrors the behaviour observed in plain fatigue [110].

A large degree of scatter in the initiation angle has been found along the length of a contact by Proudhon et al. [120] using x-ray micro tomography and it is suggested that the initiation angle of a fretting crack is strongly influenced by the local microstructure. However, crack length measurements and micrographs made of different aluminium alloys have indicated that there is no significant difference in the fretting response of alloys based on their micro structural characteristics [113].

One method of determining the number of fretting cycles required to initiate a crack that will propagate to failure is the completion of a two-stage test. In this type of investigation a fretting device is applied for a certain number of cycles in a fatigue test after which each specimen is then cycled to fracture or run out under the same alternating stress without the applied normal force [17], [121], [122].

A variation on this experiment is the test where a group of specimens are fretted with the same number of fretting cycles, following which they are ground to various depths before the test is continued in plain fatigue. Where the fretting damage has been completely removed, a run out is achieved. In certain cases removal of the fretting device leads to earlier failure by fatigue than if the device were applied continuously. The reason for this is that the clamping pressure on the fretting device results in compressive stresses at the tip of a crack which retards its progress. The retardation is a function of the clamping load [17].

2.2.4.1.1 Sites

In mechanical joints with bolted or rivet fasteners, there are three main regions of contact, i.e. between the fastener and surface of the hole in the panel, between the two panels themselves and between the fastener head and surface of the panel itself [5].

Different contact geometries have been employed in fretting fatigue tests, including bridge type pads [76], [77], [99], cylindrical pads [123], [78], [96] and variations of these.

No matter what the shape, crack initiation in fretting takes place at the surface of the component. The presence of a contact imposes a severe stress concentration at the surface, this being so localised, that the location of initiated flaws such as micro cracks can often be predicted with some considerable degree of certainty [110].

In each case, the distribution of the pressure at the contact renders certain locations in a contact area to be preferred sites for fretting damage, these usually being at or near the edges [77], [123], [124]. Examples of initiation locations with a flat-on-flat contact are shown in Figures 2.2 a) and 2.2 b).

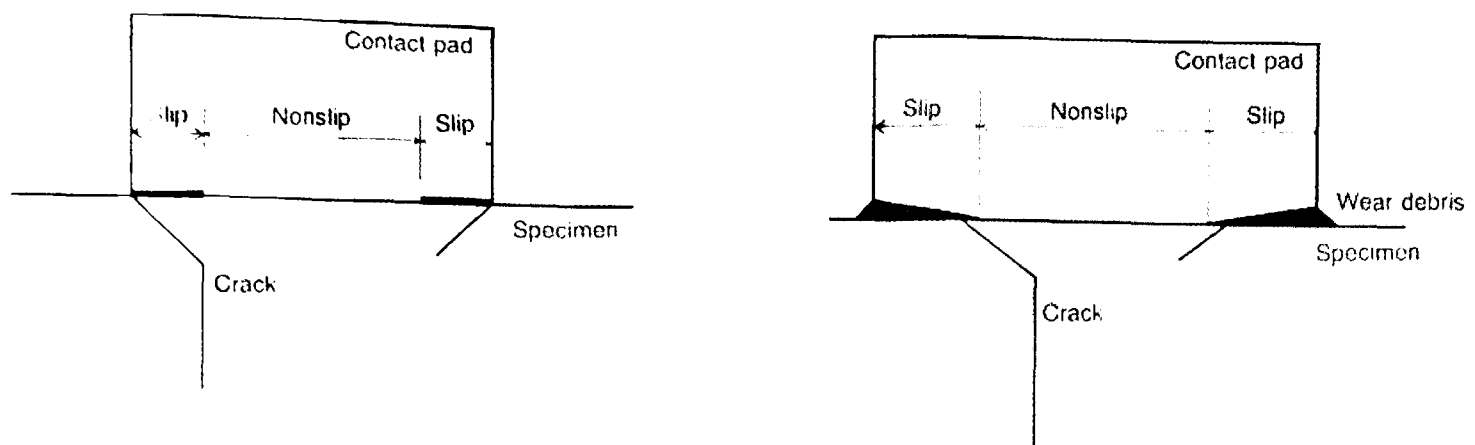


Figure 2.2: Crack initiation locations for flat-on-flat contacts [21].

Microscopic studies conducted by Taylor and Waterhouse [125] showed that the origin of fretting fatigue cracks is in the boundary between the slip and non-slip region of the contact area. Alic et al. [55] also examined fretted regions by means of scanning electron microscopy and found that cracks initiate at or near the boundary of the fretted region where it is presumed that the highest stresses and strains exist.

Wright and O'Conner [126] showed, by means of a finite element analysis, that maximum contact pressure did not occur at the edge of the contact pad, but started from somewhere inside, at the point of the maximum tangential force, a factor of two or three times the average tangential force. Use of photo elasticity techniques has also revealed a concentration of tangential forces in this region [127]. Their conclusion was that the crack initiates at the point of the maximum tangential force where the slip amplitude is also the largest [21].

The shape of a specimen also has an influence on the site of initiation. Where a specimen has a rectangular cross-section, the 90° corners themselves will have regions of stress concentration associated with them and it is therefore to be expected that cracks will initiate from these regions if the fretting pad extends beyond the edge of the specimen, leading to a corner crack [17].

2.2.4.2 Crack propagation

In fretting fatigue, the presence of intense cyclic surface friction forces virtually eliminates any crack initiation period and considerably accelerates the early phase of micro structural-dependant crack growth. The major part of fretting fatigue life is therefore considered to be spent on the propagation of fatigue cracks of the order of one grain size or more in length [128]. Visible cracks have been detected as early as within 10% of fretting fatigue life [99], which clearly indicates that the fretting fracture process is dominated by progressive stable growth of cracks and that crack propagation constitutes the major part of fretting fatigue life [85], [112].

The propagation rate of an initiated crack is greatly enhanced in the initial stages of fretting fatigue crack growth. Indeed, fretting fatigue cracks grow much faster in the early stages, than would be expected based on cyclic fatigue stresses and material characteristics alone [129]. Thus propagation is much increased by the fretting action [130].

The stresses induced by the contact can decay rapidly and the stress intensity factor range may fall during the early stages of crack growth [119]. However, this depth of influence of fretting on cracks and hence accelerated rate of crack growth has been found to exist up to a length of 30 μm – 60 μm [17], 100 μm [85] and even up to depths of a millimetre [129]. The depth of influence does depend upon test conditions such as environmental conditions, the materials used and different nominal contact pressures applied.

In any case, it is these lengths up to which acceleration of the crack growth rate due to tangential stress is negligible and after which fretting has no influence on any subsequent propagation [17].

Fretting fatigue cracks subsequently follow a distinctive path, growing to a given depth by tangential stress combined with repeated stress and then propagate with repeated stress alone prior to failure [85], as is shown in Figure 2.3, utilising nomenclature recommended by Forsyth [131].

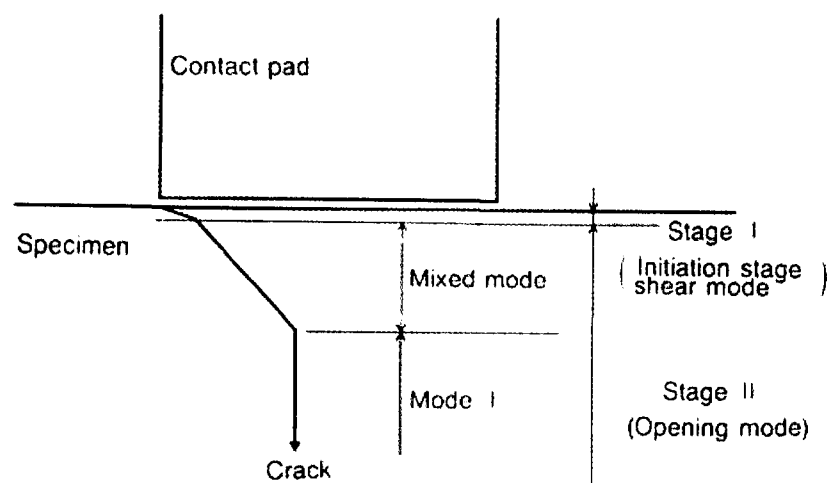


Figure 2.3: Crack propagation paths [21].

2.2.4.2.1 Stage I

In Stage I, a crack will normally be quite short and will be making the transition from the initiation phase, to the development of a proper crack straddling more than one grain [99]. Stage I growth is normally associated with very localised plasticity and the ratchetting of dislocations along persistent slip bands near the tip of the crack, this process being primarily controlled by shear, the shear stresses being predominant [45]. It is thus usually found that Stage I cracks grow along planes of maximum shear, or near maximum if the preferred planes are not oriented ideally, which for surface cracks lie at $\pm 45^\circ$ to the free surface [110].

In fretting fatigue, cracks showing predominantly Stage I or shear mode behaviour propagate in or near heavily deformed fretted regions, but show a mixture of shear and tensile mode growth [77]. Stage I development of a crack initiated by fretting is also much prolonged compared with other fatigue failures [17].

2.2.4.2.2 Stage II

Once a crack has reached a few grain diameters in size, the transition from stage I to stage II behaviour eventually takes place. It is Stage II behaviour which often dominates crack life, no endurance limit being obtained at 10^7 cycles [85]. It is here that fracture mechanics techniques are often applied to predict crack growth rates [110], as shown in Figure 2.4; Paris' equation is widely used [110].

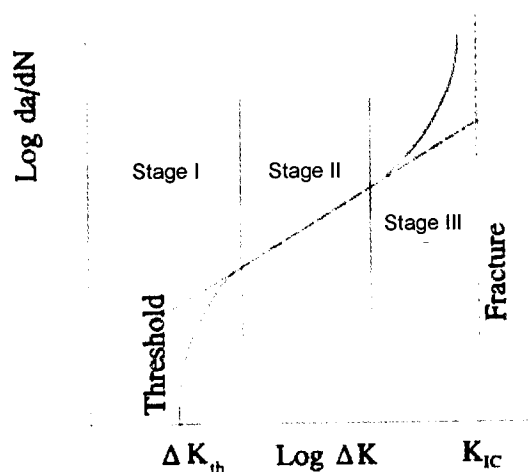


Figure 2.4: The threshold and stable stages of crack growth [110].

In fretting fatigue, small cracks initially propagate obliquely at a shallow angle to the surface of a specimen under the combined action of tangential fretting forces and cyclic body stresses, controlled by a combination of contact conditions [45]. At depths of less than $300 \mu\text{m}$, this fretting crack propagation angle shows a weak correlation with the local microstructure. This behaviour is related to the high stresses generated by the contact conditions [120].

It is often reported that these cracks propagate at angles with respect to the surface inclined at between 35° - 50° to the normal to the surface [17]. This angle is often found to be smaller than 45° when using optical micrographs [120] and when using x-ray micro tomography, stabilisation of the crack orientation has been observed with a mean value of 25° [120].

The angles of these oblique cracks depend on factors such as the combination of bulk alternating stress and contact pressure, contact width and contact material, which all influence tangential stress and hence the stress state near the contact region [21]. Oblique cracks growing to lengths of over $300\ \mu\text{m}$ [120] and up to one mm [21], without turning perpendicular to the surface have been reported. This early stage of crack propagation is significantly faster than the speed of equivalent mode I cracks [99].

In Stage II, the characteristics of the plastic deformation within the process zone ahead of the crack tip are controlled by a surrounding elastic field described by stress intensity factors, and thus propagation in Stage II is governed purely by stresses [110]. These cracks are said to grow primarily as a result of mode I loading, see Figure 2.5, at the crack tip. The stress intensity factor, K_I or rather the range of the stress intensity factor, ΔK_I is used extensively to evaluate crack propagation under mode I loading conditions.

The reported increase in the crack propagation rate of fretting fatigue cracks may be due to the presence of a mode II component. However, it is acknowledged that there is a discrepancy in the fact that although a mode II component has been identified theoretically, one has yet to be determined experimentally. The angled cracks could be due to a change in the principal stress field, as under non-proportional loading the directions of the principal stresses rotate, and the ratio between the principal stresses varies. Both the choice of crack angle and coefficient of friction, will affect the principal stress direction and hence mode I crack growth.

For mixed-mode loading, the fatigue crack growth rate may also be expressed by the Paris law, but the stress intensity factor range, ΔK_I is replaced by an equivalent stress intensity factor range ΔK_e , see Equation 2.1. C and n are material dependent constants.

$$\frac{da}{dN} = C(\Delta K_e)^n \quad \text{Equation 2.1}$$

Many methods for defining the equivalent stress intensity factor range ΔK_e for mixed-mode loadings have been proposed, but no universally accepted approach exists. However, for a known, fixed angle, based on the addition of Irwin's elastic energy release rate parameters, ΔK_e may be defined as shown in Equation 2.2, substituting the often described Equation 2.3:

$$\Delta K_e = (GE)^{\frac{1}{2}} = \left[\Delta K_I^2 + \Delta K_{II}^2 + (1 + \nu)\Delta K_{III}^2 \right]^{\frac{1}{2}} \quad \text{Equation 2.2}$$

$$\Delta K_{I,II,III} = Y_{I,II,III} \Delta \sigma \sqrt{\pi a} \quad \text{Equation 2.3}$$

Here, G is the shear modulus, E is Young's modulus and ΔK_I , ΔK_{II} and ΔK_{III} correspond to the range of the stress intensity factors for the three modes of loading. Y_I , Y_{II} and Y_{III} are geometrical factors which are functions of the crack aspect ratio, the parametric angle defining the crack, Poisson's ratio, ν and the loading conditions; $\Delta \sigma$ is a representative applied stress range and a is the crack half-length.

Hills et al. [132] have used experimental data to calculate K_I and K_{II} factors for a crack at a cylinder/flat contact and presented the information in terms of contour maps; Sheikh et al. [102] utilised finite element techniques. The maximum value of K_{II} occurs when the crack is inclined at an angle of about 45° to the free surface and from this aspect, growth under the contact is clearly favoured. The calculated K_I reaches a maximum for a crack approximately at right angles to the free surface [45].

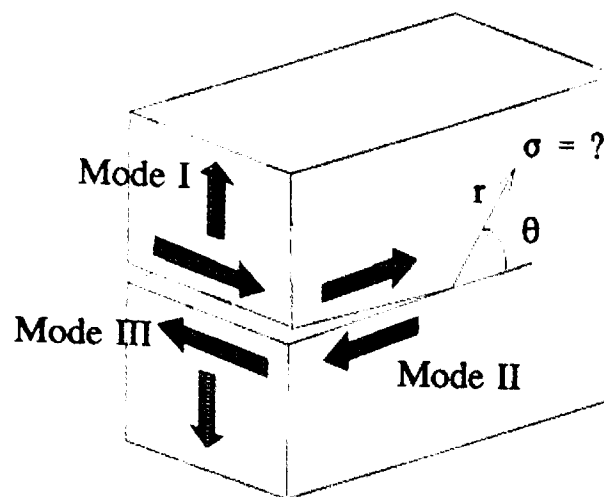


Figure 2.5: The three modes of loading of a crack tip [110].

However, these fretting fatigue cracks propagate under the influence of a contact stress field, which is limited in extent, having dimensions of the same order as the contact itself [110]. Thus eventually, when a crack reaches a certain depth, having grown beyond the immediate neighbourhood of the contact, the influence of the contact stress field will diminish to such a level that the crack will change direction under the contact, at which point tensile forces will predominate, the situation will be essentially one of plain fatigue [110] and further crack propagation will thus occur perpendicular to the applied stress since the friction forces will then be insignificant [45]. Under fatigue propagation, the crack path is observed to become very tortuous, exhibiting several straight branches, which show that the propagation here is strongly influenced by the local crystallography again [120].

2.2.4.2.3 Stage III

Eventually a fretting fatigue crack, just as a plain fatigue crack, will become so long that the crack tip plasticity zone will start to dominate the response. This signals the third stage of its life when the high ΔK values cause acceleration in the crack growth rate towards failure, as the maximum stress intensity in the cycle approaches the fracture toughness [110].

2.2.4.3 Crack closure

If the level of bulk stress in a system is relatively low, a stress intensity factor will fall with increasing crack length. In fretting fatigue, ΔK will reduce as a crack grows away from a contact and the propagation rate will be reduced. In some circumstances ΔK can fall below ΔK_{th} so that the growth of the crack ceases and the phenomenon known as self-arrest takes place [110].

For an inclined crack growing under a contact under mixed mode I/II loading as in fretting fatigue, a predicted crack closure condition is always a possibility. If the transition from mode II to mode I growth does not occur at an early stage in life, then closure and a non-propagating crack are likely to result [45].

2.2.5 Influential factors in fretting fatigue

Depending on the parameters that influence fretting fatigue, a significant reduction in fatigue life may occur as a result of fretting [18]. It has been reported that up to fifty variables may influence the magnitude and rate of the fretting fatigue process [133]. Since however, they are perceived to be the parameters of greatest importance, the roles of frictional force, contact pressure and slip have received particular attention [45]. Successful predictions of fretting fatigue life have been made using only a few parameters including: the external load, contact pressure, coefficient of friction and amplitude of slip. Consequently, the concept of a primary set of variables has been proposed, with a secondary set of variables being those which affect the fretting process through changes these variables effect in the primary set [134]. Indeed, fretting fatigue involves a highly complex interplay between mechanical, metallurgical and environmental factors, their individual contributions being quite different from those operative in plain fatigue [45].

Although a wide range of factors affect the number of cycles required for damage to accumulate, they can conveniently be grouped into three categories:

1. Mechanical factors such loads, the amplitude of micro slip, coefficient of friction, etc.
2. Material factors, including the contact, surface finish and micro structural properties of the material(s) in addition to 'bulk' properties such as yield stress or fracture toughness;
3. Environmental factors, including the background temperature and whether there are any corrosive agents present [110].

2.2.5.1 Mechanical factors

2.2.5.1.1 Axial load

Fretting fatigue tests with a fully reversed axial stress have resulted in longer fretting fatigue lives, than those of tension-tension counterparts at a given relative slip, tangential force range and axial stress range [135]. Mean stress also has a much greater effect on fretting fatigue strength than on fatigue strength. The effect of mean stress is more concerned with the propagation of fatigue cracks than with the initiation of cracks by fretting [17].

The majority of investigations carried out on fretting fatigue make use of constant amplitude stress cycles. It has been shown however, that the greater the degree of randomness, the more damaging the results. It has also been demonstrated that no non-propagating cracks are observed in fretting fatigue tests where random stress cycles are applied, whereas such cracks are not uncommon under conditions of constant amplitude [17].

A specific test on variable amplitude loading, has found that increasing the contact pressure at low frequencies, reduces fretting fatigue life, but does not have any effect at high frequencies [136].

Also, the superposition of small amplitude, high frequency cycles on a low frequency, large amplitude cycle, produced no definitive detrimental or beneficial impact on fretting fatigue resistance, when compared with a high frequency, constant amplitude test [137].

2.2.5.1.2 Frequency

Fretting fatigue lives at higher frequencies have been found to be less than those from tests conducted at lower frequencies, with a larger difference being noted at higher ratios of axial load [137].

Fretting fatigue failures in high performance turbo machinery are focussing attention on to the effects that high cycle fatigue/low cycle fatigue tangential load waveforms have on the surface mechanics and near surface stresses of fretting contacts. A relationship has been found between the number of low cycle fatigue cycles to failure and the relative high cycle fatigue frequency and amplitude [138]. The fact that a reduction in fatigue strength is lower, the lower the frequency, may be illustrated by the fact that in turbo generators, most fretting damage is thought to occur whilst running up and running down [17].

2.2.5.1.3 Friction

There are two phenomena induced by fretting between two contacting surfaces: wear and friction [21]. The coefficient of friction has been identified as the main variable in the fretting process, with the effect that other variables have on the fretting process being explained by the changes that these variables cause in the value of the coefficient of friction itself [134].

The mechanisms of friction involve the fine geometric configurations of the surfaces, as well as the physical, chemical and mechanical properties of the transient layers. This complexity is increased by the changing character of the friction phenomenon and the continuous changing of the surfaces due to wear [139].

An increase in the amplitude of the friction coefficient at a contact can intensify the process of spalling [140]. Friction also has a significant influence over the very early stages of crack growth [25]. Edwards [77] has shown that the presence of friction forces can be important in determining the rate at which short cracks grow.

Fretting fatigue damage is caused by the combination of friction stresses and repeated stresses [141]. In fretting fatigue, an alternating stress in one of the components of the contact results in an alternating strain and the only restraint on the resultant fretting movement is the level of the coefficient of friction [17]. The significance of friction forces during fretting therefore primarily arises from their effect on stresses near the contact zone [142]. The reduction in fatigue strength due to fretting has been shown to be due to the added shear stress which arises from the friction force between a pad and specimen [143]. Furthermore, as fretting fatigue cracks initiate at the highest point of tangential force on a surface in the very early stages of fatigue life and as the frictional behaviour between two components in contact controls the tangential force at the surface interface, it is said that this is the dominant factor influencing crack initiation and propagation and hence in reducing fatigue strength [21].

Under fretting conditions, stress changes exhibit some peculiarities that arise from the non-linear nature of the friction involved [142]. In most cases, the coefficient of friction is low initially, but within the first few hundred to thousands of cycles, rises and then is maintained at a steady-state [143], [124], [144]. This increase in friction has been quantified as increasing by over 300% during the first 50 cycles, whereas at 10^6 cycles, the coefficient of friction exceeded the first cycle value by a lesser 180 - 240% [145].

However, the rate at which this increase is achieved and the values involved, depends on the materials in contact [141] and an increase in the roughness of the contacting surfaces from the fretting action [144].

The plateau is due to a modification in the contact geometry and a balance of wear debris [146]. Test results for a contact between aluminium alloy 2024 T351 have indicated that the steady state coefficient of friction ranges from between 0.65 and 0.70 [147].

Friction logs are three dimensional graphs that present the variation in the coefficient of friction versus displacement and time or number of cycles and reveal the development of the coefficient of friction during a fretting fatigue test. This allows the coefficient of friction to be correlated with other influencing factors [148].

Friction is influenced by a number of other factors. The component materials and the condition of the mating surfaces determine the variation of the friction coefficient with the amplitude of slip and tangential stresses [5]. The degree of adhesion that occurs between different combinations of materials can also be shown by the initial coefficients of friction [66]. Thus the condition of mating surfaces, their composition, surface roughness, residual surface stresses and oxide or other surface films are important [17]. The number and size of any surface asperities and the strength of interfacial debris particles are also important [99].

Relative slip and normalised friction force are directly related to one another [144]. An increase in the applied relative slip as well as the applied bulk stress, and hardness of the contact materials results in an increase in the friction force [144], [149]. The position of the boundary between regions of slip and non-slip may move as fretting develops, in part because of changes in the coefficient of friction as debris is formed [17].

Friction stresses also depend on frequency [141]. An increase in contact load, frequency and temperature decreases the normalised friction force [144]. The coefficient of friction being smaller at higher frequencies is attributed to the behaviour of oxide debris [150]. The magnitude of friction forces is controlled by the cyclic variations in the applied loads, rather than the absolute magnitude [151].

In general, as far as the damage is concerned, the higher the roughness of the contact, the higher the coefficient of static friction that is observed [144] and the depth of the damaged layer formed in the initial stages of fretting fatigue is larger with a larger friction force [150]. Lowering the friction in a system is thus one of the best approaches to alleviating fretting fatigue [25]. Contact materials that contribute low friction coefficients are beneficial for fretting fatigue strength [21].

2.2.5.1.4 Normal load

Normal load is an important parameter in fretting fatigue, as it has a direct influence on life. According to results reported by Waterhouse [17], as the clamping load is increased from zero, there is a dramatic fall in the fretting fatigue limit. The fretting fatigue strength initially decreases with increasing contact pressure, but at pressures greater than some critical value the fretting fatigue strength is approximately constant. Switek [152] further demonstrated an increase in fatigue strength at higher clamping pressures due to crack closure, resulting from the introduction of compressive stresses at a crack tip, which retards progress.

Faanes and Fernando [100] observed an increase in fatigue life for contact loads above a certain level and through measurement of the friction in the contact zone predicted the effect by a crack growth model.

Nakazaw et al. [153] have shown that there is a minimum in the curve at low clamping pressures, followed by a maximum, which has been attributed to the stress concentration at the slip/non-slip boundary, which is greater when the stick region is narrow, i.e. at lower clamping stresses [17]. A normal pressure threshold in fretting fatigue was reported by Adibnazari and Hoepfner, where there is a value after which increasing the pressure does not affect life [154].

Generally speaking however, the lower the clamping load, the lower the total life [17], but below a critical normal pressure, fretting fatigue life increases as the contact load decreases and so reducing the contact pressure in a system is one of the best approaches to alleviating fretting fatigue [25], [124], [85]. For some values of normal pressure, varying the shape of a load waveform has been found to enhance the resistance of a material to fretting fatigue [155].

2.2.5.1.5 Residual stresses

Compressive residual stresses have a beneficial effect on fretting fatigue life, reducing the rate of wear [156] and slowing down the propagation of micro cracks which can lead to particle detachment [156].

Studies have shown an evolution of residual stresses in specimens initially free of residual stresses with an increasing number of cycles. Initially, higher contact loads resulted in higher residual stresses at the surface, but as the number of fretting fatigue cycles increased, compressive residual stresses increased and then stabilised. The fretting action in the contact region can thus be regarded as having the same deformation mechanism as low plasticity burnishing [157].

However, studies on specimens in which a layer of compressive residual stresses has been introduced prior to testing, have shown that stress relaxation of 20% at less than 10,000 cycles is achieved [156]. Indeed, Nowell et al. [19] have acknowledged that there is a need to predict fretting fatigue performance in the presence of residual stresses.

2.2.5.1.6 Slip

Under the influence of cyclic stresses, cyclic strains result in slip occurring between contacting surfaces. In fretting fatigue, it is the partial slip regime that is of importance and it so happens that this is the most likely situation for fatigue cracks to initiate [17]. It has been shown that full slip takes place in the first few hundreds of cycles of a fretting test [77].

The amplitude of slip between two surfaces has a significant influence on the initiation process [158]. At low amplitudes of slip, fretting is mild and long fatigue lives are recorded and the wear rate is correspondingly low [110]. When total slip occurs, wear is the predominant feature, but the initiation of a propagating fatigue crack is less likely [17]. One possible explanation for this is that any crack nuclei are being continually worn away and the accumulation of debris may act as a solid lubricant [159].

Generally speaking, fretting fatigue strength decreases with an increase in relative slip amplitude [21], [160], [149], with a critical slip range, at which fretting fatigue life is shown to be a minimum [124], sometimes observed in the region of 50 – 60 μm [161], [162]. Fretting fatigue life then increases with a further increase in the relative slip range due to the transition in the fretting regime from partial slip to gross slip [160] and associated material removal [161].

This effect however, is dependent on the magnitude of the normal pressure applied. For example, for one given normal pressure, the fretting fatigue life for one steel has been shown to decrease with increasing slip amplitude, whilst for another steel, the fretting fatigue life changed little with the amplitude of slip. At a lower normal pressure though, a minimum fretting fatigue life was observed in both materials at a slip amplitude of 20 μm [70]. Under certain load conditions the critical amplitude for an aluminium alloy has been shown to be approximately 8 μm [37].

Controlling slip is said to be a valid method of improving fretting fatigue strength [25]. It has been reported that crack formation can be prevented or retarded by ensuring that slip occurs over an entire contact [163].

However, whilst it has been shown that slip displacement can have an effect for a sliding contact [108], when fretting fatigue takes place under full slip, the contact stress distributions are uniform, hence there is no correlation between slip amplitude and the mechanical loading and thus crack growth behaviour [146].

If mechanical loading in terms of the stress intensity factor of a fretting crack varies with the degree of partial slip in the contact, then this is because the distribution of contact shear stress changes with different sizes and locations of the stick zone. The slip amplitude should thus be seen as a secondary effect and not as a direct cause to changes in fretting fatigue crack behaviour [146].

It has recently been stated by Dini and Hills, that if the primary variable controlling crack propagation is the state of stress and that nucleation is also controlled by the range of stress suffered, then there is no clear reason why the range of slip displacement should be relevant at all [108].

2.2.5.2 Material factors

2.2.5.2.1 Contact

The distribution of contact stresses across a contact is dependent on the geometry and material properties of the components in contact and [146] the distribution of contact stresses has a significant effect on fatigue life [77]. The type of contact involved is also an important fretting fatigue parameter, as it governs the confinement of debris [58].

Bramhall [59], showed that the fretting fatigue strength of an aluminium alloy was doubled when a pad with machined grooves was used as a fretting contact. The position where cracks develop depends on the nature of a contact too [17]. Cracks invariably initiate at the edge of a contact zone [124], or a slip/non-slip boundary within the contact region [17].

The geometry of the fretting pads utilised in fretting fatigue tests and models has been varied. Flat [76], [77], [99]; nominally flat with rounded corners [164], [162]; conical [164]; cylindrical [162]; and spherical [165], the latter two being the most popular in recent years. Flat contacts are unpopular nowadays, due to the singularity which appears at the edges, where the stresses are theoretically infinite; furthermore, the friction force produced on the surface of the pad generates a moment in the bridge, which can result in the uneven distribution in the contact stress [165]. Flat ended fretting surfaces may be modified by wear though [146], as due to high stress concentrations at the edges of the fretting pad, the surface of either the specimen or the fretting pad, or both, may be worn, so that concentration of stress is reduced. Neither of these issues arises when employing a cylindrical or spherical pad. There are however, few real cases of fretting fatigue where this type of contact actually exists.

Fretting fatigue life has been shown to be independent of the contact configuration though, although this is not true of the surface profile of the fretting scar [162]. However, fretting fatigue life has been found to vary with contact size [109]. Nowell and Hills [158] emphasised that fretting fatigue crack initiation will only occur when a critical contact width is exceeded [17]. It has been shown that the wider the contact width at a given normal pressure, the shorter the fatigue life at a given alternating stress. Furthermore, the value of the normal pressure required to initiate a crack is lower the broader the contact width [37]. Another critical contact size is also said to exist, whereby fatigue lives are longer than 10^7 cycles [109]. The effect of contact width appears to be affected by the surface condition, i.e. coefficient of friction [60].

According to Iyer [166], the contact semi-width is a function of the contact pressure and does not itself have any effect on fretting fatigue life. However, this work has been disputed by Hills and Nowell [167].

2.2.5.2.2 Materials

An awareness of changes in material properties, including strain hardening and a reduction in toughness during testing is necessary to understand changes observed in material behaviour during fretting fatigue [58].

Microstructure is a major factor in the fretting fatigue behaviour of a material, particularly the microstructure of the surface. However, the fretting process itself can modify that structure since both plastic deformation with attendant work hardening, as well as the generation of heat, with the possible over ageing of age-hardened materials can occur [53].

Different degrees of surface damage are possible with different contact materials [17]. In general, alloys which derive their enhanced mechanical properties by work hardening or age hardening are likely to suffer greater reduction in fatigue strength in fretting than cast or annealed materials [53]. Alloys with the highest stress-life fatigue properties exhibit a greater reduction in fatigue strength due to fretting, the total fretting fatigue life being primarily determined by the fatigue crack propagation resistance of the alloys [113].

In most cases, a good choice of material can only delay or modify the formation of fretting damage, but cannot do away with it completely [58]. Reactive metals rely on protective oxide films to provide lubrication; however, fretting continually disrupts such layers, giving a much enhanced effect in conditions normally considered non-corrosive [17]. Low notch sensitivity and a high degree of fracture toughness can also be important. Materials that are less prone to fretting damage in this respect are cast or annealed components; however, the low strength of these materials makes them unsuitable structurally.

Materials in contact with steel that are likely to cause the least damage included pure aluminium and copper. Part of their usefulness is thought to be their high thermal conductivity, which dissipates the heat generated in the contact region [17].

The conventional method of establishing the important variables which can affect fretting fatigue has been to generate *S-N* curves, with and without fretting, thereby allowing fretting fatigue strength reduction factors to be established. This method is particularly important for ranking various combinations of materials in terms of fretting fatigue performance; an indication being given of material combinations where significant fretting problems will arise or which should be avoided altogether [17].

As far as ceramics and polymers are concerned, there is limited information on their fretting fatigue performance. The static and cyclic fretting fatigue strengths in ceramics are almost coincidental when the friction force is the same [149] and data on fretting wear suggests that they are very wear resistant, this being due to their hardness and very low reactivity [168]. The elastic moduli of fibre reinforced polymers are far lower than those of metals. Amplitudes of slip recorded in fretting fatigue experiments conducted with these polymers can be as high as 700 μm and thus any damage may therefore be associated with wear [17].

2.2.5.2.3 Surface finish

Nominally flat surfaces are never so in fact, the contact between them is likely to be discontinuous, probably macroscopically due to waviness of the surfaces and microscopically owing to the texture of the surfaces [169]. Depending on the surface finish, the contact area may be made up of a large number of discrete small areas, or a few large regions [37]. Therefore, local regions of contact between high spots are likely to behave as spherical surfaces in contact [169].

It is said that it serves no useful purpose to specify the state of a surface as this will change from the first few cycles [139]. However, as analysis of a rough contact predicts a larger value of overall apparent contact size, the difference diminishing as pressure increases and a rough contact tends towards a smooth model. Furthermore, as pressure increases, the average asperity spacing falls while the average asperity size increases, which affects the slip [115].

In plain fatigue, the fatigue strength of a specimen decreases with increasing roughness, whereas the contrary is true in fretting fatigue [170]. This may be explained by the fact that a rough surface will have a lower surface strength in shear than a smooth surface, the reduction in fretting fatigue strength therefore being dependent on the radii of the asperities [171]. However, Proudhon et al. [172] report that crack initiation appears very sensitive to surface quality, a higher roughness leading to a lower value of the tangential force needed for crack initiation.

An increase in surface roughness is observed in specimens subjected to fretting fatigue under conditions of stick-slip, but surface roughness does not show an appreciable change under gross sliding. However, in order for a surface roughness methodology to be more acceptable as a means of evaluating fretting fatigue damage, more measurements to cover the whole of a fretting scar and further investigation of specimens under different fretting fatigue conditions is necessary [173].

Eddy current and ultrasonic wave techniques are used to detect cracks due to fretting fatigue damage. However, major problems with these methods are the presence of surface roughness and irregularities caused by fretting fatigue [173].

2.2.5.3 Environmental factors

Friction and wear behaviours have been shown to be affected by environmental factors. In fretting fatigue, materials have a much greater sensitivity to their environment compared with plain fatigue [53]. The environment is a contributory factor in the initiation and propagation of cracks.

The effects an environment may have on the development of fretting fatigue cracks and their propagation to failure can be summarised as follows:

- The effect on the coefficient of friction between two contacting surfaces. Reducing a coefficient of friction renders crack initiation less likely, this being achieved, for example, by encouraging the growth of protective corrosion products as in high temperature oxidation.
- The effect on the propagation of any cracks that are formed. In protective atmospheres, including a vacuum, or where cathodic protection has been applied, propagation will be retarded, despite the fact that in some cases a coefficient of friction may have been increased [17].

2.2.5.3.1 Aqueous electrolytes

In fretting, oxide films are continuously disrupted and rapid attacks can occur. The reduction in the strength of such materials in a corrosive environment such as sea water may be not much greater than in air, because the corrosive agents, oxygen and water vapour, are present in both environments [17].

In sea water a coefficient of friction will be lower and there will be a cooling effect, both of which will have an influence on crack initiation. However, once initiated by fretting, cracks grow at a faster rate in sea water than in air [174]. Entrapping liquid in a crack can enhance growth rate, keeping the faces of the crack apart under load [175]. An application of cathodic protection can reduce the propagation rate of a crack and can even retard it, this prevention of crack closure being due to the deposition of calcareous deposits within it [17].

2.2.5.3.2 Atmosphere

In tests conducted both in a vacuum and in air, the average friction coefficient, the surface roughness and wear rate were all lower in a vacuum [176]. There have been reports of a tenfold increase in fatigue life in a vacuum [177].

2.2.5.3.3 Humidity

Aluminium alloys are extremely sensitive to humidity, an increase in water vapour accelerating both the initiation and propagation of fretting fatigue cracks [128]. The effect of humidity on fretting fatigue has been attributed to its own influence on coefficients of friction, which are related to the shear strength of an oxide under high contact pressure, which in turn, is related to the heat of formation of the oxide [178]. In dry air the number of cycles required to initiate a propagating crack can be increased by several factors and the total life of a specimen increased significantly, when compared with those results achieved under normal operating conditions [17].

2.2.5.3.4 Temperature

The fatigue properties of materials are generally reduced as their temperatures are raised because of decreases in yield strength. However, exposing metals to high temperature oxidising atmospheres may promote the formation of a protective oxide on certain high temperature alloys, which brings about a large reduction in the coefficient of friction and the wear of the surfaces [179]. This more than compensates for any reduction in fatigue strength incurred.

The effect of low temperatures on the mechanical properties of metallic materials can be significant. From investigations into the fretting wear of copper and stainless steel, it is known that at low temperatures the coefficient of friction that exists between two surfaces will rise to a very high value because of the effects of severe adhesion. No loose wear particles are produced, but the considerable surface damage can be attributed to the absence of oxide films [180].

2.3 SHOT PEENING

2.3.1 An introduction to shot peening

Hand peening was undertaken to improve the durability of battle helmets, armour and weaponry thousands of years ago, as has been highlighted in review papers by Longhorn [181] and Cary [182]. However, the use of peening to improve specifically the material properties of components does not appear in the literature until the 1920s, by which time the peening of automotive components had become common practice [183]. In the mid 1920s it was observed that automotive castings that had been sand blasted clean showed increased fatigue resistance. It was not until 1927 that shot peening as a process was first documented, Herbert [184], describing the 'cloudburst process' which was used to increase the hardness of metals by raining steel balls down onto them. A German patent on steel shot blasting was subsequently published in 1929 [185].

The use of shot peening to improve fatigue resistance was first documented in 1935 by Weibel [186], who described an increase in life of shot blasted steel wire. The first systematic study of the many process parameters involved was undertaken in 1940 by Zimmerli [187], who investigated the influence of variables including: time and the diameter of the shot, on the fatigue behaviour of shot blasted steel springs. The influence of shot blasting on the fatigue resistance of aluminium alloys was first undertaken by Wiegand [188] and in 1943, Almen [189], [190], [191], introduced a device for measuring the intensity of a shot peening treatment, regardless of the input parameters, which has become the standard process control.

The residual stresses in shot peened parts were determined quantitatively for the first time in 1945 by Milburn [192] and a book on the relationship between residual stresses and fatigue was published by Almen and Black [193] in 1963.

Almen also formed the Society of Automotive Engineers' committee on shot peening; the first international conference on shot peening was held in 1981 and has occurred every three years ever since.

2.3.2 The shot peening mechanism

In the shot peening process, shot is accelerated by means of compressed air for example [194] and is then projected onto a component, striking the surface at a high velocity and imparting up to 90% of its kinetic energy to the target material [195]. The degree of deformation undergone by the target material is related to this transfer of energy and the material properties involved.

At the surface beneath the shot, the material deforms permanently, plastically. Further below the surface, an elastic response is observed and further still below the surface there is no effect. The elastically deformed layer subsequently attempts to relax as the shot rebounds, but is restrained by the plastically deformed material, the result being that a compressive residual stress is established at the surface, decaying with depth until a point at which they become tensile, as the material has to achieve a state of equilibrium in terms of internal forces and moments.

2.3.3 Shot peening effects

Shot peening deforms material plastically, leaving small craters [27]. This surface mechanical treatment results in three key changes in the surface and subsurface of the target material, related to the shot peening parameters and material conditions [196]. The performance of shot peening in terms of fatigue depends on the balance between these beneficial and detrimental effects.

2.3.3.1 Micro hardness

An increase in micro hardness has been observed due to shot peening [197], which has been attributed to changes in the microstructure [198], including distorted grains and an increase in dislocation density [199]. Micro hardness is not seen as being particularly influential on fatigue life.

2.3.3.2 Surface roughness

The dents sustained by shot peening lead to a change in surface roughness, a measure of which is given by the depth and average spacing of the indentations incurred [200]. Generally, a rougher surface yields a shorter fatigue life [71] and the level of roughness created by shot peening does affect how much gain is otherwise made as a result of the process [201]. It has been shown that a similar improvement in fatigue life achieved by shot peening can be achieved by means of burnishing, where the resultant compressive stress is less, but there is a smoother surface finish [202].

2.3.3.3 Residual stress

The plastic deformation and subsequent restrained elastic material caused by shot peening results in compressive residual stresses. The scale and depth of these compressive residual stresses have an influence on fatigue [203]. Residual stresses are believed to be the dominant factor in improving fatigue life through shot peening [196], inhibiting crack propagation [204]. Solis-Romero [197] has analysed the influence of shot peening parameters on the creation of residual stresses and required fatigue lives.

2.3.4 Influential factors in shot peening

There are six primary process parameters which are used to describe a shot peening condition [205]. The angle of incidence, media and velocity are controlled directly and adjusted to obtain the desired values of the coverage, intensity and saturation, which need to be measured in calibrating test runs.

The selection of shot peening parameters will depend on factors such as: the residual stress field desired in the subsurface layers, the geometry and material of the component and the system of forces to which the component will be subjected.

2.3.4.1 Angle of incidence

The angle at which shot impacts the surface material, has an effect on the surface finish, including the shape of the dents incurred. When the shot is fired at an angle of 90° to the surface, the resulting degree of plasticity is greatest and the indentations the deepest [206], with circular contours. If this angle is reduced, then the plasticity decreases and the dents become more elongated.

2.3.4.2 Media

Shot peening media varies in size and should be spherical to avoid sharp dents; there are specifications in industry which govern this [207]. An extensive range of materials are used, including: glass or ceramic beads, steel wire and cast iron or steel balls [208], the latter being the most widely used due to favourable material properties, including a high elastic modulus and hardness, which increase the transfer of energy from the shot to the surface.

Glass and ceramic beads are less dense, but their use results in a good surface finish, which is preferential for fatigue resistance, but costly in terms of breakages. There is a need for high quality shot in peening [209].

However, all types of shot can wear or fracture and it is suggested that peening can then be detrimental to fatigue performance [210]. It is not recommended to use steel shot topeen aluminium, as iron pick up ruins the corrosion resistance.

2.3.4.3 Velocity

The velocity at which media travels to the surface material is very important, as it governs the kinetic energy transferred to the material on impact. The component of the velocity normal to the surface material controls the intensity [211], see Section 2.3.4.5. However, although the velocity of shot can be controlled by air pressure, measuring the velocity of shot is difficult and a parameter has not yet been established for process control.

2.3.4.4 Coverage

Coverage is a description of the percentage of a surface area covered by shot in a given time. Complete coverage is deemed to have occurred when coverage reaches that maximum which is achievable theoretically, 98% [212] and coverage quoted at over 100% refers to the condition where a multiple of the time taken to achieve 98% coverage has been applied. At least 100% coverage is recommended for improved fatigue performance [213], but 200% coverage is preferable to ensure the saturation of residual stresses.

2.3.4.5 Intensity

The amount of kinetic energy transferred by a given particle of shot to a target material is referred to as the intensity [214]. The intensity in peening is measured using Almen strips and an Almen gauge [215]. Strips of nominally flat spring steel, or more recently, an aluminium alloy [212], are peened and the resultant arc height measured in the gauge. The level of intensity is given as a measure of the height, together with a letter denoting the type of strip used, as these come in three different thicknesses.

However, the same level of intensity can be achieved using a heavy shot at a low velocity and a lighter shot at a higher velocity, with differing consequences in terms of surface features and therefore for fatigue resistance. Also, different residual stress distributions can be obtained for the same level of intensity measured [213].

2.3.4.6 Saturation

Almen intensity is defined as the point at which saturation occurs [207], i.e. the point at which doubling the exposure time produces a less than 10% increase in the arc height [208]. However, saturation may be attained before 100% coverage is achieved, in which case further peening may be desirable.

2.4 SHOT PEENING AND FRETTING FATIGUE

2.4.1 An introduction to shot peening and fretting fatigue

Shot peening has been widely used as a palliative in fretting fatigue [23] for many years [216], being one of the most effective methods of reducing fretting damage [28]. As it should always provide alleviation of a fretting fatigue problem, shot peening is also often used in conjunction with other palliative treatments [23]. The resultant improvement in the fatigue life of a specimen can be over 22% [28] and it has been reported as being as much as 300 % [217]. However, the effects of shot peening on fretting fatigue have yet to be fully understood or quantified.

In 2001, de los Rios et al. [218] utilised the fretting fatigue test facility at the University of Sheffield to begin work on investigating the mechanisms of crack initiation and failure in unpeened and peened specimens.

2.4.2 The mechanism of shot peening and fretting fatigue

In designing against fretting fatigue, two strategies may be adopted, either the conditions under which cracks are initiated must be suppressed or conditions of self-arrest must be contrived [219].

Beard [25] has concluded that the increase in the fretting fatigue durability of components achieved by shot peening, is either due to the influence of peening over the principal fretting factors or a result of the improvement of resistance to crack nucleation. Gordelier and Chivers [23], agree that crack propagation is not significantly affected, as the residual surface compressive stresses are only introduced to a depth of some 0.3 mm [220]. Rather, the compressive stresses in and close to the surface offset the tensile part of the stress cycle and hence inhibit crack initiation.

Von Tein and Seibert [221] have shown that shot peening returns titanium to a previously unfretted strength. Waterhouse et al. [29] have shown that shot peening restores the fretting fatigue strength at 10^7 cycles to the value of the normal fatigue strength without fretting as well and it was thus concluded that shot peening does not prevent the initiation of cracks by the fretting action, but markedly inhibits their propagation.

Fouvry et al. [222] agreed that the introduction of compressive residual stresses appears pertinent against crack propagation, but ineffective against crack nucleation due to the activation of surface relaxation phenomena. de los Rios et al. [223] reported that the resultant increase in fretting fatigue life achieved by shot peening is caused by both retarding crack initiation and decreasing the crack propagation rate.

de los Rios et al. [218] have ascertained that the mechanisms of crack initiation and failure are different between peened and unpeened conditions in fretting fatigue. In unpeened specimens fretting fatigue cracks always take the form of three-dimensional, semi-elliptical, surface cracks and at low contact pressures only one crack initiates and propagates to failure, whereas at high contact pressures multi-crack initiation occurs [218].

Bignonnet [28] has found that shot peening shifts the fretting fatigue crack initiation point from the surface to an internal defect, thus improving the fatigue strength at the surface. de los Rios et al. [218] determined that in peened specimens, cracks initiate both at the surface and at the subsurface of components and failure is always associated with a single subsurface crack originating from the corner and propagating as a quarter elliptical crack. All surface cracks are subsequently substantially retarded or arrested by the effect of the compressive residual stresses left after shot peening [218].

The difference therefore, in crack propagation in unpeened and peened conditions, is that while in the former, surface cracks soon join to form a common front and propagate as a through thickness crack, in peened specimens they are so significantly retarded by the compressive residual stresses, that they seldom join before a failure crack subsurface overtakes [218]. Shot peening therefore, is effective in preventing the growth of fretting fatigue cracks up to a critical size, where the stress intensity factor would otherwise be high enough to propagate the crack to failure [28].

2.4.3 Influential factors in shot peening and fretting fatigue

As was stated in Section 2.2.5, it has been reported that up to fifty variables may influence the magnitude and rate of the fretting fatigue process [133]. Since, however, they are perceived to be the parameters of greatest importance, the roles of frictional force, contact pressure and slip have received particular attention [45].

2.4.3.1 Friction

The coefficient of static friction increases during the earlier part of a fretting fatigue test and then reaches a constant value due to an increase in the roughness of contact surface from the fretting action; the higher roughness of a surface from shot peening increases the coefficient of static friction still further [144].

Controlling the surface finish by means of shot peening can control the coefficient of friction to some degree and changes in the interfacial friction can be beneficial, but whether this parameter should be increased or decreased depends on a number of factors [23]. Gordelier and Chivers [224] have considered how changes in the coefficient of friction influence fretting fatigue performance, but the conflicting results, dependent on the type of contact and loading applied, only go to highlight the complexity of the problem. This phenomenon warrants further investigation.

2.4.3.2 Normal load

de los Rios et al. [218] determined that shot peened components have a similar dependence on normal load conditions as unpeened components. However, the increase in the fretting fatigue durability of components is particularly marked at low contact stresses, while at high contact stresses, the difference between peened and unpeened specimens is not as discernible.

2.4.3.3 Slip

Lee and Mall [160] discovered that shot peened specimens have longer fretting fatigue lives than unpeened specimens for a given range of relative slip, but the minimum fatigue life found is at the same value of relative slip for both conditions.

2.4.4 The effects of shot peening on fretting fatigue

As was stated in Section 2.3.3, shot peening results in three key changes in the surface and subsurface of the target material [196] and the performance of shot peening in terms of fatigue depends on the balance between these beneficial and detrimental effects.

2.4.4.1 Micro hardness

Shot peening increases surface hardness and increasing surface hardness is an advantage in fretting fatigue, if it implies an increase in the strength of the surface layers [17]. Increasing the hardness of a surface means that the material will be better able to resist the high strains arising locally from the fretting action [29]. However, it has been shown that work hardening really has only a minor role in improving fretting fatigue life [29], Mutoh et al. [225] among others stating that as cracks are known to initiate in the very early stages of fretting fatigue life, the effect of hardening of the surface layer is really rather insignificant.

2.4.4.2 Surface finish

The success of using shot peening as a palliative to improve fretting fatigue life can be attributed in part to an increase in surface roughness [226], [26], although the increase in surface roughness produced by the process is considered to be of secondary importance [28].

Waterhouse and Trowsdale [170] have found that surface roughness reduces fretting fatigue strength when compared with a polished surface, but that the greater the roughness thereafter, the higher the fatigue strength. This increase in fretting fatigue strength with increasing surface roughness has also been observed by Watanabe et al. [226], and Harris [227] has shown that in the case where especially heavy peening is applied, plain fatigue strength can be reduced, whereas fretting fatigue performance is still improved.

de los Rios et al. [218] have shown that the difference between the fretting fatigue durability of peened specimens with a rough finish compared with peened and polished specimens is dependent on the normal pressure applied. The durability of rough peened specimens is higher than that of polished peened specimens when a contact pressure of medium magnitude is applied. One possible explanation for this is that for a rough surface the contact area is reduced and with it, the possibility of crack initiation. However, when the contact pressure is low, the fretting fatigue life of a polished specimen is significantly higher, indeed approximately twice as great as that for a roughly finished component. One possible explanation for this result is that test conditions incorporating low contact pressures are close to those for plain fatigue tests, where a high surface roughness decreases fatigue durability.

On the other hand, an experimental programme to separate the effect of residual stress and surface roughness carried out by Bignonnet [28], showed that when residual stresses are relieved, fretting fatigue behaviour is similar to that observed with ground specimens.

Mutoh et al. [225] have found that when steady state wear is attained, the roughness of fretted surfaces of both polished and as peened specimens becomes almost identical; in the region of 6 μm to 8 μm . Therefore, the increase in surface roughness by shot peening can not have an important role in improving fretting fatigue strength.

Benrabah et al. [156] have stated that the beneficial effect of a residual stress induced by shot peening is in fact limited by the opposite effect of a modification to surface roughness also due to the shot peening process. A shot peened surface, will ensure that lubricants are retained more successfully than with a smooth surface though, thus enhancing the effectiveness of such applications [25].

2.4.4.3 Residual stress

The success of using shot peening as a palliative to improve fretting fatigue life can largely be attributed to the introduction of a compressive residual stress induced by the shot peening process [29].

Surface compressive stresses act to reduce the initiation and early propagation of cracks generated by imposed fatigue and fretting induced cyclic loads [23]. Introducing a compressive stress into the surface layer will offset the tensile stress generated by the sliding contact [23] and will result in less wear than where the stresses are tensile [170]. The initiation of fatigue cracks requires the attainment of a critical magnitude of local cyclic plasticity at the crack initiation site and the critical level required depends on the mean stress. This is more difficult to achieve at a shot peened surface, primarily due to the compressive residual stresses induced [218].

Compressive residual stresses can reduce the magnitude of the far field stress [28], [29] and block the growth of small surface cracks [28]. de los Rios et al. [218] have stated that crack propagation through the peened depth is also hindered due to the crack closure effect of compressive residual stress.

However, the magnitude and depth of compressive residual stresses varies immensely in line with varying shot peening conditions. Mutoh et al. [225] recorded a maximum residual stress of 420 MPa at a depth of just 0.1 mm and Chivers and Gordelier [24] have concluded that crack propagation is not significantly affected by shot peening, when residual surface compressive stresses are introduced to depths of only 0.3 mm [220].

In any case, it is necessary to adapt the shot peening conditions in relation to the distribution of the loads applied. The larger the contact size for the shot impact, the deeper the compressive stress field must be [222]. An optimum peen depth for a component that undergoes fretting will exist and be affected by the bulk and contact loads and the coefficient of friction, which affect the stresses at the edge of the contact, as well as the material properties and peen conditions [228].

Care should be taken in employing any shot peening technique. Chivers and Gordelier [24] found that by only peening two faces of a rectangular test section, a flow of material around the corner of the specimen gave rise to a re-entrant stress raiser from which cracks initiated, although when fretting pads were put in place, the associated contact stresses dominated the failures. It is also important that any compressive residual stresses are not relieved [228].

Whether or not shot peening is employed, most surfaces contain residual stress fields, but these are frequently ignored in the analysis of fretting fatigue and there is a need to predict fretting performance in the presence of residual stress, if the stress is significant [19].

2.5 OBJECTIVES

It is proposed that a comprehensive experimental and analytical study of shot peening effects on fretting fatigue is conducted, to develop of a mathematical model to predict fretting fatigue life.

In order to quantify the parameters that control the fretting fatigue phenomena, it is proposed that an experimental programme be carried out first. This work will involve conducting a series of constant normal load tests, at varying axial loads, which will provide an insight into the fretting behaviour of aluminium alloy 2024 T351, which is widely used in the aerospace industry, and aid in developing a full understanding of the influence of fastener clamping forces on fretting fatigue.

Few have investigated the true mode by which a palliative influences fretting damage and the effectiveness of palliative treatments reported are often contradictory or misleading [25]. The repetition of these tests under shot peened conditions will then quantify the effects of the surface condition. Shot peening produces a roughened surface texture. The effect that this has on the friction forces involved is not yet fully understood and residual stress is frequently ignored in the analysis of fretting fatigue [19].

The data from the test programme will aid in the testing of a model constructed to predict friction and fretting fatigue life and the benefits of shot peening: a change in surface roughness and the introduction of a compressive residual stress.

The development of general methods is important [22] and so the ultimate aim is to develop a model with simple, accessible inputs that will not require the detailed instrumentation on an aircraft.

The objectives for this research are thus to:

1. Investigate the fretting fatigue life of aluminium alloy 2024 T351 in contact with aluminium alloy 2024 T351 as a function of normal pressure and cyclic axial stress for unpeened and peened components;
2. Investigate the friction forces developed by aluminium alloy 2024 T351 in contact with aluminium alloy 2024 T351 as a function of normal pressure and cyclic axial stress for unpeened and peened components;
3. Investigate the evolution of the surface damage incurred by fretting for unpeened and peened components;
4. Explore the relationship between surface roughness and friction, with a view to predicting friction force from fretting damage;
5. Further develop the work of Faanes and Fernando [101] and predict fretting fatigue life of unpeened and peened components using Linear Elastic Fracture Mechanics for a crack normal to a surface, by incorporating the mode I and mode II stress intensity factors for fretting fatigue cracks devised by Sheikh et al. [102] by means of a finite element procedure;
6. Further develop the work of Faanes and Fernando [101] and predict fretting fatigue life of unpeened and peened components using Linear Elastic Fracture Mechanics, by incorporating a model for the friction component;
7. Further develop the work of Faanes and Fernando [101] and predict the fretting fatigue life of shot peened components using Linear Elastic Fracture Mechanics, by incorporating a model for the residual stress component.

CHAPTER

3

EXPERIMENTAL METHODOLOGY

3.1 INTRODUCTION

The aim of the experimental programme was to conduct fretting fatigue tests on aluminium alloy 2024 T351 under closely controlled conditions, to aid in the understanding of fretting behaviour of this material, the influence of fastener clamping forces on fretting fatigue and to determine the benefits obtained by shot peening the contact surface. A comprehensive test programme with specimens and pads of aluminium alloy 2024 T351 was completed for a range of six constant normal loads and three fully reversed axial loads for the unpeened condition and three constant normal loads and three fully reversed axial loads for the peened condition.

Friction forces were measured and the number of cycles to failure recorded for each combination of normal and axial load administered. Once an understanding of fretting fatigue life for both types of specimen had been established, a series of tests was also then performed for proportions of those lives, so as to study the evolution of the fretting scar. The extent of the surface damage was explored using a laser profilometer, the resultant surface profiles were then analysed utilising a program written in Visual Basic, from which maximum notch widths and depths were determined.

Studies of the fracture surfaces themselves were carried out using a Scanning Electron Microscope (SEM). The results achieved were compared with those from other test programmes [99], [218].

Historically, an experimental set-up for fretting investigations involves cyclically loading a specimen, whilst pressing symmetrically placed bridge type pads to either side of the test surface, providing a constant normal force by means of a proving ring, but neglecting the Poisson's effect and the effect of wear. When an elastic material is subjected to tension, the diameter of the material decreases, conversely, increasing when subjected to compression. Thus the applied normal load can only be approximately constant.

In 1989 a collaborative research programme began at the University of Sheffield into the fretting fatigue fracture of artificially aged BS L65 copper aluminium alloy and a biaxial fretting fatigue test facility was developed. This was unique in its ability to directly control and maintain the normal contact load on fretting pads despite any material deformation to a specimen to which a cyclic axial load was applied or any wear of the bridges [99]. Importantly, friction and slip associated with the contact of individual pad feet could be measured which enabled a thorough study of the damaging effect of friction in fretting crack growth for both micro-slip and macro-slip regimes [99].

3.2 THE FRETTING FATIGUE TESTS

3.2.1 Test rig

The fretting fatigue tests were performed on a Mayes BI-AX 200 biaxial machine, Figure 3.1, in the Lea Laboratory at the University of Sheffield. This machine has a rigid, vertical frame, which incorporates four servo-controlled hydraulic actuators, two on the horizontal axis for axial loading and two on the vertical axis. The vertical actuators provided a normal load to bridge pads via steel ball bearings, loading blocks and rollers. The BI-AX 200 is capable of a maximum dynamic load of ± 200 kN and maximum stroke length of 50 mm; the dynamic performance is such that at 200 kN a 0.4 mm stroke can be achieved at 22 Hz. A single servo valve controls each pair of actuators, so that symmetrical loading may be applied. However, to ensure this is achieved on the vertical plane a counterbalance was employed to support the weight of the lower actuator rod and grip, previously equated to a load of 786 N [229].

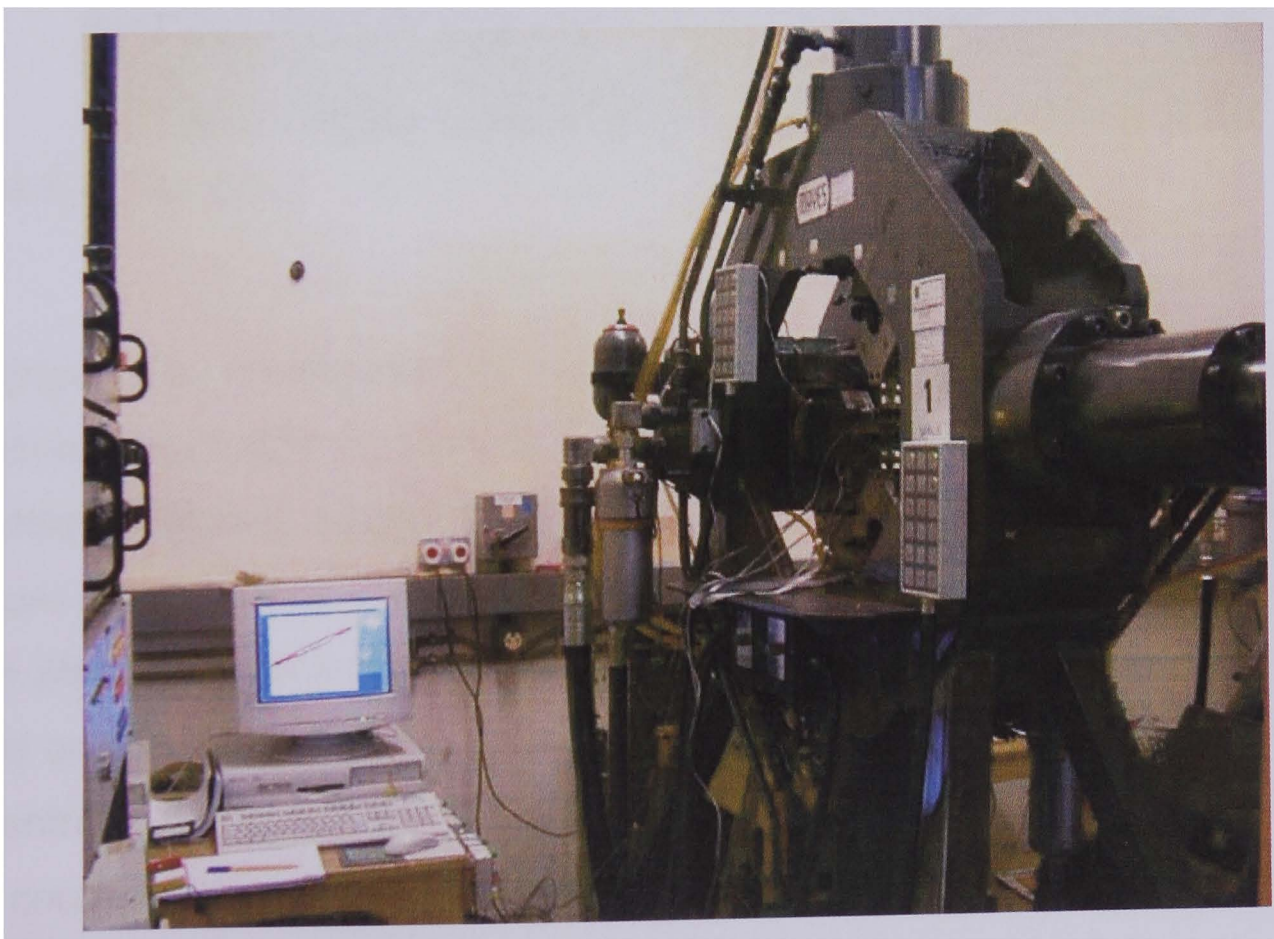


Figure 3.1: The BI-AX 200 Mayes.

3.2.2 Grips

The specimens were fixed in line between the two horizontal actuators, in grips screwed to the ends of the actuator rods, Figure 3.2. The specimens were clamped between two plates at each end, preloaded to a bolt torque of 60 Nm, creating the necessary friction to apply a maximum cyclic load of ± 80 kN [229]; the specimens were aligned with two locating pins.

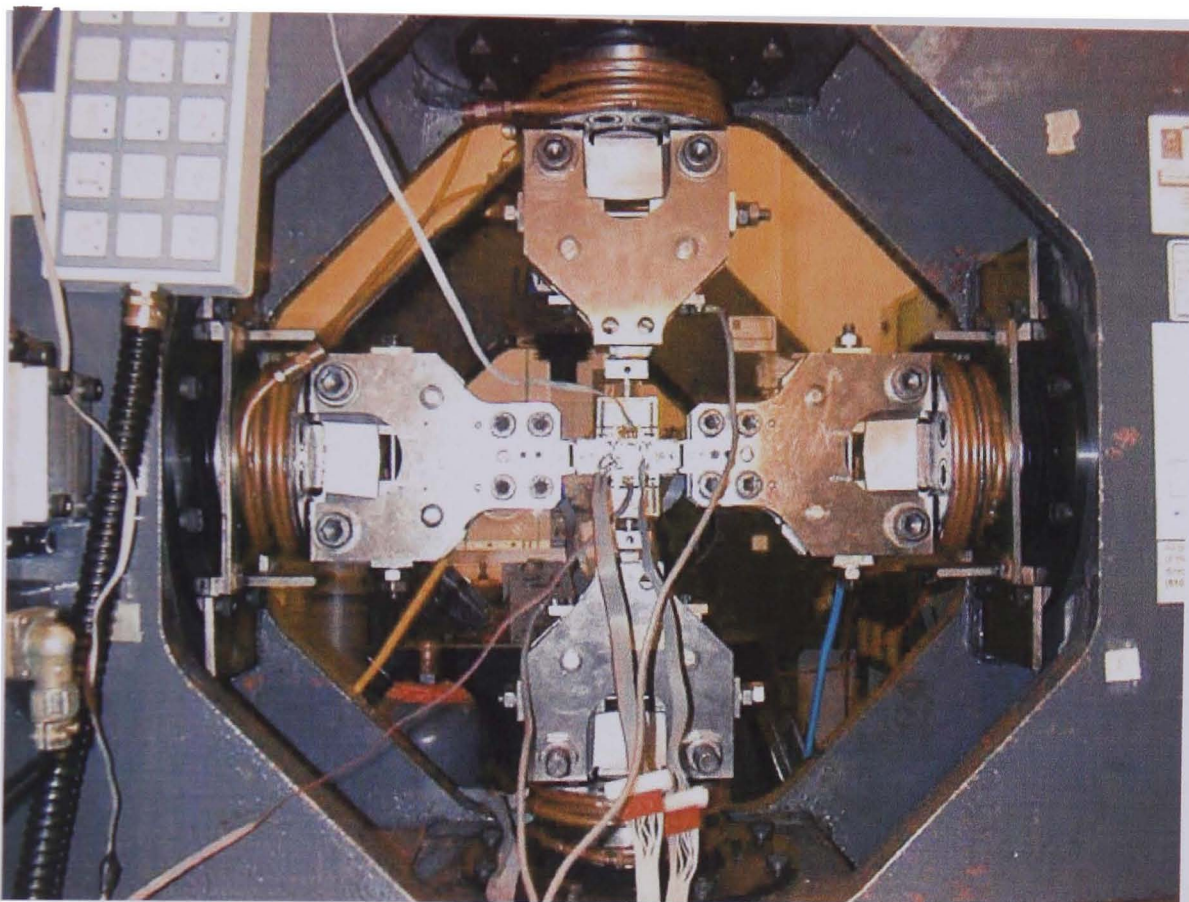


Figure 3.2: The grips.

The grips were constructed in such a manner as to eliminate backlash, and machined from EN24 (T) steel so as to sustain a maximum cyclic load of ± 200 kN whilst ensuring against fatigue failures. Sacrificial plates were inserted between the grips and the specimens to protect the grips from fretting damage. Guide plates on each horizontal actuator ensured that the specimens always stayed on the vertical plane and displacement stoppers were set to ensure that the centre of the specimens always remained in line with the vertical axis, as in load control the actuators tended to settle back against either one of the actuator ends [229].

The experimental set-up was designed in such a way as to aid the alignment of the normal load applied. Loading was applied to the bridge pads positioned on either side of the specimens by means of flat blocks set into grips screwed on to the upper and lower actuators, identical to those used on the horizontal axis. These pressed on to steel ball bearings cupped in loading blocks on the underside of which were seated a pair of rollers, which in turn rested on the bridges themselves. The rollers allowed for a symmetrical distribution of the normal load to each pad foot, but had to be aligned with each of the pad feet to avoid any bending of the bridges. Finally, Pressurex[®] film was used to check the distribution of the normal load; the colour of the film inserted under the bridge feet had to be the same colour under all four bridge feet and that colour uniform along the length of each strip. A schematic illustration of the loading arrangement is depicted in Figure 3.3.

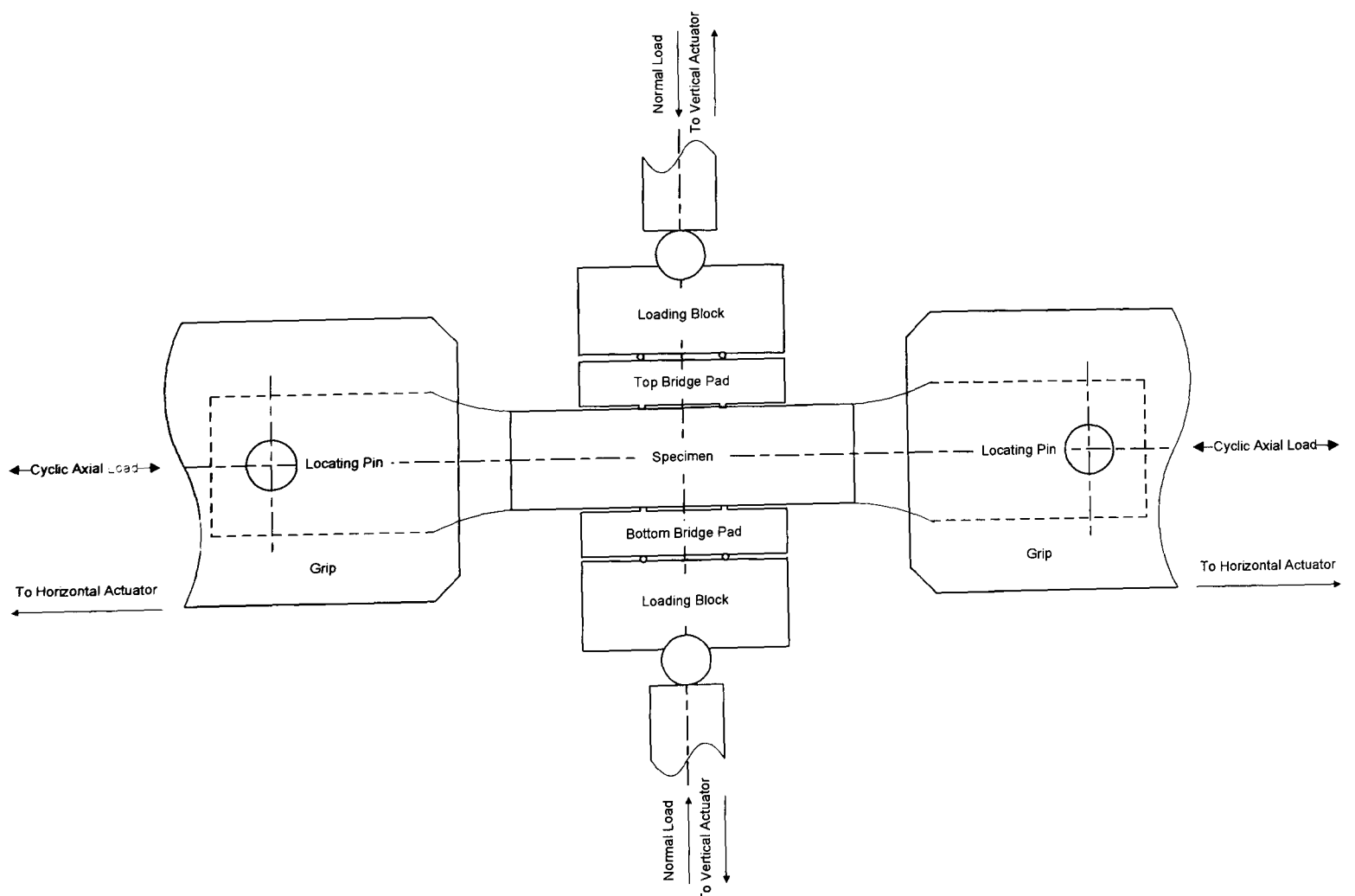


Figure 3.3: The loading arrangement.

The axial stress, σ_a , on the specimens was measured from a load cell attached to one of the actuators on the horizontal plane. The normal stress, σ_n , on the bridge pads was controlled from a load cell attached to the upper actuator on the vertical plane and monitored by means of more sensitive, independent load cells sited in each of the grips.

At a range of 20 kN, the gain of the feedback loops was found to be sufficient to correct the vertical load changes caused by minute transverse displacements of the test frame experienced in previous test programmes, which meant that a constant normal load was ensured [229].

3.2.3 Control and acquisition

Each axis of the Mayes BI-AX 200 has a separate hydraulic power supply, load cell, displacement monitor and digital control unit, such that independent management of the axes can be achieved under either modes of load or displacement control.

The digital control system was specially commissioned for this research and supplied by the Denison Mayes Group. Two Rubicons, one for each axis, were used to supply command signals and control the test conditions, ensuring, for example, the magnitude of the normal load exerted by the upper and lower actuators on the vertical axis. Although independent, these controllers were synchronised so that there were no phase difference errors between the axial and normal loads.

Specially designed software, XYPlot+, was utilised to control the inputs and outputs, with settings being made via a graphical user interface on a pair of computer monitors and a shut down procedure being automatically initiated when the distance between the horizontal actuators became greater than the length of the specimen held.

Real time information was visible on the computer screens. Data was typically sampled at a rate of 250 or 350 points over a period of between 25 to 75 cycles for every input every 300, 600 or 1,800 seconds and was recorded on a pair of hard drives for ease of processing; this could be viewed in specially designed software, XY Plot+ and da/dN.

Real time information provided included: a) the number of cycles administered; b) the displacement of each of the actuators on each axis; c) the load applied on each plane; d) the distance maintained between two actuators on the same plane; and e) via a series of independently calibrated strain gauges and bridge amplifiers, the friction associated with the upper and lower bridge pads.

The raw data files generated by the Rubicons were subsequently processed to extract the minimum, maximum and average values over the 250 to 350 data points recorded every 300 to 1,800 seconds. A programme was written in Microsoft Visual Basic specifically for this task, see Appendix B, utilising Microsoft Excel as the user interface, an icon being added to the toolbar when run.

On initialisation, the user is presented with an instruction sheet and is prompted to open one of the ASCII files generated by the Rubicons. A series of forms necessitates the entry of the number of data points recorded per cycle, the location of key data on the worksheet, including the location of the first row of data and the column containing time and the number or numbers of the columns to be analysed. Another then informs the user of what calculations are being carried out and points to where the results are being saved; a calculations worksheet is added to the workbook. For every data set from each test, the start and end times, cycle numbers, and maximum, minimum and average friction forces were thus listed, with the last line in the file being the final number of cycles to failure.

3.3 THE SPECIMENS

3.3.1 Design

A specimen is depicted in Figure 3.4; the geometry of the specimens in Figure 3.5. These were of a flat, hourglass design, selected to fit the existing test apparatus and with a test section such that the cross-sectional area was the same as that used in previous experiments [99].

Enlarged cross sections at either end of the specimens meant that the nominal axial stresses experienced in these regions were approximately 47% of those in the centre section. This reduction in stress should be sufficient to ensure that fatigue failures would not occur in the grips. Reamed holes at either end provided a means for locating the specimen in the grips of the test rig and the fillet radii from here to the test section were such that stress concentration factors in these areas were sufficiently low so that failure would always initiate from the fretting pads. The nominal length of the specimens was 190 mm; the test section was of rectangular cross-section, 8 mm x 20 mm in size [229].

The specimens were cut from the centre of a thick aluminium plate, the tensile axis machined along the direction of rolling. It was of great importance that flat surfaces were achieved to tolerances as depicted in Figure 3.5, as this was essential for proper pad contact. The specimens were also wiped clean with acetone before any testing took place.

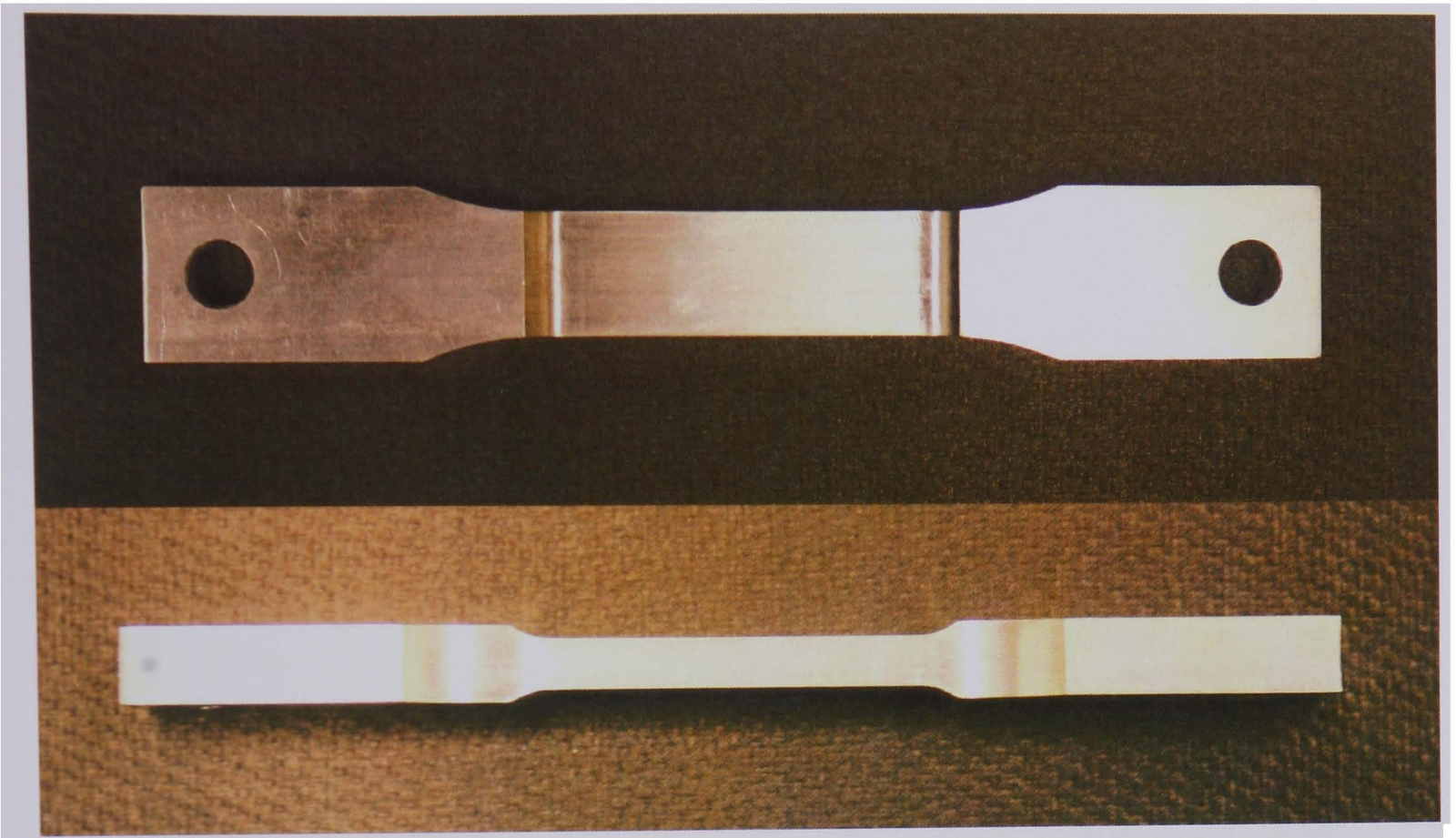


Figure 3.4: The specimen.

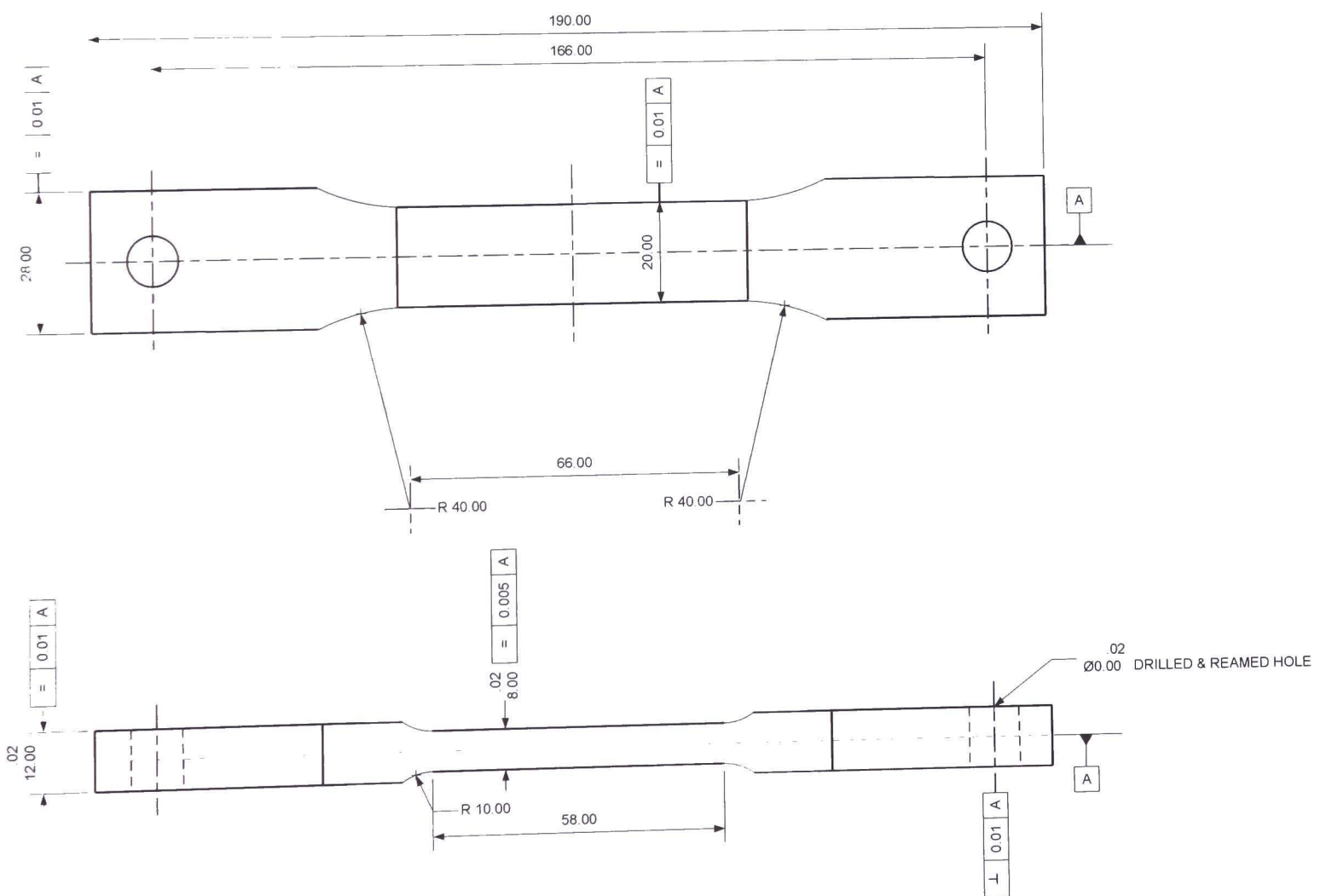


Figure 3.5: The specimen (all dimensions are in mm).

Normal load was applied to the specimens by means of two symmetrically placed bridge pads. A bridge pad is depicted in Figure 3.6; the geometry of the bridge pads in Figure 3.7. The dimensions of these were selected so as to be identical to those used in the majority of previous experiments.

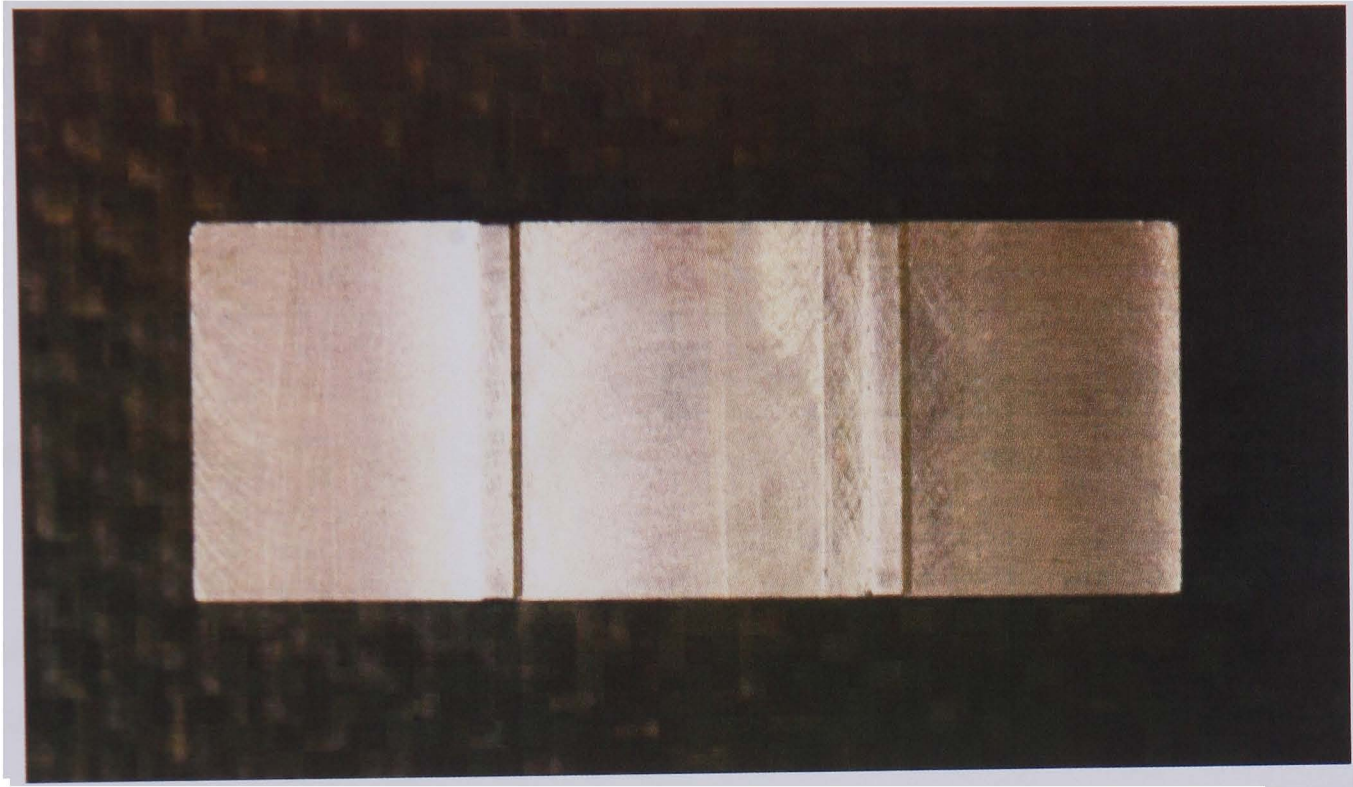


Figure 3.6: The bridge pad.

Each bridge had two feet 1.27 mm in width and 1.00 mm in height and a pad span of 16.5mm. Ensuring the same cross section for both the specimens and the pads was necessary in order to maintain the same slip amplitude under identical loading conditions.

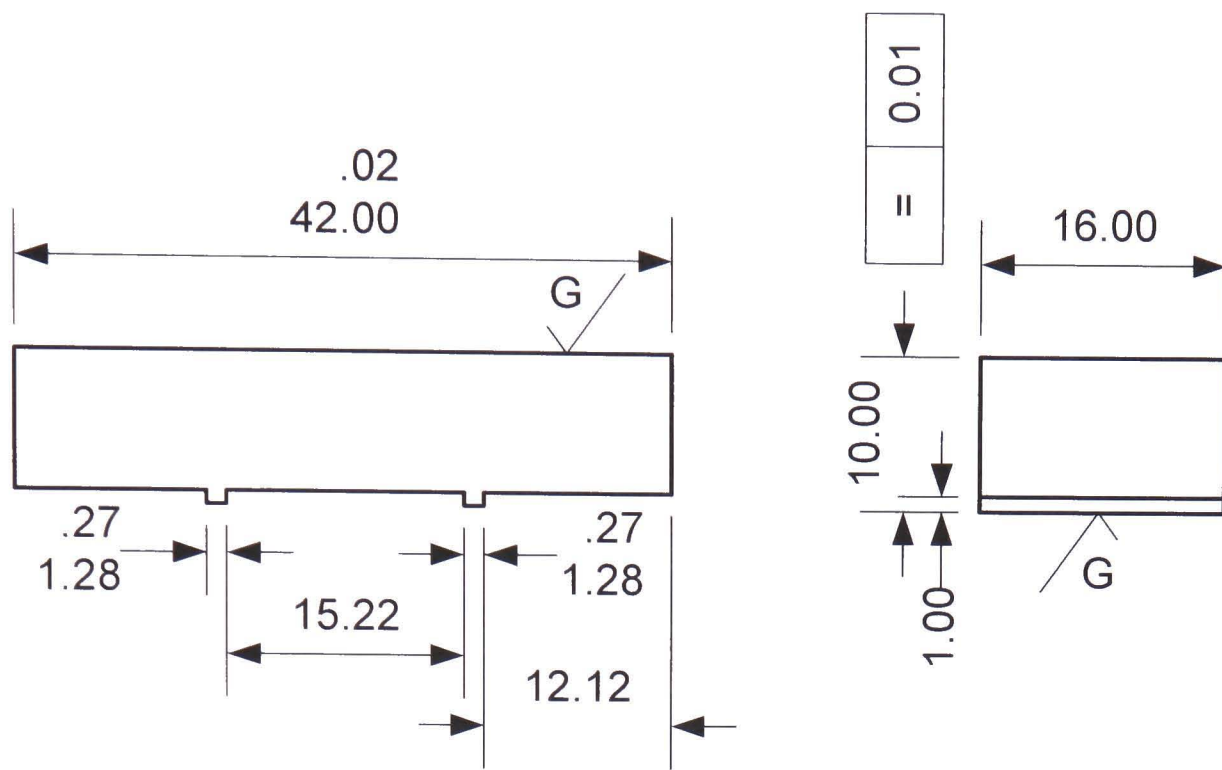


Figure 3.7: The bridge pad (all dimensions are in mm).

Strain gauges were bonded to the upper and lower surfaces of the bridges, in between the bridge feet, see Figure 3.8, the signals from which were used to measure the friction forces. Each bridge was independently calibrated utilising a Hounsfield Tensometer; example calibration curves for a top and bottom bridge pad pair are shown in Figures 3.9 and 3.10.

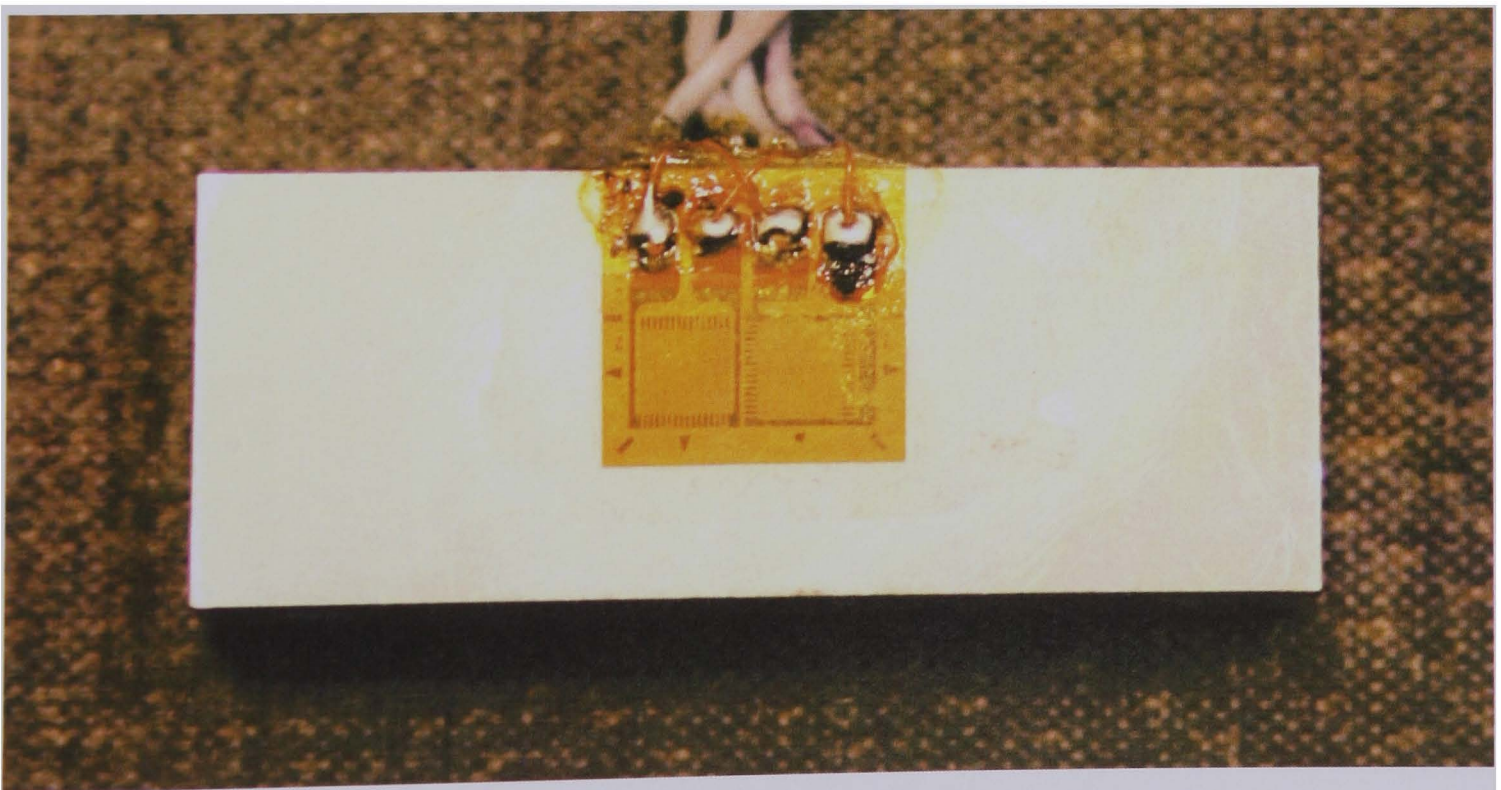


Figure 3.8: A strain gauge on the upper surface of a bridge pad.

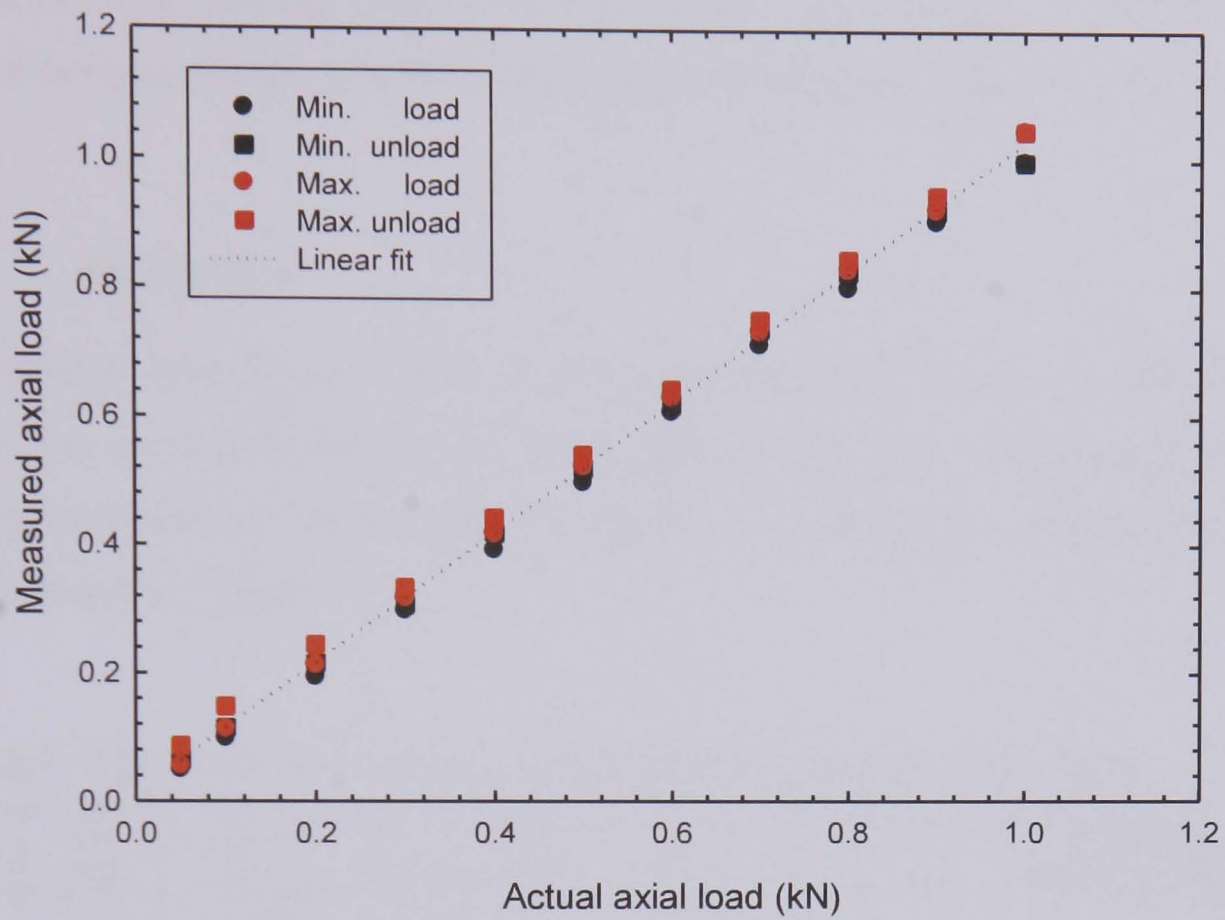


Figure 3.9: The calibration curve for a top bridge pad.

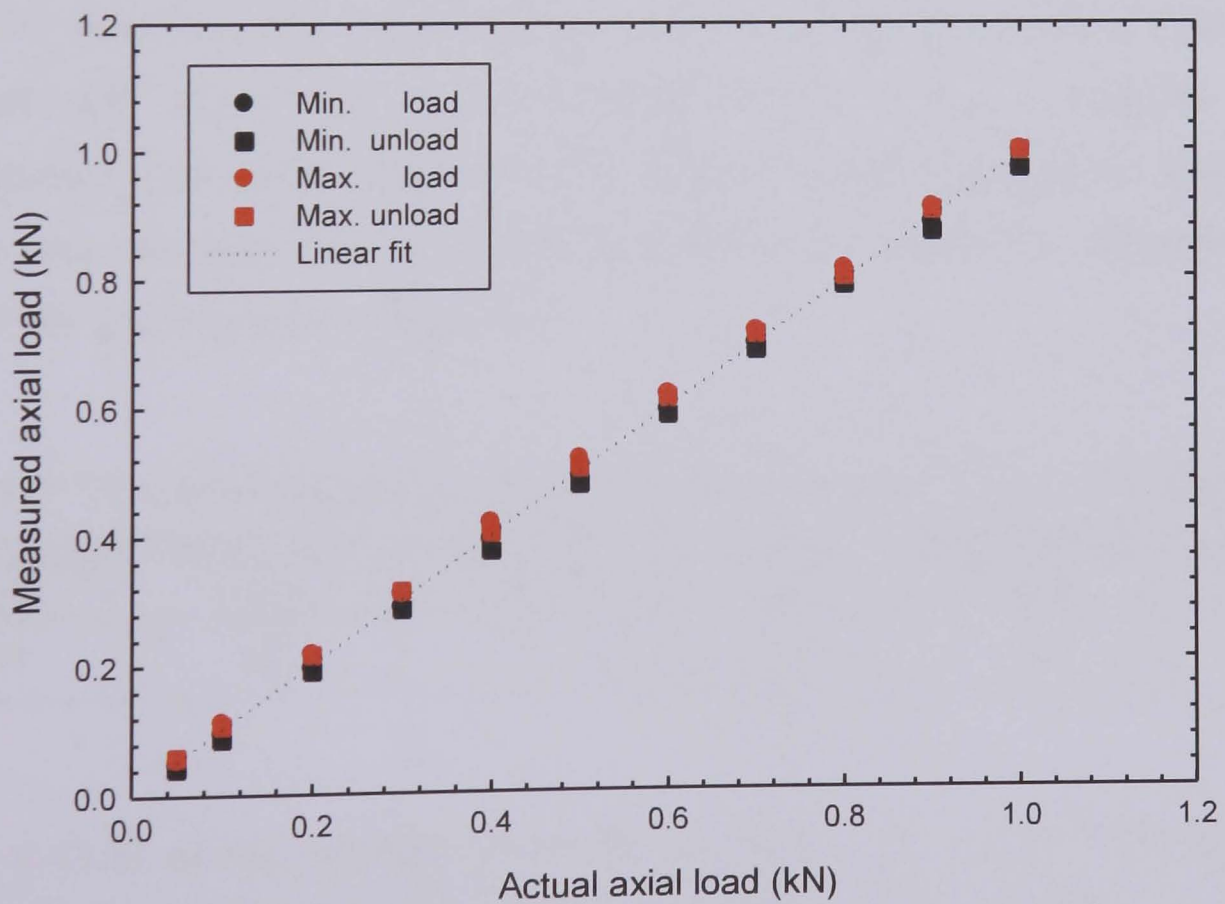


Figure 3.10: The calibration curve for a bottom bridge pad.

Bridges were reused over several tests; however, the bridge feet were reground to remove any fretting debris and ensure a flat surface and cleaned with acetone between tests. Each bridge was used approximately five times.

3.3.2 Materials

The material investigated was aluminium alloy 2024 T351, a material widely used in the aerospace industries for its good strength to weight ratio. The major alloying element for alloy 2024 is copper; the chemical composition of alloy 2024 is given in Table 3.1.

Table 3.1: The chemical composition of aluminium alloy 2024 [230].

Si (%)	Fe (%)	Cu (%)	Mn (%)	Mg (%)	Cr (%)	Zn (%)	Ti (%)	Unspecified		Al (min)
								(each)	(total)	
0.5	0.5	3.8 - 4.9	0.3 - 0.9	1.2 - 1.8	0.1	0.25	0.15	0.05	0.15	rem

Code T351 refers to the means by which the alloy has been tempered. The prefix T3 indicates that the alloy has been solution heat treated, cold worked and naturally aged to a stable condition; digits 5 and 1 indicate that no straightening has been applied to the product after it has been stretched to relieve any stresses. The resultant mechanical properties of aluminium alloy 2024 T351 are located in Table 3.2.

Table 3.2: The mechanical properties of aluminium alloy 2024 T351 [230].

Tensile strength (MPa)	Yield strength (MPa)	Elongation (%)	Hardness (HB)	Shear strength (MPa)	Fatigue strength (MPa)
470	325	20	120	285	140

Figure 3.11 is of the microstructure of aluminium alloy 2024 T351 from [231] and clearly shows the elongated grains and second-phase particles as well as a dispersion of finer precipitate which form during the aging treatment.

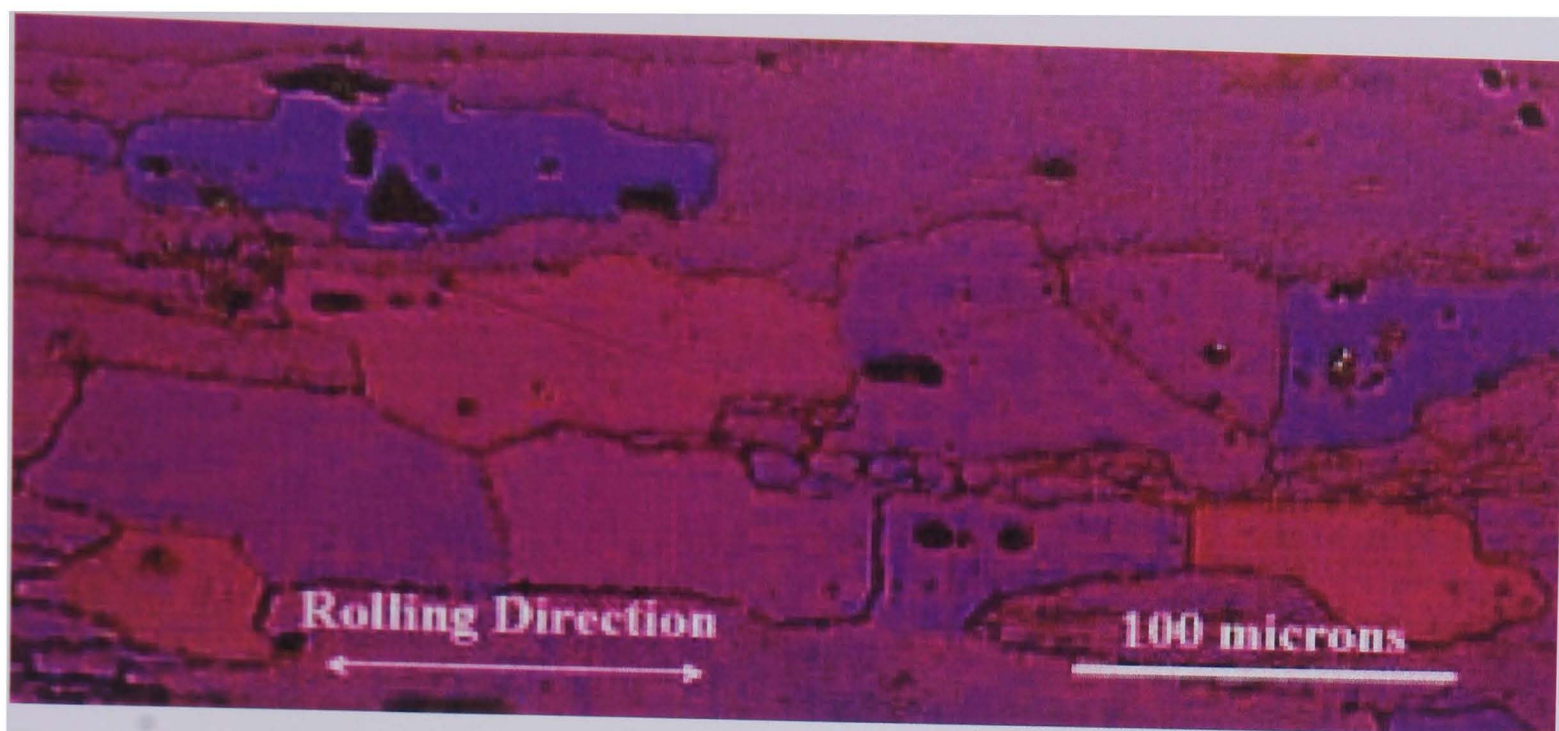


Figure 3.11: Microstructure of aluminium alloy 2024 T351.

The contacting bridge feet were manufactured from BS S98 steel or aluminium alloy 2024 T351. The former of the resultant material combinations has been used extensively in fretting experiments [232], [99] and the latter has been previously documented as well [233].

3.3.3 Shot peening parameters

All four sides of the rectangular test section were shot peened for the constant normal load test programme for peened specimens; none of the bridge feet was treated, as the deformation caused would have been too great. The shot peening parameters utilised are shown in Table Table 3.3 and were selected as a result of a concurrent investigation being carried out at the University of Sheffield [197]; these were described as being optimum for the fatigue performance of aluminium alloy 2024 T351.

Table 3.3: Shot peening parameters.

Shot (type code)	Angle (°)	Mass Flow Rate (lb/min)	Traverse Speed (mm/s)	Height (in)	Pressure (Mpa)	Coverage (%)
S110	45	10	125	6	50	200

The majority of the parameters were selected based on observations of residual stress profiles, Figure 3.12, work hardening Figure 3.13 and surface roughness. The residual stresses were determined using an incremental hole drilling method and then utilising the incremental strain method to determine the residual stress profile from the measured strains [197].

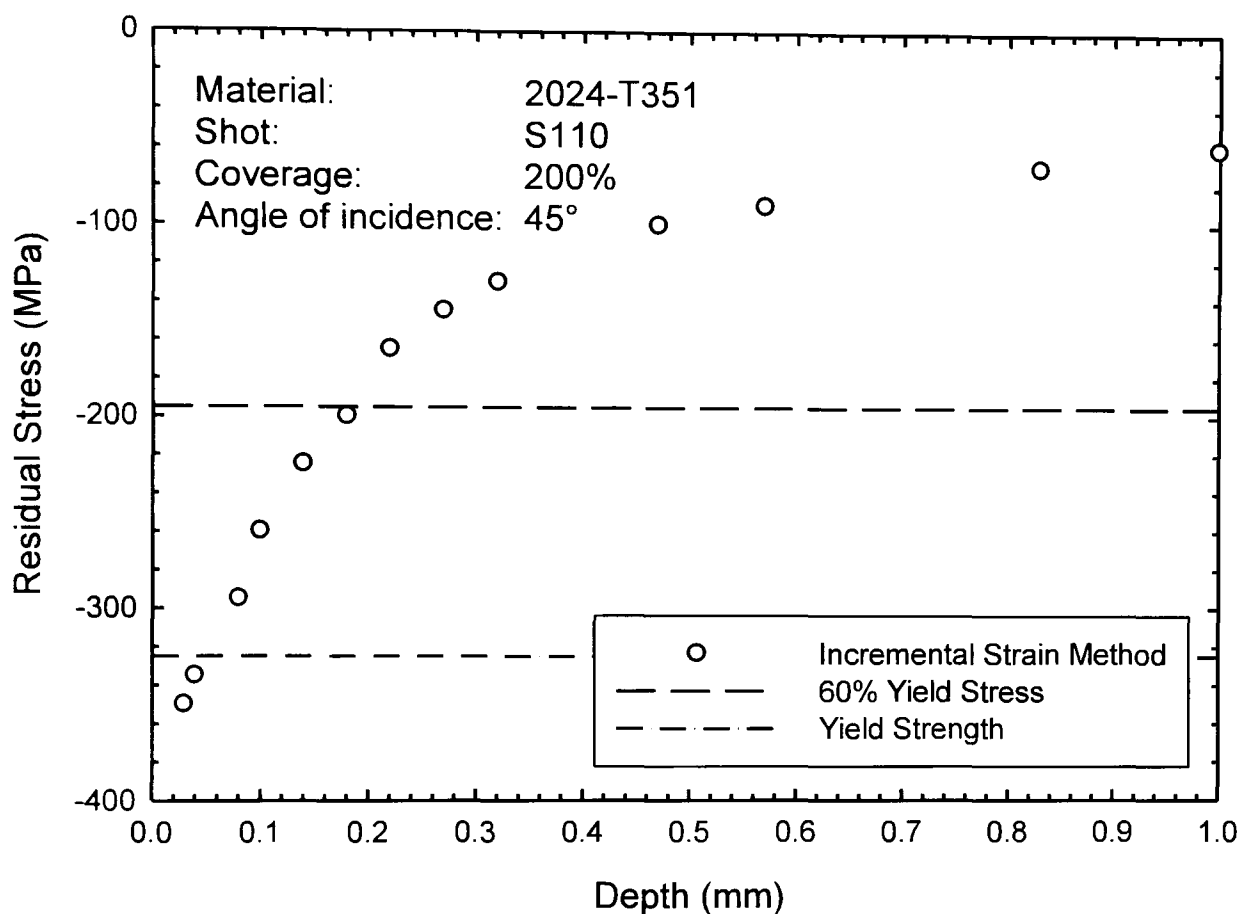


Figure 3.12: The residual stress profile for 2024 T351 optimised shot peening parameters of spherical cast steel shot type S110 [205] at 200% coverage and an angle of incidence of 45° [197].

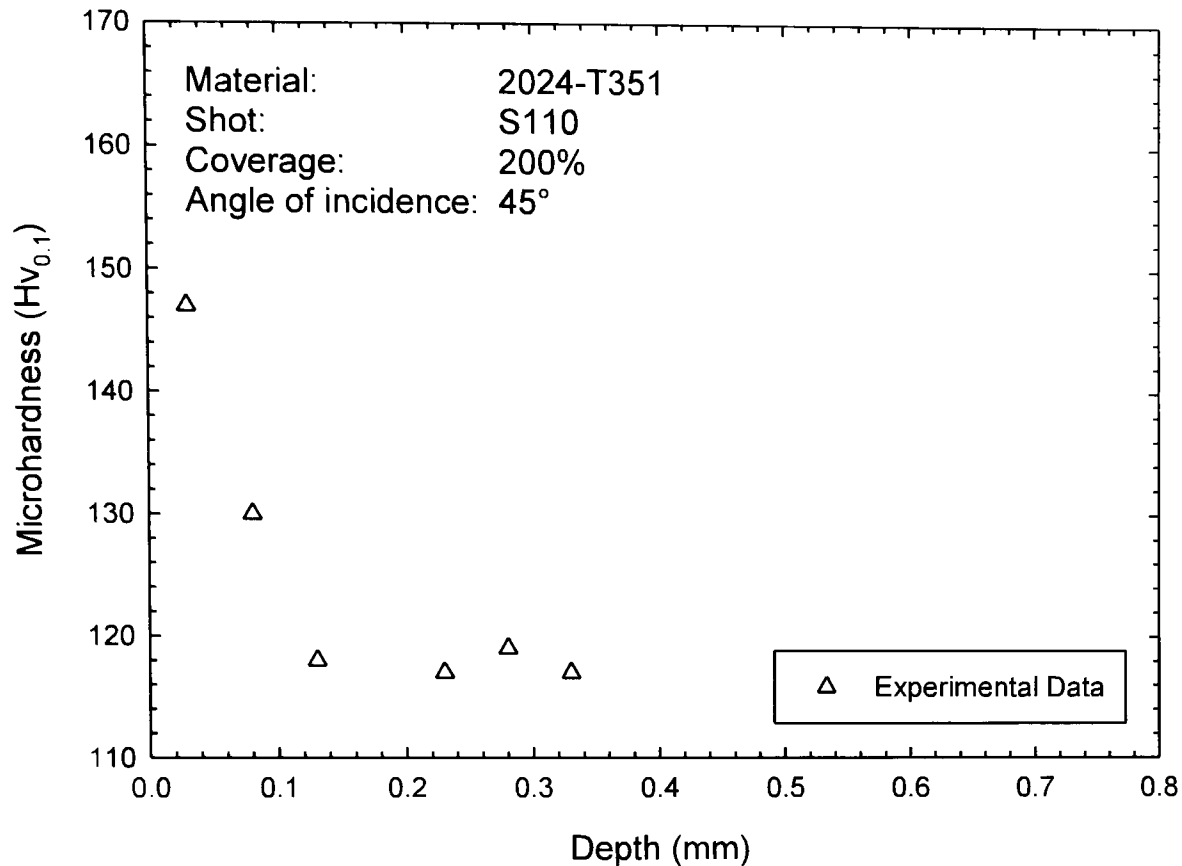


Figure 3.13: The micro hardness profile for 2024 T351 optimised shot peening parameters of spherical cast steel shot type S110 [205] at 200% coverage and an angle of incidence of 45° [197].

3.4 THE TEST PROGRAMMES

3.4.1 Test conditions

In this test programme the specimens were subjected to a sinusoidal cyclic axial stress with a stress ratio, R ($\sigma_{min}/\sigma_{max}$), of -1, at a frequency of 20 Hz. This meant that 1.0×10^6 cycles took almost 14 hours. However, the control of the loading was proven at this frequency.

The amplitude of the axial stress applied to the steel bridges was 100 MPa and ranged from 70 MPa to 125 MPa for the aluminium bridges. The normal pressure was maintained at a constant level during each test within the range of 10 MPa to 120 MPa for the steel bridges and 10 MPa to 100 MPa for the aluminium bridges. All testing was performed at room temperature.

3.4.2 Loading

3.4.2.1 Control test programme

A series of three fretting fatigue tests was carried out with bridge pads machined from BS S98 steel in flat-on-flat contact with specimens machined from aluminium alloy 2024 T351 whilst the test facility was being established. Details of these tests can be found in Table 3.4.

Table 3.4: The load conditions for the fretting fatigue tests on aluminium alloy 2024 T351 in contact with BS S98 steel.

Specimen (no.)	Normal stress (MPa)	Normal load (kN)	1/2 normal load (kN)	Axial stress (MPa)	Axial load (kN)
17	40	0.813	0.406	100	16
13	80	1.626	0.813	100	16
14	120	2.438	1.219	100	16

Failure was defined as the fracture of the specimens, rather than the achievement of a given crack length.

3.4.2.2 Constant normal load test programme

A constant normal load test programme for the unpeened specimens was devised for a total of eighteen tests, with six different normal pressure and three different axial stresses. However, in practice a total of thirty-nine tests was performed either for reproducibility or from repeating tests that suffered equipment failure. Details of the twenty-eight tests completed successfully can be found in Appendix B in tables B.1a, B.1b and B.1c. The axial and normal stresses given are obtained assuming a uniform stress distribution.

Once the constant normal load test programme for the unpeened specimens was completed, a similar, but reduced programme was devised for the shot peened specimens. A total of nine tests, with three different normal pressures and three different axial stresses was carried out. Details of these tests can be found in Appendix B tables B.2a, B.2b and B.2c.

3.4.2.3 Fretting fatigue crack measurement

A significant amount of time was spent in attempting to measure fretting fatigue crack growth employing a direct current, potential drop technique as used in previous work [234]. Using this method, the resultant increase in the electrical resistance of a cross sectional area as a crack extends is monitored. The potential difference between two points set either side of the crack rises and this potential increase is compared with a reference potential and thus crack length determined from suitable calibration curves.

Previously designed jigs [234] were mounted onto the grips, whereby four pairs of spring loaded lead wires were pressed onto either side of the specimen directly under each bridge foot. A current was passed through the specimens, insulated from the grips and the change in the electrical potential was measured in turn at each potential crack site. Since a total of sixteen pairs of leads was used on a specimen, it was necessary to switch between these signals appropriately to measure the required outputs, this being achieved by using a Time Electronics 9812 24-channel programmable switch unit. The resultant readings were disappointing due to the degree of noise.

The usefulness of the measurements taken was limited by a number of other factors as well. The application of a suitable calibration curve is an issue for example, particularly in fretting fatigue. There are a number of theoretical calibration curves based on: solutions to Laplace's equation for specific boundary conditions of a given specimen geometry, Johnson's formula applied to compact tension, centre cracked tension and single edge notched bend specimens and Gilbey and Pearson's solution, not to mention calibration curves produced by means of finite element analyses.

However, the shape of a crack front is not considered in any of these models and is random in fretting fatigue. The complex load arrangement and interaction of wear and failure mechanisms in fretting fatigue also means that experimental calibration is necessary and there was insufficient time to complete this process satisfactorily for every condition observed in this programme. In any case, the development of a fretting scar makes monitoring short cracks very difficult.

3.5 THE FRETTING FATIGUE SCARS

3.5.1 Evolutionary tests

In order to understand better the evolution of the fretting scar, a series of seventy-two interrupted fretting fatigue tests was devised for a tenth, quarter, half and three quarters of the total fretting fatigue lives found for both the unpeened and peened specimens. These were conducted at three normal pressures, 10 MPa, 40 MPa or 60 MPa and 100 MPa, these being the minimum previously applied, the maximum previously applied and that which yielded the shortest life for each axial stress. Three axial stress amplitudes, 70 MPa, 100 MPa and 125 MPa, were tested as before and all other test conditions were maintained. A new specimen and pair of bridges were used for every test so as to avoid issues of realignment and the disturbance of fretting debris. The details of the tests successfully completed with unpeened specimens can be found in Appendix C in Tables C.1a, C.1b and C.1c and with peened specimens in Appendix C in Tables C.2a, C.2b and C.2c.

3.5.2 Surface roughness measurement

Fretting scars have been studied using white light interference profilometry [235], hence an ADE Phase Shift MicroXAM™ surface mapping microscope was initially applied to gain three dimensional images of the wear scars. However, due to limitations of the technique due to variations in reflectivity, a Mitutoyo SurfTest model 301 with a mechanical stylus was used to measure the surface roughness profiles of the fretting scars, the objective being that dimensions of resultant wear features be extracted from the data. Traces from profilometers have been utilised to understand better the effect of initial surface roughness on fretting fatigue life [170] and to accommodate rough contacts in fretting fatigue analyses [115].

Although surface roughness profiles are relatively simple and inexpensive to obtain, errors inherently occur when using a mechanical stylus. The radius of the stylus in this case was 5 μm , which meant that no information was gathered on the geometry of features with an aperture of less than 10 μm in diameter. It was for this reason that after an initial test period, a laser profilometer was sought, Figure 3.14. A laser profilometer allows for non-contact characterisation of surfaces in the ranges of micrometres, with a wider scan area than with a standard confocal microscope, which typically has a resolution of between 0.2 μm and 0.5 μm .

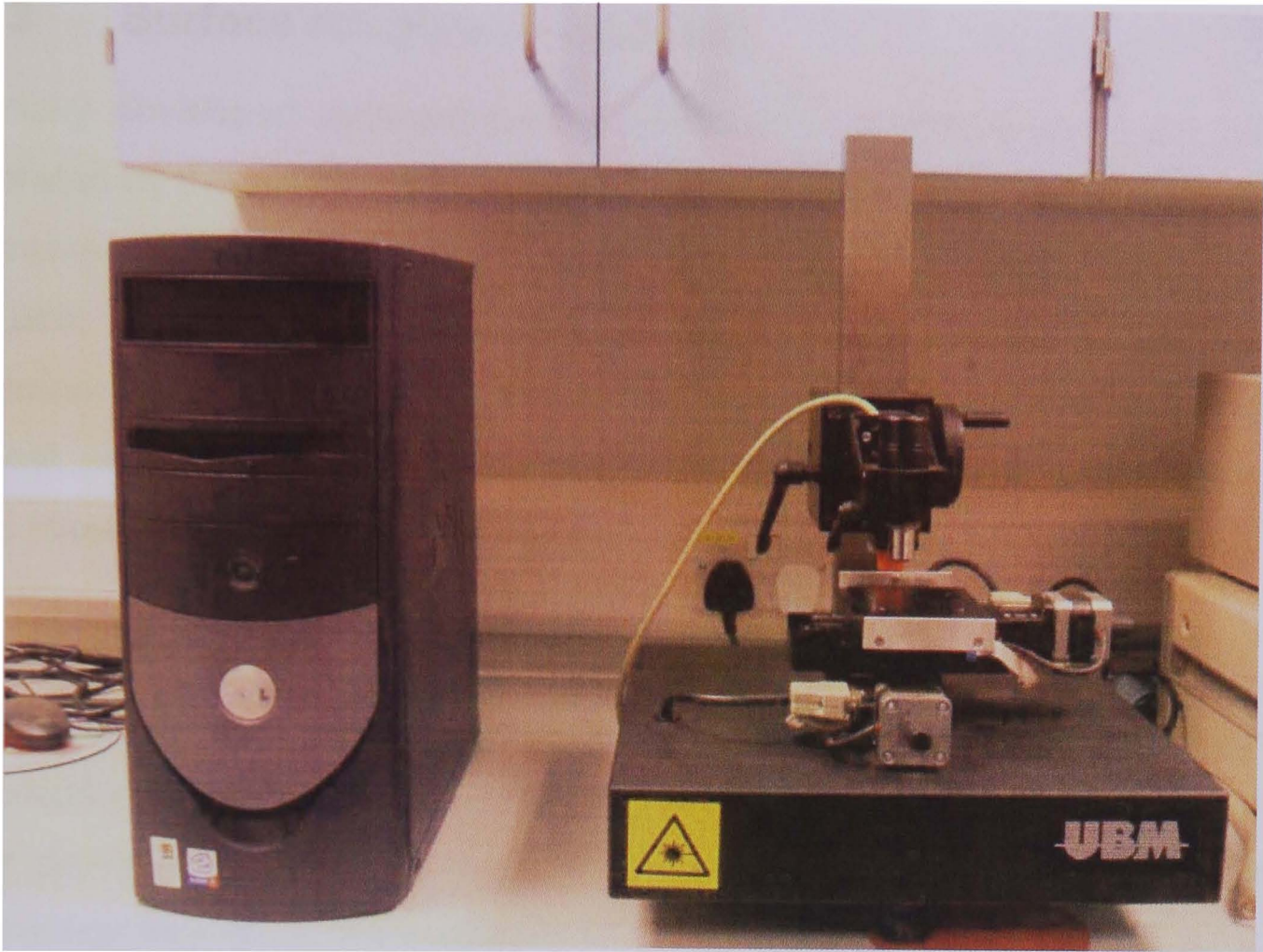


Figure3.14: The UBM laser profilometer at the Materials and Engineering Research Institute, Sheffield Hallam University.

Each specimen resulting from the evolutionary test programme was subsequently placed on a stage under a laser beam with a spot size of $1\ \mu\text{m}$, 2 mm from the lens and was moved by the stage while the sensor transmitted data on the relative heights to a measurement control unit. The data from each scan were saved to a computer file for later analysis using the data manipulation software UB Soft.

For each specimen, twelve scans were conducted. This was because each specimen had four scars, two from the upper contacts and two from the lower contacts and for consistency, each scar was traced in three different places, at the front, middle and back of each test section. This resulted in a total of 144 profiles for the unpeened specimens and 144 profiles for the peened specimens.

3.5.3 Surface roughness analysis

Specially developed software was subsequently used to analyse the profiles generated by the profilometer; whereby significant features were identified. This programme was written in Microsoft Visual Basic and utilises Microsoft Excel as the user interface. This code can be found in Appendix D. Data on the maximum notch depth found, the length of that notch and the height of the highest peaks either side of that notch were recorded. These measurements were taken from a base line of 0 mm.

First, the profiles were levelled about a centre line. Each measurement, y_M , was considered to be made up of two parts: the 'true' measurement, y_T and the 'error' in the measurement resulting from the fact that specimens lying on the bed of the laser profilometer were not level, y_E . The true measurements were therefore determined by means of Equation 3.1.

$$y_T = y_M - y_E \quad \text{Equation 3.1}$$

It was assumed that y_T was not a function of x and that therefore any change in y_M as a function of x was as a result of the error y_E . The error, y_E , was therefore estimated by performing a regression of the measurement y_M against its row number to determine the values of m and c in Equation 3.2, where x is the horizontal measurement in units of rows. The value of $mx+c$ was then simply subtracted from measurement y_M .

$$y = mx + c \quad \text{Equation 3.2}$$

The last step was to standardise the measurements such that the average measurement was zero. To do this, the average difference of the measurements from zero was found and this number subtracted from each measurement.

Next, Gaussian smoothing of the data, Equation 3.3, was conducted for several different standard deviations, 4, 8, 12, 16, 20, 24 and 30; the higher the standard deviation, the smoother the curve. To calculate the smoothed value of x at point i , a weighted sum was used over all the points in the range of $i - 120$ to $i + 120$. Each point was weighted by a Gaussian function such that the further a point was from x , the less it contributed to the smoothed value of x :

$$\bar{x}_i = \sum_{j=i-120}^{i+120} x_j \sqrt{\frac{2\pi}{\sigma^2}} \exp(-(x_i - x_j)^2 / 2\sigma^2) \quad \text{Equation 3.3}$$

A smoothing constant, σ , of 20 produced smooth profiles, but which did not hide any major features in the data, see Figures 3.15 and 3.16. For consistency, a value of 20 was used to smooth every data set.

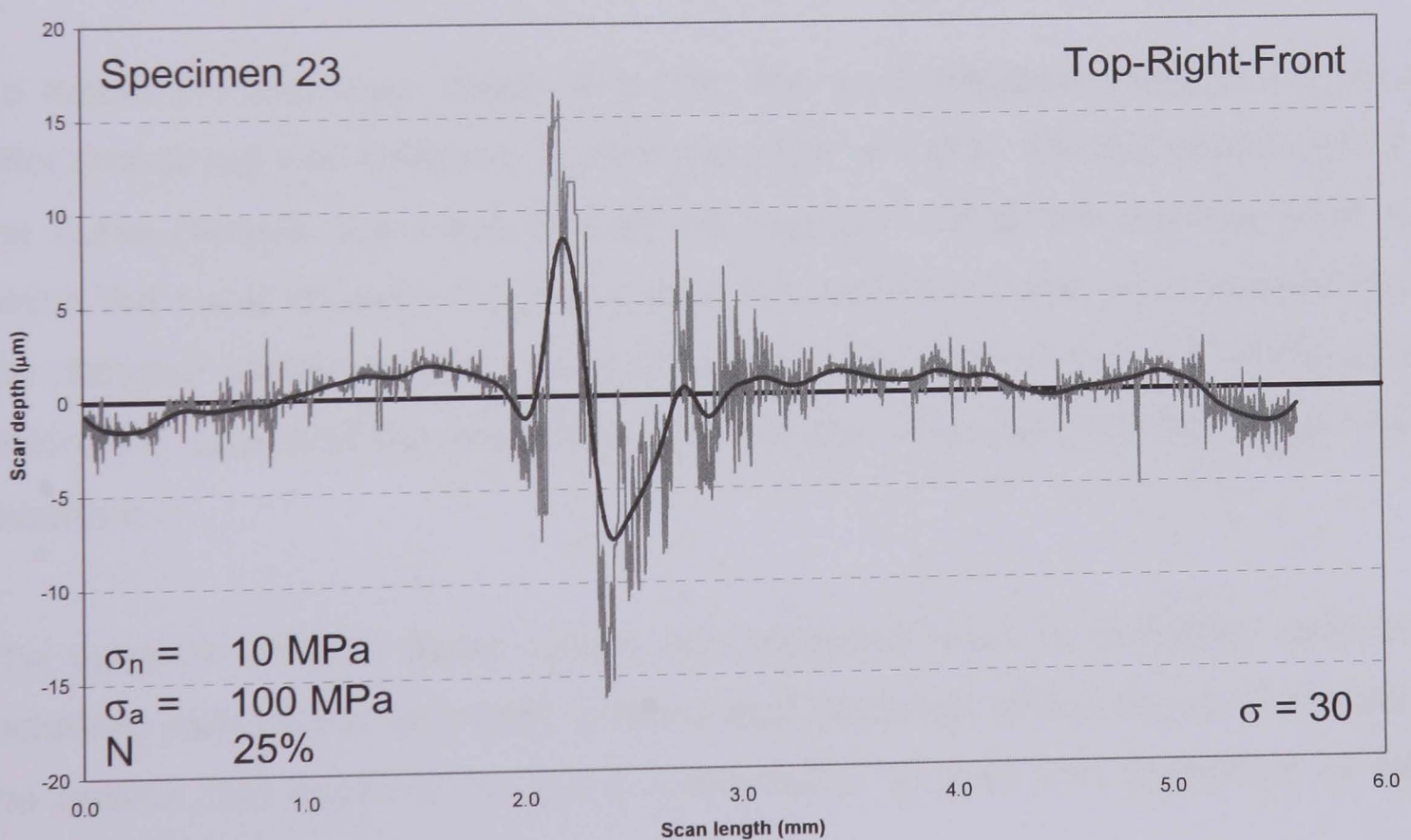


Figure 3.15: A surface roughness profile using a smoothing constant, σ , of 30.

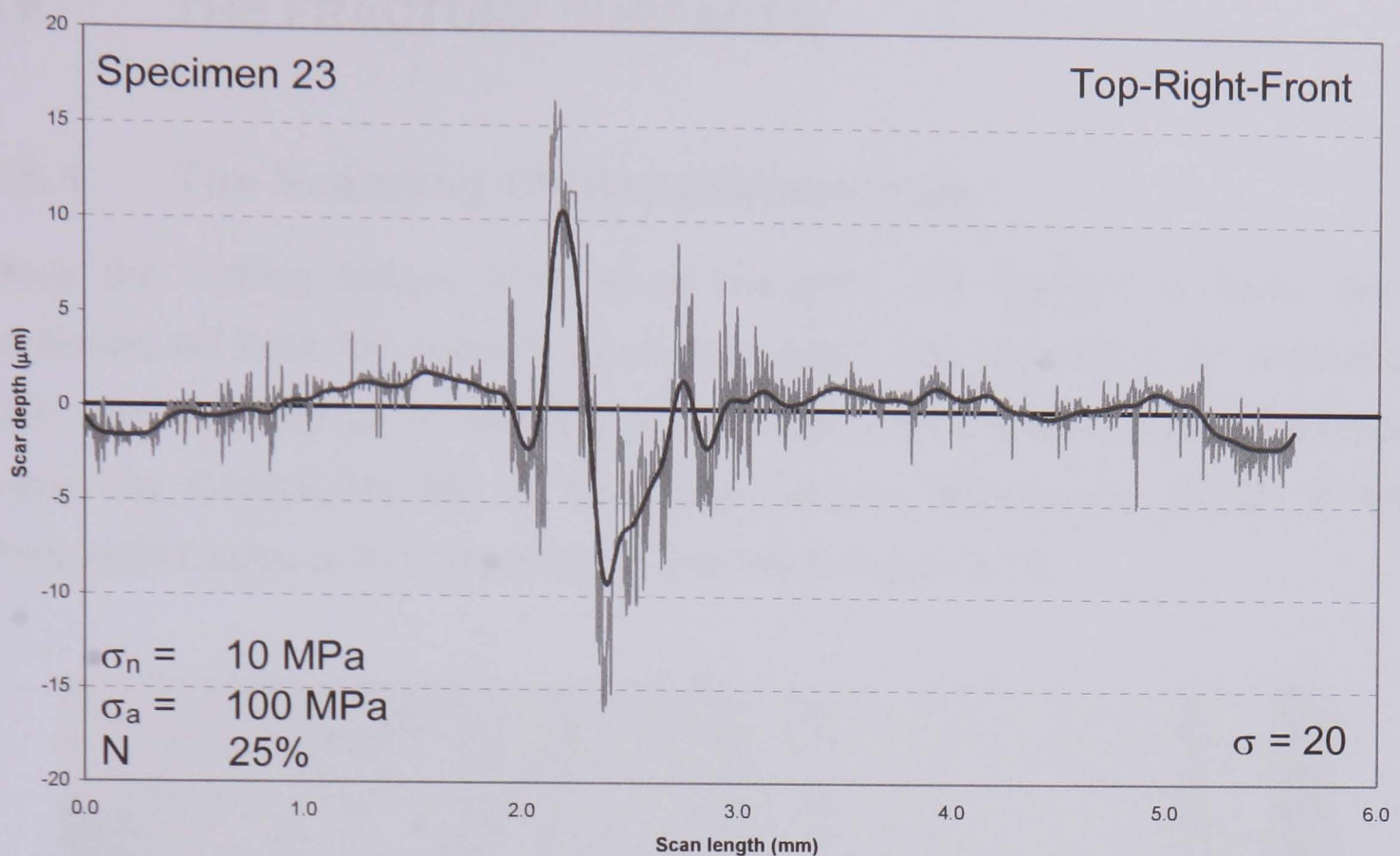


Figure 3.16: A surface roughness profile using a smoothing constant, σ , of 20.

To locate the maximum depth of a scar, the most negative value in the data after smoothing was selected. To find the width of a scar, the last point at which the curve crosses the x-axis before the minimum value and the first point at which the curve crosses the x-axis after the minimum value were located and the distance between these values calculated. The maximum value of the data before the scar and the maximum value of the data after the scar were also recorded.

The program collated these values and produced a set of individual records, including plots of the smoothed profiles and close ups of the areas of interest; the means and medians for every combination of load and proportion of life were saved to a separate file.

3.6 THE FRACTURE SURFACES

3.6.1 The Scanning Electron Microscope

Once the fretting fatigue tests were complete, the fracture surfaces were sectioned off from the main body of the specimens, cleaned in an ultrasonic bath and mounted on to backing plates; these were subsequently examined using the CAMSCAN MK II, Scanning Electron Microscope (SEM) in the Portobello Centre at the University of Sheffield, Figure 3.17.

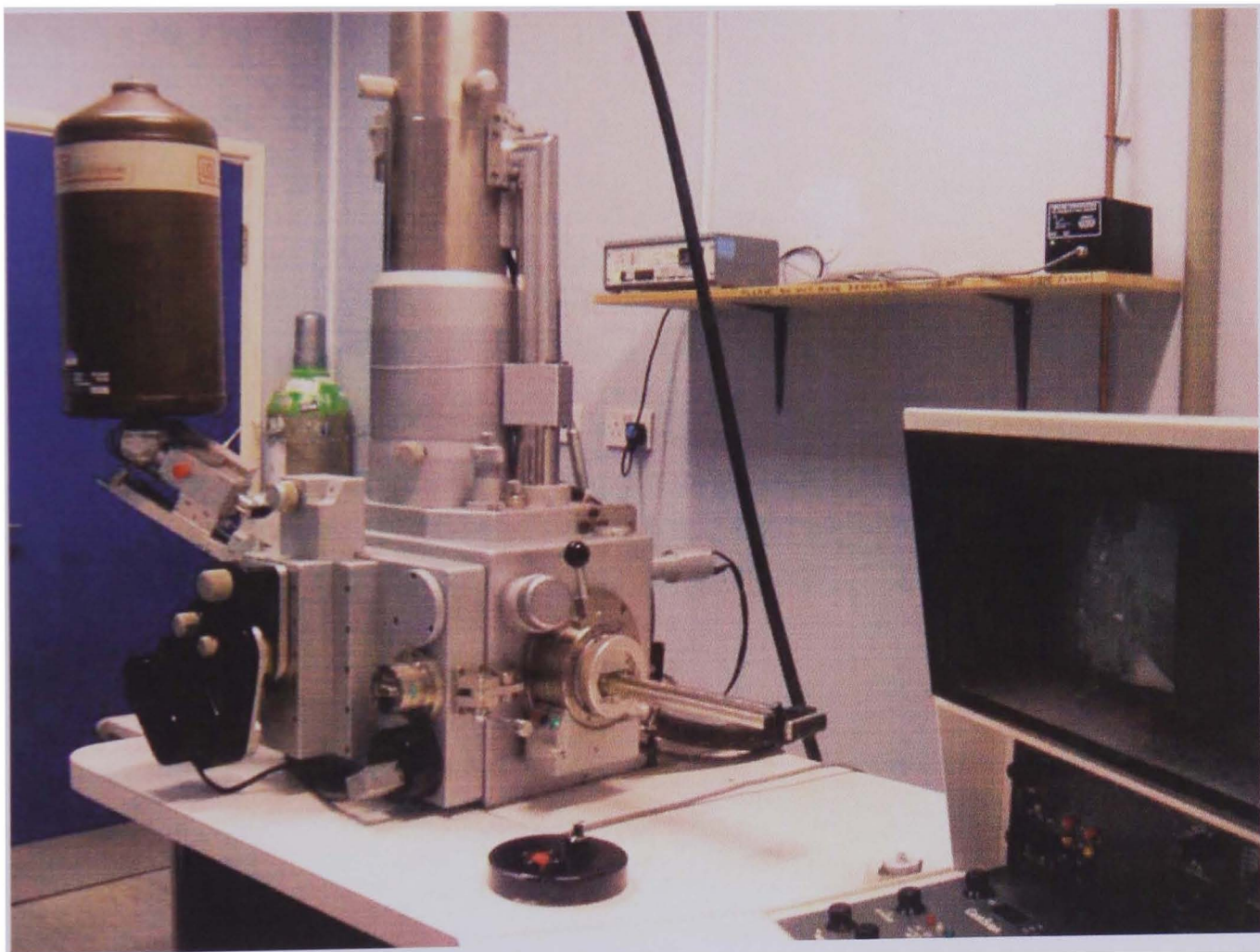


Figure 3.17: The CAMSCAN MK II, Scanning Electron Microscope.

A SEM creates images by focusing a high energy beam of electrons onto the surface of a sample and detecting signals from the interaction of the incident electrons with those of the surface of the sample. The type of signals gathered in a SEM varies and can include secondary electrons, characteristic x-rays and back scattered electrons [236].

In this research secondary electron imaging was used, this being the standard mode for this SEM, the resulting signals being rendered into two-dimensional intensity distributions producing high-resolution images of the fractured surfaces at a range of magnifications from 20 to 5,000 times; these were viewed and saved as digital images on a computer.

The characteristic three-dimensional appearance of these images was useful in aiding an understanding of the surface features of and damage to the specimens; indeed the use of scanning electron microscopy in the investigation of the fractography of fretting wear and fretting fatigue is well documented [237].

CHAPTER

4

RESULTS

4.1 INTRODUCTION

Forty fretting fatigue tests were completed in the constant normal pressure test programme. The fretting fatigue life of aluminium alloy 2024 T351 in contact with aluminium alloy 2024 T351 was determined as a function of normal pressure and cyclic axial stress for unpeened and peened components. In all cases there was a considerable reduction in fatigue strength, although less so for the peened condition. These results are presented in Section 4.2.

The sections that follow detail the subsequent analyses performed to explore some of the other influential factors. Some data on the friction forces developed as a function of normal pressure and cyclic axial stress were recorded and relationships between normal pressure and friction force and normal pressure and the friction ratio were established for the unpeened condition.

Following a further seventy-two fretting fatigue tests, surface roughness profiles of two hundred and eighty-eight wear scars were obtained. The surface damage was explored and the widths and depths of the wear scars were determined. There was a difference between the surface damage incurred by fretting for the unpeened and peened condition.

Subsequent examination of the free surfaces using a scanning electron microscope, revealed further detail of the considerable wear due to the surface contact. The wear scars indicate regions of stress concentration that could be responsible for the fast initiation and propagation of fatigue cracks.

4.2 FRETTING FATIGUE TEST RESULTS

4.2.1 Life

A total of forty fretting fatigue tests were conducted in the constant normal pressure test programme, with the primary aim to investigate the effect of a normal pressure on fatigue life. The influence of normal pressure on life was clear, as in all cases there was a considerable reduction in fatigue strength due to fretting.

4.2.1.1 Control

At the start of the test programme, three tests were conducted using a BS S98 steel bridge with a pad span of 16.5 mm, in flat-on-flat contact with aluminium alloy 2024 T351 specimens; this was to validate the experimental set-up. The resulting cycles to failure are shown in Table 4.1.

Table 4.1: The number of cycles to failure for the fretting fatigue tests with a BS S98 steel bridge in contact with an aluminium alloy 2024 T351 specimen.

Specimen (no.)	Normal stress (MPa)	Normal load (kN)	1/2 normal load (kN)	Axial stress (MPa)	Axial load (kN)	Cycles to failure (no.)
17	40	0.813	0.406	100	16	190,709
13	80	1.626	0.813	100	16	99,232
14	120	2.438	1.219	100	16	238,499

The results attained were comparable with data reported by Faanes and Fernando [100] for a BS S98 steel bridge with a pad span of 16.5 mm, in flat-on-flat contact with BS L65 4 % copper aluminium alloy specimens under the same load conditions, Figure 4.1, thus negating the need to repeat all previous tests.

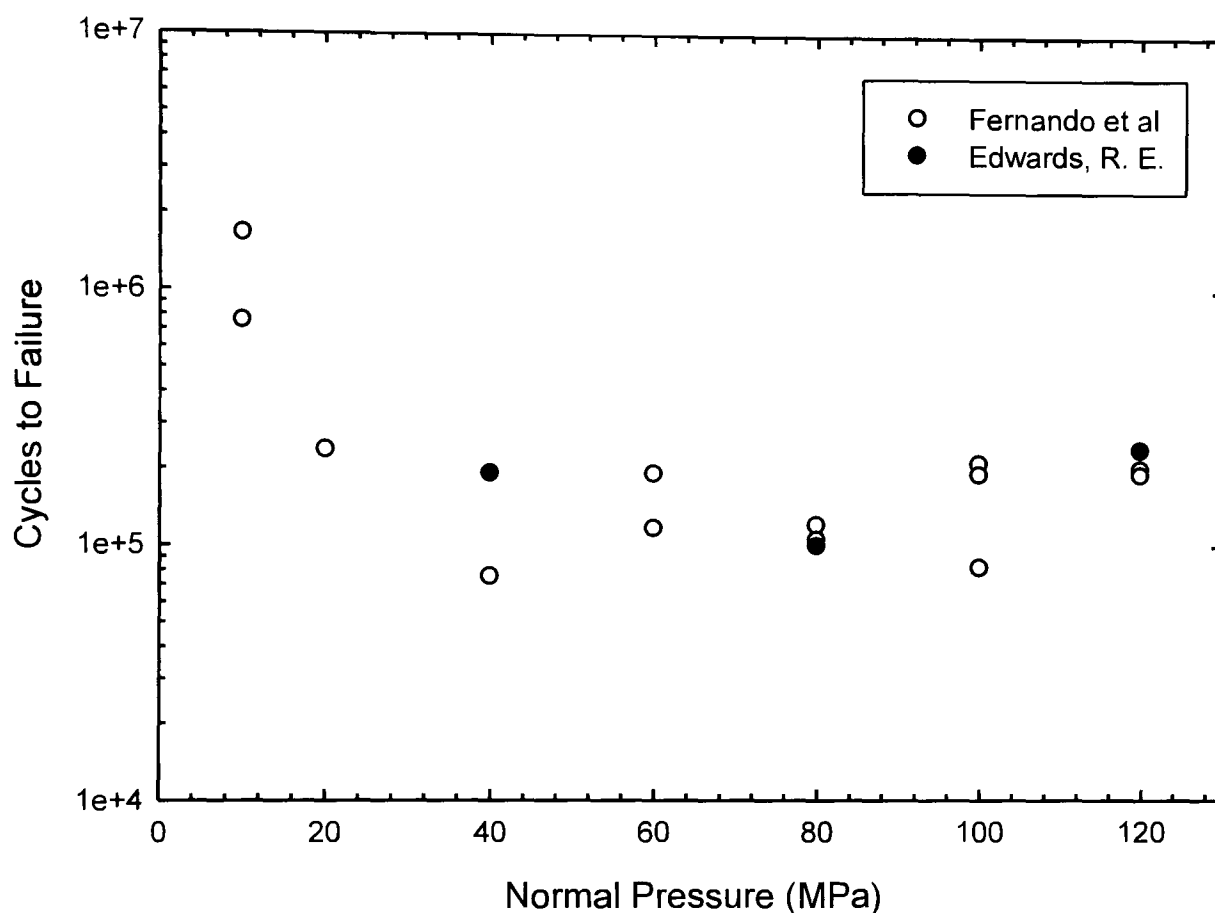


Figure 4.1: A comparison of the number of cycles to failure determined from this research and by Faanes and Fernando [100] for fretting fatigue tests with a BS S98 steel bridge in contact with an aluminium alloy 2024 T351 specimen subjected to an axial stress amplitude of 100 MPa.

4.2.1.2 Unpeened

Experiments using aluminium alloy 2024 T351 in flat-on-flat contact with aluminium alloy 2024 T351 were performed after the control test programme. The fretting fatigue lives for the constant normal pressure test programme of these thirty-one unpeened specimens are given in Appendix E, tables E.1a, E.1b and E.1c.

A summary of the results attained at axial stress amplitudes of 70 MPa, 100 MPa and 125 MPa using unpeened aluminium alloy 2024 T351 in flat-on-flat contact with unpeened aluminium alloy 2024 T351 is given in Figure 4.2.

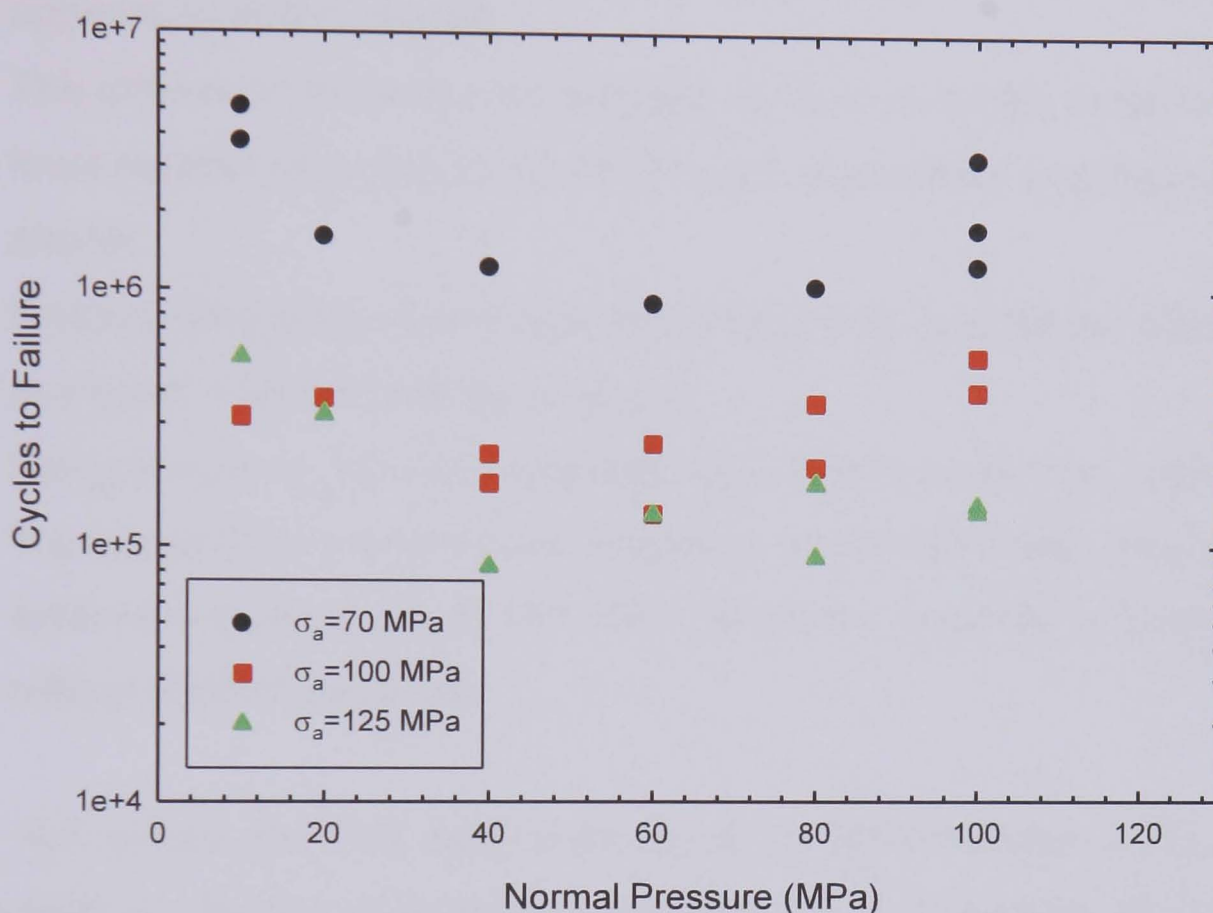


Figure 4.2: The experimental results for fretting fatigue tests conducted with an aluminium alloy 2024 T351 bridge subjected to a range of normal pressures in contact with an aluminium alloy 2024 T351 specimen subjected to axial stress amplitudes of 70 MPa, 100 MPa and 125 MPa.

An analysis of the results presented in figure 4.2 indicates that:

- The results for all three axial stress amplitudes applied exhibit a characteristic life distribution, whereby the number of cycles to failure decreases with an increase in normal pressure up to a critical value, whereupon a further increase in normal pressure leads to an increase in life;

- The critical normal pressure giving the shortest life for an axial stress amplitude of 100 MPa is at 40 MPa, 40% of the applied axial stress amplitude. For axial stress amplitudes of 70 MPa and 125 MPa that turning point is at 60 MPa, 85% and 50% of the axial stress amplitude respectively. Indeed the curve for the axial stress amplitude of 100 MPa appears to shift to the left;
- The difference between the greatest number of cycles to failure and the least number of cycles to failure for each axial stress amplitude applied is similar;
- Fretting fatigue life decreases with increasing axial stress amplitude for any given constant normal pressure;
- Fatigue lives at normal pressures above their respective critical values are higher for an axial stress amplitude of 100 MPa than they are for an axial stress amplitude of 125 MPa, whilst the opposite is true below the critical normal pressures.

Figure 4.3 shows the $S-N$ data determined by Solis-Romero [197], for plain fatigue tests conducted on unpeened specimens at a stress ratio of $R = 0.1$.

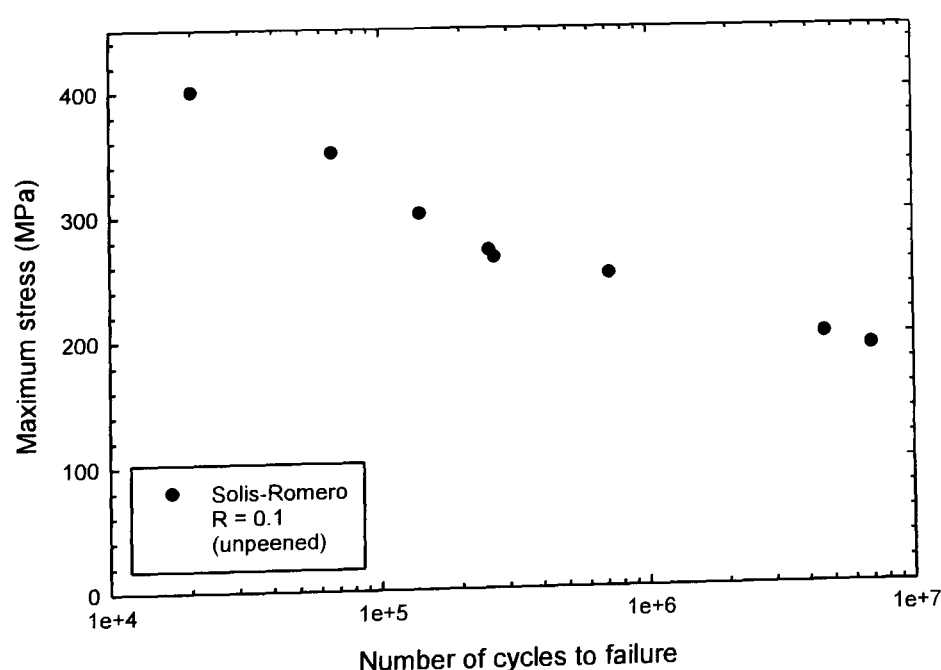


Figure 4.3: Plain fatigue $S-N$ data determined by Solis-Romero for aluminium alloy 2024 T351 for a stress ratio of $R = 0.1$.

In order to determine the $S-N$ plain fatigue curve for aluminium alloy 2024 T351 at a stress ratio of $R = -1$, the mean stresses, σ_m , and stress amplitudes, σ_a , were calculated from the data recorded by Solis-Romeo [197] for a stress ratio $R = 0.1$, utilising Equation 4.1, as is shown in Table 4.2.

$$R = \frac{\sigma_{\min}}{\sigma_{\max}} \quad \text{Equation 4.1}$$

Table 4.2: The mean stresses, σ_m , and stress amplitudes, σ_a , calculated from the data from Solis-Romeo for a stress ratio $R = 0.1$

N_f	σ_{\max}	R	σ_{\min}	σ_m	σ_a
20,227	400	0.1	40	220	180
66,760	350	0.1	35	193	158
140,990	300	0.1	30	165	135
254,920	270	0.1	27	149	122
266,900	264	0.1	26	145	119
721,645	250	0.1	25	138	113
4,640,000	200	0.1	20	110	90
7,000,000	190	0.1	19	105	86

By plotting this data and drawing a series of straight lines between the tensile strength, σ_u , of the material at $\sigma_a = 0$ and the data for $R = 0.1$, the stress amplitudes for the case of zero mean stress were thus determined at the intercept of the curve at $\sigma_m = 0$, as is shown in Figure 4.4.

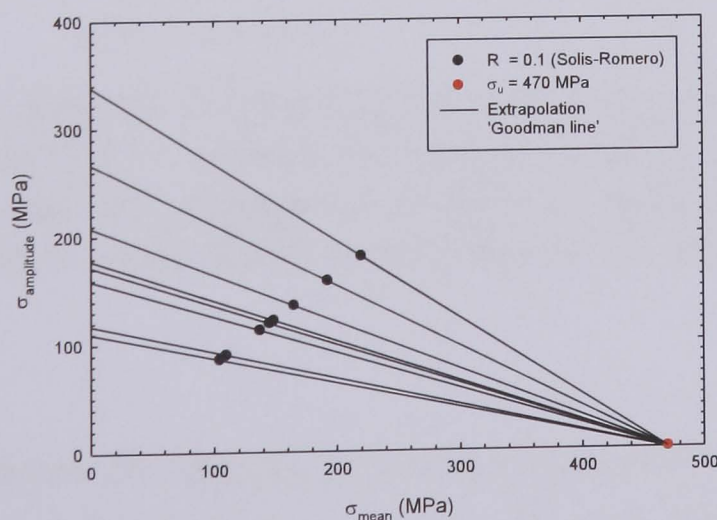


Figure 4.4: Interpolation of the data for $R = 0.1$ on a constant-life diagram, in order to determine that for $R = -1$.

The fretting fatigue tests were conducted at a stress ratio of $R = -1$. The values of σ_a at $\sigma_m = 0$, are therefore a direct estimate of the values of σ_a that would have been determined had the bridge pads not been applied.

Figures 4.5 and 4.6 show the $S-N$ data for all fretting fatigue tests conducted on unpeened specimens. Figure 4.5 compares this data with the $S-N$ curve for plain fatigue derived from the data published by Solis-Romero [197], in contrast with that published by Dowling [238]. This figure demonstrates fretting fatigue failures at stresses well below the fatigue strength of aluminium alloy 2024 T351 of 140 MPa.

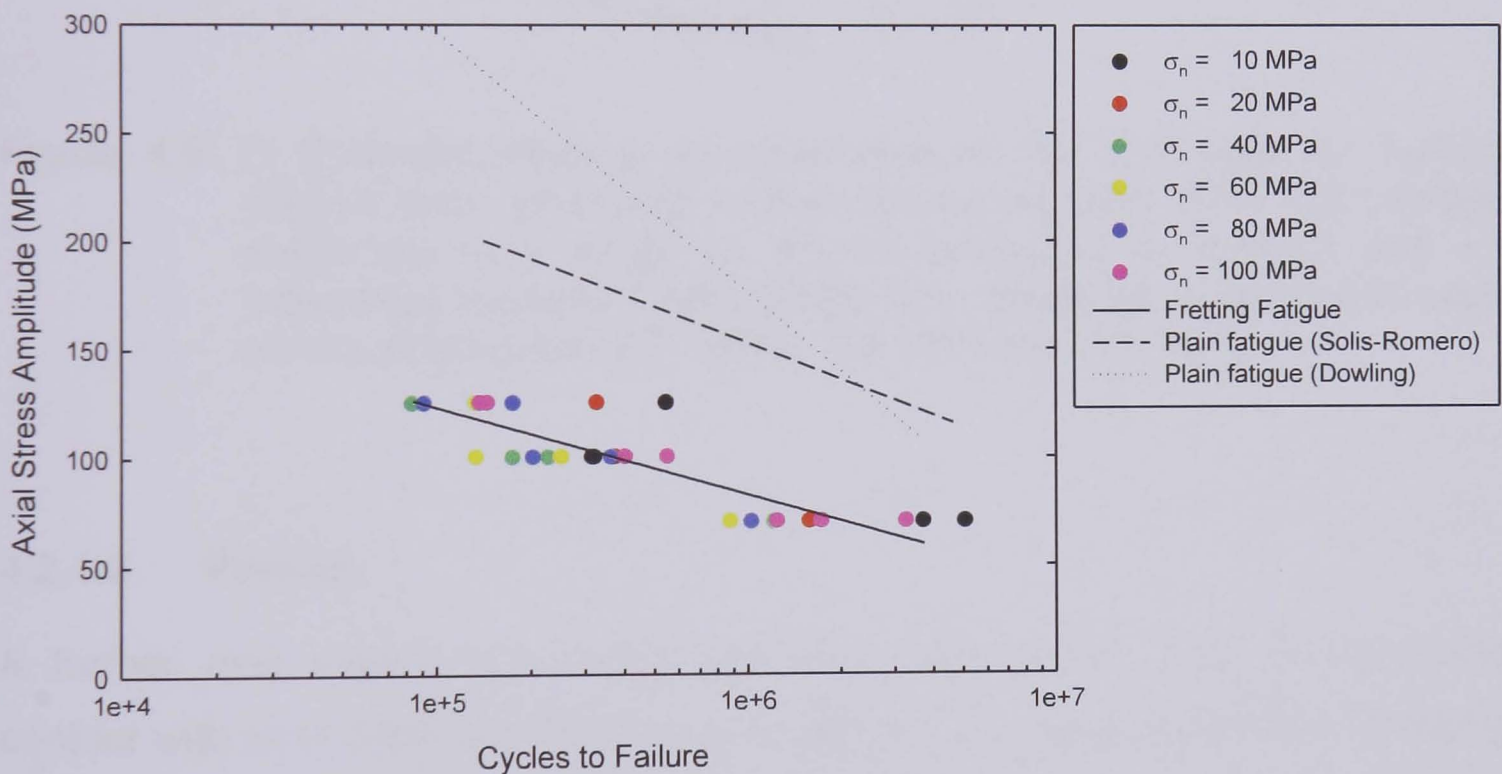


Figure 4.5: The $S-N$ data for fretting fatigue tests conducted with an aluminium alloy 2024 T351 bridge subjected to a range of normal pressures in contact with an unpeened aluminium alloy 2024 T351 specimen subjected to axial stress amplitudes of 70 MPa, 100 MPa and 125 MPa.

Figure 4.6 encompasses all data as previously documented in Figures 4.2 and 4.5. A surface plot has been fitted between these points, demonstrating the scope of the information determined and resulting in a useful reference map.

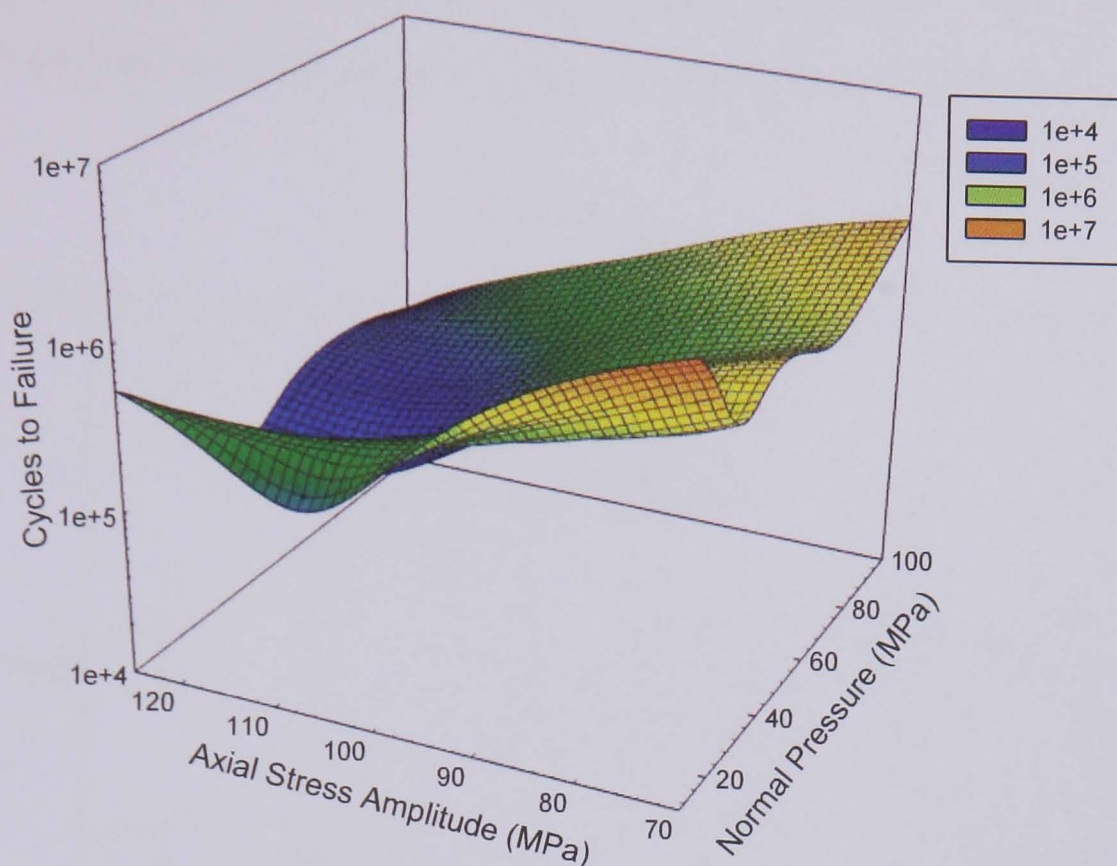


Figure 4.6: A three-dimensional representation of the S-N data for fretting fatigue tests conducted with an aluminium alloy 2024 T351 bridge subjected to a range of normal pressures in contact with an unpeened aluminium alloy 2024 T351 specimen subjected to axial stress amplitudes of 70 MPa, 100 MPa and 125 MPa.

4.2.1.3 Peened

A further nine experiments using aluminium alloy 2024 T351 in flat-on-flat contact with shot peened aluminium alloy 2024 T351 were performed following those on the unpeened specimens. For each of the three axial stress amplitudes applied before, the minimum, maximum and critical normal pressures previously determined were applied. The fretting fatigue test results from this constant normal pressure test programme are given in Appendix E, tables E.2a, E.2b and E.2c.

A summary of the results attained at axial stress amplitudes of 70 MPa, 100 MPa and 125 MPa using unpeened aluminium alloy 2024 T351 in flat-on-flat contact with peened aluminium alloy 2024 T351 is given in Figure 4.7.

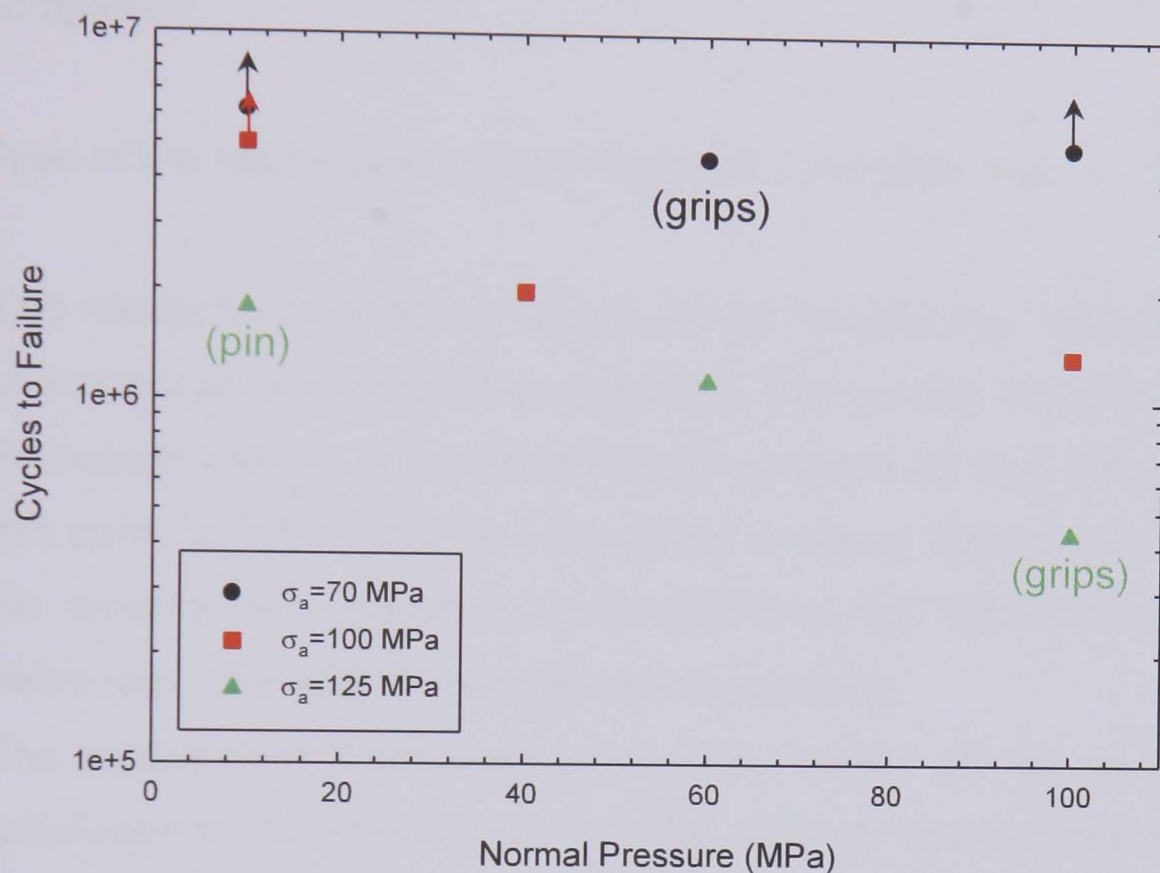


Figure 4.7: The experimental results for fretting fatigue tests conducted with an aluminium alloy 2024 T351 bridge subjected to a range of normal pressures in contact with a peened aluminium alloy 2024 T351 specimen subjected to axial stress amplitudes of 70 MPa, 100 MPa and 125 MPa.

Two of the tests conducted at an axial stress amplitude of 70 MPa were halted when over 5×10^6 cycles was reached and the third resulted in failure, not at the peened test section, but at an unpeened area in the grips. These tests were not repeated due to restrictions on time.

The test conducted at an axial stress amplitude of 100 MPa and a normal pressure of 10 MPa was halted when 5×10^6 cycles were reached; the other two test conditions resulted in failure.

The test conducted at an axial stress amplitude of 125 MPa and a normal pressure of 0.1 kN was halted by the failure of one of the steel locating pins, the test conducted at a normal pressure of 100 MPa resulted in failure, not at the peened test section, but at an unpeened area in the grips, but was not repeated due to restrictions on time; the test conducted at a normal pressure of 60 MPa ran to completion.

An analysis of the results presented in Figure 4.7 indicates that:

- The results for axial stress amplitudes of 70 MPa and 100 MPa exhibit a characteristic life distribution, whereby the number of cycles to failure decreases with an increase in normal pressure up to a critical value. At this point, a further increase in normal pressure leads to an increase in life, whereas for an axial stress amplitude of 125 MPa there is a marked decrease in life with increasing normal pressure;
- The critical normal pressure giving the shortest life for an axial stress amplitude of 70 MPa is at 60 MPa, 85% of the applied axial stress amplitude. For an axial stress amplitude of 100 MPa that point is probably around 80 MPa, 80% of the applied axial stress amplitude, indeed the curve for the axial stress amplitude of 100 MPa appears to shift to the right;
- Fretting fatigue life decreases with increasing axial stress amplitude for any given constant normal pressure;
- Fatigue lives at normal pressures above their respective critical values are higher for an axial stress amplitude of 70 MPa than they are for an axial stress amplitude of 100 MPa, whilst below the critical normal pressures the values of these fatigue lives tend together.

Figures 4.8 and 4.9 show the $S-N$ data for all tests conducted on peened specimens, demonstrating fatigue failures at stresses still well below the yield stress of aluminium alloy 2024 T351.

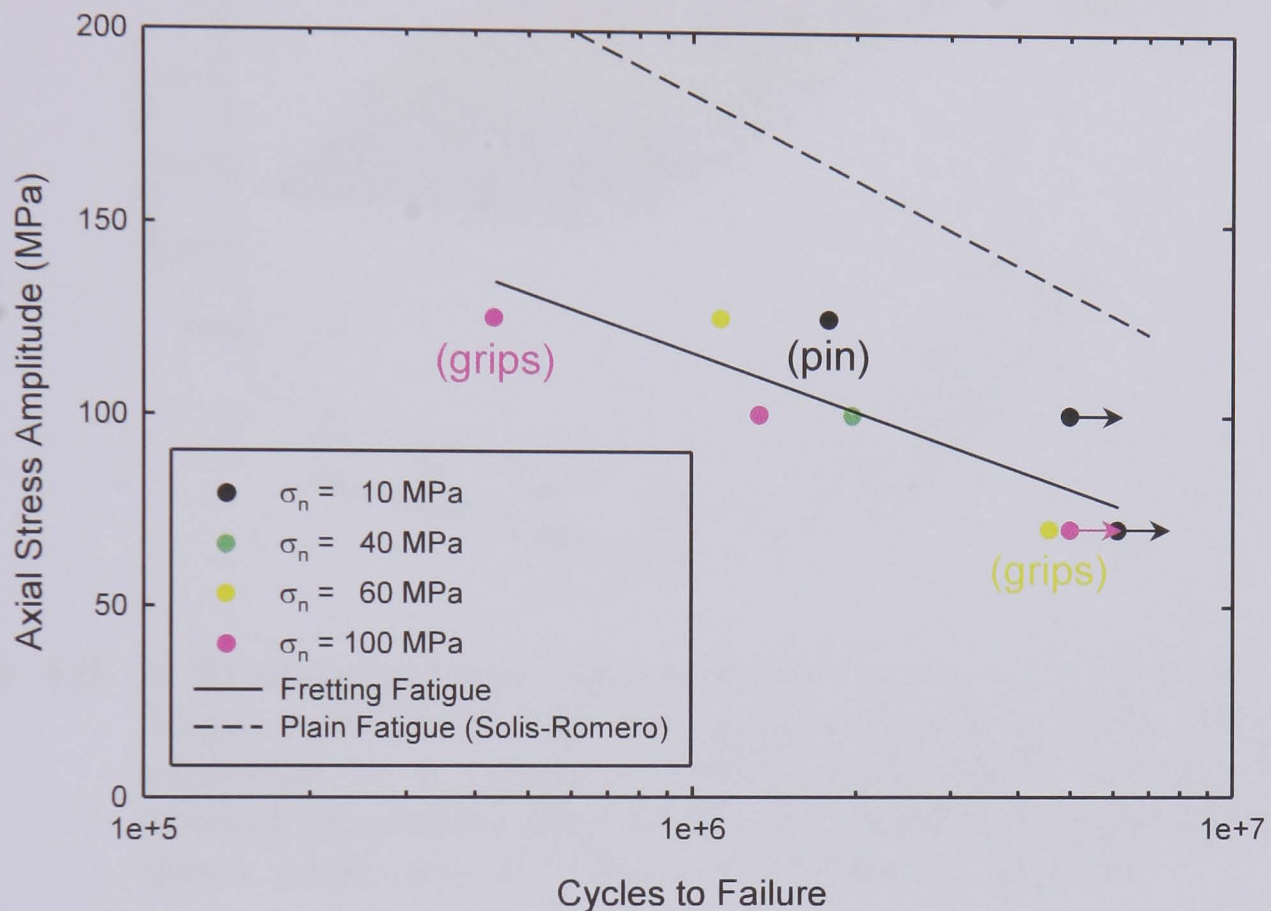


Figure 4.8: The $S-N$ data for fretting fatigue tests conducted with an aluminium alloy 2024 T351 bridge subjected to a range of normal pressures in contact with an peened aluminium alloy 2024 T351 specimen subjected to axial stress amplitudes of 70 MPa, 100 MPa and 125 MPa. Both fretting and plain fatigue lives are determined for the peened condition.

Figure 4.9 encompasses all data as previously documented in Figures 4.7 and 4.8. A surface plot has been fitted between these points, demonstrating the scope of the information determined and resulting in a useful reference map.

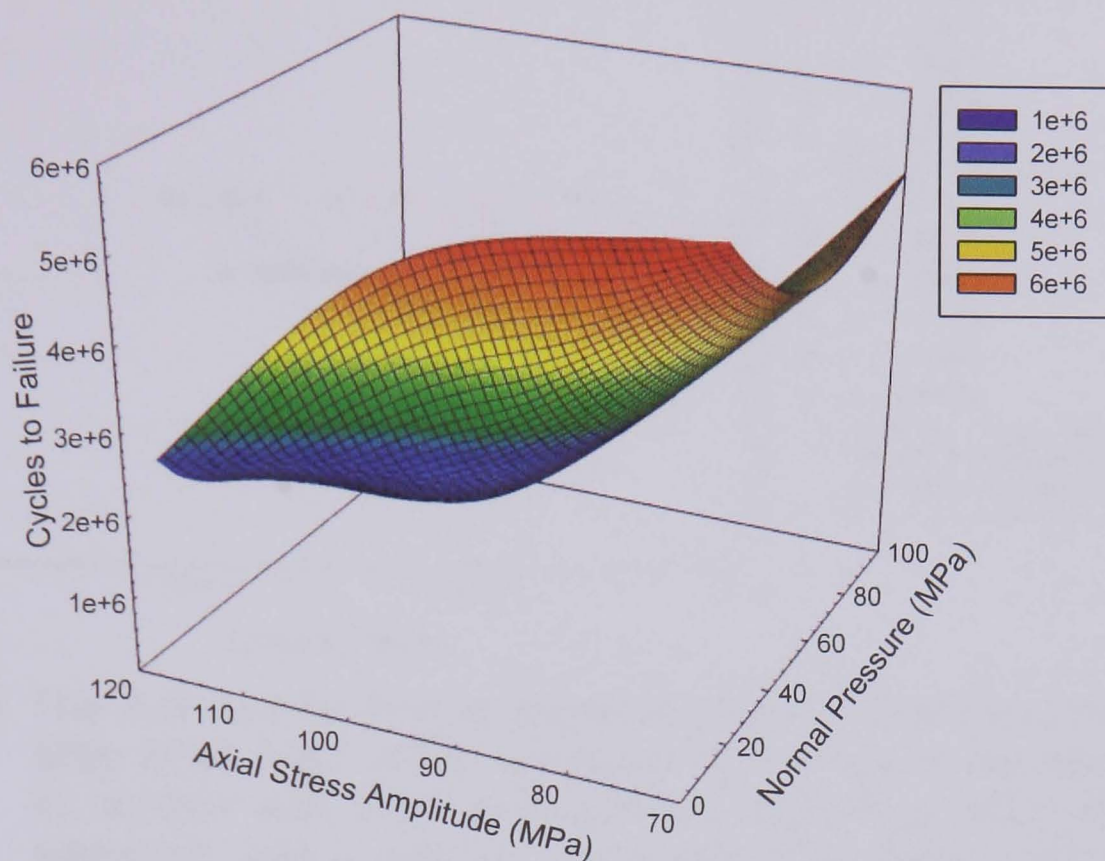


Figure 4.9: A three-dimensional representation of the $S-N$ data for fretting fatigue tests conducted with an aluminium alloy 2024 T351 bridge subjected to a range of normal pressures in contact with a peened aluminium alloy 2024 T351 specimen subjected to axial stress amplitudes of 70 MPa, 100 MPa and 125 MPa.

Figure 4.10 shows the $S-N$ data for all tests conducted on both unpeened and peened specimens, demonstrating a marked improvement in fatigue life due to shot peening, but with the same dependency on normal pressure.

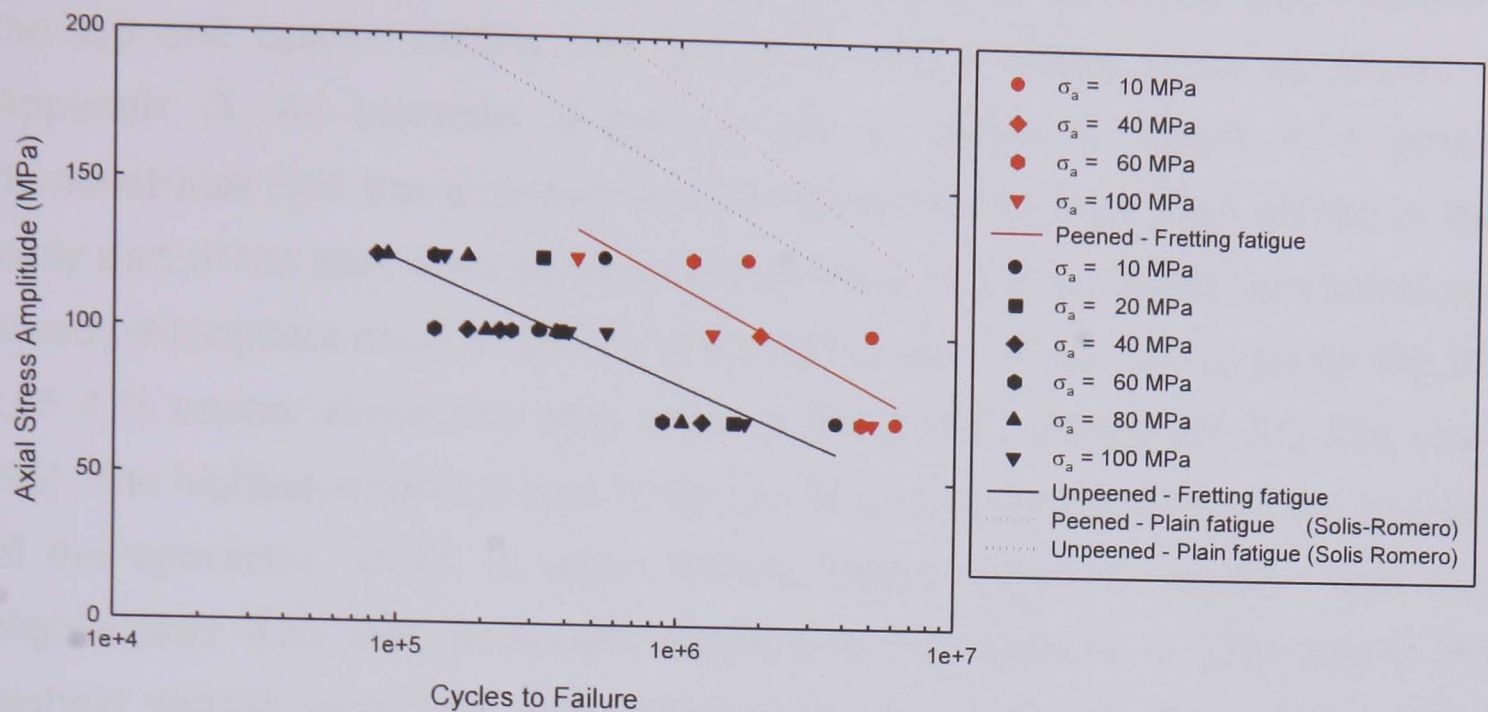


Figure 4.10: The S-N data for fretting fatigue tests conducted with an aluminium alloy 2024 T351 bridge subjected to a range of normal pressures in contact with both an unpeened aluminium alloy 2024 T351 specimen and a peened aluminium alloy 2024 T351 specimen subjected to axial stress amplitudes of 70 MPa, 100 MPa and 125 MPa.

4.2.2 Friction

It has been reported that friction force plays a critical role in fretting crack initiation [155], therefore a primary aim of this test programme was to investigate the effect of friction on fretting fatigue life.

Data on the friction forces developed were recorded successfully for twenty-six out of the thirty-one fretting fatigue tests conducted with unpeened specimens. These included: all three of the control tests conducted using a BS S98 steel bridge, six out of the nine tests conducted with an axial stress amplitude of 70 MPa, all of the eleven tests conducted with an axial stress amplitude of 100 MPa and six out of the eight tests conducted with an axial stress amplitude of 125 MPa. These results can be found in Appendix F. Due to a corruption of the data acquisition software, no data is available for the peened case.

The evolution of the friction forces over the life of each specimen was traced for the top and bottom fretting pad for every one of these tests, as shown in Appendix G. An example of such a plot is shown in Figure 4.11, which demonstrates that the amplitude of the friction forces increased rapidly in the early part of the test, then decreased with wear and then settled and remained steady throughout most of the life of the specimen, as was the case for the BS L65 4 % copper aluminium alloy when in flat-on-flat contact with BS S98 steel [99]. The highest amplitude was observed at approximately 13 % of the total life of the specimen, which is when fretting debris began to appear. This was slightly later than that previously reported by Fernando et al. [99], where the highest friction amplitude was observed at approximately 5 – 10 % of the lifetime.

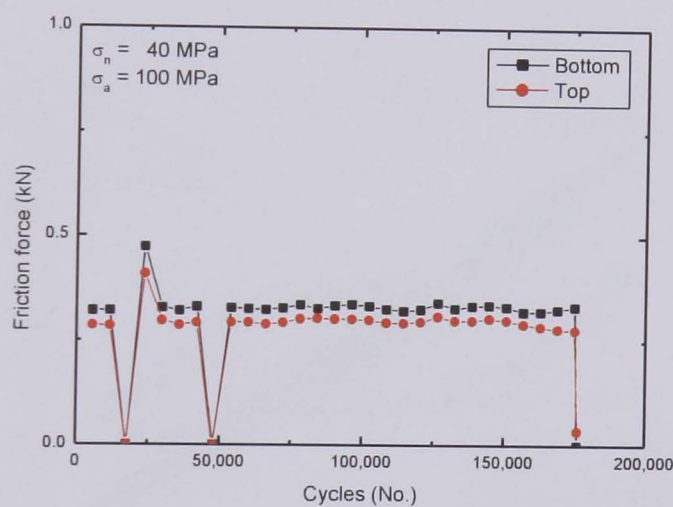


Figure 4.11: The evolution of the friction forces for both the top and bottom fretting pads, over the life of a specimen subjected to a normal pressure of 40 MPa and an axial stress amplitude of 100 MPa.

In general, stable friction behaviour was observed for both fretting pads during the major part of each lifetime, although the friction force transmitted by the bottom fretting pad was marginally greater than that transmitted by the top pad. The degree of stability of the friction force behaviour did vary from test to test. Indeed, in some tests a periodic change in mean friction force was noted.

In most cases though, a significant reduction in friction force was observed, during the final period before the fracture of the specimen, which could be attributed to the presence of a growing crack and the subsequent alteration in slip characteristics. Despite there being only one dominant crack in each of the specimens, approximately the same friction behaviour was observed for both the top and bottom fretting pads.

Hysteresis loops of friction force versus axial stress were subsequently plotted for the top and bottom fretting pad for each of these tests, as shown in Appendix H. An example of such a plot is shown in Figure 4.12, where the hysteresis loops at 3 %, 25 %, 50 %, 75 % and 97 % of the total fretting fatigue life are shown for a specimen subjected to a normal pressure of 80 MPa and an axial stress of ± 100 MPa.

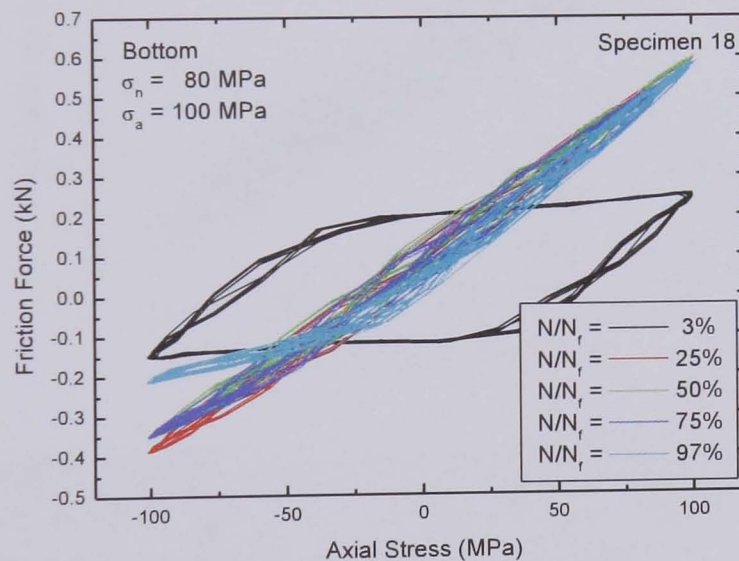


Figure 4.12: The axial stress versus friction force hysteresis loops for the bottom fretting bridge, for 3 %, 25 %, 50 %, 75 % and 97 % of the total fretting fatigue life of specimen number 18.

The hysteresis loops for the early stages of this test, demonstrate classic distinct micro-slip and macro-slip behaviours, which become less apparent during subsequent loading, as was the case for the BS L65 4 % copper aluminium alloy when in flat-on-flat contact with BS S98 steel [99].

A wider hysteresis loop is observed at the beginning of the test, with a gradual reduction in the hysteresis as the cycling progresses. In almost all tests, stable hysteresis behaviour was achieved within a few thousands of loading cycles. The drastic reduction in the friction force experienced during the tensile part of the loading cycle towards the final stages of this test may be indicative of significant cracking.

Figure 4.13 is the corresponding plot for the upper bridge pad in this test. This shows that the force transmitted by the lower pad was greater than that of the upper one.

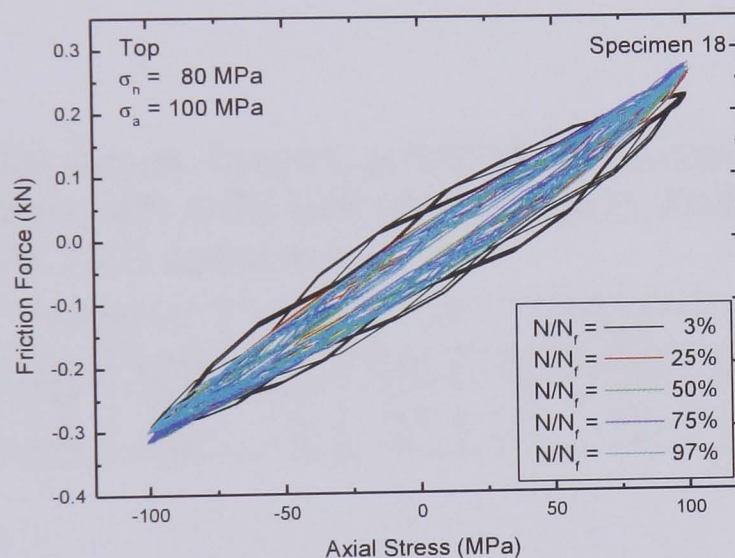


Figure 4.13: The axial stress versus friction force hysteresis loops for the top fretting bridge, for 3 %, 25 %, 50 %, 75 % and 97 % of the total fretting fatigue life of specimen number 18.

From these hysteresis loops, the overall maximum and minimum friction forces could be determined for both the top and bottom fretting pads when stable behaviour was observed, and thus the average friction force range and amplitude for each combination of normal pressure and axial stress. A friction ratio was also calculated from the normal pressure applied.

Following the corroboration of results from a control set with data published by Fernando et al. [99], the relationships between the maximum friction force and normal pressure and the friction force amplitude and normal pressure were subsequently investigated for both the top and bottom fretting pads in every case.

4.2.2.1 Control

The maximum and minimum friction forces determined for the three preliminary tests conducted using a BS S98 steel bridge with a pad span of 16.5 mm, in flat-on-flat contact with aluminium alloy 2024 T351 specimens are shown in Table 4.4, together with the ranges, amplitudes and ratios subsequently calculated.

Table 4.4: The friction forces, ranges, amplitudes and coefficients for the fretting fatigue tests with a BS S98 steel bridge in contact with an aluminium alloy 2024 T351 specimen.

Specimen (no.)	Normal stress (MPa)	Axial stress (MPa)	Friction force max. (kN)		Friction force min. (kN)		Friction amplitude (kN)			Friction coefficient (μ)		
			Top	Bottom	Top	Bottom	Top	Bottom	Average	Top	Bottom	Average
17	40	100	0.364	0.534	-0.336	-0.441	0.350	0.487	0.418	0.861	1.199	1.030
13	80	100	0.718	0.880	-0.721	-0.695	0.720	0.787	0.753	0.885	0.968	0.927
14	120	100	5.458	0.901	-0.746	-1.203	3.102	1.052	2.077	2.544	0.863	1.703

The results attained were compared with the data reported by Fernando et al. [99] for a BS S98 steel bridge with a pad span of 16.5 mm, in flat-on-flat contact with BS L65 4 % copper aluminium alloy specimens under the same load conditions, and were shown to be in good agreement, apart from the top pad in test 14, see Figure 4.14.

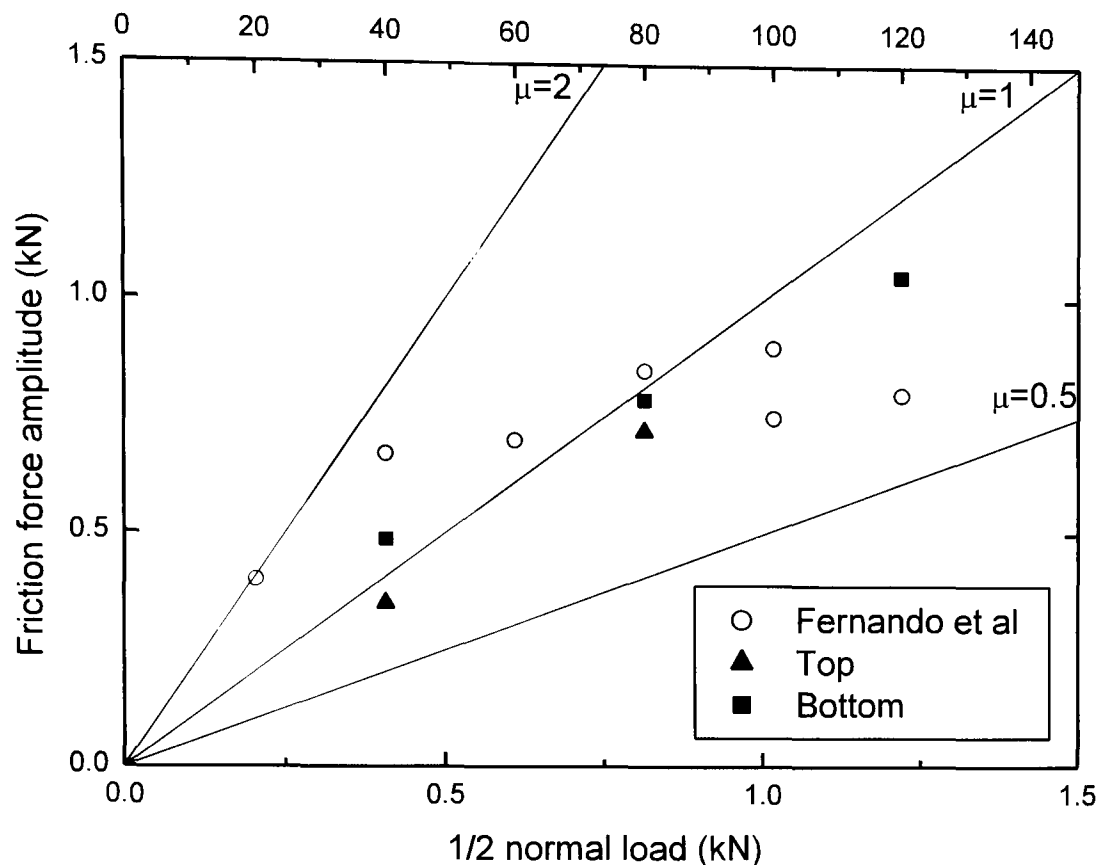


Figure 4.14: A comparison of the friction force amplitudes derived from the maximum and minimum friction forces determined for each test and by Fernando et al. [99] for fretting fatigue tests with a BS S98 steel bridge in contact with an aluminium alloy 2024 T351 specimen subjected to an axial stress amplitude of 100 MPa.

An analysis of the results presented in figure 4.14 indicates that:

- An increase in normal pressure tends to decrease the coefficient of friction in the original case, whereas the coefficient of friction is maintained in the new data set;
- The coefficient of friction for a normal pressure of 80 MPa is approximately equal to 1 in the original case and also in the new data set;
- In both cases, the amplitude of the friction forces generally increases with the magnitude of the applied normal pressure;
- The amplitudes of the friction forces for the steel bridge are greater than those for the aluminium bridge.

4.2.2.2 Unpeened

The friction forces for twenty-three of the twenty-eight unpeened specimens in the constant normal pressure test programme are given in Appendix F, tables F.1a, F.1b and F.1c. The friction forces were derived assuming a uniform distribution over the whole contact area; the friction ratios were defined using the amplitudes of the friction forces and the values of normal load on a pad applied. However, although coefficients of friction are stated, strictly these may only be defined when macro slip occurs, such that the values given by ratio of the friction force, F , between the surfaces in contact to the normal force, $N/2$ are true.

For an axial stress amplitude of 70 MPa, data were generally recorded at a rate of between 250 and 350 data points every 300, 600 or 1,800 seconds. These data sets are reliable for 3% of life for a normal pressure of 60 MPa, 25% of life for a normal pressure of 10 MPa, 50% of life for normal pressures of 80 MPa and 100 MPa and 100% for normal pressures of 20 MPa and 40 MPa. The dependence of the friction force on the normal pressure applied is shown in Figures 4.15 and 4.16. This behaviour is in good agreement with previous results [99].

For an axial stress amplitude of 100 MPa, data were recorded at a rate of 350 data points every 300 seconds. These data sets are complete for all normal pressures applied. The dependence of the friction force on the normal pressure applied is shown in Figures 4.17 and 4.18. This behaviour is in good agreement with previous results [99].

For an axial stress amplitude of 125 MPa, data were recorded at a rate of 350 data points every 300 seconds. These data sets are reliable for 3% of life for a normal pressure of 60 MPa, 25% of life for a normal pressure of 100 MPa and 100% for normal pressures of 10 MPa, 20 MPa, 40 MPa and 80 MPa. The dependence of the friction force on the normal pressure applied is shown in Figures 4.19 and 4.20. This behaviour is in good agreement with previous results [99].

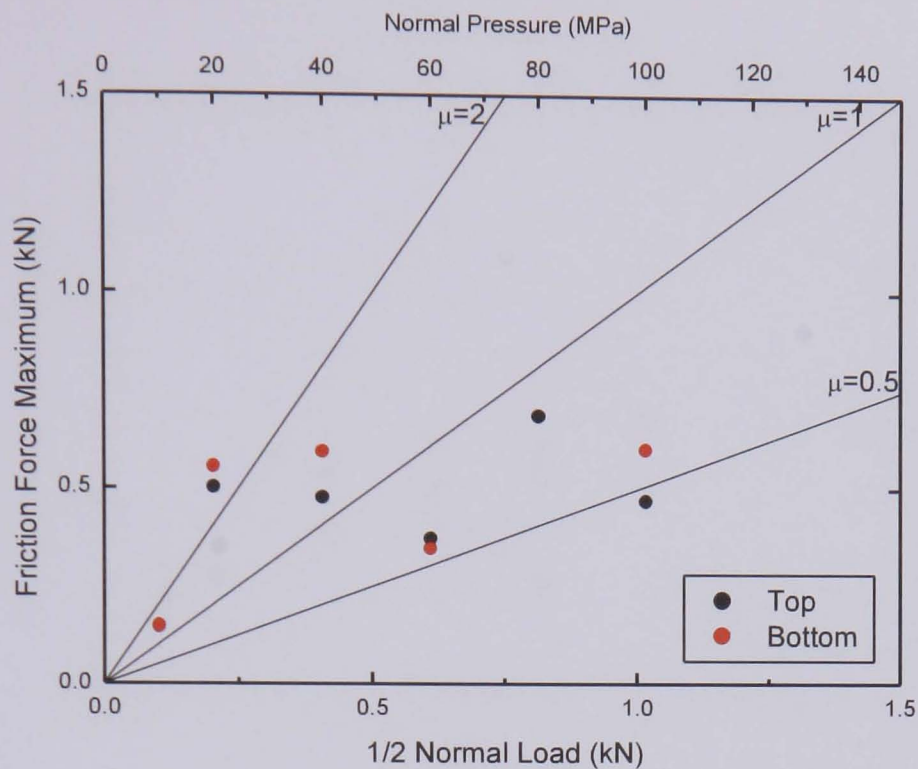


Figure 4.15: The maximum friction forces recorded from the upper and lower bridge pads in fretting fatigue tests conducted with an aluminium alloy 2024 T351 bridge in contact with an unpeened aluminium alloy 2024 T351 specimen subjected to an axial stress amplitude of 70 MPa.

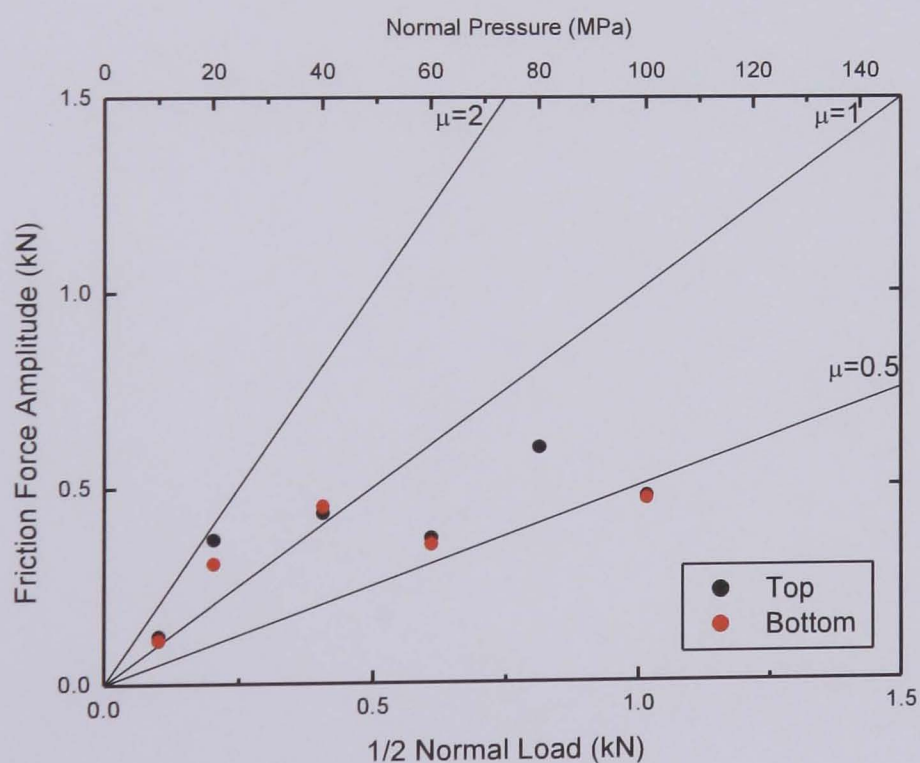


Figure 4.16: The friction force amplitudes calculated for fretting fatigue tests conducted with an aluminium alloy 2024 T351 bridge in contact with an unpeened aluminium alloy 2024 T351 specimen subjected to an axial stress amplitude of 70 MPa.

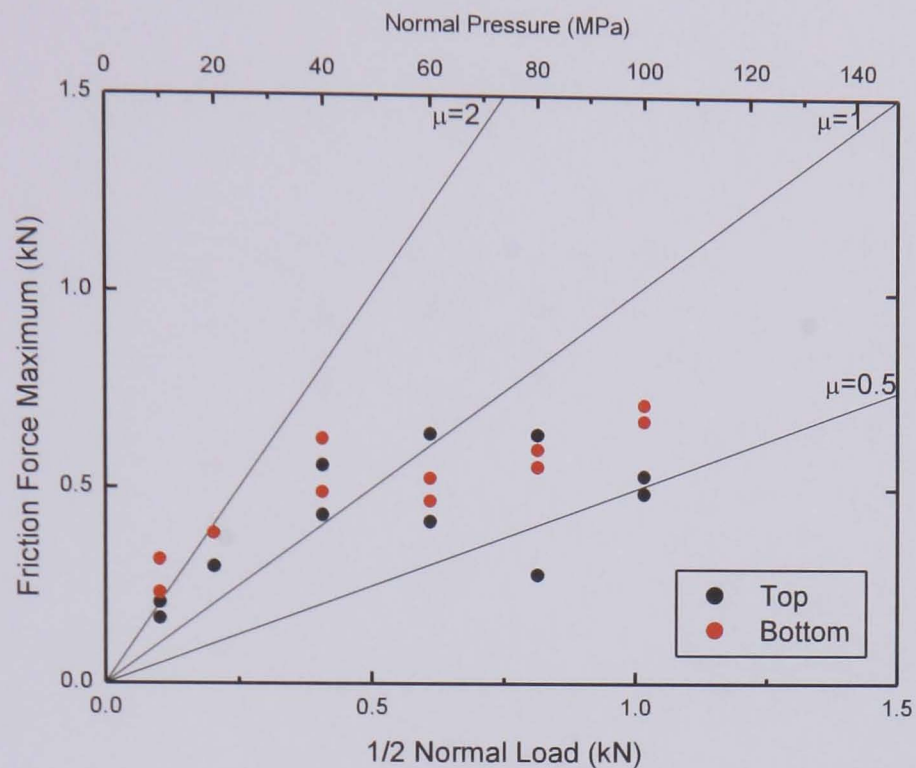


Figure 4.17: The maximum friction forces recorded from the upper and lower bridge pads in fretting fatigue tests conducted with an aluminium alloy 2024 T351 bridge in contact with an unpeened aluminium alloy 2024 T351 specimen subjected to an axial stress amplitude of 100 MPa.

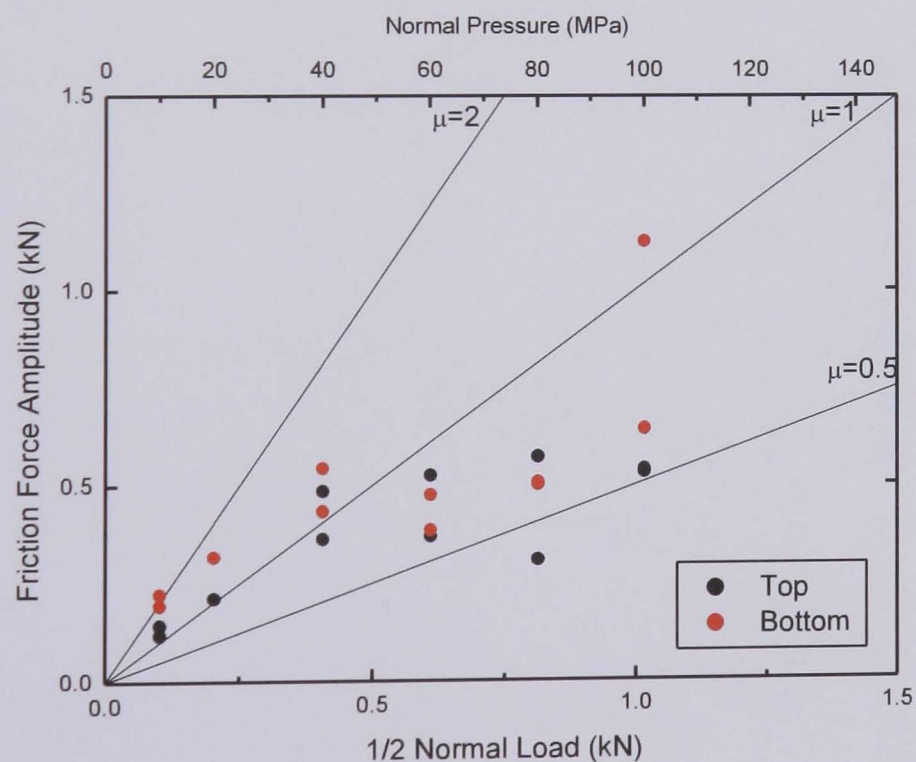


Figure 4.18: The friction force amplitudes calculated for fretting fatigue tests conducted with an aluminium alloy 2024 T351 bridge in contact with an unpeened aluminium alloy 2024 T351 specimen subjected to an axial stress amplitude of 100 MPa.

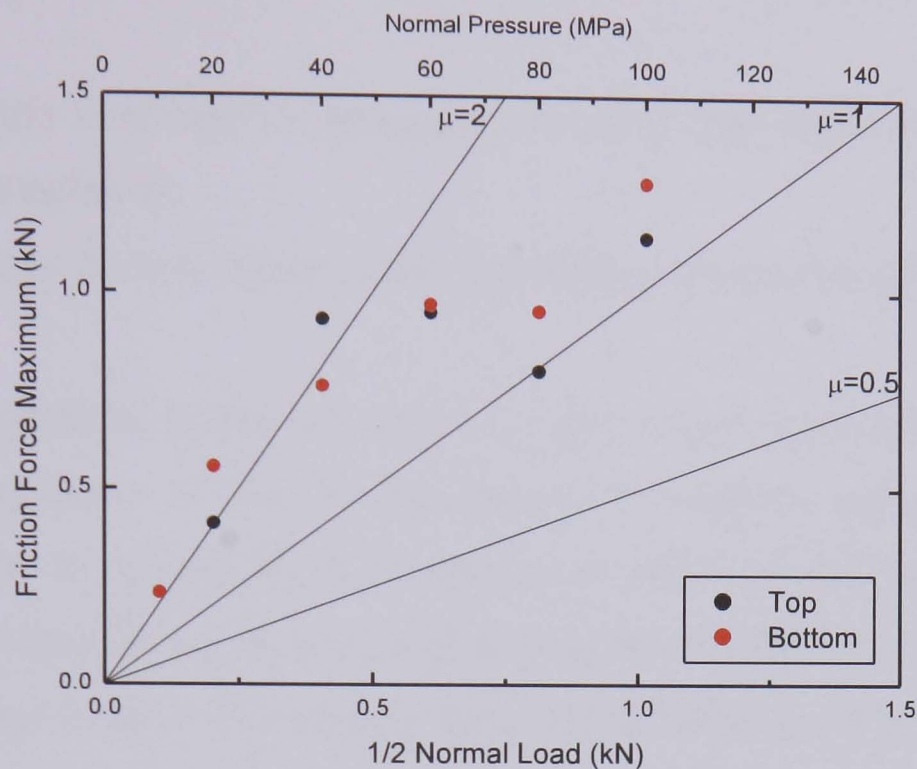


Figure 4.19: The maximum friction forces recorded from the upper and lower bridge pads in fretting fatigue tests conducted with an aluminium alloy 2024 T351 bridge in contact with an unpeened aluminium alloy 2024 T351 specimen subjected to an axial stress amplitude of 125 MPa.

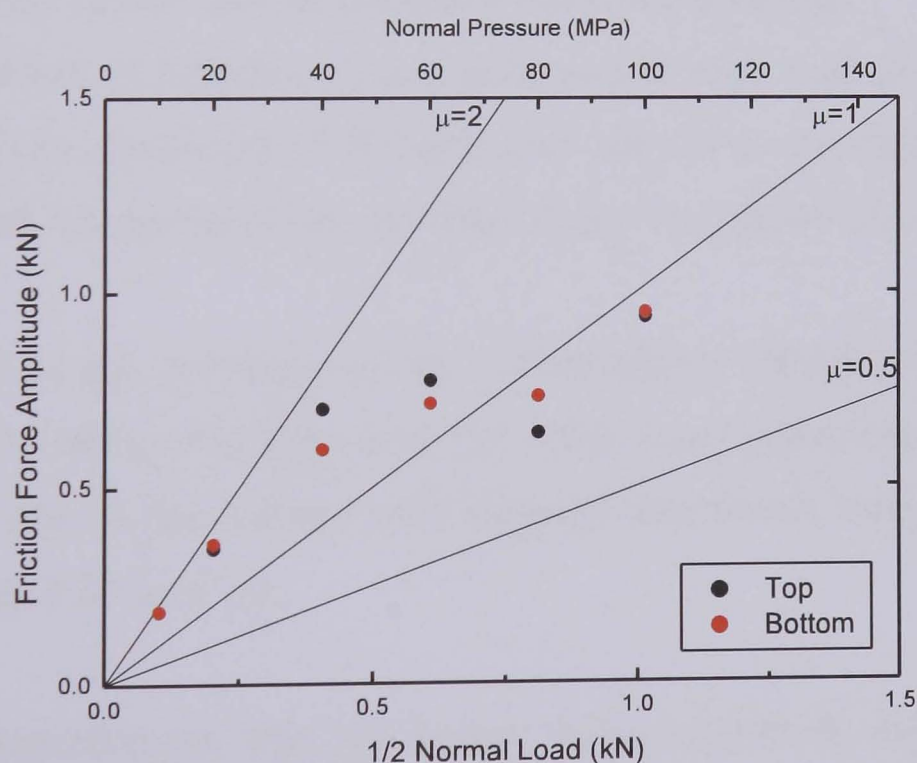


Figure 4.20: The friction force amplitudes calculated for fretting fatigue tests conducted with an aluminium alloy 2024 T351 bridge in contact with an unpeened aluminium alloy 2024 T351 specimen subjected to an axial stress amplitude of 125 MPa.

Analyses of the results presented in figures 4.15 to 4.20 indicate that:

- The trends in behaviour between the upper and lower bridge pads are in good agreement;
- The higher friction forces were generally observed with the lower bridge pads;
- The magnitude of the maximum friction forces generally increases with the magnitude of the normal pressure applied, although some later reduction in amplitude is observed at high normal pressures with the upper bridge pad at axial stress amplitudes of 100 MPa and 125 MPa;
- The magnitude of the friction force amplitudes generally increases with the magnitude of the normal pressure applied, although some later reduction in amplitude is observed at high normal pressures with the upper bridge pad at axial stress amplitudes of 100 MPa and 125 MPa;
- A coefficient of friction of 2 is achieved at low normal pressures;
- High coefficients of friction are obtained at low normal pressures, but this decreases as the normal pressure applied increases;
- A coefficient of friction of 0.5 is achieved at high normal pressures for an axial stress amplitude of 70 MPa and 100 MPa, whereas a coefficient of friction of 1 is achieved for an axial stress amplitude of 125 MPa.

A summary of all the average results subsequently calculated for axial stress amplitudes of 70 MPa, 100 MPa and 125 MPa using unpeened aluminium alloy 2024 T351 in flat-on-flat contact with peened aluminium alloy 2024 T351 are given in Figures 4.21 to 4.28.

Figure 4.21 demonstrates that the friction force amplitude generally increases with the magnitude of the applied normal pressure, or one half of the applied normal load per bridge foot, in line with the axial stress amplitude.

For an axial stress amplitude of 70 MPa, the coefficient of friction at low normal pressures is approximately equal to 1, dropping down to 0.5 at high normal pressures. For an axial stress amplitude of 100 MPa, the coefficient of friction at low normal pressures is approximately equal to 2, dropping down to 0.7 at high normal pressures. For an axial stress amplitude of 125 MPa, the coefficient of friction at low normal pressures is approximately equal to 2, dropping down to 1 at high normal pressures.

In all cases, an increase in normal pressure tends to decrease the coefficient of friction. The rate of this decrease is related to the applied axial stress amplitude, being greatest at 70 MPa and less pronounced at the higher axial stresses.

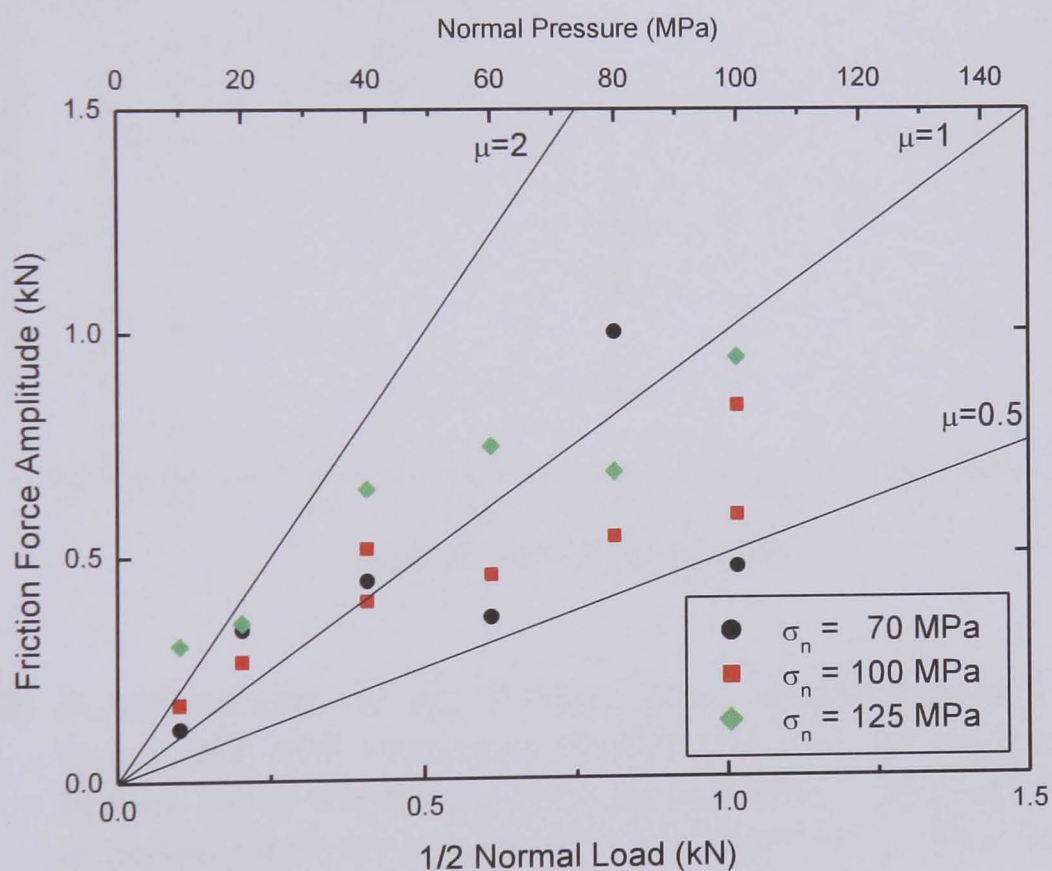


Figure 4.21: A comparison of the friction force amplitudes derived from the maximum and minimum friction forces determined for fretting fatigue tests conducted with an aluminium alloy 2024 T351 bridge in contact with an unpeened aluminium alloy 2024 T351 specimen subjected to axial stress amplitudes of 70 MPa, 100 MPa and 125 MPa.

Figure 4.22 highlights the influence of the axial stress amplitude on the friction force amplitude. There is a good degree of correlation between the axial stress amplitude and the normal pressures applied and the resultant friction force amplitudes observed in all cases; the average friction force amplitude is shown to be at a maximum for the maximum normal pressures applied and at a minimum for the minimum normal pressures applied for all axial stress amplitudes.

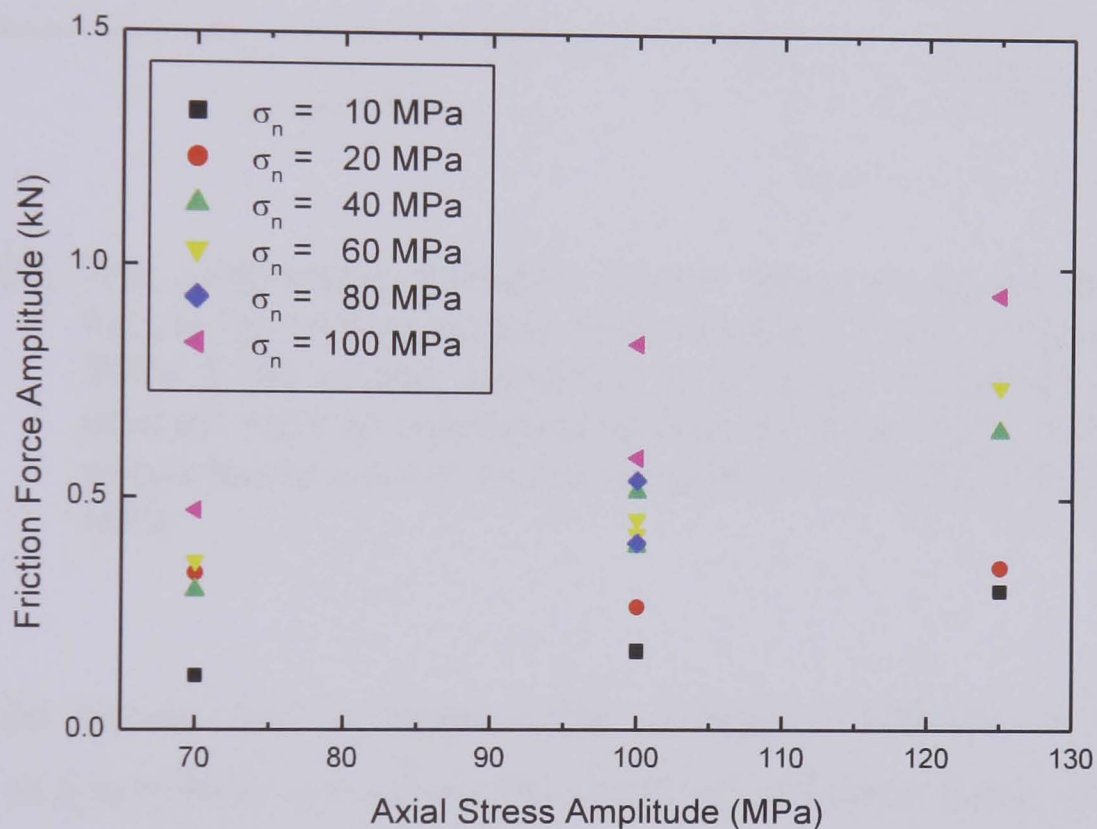


Figure 4.22: A comparison of the friction force amplitudes derived from the maximum and minimum friction forces determined for fretting fatigue tests conducted with an aluminium alloy 2024 T351 bridge in contact with an unpeened aluminium alloy 2024 T351 specimen subjected to a range of normal pressures.

Figure 4.23 demonstrates a degree of correlation between friction force amplitude and cycles to failure; the lower the number of cycles to failure, the greater the magnitude of the friction forces observed.

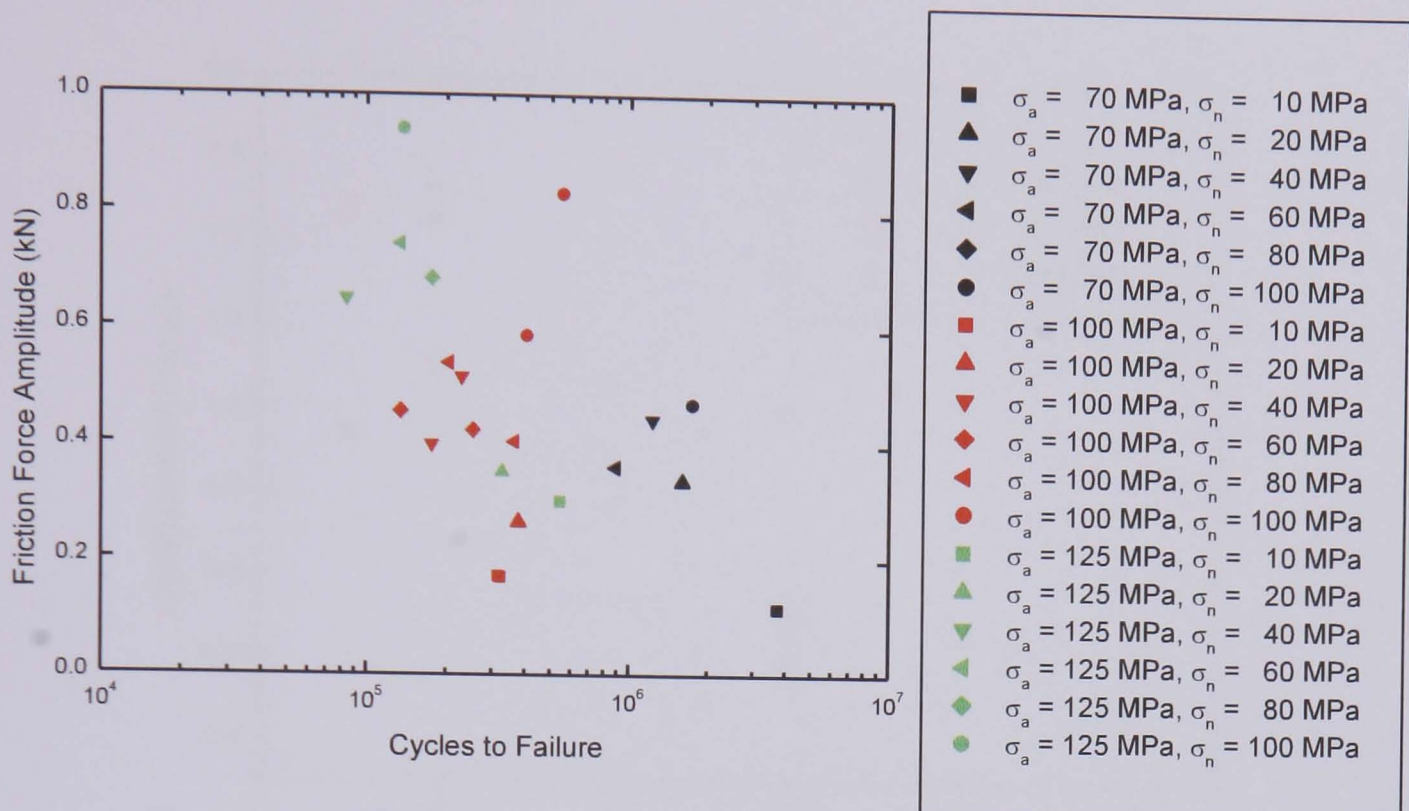


Figure 4.23: The relationship between friction force amplitude and cycles to failure for fretting fatigue tests conducted with an aluminium alloy 2024 T351 bridge subjected to a range of normal pressures in contact with an unpeened aluminium alloy 2024 T351 specimen subjected to axial stress amplitudes of 70 MPa, 100 MPa and 125 MPa.

Figure 4.24 shows that a higher total average coefficient of friction was observed at low normal pressures, the maximum recorded being approximately equal to 1.8, whereas for the BS L65 4 % copper aluminium alloy when in flat-on-flat contact with BS S98 steel this value was approximately equal to 2 [99]. The increase in the value of the friction coefficients with axial stress amplitude is compatible with the reduction in fretting fatigue life observed at the three different axial stress amplitudes.

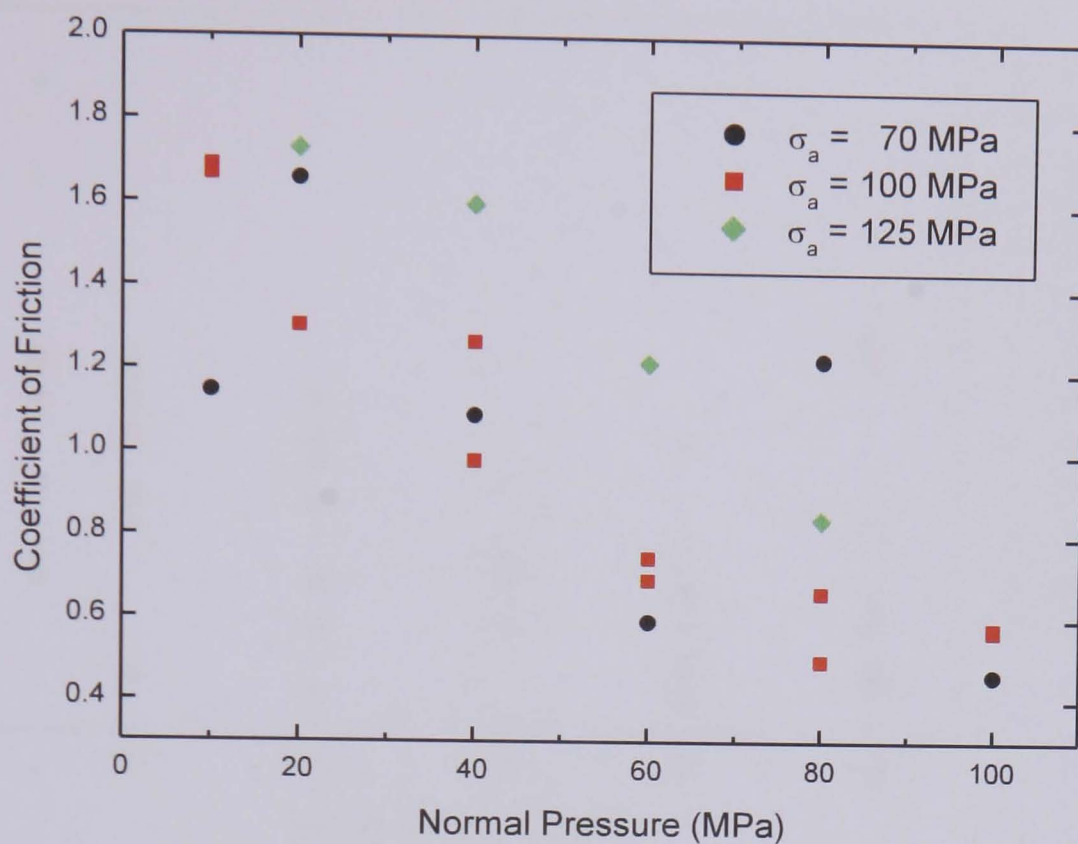


Figure 4.24: A comparison of the total average coefficients of friction calculated for fretting fatigue tests conducted with an aluminium alloy 2024 T351 bridge in contact with an unpeened aluminium alloy 2024 T351 specimen subjected to axial stress amplitudes of 70 MPa, 100 MPa and 125 MPa.

However, the evolution of the coefficients of friction over the life of each specimen was also investigated for the top and bottom fretting pad for every one of these tests, as shown in Appendix I. Figure 4.25 summarises these data, which shows that the highest average coefficient of friction, 2.7, was observed at a normal pressure of 10 MPa and an axial stress amplitude of 125 MPa, at 75% of the life of that test, although there is little difference between this reading and that taken at 3%. In contrast, the next highest average coefficient of friction was observed at a normal pressure of 100 MPa and an axial stress amplitude of 100 MPa. There is no clear correlation in the value of the friction coefficients with time.

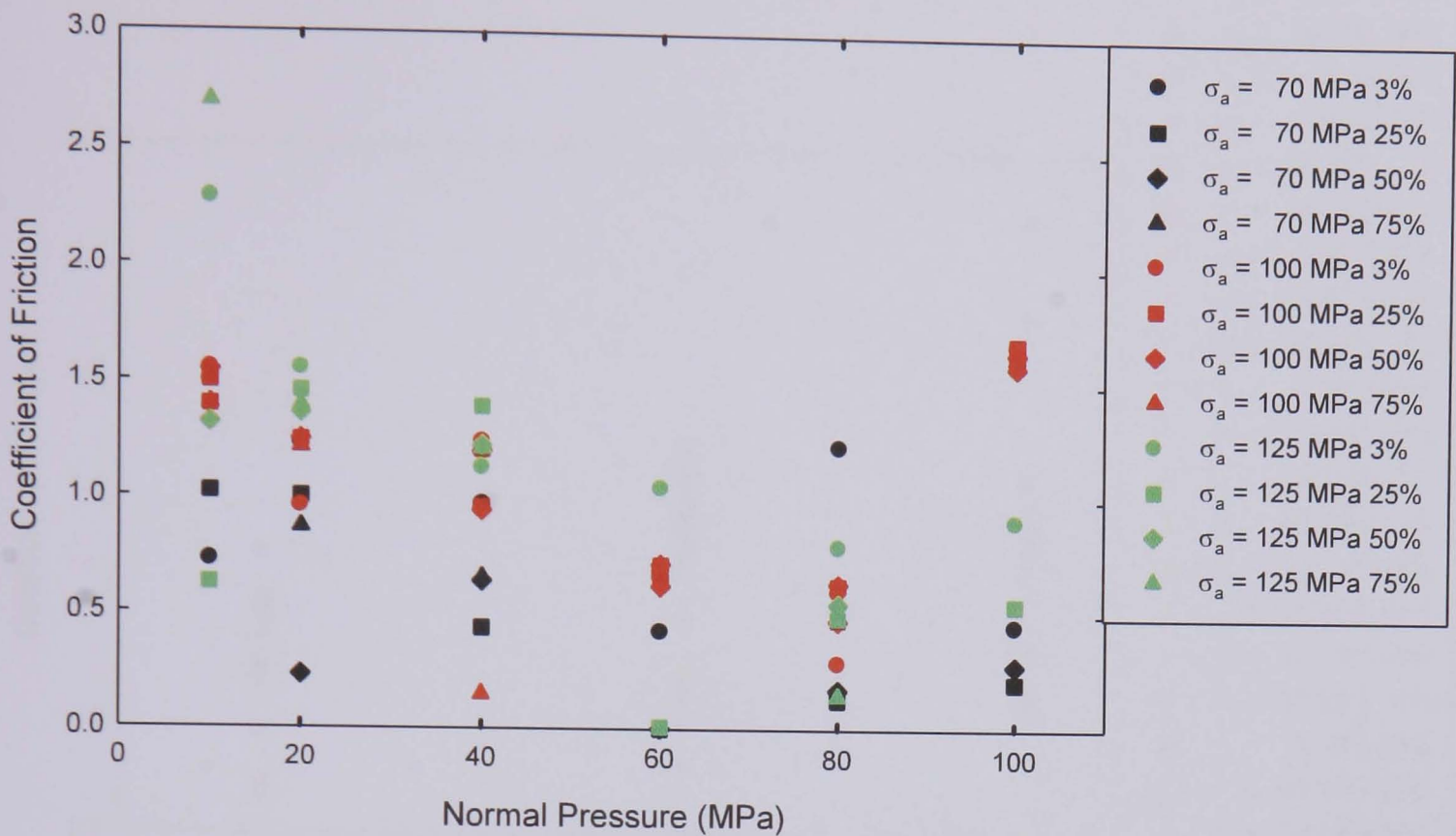


Figure 4.25: A comparison of the average coefficients of friction calculated over time for fretting fatigue tests conducted with an aluminium alloy 2024 T351 bridge in contact with an unpeened aluminium alloy 2024 T351 specimen subjected to axial stress amplitudes of 70 MPa, 100 MPa and 125 MPa.

Figure 4.26 highlights the influence of the axial stress amplitude on the coefficient of friction, an increase in axial stress amplitude resulted in an increase in the coefficient of friction. There is no correlation between the normal pressure and the coefficient of friction for an axial stress amplitude of 70 MPa, however, for an axial stress amplitude of 125 MPa, an increase in the normal pressure applied, led to a decrease in the coefficient of friction and for an axial stress amplitude of 100 MPa, an increase in the normal pressure applied, led to a decrease in the coefficient of friction up until a normal pressure of 100 MPa was applied, where the highest coefficients of friction for that axial stress amplitude were observed. There is no clear correlation in the value of the friction coefficients with time in any case.

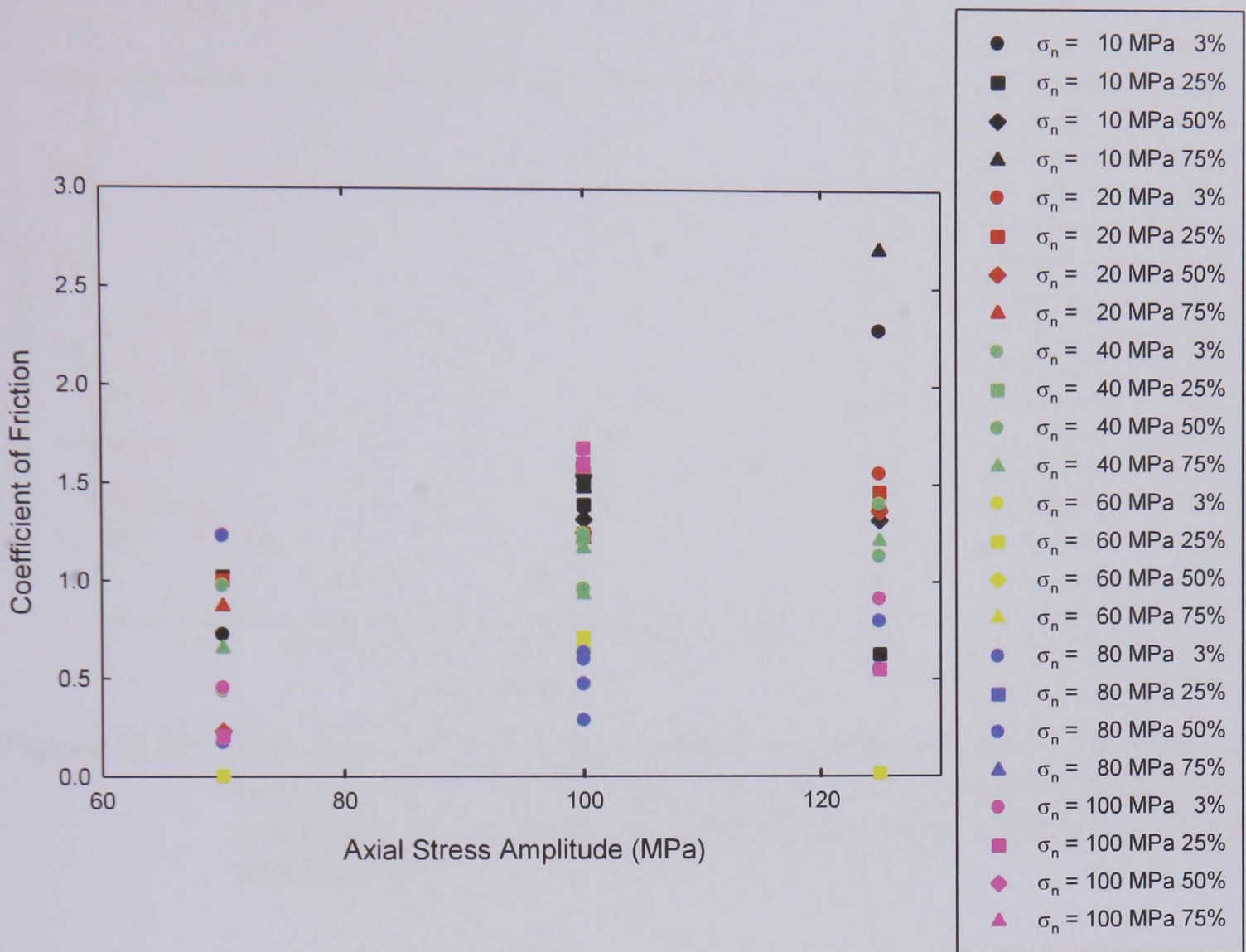


Figure 4.26: A comparison of the average coefficients of friction calculated over time for fretting fatigue tests conducted with an aluminium alloy 2024 T351 bridge in contact with an unpeened aluminium alloy 2024 T351 specimen subjected to a range of normal pressures.

Figures 4.27 and 4.28 demonstrate that there is no correlation between the coefficient of friction and percentage life.

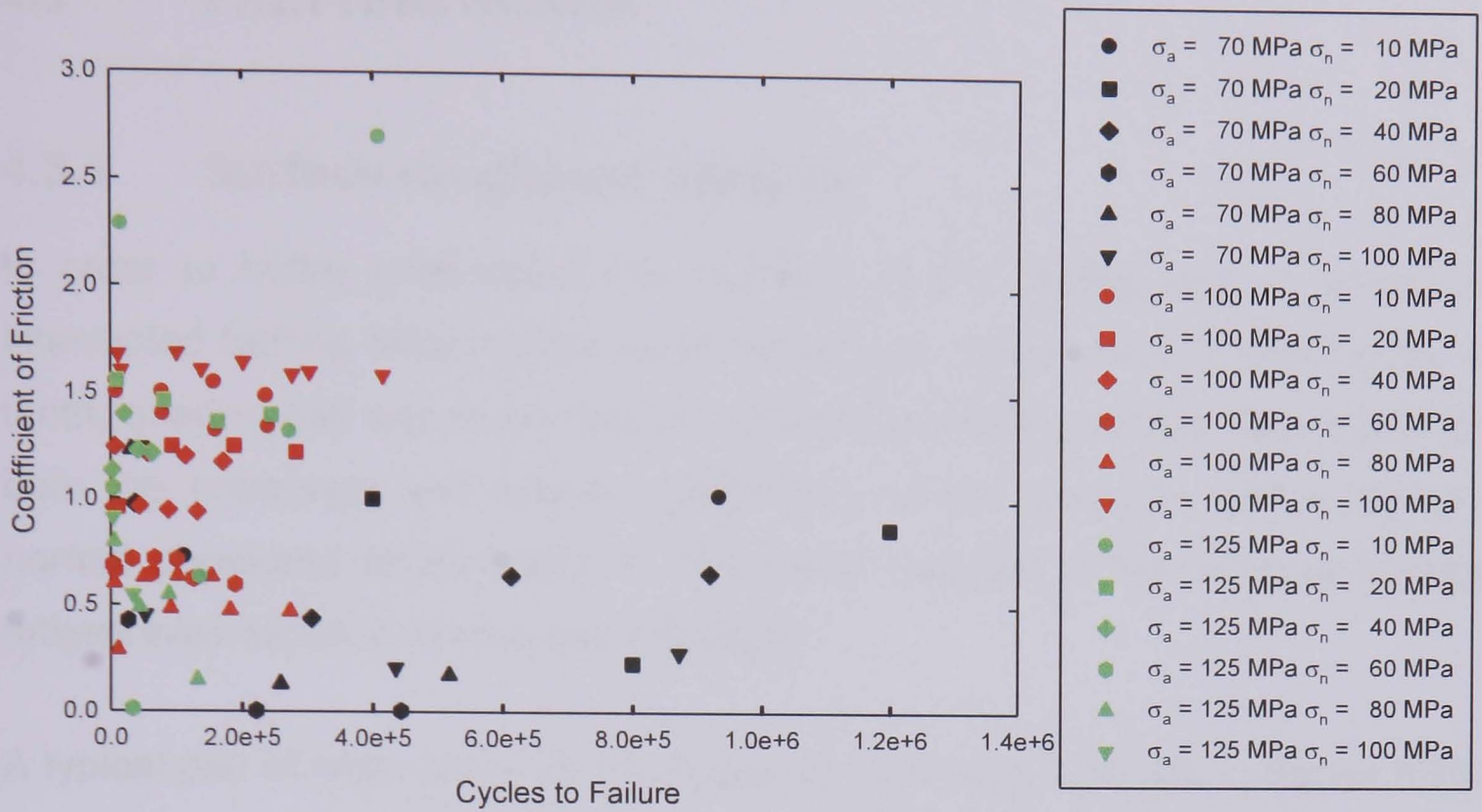


Figure 4.27: The evolution, in terms of the number of cycles applied, of coefficients of friction over the lives of unpeened specimens subjected to a range of normal pressures and axial stress amplitudes.

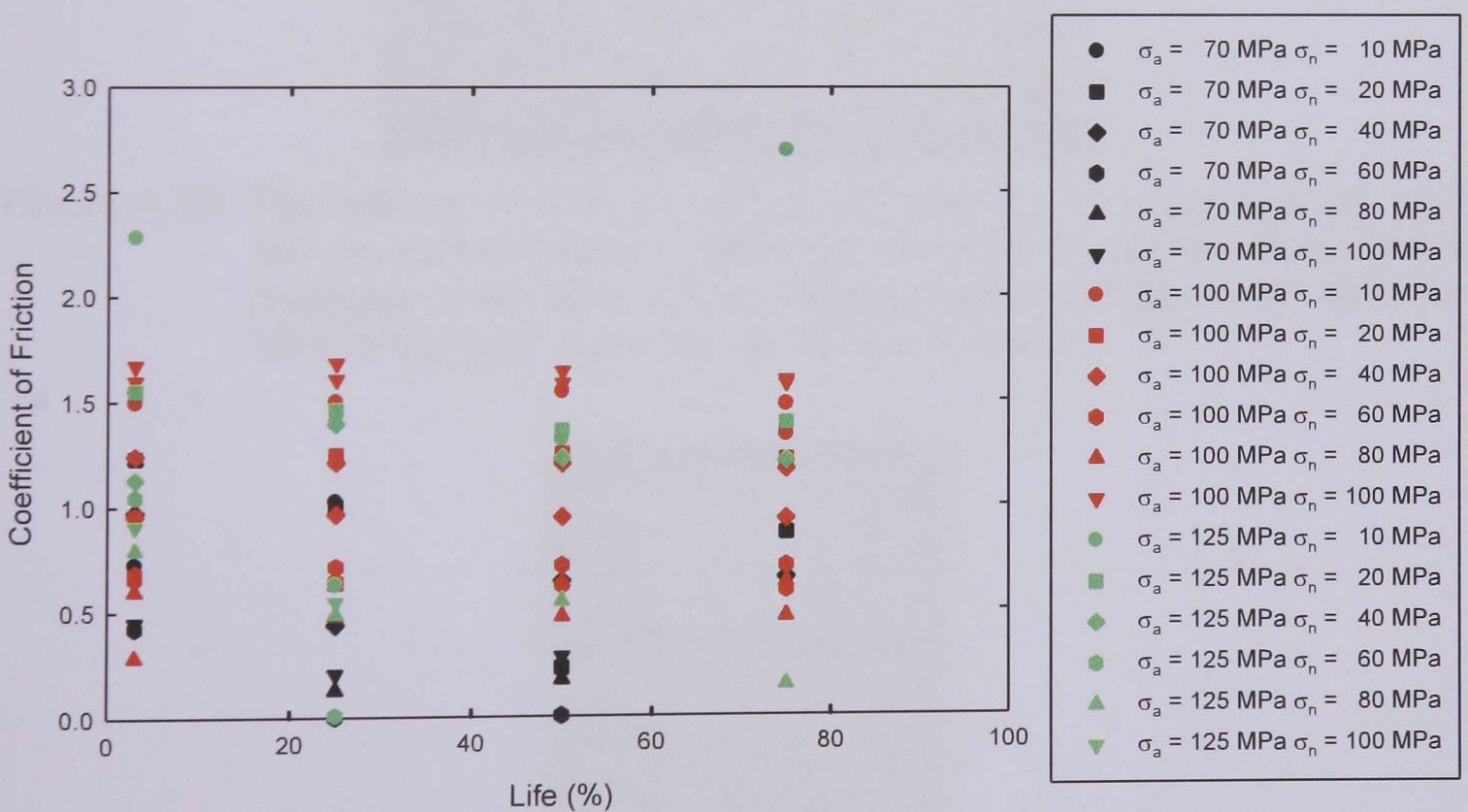


Figure 4.28: The evolution, in terms of the number of percentage life, of coefficients of friction over the lives of unpeened specimens subjected to a range of normal pressures and axial stress amplitudes.

4.3 FRETTING SCARS

4.3.1 Surface roughness analysis

In order to better understand the evolution of the fretting scar, a series of interrupted fretting fatigue tests were carried out. These were completed for a tenth, quarter, half and three quarters of the total fretting fatigue lives found for both the unpeened and peened specimens, at the minimum and maximum normal pressures applied and at that which resulted in the shortest fretting fatigue lives for each axial stress amplitude.

A typical pair of wear scars on an unpeened specimen is shown in Figure 4.29; a typical set of wear scars on a pair of bridges is shown in Figure 4.30.

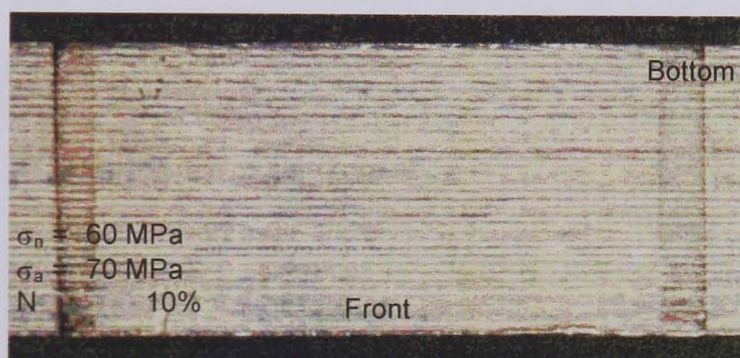


Figure 4.29: The wear scar from an unpeened bridge with a pad span of 16.5 mm in contact with an unpeened specimen subjected to a normal pressure of 60 MPa and an axial stress amplitude of 70 MPa for 10% of the total expected life of that specimen.



Figure 4.30: The wear scars from an unpeened bridge with a pad span of 16.5 mm having been in contact with a peened specimen subjected to a normal pressure of 100 MPa and an axial stress amplitude of 100 MPa for 25% of the total expected life of that specimen.

Surface roughness analyses were performed, with each of the four scars on every test specimen being traced utilising a UBM laser profilometer, with a scan length of 5.6 mm. The objective was that dimensions of resultant wear features be extracted from the data, to provide an understanding of the development of the fretting scars on the specimens due to the friction between the bridge pads and the free surfaces. These measurements included: the depth and width of the scar about a base line; the height of peaks that were observed to form either side of the scar; the total peak to valley depth; the total width and the angle of the notch. These results can be found in Appendix J; definitions in Figure 4.44 and Equation 4.2.

Each scar was traced in three different places, i.e. at the front, middle and back of each test section, see Figure 4.31. This resulted in a total of 288 profiles for all of the specimens.

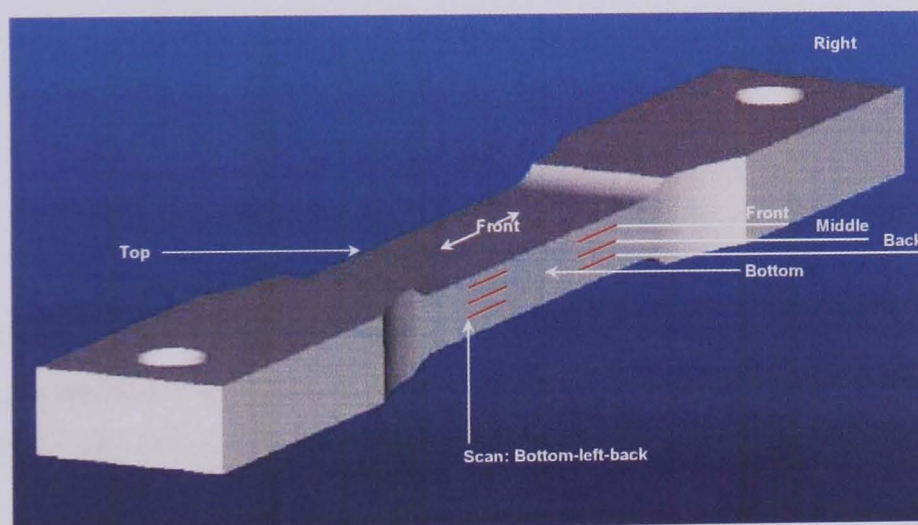


Figure 4.31: The location of the 12 surface roughness scans taken for every test specimen in the evolutionary test programme.

Figures 4.32 to 4.34, demonstrate that there was no difference between the greatest peak to valley depths measured and the position of those measurements taken for each combination of normal pressure and axial stress amplitude.

Figures 4.35 to 4.37, demonstrate that there was no correlation between the greatest notch widths measured and the position of those measurements taken for each combination of normal pressure and axial stress amplitude.

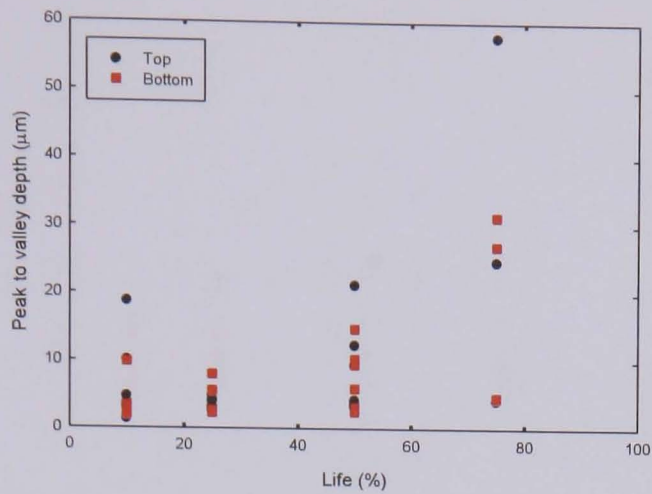


Figure 4.32: The evolution of notch peak to valley depth over the life of unpeened specimens subjected to a normal pressure of 10 MPa and an axial stress amplitude of 70 MPa.

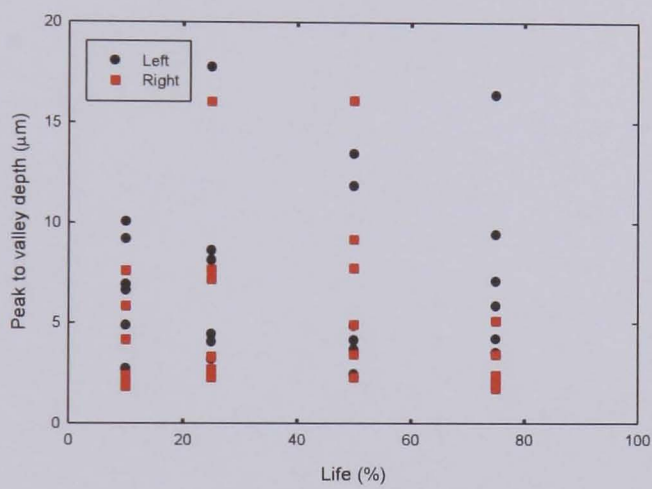


Figure 4.33: The evolution of notch peak to valley depth over the life of unpeened specimens subjected to a normal pressure of 40 MPa and an axial stress amplitude of 100 MPa.

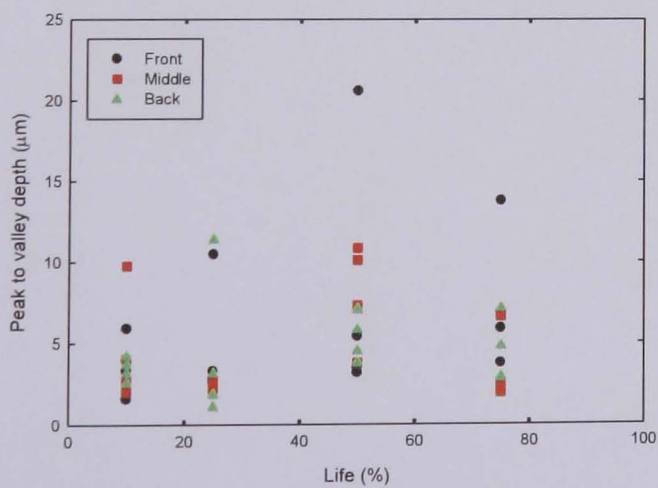


Figure 4.34: The evolution of notch peak to valley depth over the life of unpeened specimens subjected to a normal pressure of 100 MPa and an axial stress amplitude of 125 MPa.

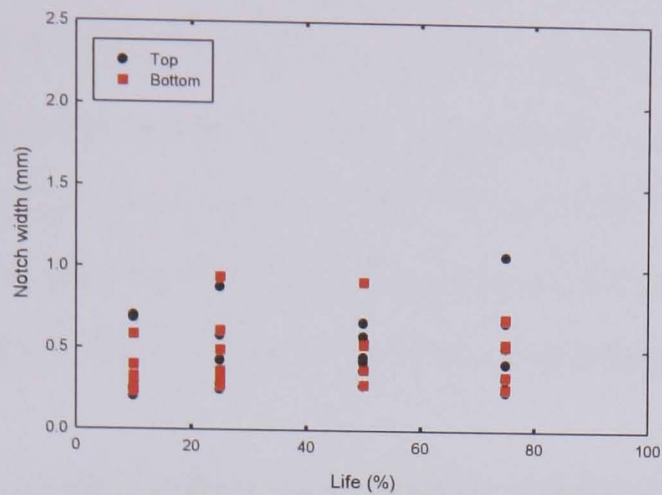


Figure 4.35: The evolution of the notch width over the life of peened specimens subjected to a normal pressure of 100 MPa and an axial stress amplitude of 70 MPa.

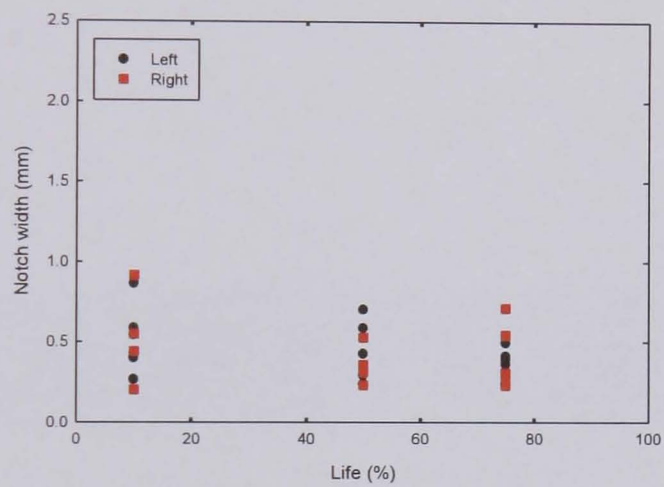


Figure 4.36: The evolution of the notch width over the life of peened specimens subjected to a normal pressure of 40 MPa and an axial stress amplitude of 100 MPa.

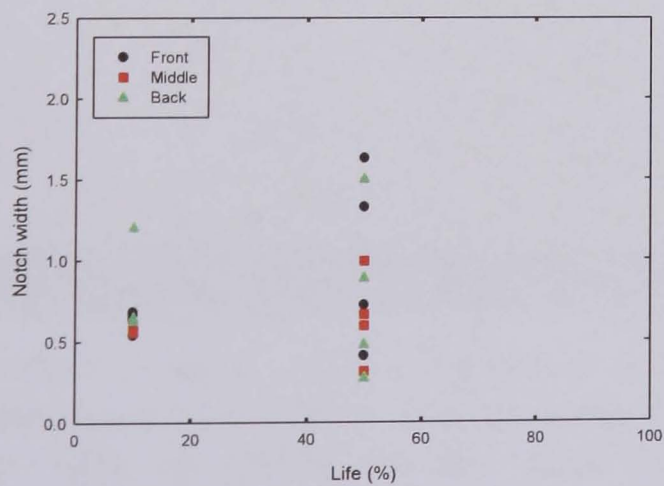


Figure 4.37: The evolution of the notch width over the life of peened specimens subjected to a normal pressure of 10 MPa and an axial stress amplitude of 125 MPa.

For each condition the evolution of the surface damage was investigated in terms of percentage life. The wear scars on two peened specimens are shown in Figure 4.38. Both specimens have been subjected to a normal pressure of 10 MPa and an axial stress amplitude of 125 MPa, one for 10% of the total life determined in the constant normal load test programme, the other for 100% of the total life determined in the constant normal load test programme.

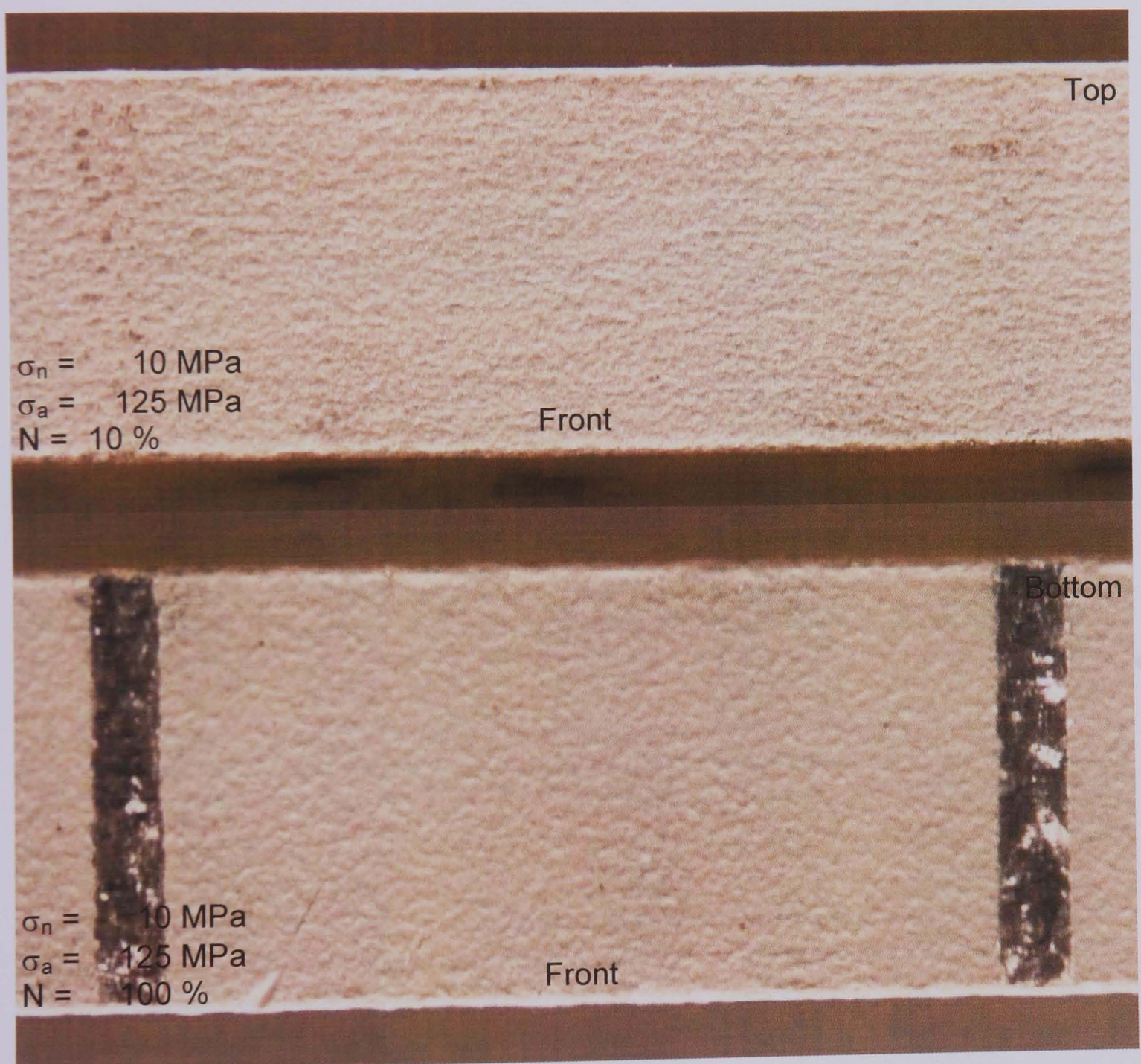


Figure 4.38: The evolution of wear scars on peened specimens subjected to a normal pressure of 10 MPa and an axial stress amplitude of 125 MPa for 10% to 100% of the total expected life of those specimens.

The influence of the normal pressure on the surface damage was also investigated, as is demonstrated in Figure 4.39.

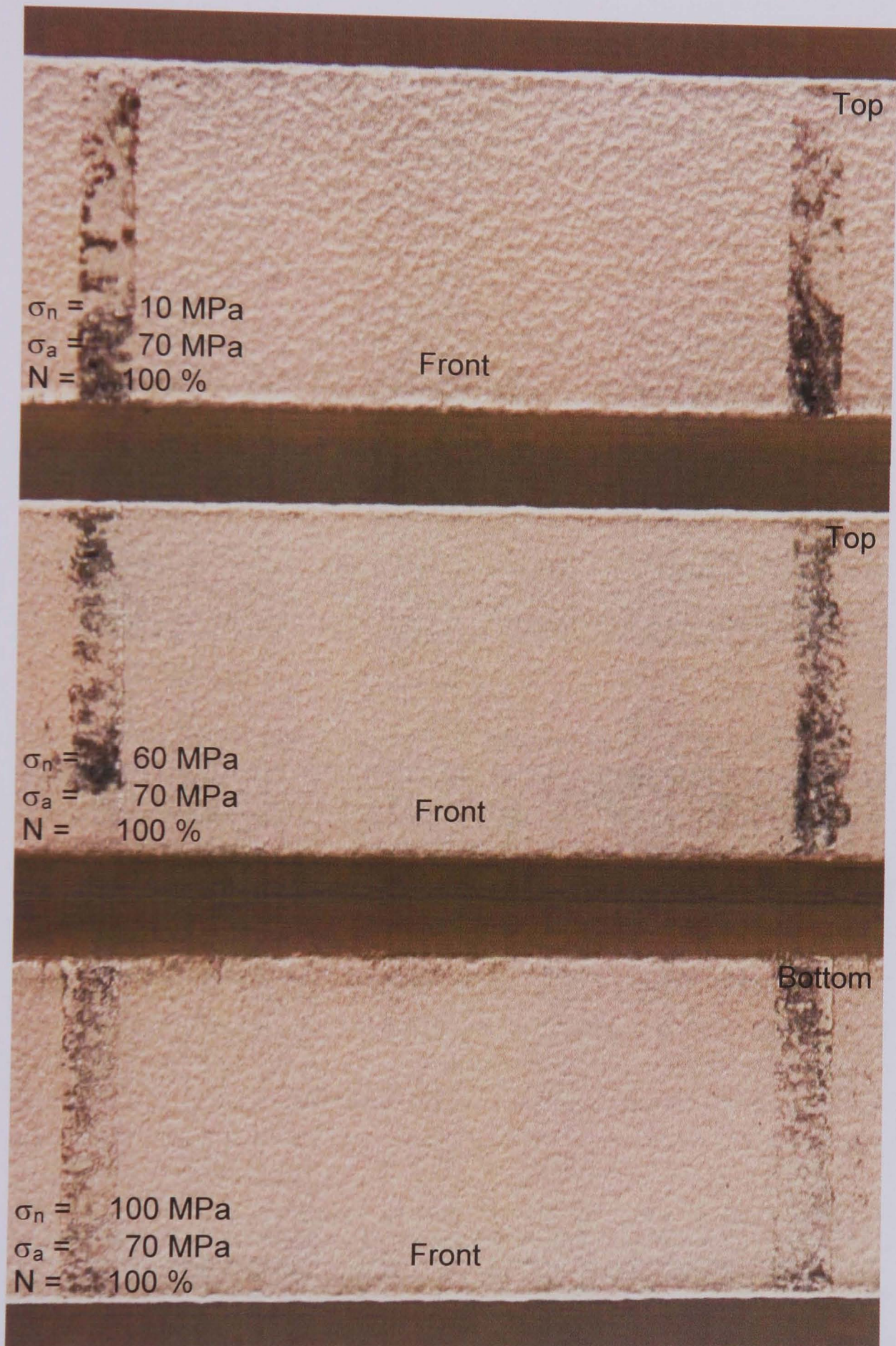


Figure 4.39: The effect of normal pressure on wear scars on peened specimens subjected to normal pressures of 10 MPa, 60 MPa and 100 MPa and an axial stress amplitude of 70 MPa for 100% of expected life.

The influence of the axial stress amplitude on the surface damage was studied too, as is shown in Figure 4.40.

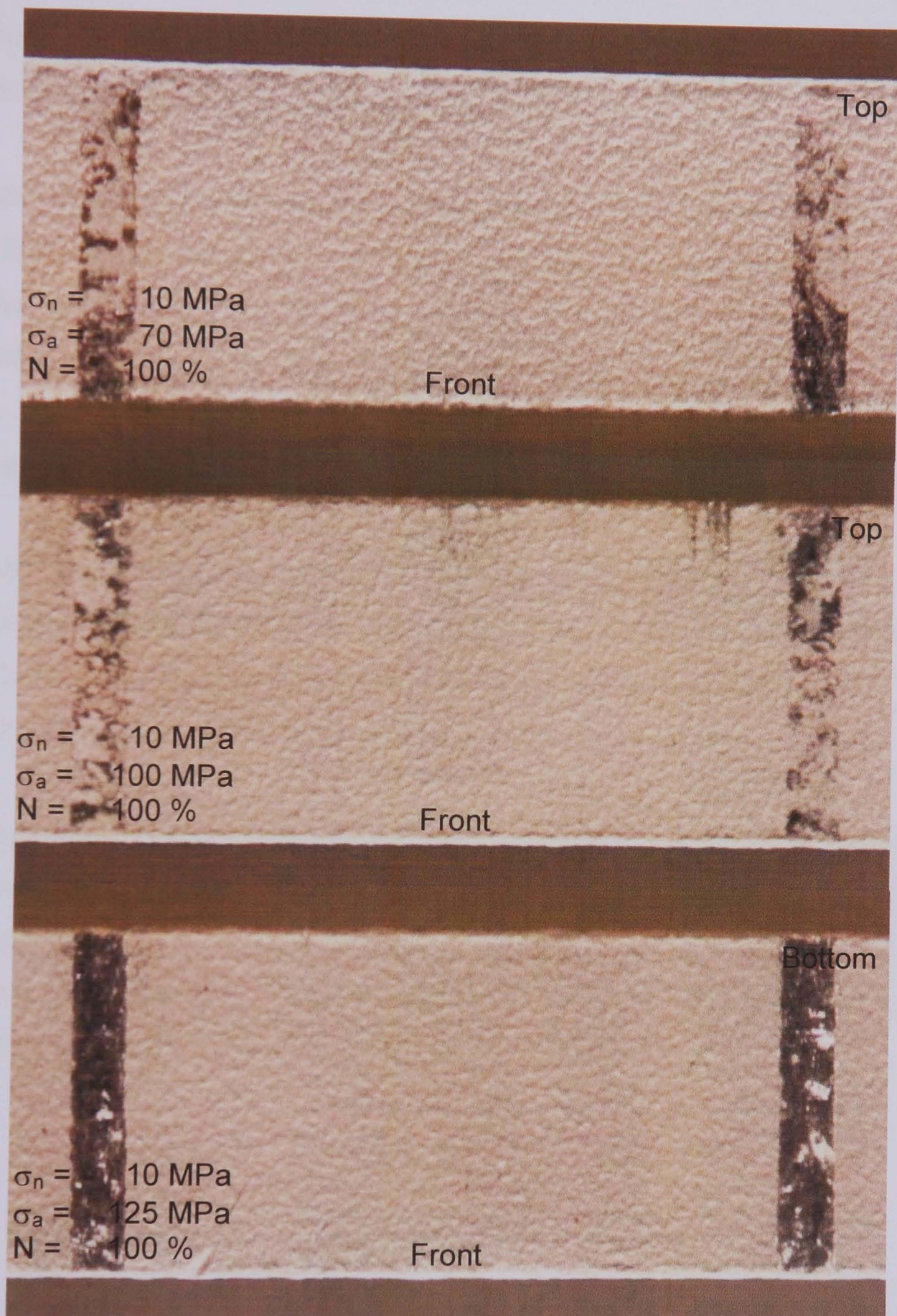


Figure 4.40: The effect of axial stress on wear scars on peened specimens subjected to a normal pressure of 10 MPa and axial stress amplitudes of 70 MPa, 100 MPa and 125 MPa for 100% of expected life.

4.3.1. Unpeened

Thirty-six unpeened specimens were analysed in this programme, resulting in a total of: 12 profiles for each combination of normal pressure, axial stress amplitude and percentage life, 48 profiles in total for each normal pressure and 144 profiles for each axial stress amplitude applied.

Specially developed software was used to analyse the profiles generated by the UBM laser profilometer, whereby significant features were identified; this code is in Appendix D. Specifically, data on the total peak to valley depth of the scar and the total width of the scar are given in Appendix J, Tables J.1, 2 and 3a, J.1, 2, and 3b and J.1, 2 and 3c; the maximum and minimum values for each data set are also given.

However, for axial stress amplitudes of 70 MPa, 100 MPa and 125 MPa, figures are not given for a number of notch widths, twenty percent, eight percent and thirty-three percent of the figures accordingly, due to the fact that these profiles did not cross the x axis in the region specified.

This data was subsequently investigated to establish the relationship between wear and time. Plots of notch peak to valley depth versus percentage life for each combination of load are shown in Appendix K and plots of notch width versus percentage life for each combination of load are shown in Appendix L. Typical profiles are shown in Figures 4.41 and 4.42.

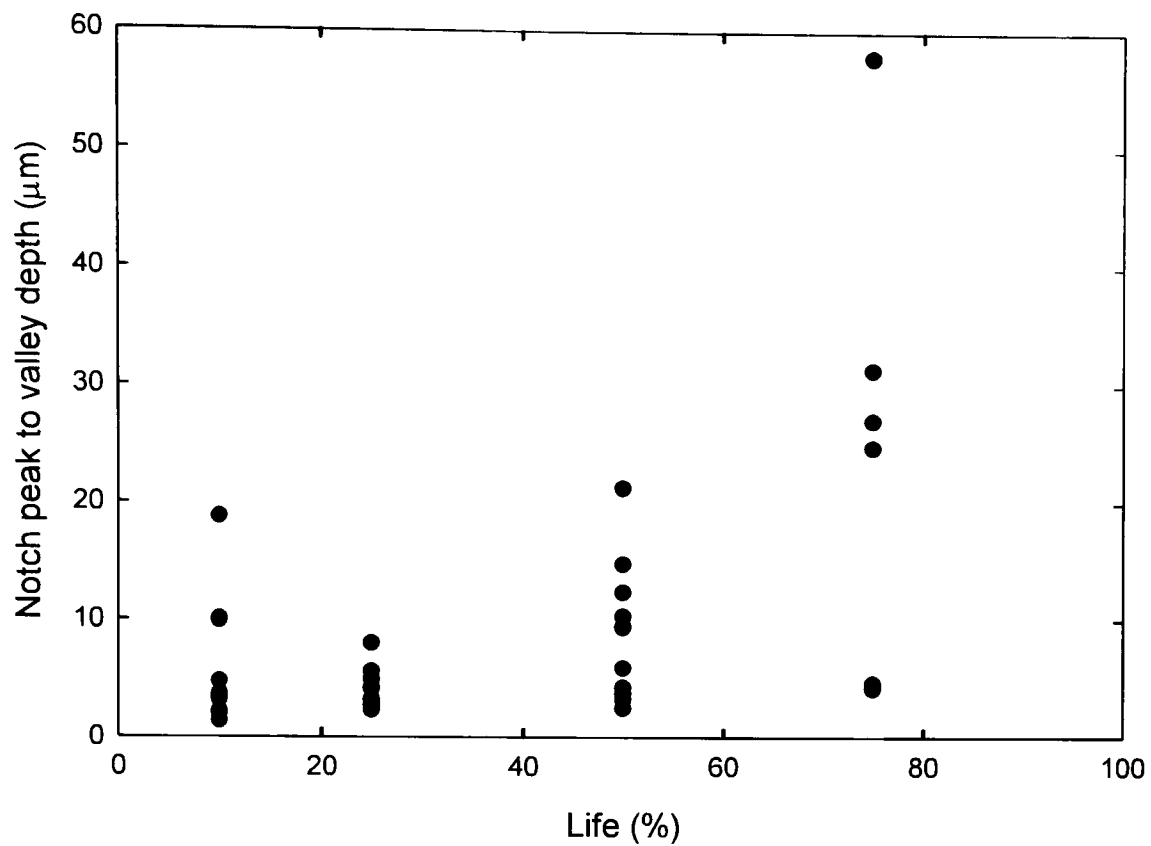


Figure 4.41: The evolution of notch peak to valley depth over the life of unpeened specimens subjected to a normal pressure of 10 MPa and an axial stress amplitude of 70 MPa.

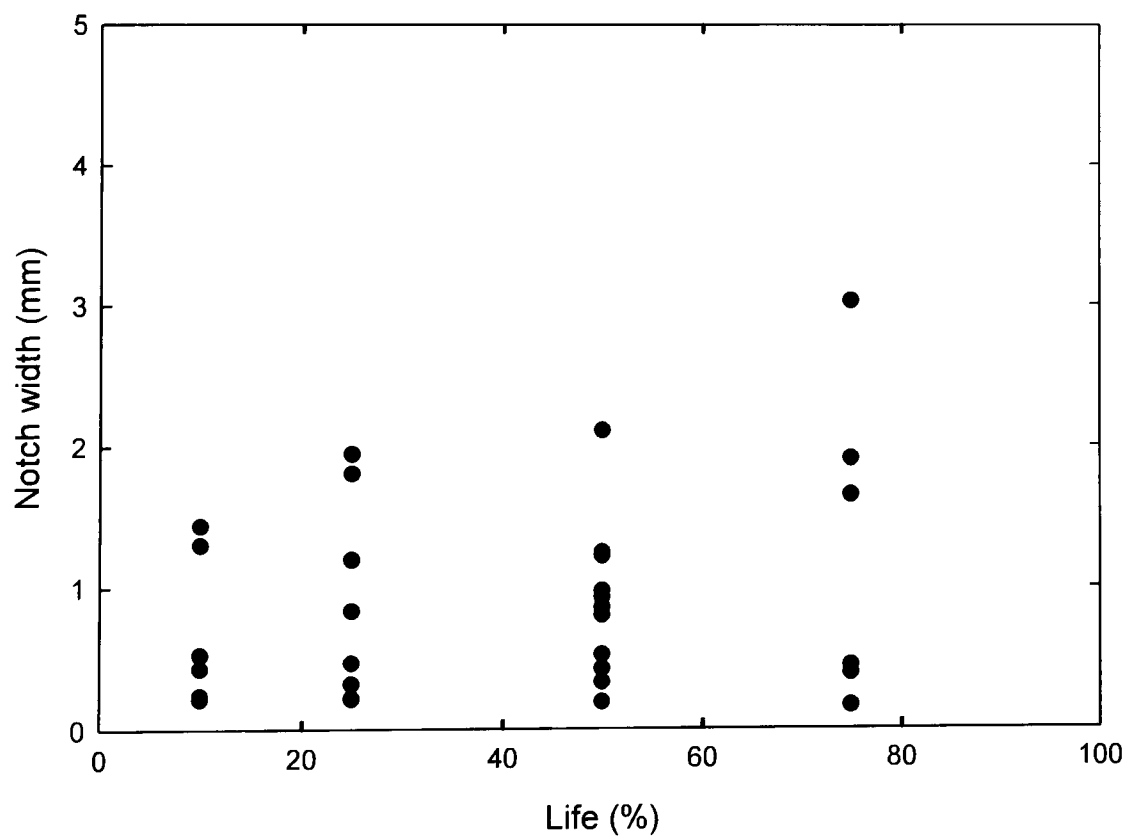


Figure 4.42: The evolution of notch width over the life of unpeened specimens subjected to a normal pressure of 10 MPa and an axial stress amplitude of 70 MPa.

For the greatest notch depths found for each combination of normal pressure and axial stress and percentage life for the unpeened condition, the resultant plots together with a corresponding magnified view of the areas of interest found are shown in Appendix M. A typical profile is shown in Figure 4.43; a magnified view of the primary notch found on this plot is shown in Figure 4.44. The grey line is the original trace line; the black line is the profile smoothed for analysis purposes. These figures depict two primary notches in the centre of the trace, the deepest of which has peaks of material pushed up on either side.

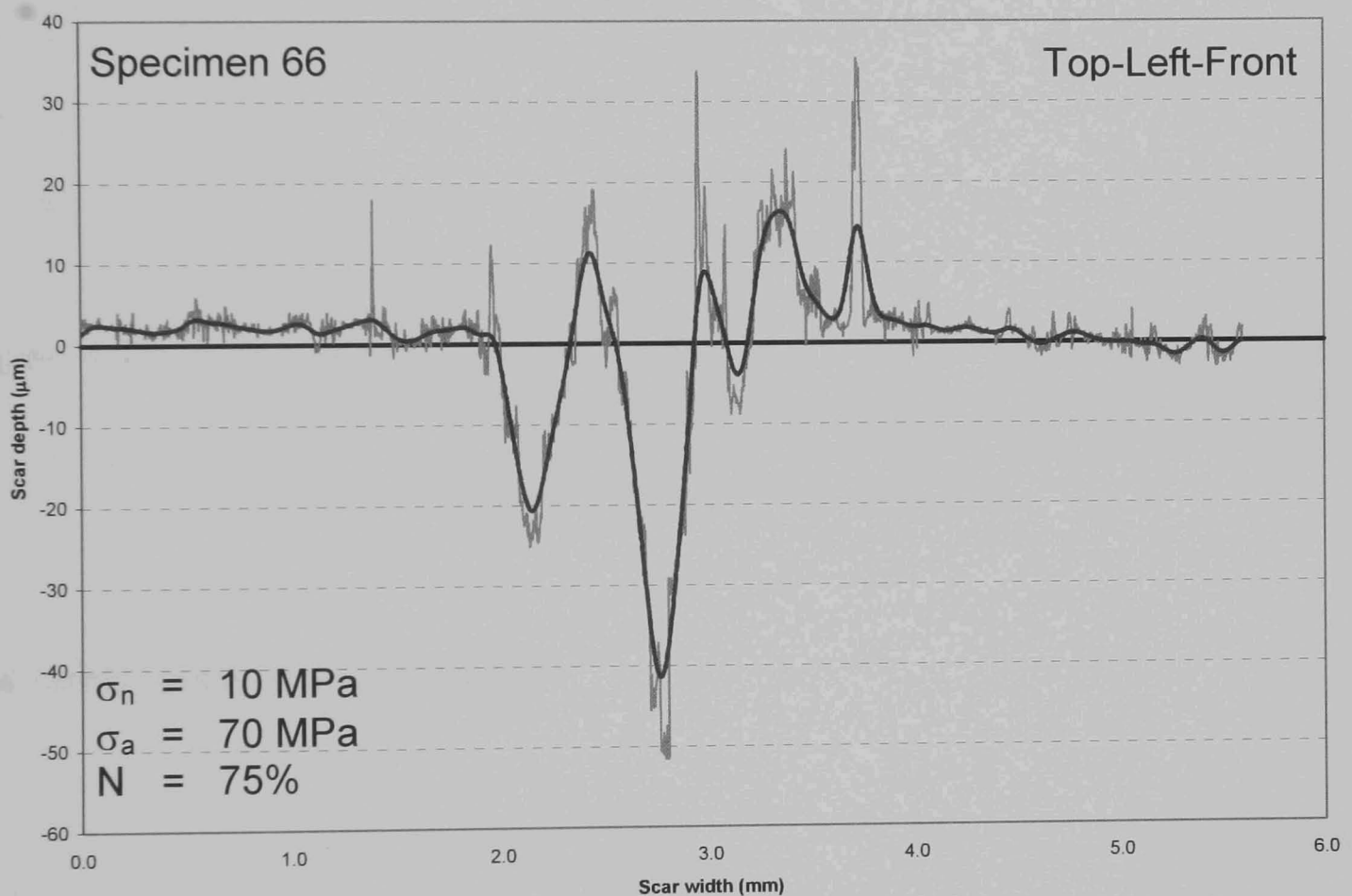


Figure 4.43: The surface roughness profile of an unpeened specimen subjected to a normal pressure of 10 MPa and an axial stress amplitude of 70 MPa for 75% of the total expected life of that specimen.

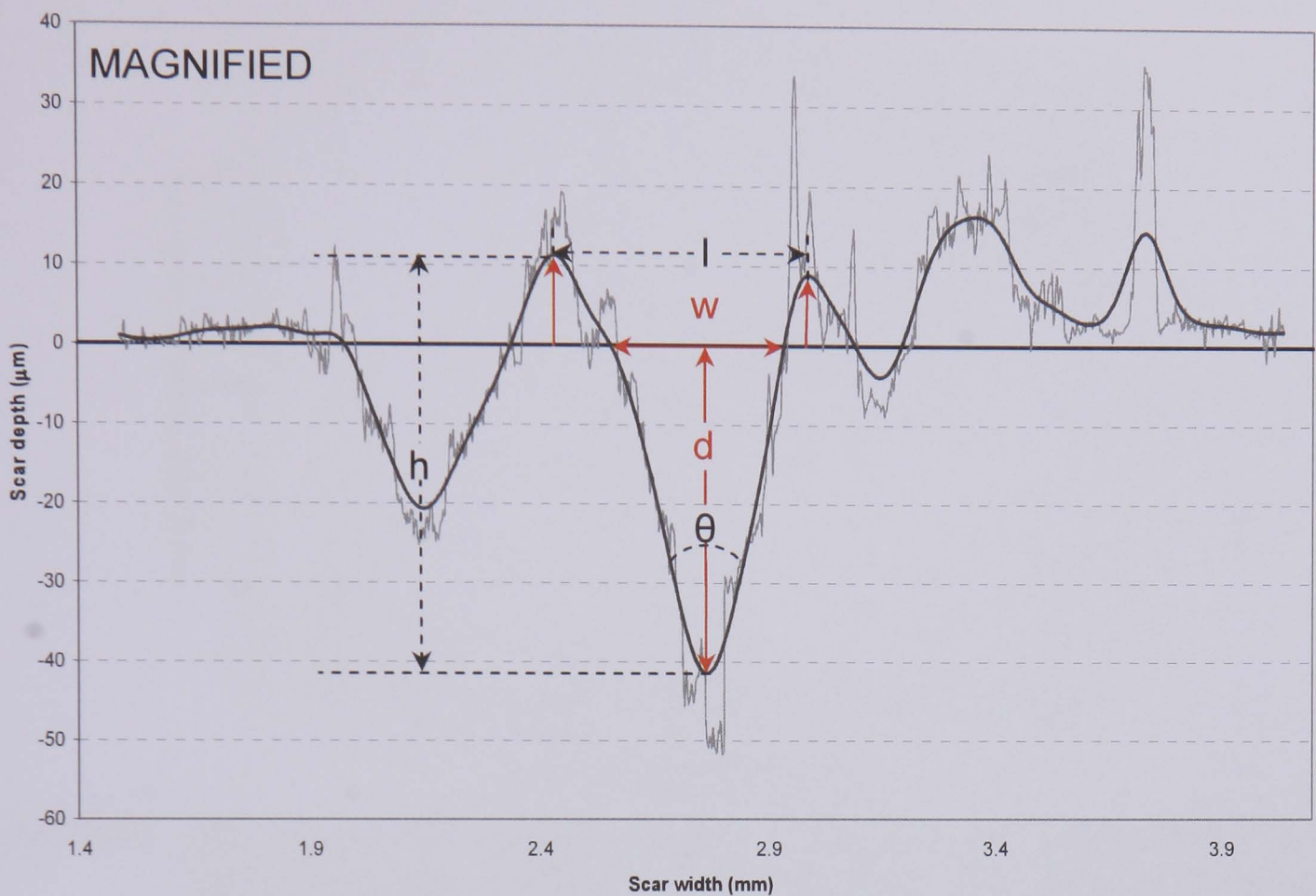


Figure 4.44: A magnified view highlighting the areas of interest on the surface roughness profile of an unpeened specimen subjected to a normal pressure of 10 MPa and an axial stress amplitude of 70 MPa for 75% of the total expected life of that specimen.

The notch angle, θ , is defined by:

$$\theta = 2 \tan^{-1} \left(\frac{w}{2d} \right) \quad \text{Equation 4.2}$$

The dependence of the notch peak to valley depth on the normal pressure applied for an axial stress amplitude of 70 MPa is shown in Figure 4.45, for an axial stress amplitude of 100 MPa is shown in Figure 4.46 and for an axial stress amplitude of 125 MPa is shown in Figure 4.47.

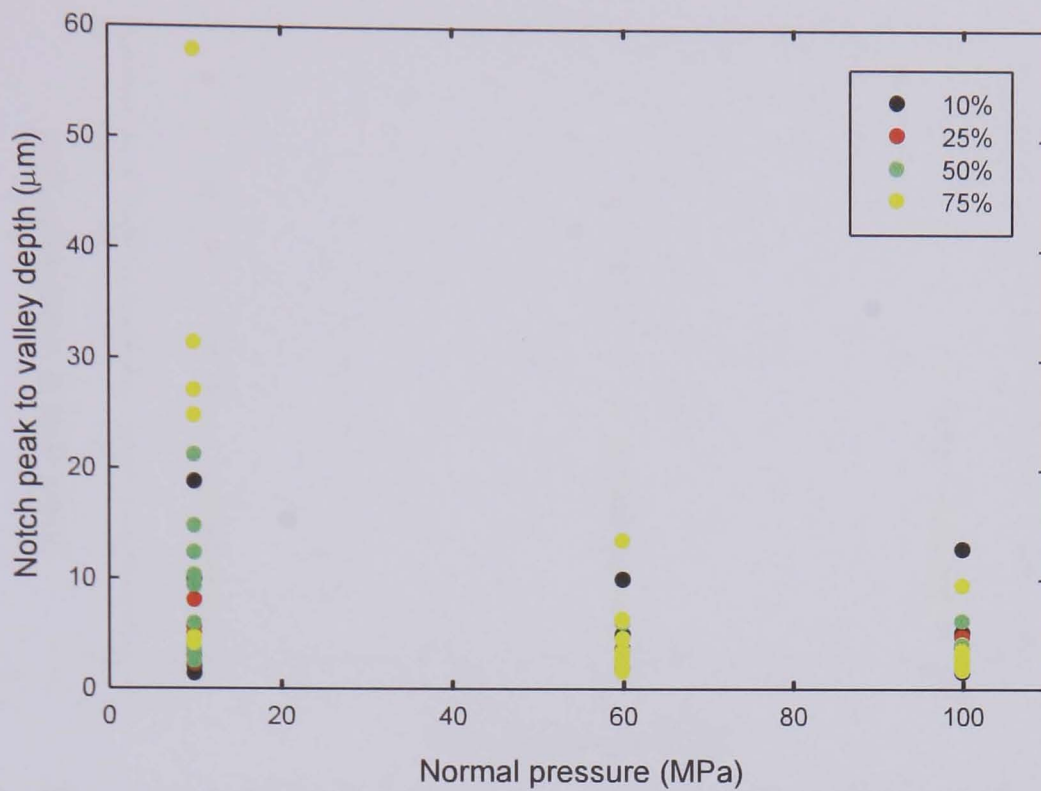


Figure 4.45: The notch peak to valley depths resulting from fretting fatigue tests conducted with an aluminium alloy 2024 T351 bridge in contact with an unpeened aluminium alloy 2024 T351 specimen subjected to an axial stress amplitude of 70 MPa.

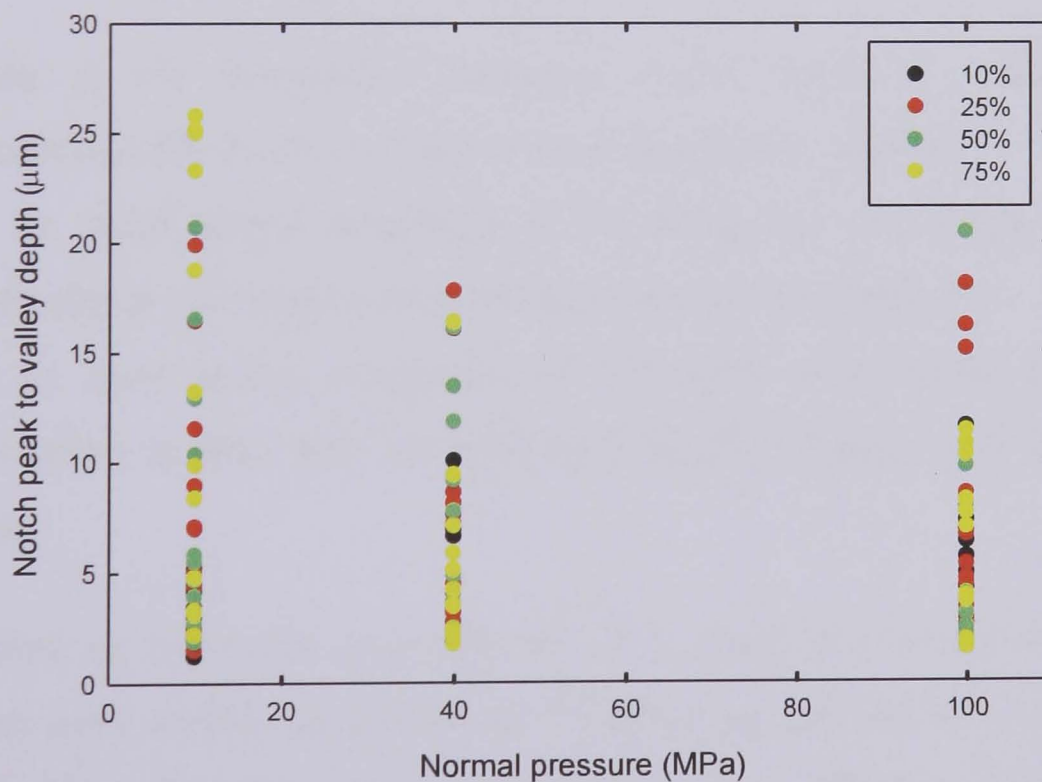


Figure 4.46: The notch peak to valley depths resulting from fretting fatigue tests conducted with an aluminium alloy 2024 T351 bridge in contact with an unpeened aluminium alloy 2024 T351 specimen subjected to an axial stress amplitude of 100 MPa.

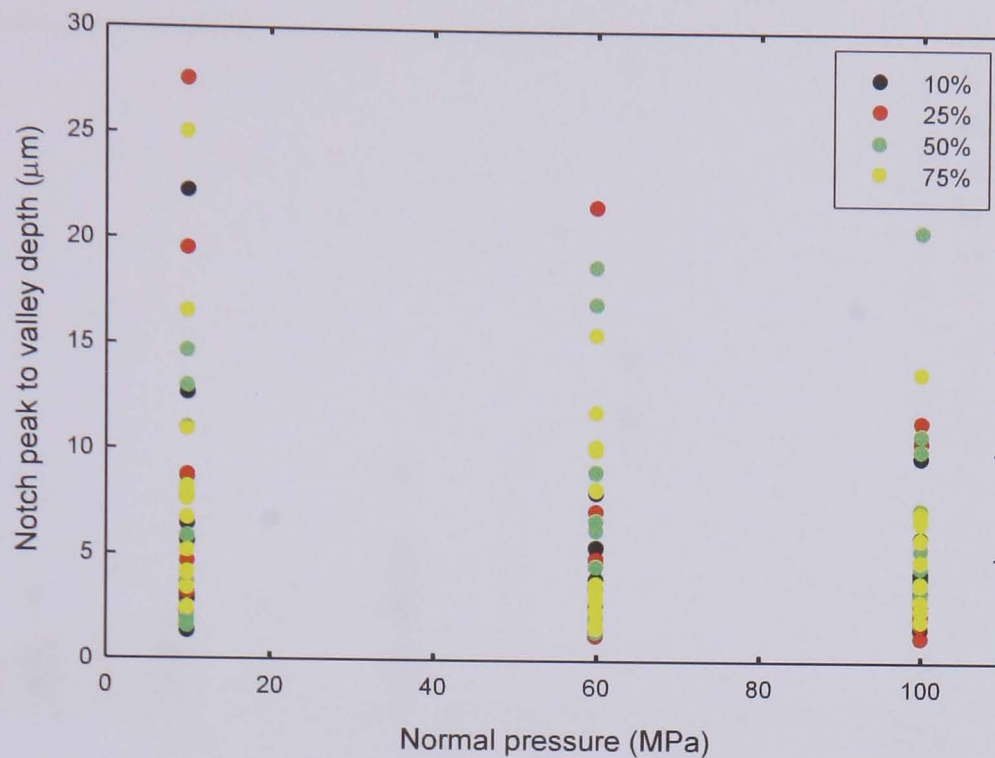


Figure 4.47: The notch peak to valley depths resulting from fretting fatigue tests conducted with an aluminium alloy 2024 T351 bridge in contact with an unpeened aluminium alloy 2024 T351 specimen subjected to an axial stress amplitude of 125 MPa.

Analyses of the results presented in Figures 4.45, 4.46 and 4.47 indicate that:

- There is no correlation between notch peak to valley depth and percentage life for any of the normal pressures applied;
- For an axial stress amplitude of 70 MPa and 125 MPa notch peak to valley depth decreases with increasing normal pressure;
- For an axial stress amplitude of 100 MPa notch peak to valley depth decreases a little with increasing normal pressure and then increases again.

The formation of the scars over the life of a specimen was also investigated. Plots for an axial stress amplitude of 70 MPa are shown in Figures 4.48 and 4.49, which show that for a normal pressure of 10 MPa, notch peak to valley depth increases with the number of cycles applied and these values are above those resulting from the other two normal pressures applied. The greatest peak to valley depth recorded for this axial stress amplitude was 58 μm .

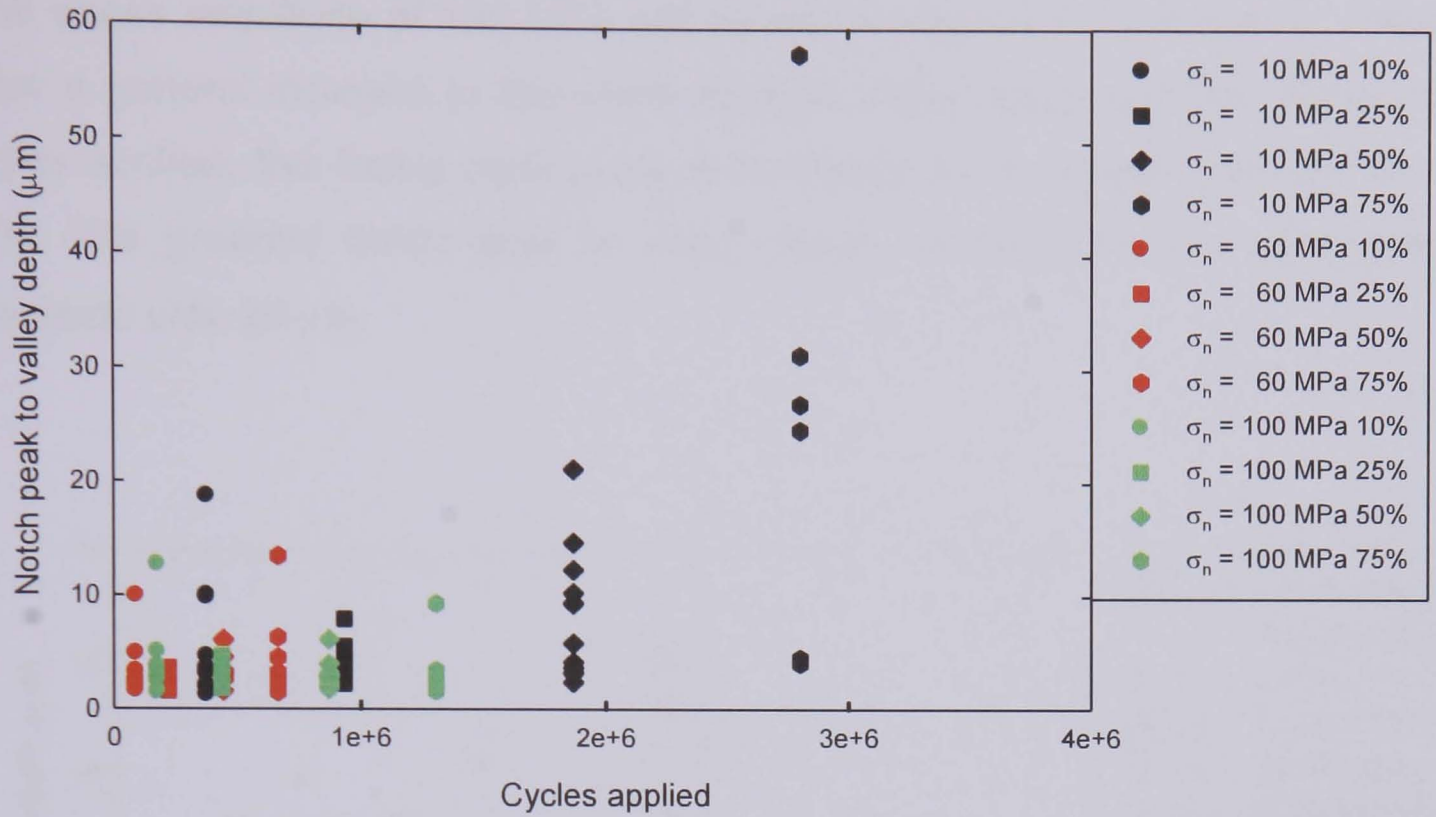


Figure 4.48: The evolution, in terms of the number of cycles applied, of notch peak to valley depth over the lives of unpeened specimens subjected to three normal pressures and an axial stress amplitude of 70 MPa.

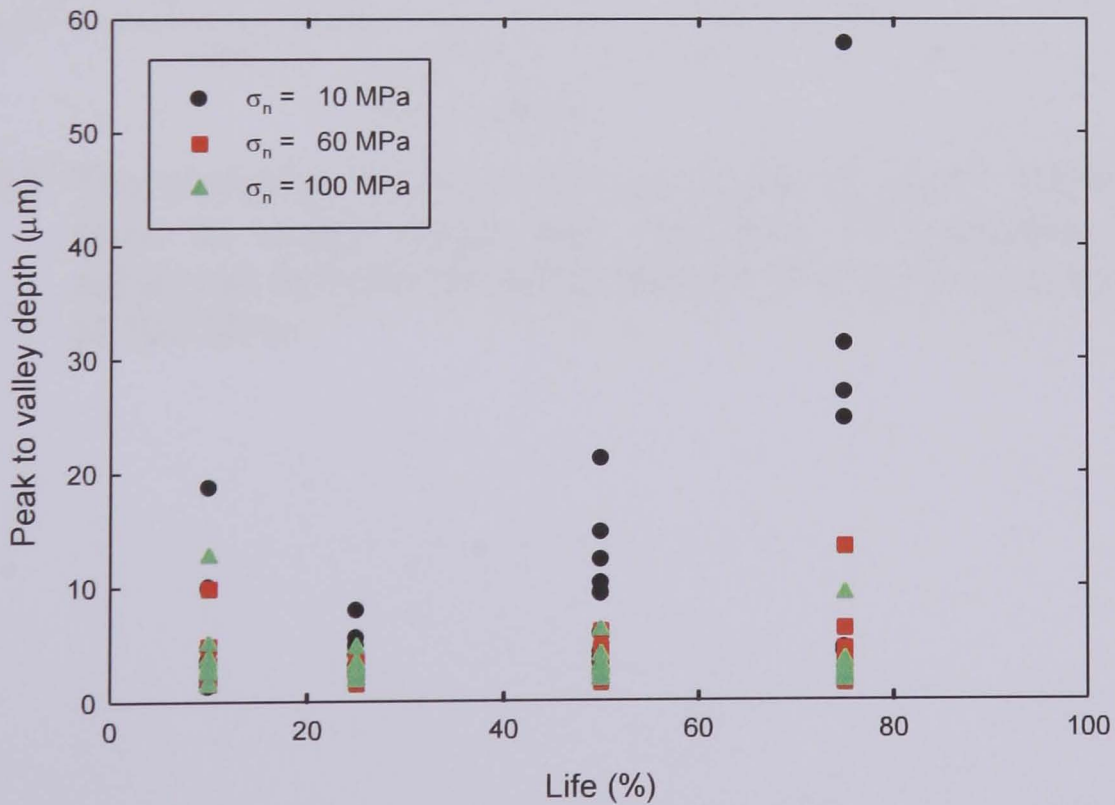


Figure 4.49: The evolution, in terms of percentage life, of notch peak to valley depth over the lives of unpeened specimens subjected to three normal pressures and an axial stress amplitude of 70 MPa.

Plots demonstrating the formation of the scars over the life of a specimen for an axial stress amplitude of 100 MPa are shown in Figures 4.50 and 4.51. These show a general increase in the notch peak to valley depth with the number of cycles applied, this being particularly pronounced for a normal pressure of 10 MPa. The greatest notch peak to valley depth recorded for this axial stress amplitude was 26 μm .

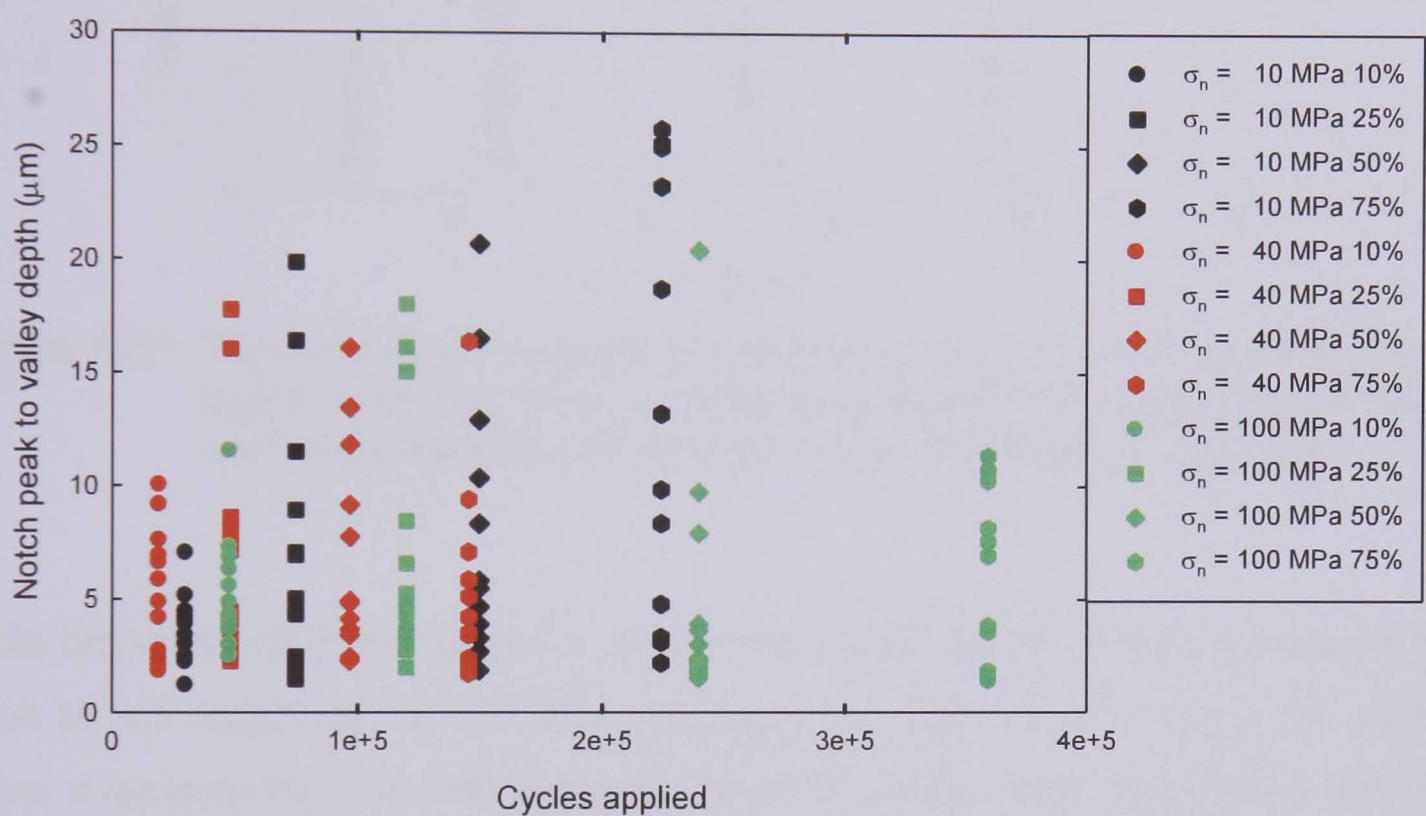


Figure 4.50: The evolution, in terms of the number of cycles applied, of notch peak to valley depth over the lives of unpeened specimens subjected to three normal pressures and an axial stress amplitude of 100 MPa.

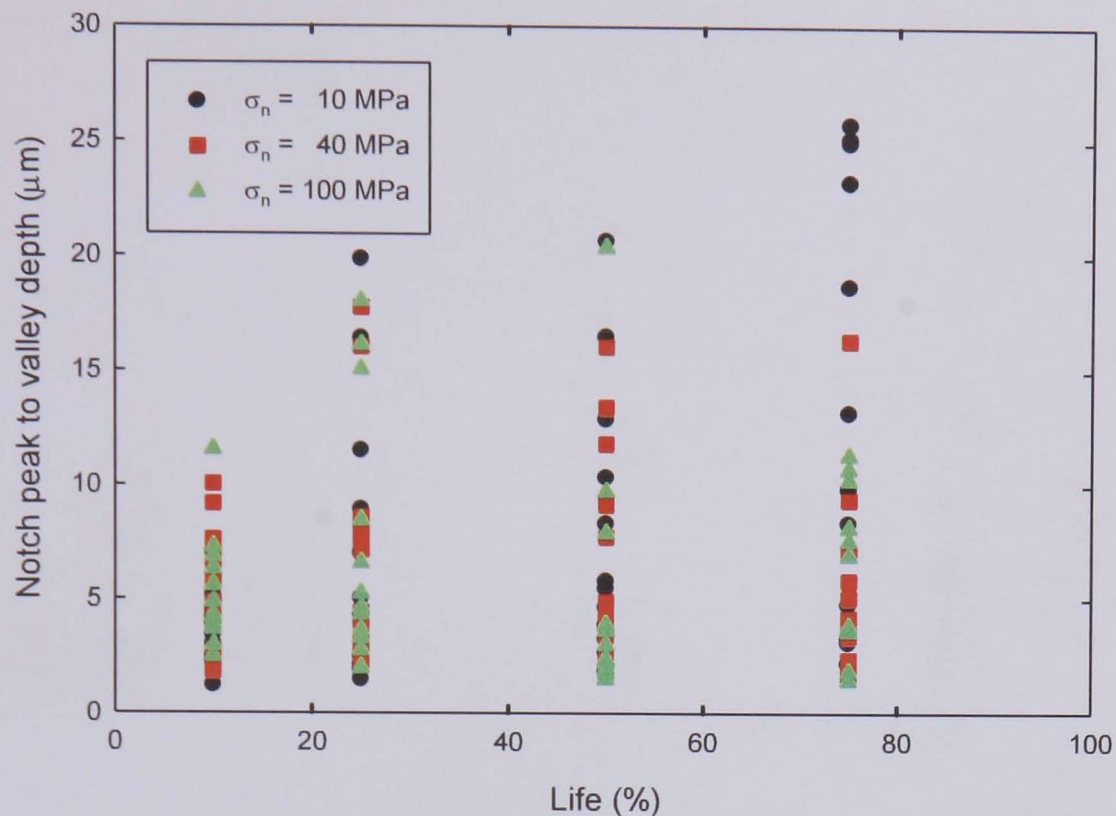


Figure 4.51: The evolution, in terms of percentage life, of notch peak to valley depth over the lives of unpeened specimens subjected to three normal pressures and an axial stress amplitude of 100 MPa.

Plots demonstrating the formation of the scars over the life of a specimen for an axial stress amplitude of 125 MPa are shown in Figures 4.52 and 4.53, which show a general trend in that the notch peak to valley depth decreases with the number of cycles applied up to 50% of expected life, after which notch peak to valley depth increases again. The greatest notch peak to valley depth recorded for this axial stress amplitude was 32 μm .

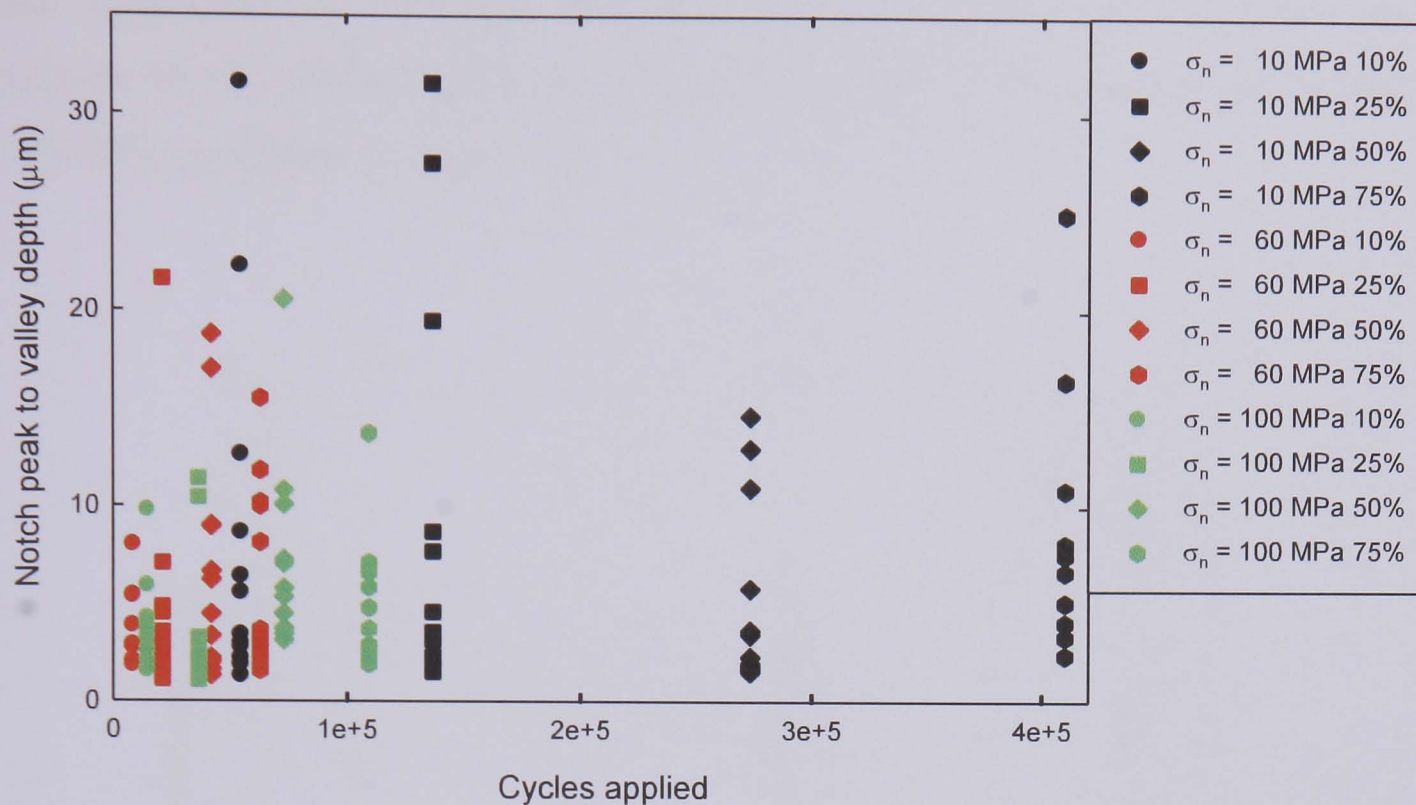


Figure 4.52: The evolution, in terms of the number of cycles applied, of notch peak to valley depth over the life of unpeened specimens subjected to three normal pressures and an axial stress amplitude of 125 MPa.

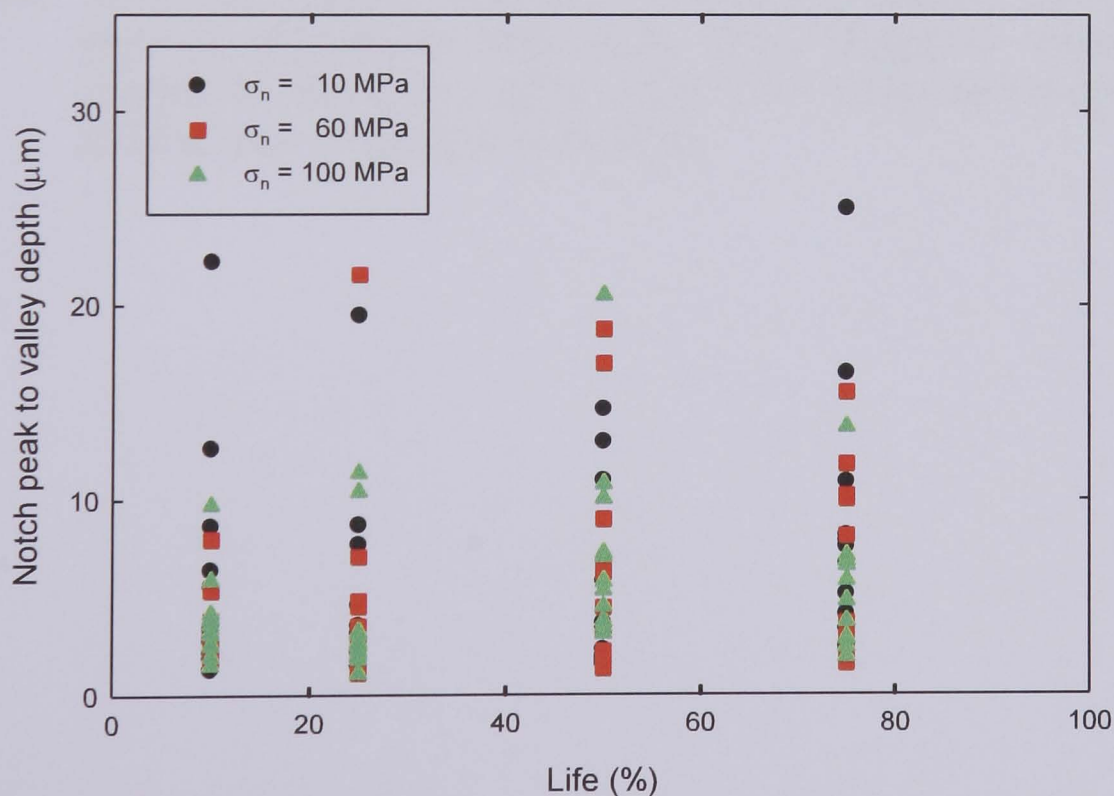


Figure 4.53: The evolution, in terms of percentage life, of notch peak to valley depth over the life of unpeened specimens subjected to three normal pressures and an axial stress amplitude of 125 MPa.

The dependence of the notch width on the normal pressure applied for an axial stress amplitude of 70 MPa is shown in Figure 4.54, for an axial stress amplitude of 100 MPa is shown in Figure 4.55 and for an axial stress amplitude of 125 MPa is shown in Figure 4.56.

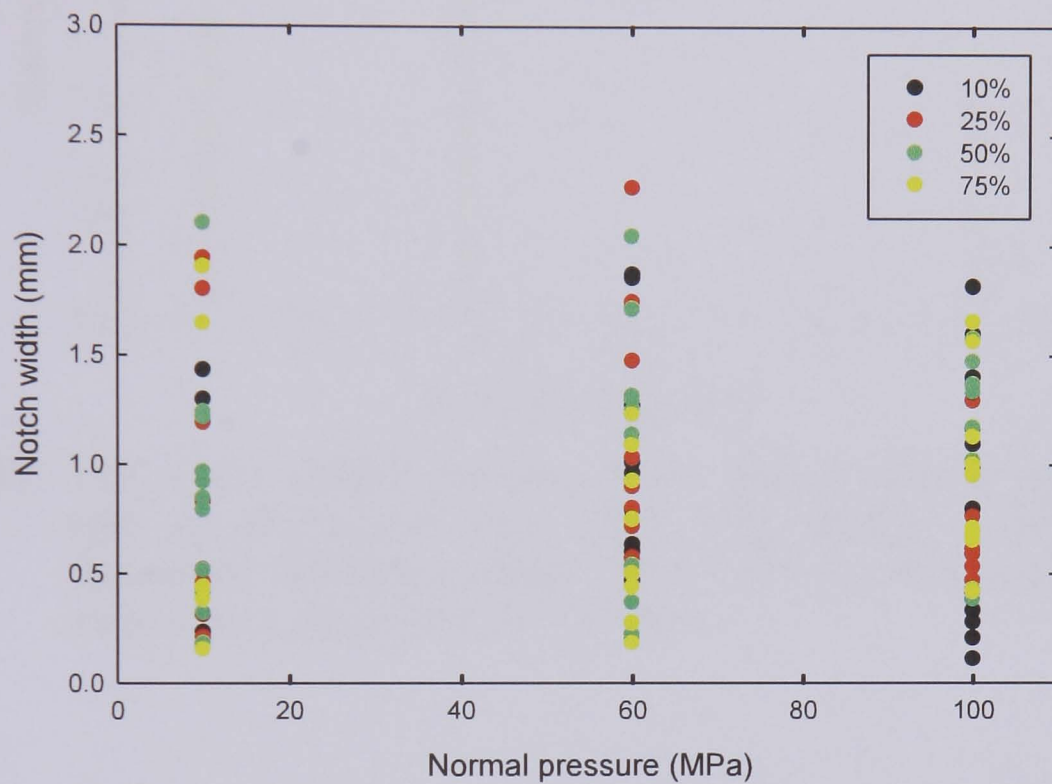


Figure 4.54: The notch widths resulting from fretting fatigue tests conducted with an aluminium alloy 2024 T351 bridge in contact with an unpeened aluminium alloy 2024 T351 specimen subjected to an axial stress amplitude of 70 MPa.

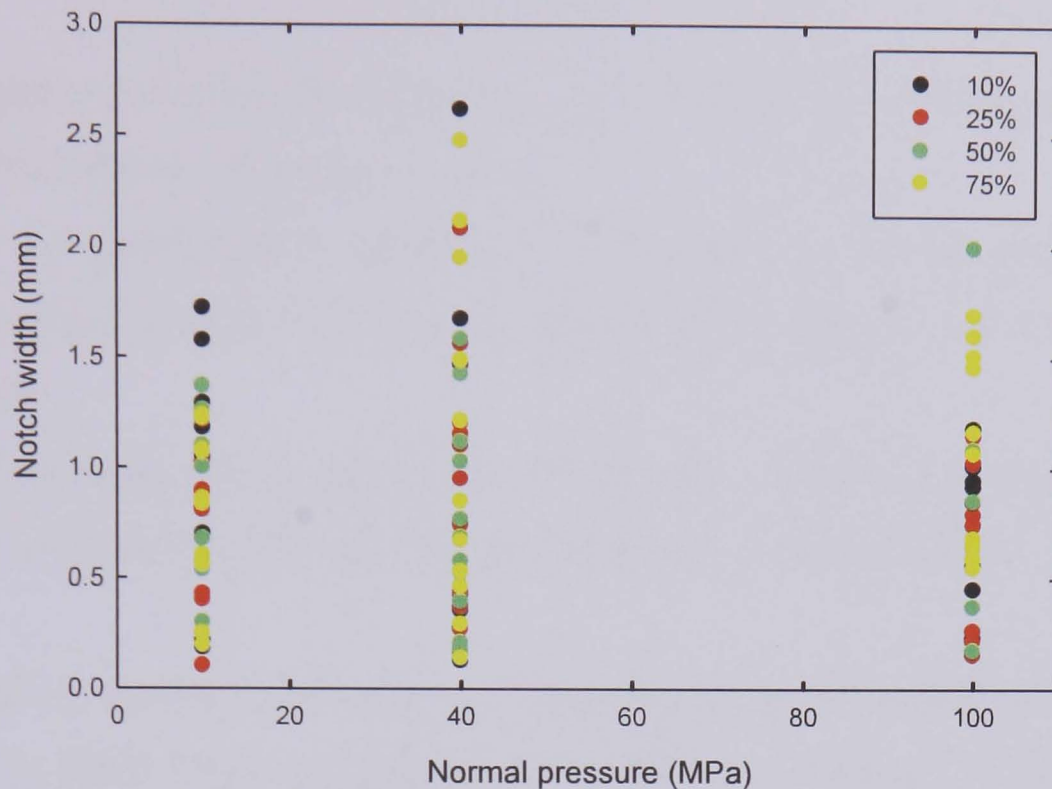


Figure 4.55: The notch widths resulting from fretting fatigue tests conducted with an aluminium alloy 2024 T351 bridge in contact with an unpeened aluminium alloy 2024 T351 specimen subjected to an axial stress amplitude of 100 MPa.

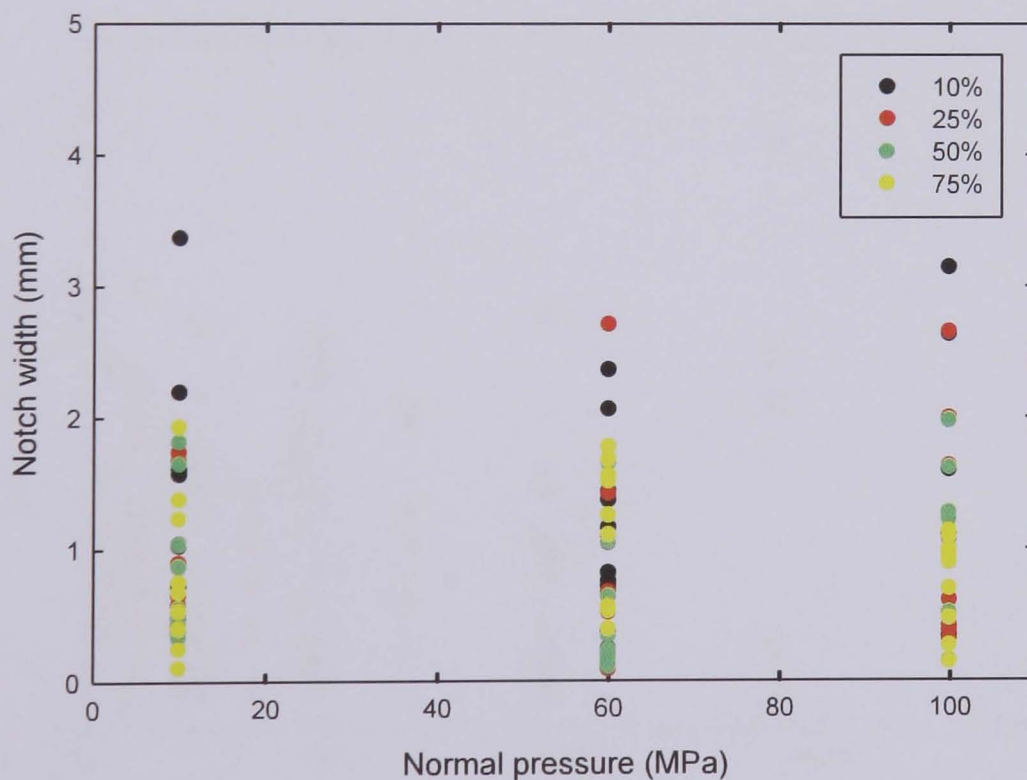


Figure 4.56: The notch widths resulting from fretting fatigue tests conducted with an aluminium alloy 2024 T351 bridge in contact with an unpeened aluminium alloy 2024 T351 specimen subjected to an axial stress amplitude of 125 MPa.

Analyses of the results presented in Figures 4.54, 4.55 and 4.56 indicate that:

- There is no correlation between notch width and percentage life for any of the normal pressures applied;
- For an axial stress amplitude of 70 MPa and 100 MPa notch width increases a little with increasing normal pressure and then decreases again;
- For an axial stress amplitude of 125 MPa, notch width decreases a little with increasing normal pressure and then increases again.

The formation of the scars over the life of a specimen was also investigated. Plots for an axial stress amplitude of 70 MPa are shown in Figures 4.57 and 4.58, which show no significant change in the notch width with the number of cycles applied. The greatest notch width recorded for this axial stress amplitude was 3 mm.

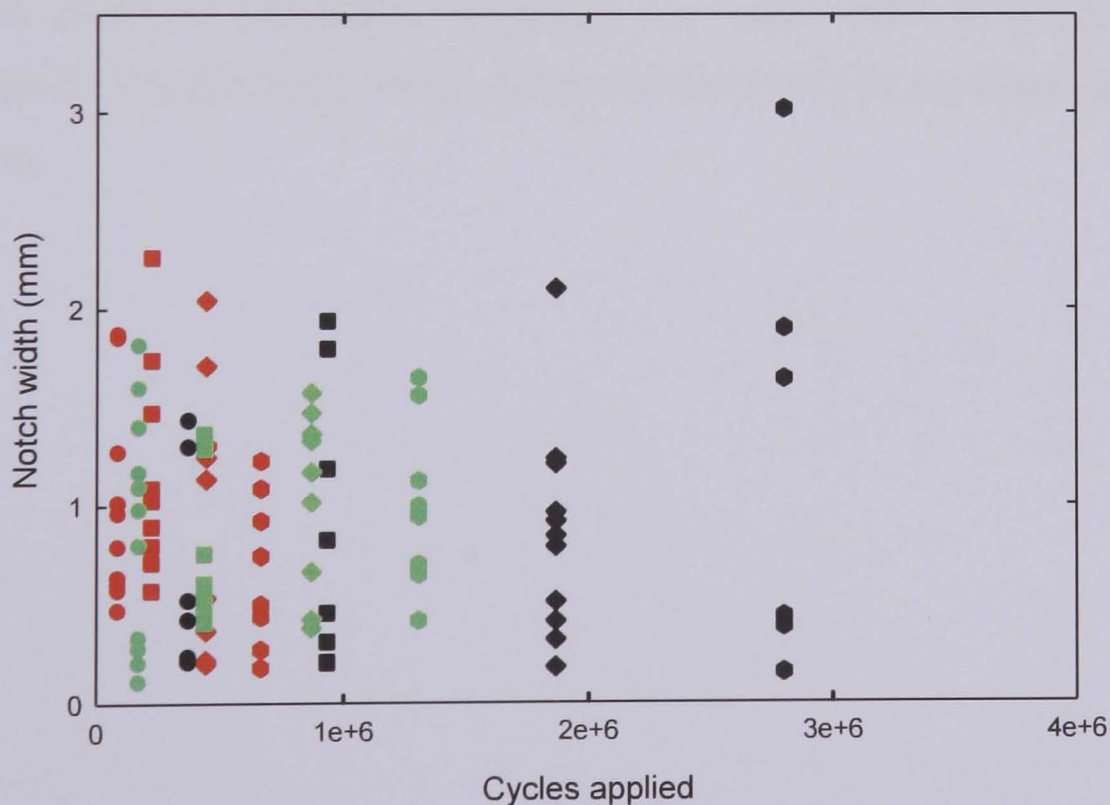


Figure 4.57: The evolution, in terms of the number of cycles applied, of notch width over the lives of unpeened specimens subjected to three normal pressures and an axial stress amplitude of 70 MPa.

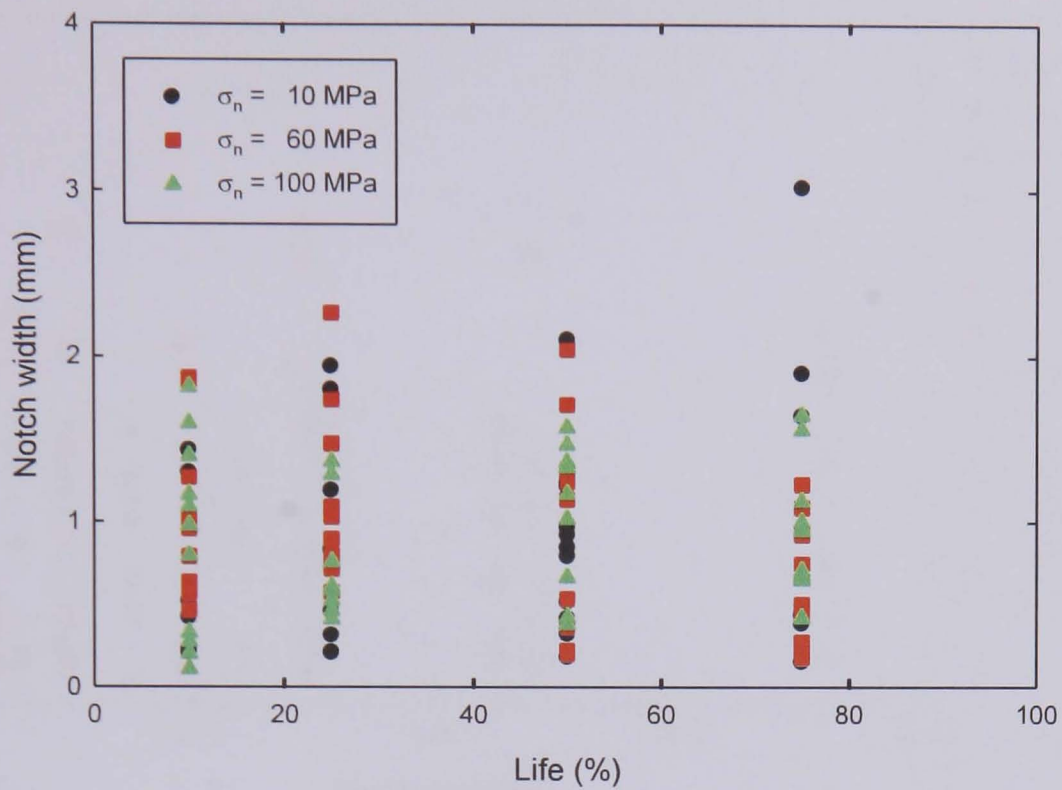


Figure 4.58: The evolution, in terms of percentage life, of notch width over the lives of unpeened specimens subjected to three normal pressures and an axial stress amplitude of 70 MPa.

Plots for an axial stress amplitude of 100 MPa are shown in Figures 4.59 and 4.60, which show no correlation between the notch width and the number of cycles applied. The greatest notch width recorded for this axial stress amplitude was 2.6 mm.

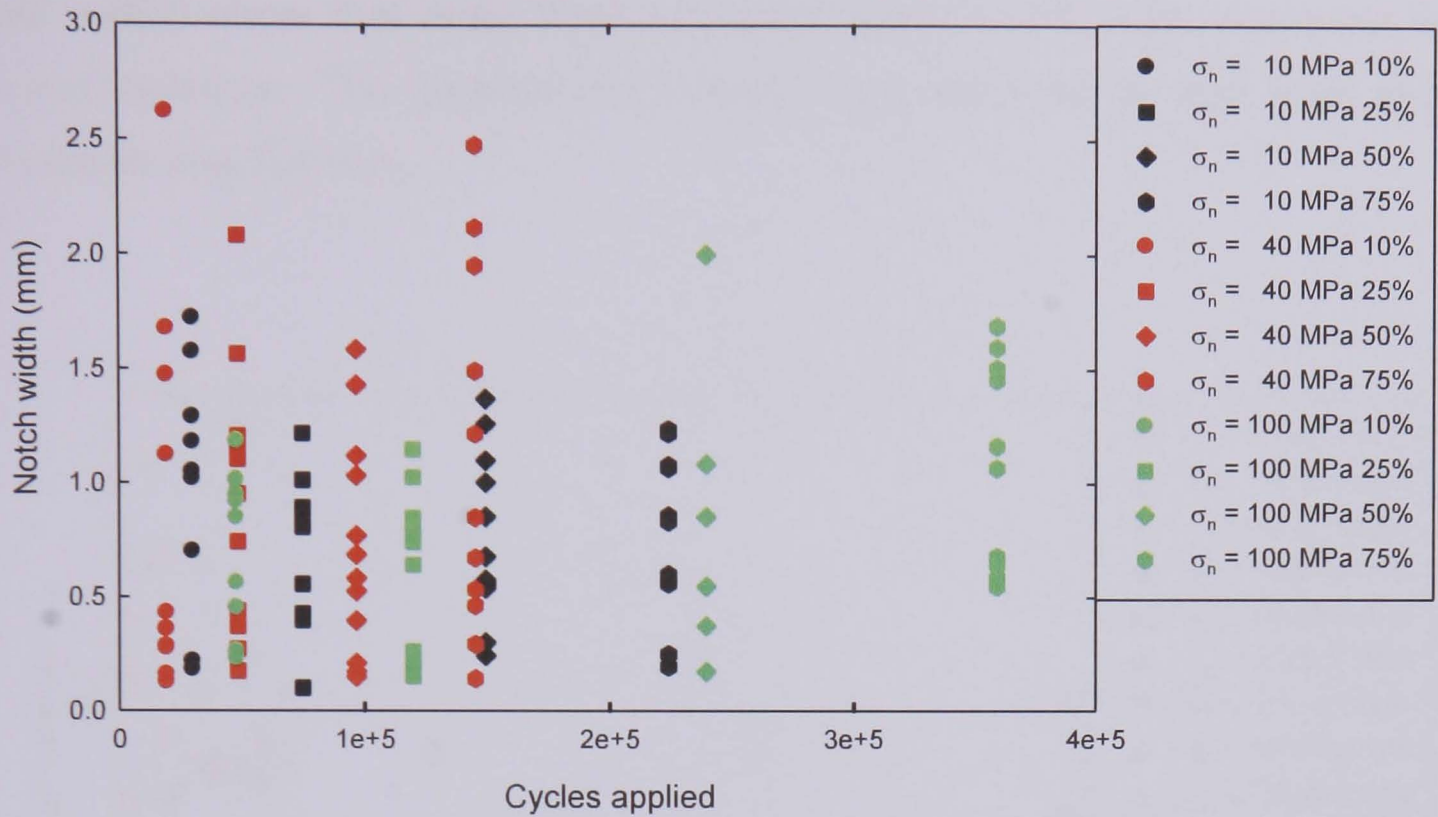


Figure 4.59: The evolution, in terms of the number of cycles applied, of notch width over the lives of unpeened specimens subjected to three normal pressures and an axial stress amplitude of 100 MPa.

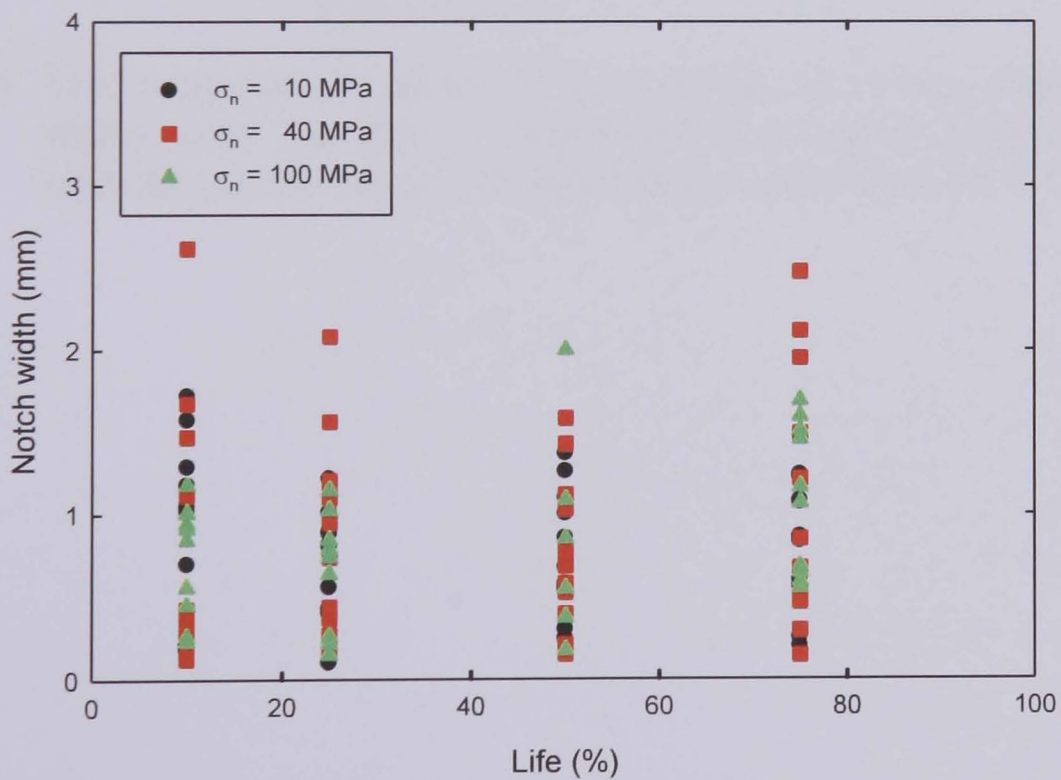


Figure 4.60: The evolution, in terms of percentage life, of notch width over the lives of unpeened specimens subjected to three normal pressures and an axial stress amplitude of 100 MPa.

Plots for an axial stress amplitude of 125 MPa are shown in Figures 4.61 and 4.62, which show that apart from one stray point, notch width increases with normal pressure. The greatest notch width was recorded for this axial stress amplitude was 3.4 mm.

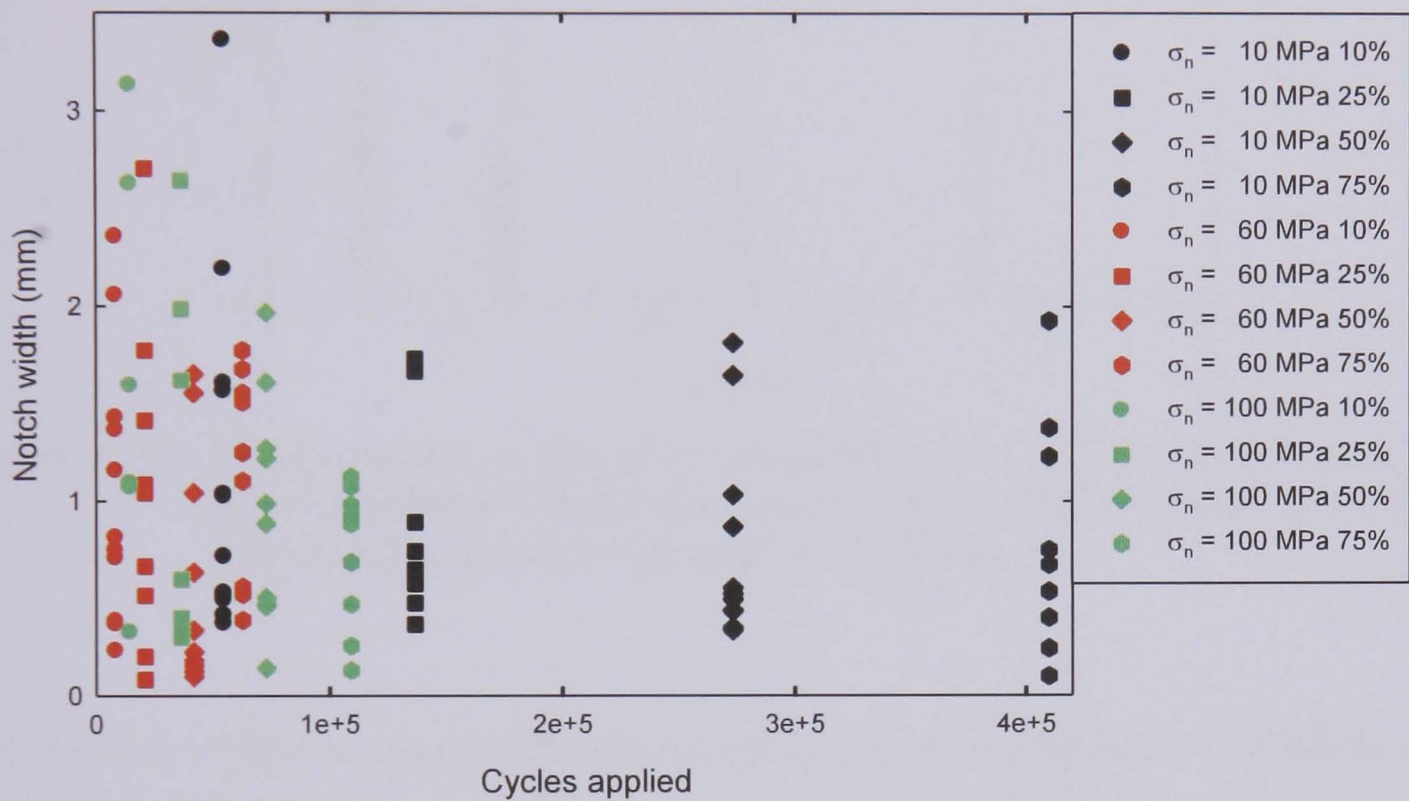


Figure 4.61: The evolution, in terms of the number of cycles applied, of notch width over the life of unpeened specimens subjected to three normal pressures and an axial stress amplitude of 125 MPa.

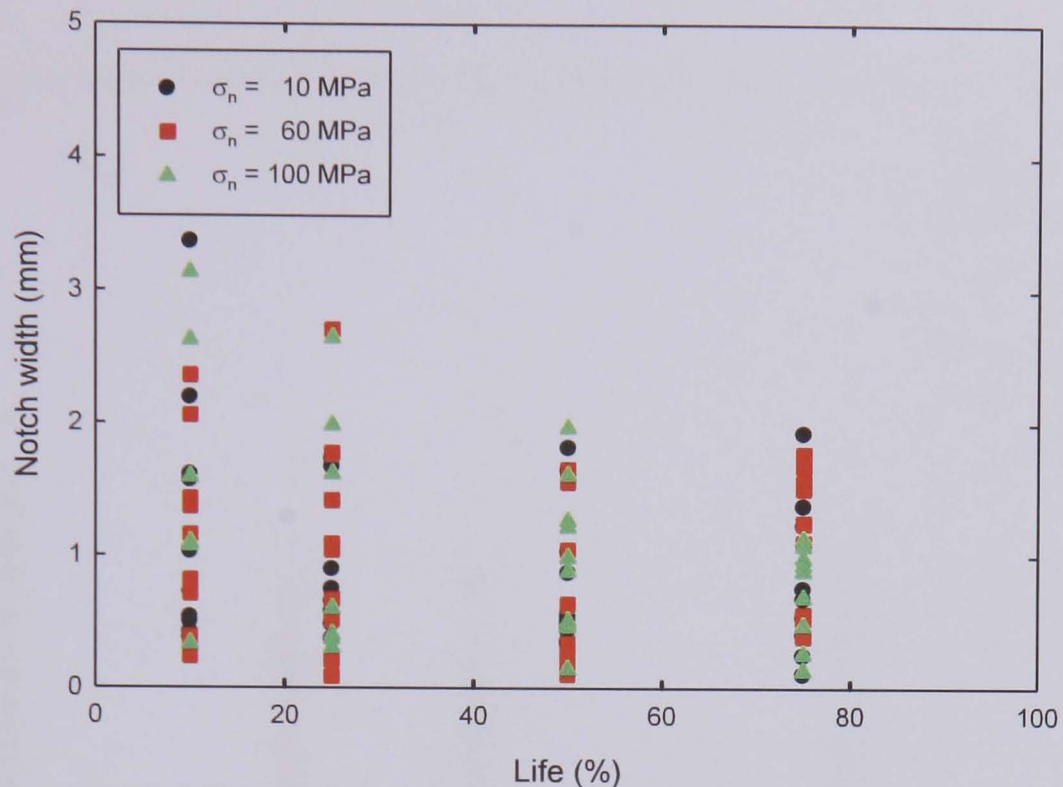


Figure 4.62: The evolution, in terms of percentage life, of notch width over the life of unpeened specimens subjected to three normal pressures and an axial stress amplitude of 125 MPa.

A summary of all the results attained at axial stress amplitudes of 70 MPa, 100 MPa and 125 MPa using unpeened aluminium alloy 2024 T351 in flat-on-flat contact with unpeened aluminium alloy 2024 T351 are given in Figures 4.63 to 4.66.

Figure 4.63 demonstrates that in all cases notch peak to valley depth decreases marginally with the increasing magnitude of the normal pressure applied. The rate of this decrease is related to the applied axial stress amplitude, being greatest at 70 MPa and less pronounced at higher axial stress amplitudes, where the trends observed are almost identical. The maximum notch peak to valley depth recorded was 58 μm for a normal pressure of 10 MPa and an axial stress amplitude of 70 MPa. There is a decreasing degree of spread in the measurements taken with increasing normal pressure.

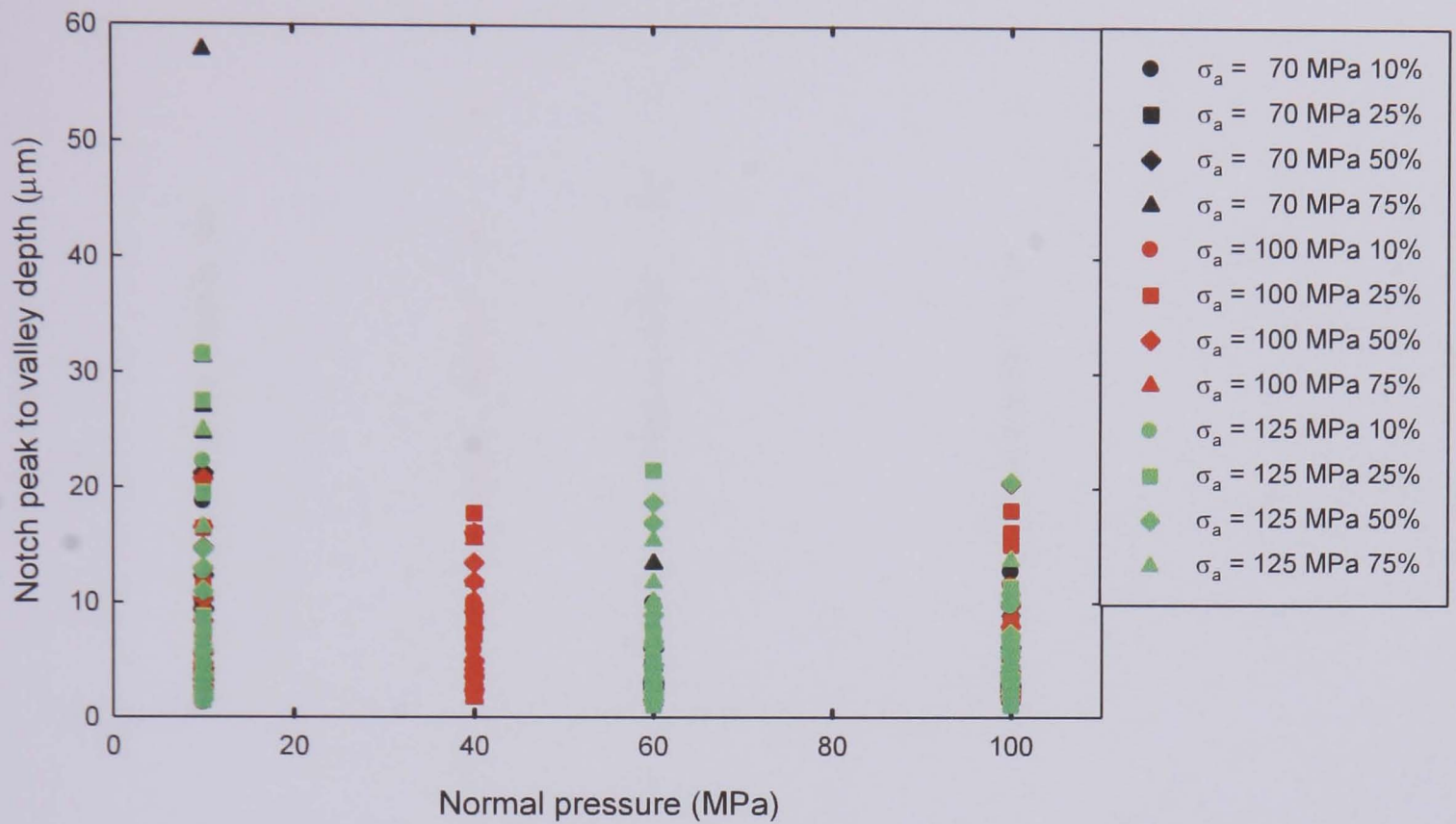


Figure 4.63: A comparison of the notch peak to valley depths resulting from fretting fatigue tests conducted with an aluminium alloy 2024 T351 bridge in contact with an unpeened aluminium alloy 2024 T351 specimen subjected to axial stress amplitudes of 70 MPa, 100 MPa and 125 MPa.

Figure 4.64 demonstrates that that in all cases, notch width has little dependence on normal pressure. The maximum notch width recorded was 3.4 mm for a normal pressure of 60 MPa and an axial stress amplitude of 125 MPa. There is the least scatter in the measurements taken at the maximum normal pressure.

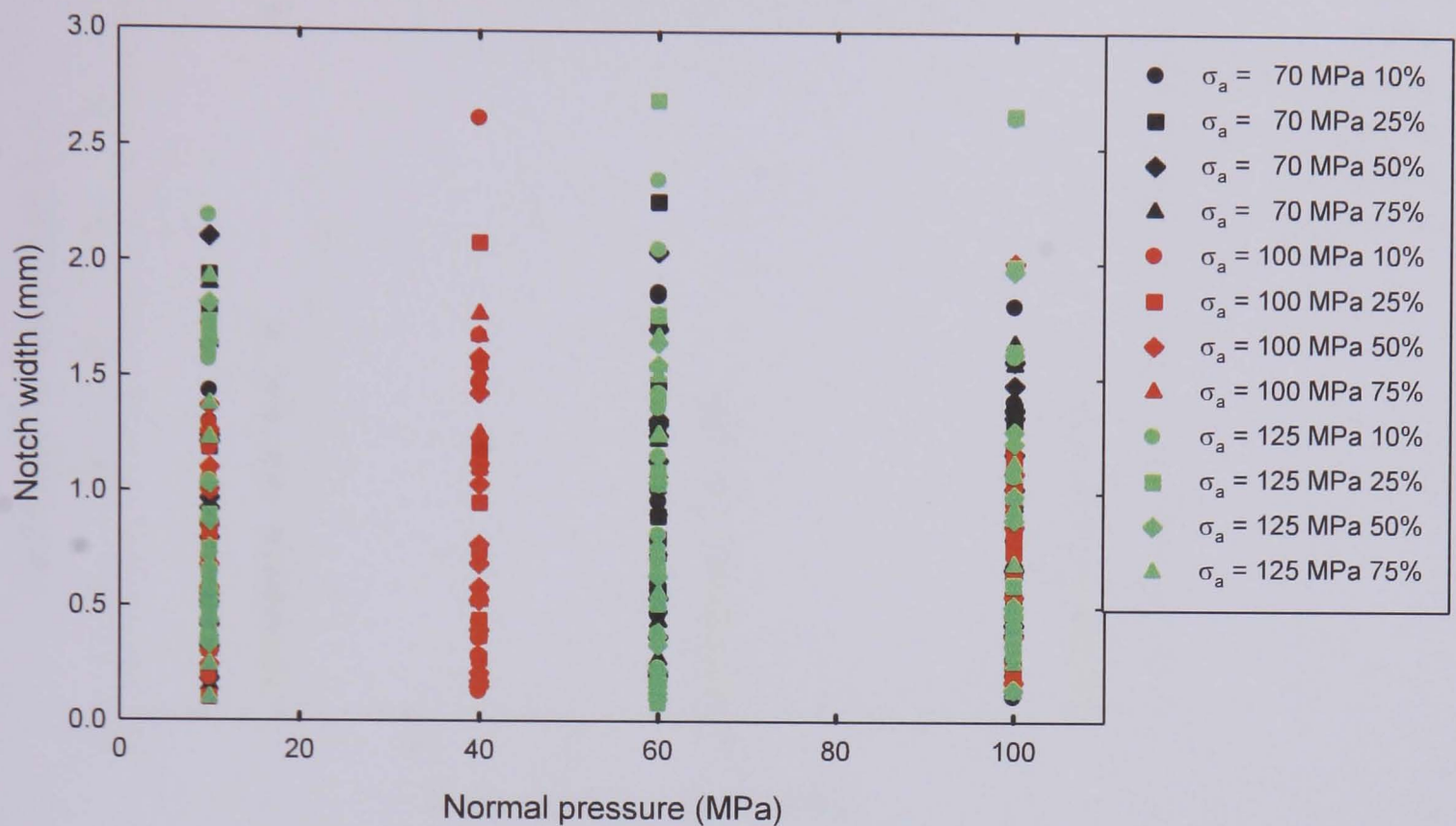


Figure 4.64: A comparison of the notch widths resulting from fretting fatigue tests conducted with an aluminium alloy 2024 T351 bridge in contact with an unpeened aluminium alloy 2024 T351 specimen subjected to axial stress amplitudes of 70 MPa, 100 MPa and 125 MPa.

Figure 4.65 shows the influence of axial stress on notch peak to valley depth. There does not appear to be a great deal of correlation between the normal pressures applied and the resultant notch peak to valley depths observed in each case, although notch peak to valley depth is shown to be at a maximum for the minimum normal pressures applied for axial stress amplitudes of 70 MPa and 125 MPa. To this end, for a normal pressure of 10 MPa, notch peak to valley depth decreases marginally with an increase in axial stress up to a critical normal pressure, after which notch peak to valley depth increases marginally again. For normal pressures of 60 MPa and 100 MPa, notch peak to valley depth increases marginally with increasing axial stress.

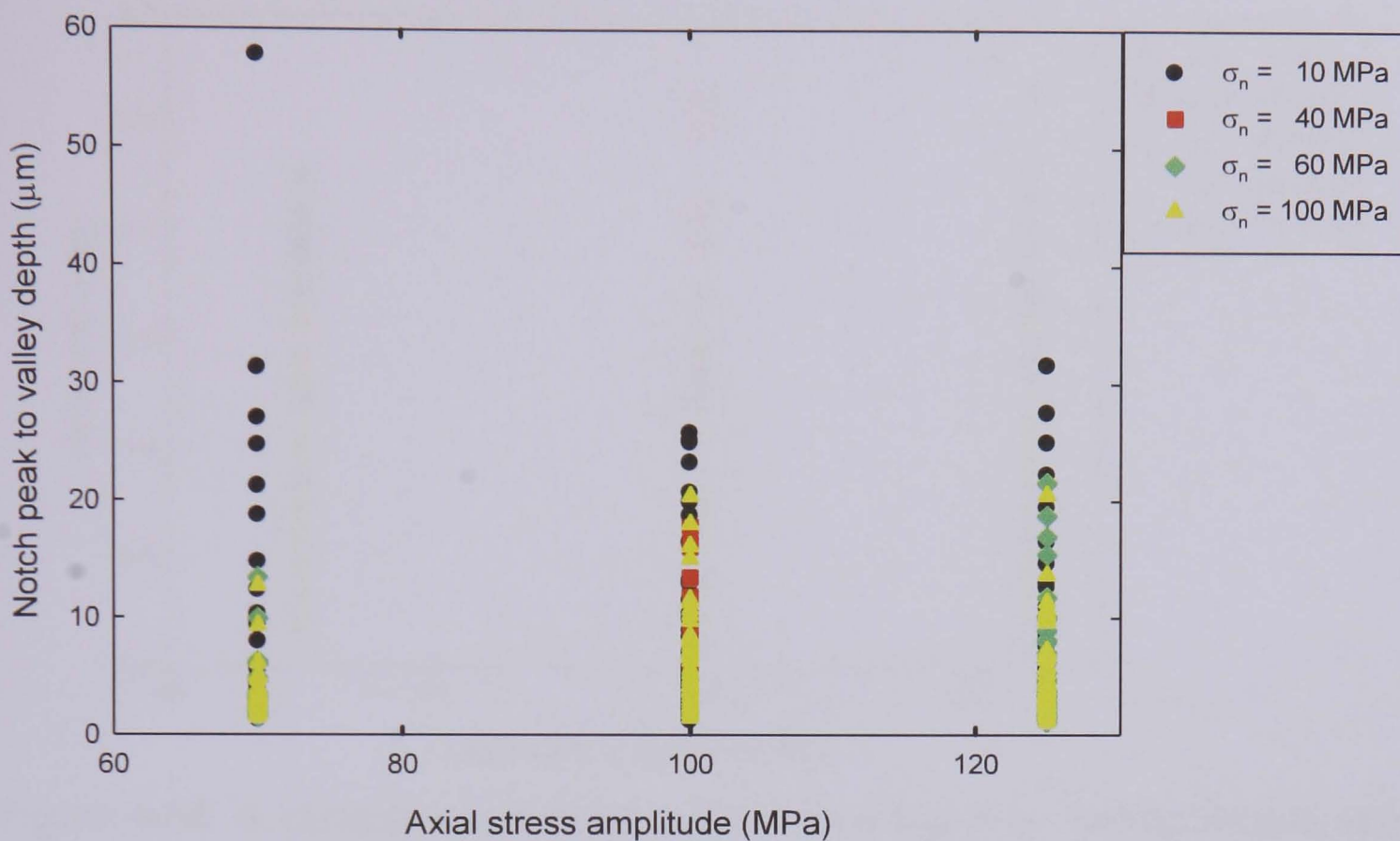


Figure 4.65: A comparison of notch peak to valley depths resulting from fretting fatigue tests conducted with an aluminium alloy 2024 T351 bridge in contact with an unpeened aluminium alloy 2024 T351 specimen subjected to normal pressures of 10 MPa, 40 MPa or 60 MPa and 100 MPa.

Figure 4.66 shows the influence of axial stress on notch width. There does not appear to be a great deal of correlation between the normal pressures applied and the resultant notch widths observed in each case.

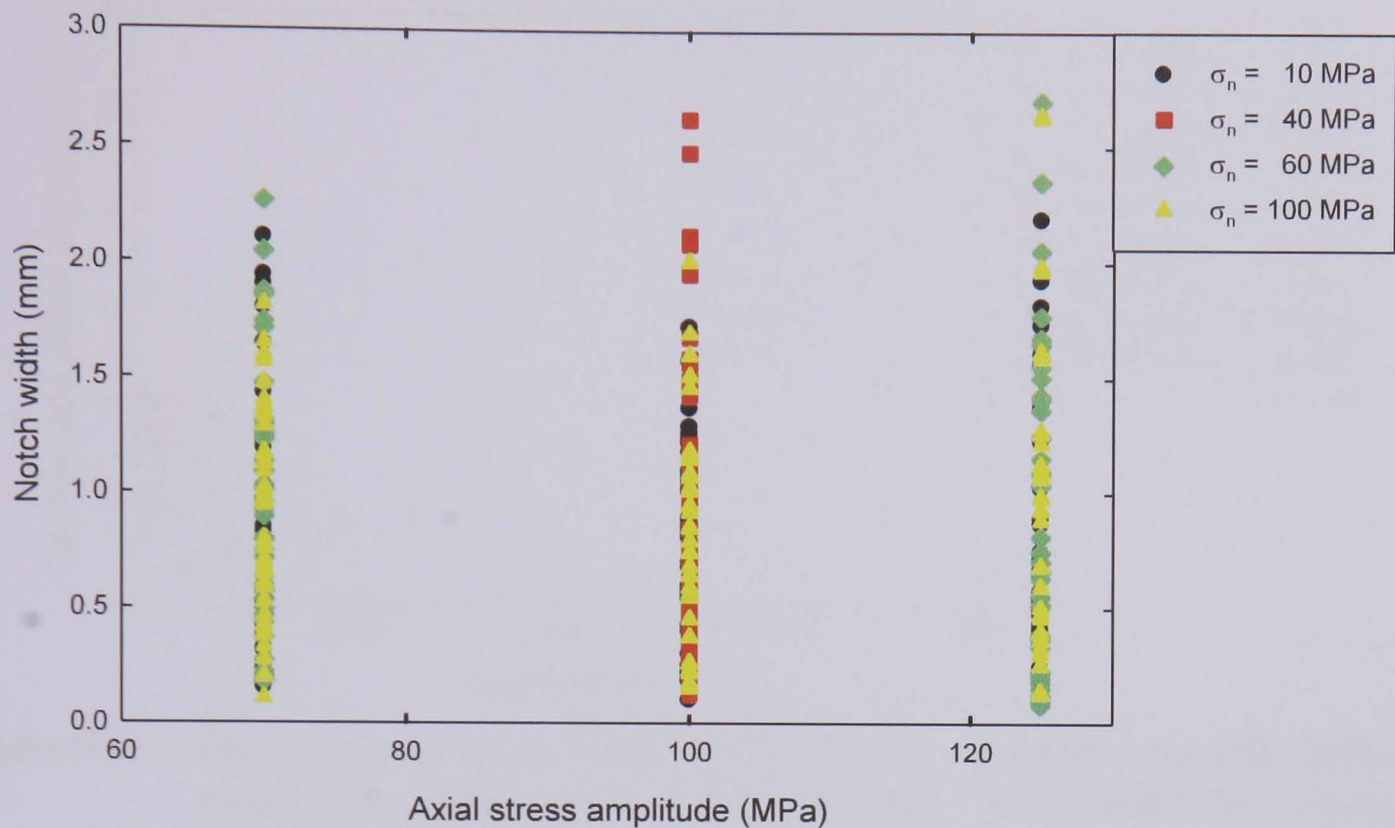


Figure 4.66: A comparison of notch widths resulting from fretting fatigue tests conducted with an aluminium alloy 2024 T351 bridge in contact with an unpeened aluminium alloy 2024 T351 specimen subjected to normal pressures of 10 MPa, 40 MPa or 60 MPa and 100 MPa.

Figures 4.67 and 4.68 demonstrate a degree of correlation between the maximum notch peak to valley depth and cycles to failure. For an axial stress amplitude of 70 MPa, the higher the number of cycles to failure, the greater the magnitude of the maximum notch peak to valley depth observed. This trend is also apparent in Figures 4.69 and 4.70, which show the relationship between the mean notch peak to valley depth and cycles to failure.

Figures 4.71 and 4.72 demonstrate a correlation between the maximum notch width and cycles to failure. For an axial stress amplitude of 70 MPa, the higher the number of cycles to failure, the greater the magnitude of the maximum notch width observed, at least at 10 MPa normal pressure. However, there is no direct correlation between mean notch width and cycles to failure, as is shown in Figures 4.73 and 4.74.

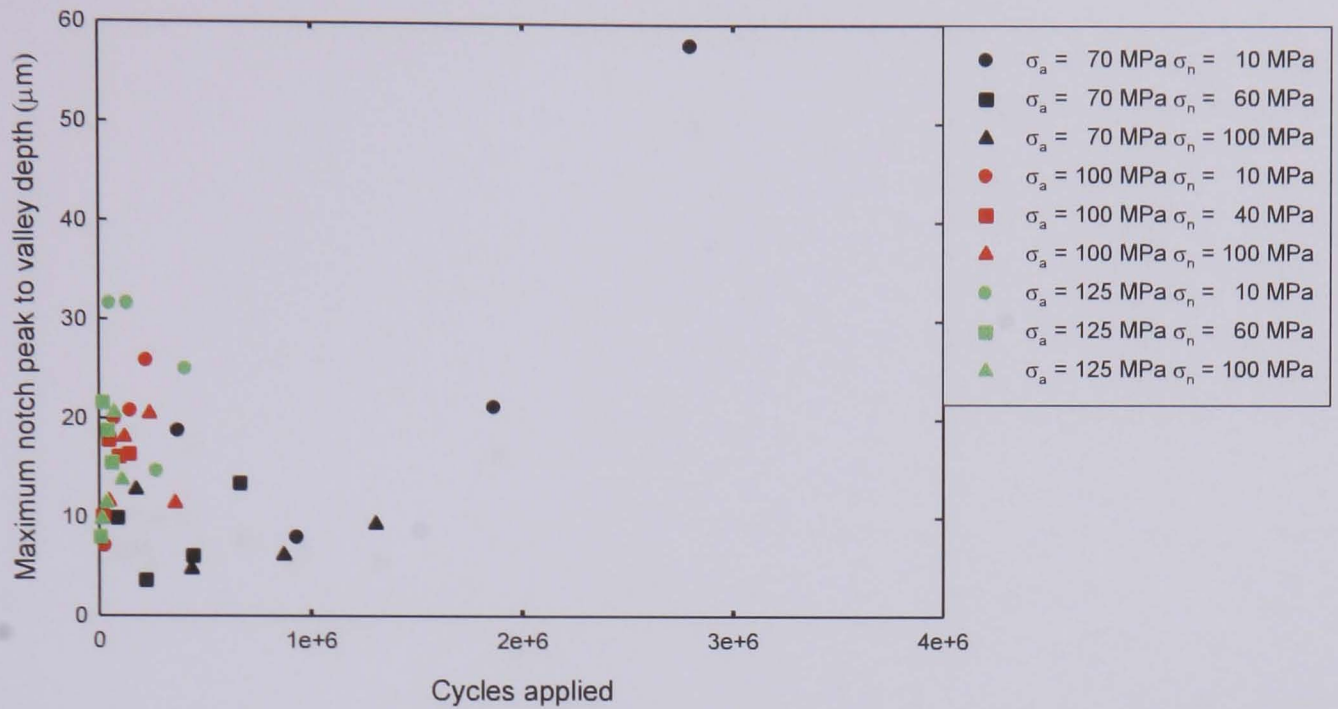


Figure 4.67: The relationship, in terms of the number of cycles applied, between maximum notch peak to valley depth and cycles to failure for fretting fatigue tests conducted with an aluminium alloy 2024 T351 bridge subjected to a range of normal pressures in contact with an unpeened aluminium alloy 2024 T351 specimen subjected to axial stress amplitudes of 70 MPa, 100 MPa and 125 MPa.

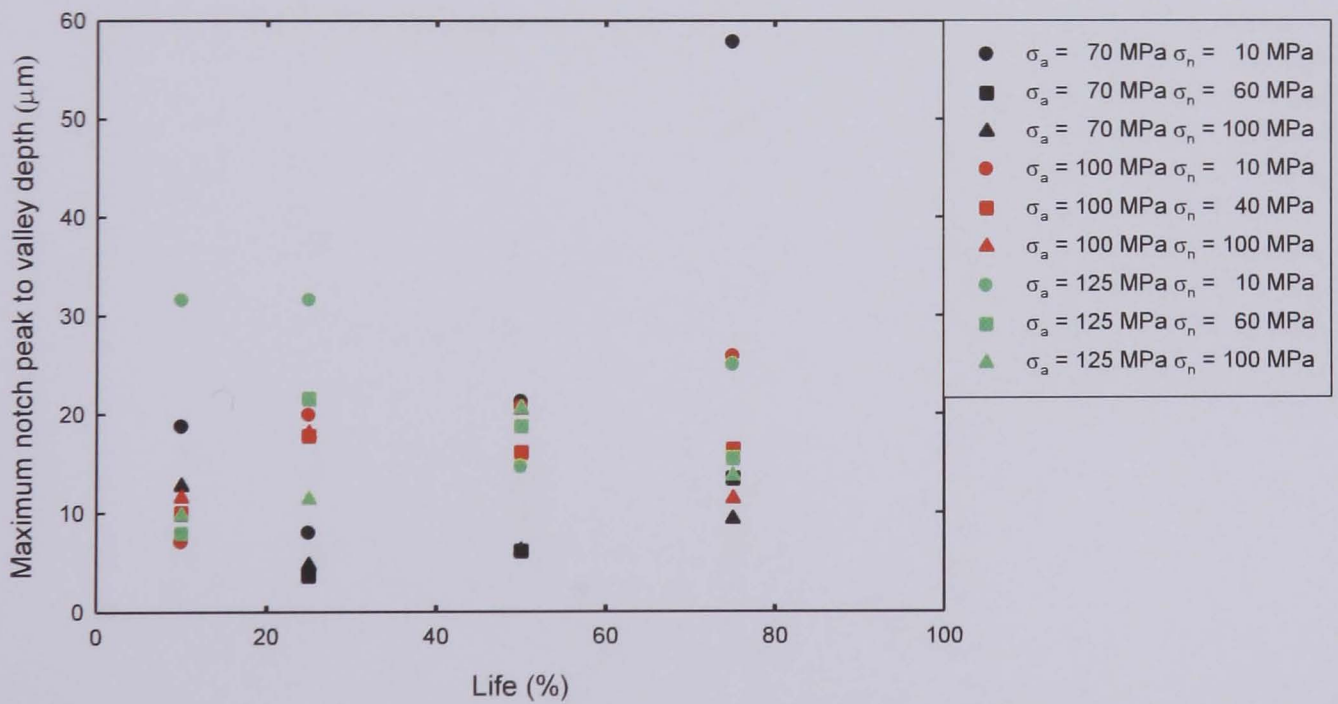


Figure 4.68: The relationship, in terms of percentage life, between maximum notch peak to valley depth and cycles to failure for fretting fatigue tests conducted with an aluminium alloy 2024 T351 bridge subjected to a range of normal pressures in contact with an unpeened aluminium alloy 2024 T351 specimen subjected to axial stress amplitudes of 70 MPa, 100 MPa and 125 MPa.

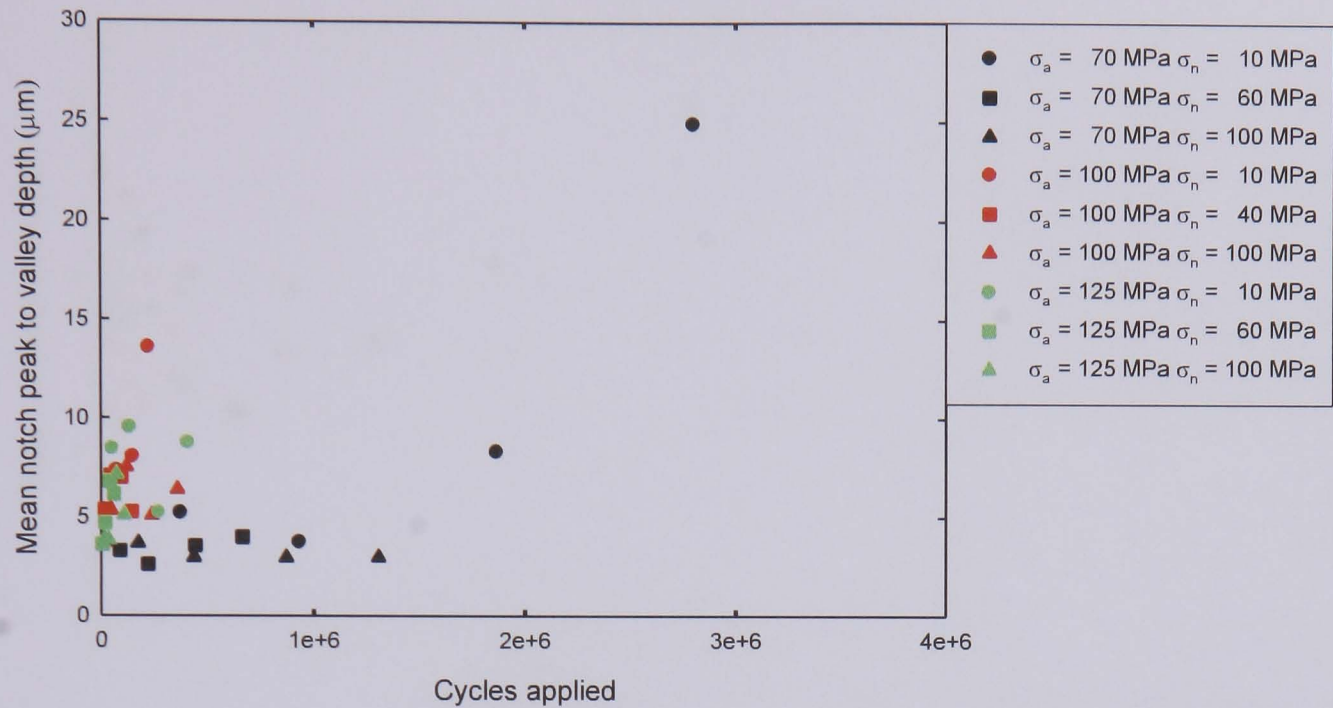


Figure 4.69: The relationship, in terms of the number of cycles applied, between mean notch peak to valley depth and cycles to failure for fretting fatigue tests conducted with an aluminium alloy 2024 T351 bridge subjected to a range of normal pressures in contact with an unpeened aluminium alloy 2024 T351 specimen subjected to axial stress amplitudes of 70 MPa, 100 MPa and 125 MPa.

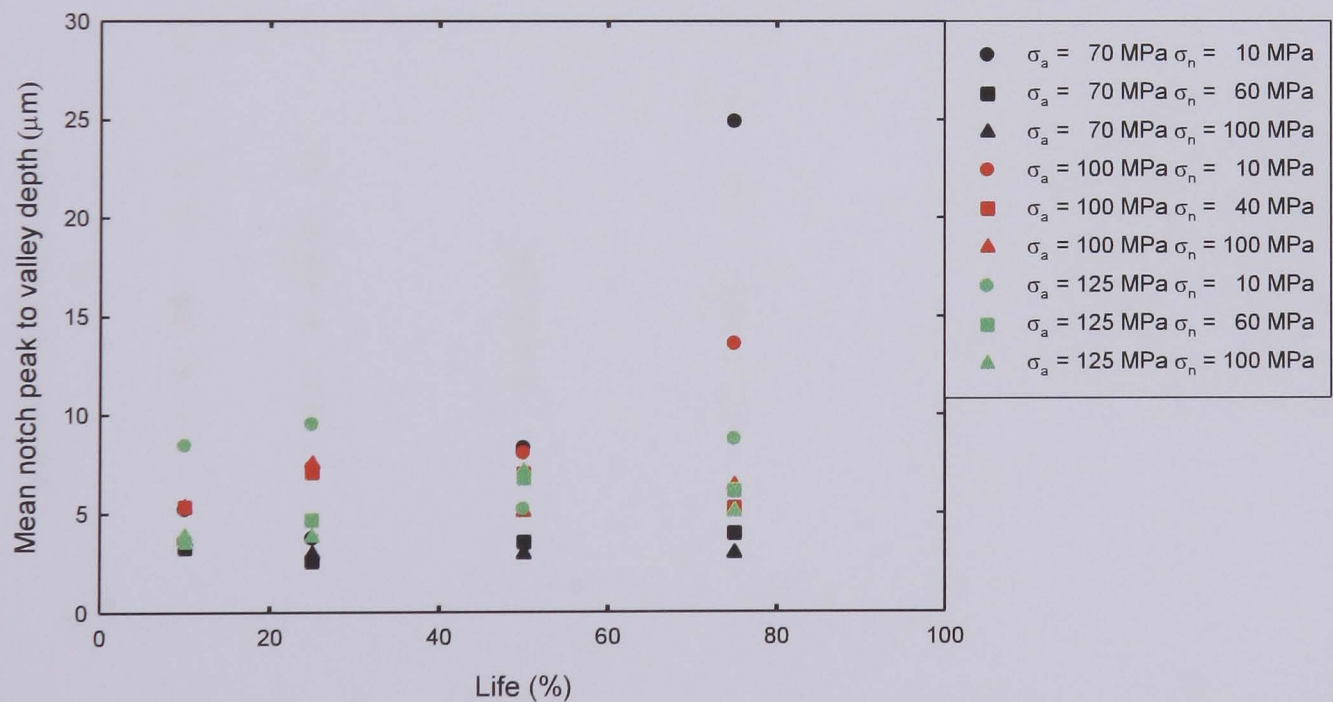


Figure 4.70: The relationship, in terms of percentage life, between mean notch peak to valley depth and cycles to failure for fretting fatigue tests conducted with an aluminium alloy 2024 T351 bridge subjected to a range of normal pressures in contact with an unpeened aluminium alloy 2024 T351 specimen subjected to axial stress amplitudes of 70 MPa, 100 MPa and 125 MPa.

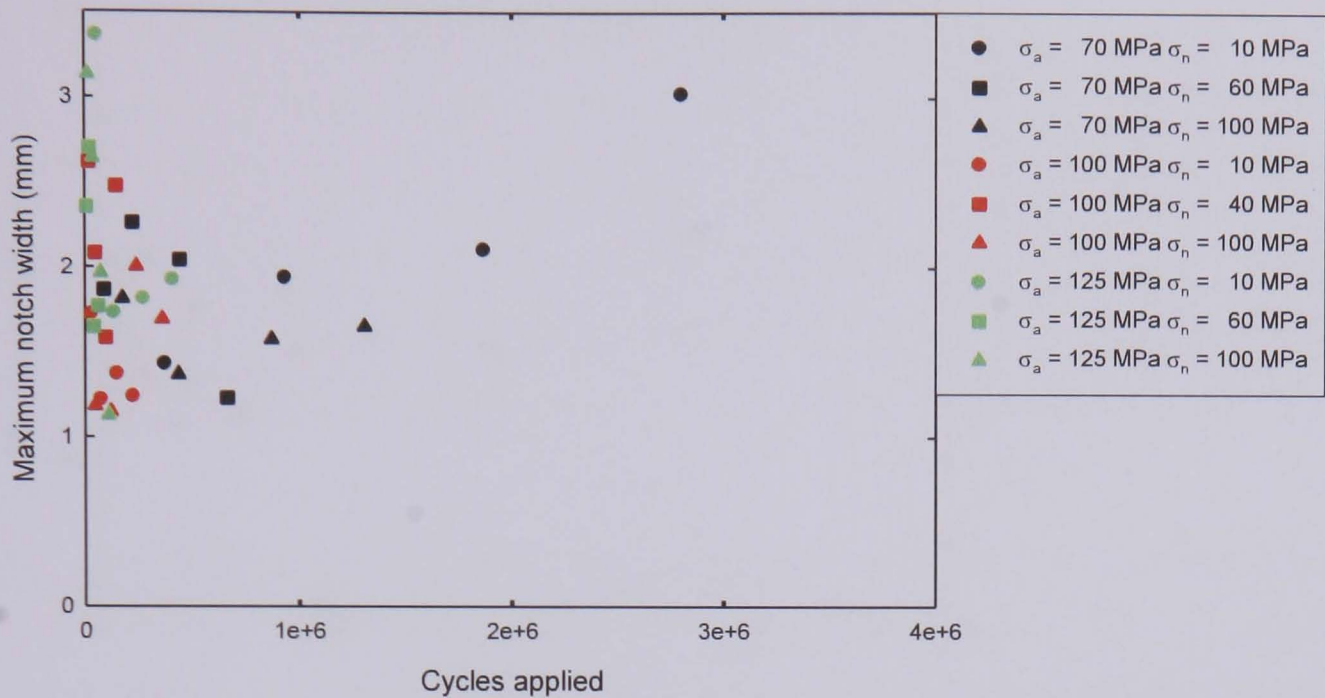


Figure 4.71: The relationship, in terms of the number of cycles applied, between maximum notch width and cycles to failure for fretting fatigue tests conducted with an aluminium alloy 2024 T351 bridge subjected to a range of normal pressures in contact with an unpeened aluminium alloy 2024 T351 specimen subjected to axial stress amplitudes of 70 MPa, 100 MPa and 125 MPa.

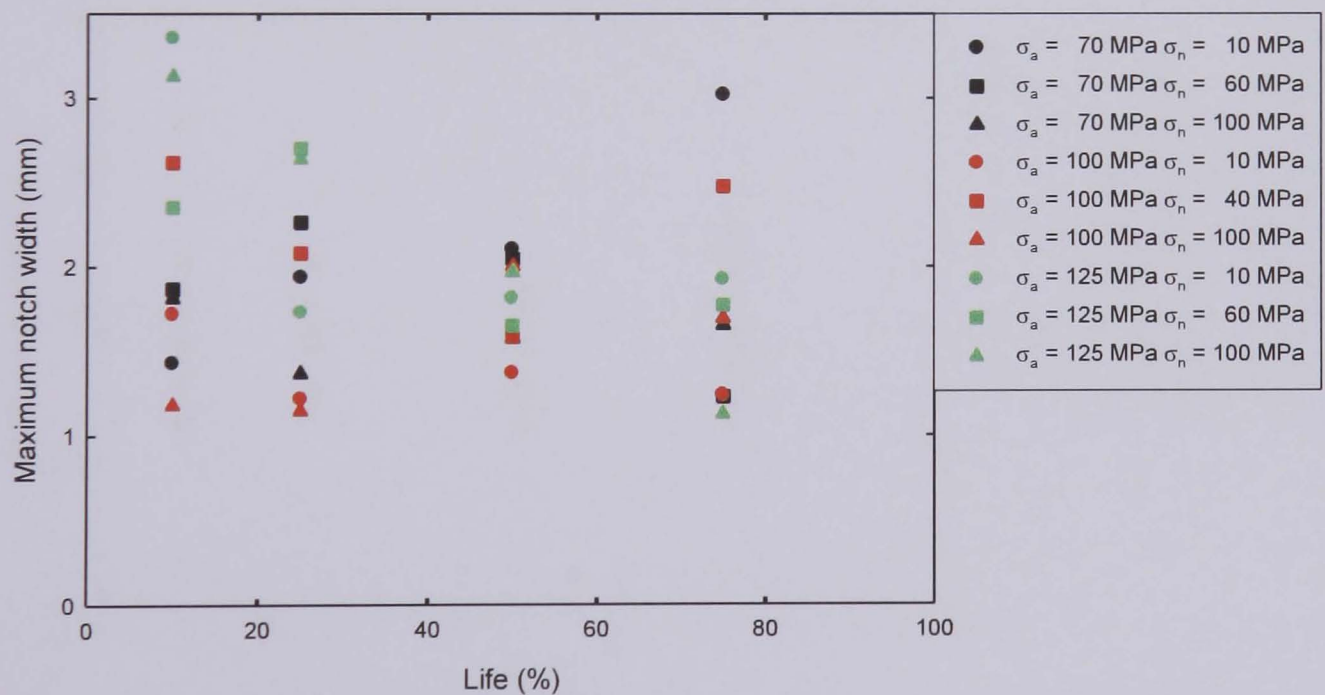


Figure 4.72: The relationship, in terms of percentage life, between maximum notch width and cycles to failure for fretting fatigue tests conducted with an aluminium alloy 2024 T351 bridge subjected to a range of normal pressures in contact with an unpeened aluminium alloy 2024 T351 specimen subjected to axial stress amplitudes of 70 MPa, 100 MPa and 125 MPa.

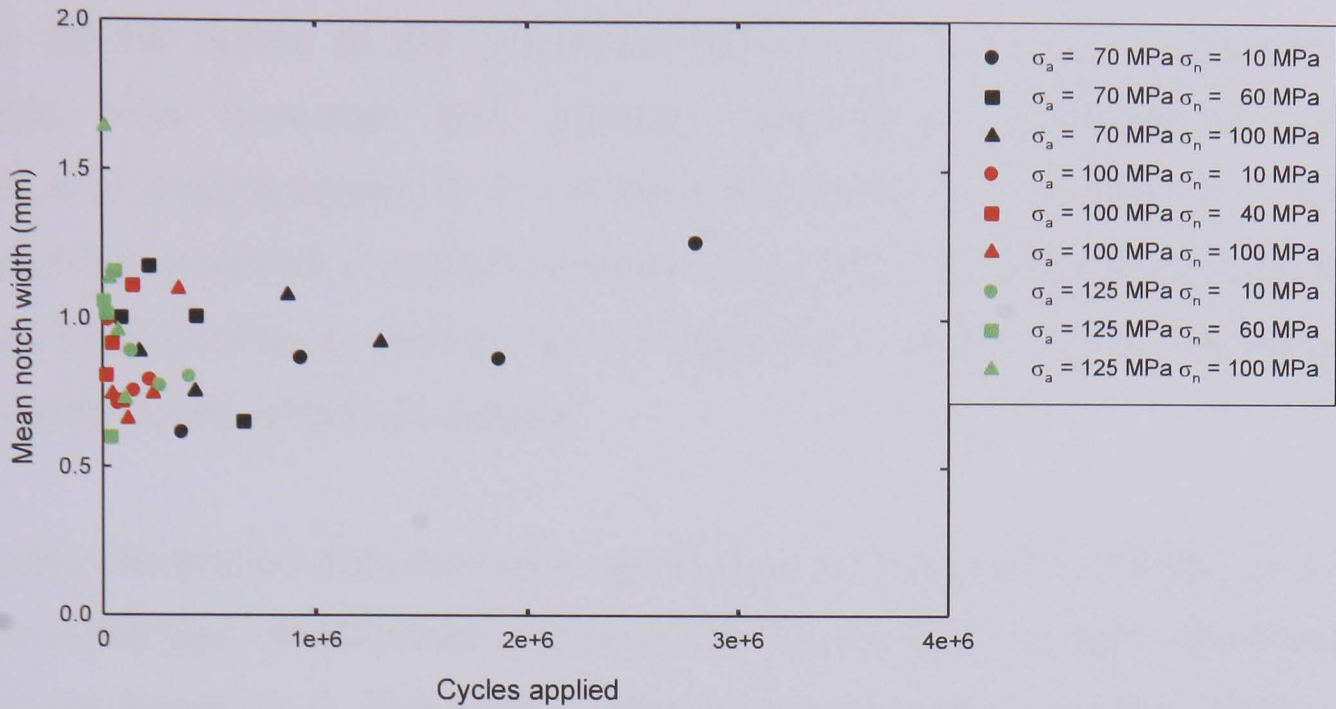


Figure 4.73: The relationship, in terms of the number of cycles applied, between mean notch width and cycles to failure for fretting fatigue tests conducted with an aluminium alloy 2024 T351 bridge subjected to a range of normal pressures in contact with an unpeened aluminium alloy 2024 T351 specimen subjected to axial stress amplitudes of 70 MPa, 100 MPa and 125 MPa.

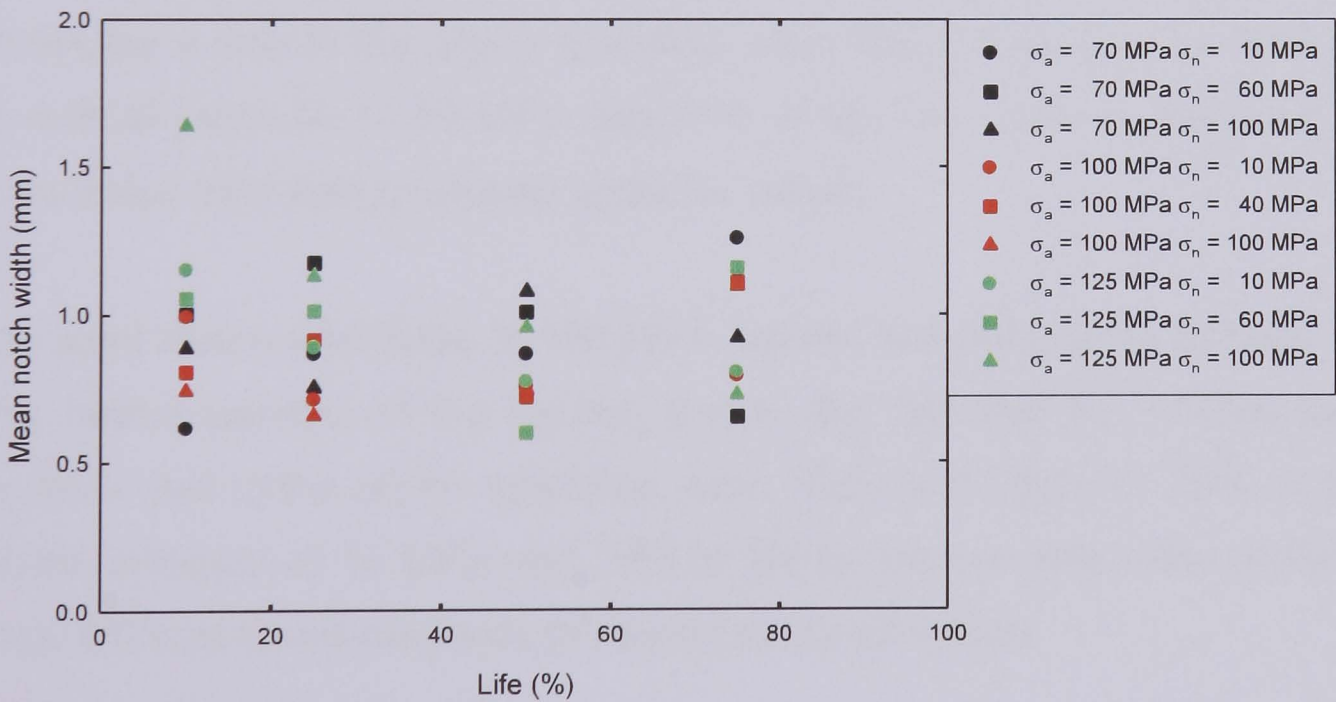


Figure 4.74: The relationship, in terms of percentage life, between mean notch width and cycles to failure for fretting fatigue tests conducted with an aluminium alloy 2024 T351 bridge subjected to a range of normal pressures in contact with an unpeened aluminium alloy 2024 T351 specimen subjected to axial stress amplitudes of 70 MPa, 100 MPa and 125 MPa.

4.3.1.3 Peened

Once all the scans of the unpeened specimens had been completed, the process was repeated with peened specimens. Twenty-seven peened specimens were analysed in this programme, resulting in a total of: 12 profiles for each combination of normal pressure, axial stress amplitude and percentage life, 24 to 48 profiles in total for each normal pressure and up to 144 profiles for each axial stress amplitude applied.

Specially developed software was again used to analyse the profiles generated by the UBM laser profilometer, whereby significant features were identified; this code is in Appendix D. Specifically, data on the total peak to valley depth of the scar and the total width of the scar are given in Appendix J, Tables J.4, 5 and 6a, J.4, 5 and 6b and J.4, 5 and 6c; the maximum and minimum values for each data set are also given.

However, for an axial stress amplitude of 70 MPa, figures are missing for five notch widths, seven percent of the figures, due to the fact that the profiles did not cross the x axis in the region specified. Also, there is no data for 50% of life for a normal pressure of 10 MPa and 75% of life for a normal pressure of 60 MPa as these data sets produced spurious results.

For an axial stress amplitude of 100 MPa, figures are missing for thirteen notch widths, twelve percent of the figures, due to the fact that the profiles did not cross the x axis in the region specified. Also, there is no data for 75% of life for a normal pressure of 10 MPa and 25% of life for normal pressures of 60 MPa and 100 MPa as these data sets produced spurious results.

For an axial stress amplitude of 125 MPa, figures are missing for eleven notch widths, eleven percent of the figures, due to the fact that the profiles did not cross the x axis in the region specified. Also, there is no data for 25% and 75% of life for a normal pressure of 10 MPa and 75% of life for normal pressures of 60 MPa and 100 MPa as these data sets produced spurious results.

This data was subsequently investigated to establish the relationship between wear and time. Plots of notch peak to valley depth versus percentage life for each combination of load are shown in Appendix K and plots of notch width versus percentage life for each combination of load are shown in Appendix L. Typical profiles are shown in Figures 4.75 and 4.76.

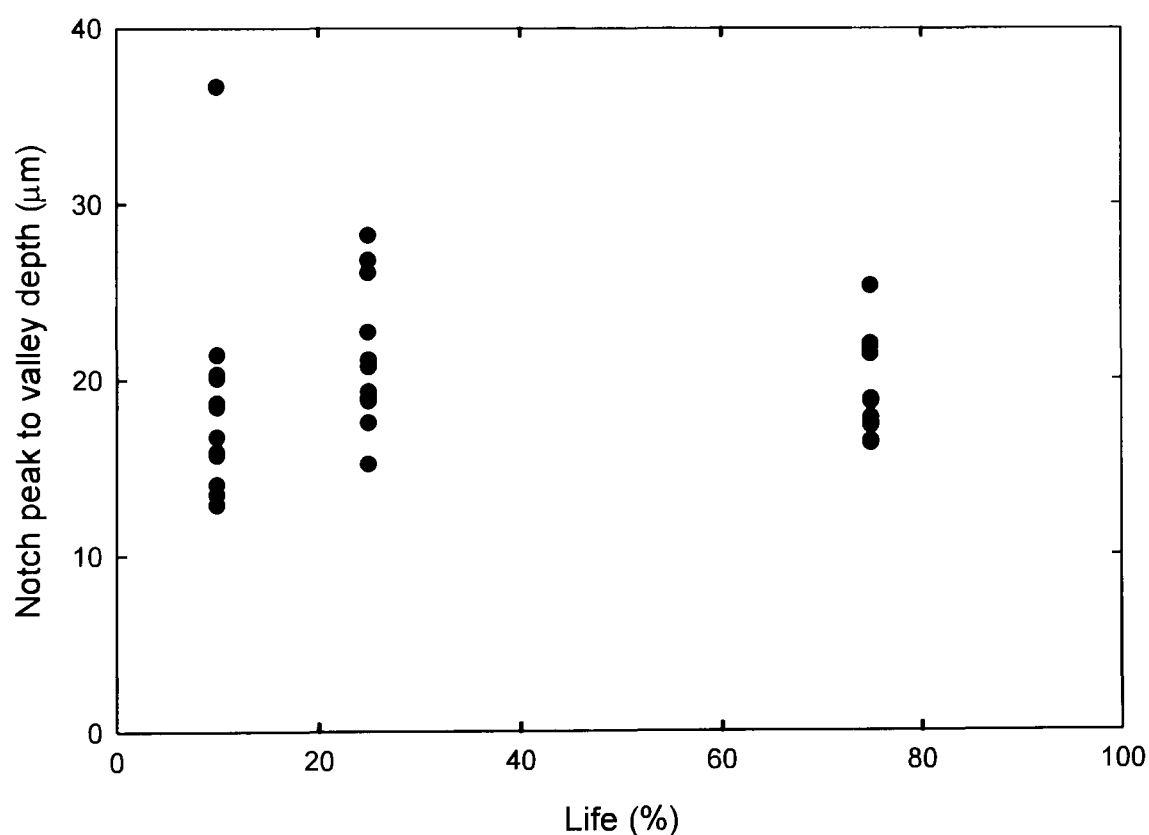


Figure 4.75: The evolution of notch peak to valley depth over the life of peened specimens subjected to a normal pressure of 10 MPa and an axial stress amplitude of 70 MPa.

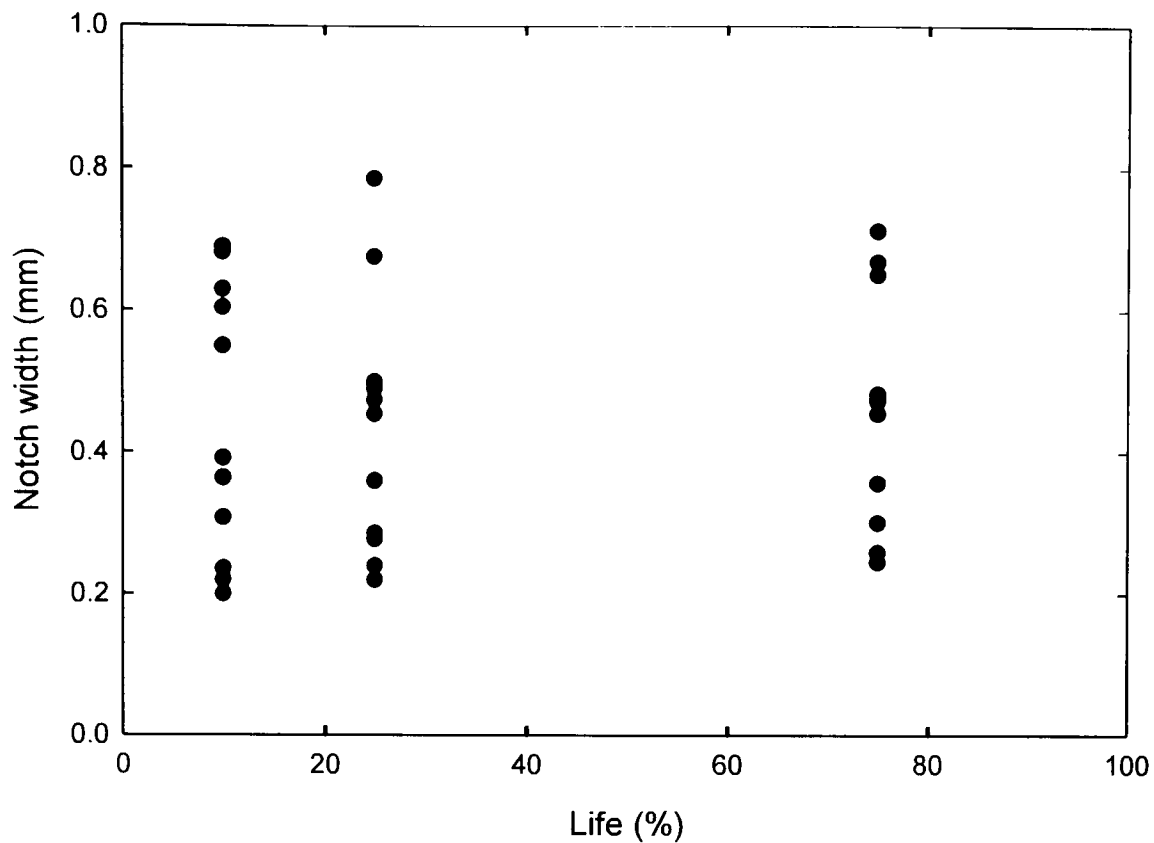


Figure 4.76: The evolution of notch width over the life of peened specimens subjected to a normal pressure of 10 MPa and an axial stress amplitude of 70 MPa.

For the greatest notch depths found for each combination of load and percentage life, the resultant plots together with a corresponding magnified view of the areas of interest found are shown in Appendix M. A profile resulting from identical loading to that in Figures 4.75 and 4.76 is shown in Figure 4.77; a magnified view of the primary notch found on this plot is shown in Figure 4.78. The grey line is the original trace line; the black line is the profile smoothed for analysis purposes. These figures depict a significantly roughened surface with a number of notches present, the deepest of which has small peaks of material pushed up on either side.

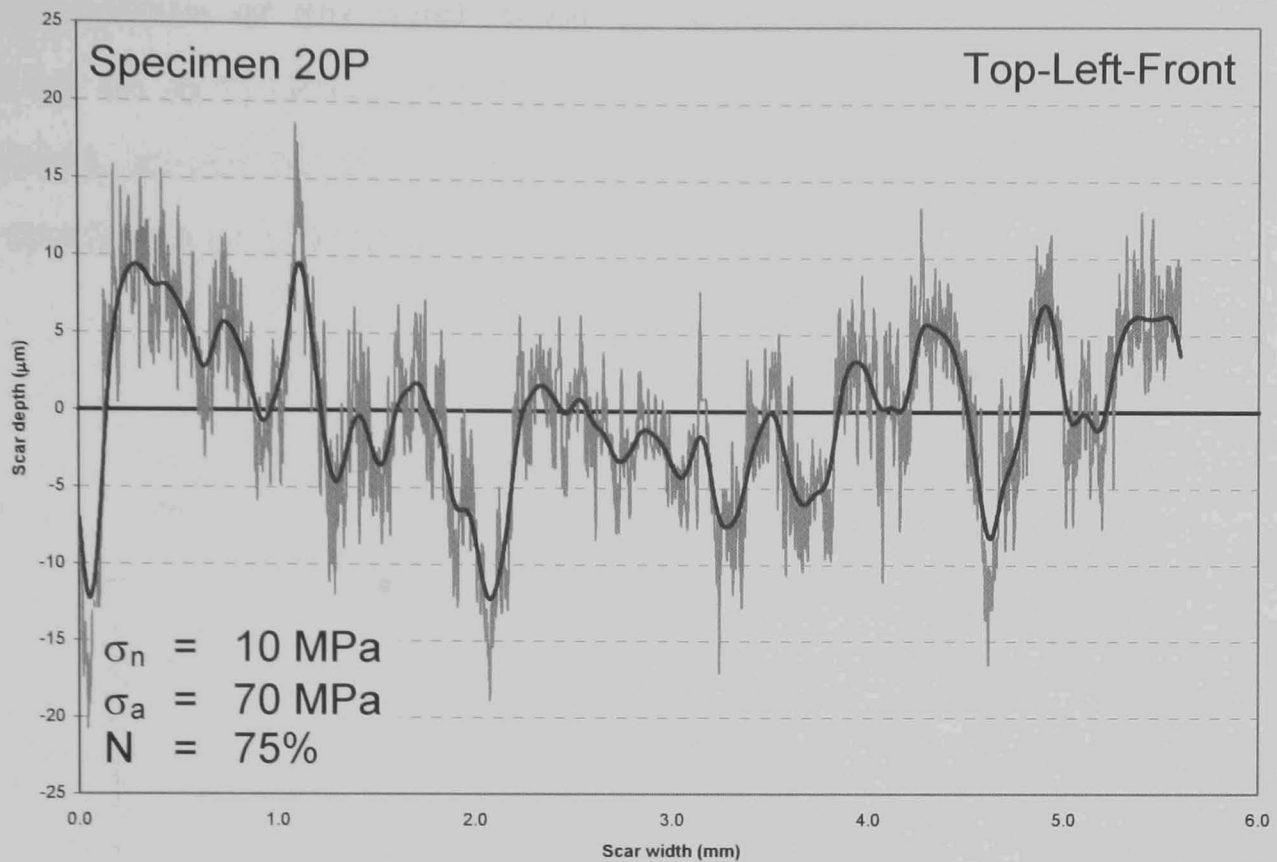


Figure 4.77: The surface roughness profile of a peened specimen subjected to a normal pressure of 10 MPa and an axial stress amplitude of 70 MPa for 75% of the total expected life of that specimen.

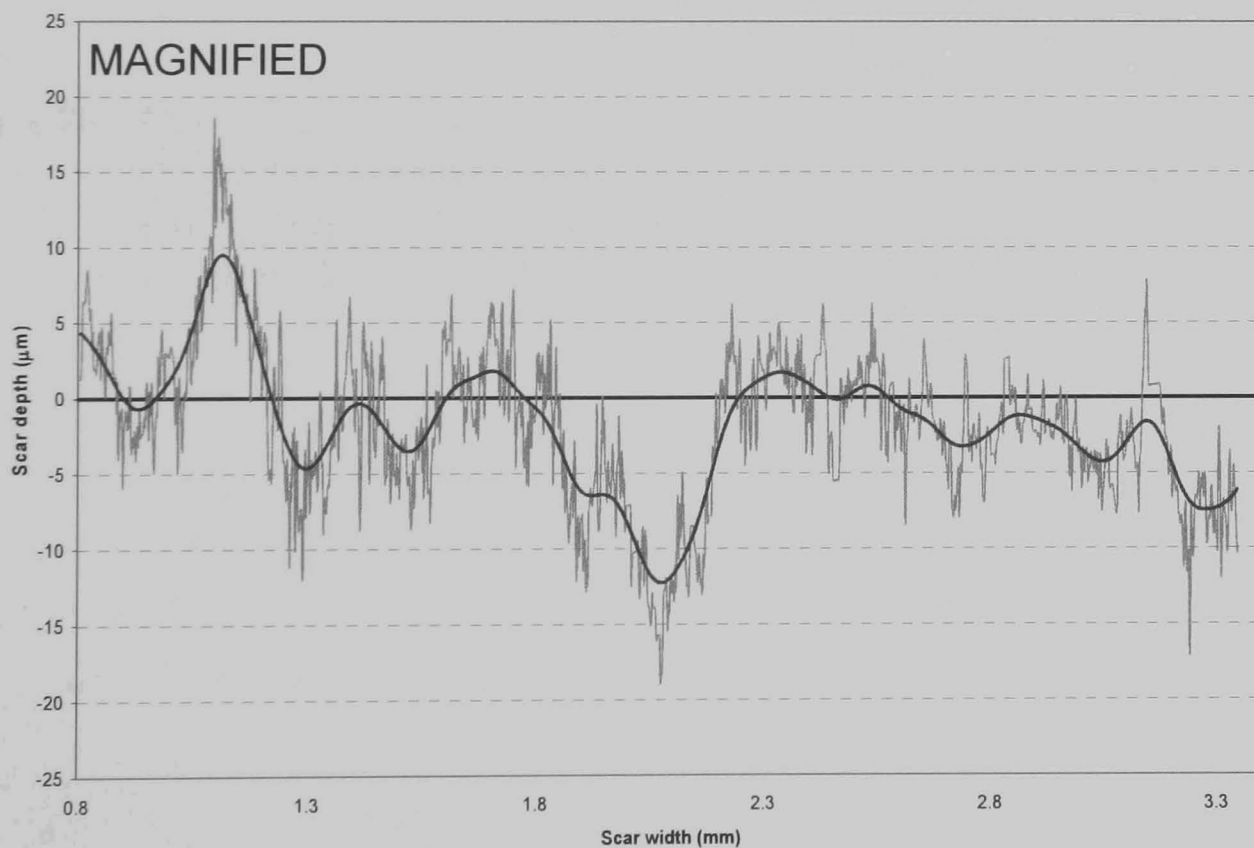


Figure 4.78: A magnified view highlighting the areas of interest on the surface roughness profile of a peened specimen subjected to a normal pressure of 10 MPa and an axial stress amplitude of 70 MPa for 75% of the total expected life of that specimen.

The dependence of the notch peak to valley depth on the normal pressure applied for an axial stress amplitude of 70 MPa is shown in Figure 4.79, for an axial stress amplitude of 100 MPa is shown in Figure 4.80 and for an axial stress amplitude of 125 MPa is shown in Figure 4.81.

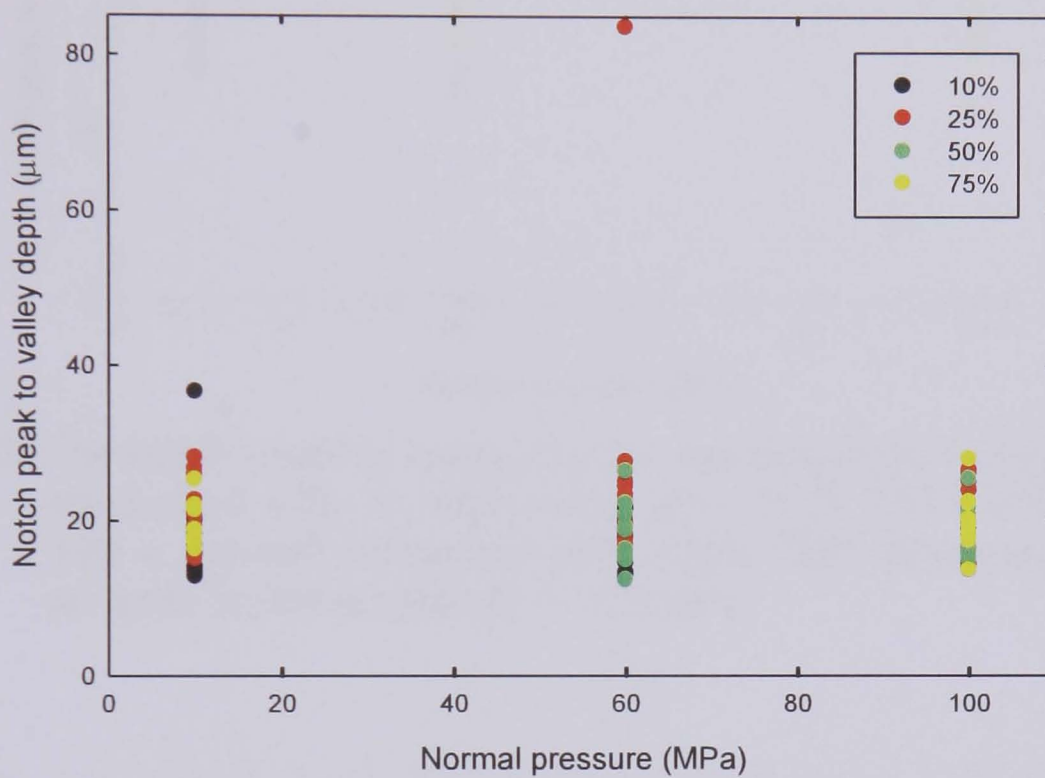


Figure 4.79: The notch peak to valley depths resulting from fretting fatigue tests conducted with an aluminium alloy 2024 T351 bridge in contact with a peened aluminium alloy 2024 T351 specimen subjected to an axial stress amplitude of 70 MPa.

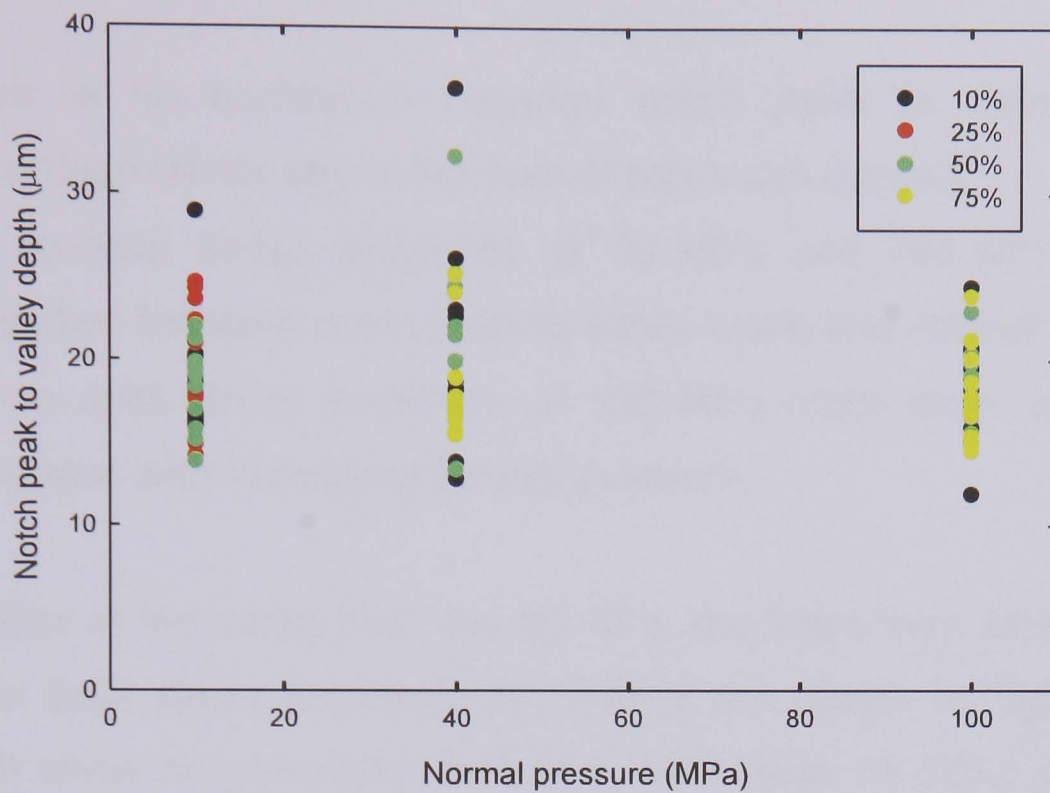


Figure 4.80: The notch peak to valley depths resulting from fretting fatigue tests conducted with an aluminium alloy 2024 T351 bridge in contact with a peened aluminium alloy 2024 T351 specimen subjected to an axial stress amplitude of 100 MPa.

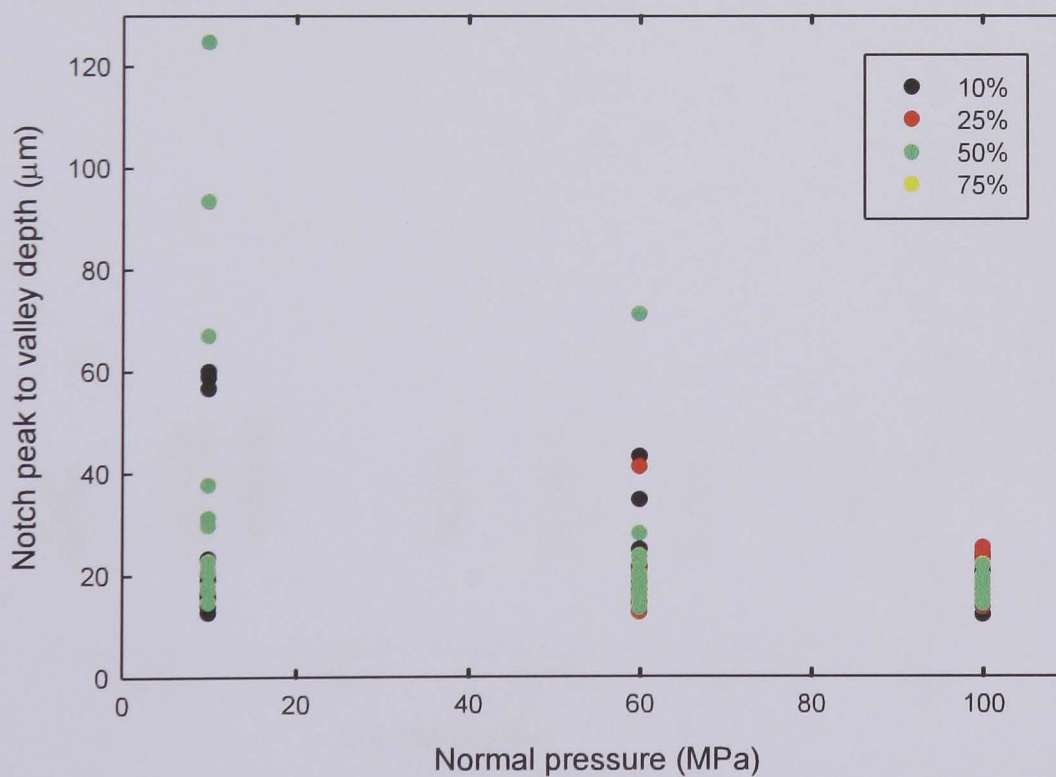


Figure 4.81: The notch peak to valley depths resulting from fretting fatigue tests conducted with an aluminium alloy 2024 T351 bridge in contact with a peened aluminium alloy 2024 T351 specimen subjected to an axial stress amplitude of 125 MPa.

Analyses of the results presented in Figures 4.79, 4.80 and 4.81 indicate that:

- There is no correlation between notch peak to valley depth and percentage life for any of the normal pressures applied;
- For an axial stress amplitude of 70 MPa and 100 MPa there is no correlation between notch peak to valley depth and normal pressure;
- For an axial stress amplitude of 125 MPa notch peak to valley depth decreases with increasing normal pressure.

The formation of the scars over the life of a specimen was also investigated. Plots for an axial stress amplitude of 70 MPa are shown in Figures 4.82 and 4.83, which show no correlation between notch peak to valley depth and the number of cycles applied. The greatest peak to valley depth recorded for this axial stress amplitude was 84 μm .

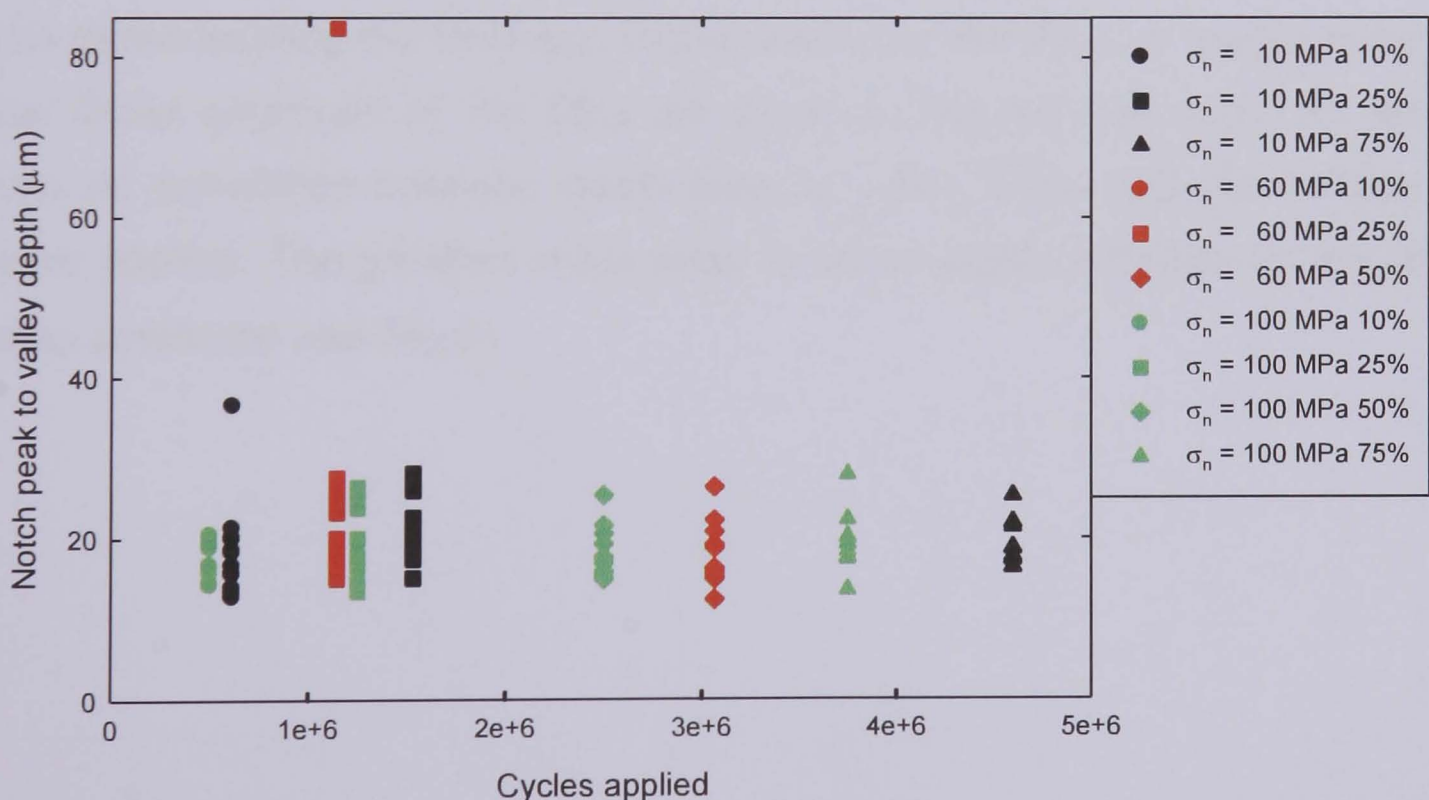


Figure 4.82: The evolution, in terms of the number of cycles applied, of notch peak to valley depth over the lives of peened specimens subjected to three normal pressures and an axial stress amplitude of 70 MPa.

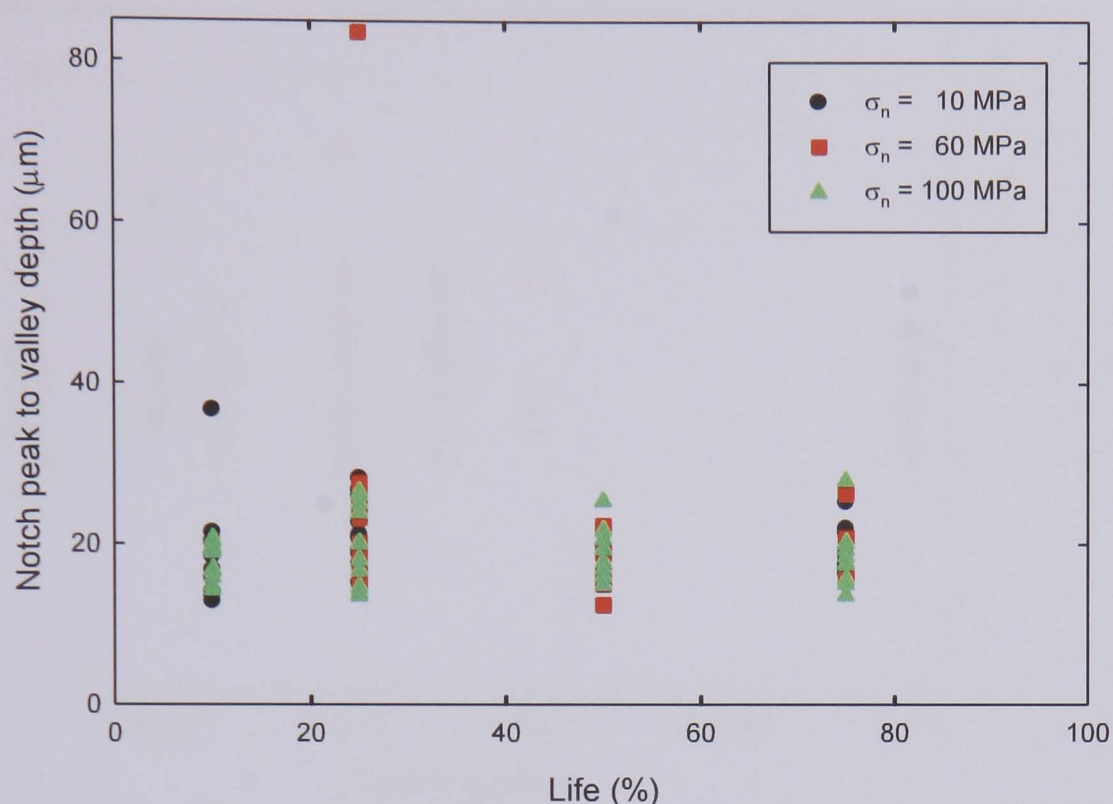


Figure 4.83: The evolution, in terms of percentage life, of notch peak to valley depth over the lives of peened specimens subjected to three normal pressures and an axial stress amplitude of 70 MPa.

Plots demonstrating the formation of the scars over the life of a specimen for an axial stress amplitude of 100 MPa are shown in Figures 4.84 and 4.85, which show no correlation between notch peak to valley depth and the number of cycles applied. The greatest notch peak to valley depth recorded for this axial stress amplitude was 36 μm

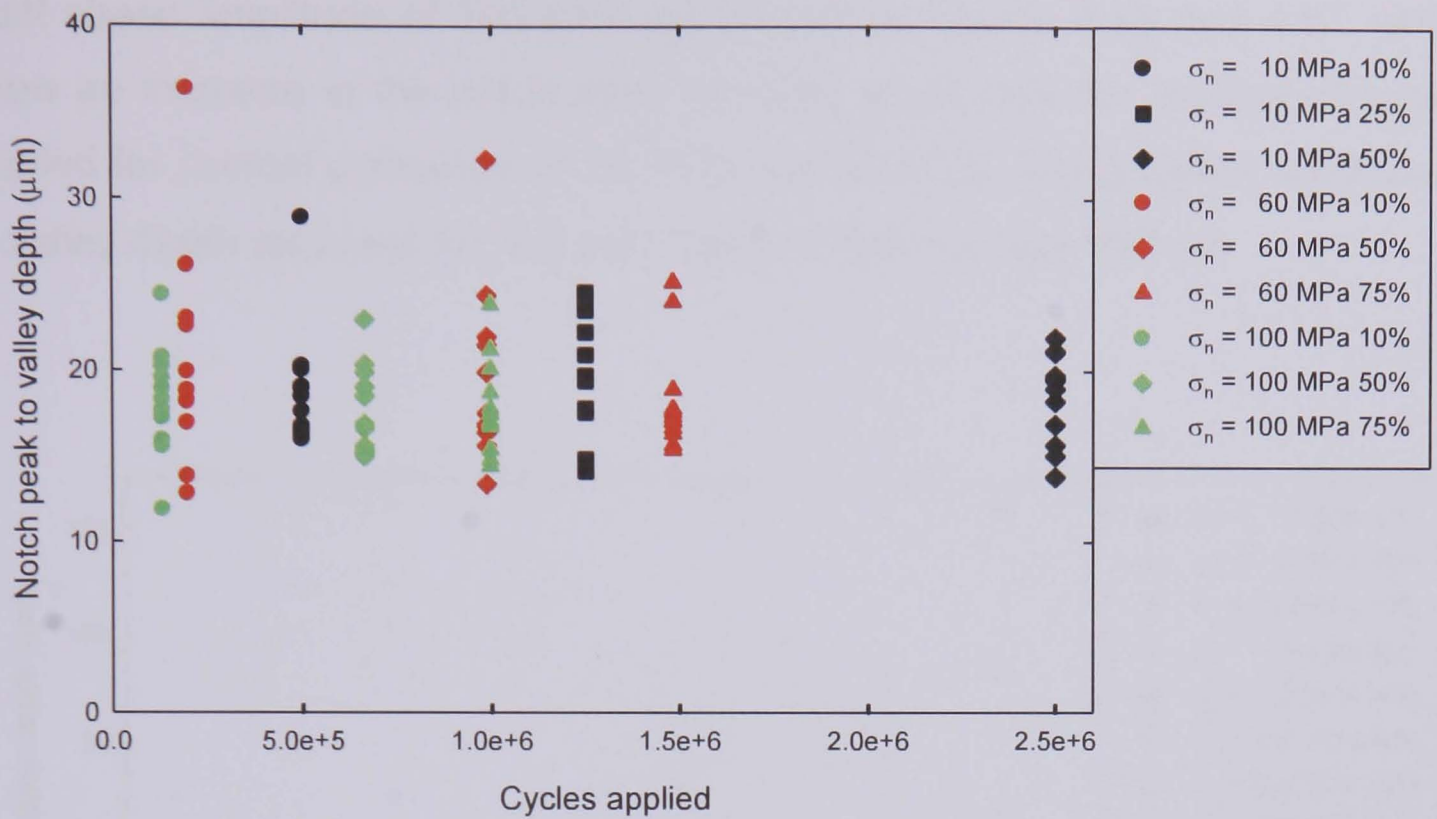


Figure 4.84: The evolution, in terms of the number of cycles applied, of notch peak to valley depth over the lives of peened specimens subjected to three normal pressures and an axial stress amplitude of 100 MPa.

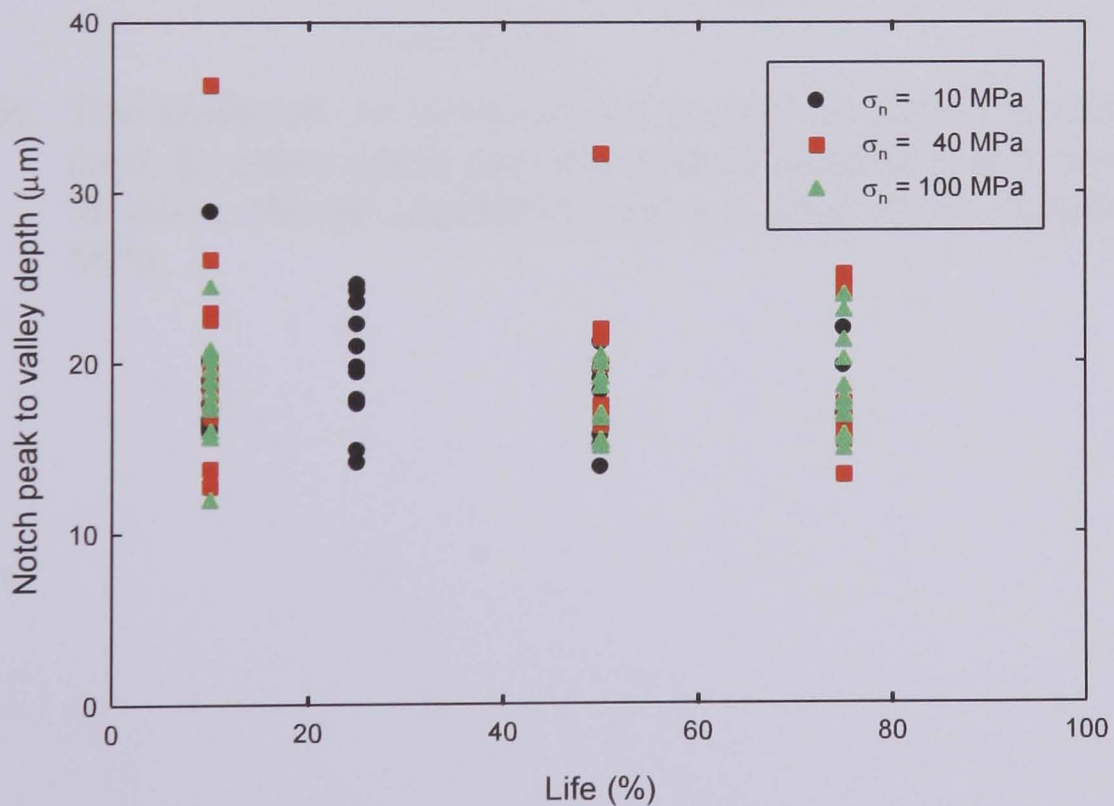


Figure 4.85: The evolution, in terms of percentage life, of notch peak to valley depth over the lives of peened specimens subjected to three normal pressures and an axial stress amplitude of 100 MPa.

Plots demonstrating the formation of the scars over the life of a specimen for an axial stress amplitude of 125 MPa are shown in Figures 4.86 and 4.87, which show an increase in the notch peak to valley depth and the number of cycles applied for normal pressures of 10 MPa and 60 MPa. The greatest notch peak to valley depth recorded for this axial stress amplitude was 125 μm

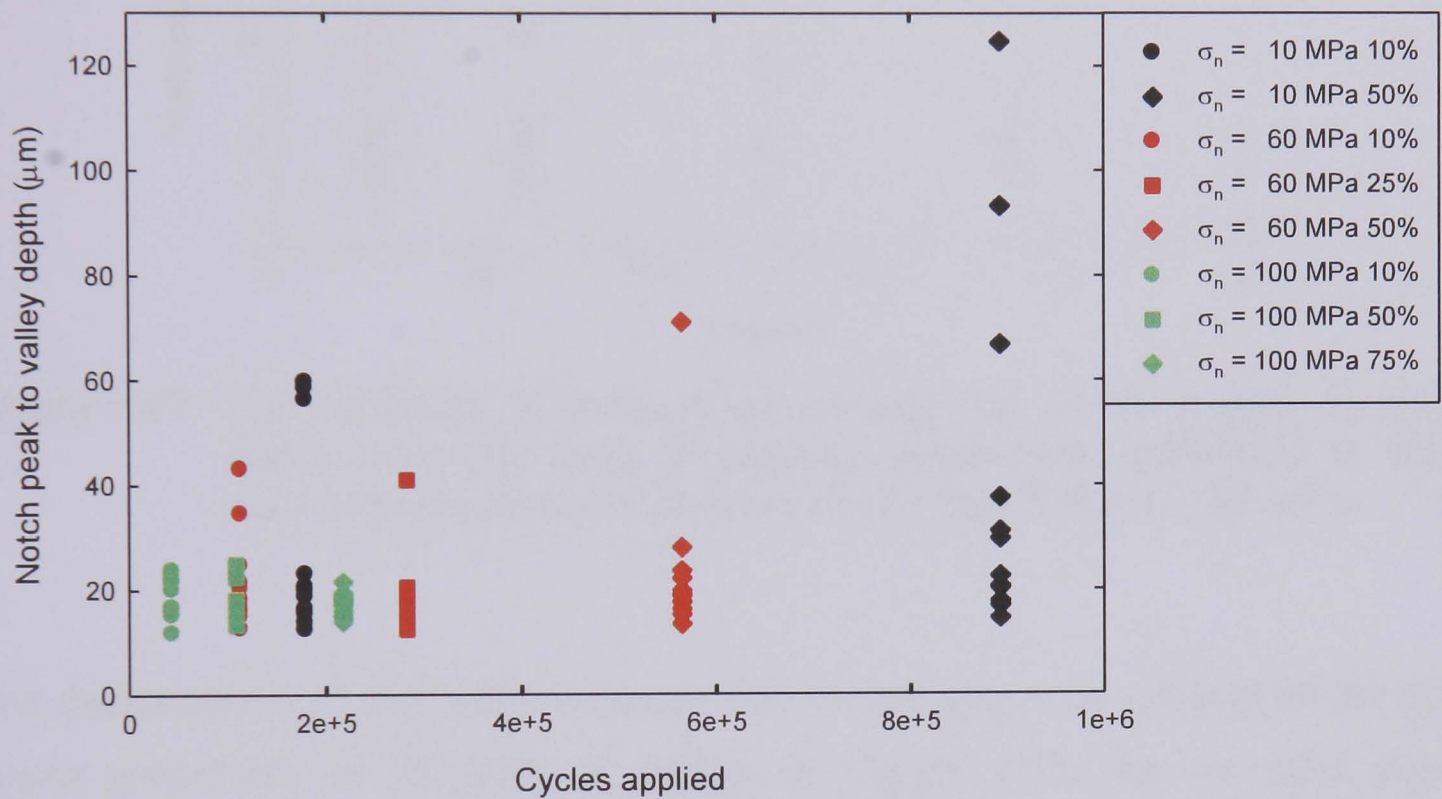


Figure 4.86: The evolution, in terms of the number of cycles applied, of notch peak to valley depth over the lives of peened specimens subjected to three normal pressures and an axial stress amplitude of 125 MPa.

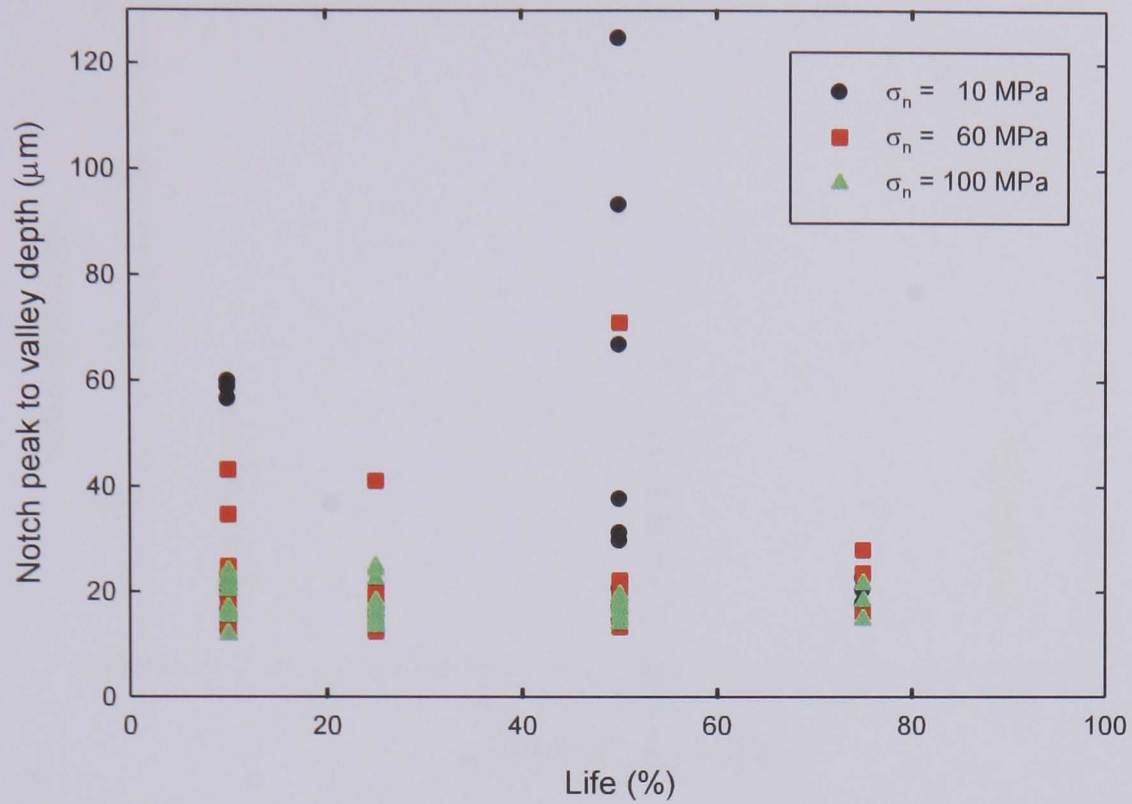


Figure 4.87: The evolution, in terms of percentage life, of notch peak to valley depth over the lives of peened specimens subjected to three normal pressures and an axial stress amplitude of 125 MPa.

The dependence of the notch width on the normal pressure applied for an axial stress amplitude of 70 MPa is shown in Figure 4.88, for an axial stress amplitude of 100 MPa is shown in Figure 4.89 and for an axial stress amplitude of 125 MPa is shown in Figure 4.90.

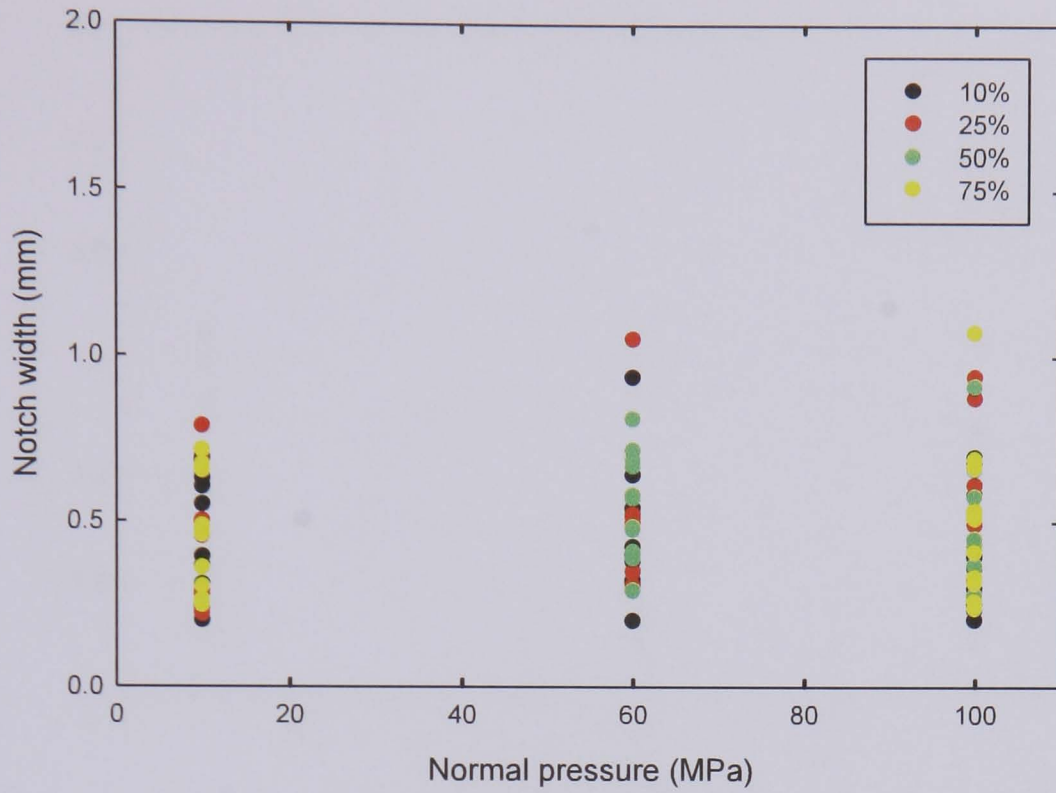


Figure 4.88: The notch widths resulting from fretting fatigue tests conducted with an aluminium alloy 2024 T351 bridge in contact with a peened aluminium alloy 2024 T351 specimen subjected to an axial stress amplitude of 70 MPa.

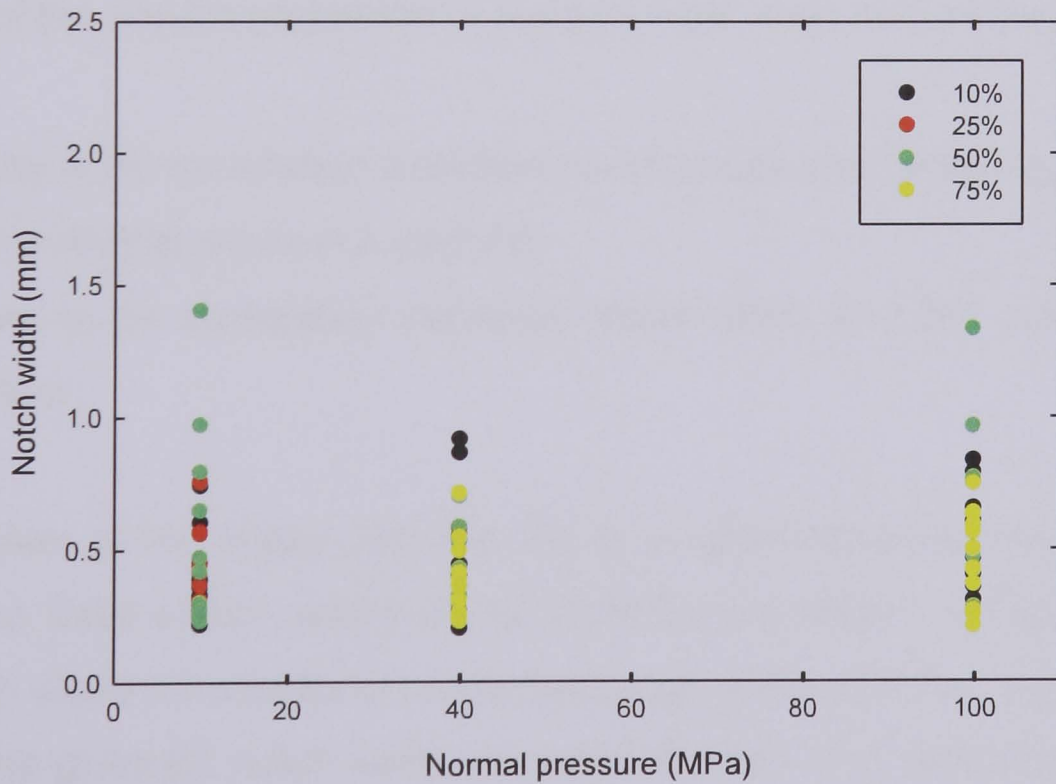


Figure 4.89: The notch widths resulting from fretting fatigue tests conducted with an aluminium alloy 2024 T351 bridge in contact with a peened aluminium alloy 2024 T351 specimen subjected to an axial stress amplitude of 100 MPa.

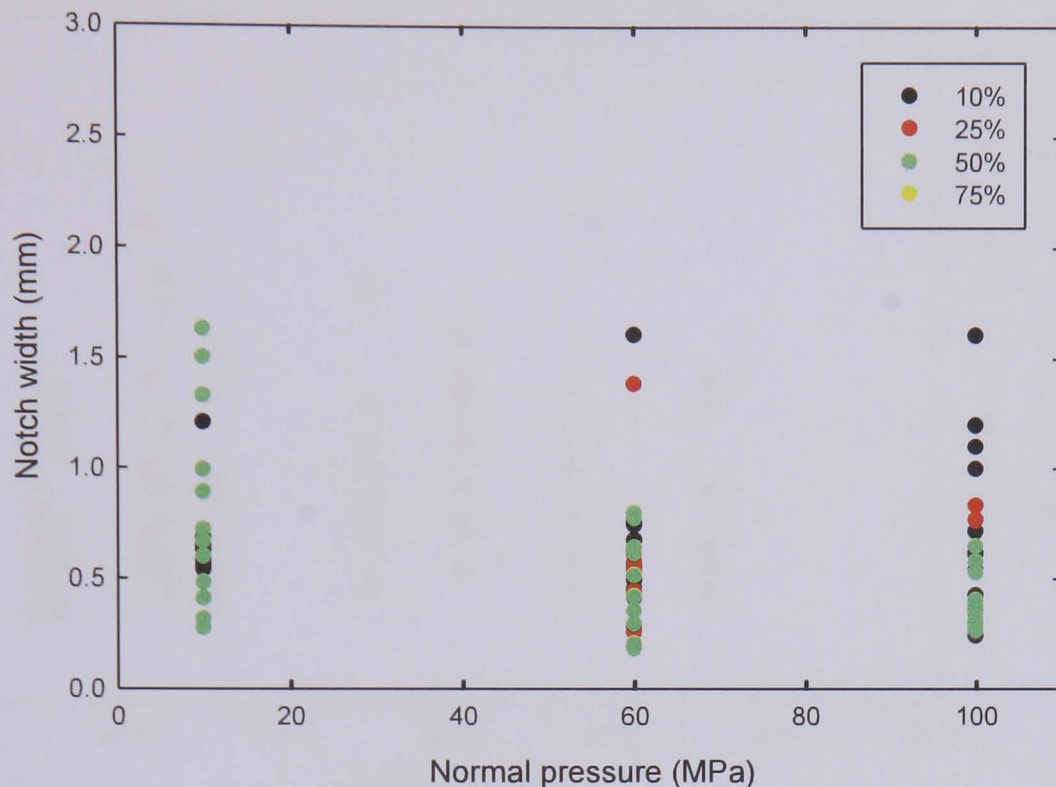


Figure 4.90: The notch widths resulting from fretting fatigue tests conducted with an aluminium alloy 2024 T351 bridge in contact with a peened aluminium alloy 2024 T351 specimen subjected to an axial stress amplitude of 125 MPa.

Analyses of the results presented in Figures 4.88, 4.89 and 4.90 indicate that:

- There is no correlation between notch width and percentage life for any of the normal pressures applied;
- There is no correlation between notch width and the normal pressure applied.

The formation of the scars over the life of a specimen was also investigated. Plots for an axial stress amplitude of 70 MPa are shown in Figures 4.91 and 4.92, which show no correlation between notch width and the number of cycles applied. The greatest notch width recorded for this axial stress amplitude was 1.07 mm.

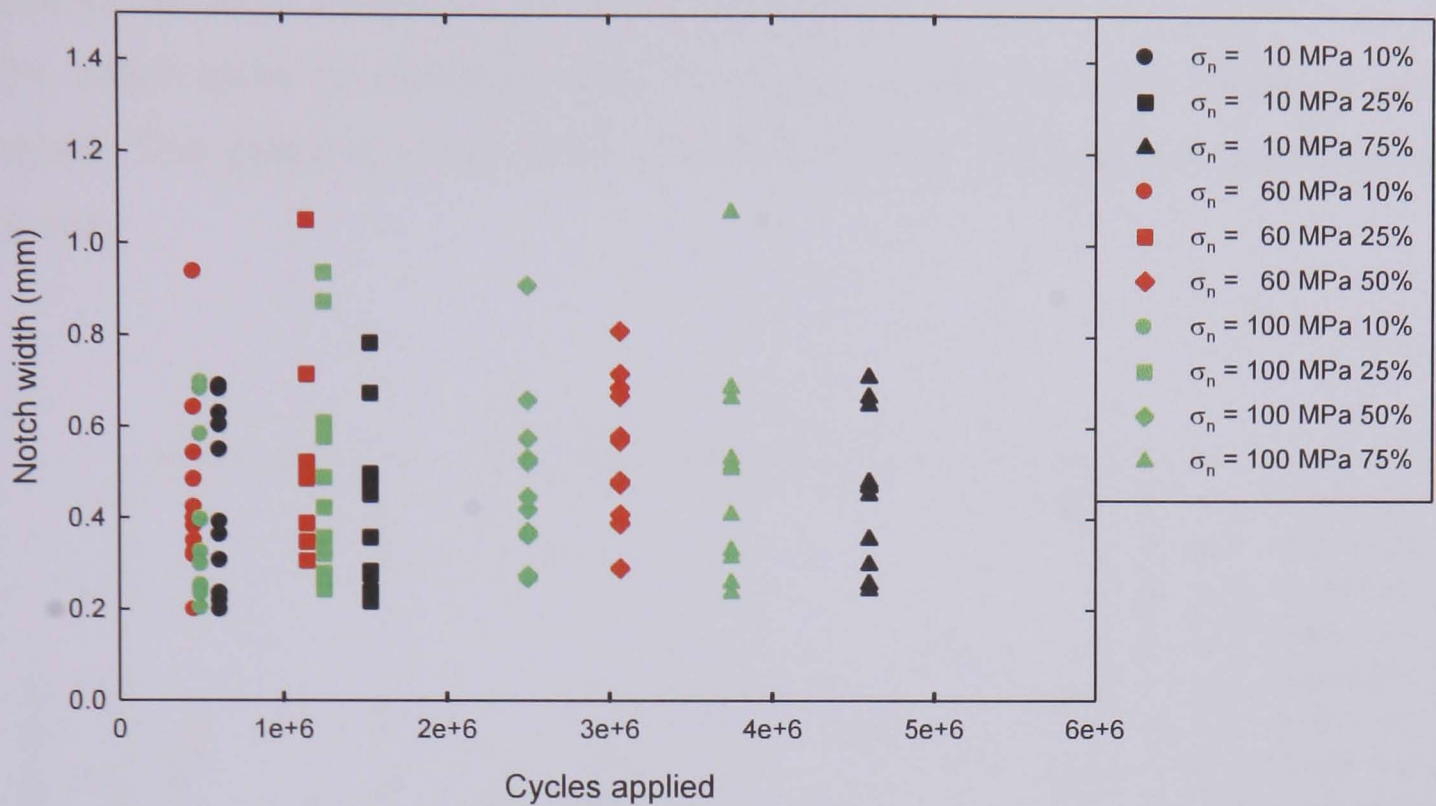


Figure 4.91: The evolution, in terms of the number of cycles applied, of notch width over the lives of peened specimens subjected to three normal pressures and an axial stress amplitude of 70 MPa.

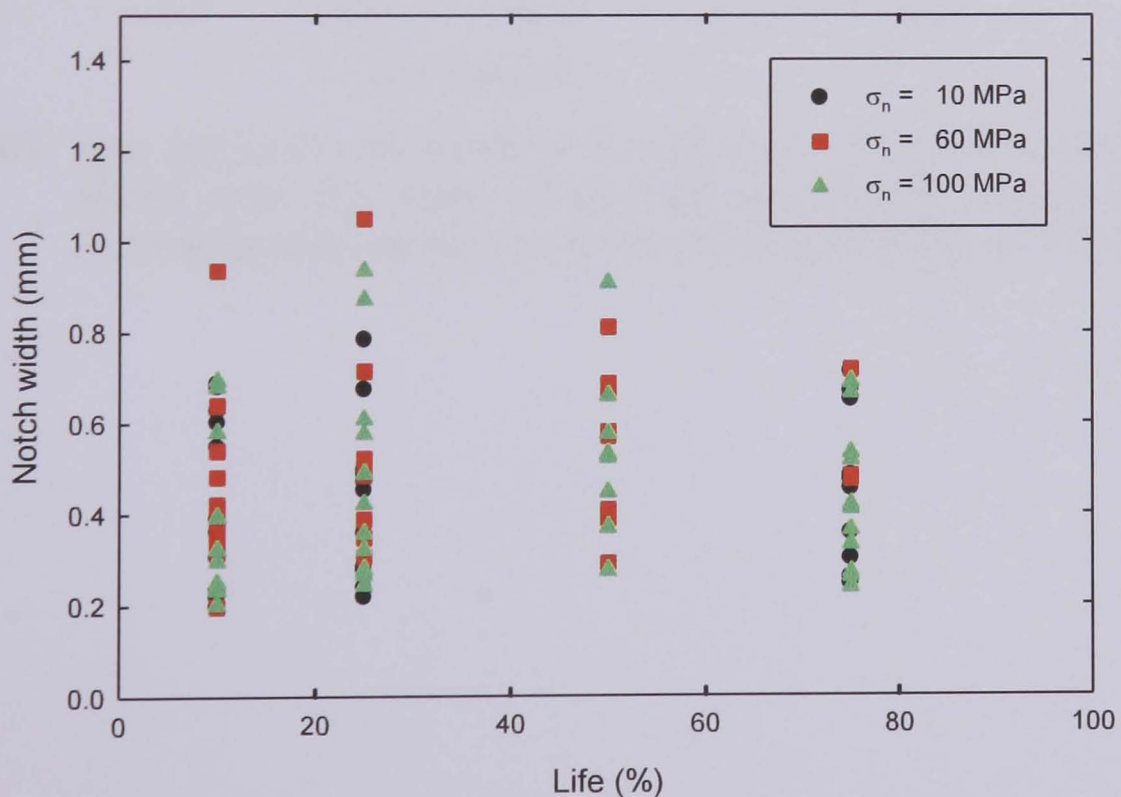


Figure 4.92: The evolution, in terms of percentage life, of notch width over the lives of peened specimens subjected to three normal pressures and an axial stress amplitude of 70 MPa.

The formation of the scars over the life of a specimen was also investigated. Plots for an axial stress amplitude of 100 MPa are shown in Figures 4.93 and 4.94, which show no correlation between notch width and the number of cycles applied. The greatest notch width recorded for this axial stress amplitude was 1.4 mm.

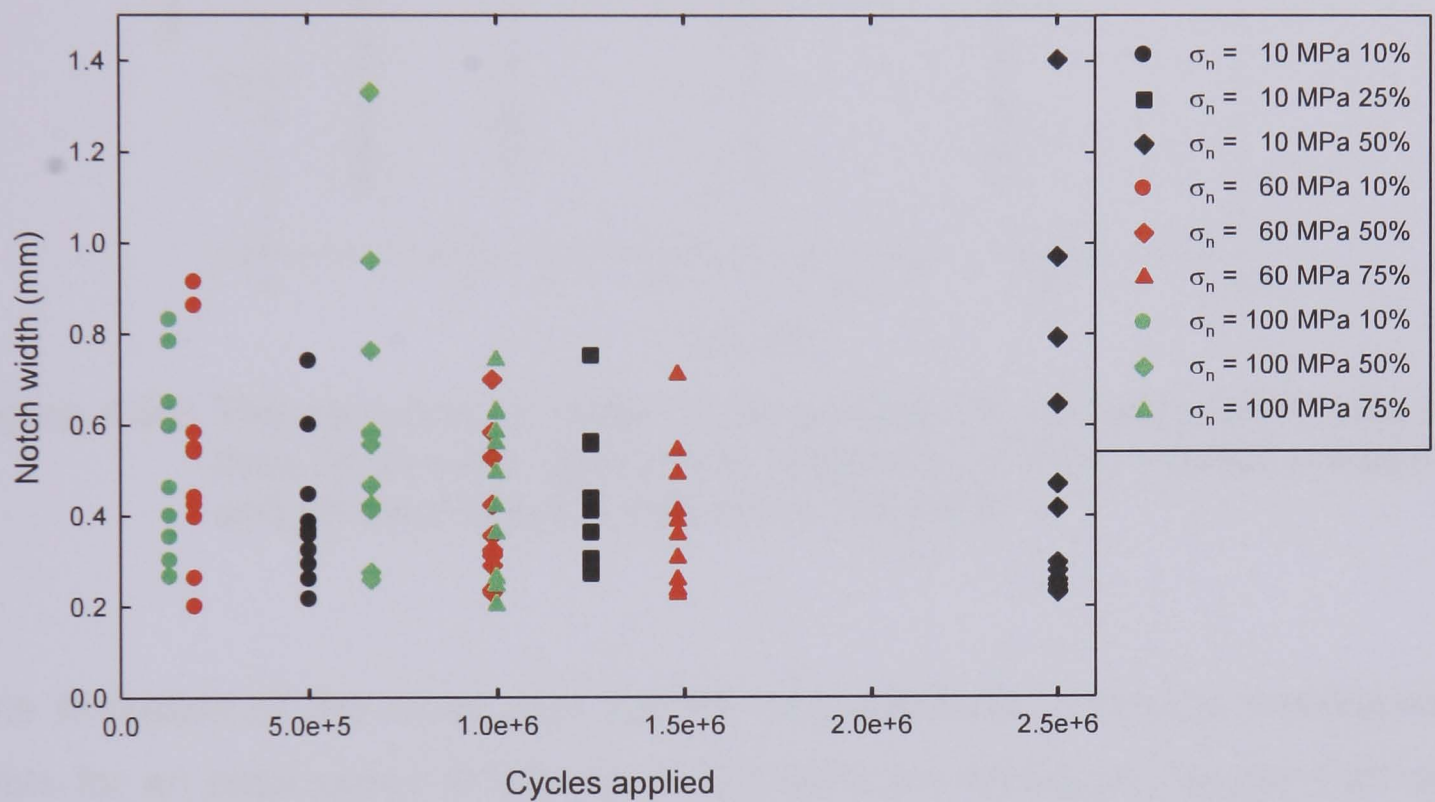


Figure 4.93: The evolution, in terms of the number of cycles applied, of notch width over the lives of peened specimens subjected to three normal pressures and an axial stress amplitude of 100 MPa.

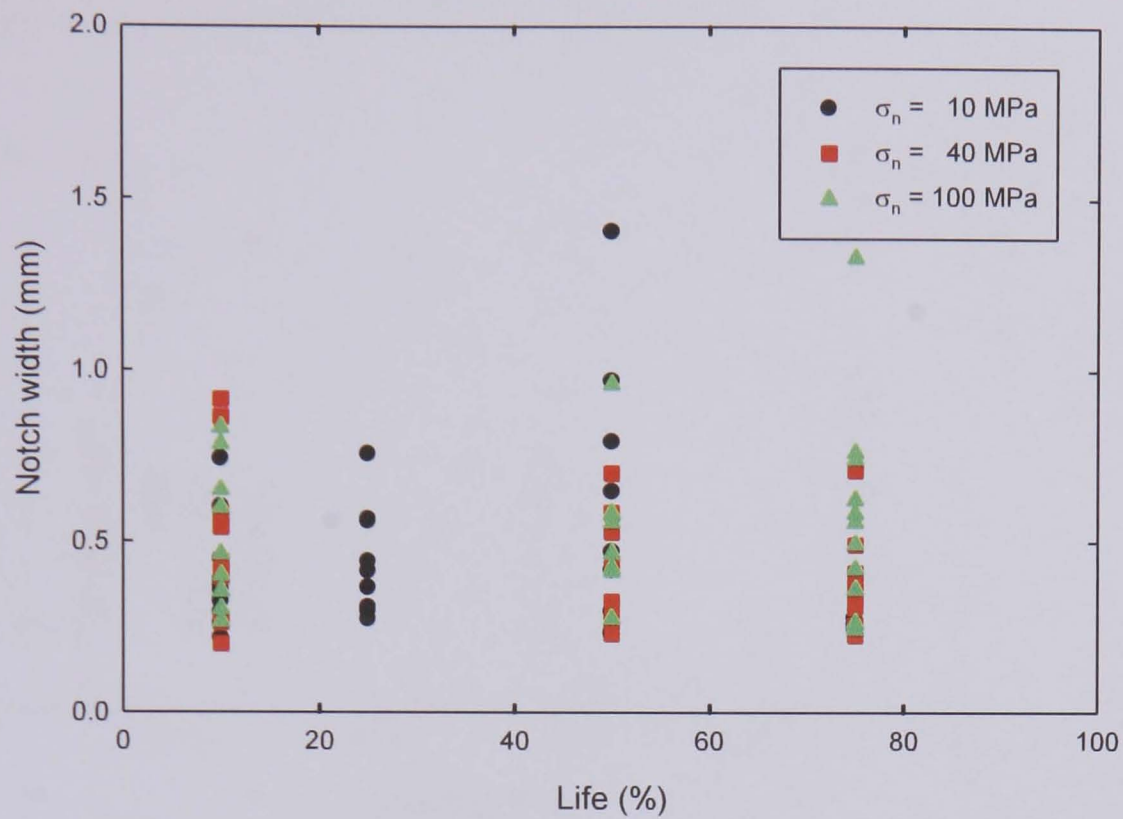


Figure 4.94: The evolution, in terms of percentage life, of notch width over the lives of peened specimens subjected to three normal pressures and an axial stress amplitude of 100 MPa.

The formation of the scars over the life of a specimen was also investigated. Plots for an axial stress amplitude of 125 MPa are shown in Figures 4.95 and 4.96, which show no correlation between notch width and the number of cycles applied, except at 10 MPa normal pressure, where notch width develops with further cycling. The greatest notch width recorded for this axial stress amplitude was 1.63 mm.

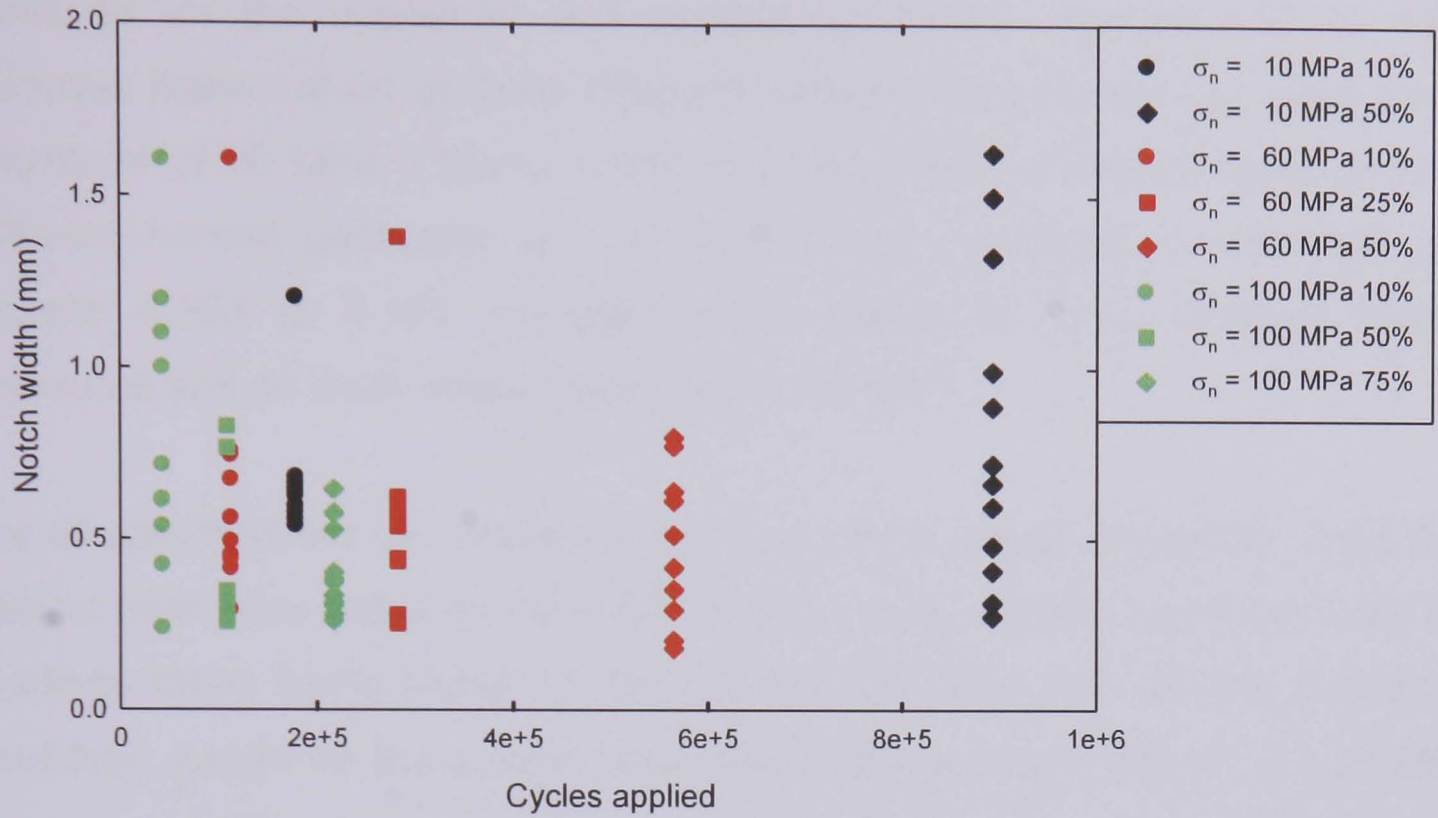


Figure 4.95: The evolution, in terms of the number of cycles applied, of notch width over the lives of peened specimens subjected to three normal pressures and an axial stress amplitude of 125 MPa.

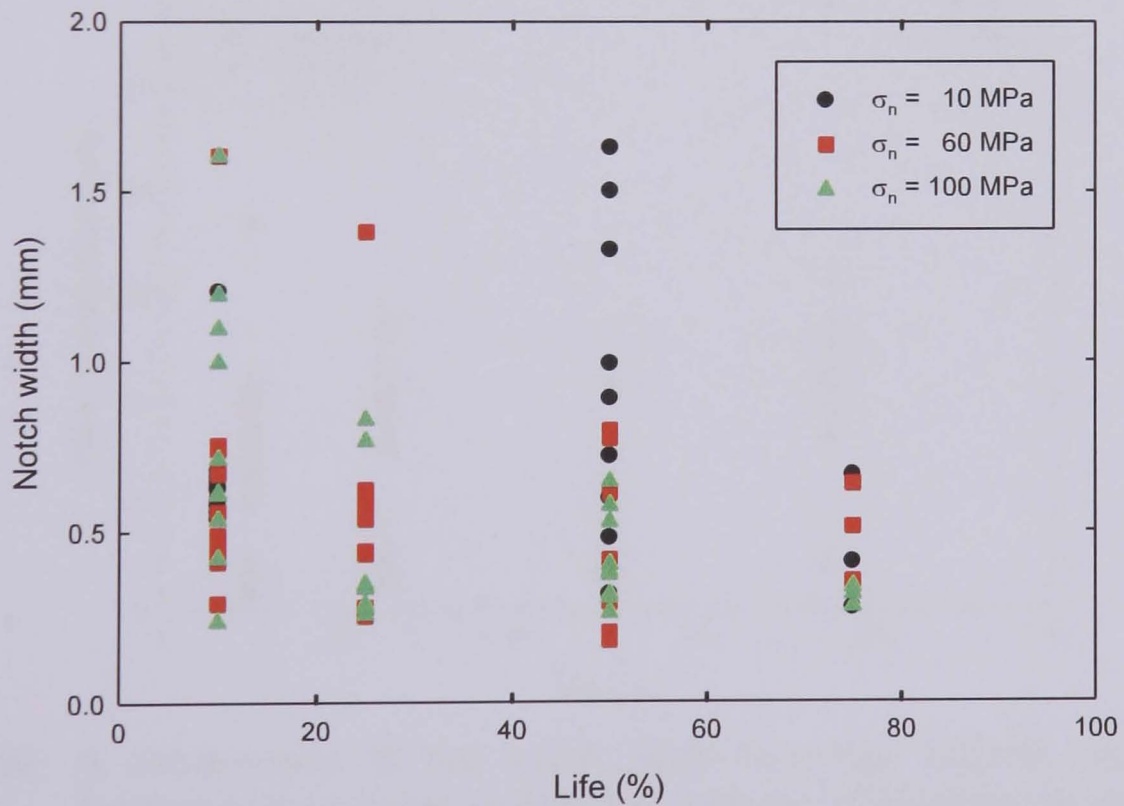


Figure 4.96: The evolution, in terms of percentage life, of notch width over the lives of peened specimens subjected to three normal pressures and an axial stress amplitude of 125 MPa.

Figures 4.97 to 4.105 compare the values of notch peak to valley depth achieved for the unpeened and peened conditions. Figures 4.97 to 4.99, compare these values at three different normal pressures and an axial stress amplitude of 70 MPa, Figures 4.100 to 4.102, compare these values at three different normal pressures and an axial stress amplitude of 100 MPa and Figures 4.103 to 4.105, compare these values at three different normal pressures and an axial stress amplitude of 125 MPa.

For all combinations of normal pressure and axial stress amplitude, there is a distinct difference between the notch peak to valley depths achieved, with the readings taken being higher for the peened condition than for the unpeened condition, except for the special case identified previously, where $\sigma_a = 70$ MPa and $\sigma_n = 10$ MPa, where the notch peak to valley depth increases throughout life, see Figure 4.109.

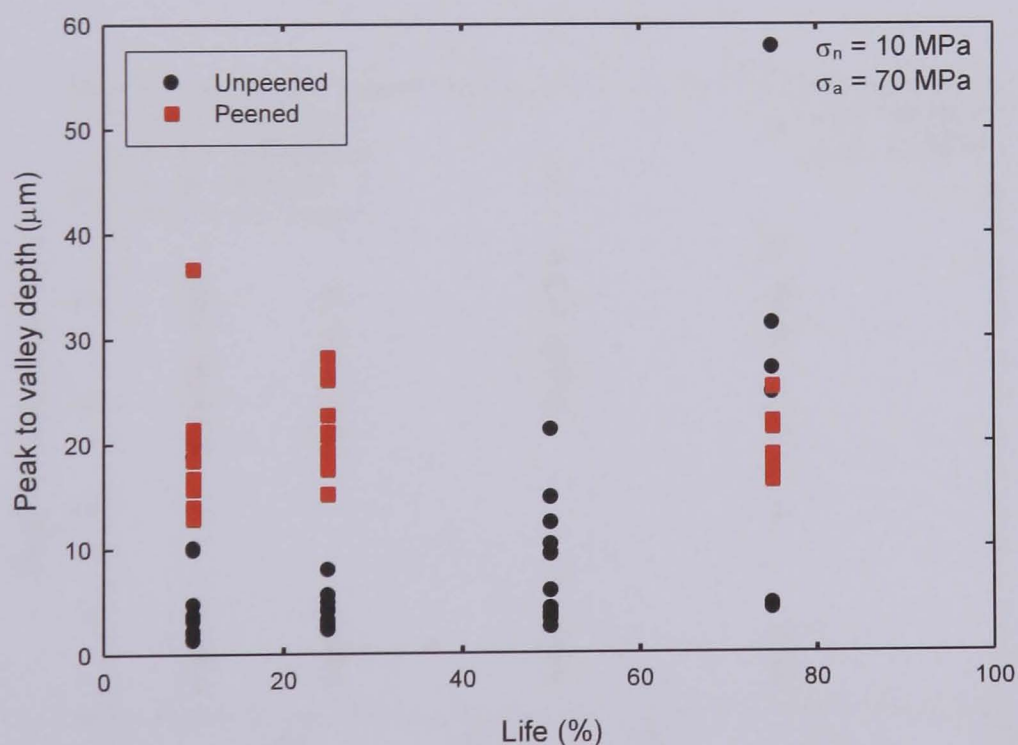


Figure 4.97: A comparison of the notch peak to valley depths resulting from fretting fatigue tests conducted with an aluminium alloy 2024 T351 bridge in contact with both unpeened and peened aluminium alloy 2024 T351 specimens subjected to a normal pressure of 10 MPa and an axial stress amplitude of 70 MPa.

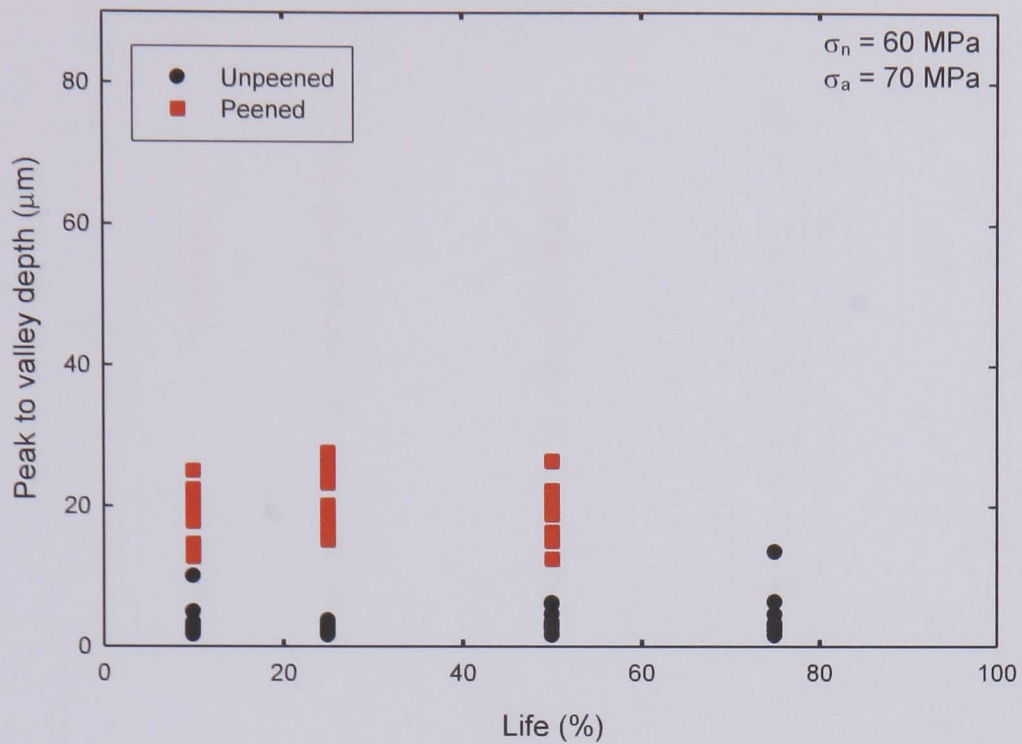


Figure 4.98: A comparison of the notch peak to valley depths resulting from fretting fatigue tests conducted with an aluminium alloy 2024 T351 bridge in contact with both unpeened and peened aluminium alloy 2024 T351 specimens subjected to a normal pressure of 60 MPa and an axial stress amplitude of 70 MPa.

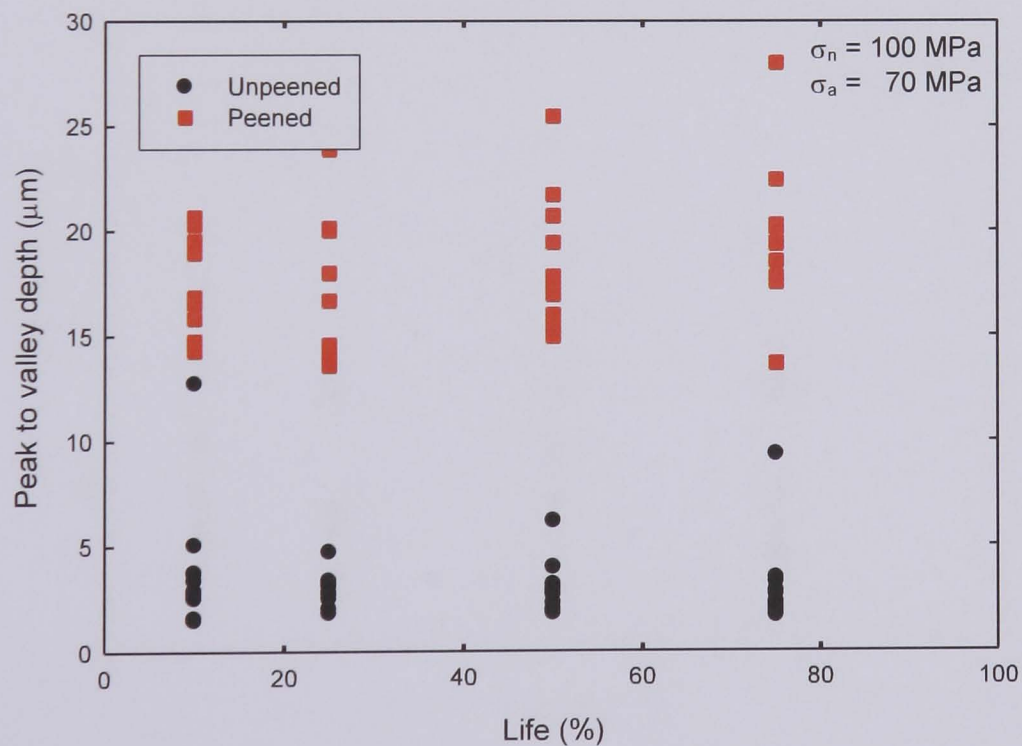


Figure 4.99: A comparison of the notch peak to valley depths resulting from fretting fatigue tests conducted with an aluminium alloy 2024 T351 bridge in contact with both unpeened and peened aluminium alloy 2024 T351 specimens subjected to a normal pressure of 100 MPa and an axial stress amplitude of 70 MPa.

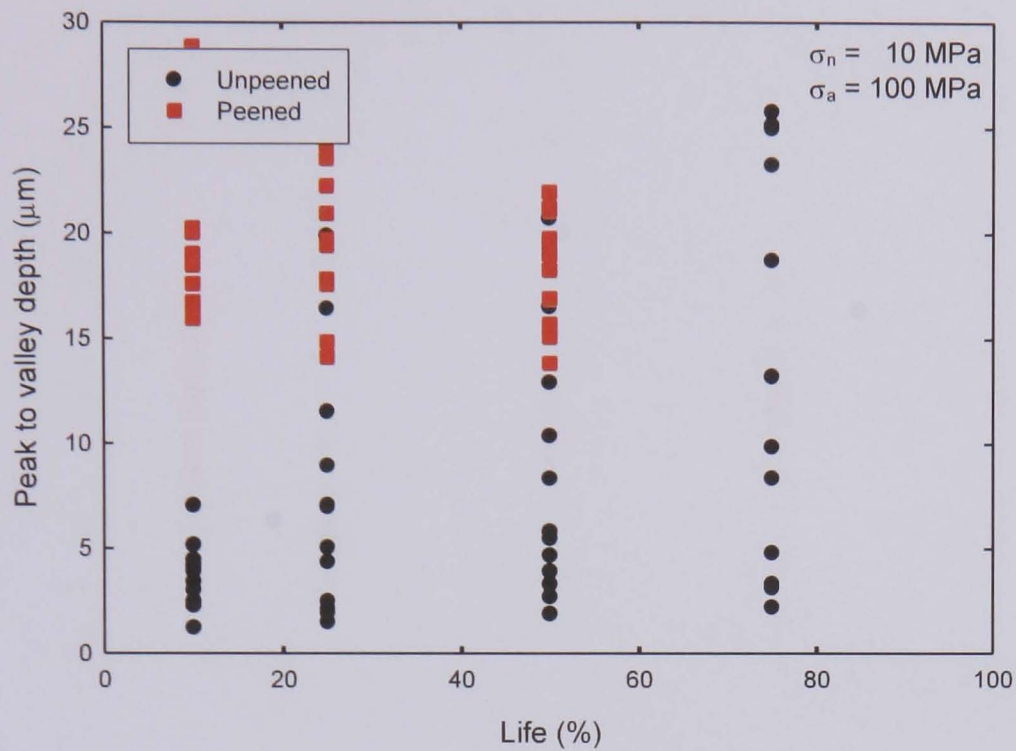


Figure 4.100: A comparison of the notch peak to valley depths resulting from fretting fatigue tests conducted with an aluminium alloy 2024 T351 bridge in contact with both unpeened and peened aluminium alloy 2024 T351 specimens subjected to a normal pressure of 10 MPa and an axial stress amplitude of 100 MPa.

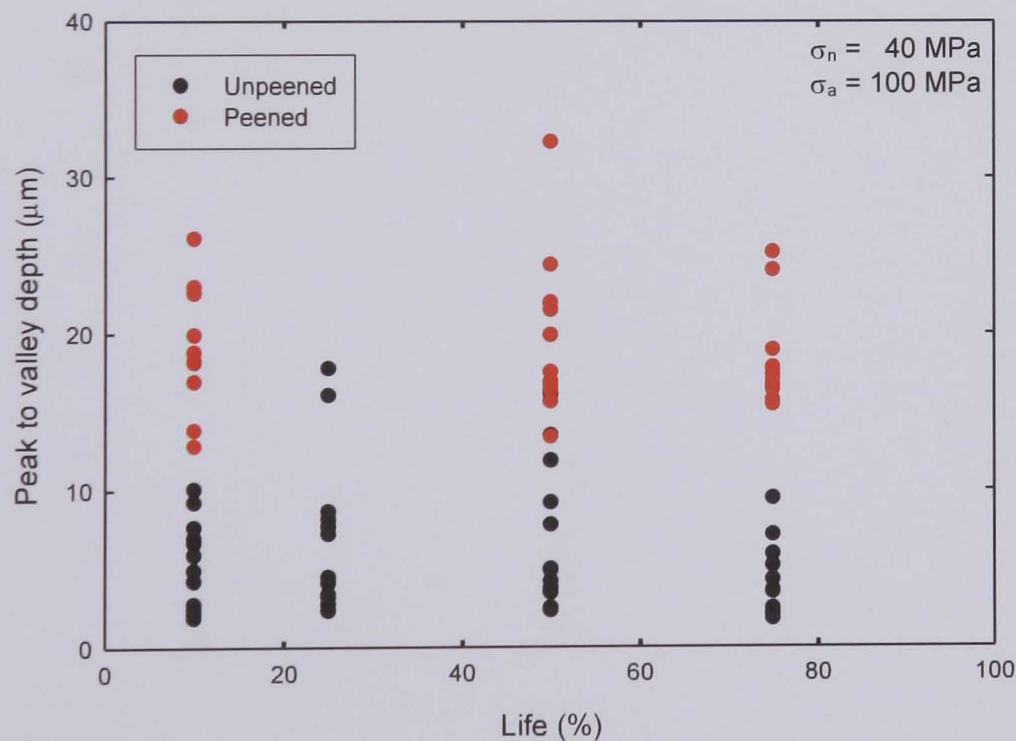


Figure 4.101: A comparison of the notch peak to valley depths resulting from fretting fatigue tests conducted with an aluminium alloy 2024 T351 bridge in contact with both unpeened and peened aluminium alloy 2024 T351 specimens subjected to a normal pressure of 40 MPa and an axial stress amplitude of 100 MPa.

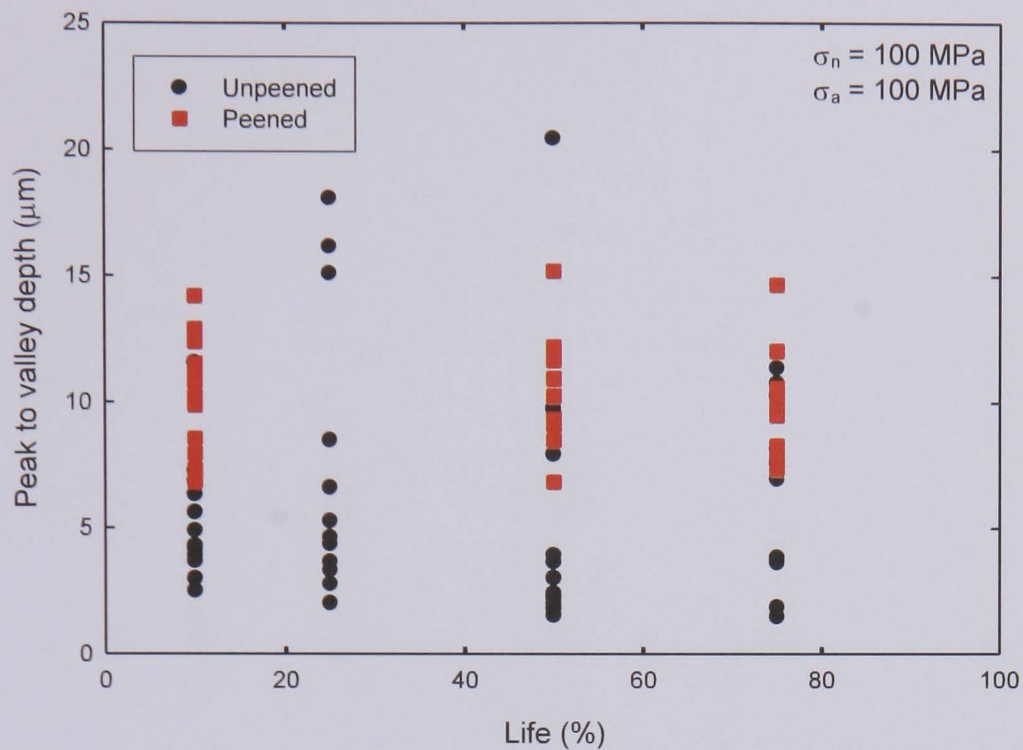


Figure 4.102: A comparison of the notch peak to valley depths resulting from fretting fatigue tests conducted with an aluminium alloy 2024 T351 bridge in contact with both unpeened and peened aluminium alloy 2024 T351 specimens subjected to a normal pressure of 100 MPa and an axial stress amplitude of 100 MPa.

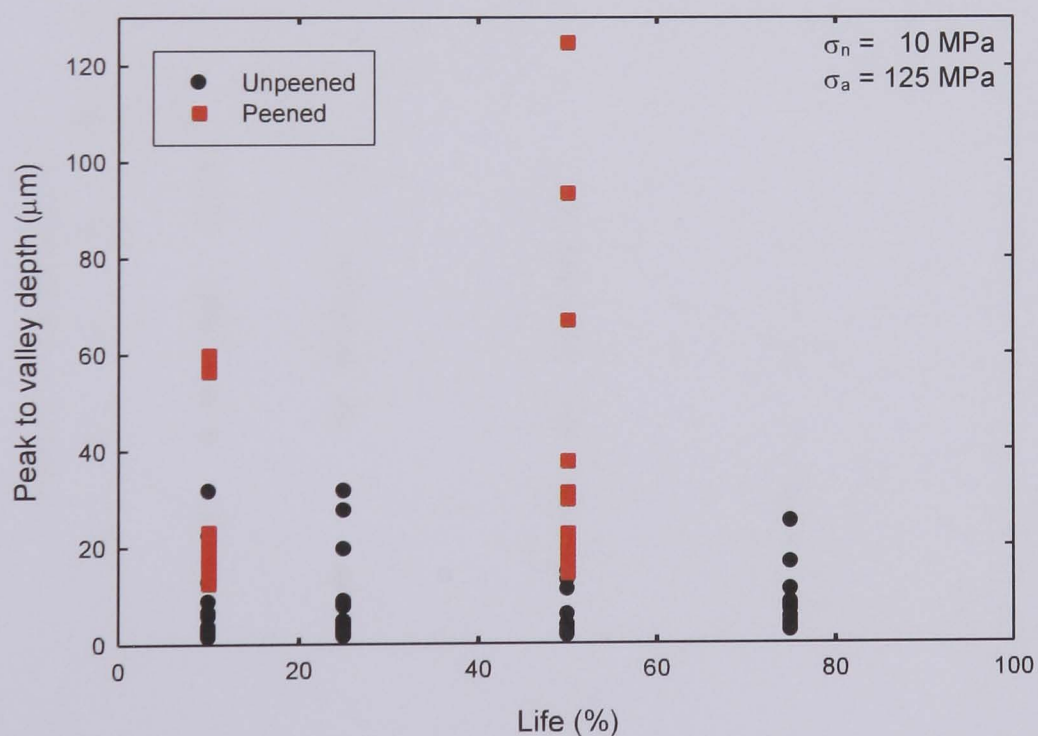


Figure 4.103: A comparison of the notch peak to valley depths resulting from fretting fatigue tests conducted with an aluminium alloy 2024 T351 bridge in contact with both unpeened and peened aluminium alloy 2024 T351 specimens subjected to a normal pressure of 10 MPa and an axial stress amplitude of 125 MPa.

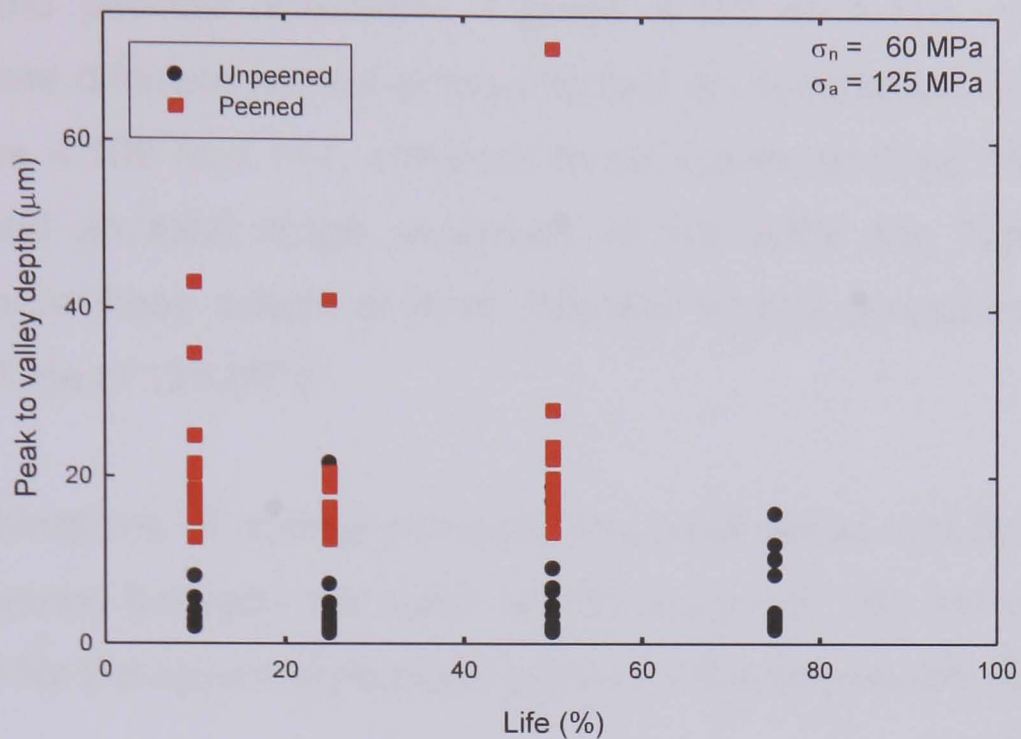


Figure 4.104: A comparison of the notch peak to valley depths resulting from fretting fatigue tests conducted with an aluminium alloy 2024 T351 bridge in contact with both unpeened and peened aluminium alloy 2024 T351 specimens subjected to a normal pressure of 60 MPa and an axial stress amplitude of 125 MPa.

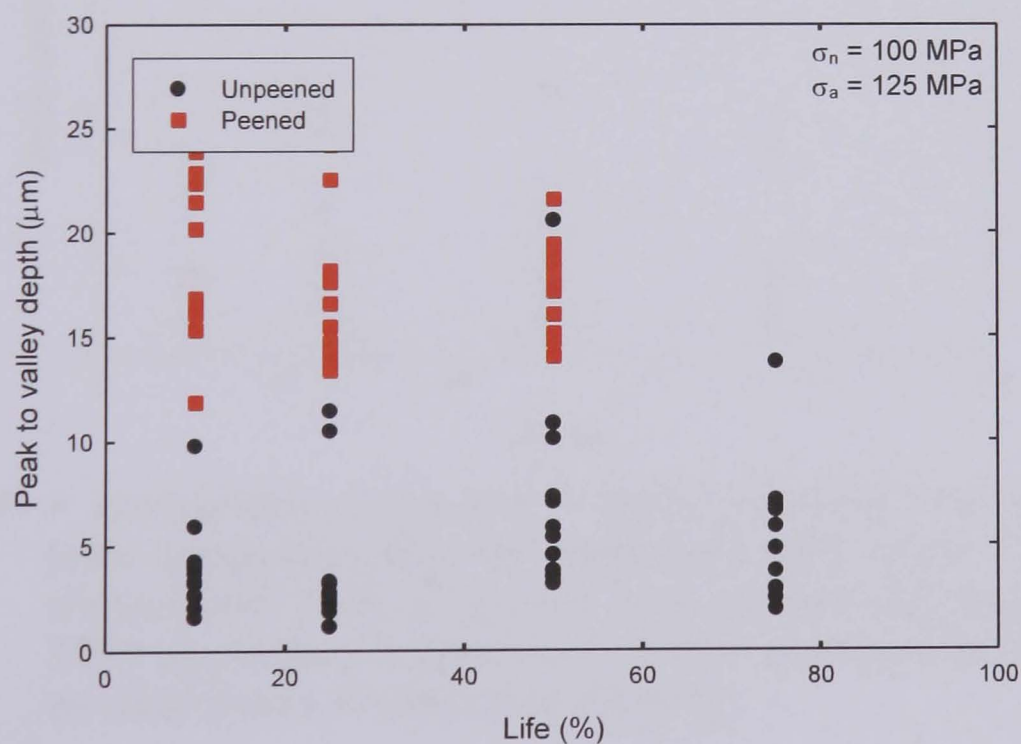


Figure 4.105: A comparison of the notch peak to valley depths resulting from fretting fatigue tests conducted with an aluminium alloy 2024 T351 bridge in contact with both unpeened and peened aluminium alloy 2024 T351 specimens subjected to a normal pressure of 100 MPa and an axial stress amplitude of 125 MPa.

Figures 4.106 to 4.114 compare the values of notch width achieved for the unpeened and peened conditions. Figures 4.106 to 4.120, compare these values at three different normal pressures and an axial stress amplitude of 70 MPa, Figures 4.109 to 4.111, compare these values at three different normal pressures and an axial stress amplitude of 100 MPa and Figures 4.112 to 4.114, compare these values at three different normal pressures and an axial stress amplitude of 125 MPa.

For all combinations of normal pressure and axial stress amplitude, there is a distinct difference between the notch widths achieved, with the readings taken being higher for the unpeened condition than for the peened condition.

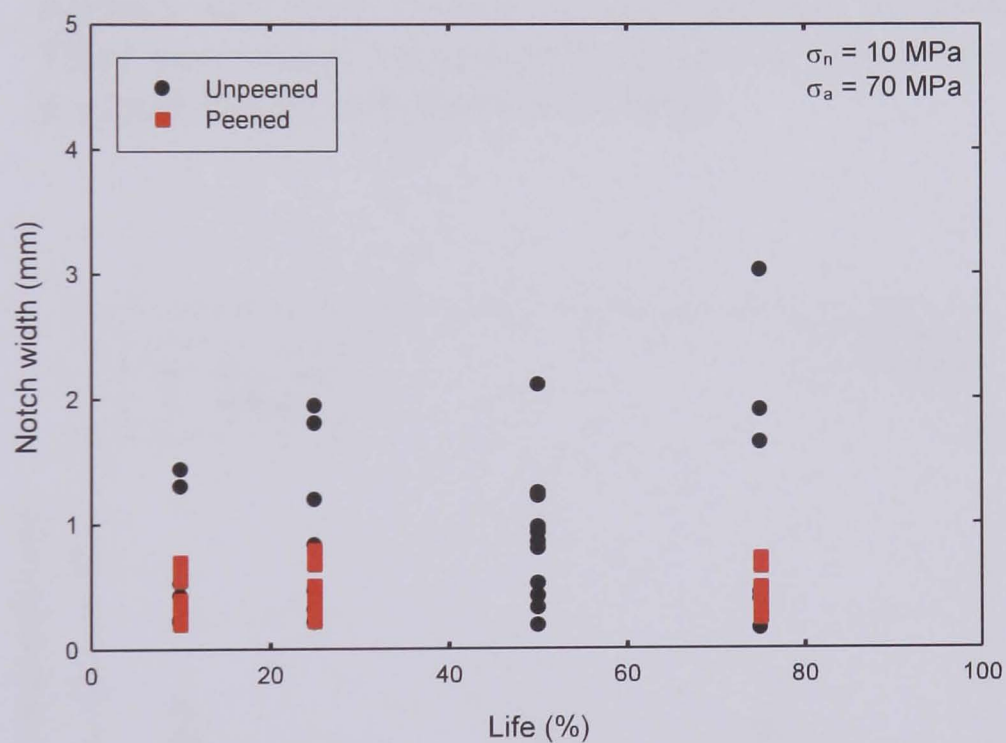


Figure 4.106: A comparison of the notch widths resulting from fretting fatigue tests conducted with an aluminium alloy 2024 T351 bridge in contact with both unpeened and peened aluminium alloy 2024 T351 specimens subjected to a normal pressure of 10 MPa and an axial stress amplitude of 70 MPa.

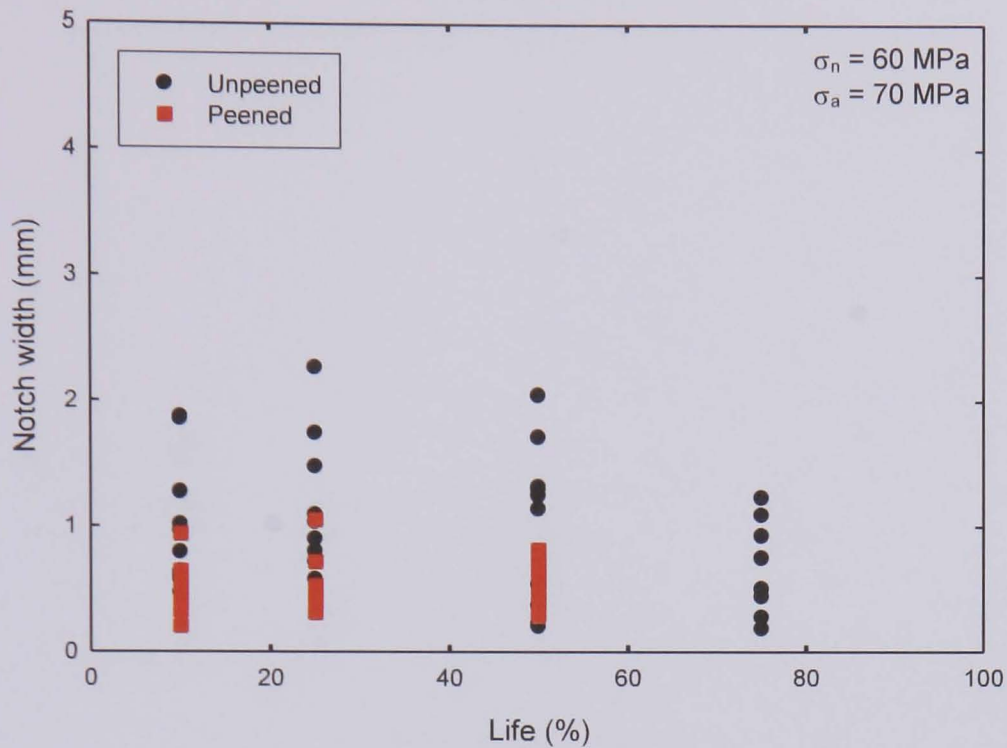


Figure 4.107: A comparison of the notch widths resulting from fretting fatigue tests conducted with an aluminium alloy 2024 T351 bridge in contact with both unpeened and peened aluminium alloy 2024 T351 specimens subjected to a normal pressure of 60 MPa and an axial stress amplitude of 70 MPa.

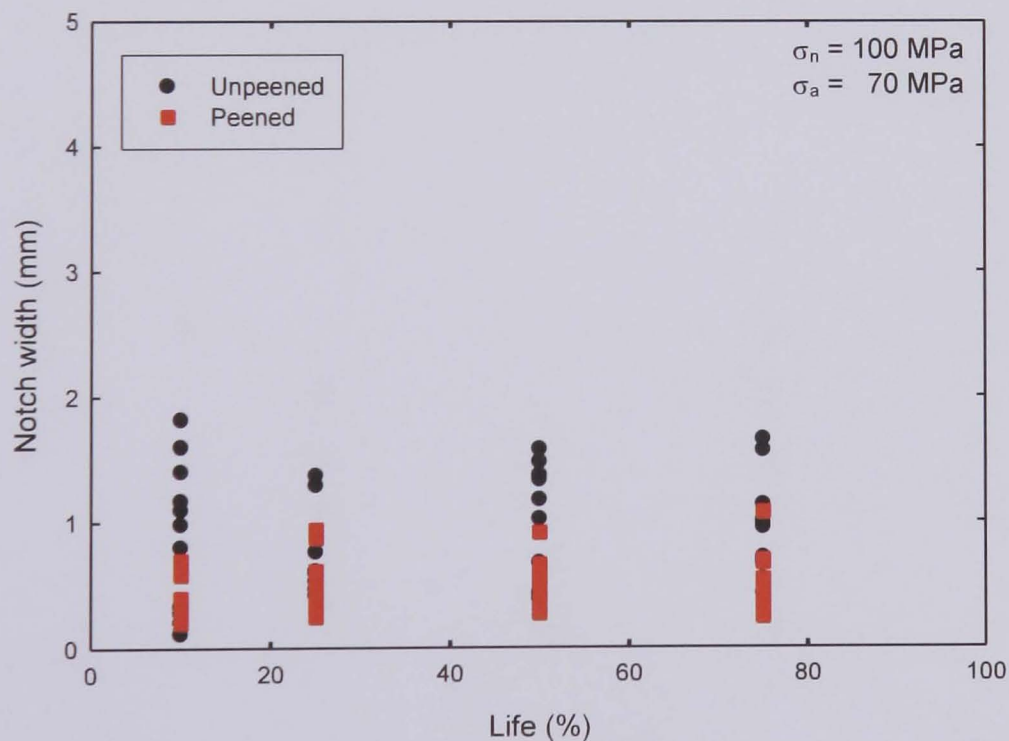


Figure 4.108: A comparison of the notch widths resulting from fretting fatigue tests conducted with an aluminium alloy 2024 T351 bridge in contact with both unpeened and peened aluminium alloy 2024 T351 specimens subjected to a normal pressure of 100 MPa and an axial stress amplitude of 70 MPa.

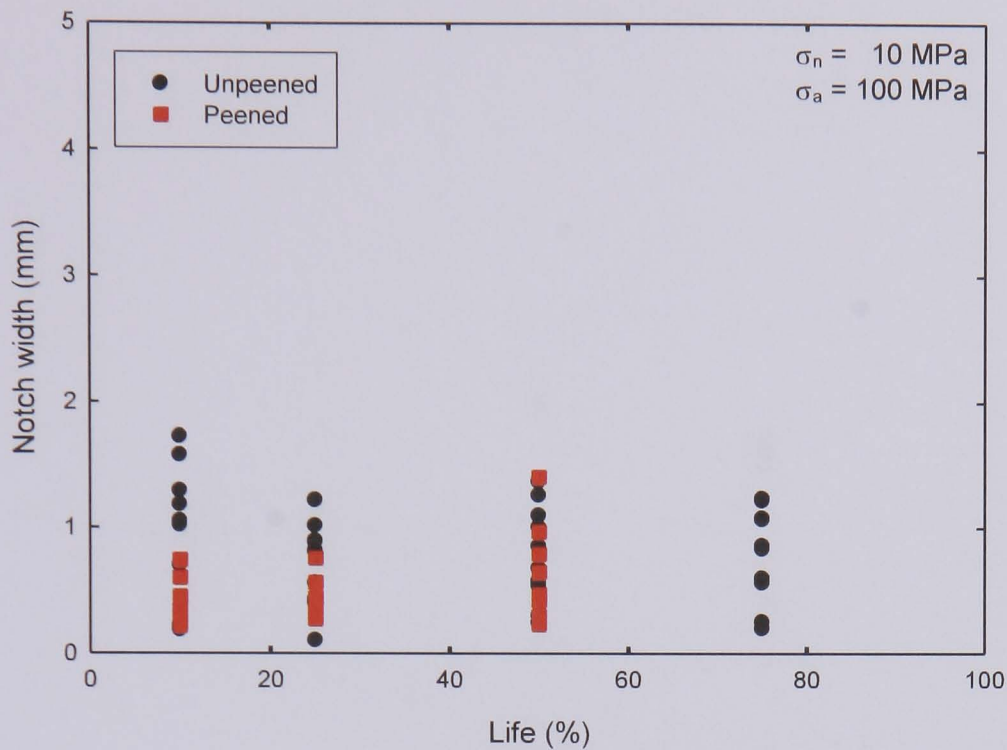


Figure 4.109: A comparison of the notch widths resulting from fretting fatigue tests conducted with an aluminium alloy 2024 T351 bridge in contact with both unpeened and peened aluminium alloy 2024 T351 specimens subjected to a normal pressure of 10 MPa and an axial stress amplitude of 100 MPa.

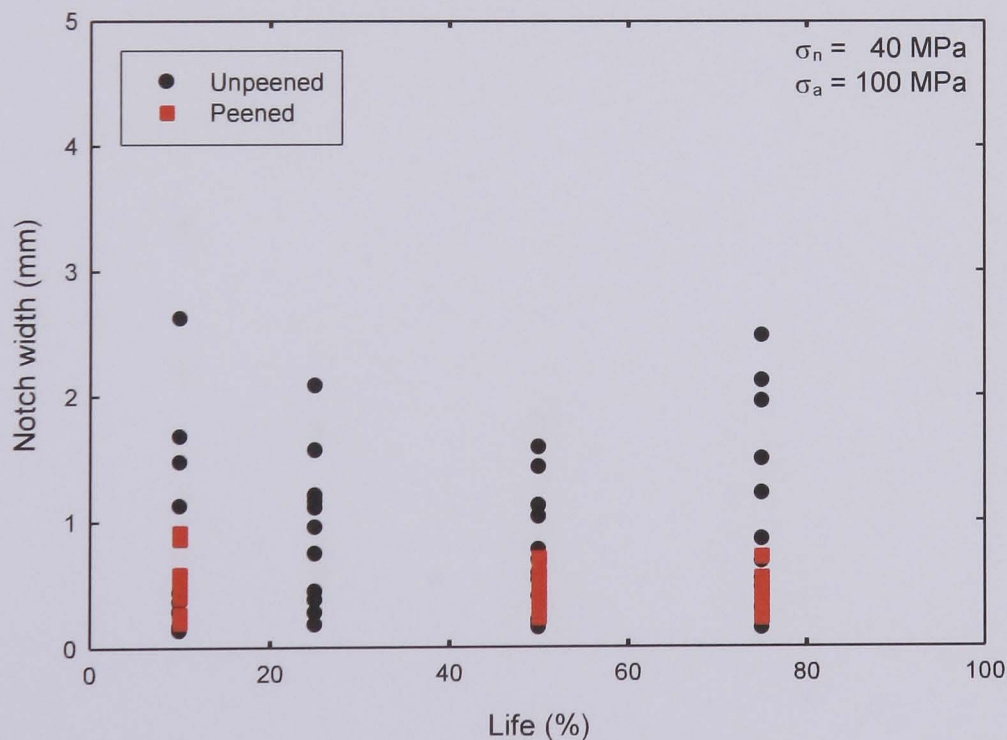


Figure 4.110: A comparison of the notch widths resulting from fretting fatigue tests conducted with an aluminium alloy 2024 T351 bridge in contact with both unpeened and peened aluminium alloy 2024 T351 specimens subjected to a normal pressure of 40 MPa and an axial stress amplitude of 100 MPa.

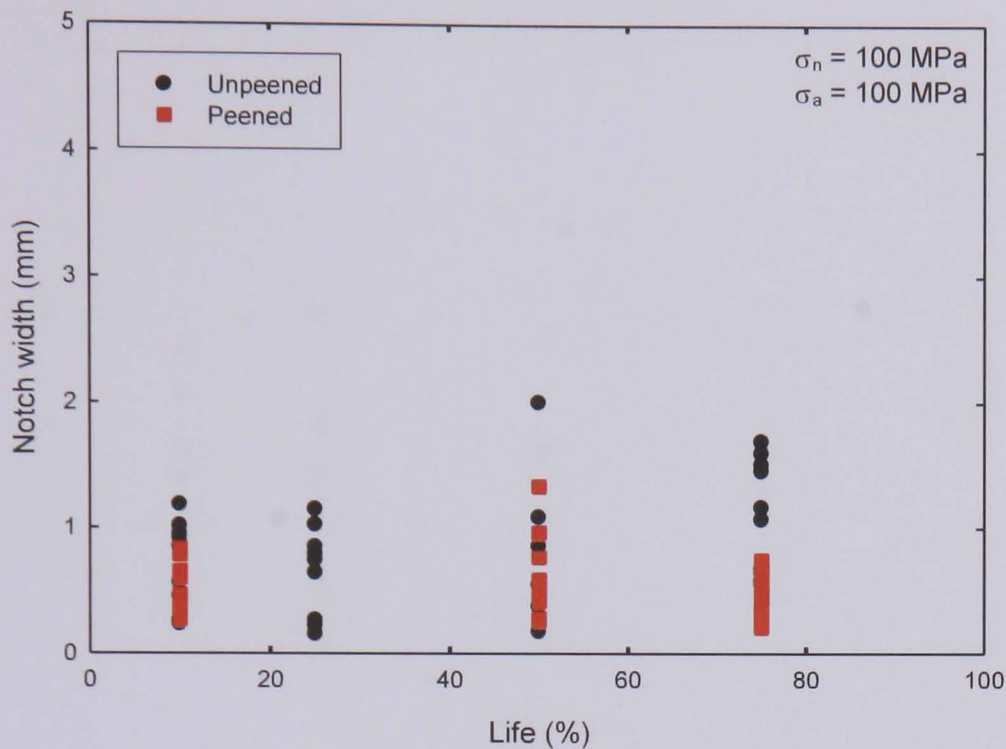


Figure 4.111: A comparison of the notch widths resulting from fretting fatigue tests conducted with an aluminium alloy 2024 T351 bridge in contact with both unpeened and peened aluminium alloy 2024 T351 specimens subjected to a normal pressure of 100 MPa and an axial stress amplitude of 100 MPa.

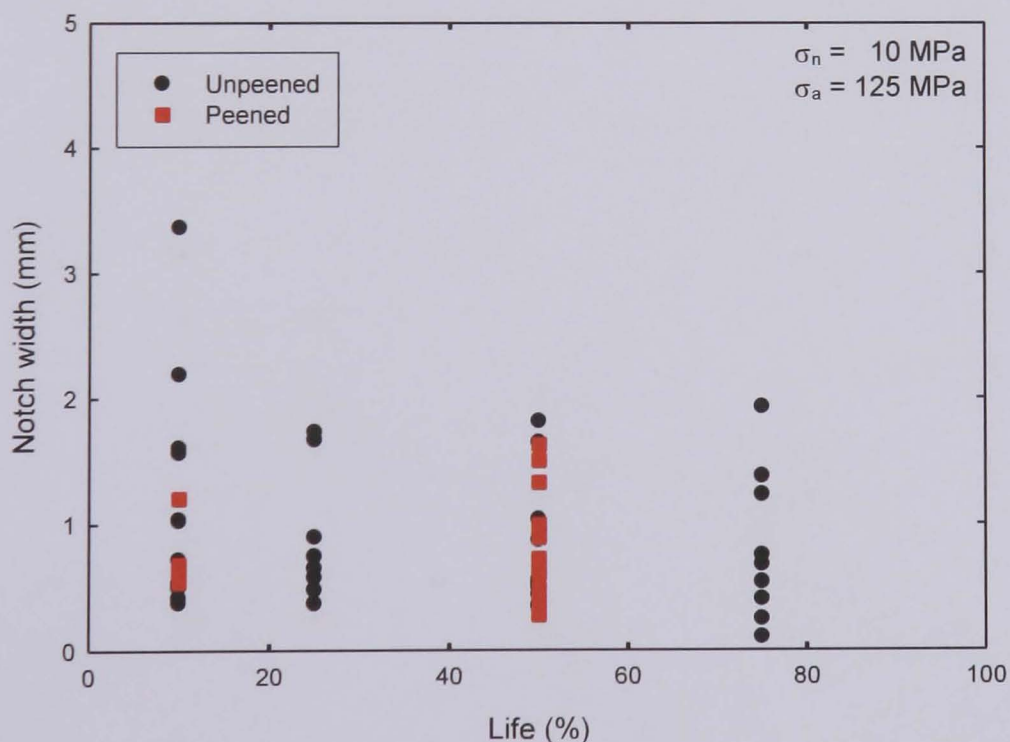


Figure 4.112: A comparison of the notch widths resulting from fretting fatigue tests conducted with an aluminium alloy 2024 T351 bridge in contact with both unpeened and peened aluminium alloy 2024 T351 specimens subjected to a normal pressure of 10 MPa and an axial stress amplitude of 125 MPa.

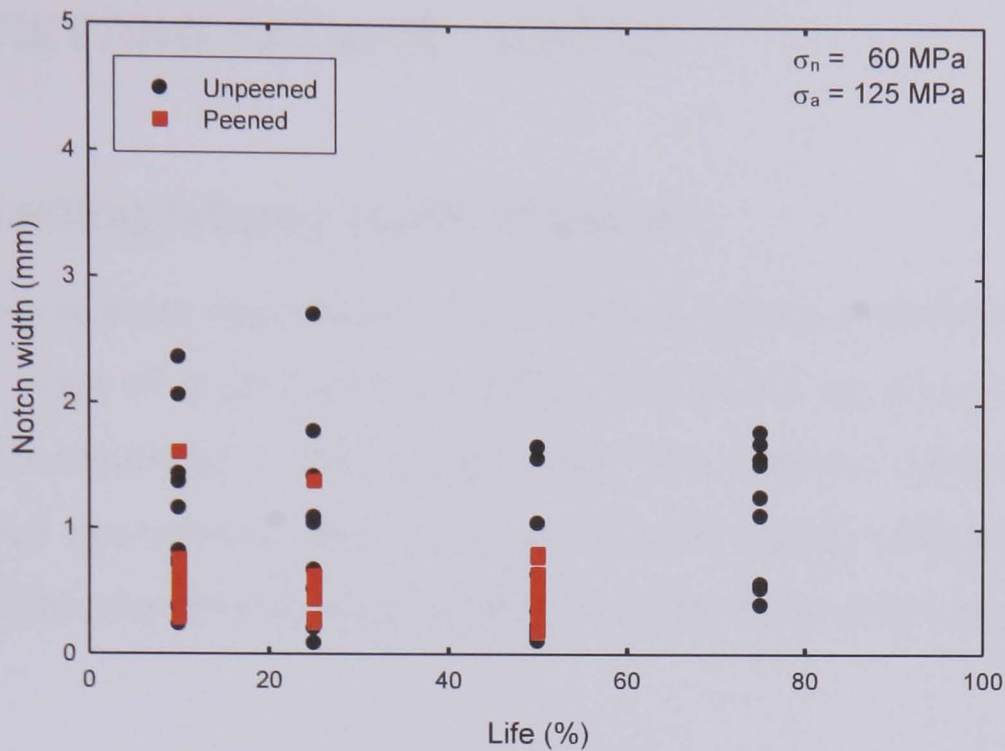


Figure 4.113: A comparison of the notch widths resulting from fretting fatigue tests conducted with an aluminium alloy 2024 T351 bridge in contact with both unpeened and peened aluminium alloy 2024 T351 specimens subjected to a normal pressure of 60 MPa and an axial stress amplitude of 125 MPa.

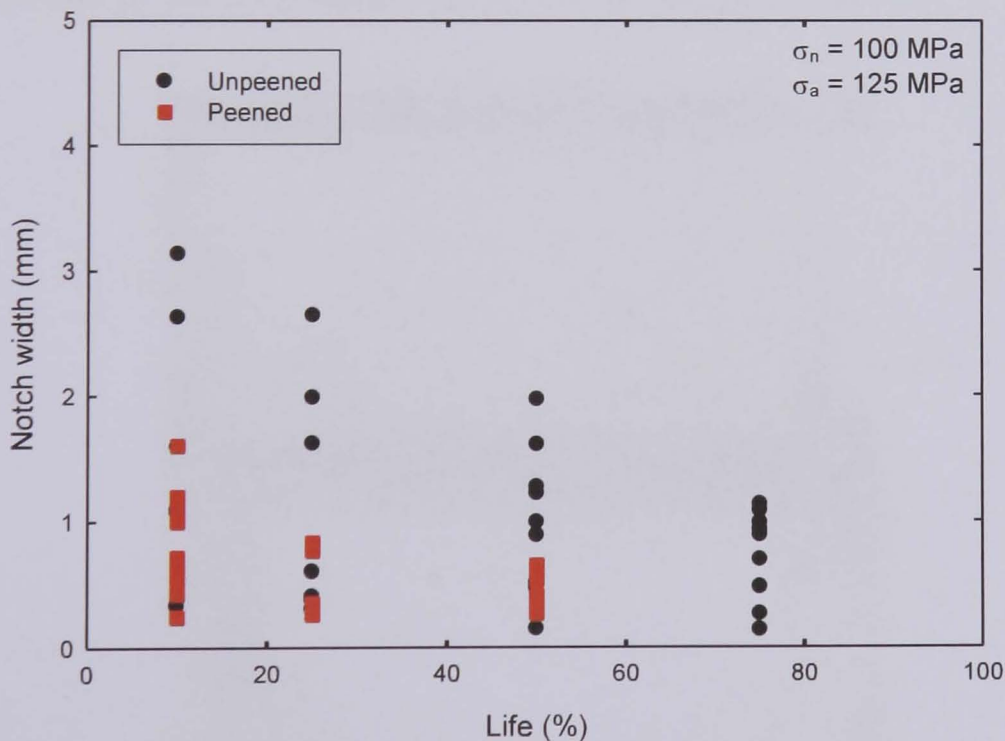


Figure 4.114: A comparison of the notch widths resulting from fretting fatigue tests conducted with an aluminium alloy 2024 T351 bridge in contact with both unpeened and peened aluminium alloy 2024 T351 specimens subjected to a normal pressure of 100 MPa and an axial stress amplitude of 125 MPa.

4.4 FRETTING FATIGUE CRACKS

4.4.1 Fretting fatigue crack initiation

In fretting fatigue tests reported in the literature, cracks invariably initiate at, or close to, the edge of a contact zone [99], [219], [124], as shown in Figure 2.3. This was also observed in this study in the two material combinations tested with unpeened specimens. The dominant cracks, which ultimately resulted in the failure of the specimens, always initiated at an outer edge of one of the four bridge feet.

Figure 4.115 is an example of such a failure. However, whilst the first crack initiated from the leading edge of the left hand bridge foot in contact with the top surface area, at some time another crack initiated at the edge of the right hand bridge foot (shown on the left hand side of the lower image in Figure 4.115) diagonally across from the first on the bottom surface area. This second catastrophic crack grew to a length of approximately 17.5 mm.

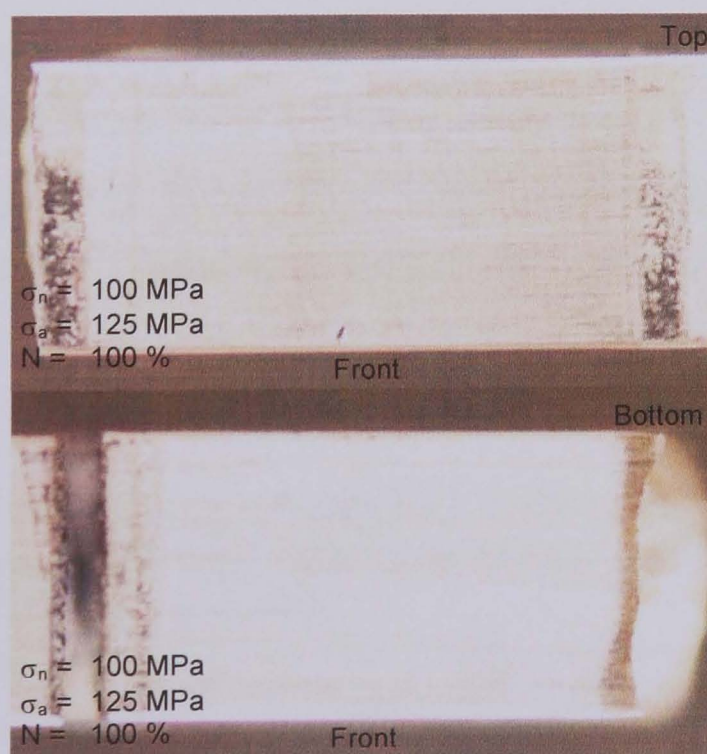


Figure 4.115: Crack initiation at the leading edge of the contact area on an unpeened specimen, on the top surface and simultaneously on the bottom surface.

Figure 4.116 shows an example of failure in a peened specimen. Here, the fatal crack initiated from the leading edge of the right hand bridge foot in contact with the top surface area.



Figure 4.116: Crack initiation at the leading edge of the contact area on the top surface of a peened specimen.

For both surface conditions, failures occurred at both the upper left hand, lower left hand, upper right hand and lower right hand bridge feet. Table 4.3 is a record of the locations of the cracks that occurred as a result of contact between the control set. Figure 4.117 shows the locations of the cracks that occurred as a result of the fretting fatigue tests conducted with aluminium alloy 2024 T351 bridges in contact with unpeened aluminium alloy 2024 T351 specimens. Table 4.4 is a record of the locations of the three cracks that initiated and propagated to failure as a result of the fretting fatigue tests with aluminium alloy 2024 T351 bridges in contact with peened aluminium alloy 2024 T351 specimens.

Table 4.3: The locations of the cracks that initiated as a result of the fretting fatigue tests with a BS S98 steel bridge in contact with an aluminium alloy 2024 T351 specimen.

Specimen (no.)	Normal stress (MPa)	Axial stress (MPa)	Top		Bottom	
			Left	Right	Left	Right
17	40	100			✓	
13	80	100	✓			
14	120	100	✓			

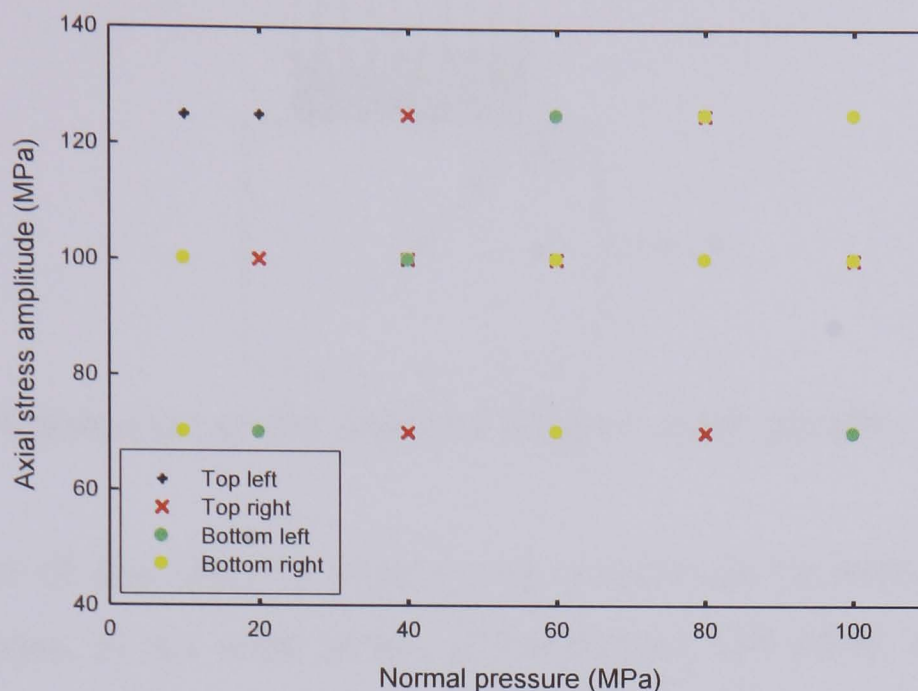


Figure 4.117: The locations of the cracks that initiated as a result of the fretting fatigue tests with aluminium alloy 2024 T351 bridges in contact with unpeened aluminium alloy 2024 T351 specimens.

Table 4.4: The locations of the cracks that initiated as a result of the fretting fatigue tests with aluminium alloy 2024 T351 bridges in contact with peened aluminium alloy 2024 T351 specimens.

Specimen (no.)	Normal stress (MPa)	Axial stress (MPa)	Top		Bottom	
			Left	Right	Left	Right
8P	60	100		✓		
4P	100	100				✓
10P	40	125	✓			

4.4.2 Fretting fatigue crack propagation

Observations were made regarding the shape of the subsequent crack paths and information gained from examining the fracture surfaces. It was found that fretting fatigue cracks initiated at angles of greater than 90° to the contact surface when in stage I, growing at angles beneath the pad feet, but propagated nearly normal to the surface when in stage II, perpendicular to the orientation of the axial stress. The orientation of the cracks is defined by the angle between the crack and the free surface as is shown in Figure 4.118.

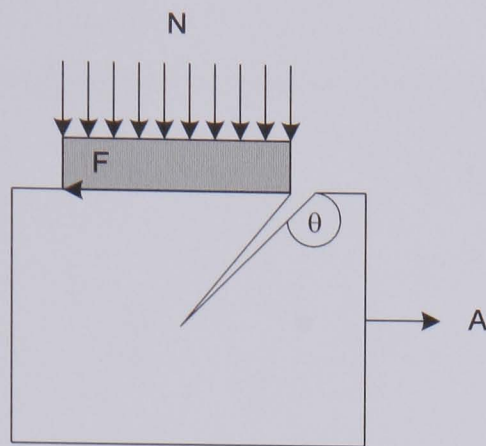


Figure 4.118: A definition of the angle of Stage I crack growth.

The orientation of the stage I cracks was subsequently examined for various normal pressures, at an axial stress amplitude of 100 MPa, by sectioning the fractured specimens, see Figure 4.119 and Appendix N.

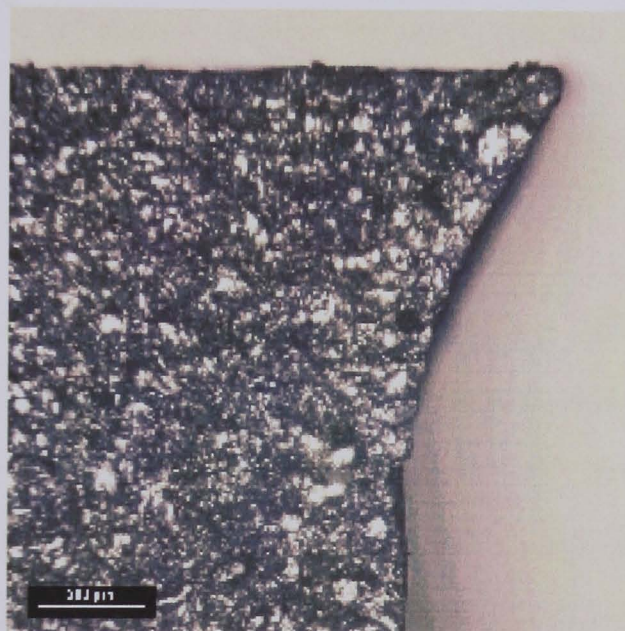


Figure 4.119: The morphology of a fretting fatigue crack.

The cracks formed by the aluminium bridges initiated at angles to the free surface ranging from 100° to 120° , depending on the magnitude of the normal pressure applied, see Figure 4.120. The results obtained were comparable with the data reported by Faanes and Fernando [100] for a BS S98 steel bridge with a pad span of 16.5 mm, in flat-on-flat contact with BS L65 4% copper aluminium alloy specimens under the same load conditions. The orientation of these stage I cracks was subsequently examined using a finite element model, described in Chapter 5.

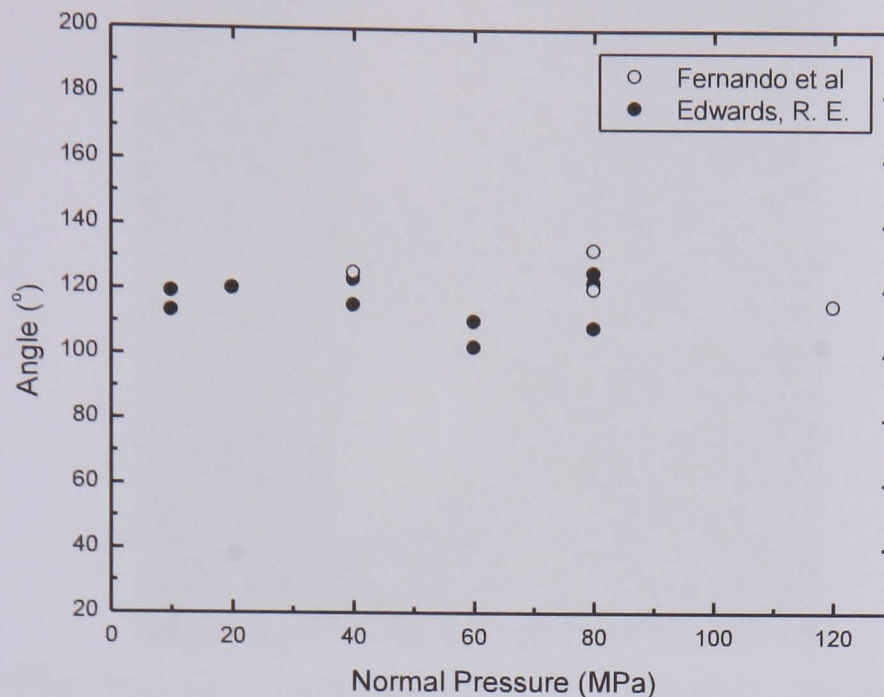


Figure 4.120: A comparison of the variation, with normal pressure, of the direction of initial crack growth determined from this research and by Fernando et al. [100] for fretting fatigue tests conducted at an axial stress amplitude of 100 MPa.

By further examination of the fracture surfaces, patterns were established between the normal pressures and axial stresses applied and the number of crack initiation sites. It was determined that at low normal pressures at axial stresses up to an amplitude of 100 MPa, there was a tendency for only one dominant surface crack to initiate and propagate to failure, as shown in Figure 4.121. For both material combinations tested, the fretting fatigue cracks observed were predominantly three-dimensional semi elliptical surface cracks. The dimensions of the specimens is shown in Figure 3.5.

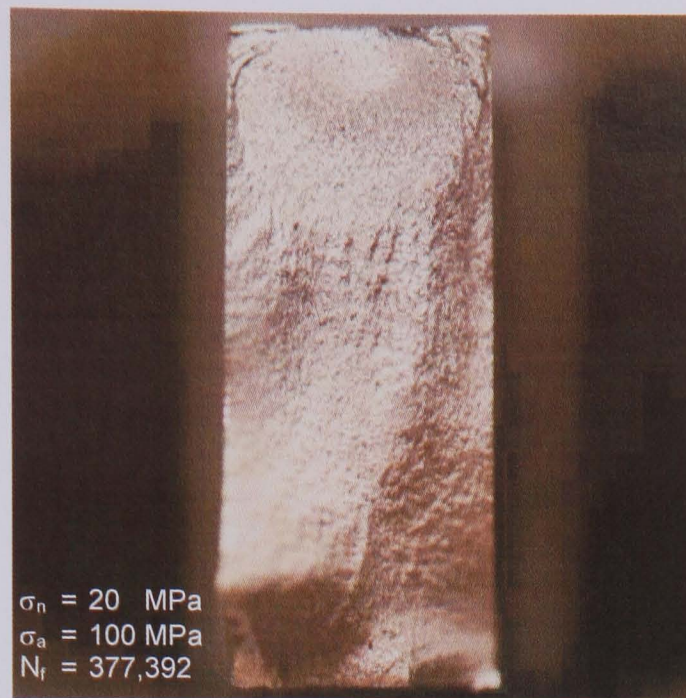


Figure 4.121: The fracture surface of an unpeened specimen having been subjected to a normal pressure of 20 MPa and an axial stress amplitude of 100 MPa.

At normal pressures in the middle of the range tested, two or three dominant surface cracks were found, see Figure 4.122, while at high normal pressures there were multiple crack initiation points along the fretting scars and thus, the dominant cracks propagated as through section cracks. An example of such a fracture surface is shown in Figure 4.123.

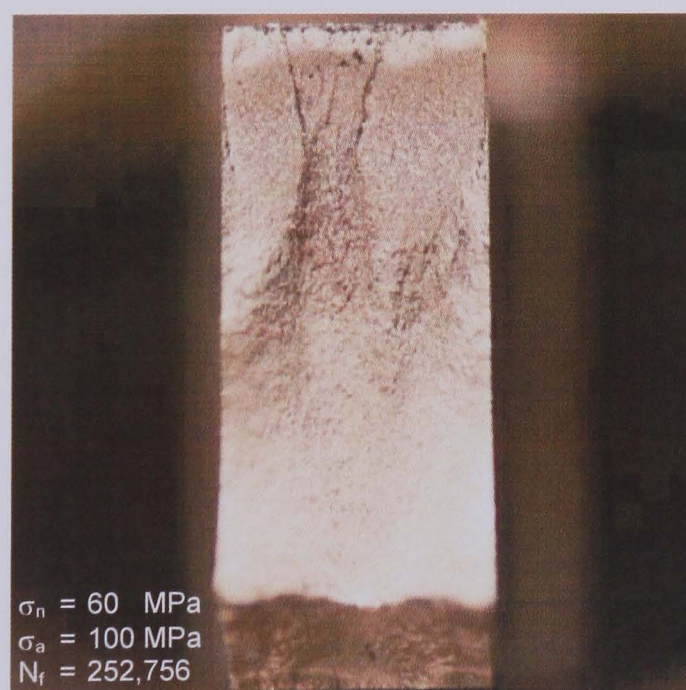


Figure 4.122: The fracture surface of an unpeened specimen having been subjected to a normal pressure of 60 MPa and an axial stress amplitude of 100 MPa.

The behaviour shown in Figure 4.123 is characteristic of that observed for all normal pressures when an axial stress amplitude of 125 MPa was applied.

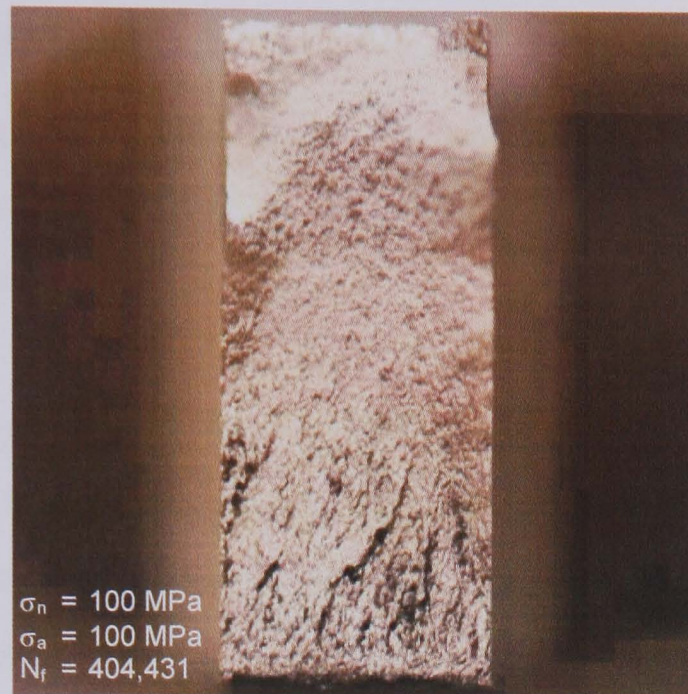


Figure 4.123: The fracture surface of an unpeened specimen having been subjected to a normal pressure of 100 MPa and an axial stress amplitude of 100 MPa.

There was a more limited supply of peened specimens, but from those studied, cracks appeared to initiate sub surface, see Figure 4.124. Images of all the fracture surfaces can be found in Appendix O.

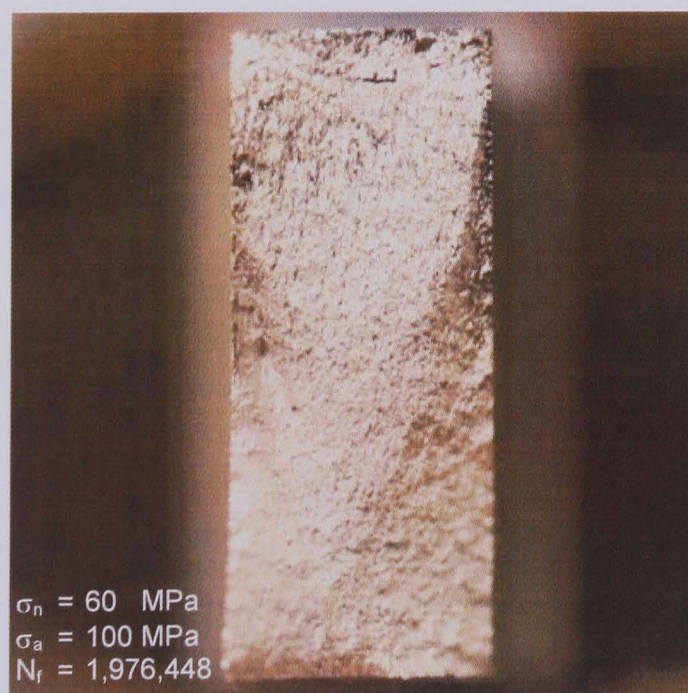


Figure 4.124: The fracture surface of a peened specimen having been subjected to a normal pressure of 60 MPa and an axial stress amplitude of 100 MPa

4.5 FRACTURE SURFACES

4.5.1 Topography

In order to gain detailed information regarding the fracture mechanisms, microscopic examinations of the specimens were carried out on a CAMSCAN MK II, scanning electron microscope.

Twenty one aluminium alloy 2024 T351 specimens were examined: three that had been in flat-on-flat contact with BS S98 steel bridges and eighteen that had been in flat-on-flat contact with aluminium alloy 2024 T351 bridges, one for each combination of normal pressure and axial stress applied, see Appendix P.

The specimens that had been in flat-on-flat contact with BS S98 steel bridges, had been subjected to an axial stress amplitude of 100 MPa and normal pressures of 40, 80 and 120 MPa, 80 MPa being the critical loading condition that resulted in the shortest fretting fatigue life for this loading arrangement.

The specimens that had been in flat-on-flat contact with aluminium alloy 2024 T351 bridges had been subjected to normal pressures of 10, 20, 40, 60, 80 and 100 MPa. For an axial stress amplitude of 100 MPa, 40 MPa was the critical loading condition that resulted in the shortest fretting fatigue life.

In all cases there was a high degree of surface degradation, see Appendix Q. As shown in Figures 4.6 and 4.116, the wear scars were typically black, suggesting the presence of oxide debris. At higher magnifications, there was also evidence of metal adhesion, as shown in Figure 4.125.



Figure 4.125: Evidence of adhesion relating to specimen number 105; an aluminium alloy 2024 T351 specimen in contact with an aluminium alloy 2024 T351 bridge subjected to a normal pressure of 20 MPa and an axial stress amplitude of 70 MPa.

There was evidence of smearing too, as is shown in Figure 4.126, where the friction forces will have been large, causing tangential stresses in the surface layers [100]. Surface cracks were also found, see Figure 4.127. Crack initiation occurred at the edge of the wear scars.

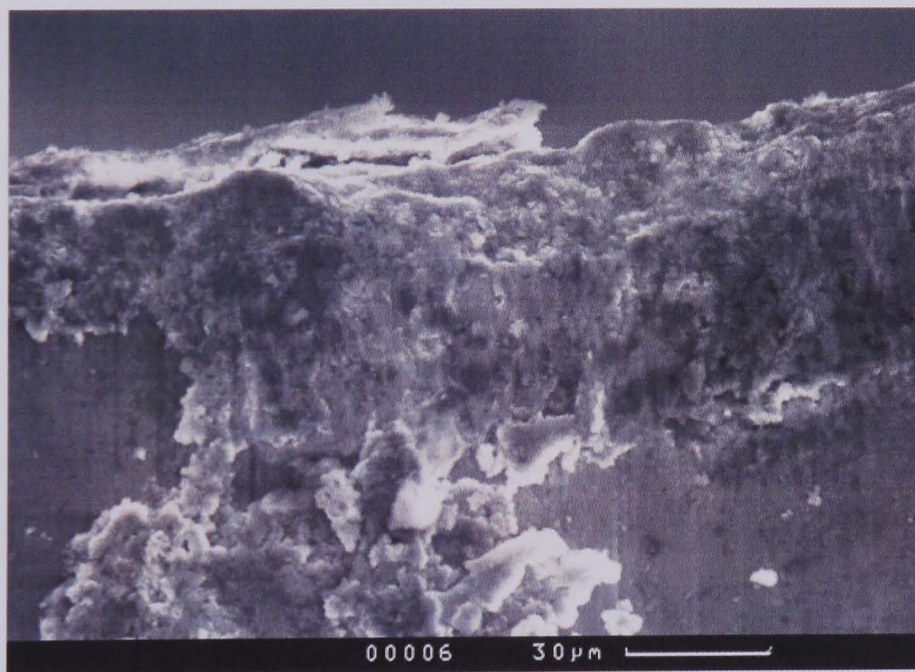


Figure 4.126: Evidence of smearing relating to specimen number 40; an aluminium alloy 2024 T351 specimen in contact with an aluminium alloy 2024 T351 bridge subjected to a normal pressure of 20 MPa and an axial stress amplitude of 125 MPa.

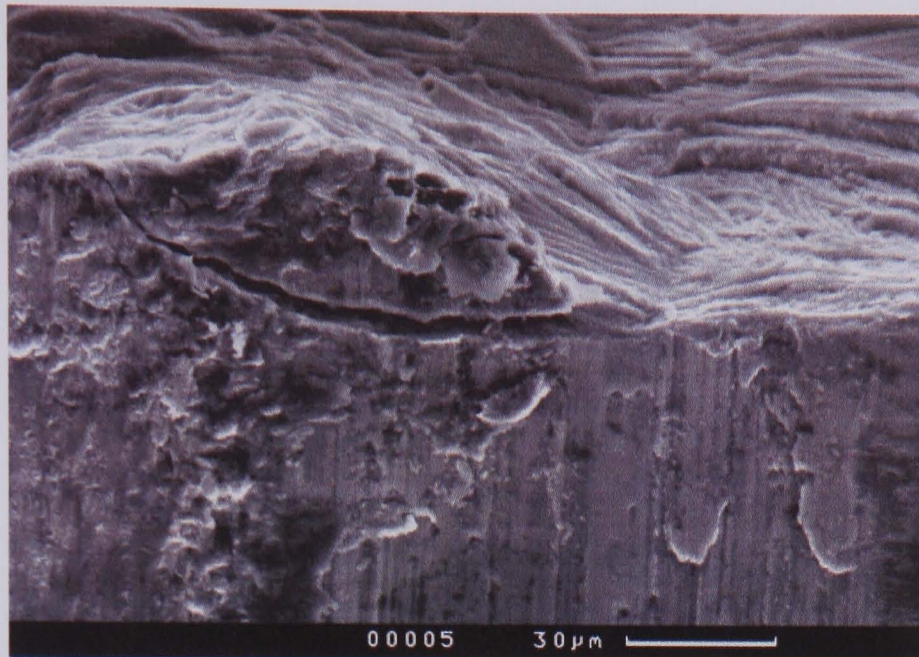


Figure 4.127: Evidence of surface cracking relating to specimen number 54; an aluminium alloy 2024 T351 specimen in contact with an aluminium alloy 2024 T351 bridge subjected to a normal pressure of 100 MPa and an axial stress amplitude of 70 MPa

As these were fretting fatigue tests, damage to the fracture surfaces was also observed in regions near to the bridge-specimen interface, see Appendix R. A greater degree of rubbing was apparent when using a BS S98 steel bridge as opposed to an aluminium alloy 2024 T351 bridge, as is demonstrated by comparing Figures 4.128 and 4.129.

This rubbing near to the fretting scars is thought to be due to the shear from the loading and the opening and closing motion of the crack. As part of the loading cycle was compressive, there was always the added complication that the newly formed fracture surfaces could be forced together so obliterating the primary features of the crack extensions. This is a problem in all cyclic fatigue involving ductile separation at the crack tip [236].



Figure 4.140: A region of rubbing corresponding to specimen number 17; an aluminium alloy 2024 T351 specimen in contact with a BS S98 steel bridge subjected to a normal pressure of 40 MPa and an axial stress amplitude of 100 MPa.

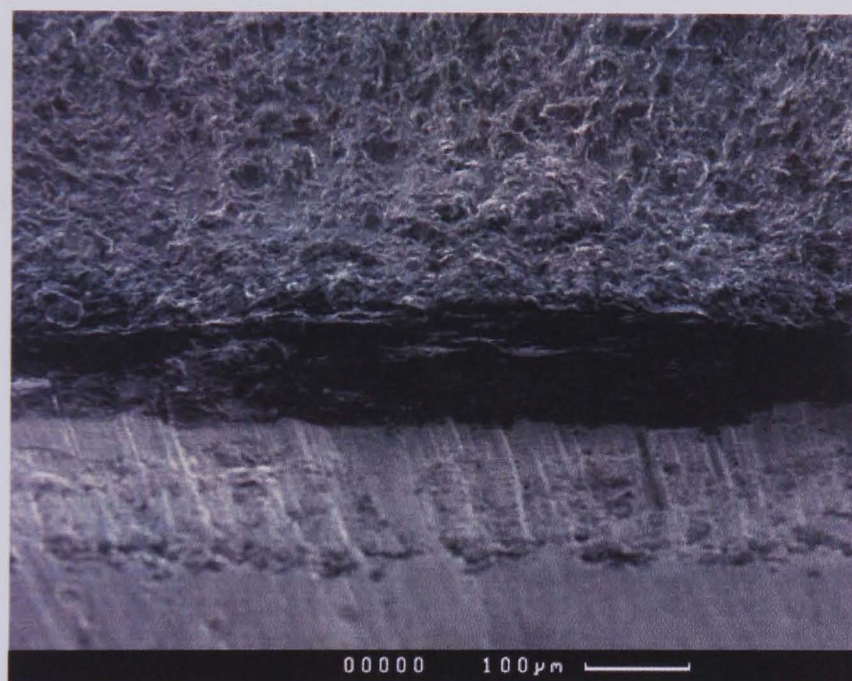


Figure 4.141: A region of rubbing corresponding to specimen number 11; an aluminium alloy 2024 T351 specimen in contact with an aluminium alloy 2024 T351 bridge subjected to a normal pressure of 20 MPa and an axial stress amplitude of 100 MPa.

As shown previously in Figure 4.121, at low normal pressures there was a tendency for only one dominant surface crack to initiate and propagate to failure.

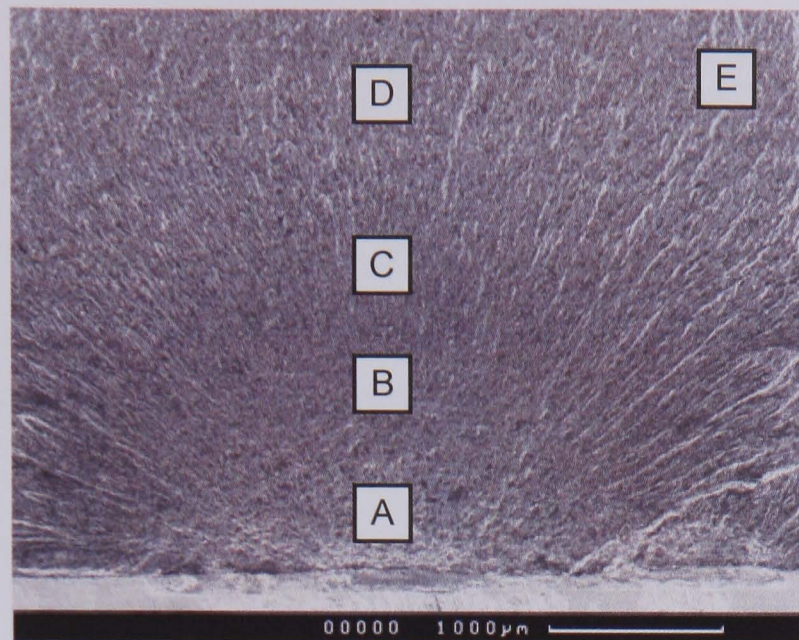


Figure 4.142: A fractograph of the fretting fatigue crack initiation site relating to specimen number 11; an aluminium alloy 2024 T351 specimen in contact with an aluminium alloy 2024 T351 bridge subjected to a normal pressure of 20 MPa and an axial stress amplitude of 100 MPa.

At high normal pressures there were multiple crack initiation points along the fretting scars and thus the dominant cracks propagated as through section cracks. An example of such a fracture surface is shown in Figure 4.123 and in Figure 4.143.

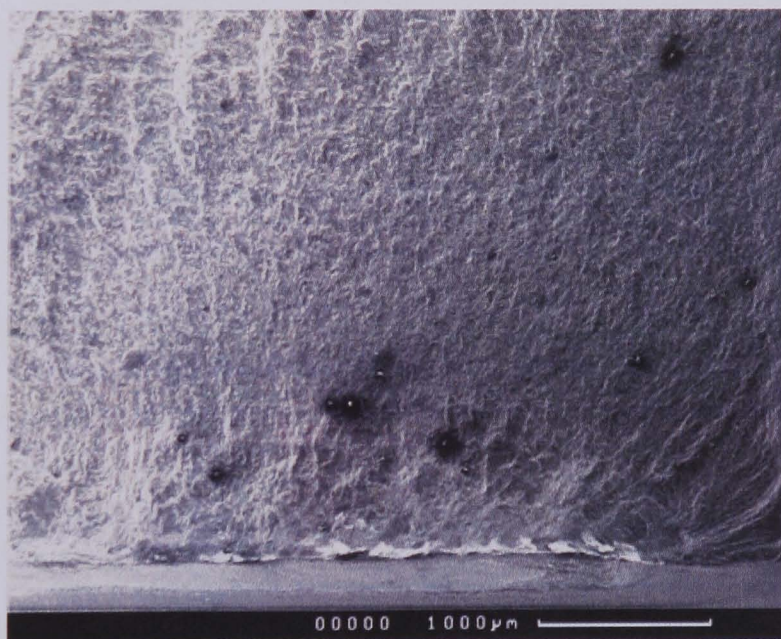


Figure 4.143: A fractograph of the fretting fatigue crack initiation site relating to specimen number 14; an aluminium alloy 2024 T351 specimen in contact with a BS S98 steel bridge subjected to a normal pressure of 120 MPa and an axial stress amplitude of 100 MPa.

Regions of stage I propagation were visible from all of the SEM images, as shown in Appendix S and Figure 4.144 (A), which is part of the fracture surface depicted in Figure 4.142. Cracks grew along crystallographic shear planes at angles in the region of 20 to 40 degrees to the free surface. A crystallographic fracture formed during stage I propagation shows planar facets when the fracture occurs along single crystallographic planes [236]. In addition to the crystallographic facets, Figure 4.144 (A) shows regions of rubbing due to the mismatch of the fracture surfaces.



Figure 4.144: (A): A fractograph demonstrating a region of stage I crack propagation relating to specimen number 13; an aluminium alloy 2024 T351 specimen in contact with a BS S98 steel bridge subjected to a normal pressure of 80 MPa and an axial stress amplitude of 100 MPa.

Regions of stage II propagation, tensile dominant fracture were also visible on the SEM images, where Mode I crack growth was observed and there was a change in propagation direction to be roughly perpendicular to the applied tensile stresses, as shown in Appendix T and Figure 4.145 (B), which is part of the fracture surface depicted in Figure 4.142.

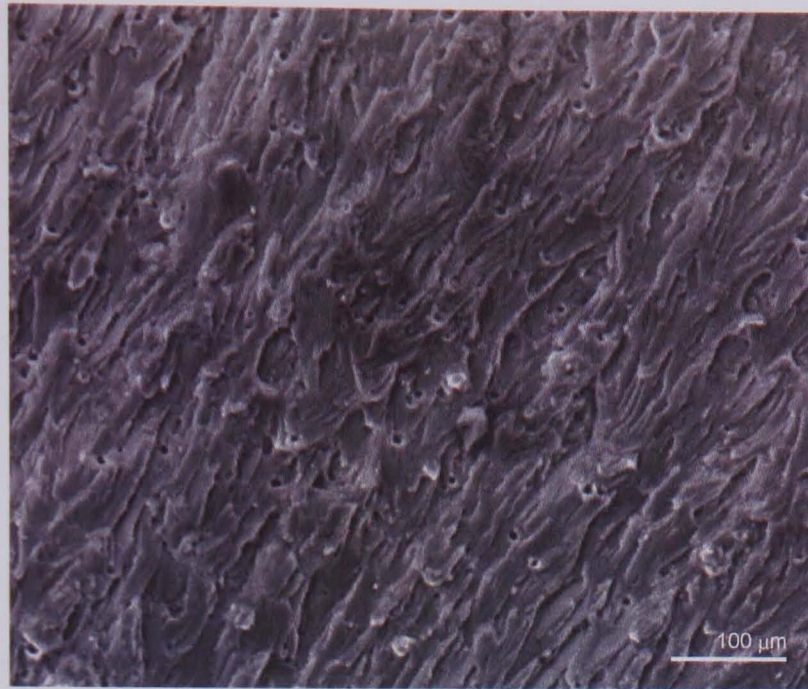


Figure 4.145: (B): A fractograph demonstrating a region of stage II crack propagation relating to specimen number 1; an aluminium alloy 2024 T351 specimen in contact with a BS S98 steel bridge subjected to a normal pressure of 80 MPa and an axial stress amplitude of 100 MPa.

The regions of the fracture surfaces that formed during stage II propagation were characterised by striation markings, as shown in Appendix U, each striation representing the distance the crack has moved in a single stress cycle. Figure 4.146 (C) is an electron fractograph, which is part of the fracture surface depicted in Figure 4.142 and demonstrates a regular striated pattern. It is possible to estimate crack propagation rate, da/dN , by taking measurements of the spacing of striations on a fracture surface. However, within a small area, the spacing of striations can vary widely and therefore a significant number of images are required in order that an average can be taken [237]. Endo and Goto [85] and Leadbeater et al. [237] have subsequently found that fretting fatigue cracks are accelerated by the fretting action whilst growing at an angle, indicating that fretting stresses at the surface affect both crack direction and crack propagation rates.

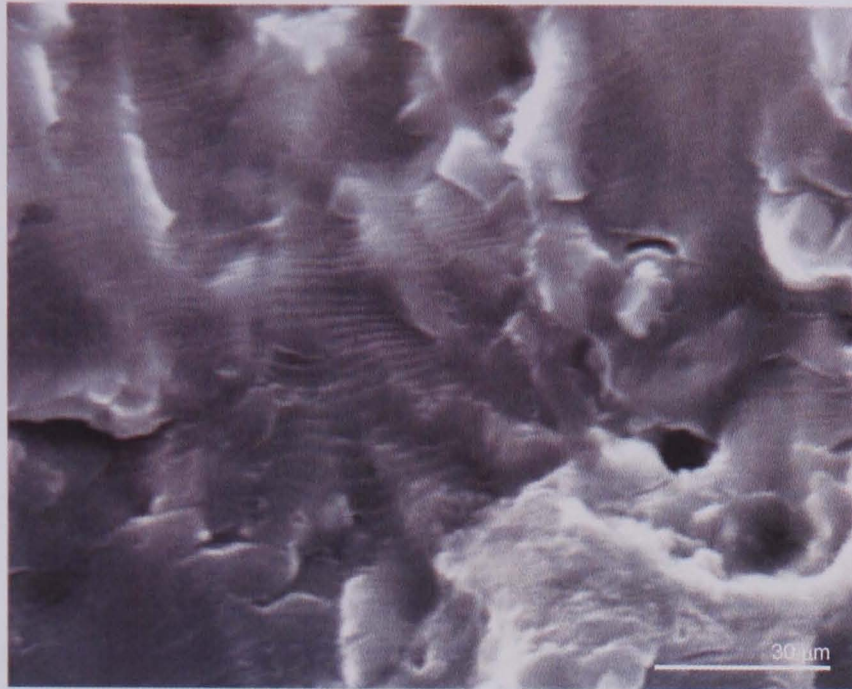


Figure 4.146: (C): A fractograph illustrating a region of striations corresponding to specimen number 17; an aluminium alloy 2024 T351 specimen in contact with a BS S98 steel bridge subjected to a normal pressure of 40 MPa and an axial stress amplitude of 100 MPa.

The transition to unstable fracture in the final stages of fatigue failure is clearly visible on a fracture surface because it is associated with an abrupt change in the separation processes at the crack tip [236]. The regions of rapid failure of the aluminium alloy 2024 T351 specimens were characterised by their dull and fibrous texture and covered the vast majority of the fracture surfaces. Fast failure was confirmed by the absence of gross plastic deformation. A region of tensile failure is shown in Figure 4.147 (D) and a region of shear failure is shown in Figure 4.148 (E), both of which are part of the fracture surface depicted in Figure 4.142.

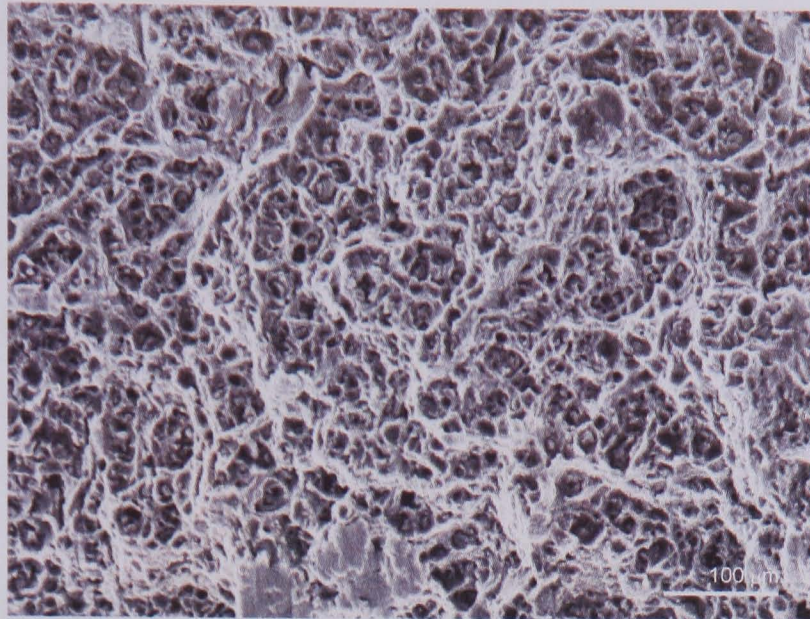


Figure 4.147: (D): A fractograph demonstrating a region of unstable tensile fracture relating to specimen number 13; an aluminium alloy 2024 T351 specimen in contact with a BS S98 steel bridge subjected to a normal pressure of 80 MPa and an axial stress amplitude of 100 MPa.

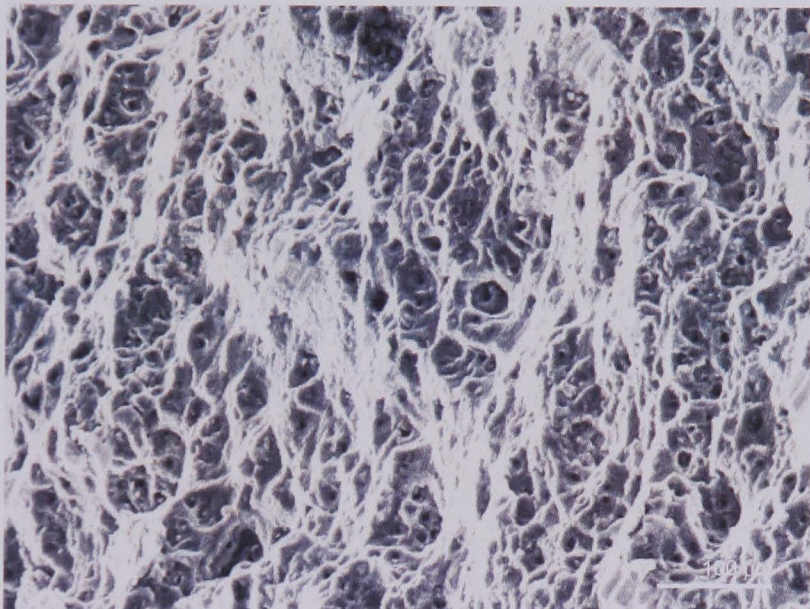


Figure 4.148: (E): A fractograph demonstrating a region of unstable shear fracture relating to specimen number 13; an aluminium alloy 2024 T351 specimen in contact with a BS S98 steel bridge subjected to a normal pressure of 80 MPa and an axial stress amplitude of 100 MPa.

By applying a topographical filter in Jasc® Paint Shop Pro™ the boundaries between the propagation regions in Figure 4.142 were more easily distinguished and by using the image analysis software SigmaScan, the lengths of Stage I and Stage II were measured.

For this aluminium alloy 2024 T351 specimen, having been in contact with an aluminium alloy 2024 T351 bridge and subjected to a normal pressure of 20 MPa and an axial stress amplitude of 100 MPa, Stage I, angled crack growth was measured at 1.46 mm, for an Al-4%Cu-1%Mg alloy this has previously been reported at 0.5 mm [237]. Stage II, where the crack propagates perpendicularly to the applied axial stress, was estimated as being approximately 3.04 mm in length, or radius, see Figure 4.149.

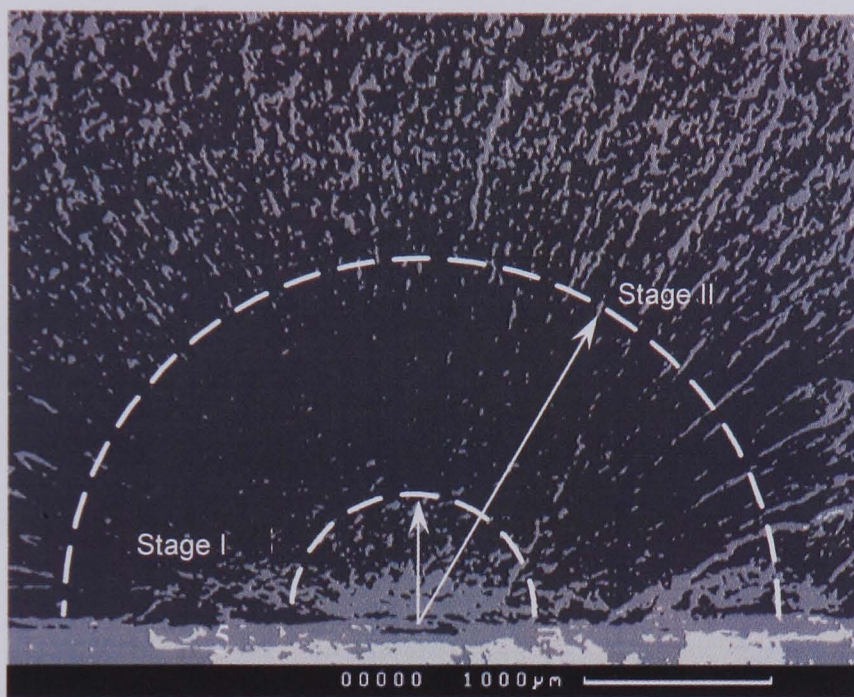


Figure 4.149: A topographic image of specimen number 11, an aluminium alloy 2024 T351 specimen in contact with an aluminium alloy 2024 T351 bridge subjected to a normal pressure of 20 MPa and an axial stress amplitude of 100 MPa, showing an area of stage I crack growth and stage II propagation.

CHAPTER

5

MODELLING

5.1 INTRODUCTION

It has been demonstrated that fretting fatigue leads to surface and near surface degradation, which has a detrimental effect on fatigue strength. In this test programme, dominant fretting fatigue cracks initiated at the outer edges of every contact for every combination of normal pressure and axial stress applied and grew at an angle beneath the contact during Stage I, before turning, and continuing their growth perpendicularly to the direction of the axial load during Stage II. This behaviour has been well documented [100], [240] and an example of such a crack is shown in Figure 4.119.

The orientation of the dominant cracks whilst in Stage I was examined for various normal pressures as is summarised in Figure 4.120; the orientation of the cracks is defined as the angle between the crack and the free surface, see Figure 4.118. The cracks formed by the aluminium bridges initiated at angles to the free surface ranged from 100° to 120° , depending on the magnitude of the normal pressure applied.

To investigate further the sites and direction of crack growth recorded in Figure 4.120, the stress distribution, during cyclic loading, over the geometry of the specimen depicted in Figure 3.5 has been examined. Two-dimensional, elastic finite element analyses were carried out under plane strain conditions using a finite element mesh constructed using the commercial finite element package ANSYS. The results concurred with the measurements made on actual specimens.

It is postulated that at any angle, the initiation of fretting fatigue cracks is not least due to an increase in normal and friction stresses at the leading edge of a contact [102] and that these cracks initiate very early on in life [99], [102]. The fretting fracture process is therefore assumed to be dominated by crack growth [17], [99], the high stress concentration at the contact zone accelerating this crack propagation.

The fracture mechanics approach is therefore appropriate for the prediction of fretting fatigue life. In 1979 Rooke and Jones [241], derived solutions in the form of polynomial functions for mode I and mode II stress intensity factors, for a crack at the edge of a sheet, subjected to localized fretting forces. Indeed, fracture mechanics has been used to perform fretting fatigue life calculations by a large number of researchers, including: Endo and Goto [85], Edwards [77], Nix and Lindley [242], Hattori et al. [97], Faanes and Fernando [101], Nicholas et al. [243], Conner et al. [244], Attia [245], Giummarra and Brockenbrough [246] and Chambon and Journet [247].

Faanes and Fernando [101] demonstrated that mode I crack growth described fretting fatigue crack growth behaviour well. However, it was suggested that investigations of the influence of mixed mode crack growth be carried out.

In 1994, Sheikh et al. [102] developed a finite element procedure for the determination of stress intensity factors for fretting fatigue cracks. In this chapter, an attempt is made to predict fretting fatigue life using a linear elastic fracture mechanics based methodology, with mode I and mode II elastic stress intensity factors, K_I and K_{II} , being determined for a crack inclined to the normal at 22.5° , that is to the free surface at 112.5° , for all combinations of loading applied and recorded during testing, from data published by Sheikh et al [102].

Faanes and Fernando [101] experimented with changing the initial flaw size in a series of fracture mechanics models in order that the corresponding $S-N$ curves fitted material data and an estimate of the initial damage was made here, with the application of x , a multiple of the grain size, d , incorporating a whole host of factors including Stage I cracking and friction, hardening, and a measure of fretting damage or wear.

Components of fretting forces: the alternating, hence damaging, axial stress in the specimen, σ_a and frictional stress at the contacting surfaces, σ_f and the static, compressive normal stress, σ_n , were then incorporated in stress intensity factors K_I and K_{II} at the tip of an inclined crack as if grown from the leading edge of a fretting pad. The fretting fatigue life of aluminium alloy 2024 T351 was subsequently investigated for six normal and three axial loading conditions; these being compared with the experimental results and shown to be in good agreement.

It has subsequently been demonstrated that friction has a significant influence on the very early stages of crack growth; indeed, it has been shown that lowering the friction in a system is one of the best approaches to alleviating fretting fatigue [25]. Friction is influenced by the condition of mating surfaces, the composition of component materials, surface roughness, residual surface stresses and oxides or other surface films [17].

Relationships between fretting wear and the friction ratio σ_f/σ_n have thus been established and used to predict the fretting fatigue life for the peened condition under three normal and three axial loading conditions; these were compared with the experimental results and were conservative.

A detrimental effect of the shot peening process is an increase in surface roughness and wear. However, in 1959, Matterson and Roberts [248] demonstrated that an improvement in the fatigue strength of a shot peened steel could largely be attributed to compressive residual stresses. Crack growth is influenced by a compressive residual stress distribution in the surface layer; this prolongs the time to crack initiation and retards crack growth [249].

The shot peening parameters utilised here are shown in Table 3.3 and were selected as a result of an investigation carried out concurrently at the University of Sheffield [197]. The residual stress profile determined for these conditions by Solis-Romero [197], has also been incorporated in the predictions, which show excellent agreement when compared with the experimental results in this chapter.

5.2 FRETTING FATIGUE CRACKS

5.2.1 Finite Element Analyses

5.2.1.1 Model

In 1895, Hertz [250] determined the calculation of the state of stress produced by both spherical and cylindrical contacts; the analysis of the Hertzian contact under conditions of partial slip was conducted by Mindlin [41] in 1949 and was used by Johnson in his investigation of fretting in 1955 [42]. However, other than for Hertzian contacts, analytical solutions of contact conditions, even for relatively simple geometries, are unavailable.

For example, flat on flat contact problems have been shown by Hills and Nowell to be unsolvable in a closed form [110]. Analysis of the potential for fretting of real, highly complex assemblies found in practice, may, therefore, be carried out by numerical methods [45]. Finite element, and for that matter boundary element methods of crack analysis are special applications of more general stress analysis techniques [251].

Consequently, a quarter of the fretting fatigue specimen and bridge set-up was modelled using the finite element package ANSYS; the finite element mesh is demonstrated in Figure 5.1. Two dimensional, structural, solid isoparametric, quadrilateral elements with eight nodes apiece and having two degrees of freedom per node, were used throughout, except at the boundary between the specimen and the bridge, where point-to-point contact elements were specified. The inclusion of mid-side nodes meant that a degree of accuracy could be achieved greater than would have been using linear elements, but consequentially the computational time was increased. The total number of elements used for the model was 795, resulting in a total of 2,466 nodes. Here the x-axis denoted the axial direction for the specimen and the y-axis the direction of the normal load applied.

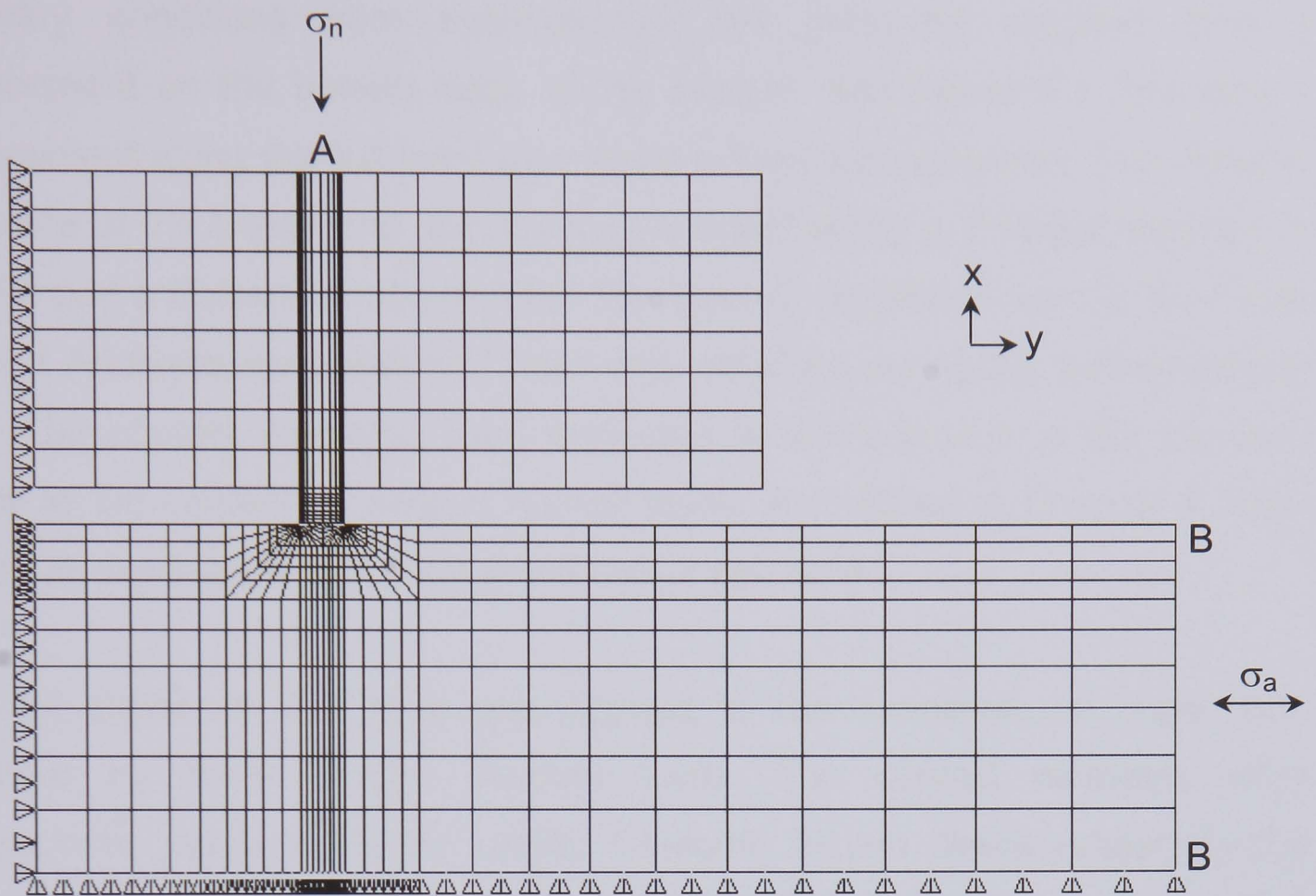


Figure 5.1: The complete finite element mesh of the fretting specimen and bridge, showing one quarter of the test sample working section.

The mesh was refined over the critical contact area, the interface between the specimen and the bridge pad, with a particular focus on the areas at the edge of the pad, where regions of stress concentrations were expected to arise, see Figure 5.2. This was to ensure a satisfactory degree of accuracy, without waste.

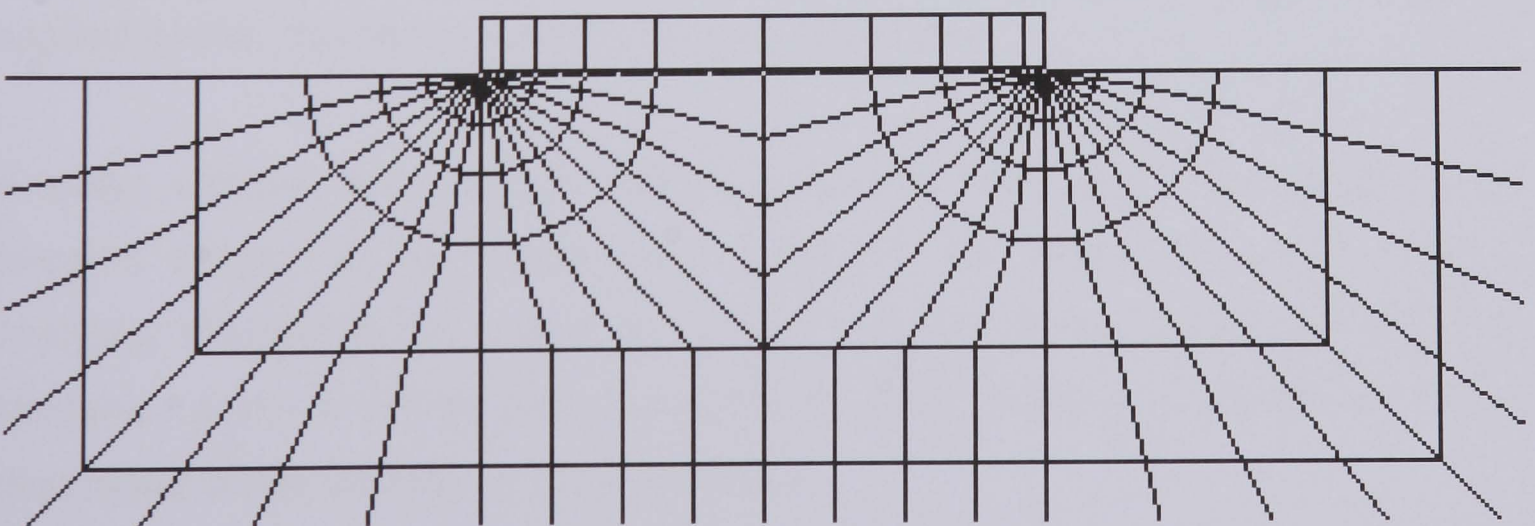


Figure 5.2: The critical region of the finite element mesh of the fretting specimen and bridge.

Boundary conditions from symmetry of the geometry requires zero y displacement on the bottom edge of the sample, see Figure 5.1 and zero x displacement along the left hand side of the bridge and specimen. The material properties of the bridge and specimen were specified by a Young's modulus of 70 GPa and a Poisson's ratio of 0.33. The loading conditions used in the Finite Element Analyses were selected from data obtained during the fretting fatigue tests. The contact elements were subjected to compression in the direction normal to the contact as various normal loads, as outlined in Chapter 3, were applied as point loads to the top of the bridge pad at 'A'.

An axial stress of 100 MPa was applied to the specimen on edge 'BB,' simulated by finely divided discrete loads. The contact elements were subsequently subjected to an elastic Coulomb friction stress (shear) in the tangential direction and a coefficient of friction was specified for each analysis, with those values being selected from Table F.1b in order for the results achieved to be comparable with those obtained from the experimental test programme.

In running the analyses used to determine the sites of crack initiation and initial directions of crack growth, the following assumptions were made: a) that the loads were uniformly distributed along the fretting pad in the z direction, b) that the surfaces of the components were perfectly flat, c) that rigid Coulomb friction applied and d) that the materials behaved elastically.

A static solution was sought initially; solutions were then also obtained at stepped stages of the cyclic load, whereby full, two-dimensional, elastic analyses simulating the interaction of the various applied loads between the specimen and the bridge pad, for all those tests undertaken practically, were processed under conditions of plane strain.

5.2.2 Results

5.2.2.1 Calibration

By applying coefficients of friction defined during testing, friction forces were simulated numerically by integrating the shear stresses along the contact interface; an example of these results is presented in Figure 5.3. In Figure 5.3, the friction response obtained from the finite element analyses is compared with experimental results for both the steel and aluminium bridges. These friction forces correspond to an early stage of fatigue life and were obtained for a normal pressure of 60 MPa and a maximum axial stress of 100 MPa. The curves for both types of bridge form typical hysteresis loops with the amplitude of the friction force for the steel bridge being greater than that for the aluminium bridge. The responses obtained with the finite element analyses were in good agreement with the behaviour observed experimentally and it was therefore concluded that any further results from the finite element model could be considered to be reliable.

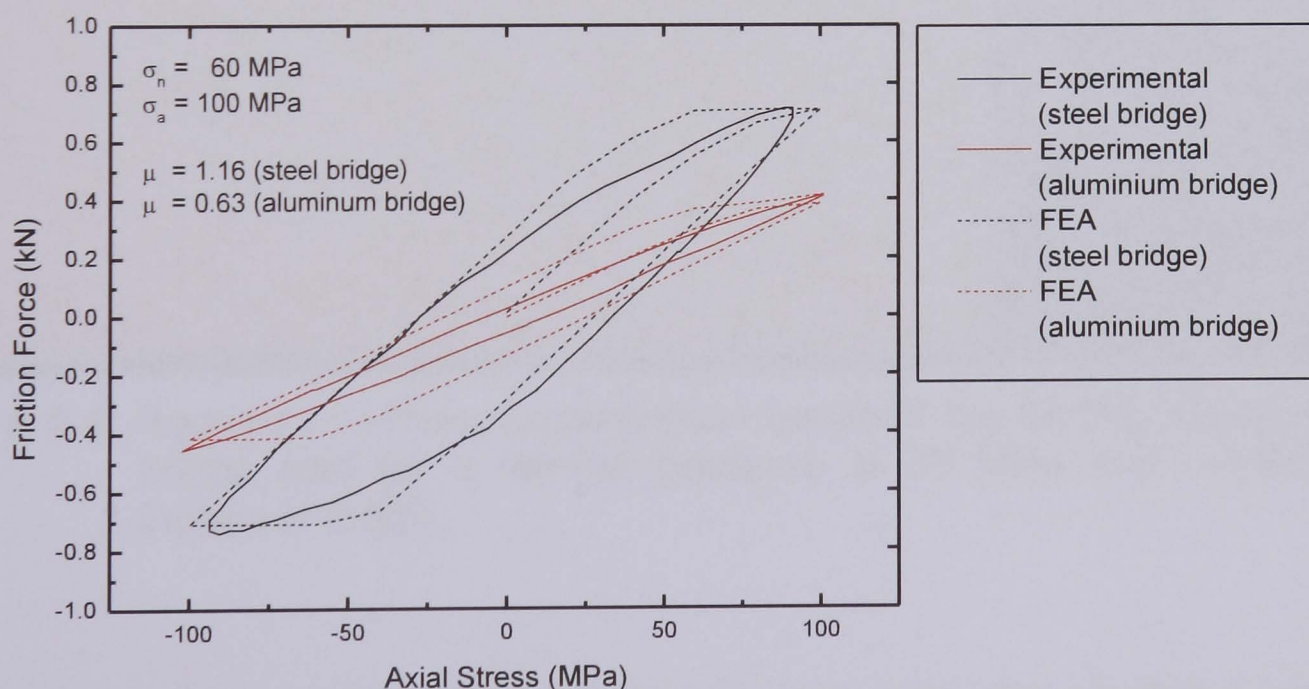


Figure 5.3: The friction force responses obtained from the experiments and subsequent finite element analyses.

5.2.2.2 Direction of fretting fatigue crack growth

In order to be able to predict the site and initial propagation direction of a fretting fatigue crack, potential damage parameters needed to be quantified. From the results of the finite element analyses, the cyclic load stress distributions over the contact interface between bridge and specimen were examined. In addition to the friction forces, the tangential and shear stresses were displayed graphically along with any deflection encountered. These were plotted initially as a series of stress contours, so that regions of stress concentration at the interface of the fretting specimen and bridge pad were clearly highlighted, as is shown in Figure 5.4.

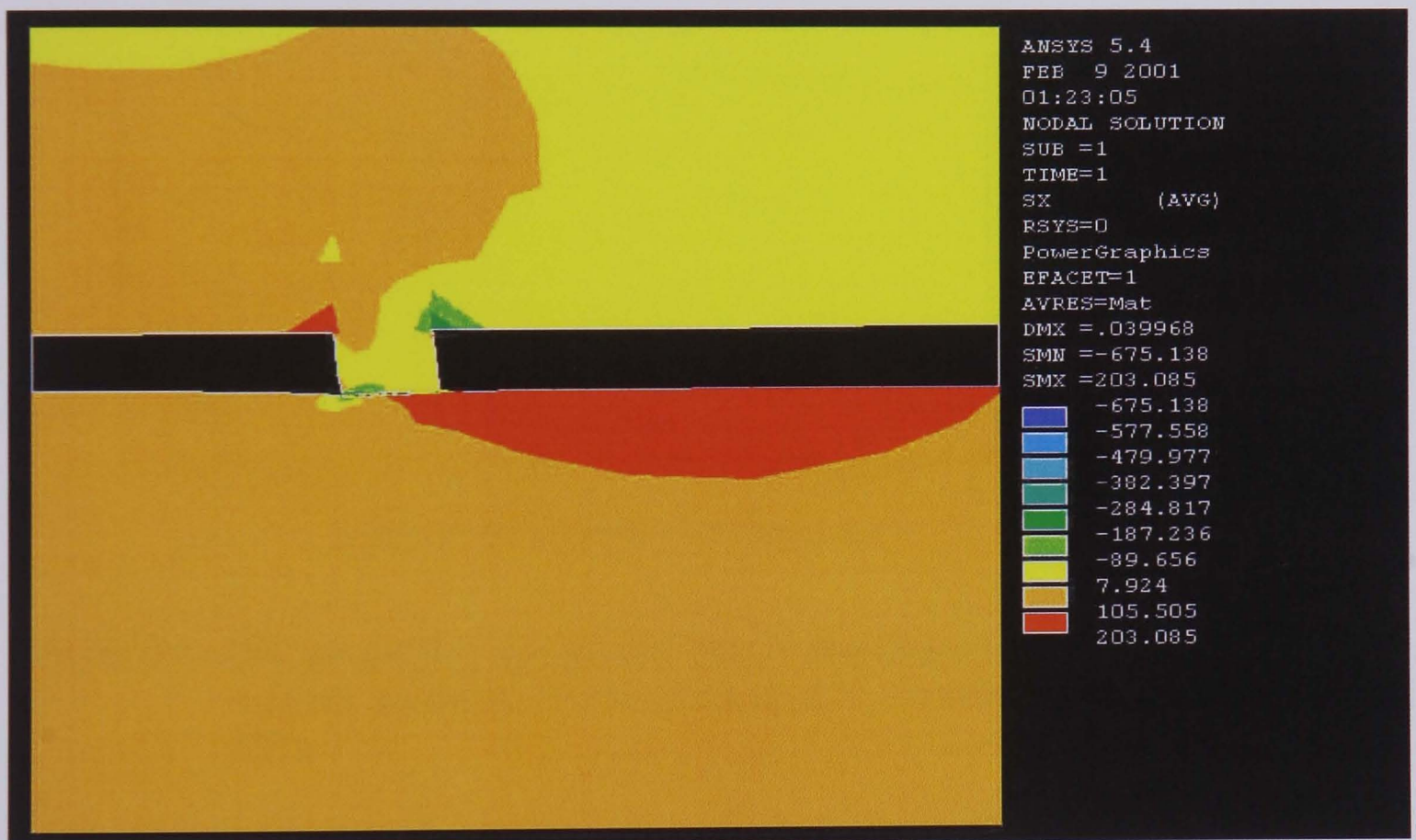


Figure 5.4: Regions of stress concentration between the fretting specimen and bridge pad for a normal pressure of 80 MPa and coefficient of friction of 0.580.

Data relating to the distribution of the stresses over the contact area were plotted for every combination of normal pressure and friction ratio at each step of the applied cyclic axial stress: 0 MPa, 100 MPa, 0 MPa and -100 MPa.

Figure 5.5 presents the tangential and shear stress distributions along the contact where the cyclic axial stress was at its maximum. It shows that these stresses have peak values at only one of the edges of the pad, the leading edge, which differs from the case of zero axial stress where there were peaks at both edges. This implies that the value and location of the maximum tangential stress, $\sigma_{\theta\theta max}$, changes during cyclic loading along the contact interface according to the magnitude of the normal pressure applied.

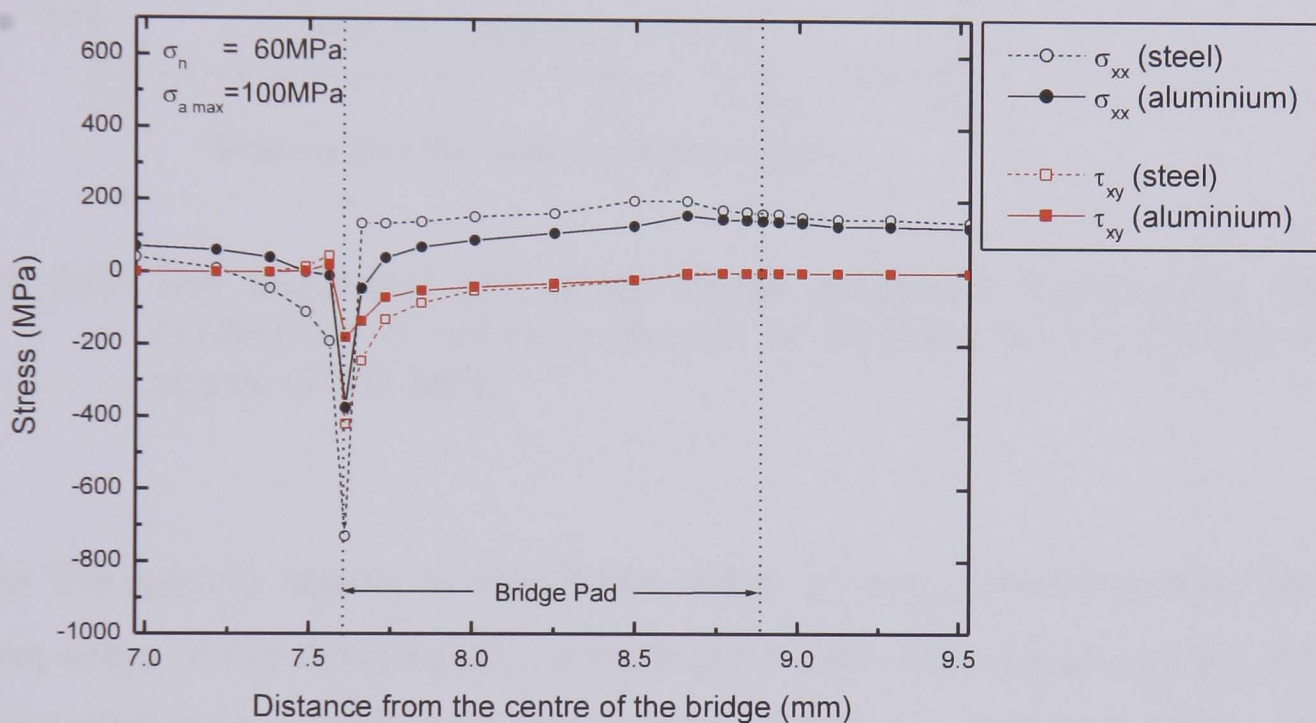


Figure 5.5: The tangential and shear stress distributions over the contact for a normal pressure of 60 MPa and a maximum axial stress of 100 MPa.

The maximum effective amplitude of tangential stress perpendicular to the crack trajectory, $\Delta\sigma_{\theta\theta*max}$ was identified by Dubourg and Lamacq [252] as a possible parameter for predicting the direction of crack propagation during stage II crack growth. In this case, the distribution of the tangential stress range, $\Delta\sigma_{xx}$ was plotted, together with the shear stress range, $\Delta\tau_{xy}$, as a function of the length of the contact region, with data obtained from the results of the finite element analyses, an example of which is shown in Figure 5.6.

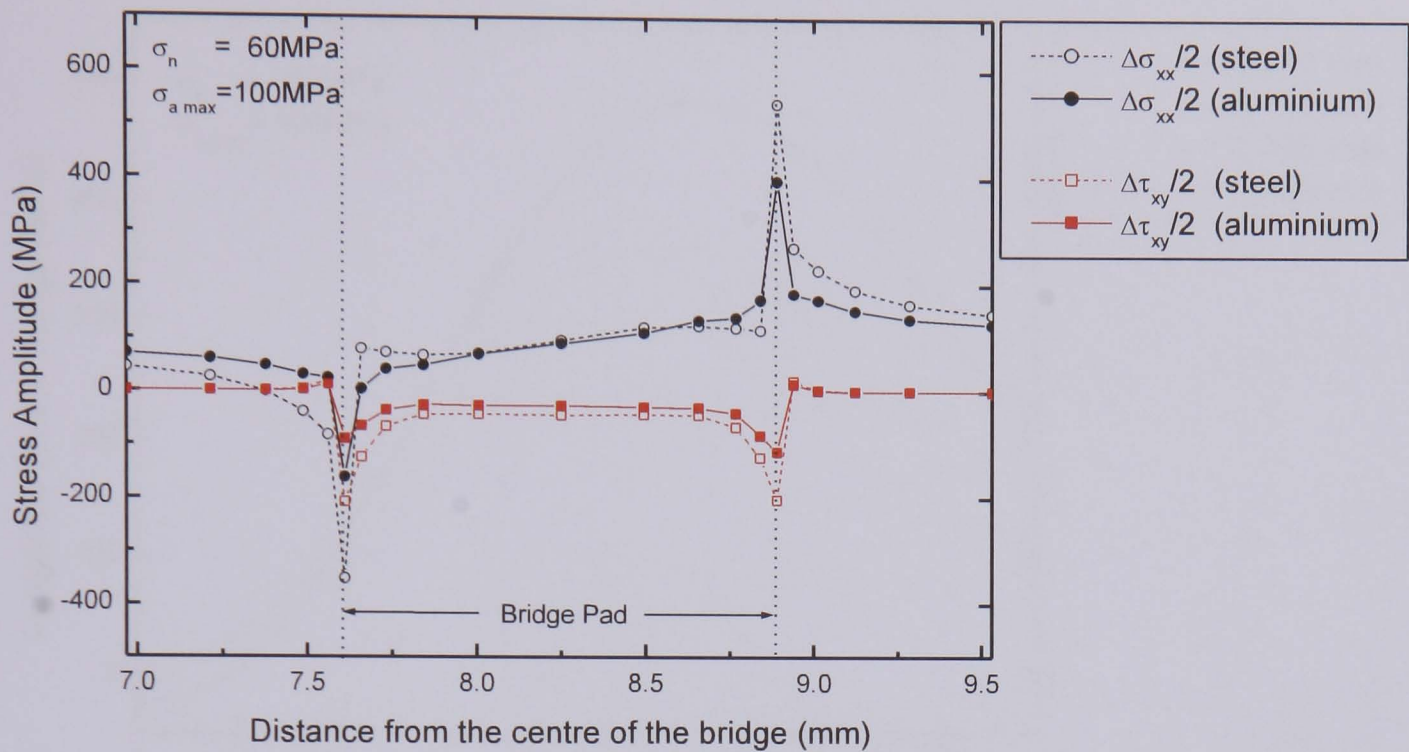


Figure 5.6: The tangential and shear stress amplitude distributions over the contact for a normal pressure of 60 MPa and a maximum axial stress of 100 MPa.

Figure 5.6 clearly shows a maximum value of $\Delta\sigma_{xx}$, corresponding with the leading edge of the bridge pad. Comparisons with observations made from the experimental tests, confirmed this site as being the primary crack initiation location.

By studying the variation of $\Delta\sigma_{xx}$ with angular locations below the leading edges of the bridge feet at various depths as shown in Figure 5.7, it was subsequently possible to identify the initial direction of crack growth.

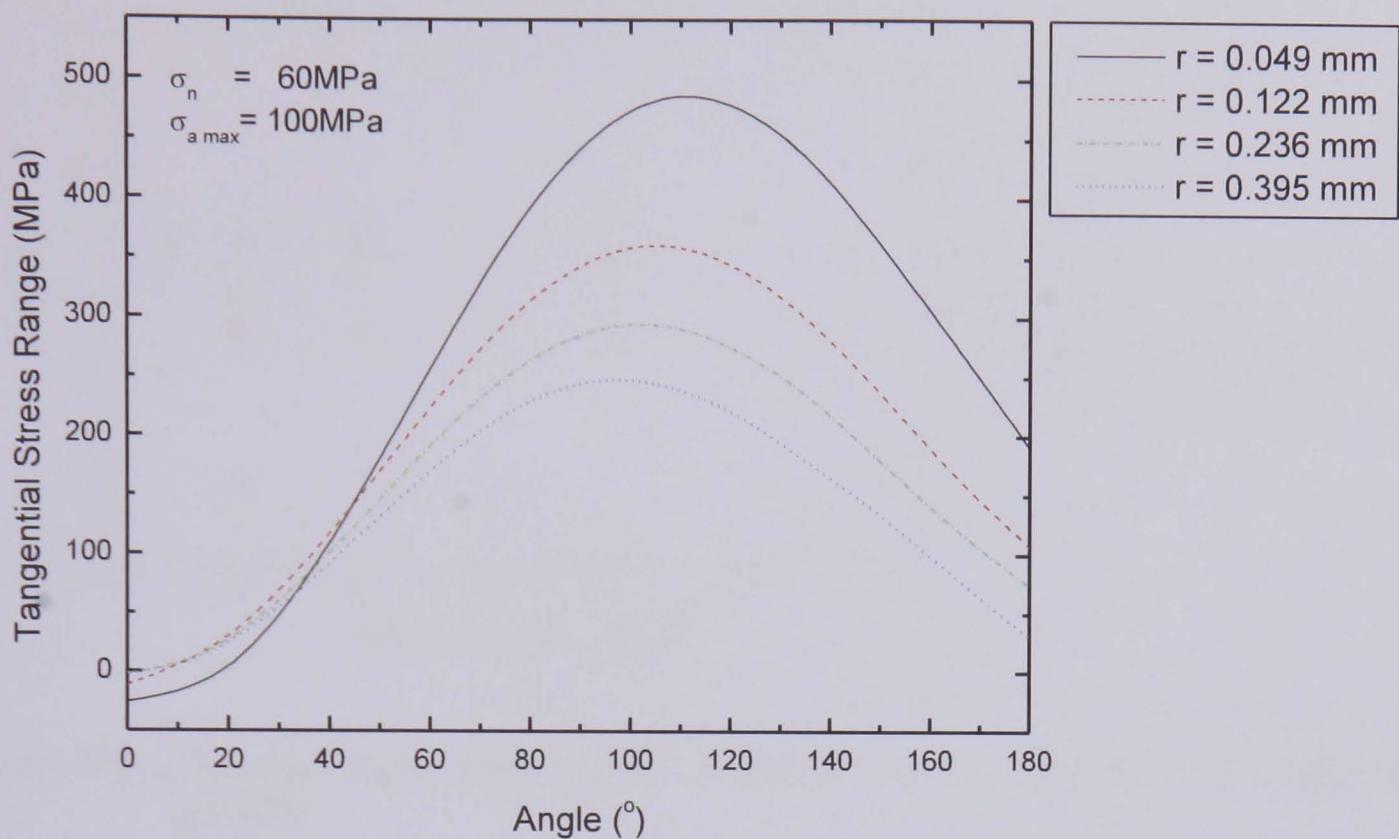


Figure 5.7: The relationship between the tangential stress range and various angles below the leading edge of a bridge pad at various depths for a normal pressure of 60 MPa and a maximum axial stress of 100 MPa.

These results are summarized in Figure 5.8 where they are compared with test data previously reported by Fernando et al. for BS L65 4 % copper aluminium alloy in flat-on-flat contact with BS S98 steel [99] as well as with the initial direction of crack growth data obtained from this test programme. It shows that initial crack directions at normal pressures investigated for both contact materials coincide with the direction the maximum value of the tangential stress range, $\Delta\sigma_{\theta\theta max}$.

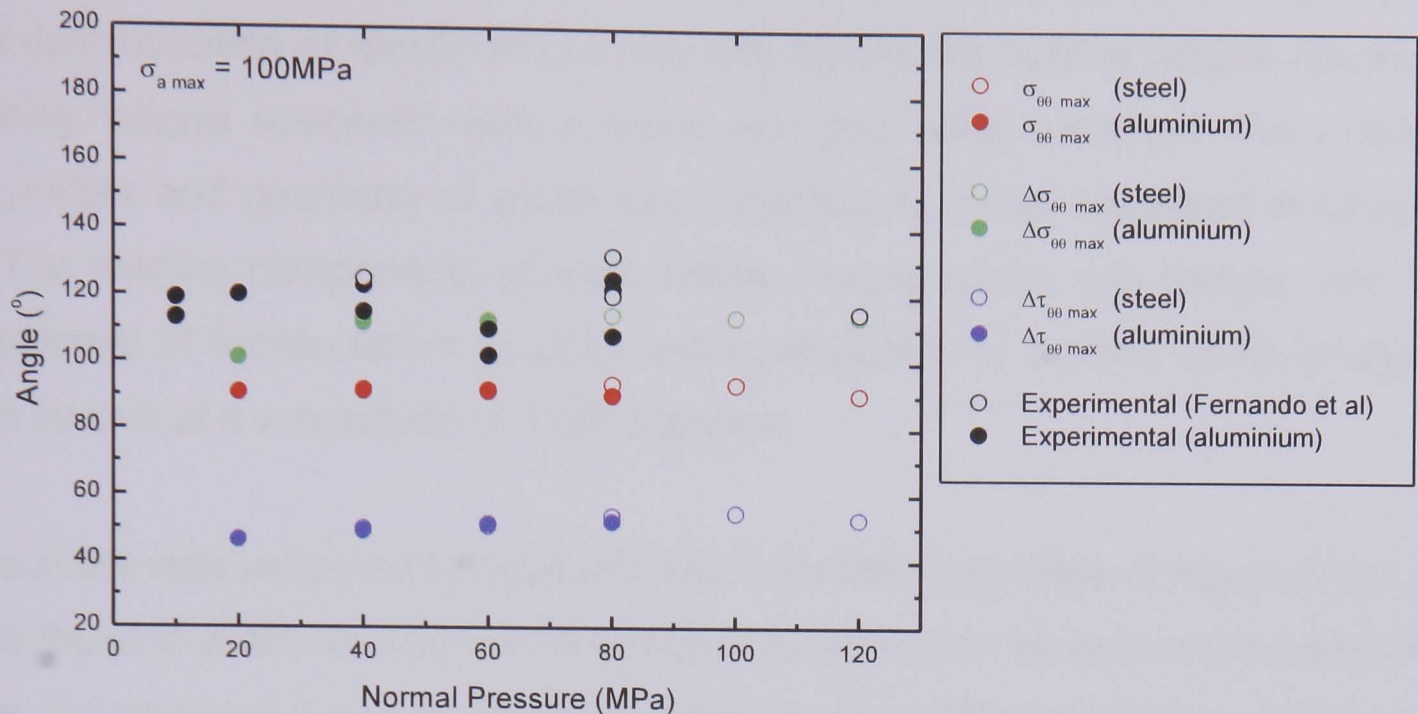


Figure 5.8: The variation, with normal pressure, of the direction of initial crack growth.

5.3 FRETTING FATIGUE LIFE

5.3.1 Unpeened

5.3.1.1 Elastic Stress Intensity Factors

The fretting fatigue cracks examined in Chapter 4 and in Section 5.2 predominantly stem from the leading edge of the fretting contact. These cracks are also shown to propagate as inclined and then normal edge cracks, demonstrating that fretting cracks initially grow under a combination of mode I, tensile and mode II, shear fatigue loading, before turning to a mode I plane prior to propagating to failure. When applying linear elastic fracture mechanics techniques to a fretting problem, the magnitude of the axial load, normal load and friction force need to be considered and both stress intensity factors K_I and K_{II} are subsequently required.

In 1994, Sheikh et al. [102] developed a suitable finite element procedure for the determination of elastic stress intensity factors for fretting fatigue cracks. A fretting fatigue specimen with a crack and pad were modelled, the material properties and geometry of which were identical to those described in Chapter 3. The loading components of axial stress, normal stress and friction, with the coefficient of friction taken as unity, were simulated for a plane strain analysis, one by one at a magnitude of 1 GPa apiece.

The crack was assumed to have initiated from the outer edge of the pad foot, as was found in practice, and was subsequently advanced by incremental amounts from 0.1 mm to 2.0 mm to obtain the strain energy release rates G_I and G_{II} , see Equations 5.1 and Equation 5.2, from which the stress intensity factors were obtained for a range of crack lengths.

$$G_I = \frac{K_I^2}{E'}, \quad G_{II} = \frac{K_{II}^2}{E'} \quad \text{Equation 5.1}$$

$$E' = \frac{E}{(1 - \nu^2)} \quad \text{Equation 5.2}$$

Among the analyses performed, values of K_I and K_{II} were obtained for a pad span of 16.5 mm, a uniform, constant normal load and a crack stemming from the leading edge of the pad at an angle of 22.5°. K_I and K_{II} v crack length, a , data for the individual unit load cases, axial load, σ_a , normal load, σ_n and friction load, σ_f were published and are given in Tables 5.1, 5.2 and 5.3.

These results quote K in terms of $\text{GPa}\sqrt{\text{mm}}$, arising from modelling a 1 mm crack with 1 GPa stress applied, Equation 5.3.

$$K_I = Y_I \sigma \sqrt{\pi a} = Y_I \sqrt{\pi}, \quad K_{II} = Y_{II} \sigma \sqrt{\pi a} = Y_{II} \sqrt{\pi} \quad \text{Equation 5.3}$$

The geometrical parameters Y_I and Y_{II} were subsequently calculated by means of Equation 5.4, independent of the units of K ; these too are given in Tables 5.1, 5.2 and 5.3.

$$Y_I = \frac{K_I}{\sqrt{\pi}}, \quad Y_{II} = \frac{K_{II}}{\sqrt{\pi}} \quad \text{Equation 5.4}$$

Table 5.1: K_I , K_{II} and a data for an applied axial stress of 1 GPa extracted from a graph published by Sheikh et al. [102], together with Y_I and Y_{II} figures calculated by means of Equation 5.4.

a (mm)	$K_{I \text{ axial}}$ (GPa $\sqrt{\text{mm}}$)	$K_{II \text{ axial}}$ (GPa $\sqrt{\text{mm}}$)	$Y_{I \text{ axial}}$	$Y_{II \text{ axial}}$
0.1	0.525	-0.16	0.30	-0.09
0.2	0.75	-0.2	0.42	-0.11
0.3	0.95	-0.24	0.54	-0.14
0.4	1.075	-0.28	0.61	-0.16
0.5	1.225	-0.32	0.69	-0.18
0.6	1.35	-0.34	0.76	-0.19
0.7	1.45	-0.38	0.82	-0.21
0.8	1.55	-0.4	0.87	-0.23
0.9	1.65	-0.43	0.93	-0.24
1	1.725	-0.45	0.97	-0.25
1.1	1.825	-0.47	1.03	-0.27
1.2	1.9	-0.49	1.07	-0.28
1.3	1.975	-0.5	1.11	-0.28
1.4	2.05	-0.52	1.16	-0.29
1.5	2.15	-0.54	1.21	-0.30
1.6	2.2	-0.56	1.24	-0.32
1.7	2.275	-0.58	1.28	-0.33
1.8	2.35	-0.6	1.33	-0.34
1.9	2.375	-0.62	1.34	-0.35
2	2.45	-0.64	1.38	-0.36

Table 5.2: K_I , K_{II} and a data for a normal pressure of 1 GPa extracted from a graph published by Sheikh et al. [102], together with Y_I and Y_{II} figures calculated by means of Equation 5.4.

a (mm)	$K_{I \text{ normal}}$ (GPa $\sqrt{\text{mm}}$)	$K_{II \text{ normal}}$ (GPa $\sqrt{\text{mm}}$)	$Y_{I \text{ normal}}$	$Y_{II \text{ normal}}$
0.1	-0.43	-0.25	-0.24	-0.14
0.2	-0.59	-0.36	-0.33	-0.20
0.3	-0.7	-0.46	-0.39	-0.26
0.4	-0.77	-0.54	-0.43	-0.30
0.5	-0.83	-0.61	-0.47	-0.34
0.6	-0.87	-0.67	-0.49	-0.38
0.7	-0.88	-0.72	-0.50	-0.41
0.8	-0.89	-0.75	-0.50	-0.42
0.9	-0.9	-0.78	-0.51	-0.44
1	-0.88	-0.81	-0.50	-0.46
1.1	-0.86	-0.83	-0.49	-0.47
1.2	-0.84	-0.83	-0.47	-0.47
1.3	-0.82	-0.84	-0.46	-0.47
1.4	-0.8	-0.85	-0.45	-0.48
1.5	-0.78	-0.86	-0.44	-0.49
1.6	-0.76	-0.87	-0.43	-0.49
1.7	-0.74	-0.87	-0.42	-0.49
1.8	-0.72	-0.87	-0.41	-0.49
1.9	-0.71	-0.86	-0.40	-0.49
2	-0.69	-0.85	-0.39	-0.48

Table 5.3: K_I , K_{II} and a data for a resultant friction stress of 1 GPa extracted from a graph published by Sheikh et al. [102], together with Y_I and Y_{II} figures calculated by means of Equation 5.4.

a (mm)	$K_{I \text{ friction}}$ (GPa $\sqrt{\text{mm}}$)	$K_{II \text{ friction}}$ (GPa $\sqrt{\text{mm}}$)	$Y_{I \text{ friction}}$	$Y_{II \text{ friction}}$
0.1	1.26	0.08	0.71	0.05
0.2	1.42	0.2	0.80	0.11
0.3	1.48	0.31	0.84	0.17
0.4	1.47	0.38	0.83	0.21
0.5	1.43	0.44	0.81	0.25
0.6	1.38	0.48	0.78	0.27
0.7	1.34	0.51	0.76	0.29
0.8	1.28	0.52	0.72	0.29
0.9	1.21	0.53	0.68	0.30
1	1.15	0.545	0.65	0.31
1.1	1.1	0.545	0.62	0.31
1.2	1.04	0.54	0.59	0.30
1.3	0.98	0.53	0.55	0.30
1.4	0.94	0.525	0.53	0.30
1.5	0.9	0.515	0.51	0.29
1.6	0.85	0.505	0.48	0.28
1.7	0.83	0.5	0.47	0.28
1.8	0.79	0.49	0.45	0.28
1.9	0.76	0.48	0.43	0.27
2	0.73	0.47	0.41	0.27

Each individual Y_I and Y_{II} curve has been fitted using a range of polynomial equations up to an order of ten, see Equation 5.5, as shown in Figures 5.9, 5.11 and 5.13 for the Y_I values and 5.10, 5.12 and 5.14 for the Y_{II} values. Reasonable agreement was achieved with fourth order equations, however, as the curves were not to be extended beyond the length of the 2 mm crack defined by Sheikh et al. [102], it was decided that the most accurate fit achievable could be applied without any risk of instability.

$$y = -A + Bx + Cx^2 - Dx^3 + Ex^4 - Fx^5 + Gx^6 - Hx^7 + Ix^8 - Jx^9 + Kx^{10} \quad \text{Equation 5.5}$$

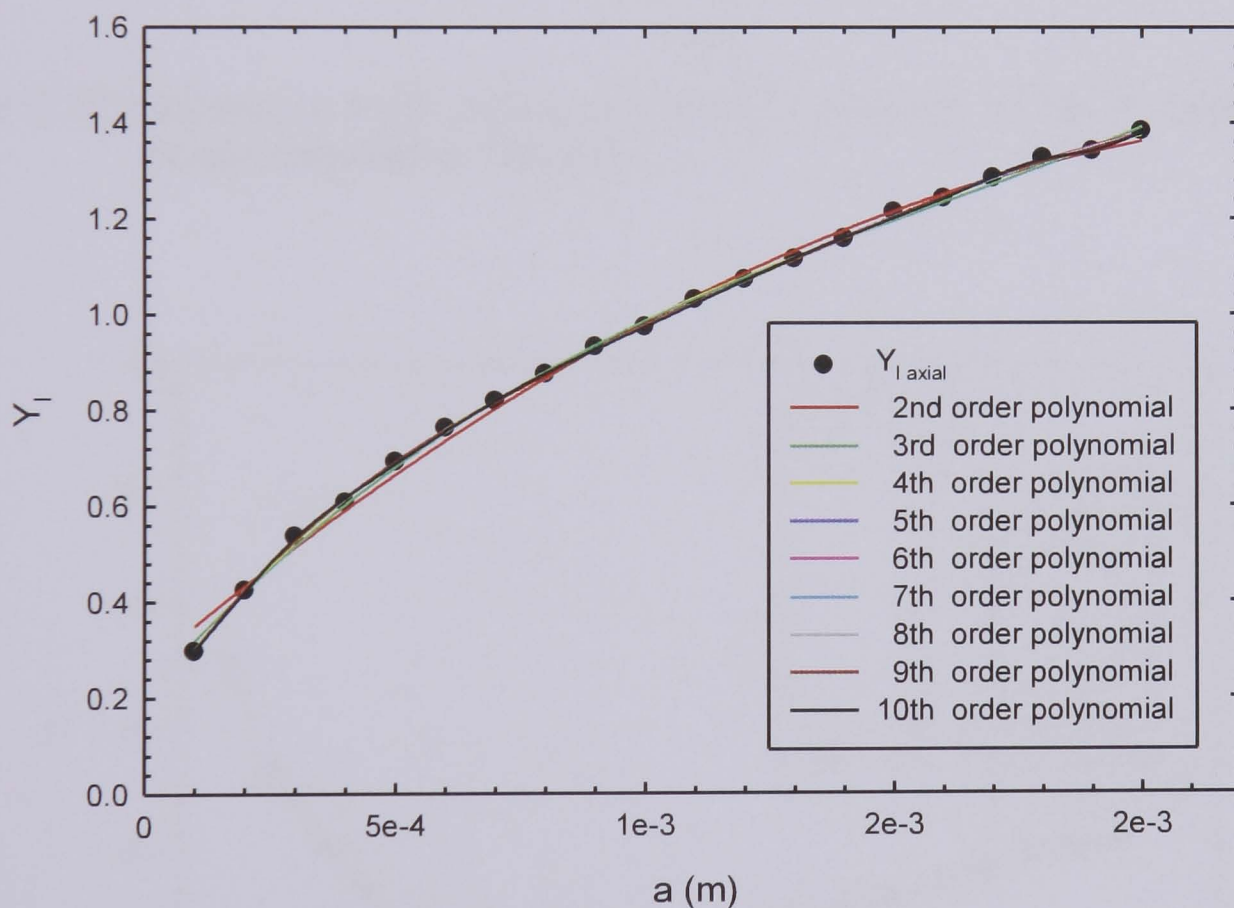


Figure 5.9: Second to tenth order polynomial curve fits of the Y_I data for axial stress detailed in Table 5.1.

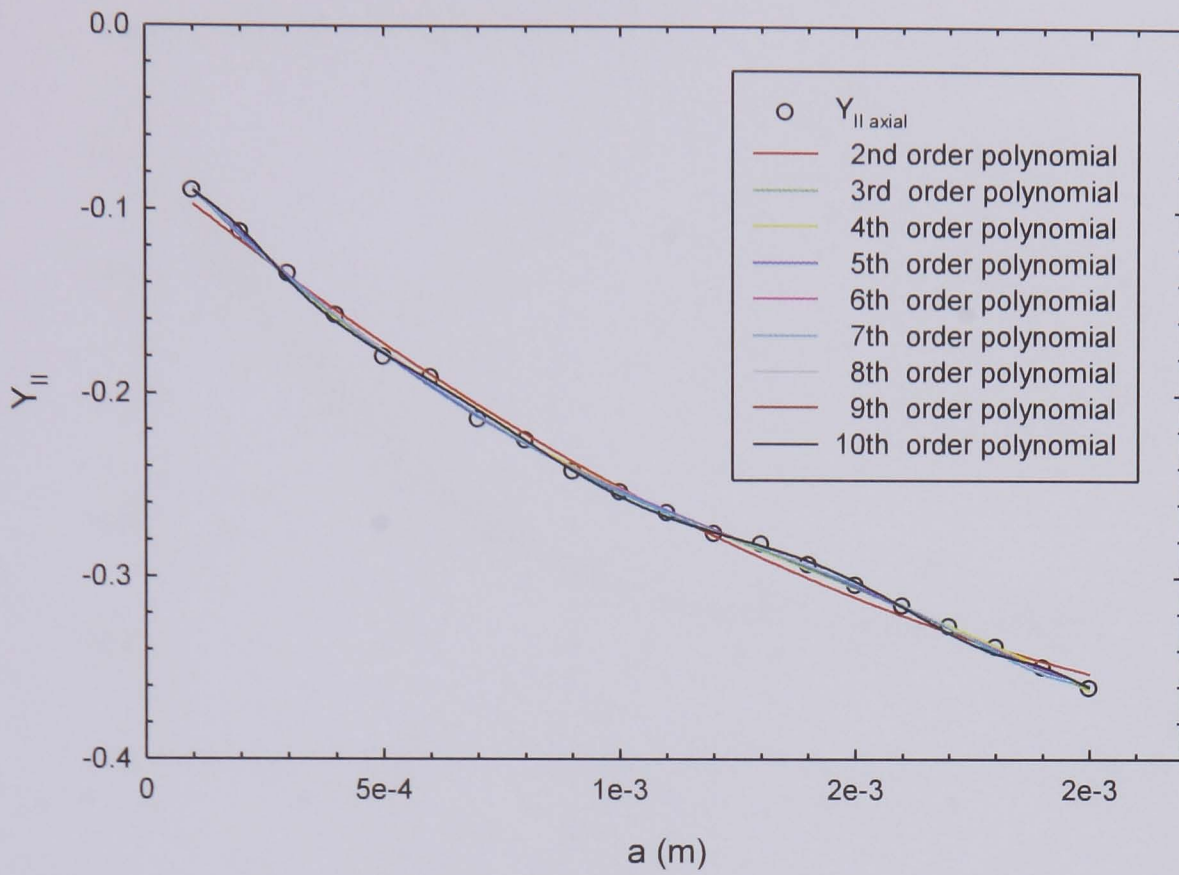


Figure 5.10: Second to tenth order polynomial curve fits of the Y_{II} data for axial stress detailed in Table 5.1.

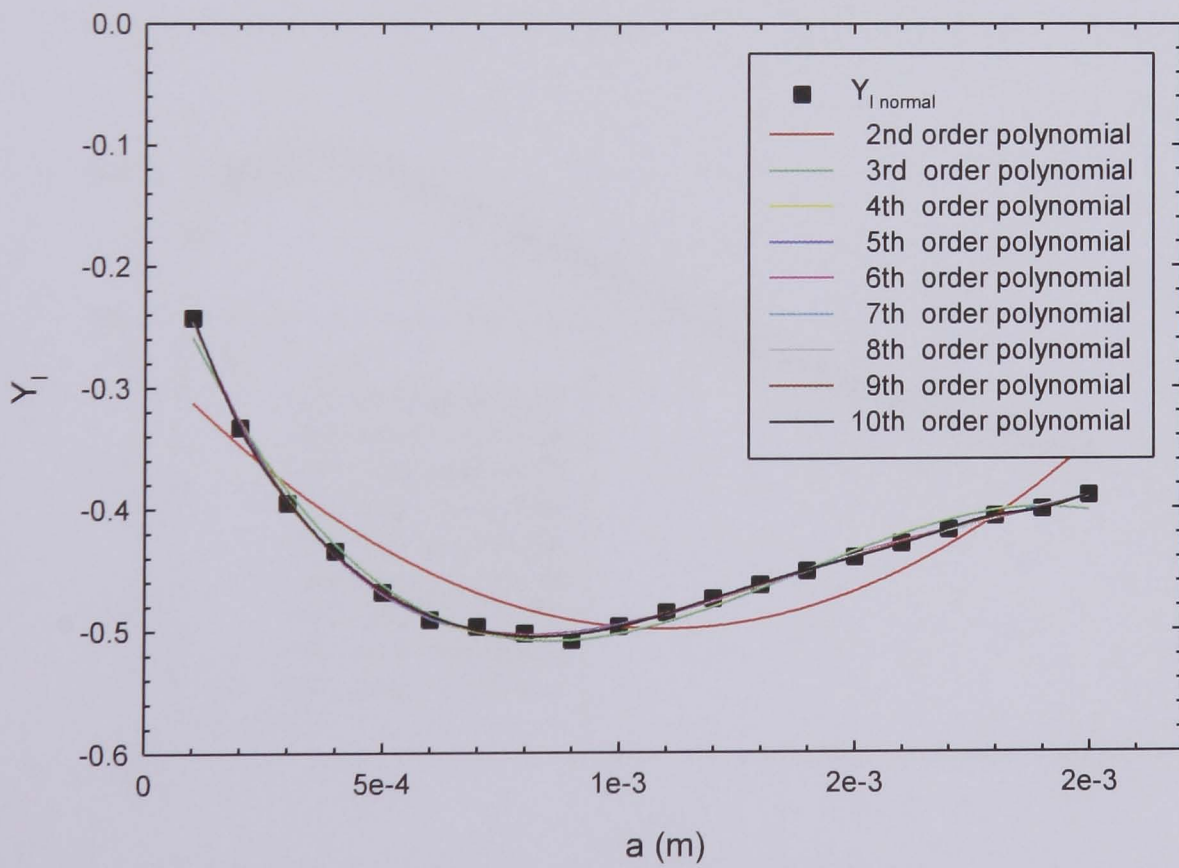


Figure 5.11: Second to tenth order polynomial curve fits of the Y_I data for normal stress detailed in Table 5.2.

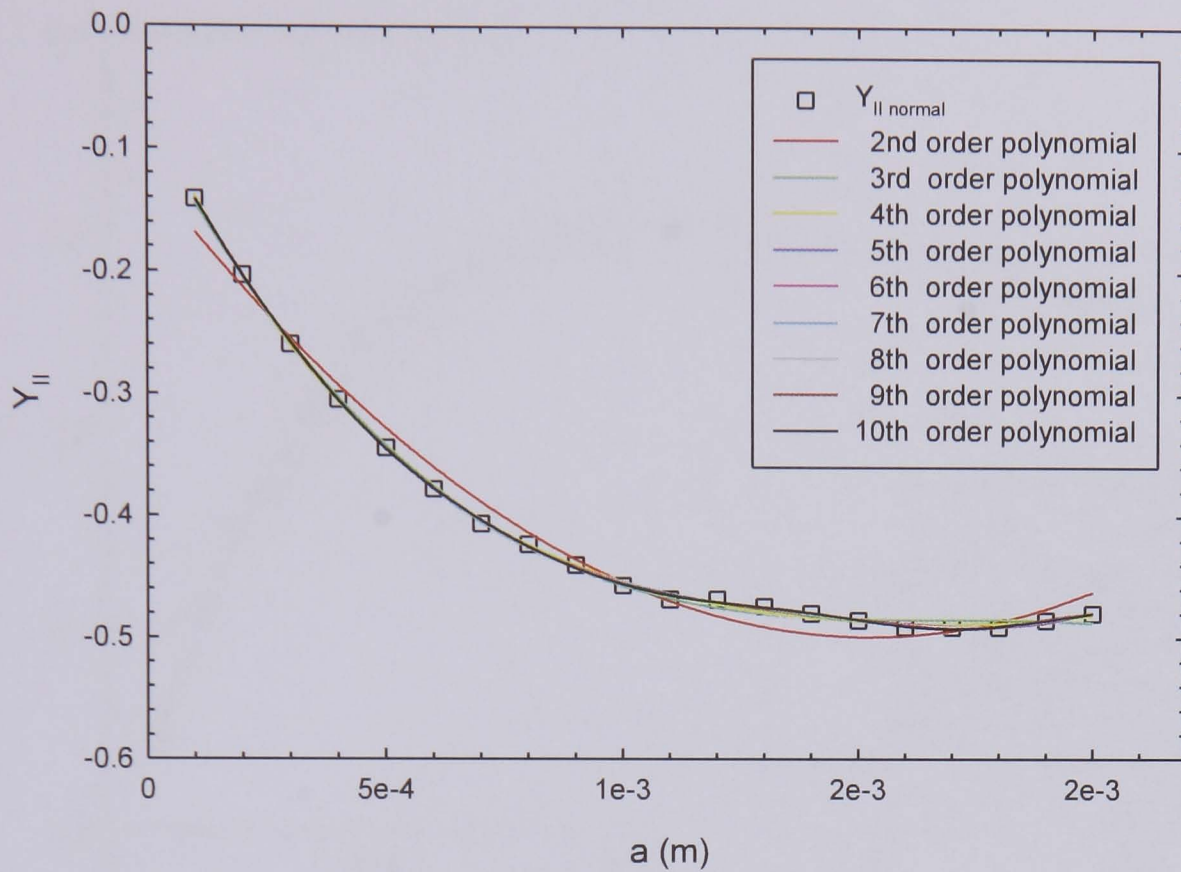


Figure 5.12: Second to tenth order polynomial curve fits of the Y_{II} data for normal stress detailed in Table 5.2.

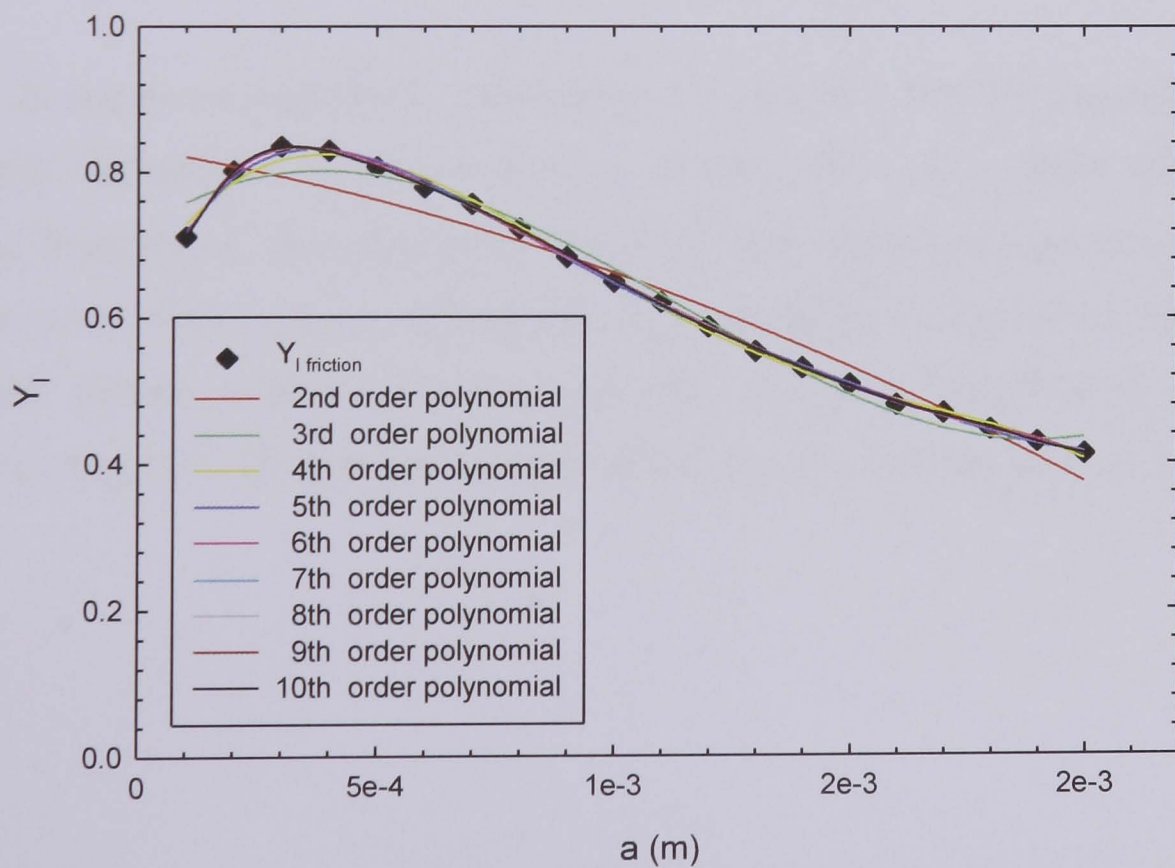


Figure 5.13: Second to tenth order polynomial curve fits of the Y_I data for friction stress detailed in Table 5.3.

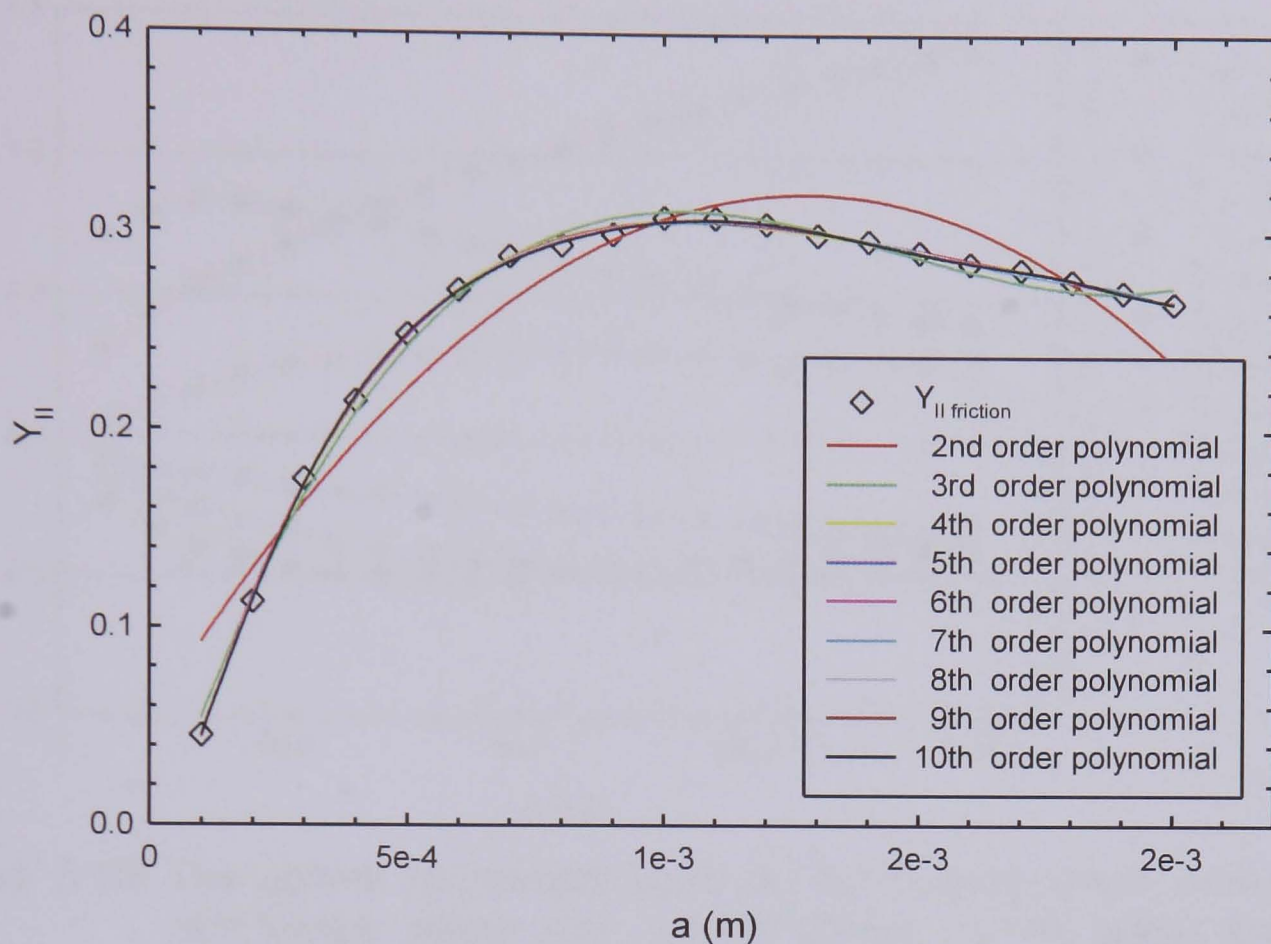


Figure 5.14: Second to tenth order polynomial curve fits of the Y_{II} data for friction stress detailed in Table 5.3.

Y_I and Y_{II} were subsequently calculated for specific values of crack length, a , using the constants derived from the curves and the optima subsequently selected from those demonstrating the least difference between the data values and the curve fitted values; equations for each geometrical factor were thereby achieved. These detailed analyses can be found in Appendix V; the curves chosen in Figure 5.15 and the related constants are summarised in Table 5.4.

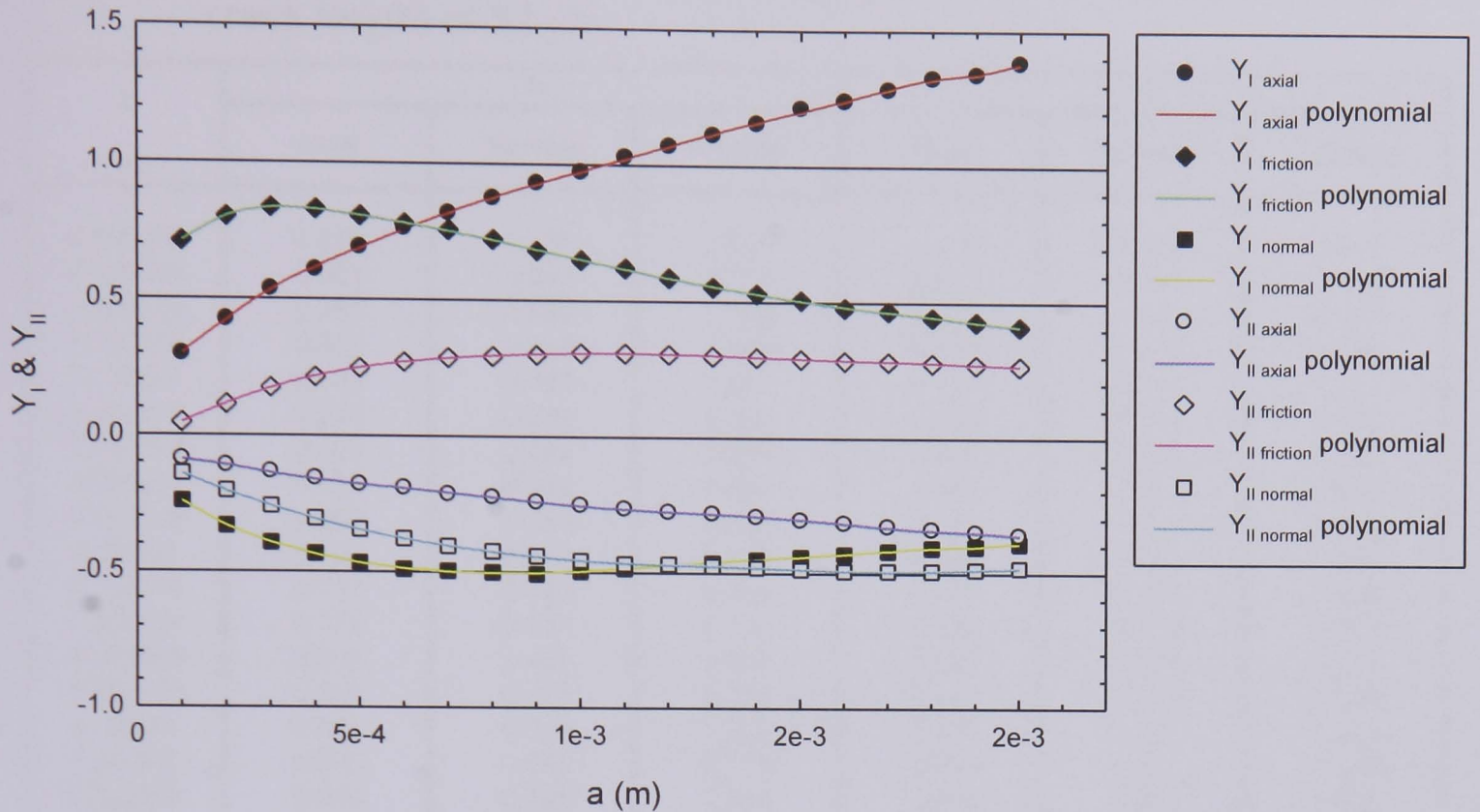


Figure 5.15: The optima polynomial curve fits for Y_I axial stress, normal stress and friction stress and Y_{II} axial stress, normal stress and friction stress.

Table 5.4: The coefficients of the optima polynomial curve fits for Y_I axial stress, normal stress and friction stress and Y_{II} axial stress, normal stress and friction stress.

Coefficient	Y_I			Y_{II}		
	Axial	Normal	Friction	Axial	Normal	Friction
A	3.523762E-01	-6.940012E-02	5.946026E-01	-6.669092E-02	-3.579200E-02	-2.226271E-02
B	-2.972166E+03	-2.519691E+03	8.476127E+02	-2.245669E+02	-1.552783E+03	5.840282E+02
C	3.761530E+07	1.087826E+07	7.332426E+06	-8.227373E+04	7.495312E+06	1.460852E+06
D	-1.678874E+11	-3.756751E+10	-5.542654E+10	2.365289E+08	-3.190279E+10	-6.916605E+09
E	4.225591E+14	8.832361E+13	1.600005E+14	-1.428202E+11	8.304006E+13	1.267639E+13
F	-6.576089E+17	-1.363903E+17	-2.602423E+17	2.741509E+13	-1.332101E+17	-1.462234E+16
G	6.548267E+20	1.382643E+20	2.614183E+20		1.352701E+20	1.222723E+19
H	-4.177144E+23	-9.078764E+22	-1.655373E+23		-8.706070E+22	-7.616228E+21
I	1.650305E+26	3.704614E+25	6.442031E+25		3.436861E+25	3.277550E+24
J	-3.675254E+28	-8.516033E+27	-1.408009E+28		-7.583474E+27	-8.360368E+26
K	3.525574E+30	8.411684E+29	1.323605E+30		7.156708E+29	9.280659E+28

The geometrical parameters Y_I and Y_{II} were calculated starting at and incrementing by, a crack length, a , of $52 \mu\text{m}$, the average grain width for aluminium alloy 2024 T351, see Table 5.5.

Table 5.5: Y_I , Y_{II} and a data for axial, normal and friction stresses, starting at a crack length of 52 μm .

a (m)	Y_I			Y_{II}		
	Axial	Normal	Friction	Axial	Normal	Friction
0						
0.000052	0.279	-0.176	0.652	-0.079	-0.100	0.011
0.000104	0.303	-0.247	0.716	-0.091	-0.144	0.048
0.000156	0.365	-0.299	0.769	-0.103	-0.178	0.084
0.000208	0.432	-0.339	0.806	-0.115	-0.208	0.119
0.00026	0.493	-0.372	0.827	-0.127	-0.237	0.151
0.000312	0.545	-0.399	0.835	-0.139	-0.264	0.178
0.000364	0.590	-0.423	0.834	-0.150	-0.289	0.202
0.000416	0.629	-0.443	0.826	-0.161	-0.313	0.223
0.000468	0.666	-0.459	0.815	-0.172	-0.334	0.240
0.00052	0.702	-0.472	0.802	-0.182	-0.352	0.254
0.000572	0.737	-0.483	0.789	-0.191	-0.369	0.265
0.000624	0.772	-0.491	0.775	-0.200	-0.384	0.274
0.000676	0.805	-0.497	0.760	-0.209	-0.398	0.282
0.000728	0.836	-0.501	0.744	-0.217	-0.410	0.288
0.00078	0.865	-0.504	0.727	-0.225	-0.421	0.293
0.000832	0.893	-0.505	0.710	-0.232	-0.431	0.298
0.000884	0.919	-0.504	0.692	-0.239	-0.440	0.301
0.000936	0.944	-0.502	0.674	-0.245	-0.448	0.303
0.000988	0.968	-0.498	0.655	-0.251	-0.455	0.305
0.00104	0.993	-0.493	0.637	-0.257	-0.460	0.306
0.001092	1.018	-0.488	0.620	-0.263	-0.464	0.306
0.001144	1.043	-0.481	0.603	-0.268	-0.468	0.306
0.001196	1.069	-0.475	0.587	-0.273	-0.470	0.305
0.001248	1.093	-0.468	0.571	-0.279	-0.473	0.303
0.0013	1.117	-0.462	0.557	-0.284	-0.475	0.301
0.001352	1.140	-0.456	0.543	-0.290	-0.477	0.298
0.001404	1.162	-0.450	0.529	-0.295	-0.479	0.295
0.001456	1.183	-0.445	0.516	-0.300	-0.482	0.292
0.001508	1.204	-0.440	0.503	-0.306	-0.485	0.290
0.00156	1.226	-0.434	0.492	-0.312	-0.488	0.287
0.001612	1.248	-0.428	0.481	-0.318	-0.491	0.285
0.001664	1.271	-0.422	0.471	-0.324	-0.492	0.283
0.001716	1.293	-0.415	0.462	-0.330	-0.492	0.281
0.001768	1.313	-0.409	0.454	-0.336	-0.491	0.279
0.00182	1.329	-0.405	0.444	-0.342	-0.489	0.276
0.001872	1.339	-0.402	0.434	-0.347	-0.487	0.273
0.001924	1.346	-0.400	0.423	-0.353	-0.484	0.269
0.001976	1.362	-0.395	0.414	-0.358	-0.481	0.266
0.002028	1.417	-0.378	0.414	-0.363	-0.476	0.266

These geometric parameters were determined by Sheikh et al. [102] from stress intensity factors that were derived from strain energy release rates which are directionless scalars. However, in further considering the load arrangement as depicted in Figure 5.16, the sign conventions employed in this figure make the value of K_{II} due to friction equal to $-Y_{Ifraction} \mu \sigma \sqrt{\pi a}$ and this negative will be used in this study.

The negative values for K_{II} for axial, normal and friction stress components, all imply anti-clockwise shear on the crack plane.

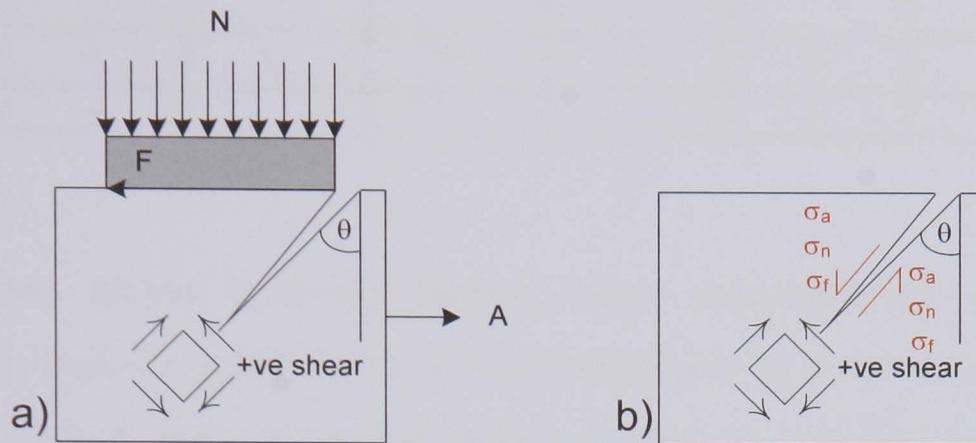


Figure 5.16: a) The load arrangement, indicating the direction of positive shear, b) The resolved stresses on the crack plane.

By substituting values of axial pressure, normal pressure and friction coefficient into Equations 5.6 and 5.7, values of K_I and K_{II} were subsequently calculated for all combinations of axial and normal loading applied and friction force recorded during testing, as detailed in Chapters 3 and 4.

$$K_I = \sigma_a Y_{Iaxial} \sqrt{\pi a}, \quad K_I = \sigma_n Y_{Inormal} \sqrt{\pi a}, \quad K_I = \mu \sigma_n Y_{Ifriiction} \sqrt{\pi a} \quad \text{Equation 5.6}$$

$$K_{II} = \sigma_a Y_{IIaxial} \sqrt{\pi a}, \quad K_{II} = \sigma_n Y_{IInormal} \sqrt{\pi a}, \quad K_{II} = -\mu \sigma_n Y_{IIfriction} \sqrt{\pi a} \quad \text{Equation 5.7}$$

As the principle of superposition applies in Linear Elastic Fracture Mechanics for open cracks, the individual stress intensity factors were combined to obtain the total stress intensity factors for each mode, giving the sign values summarised in Table 5.6. The resultant values of K_I and K_{II} are detailed in Appendix W.

Table 5.6: The sign values obtained from the superposition of the individual stress intensity factors for a tensile σ_a and a uniformly distributed σ_n . The friction stress σ_f , assumes sliding when macro slip occurs.

σ_a		σ_n		σ_f	
K_I	K_{II}	K_I	K_{II}	K_I	K_{II}
+	-	-	-	+	-

The equivalent stress intensity factors were subsequently calculated using Equation 5.8, see Chapter 2, for all combinations of axial and normal loading applied and friction force recorded during testing, as detailed in Chapters 3 and 4. Under reversed loading, cracks only open during the tensile realm, hence K_I was only evaluated where $K_I > 0$. However, in mode II, the maximum and minimum elements of a fully reversed, frictionless, sliding cycle can be equally as damaging, hence for fatigue analysis, K_{II} was considered as a range, see equation 5.9, noting that σ_n remains constant through the cycle. The resultant values of K_e are depicted in Figures 5.17, 5.18 and 5.19.

$$\Delta K_e = \sqrt{\Delta K_I^2 + \Delta K_{II}^2} \quad \text{Equation 5.8}$$

$$\frac{\Delta K_{II}}{\sqrt{\pi a}} = (Y_a \sigma_a + (-Y_f \sigma_f) + Y_n \sigma_n)_{\max} - (-Y_a \sigma_a - (-Y_f \sigma_f) + Y_n \sigma_n)_{\min} \quad \text{Equation 5.9}$$

Here we assume that $\sigma_{f \min} = -\sigma_{f \max} = \frac{1}{2} \Delta \sigma_f$ for later analyses. In this study,

$K_{I \min}$ was always zero, since axial stress was always fully reversed.

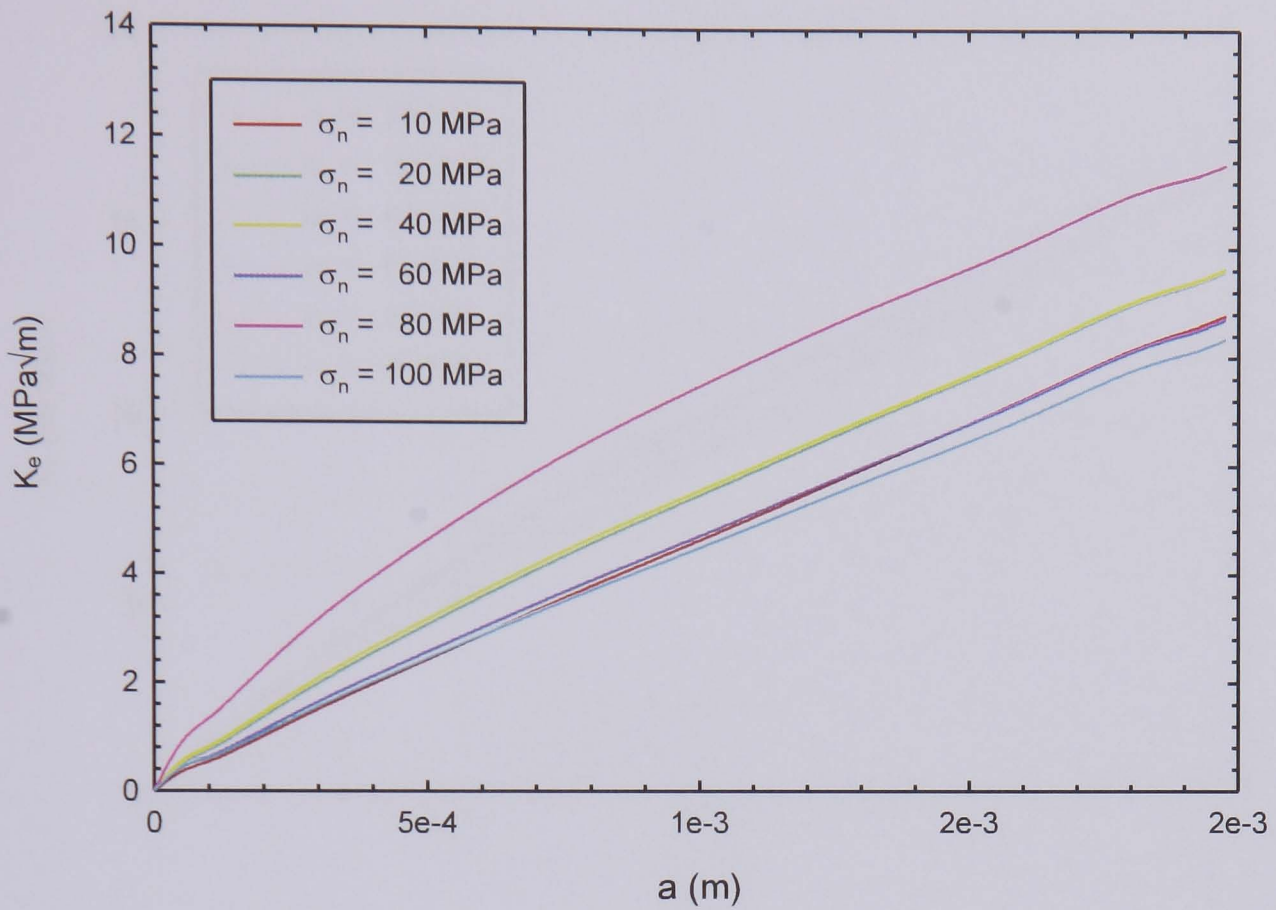


Figure 5.17: K_e v a for a range of normal stresses and an axial stress of 70 MPa and experimentally measured friction coefficients.

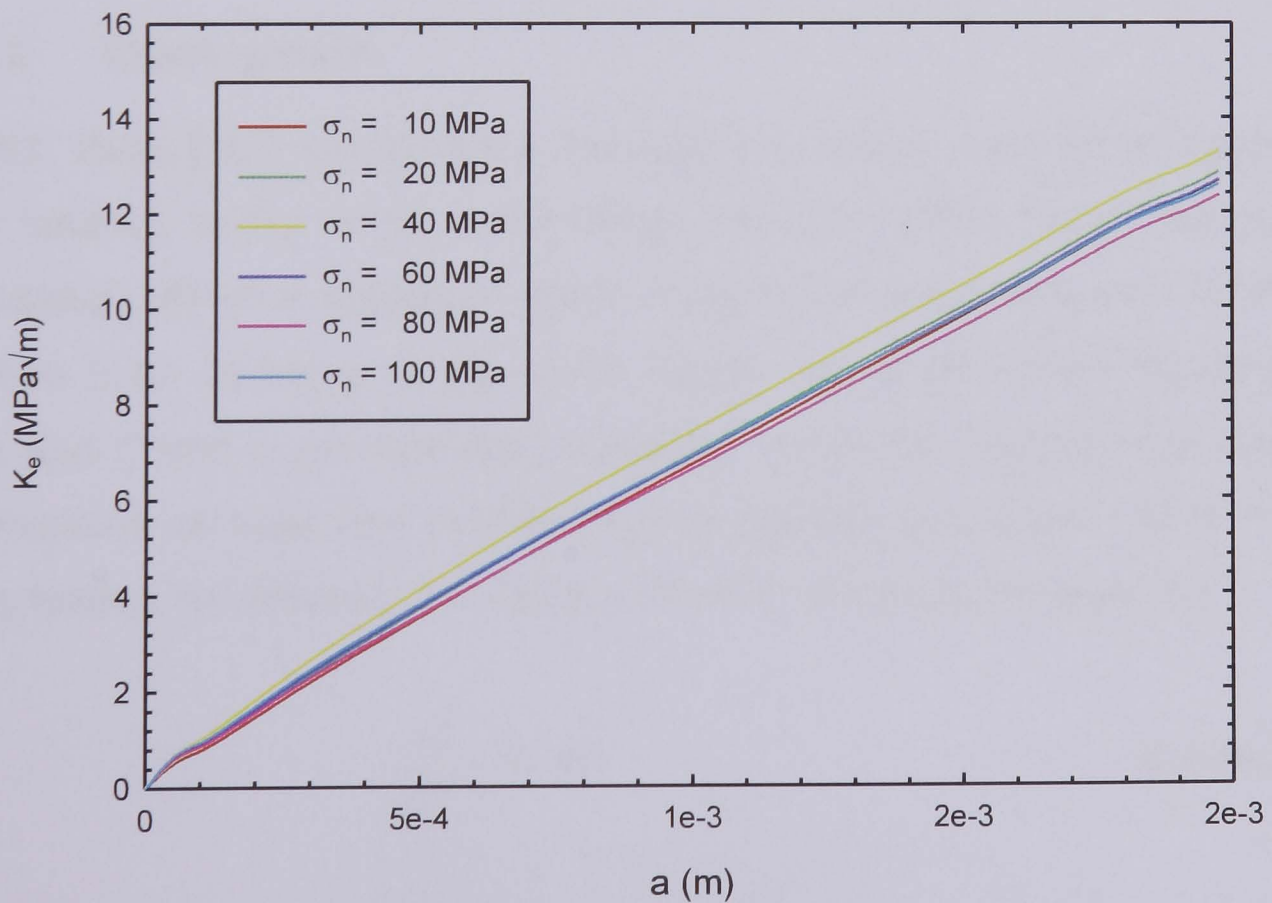


Figure 5.18: K_e v a for a range of normal stresses and an axial stress of 100 MPa experimentally measured friction coefficients.

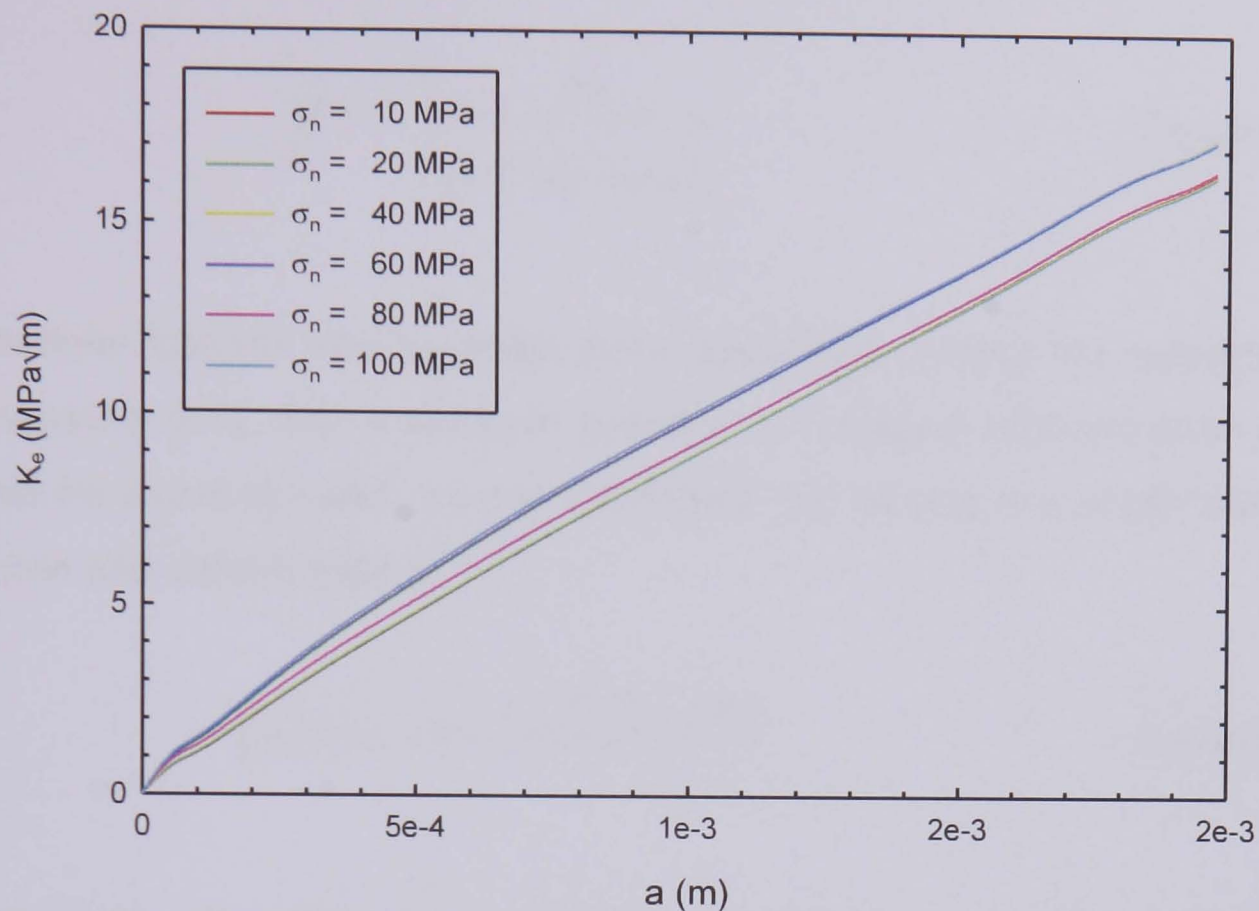


Figure 5.19: K_e v a for a range of normal stresses and an axial stress of 125 MPa experimentally measured friction coefficients.

5.3.1.2 Crack growth

In 1961, Paris [253] introduced a formula that relates crack growth rate during cyclic loading, to the range of the stress intensity factor. Paris' Law quantifies the residual life of a specimen given a particular crack size and is shown in Equation 5.10, where a , is the crack length, ΔK , is the stress intensity factor range and C and n are material constants. Values of crack growth rate for all combinations of axial and normal loading applied and friction force recorded during testing, as detailed in Chapters 3 and 4, are given in Appendix X.

$$\frac{da}{dN} = C\Delta K^n \quad \text{Equation 5.10}$$

Integrating Equation 5.10 over the crack size, results in Equation 5.11.

$$\int_0^{N_f} dN = \int_{a_i}^{a_f} \frac{da}{(CY^n \Delta \sigma^n (\pi a)^{\frac{n}{2}})} \quad \text{Equation 5.11}$$

This definite integral was approximately calculated utilising the trapezium rule, see Equation 5.12. For a concave function, an integral approximated with this rule will be overestimated, as the trapezoids will include the whole area under the curve and extend over it.

$$\int_a^b f(x)dx \approx (b-a) \frac{f(a) + f(b)}{2} \quad \text{Equation 5.12}$$

An alternative, the Simpson's rule, was therefore also utilised, so that the difference between the values for life, N_f , could be optimised, thus ensuring convergence of the numerical integration. Theoretical values of the number of cycles to failure were subsequently determined for all combinations of axial and normal loading applied and friction force recorded during testing, detailed in Chapters 3 and 4, as shown in Appendix Y. The resultant plots, together with the experimental data points are shown in Figures 5.20, 5.21 and 5.22.

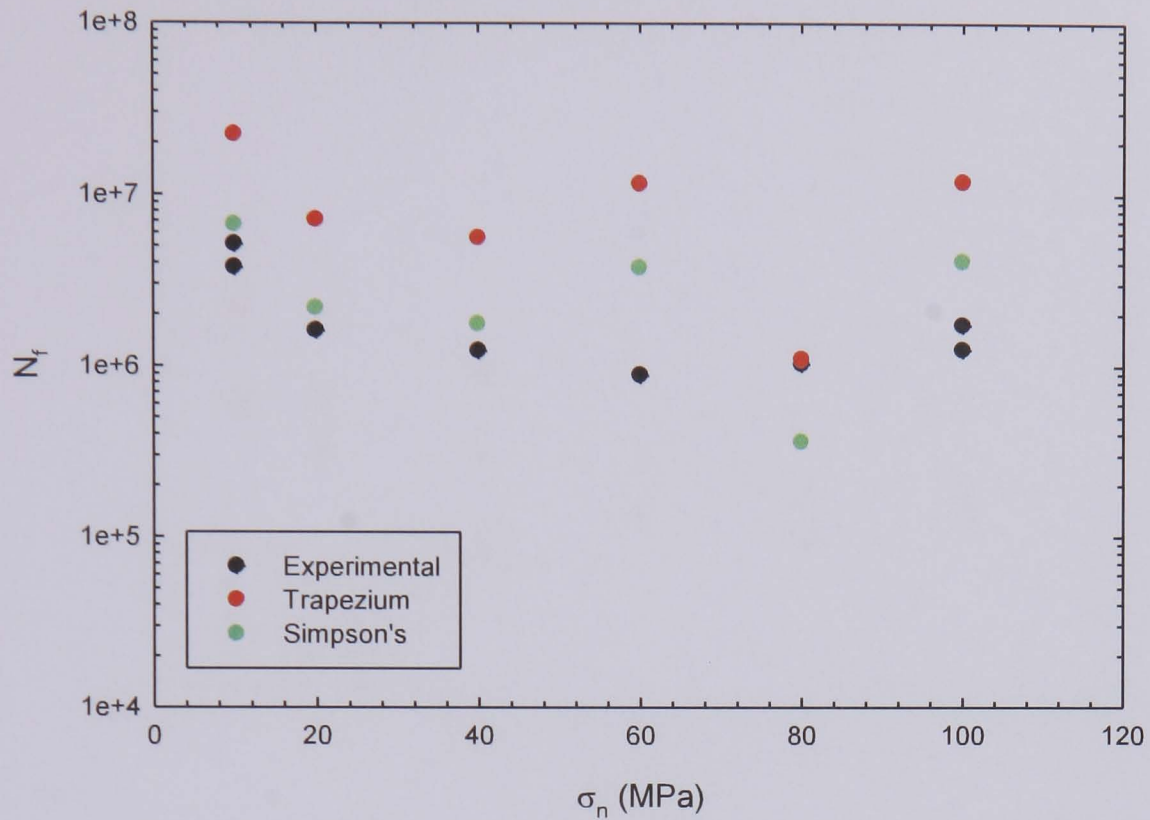


Figure 5.20: Experimental data points of N_f v σ_n and those determined experimentally using both the Trapezium rule and Simpson's rule for an axial stress of 70 MPa.

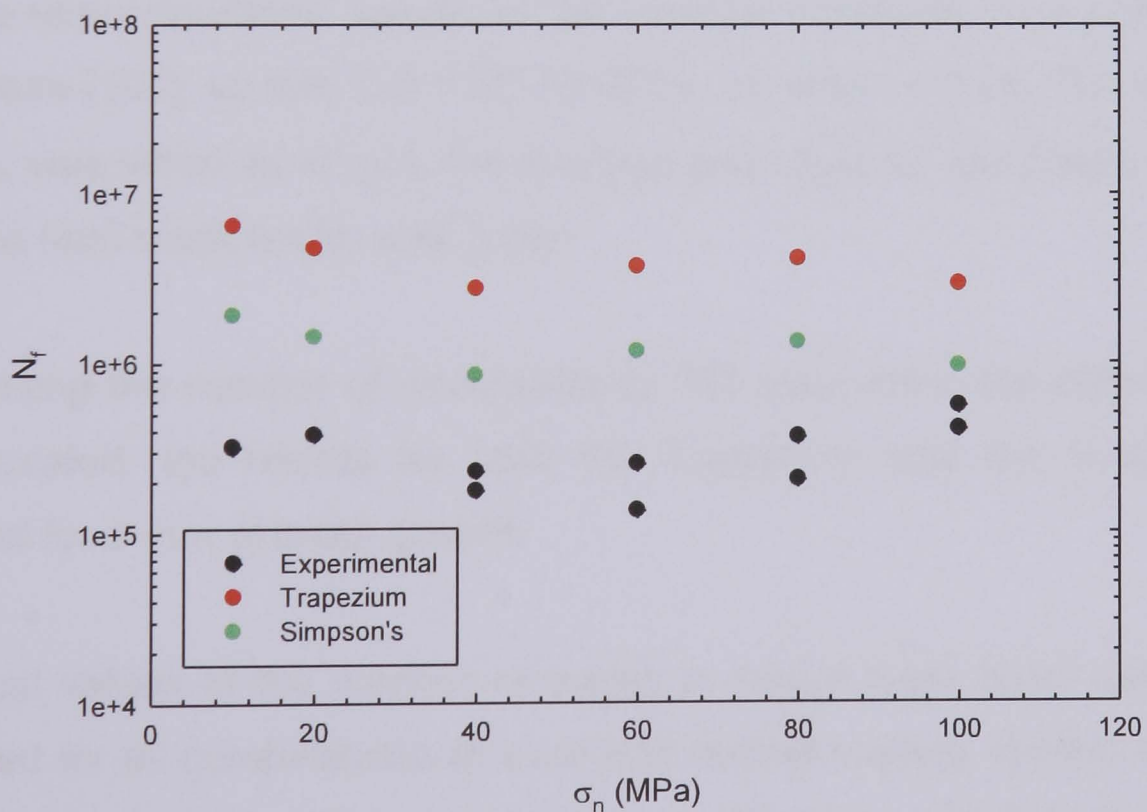


Figure 5.21: Experimental data points of N_f v σ_n and those determined experimentally using both the Trapezium rule and Simpson's rule for an axial stress of 100 MPa.

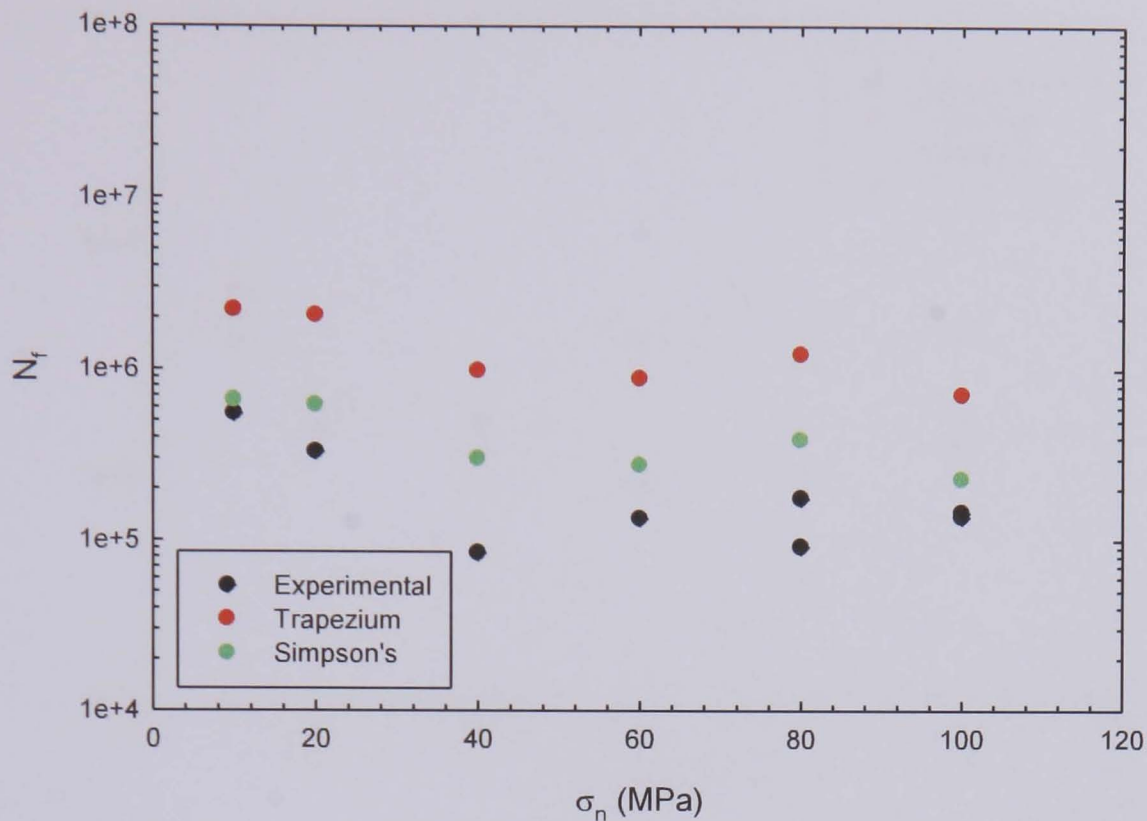


Figure 5.22: Experimental data points of N_f v σ_n and those determined experimentally using both the Trapezium rule and Simpson's rule for an axial stress of 125 MPa.

For these approximations, values for the material constants were selected from the literature [101], so that $C = 1.8E-10$ (MPa, m) and $n = 3.25$. The initial crack length, a_i , was taken as $52 \mu\text{m}$, the average grain size for aluminium alloy 2024 T351. The final crack length was 2 mm.

By increasing the number of increments to 100 over which the definite integral was calculated, the results for both the Trapezium and the Simpson rules converged for 2 mm of crack growth.

Theoretical values of the number of cycles to failure were again subsequently determined for all combinations of axial and normal loading applied and friction force recorded during testing, as detailed in Chapters 3 and 4. The resultant plots, together with the experimental data points are shown in Figures 5.23, 5.24 and 5.25.

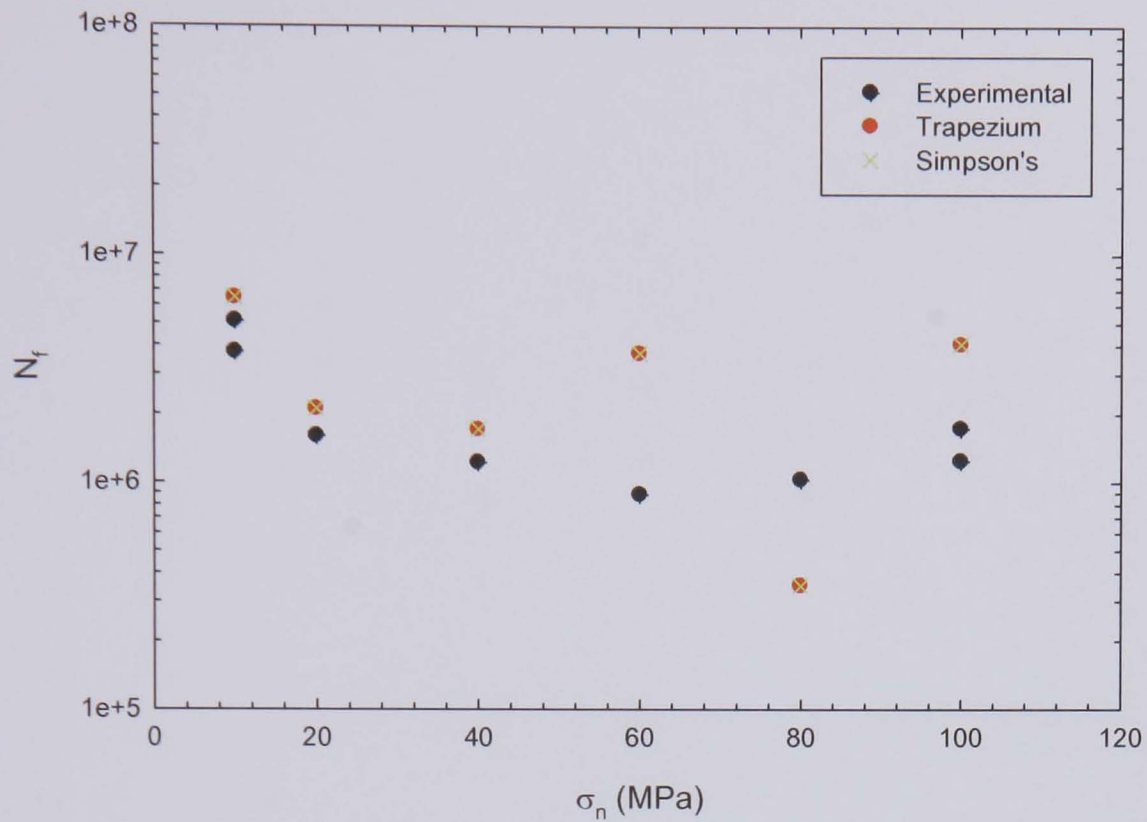


Figure 5.23: Experimental data points of N_f v σ_n and those converged using both the Trapezium rule and Simpson's rule for an axial stress of 70 MPa.

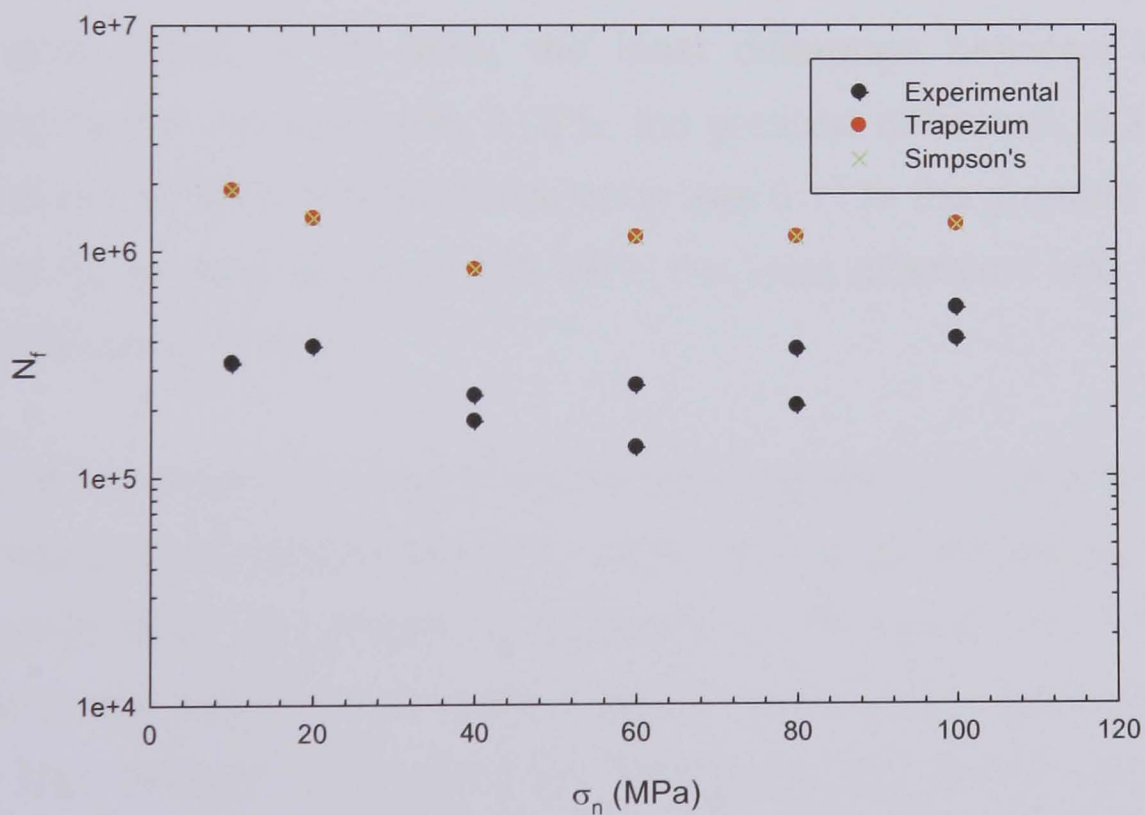


Figure 5.24: Experimental data points of N_f v σ_n and those converged using both the Trapezium rule and Simpson's rule for an axial stress of 100 MPa.

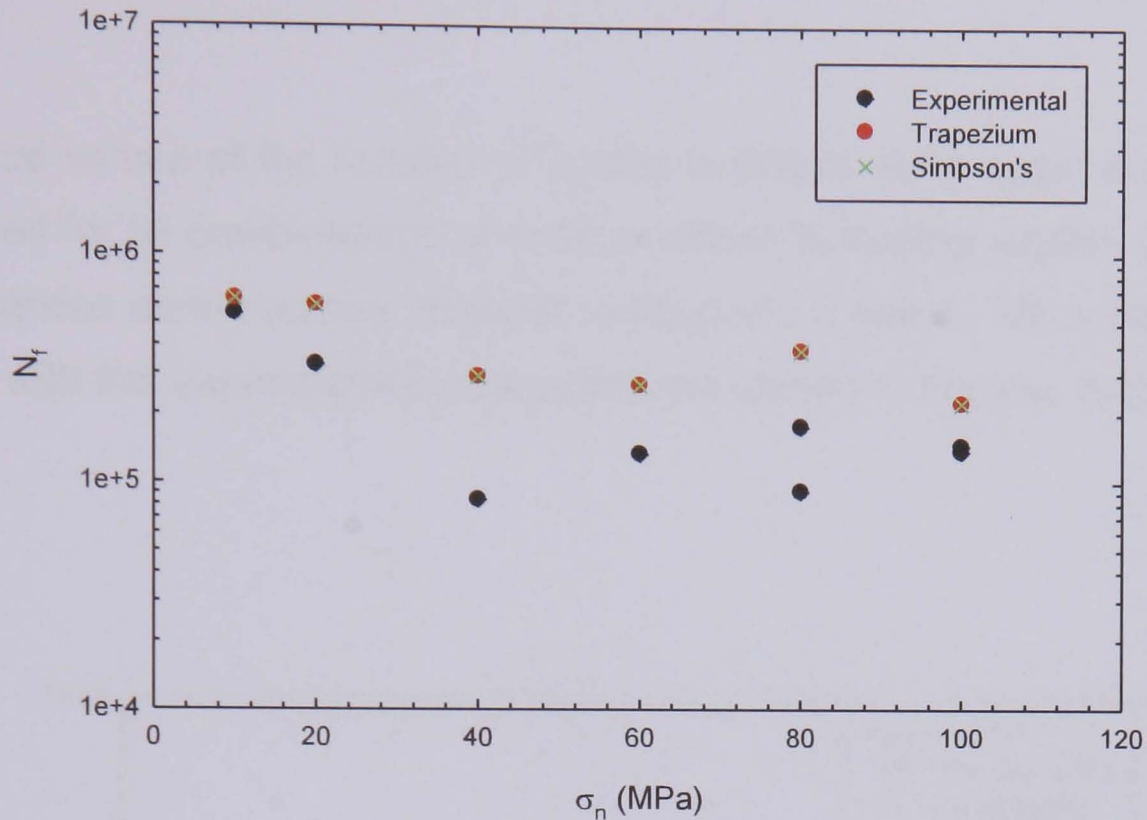


Figure 5.25: Experimental data points of N_f v σ_n and those converged using both the Trapezium rule and Simpson's rule for an axial stress of 125 MPa.

For an axial stress of 70 MPa, the least difference between the results determined by the two rules was 0.08%, the greatest difference, 0.22%; for an axial stress of 100 MPa, the least difference was 0.11%, the greatest difference, 0.14% and for an axial stress of 125 MPa, the least difference was 0.06%, the greatest difference, 0.10%.

Faanes and Fernando [101] experimented with changing the initial flaw size in a series of fracture mechanics models in order that the corresponding $S-N$ curves fitted material data. The difference between the theoretical and experimental results here was subsequently addressed by adjusting the initial crack length applied. The average grain size for aluminium alloy 2024 T351, d , was multiplied by a factor x , see Equation 5.13 and using the Goal Seek function in Microsoft Excel, the optimum value of x was sought, by forcing to 0 the sum of the log of the least squares between the experimental and theoretical values of life for each normal load.

$$a_i = xd$$

Equation 5.13

Theoretical values of the number of cycles to failure were again subsequently determined for all combinations of axial and normal loading applied and friction force recorded during testing, detailed in Chapters 3 and 4. The resultant plots, together with the experimental data points are shown in Figures 5.26, 5.27 and 5.28.

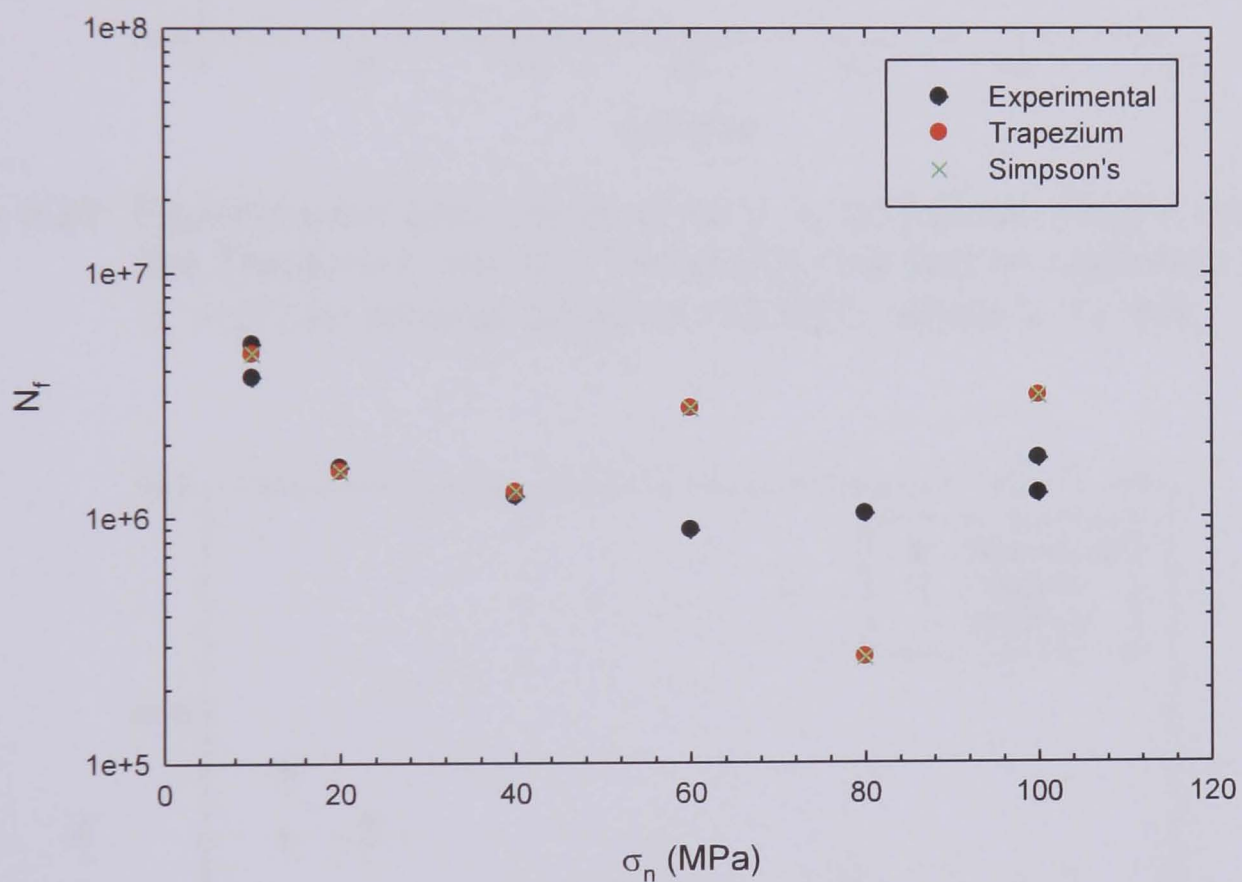


Figure 5.26: Experimental data points of N_f v σ_n and those sought using both the Trapezium rule and Simpson's rule and an optimised value of $a_i = xd$, for an axial stress of 70 MPa, where $x = 1.258$.

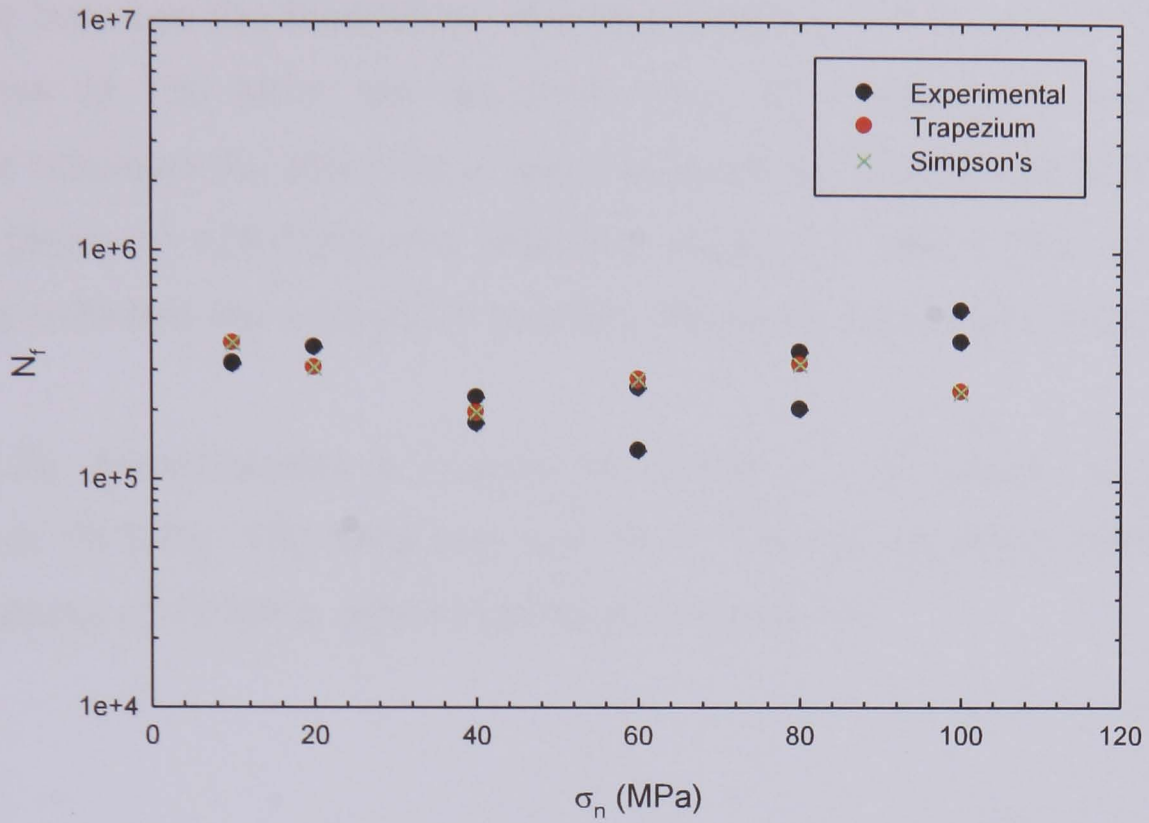


Figure 5.27: Experimental data points of N_f v σ_n and those sought using both the Trapezium rule and Simpson's rule and an optimised value of $a_i = xd$, for an axial stress of 100 MPa, where $x = 2.446$.

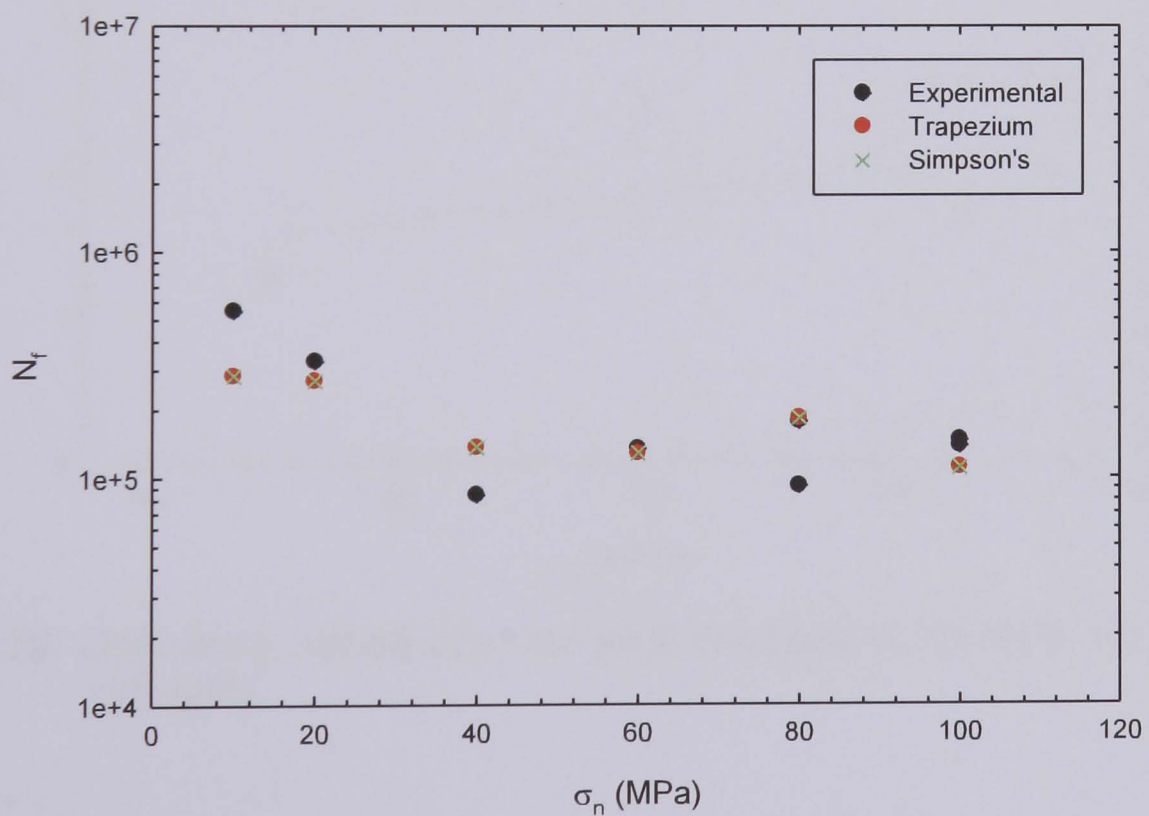


Figure 5.28: Experimental data points of N_f v σ_n and those sought using both the Trapezium rule and Simpson's rule and an optimised value of $a_i = xd$, for an axial stress of 125 MPa, where $x = 1.682$.

For an axial stress of 70 MPa, the resultant value of x was 1.258 and the least difference between the theoretical and experimental results was 3.57%. For an axial stress of 100 MPa, the resultant value of x was 2.446 and the least difference between the theoretical and experimental results was 8.83% and for an axial stress of 125 MPa, the resultant value of x was 1.682 and the least difference between the theoretical and experimental results was 3.31%.

Figure 5.29 demonstrates a degree of scatter in the values of x for axial stresses of 70 MPa, 100 MPa and 125 MPa. The lowest value corresponds to an axial stress of 70 MPa, which results in longer lives.

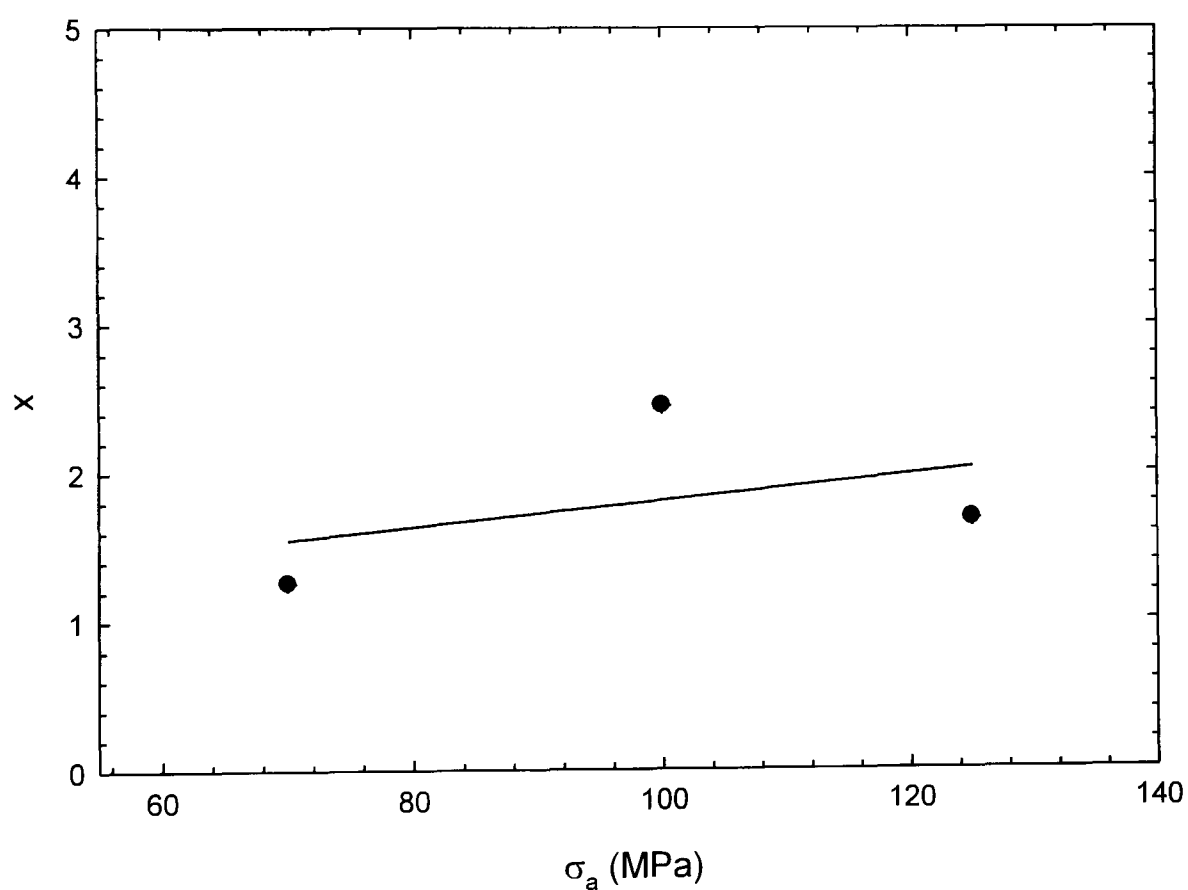


Figure 5.29: Optimised values of x , for axial stresses of 70 MPa, 100 MPa and 125 MPa.

5.3.1.3 Friction predictions

In a study of friction force during fretting fatigue, Lee and Mall [144] concluded that the coefficient of static friction increases during the earlier part of a fretting fatigue test and then reaches a constant value due to an increase in the roughness of contact surface from the fretting action.

Figure 5.30 shows the relationship between the average wear depth measured for each combination of axial stress and normal pressure as detailed in Appendix C and the average friction ratios recorded for the same load conditions as detailed in Appendix F.

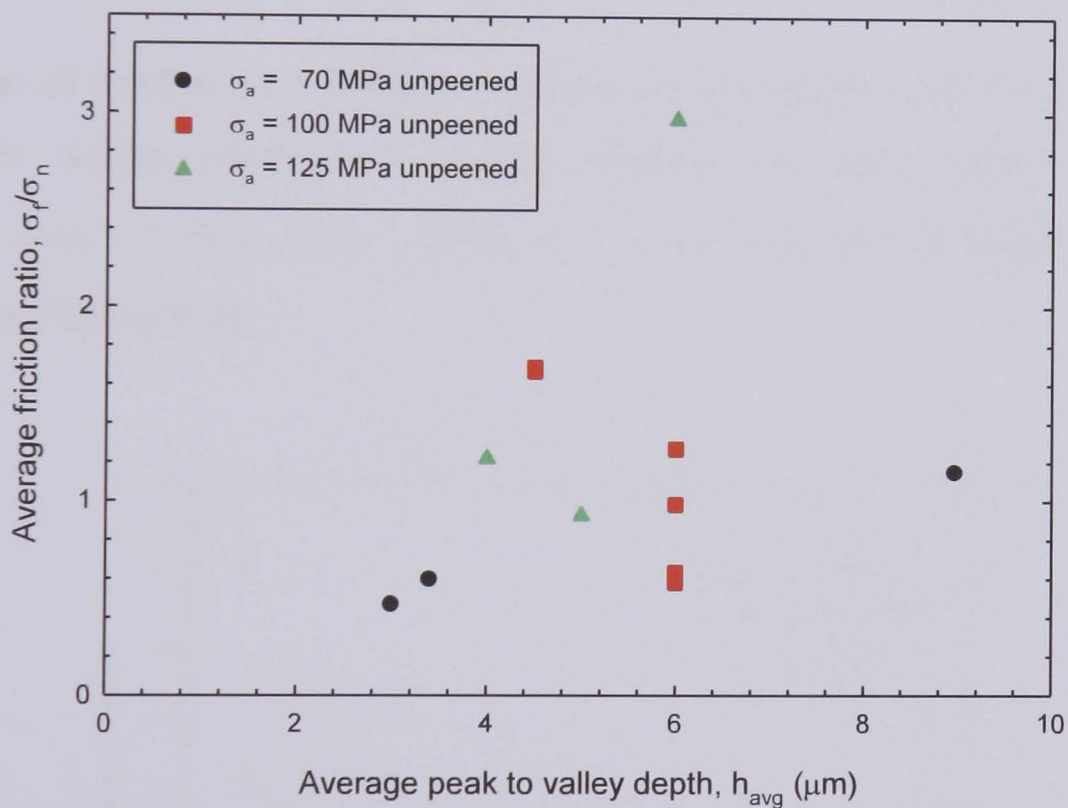


Figure 5.30: The relationship between the average friction ratios recorded in the load test programme and the average peak to valley depths measured in the surface roughness analyses.

A fair degree of scatter is apparent, which was reduced by plotting the maximum wear depth measured as is shown in Figure 5.31. The values of the friction ratios determined using the average values were generally maintained.

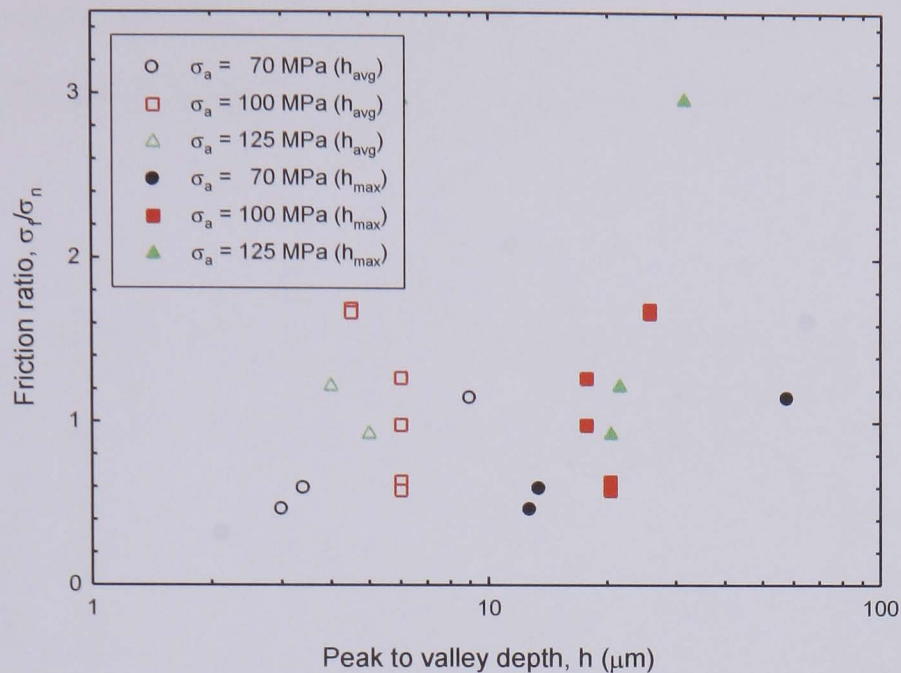


Figure 5.31: The relationship between the average friction ratios recorded in the load test programme and the average and maximum peak to valley depths measured in the surface roughness analyses.

The degree of scatter was further reduced by considering that in the values of the friction ratios measured during testing. A trend line of the form $y = 1.396E - 04x^2 - 2.730E - 02x + 1.894E + 01$ was fitted to the experimental data as shown in Figure 5.32.

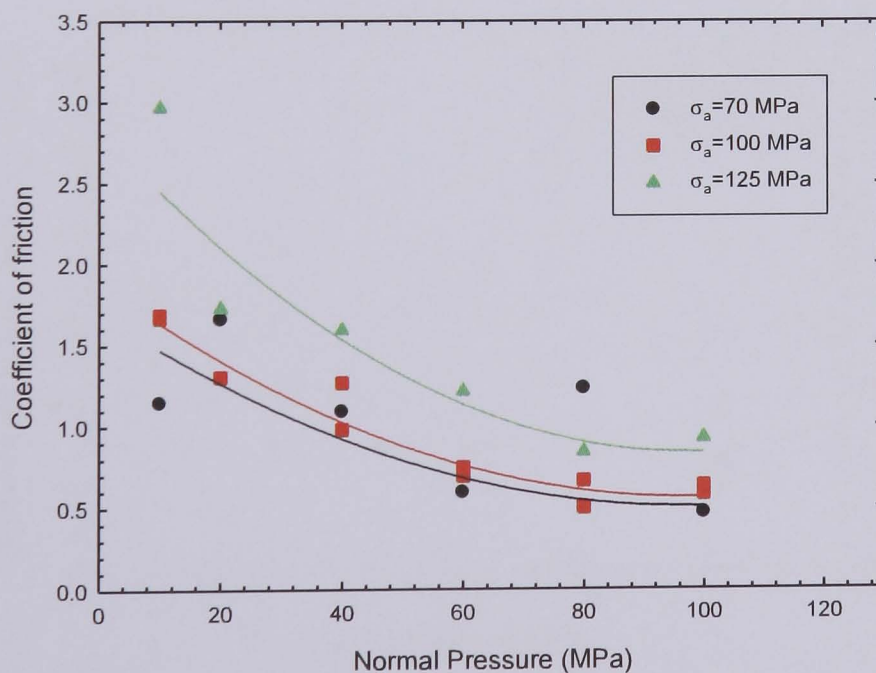


Figure 5.32: A comparison of fitted data of the total average coefficients of friction calculated for specimens subjected to axial stress amplitudes of 70 MPa, 100 MPa and 125 MPa.

These data were plotted with wear depth, both the average and maximum values as is shown in Figures 5.31 and 5.32 respectively. There is a better degree of correlation between the fitted friction ratios and the maximum wear depths.

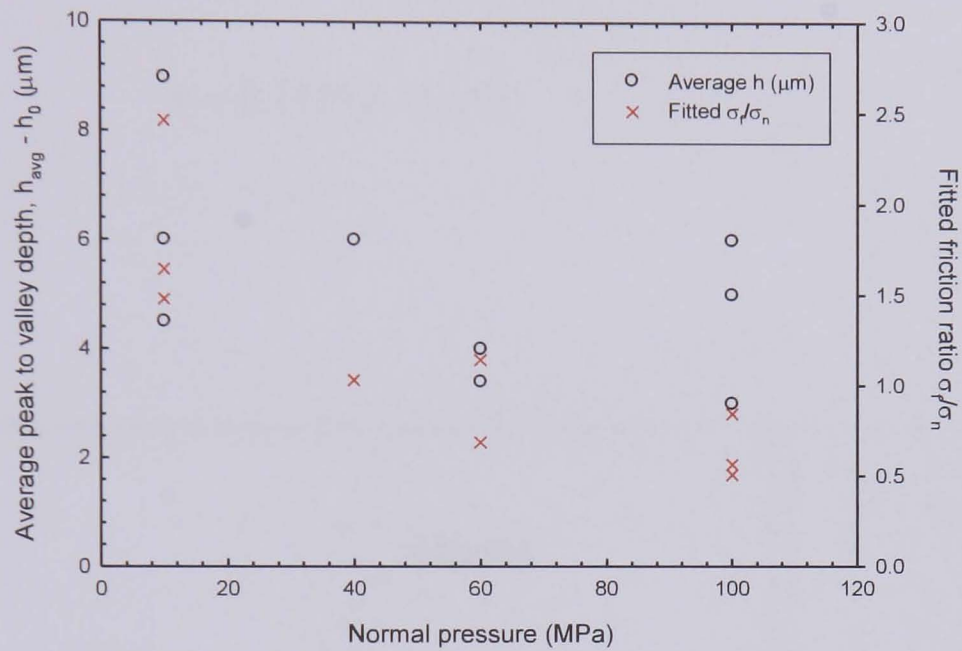


Figure 5.31: Correlation between the friction ratios fitted to that data recorded in the load test programme and the average peak to valley depths measured in the surface roughness analyses for various normal pressures.

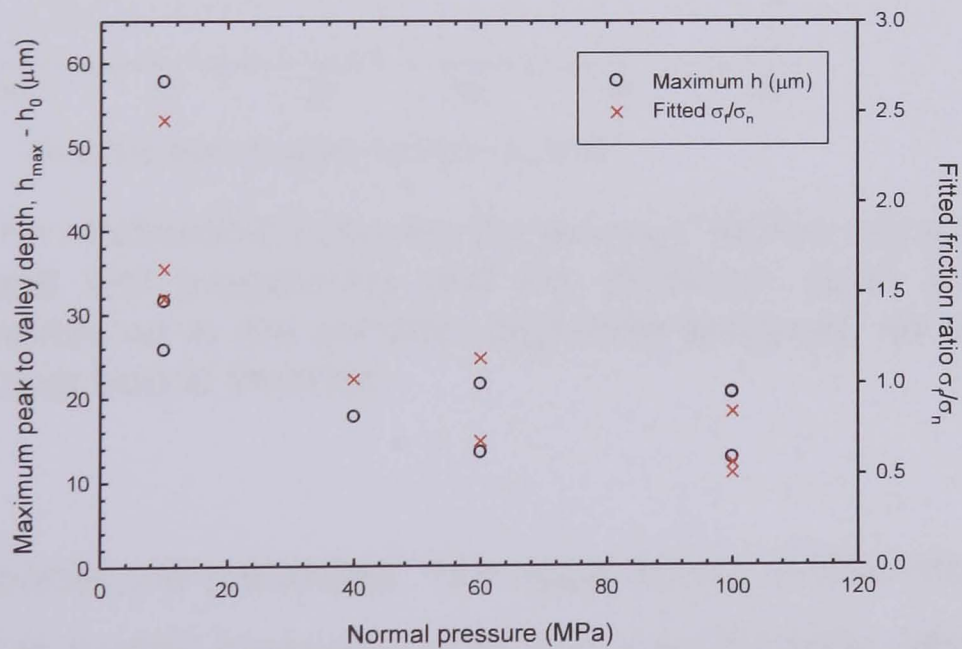


Figure 5.32: Correlation between the friction ratios fitted to that data recorded in the load test programme and the maximum peak to valley depths measured in the surface roughness analyses for various normal pressures.

Figure 5.33 demonstrates the linear relationship between the maximum wear depth measured for each combination of axial stress and normal pressure as detailed in Appendix C and the average friction ratios recorded for the same load conditions as detailed in Appendix F. The equation of this line shown is Equation 5.14.

$$y = 0.1157x - 1.215$$

Equation 5.14

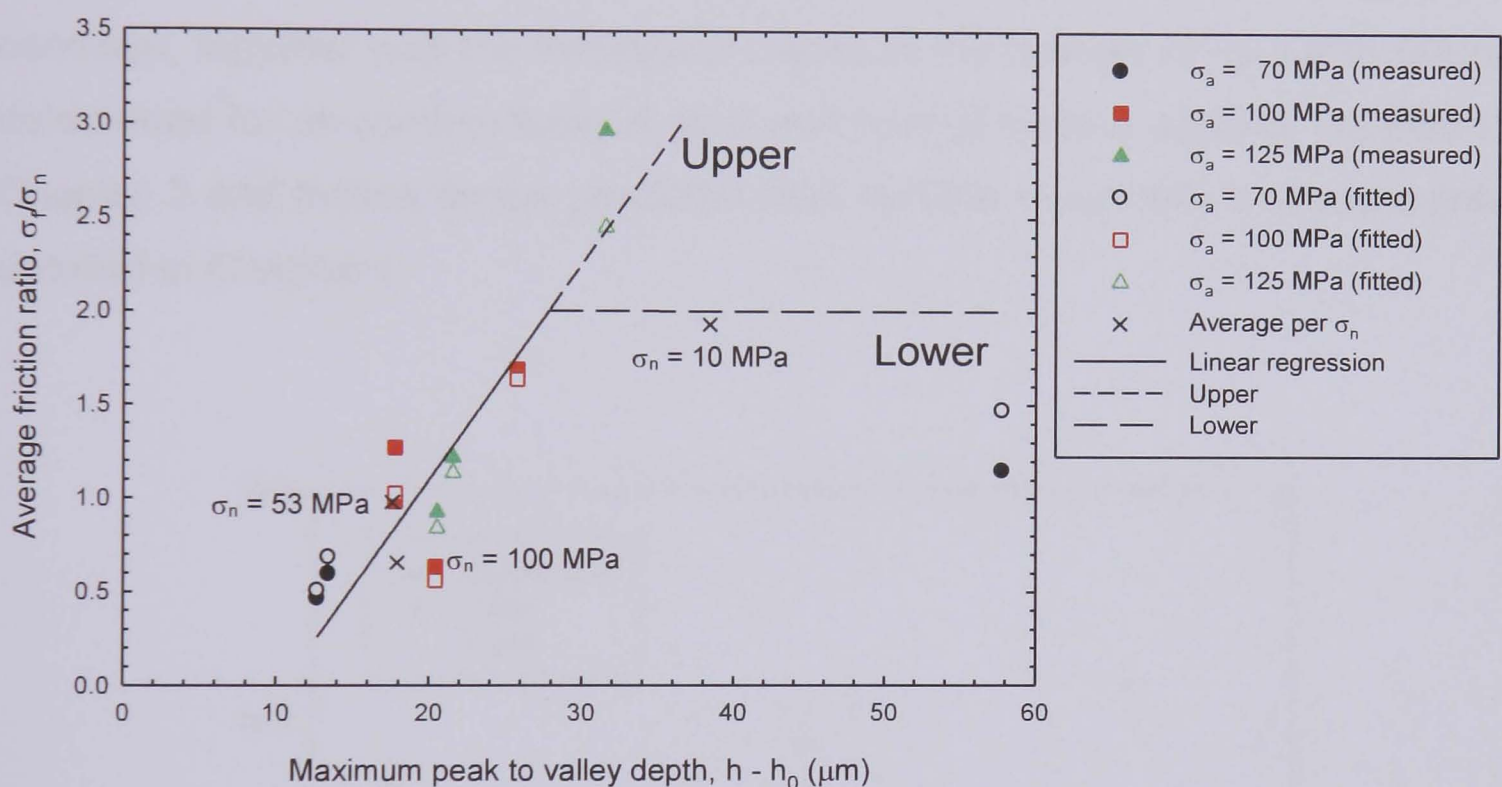


Figure 5.33: The relationship between the average friction ratios recorded in the load test programme and the maximum peak to valley depths measured in the surface roughness analyses, showing upper and lower bound theories.

Two bound theories are presented. The upper bound is fitted through that data corresponding to normal pressures of 40 MPa and 60 MPa, and 100 MPa and the lower bound is fitted through that data corresponding to a normal pressure of 10 MPa for all three axial stresses applied.

It is postulated that the higher values occur when the bridge pads undergo sliding, producing a greater degree of wear and butt up against the ends of deep grooves, see Figure 5.34.

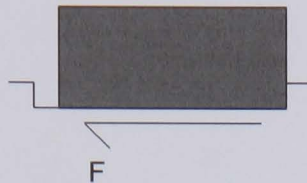


Figure 5.34: A bridge pad butted up against the edge of a groove.

Figures 5.35, 5.38 and 5.39, show experimental data points for the unpeened condition, together with the theoretical values of the number of cycles to failure determined for all combinations of axial and normal loading applied, detailed in Chapter 3 and friction forces predicted from surface roughness measurements detailed in Chapter 4.

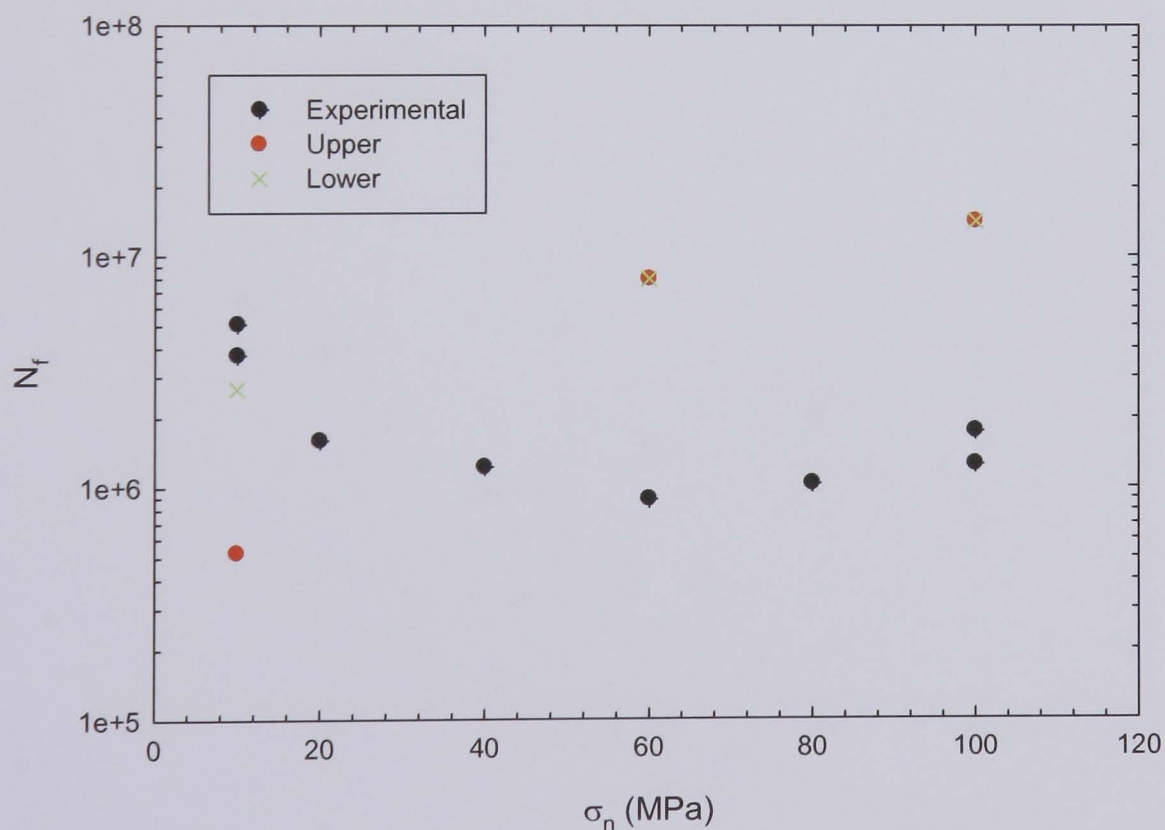


Figure 5.35: Experimental data points of N_f v σ_n and those determined by incorporating values of σ_f established from the maximum notch depths for an axial stress of 70 MPa.

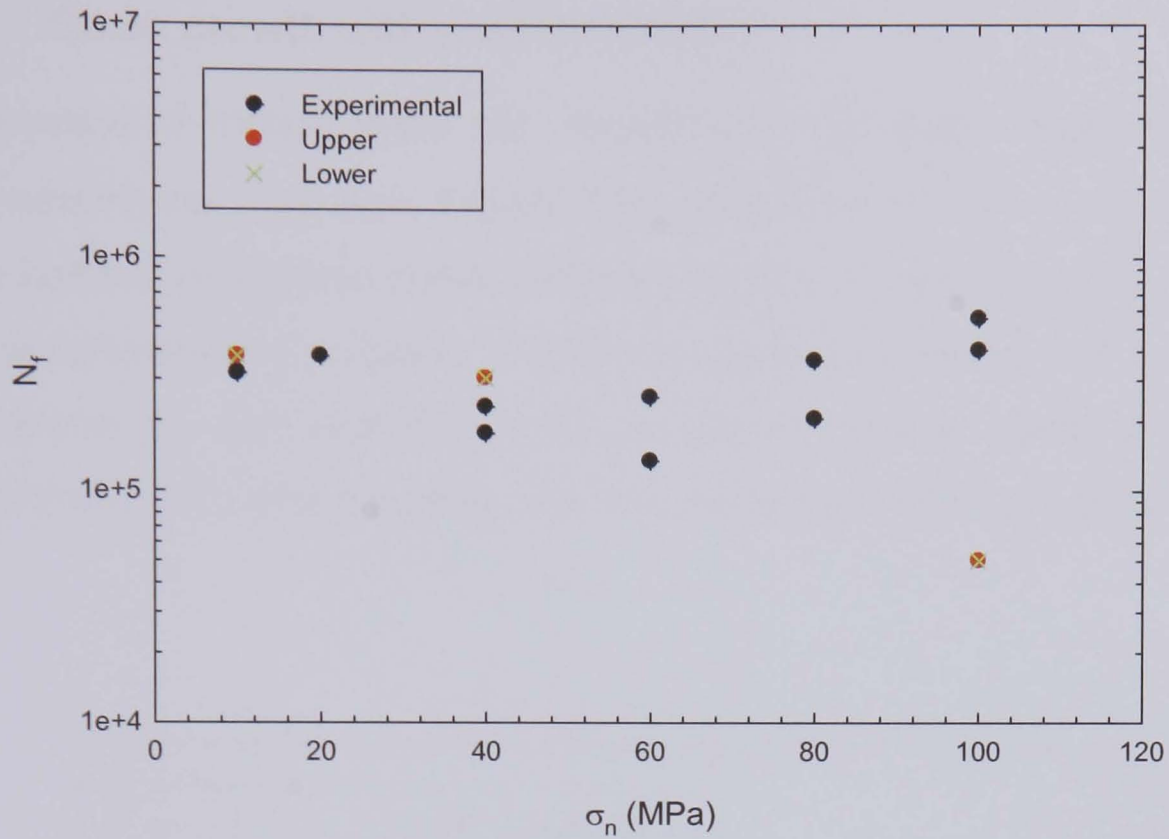


Figure 5.36: Experimental data points of N_f v σ_n and those determined by incorporating values of σ_f established from the maximum notch depths for an axial stress of 100 MPa.

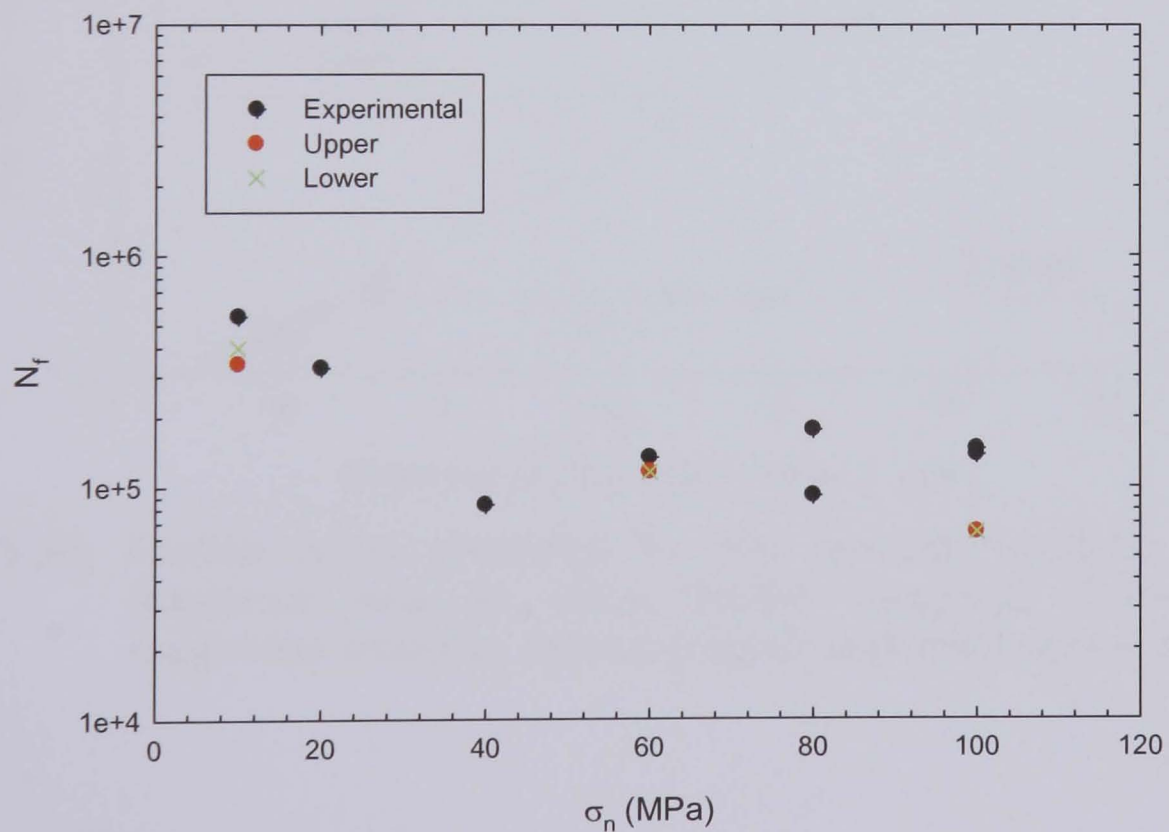


Figure 5.37: Experimental data points of N_f v σ_n and those determined by incorporating values of σ_f established from the maximum notch depths for an axial stress of 125 MPa.

5.3.2 Peened

5.3.2.1 Crack growth with predicted friction

Measurements of friction were not recorded for the tests conducted on shot peened specimens. However, Figure 5.38 shows the values of σ_f/σ_n predicted from the surface roughness measurements for the peened condition, minus the difference between the increase in surface roughness due to the shot peening process alone, h_0 . Lee and Mall [144] concluded that the higher roughness of contact surface from shot peening also increases the coefficient of static friction.

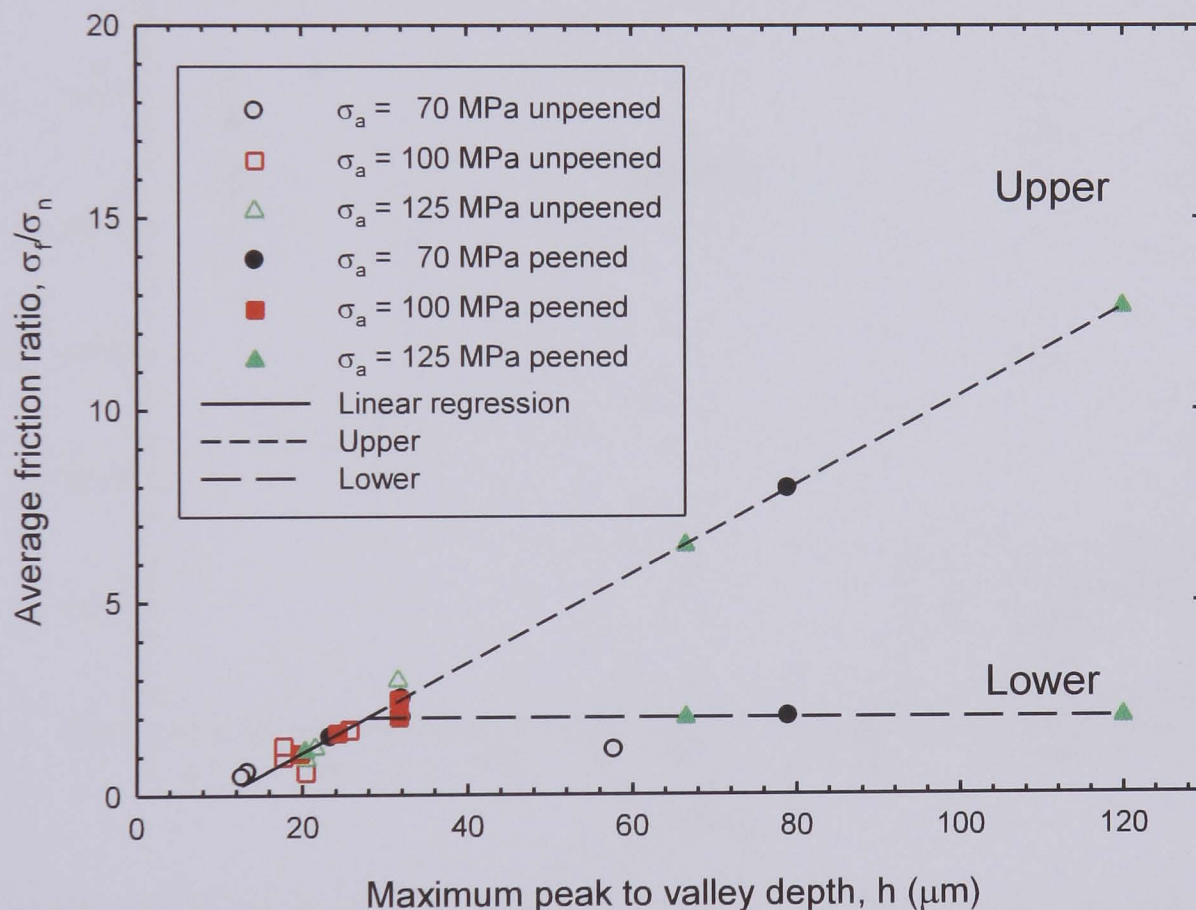


Figure 5.38: Friction ratios predicted for the peened condition from the maximum peak to valley depths measured in the surface roughness analyses, showing upper and lower bound theories.

Figures 5.39, 5.40 and 5.41 show experimental data points for the peened condition, together with the theoretical values of the number of cycles to failure determined for all combinations of axial and normal loading applied, detailed in Chapter 3 and friction forces predicted from surface roughness measurements detailed in Chapter 4. Sensitivity to friction is demonstrated; the data points shown in red represent those values predicted from the linear relationship and the data points shown in green represent those values limited by Coulomb friction.

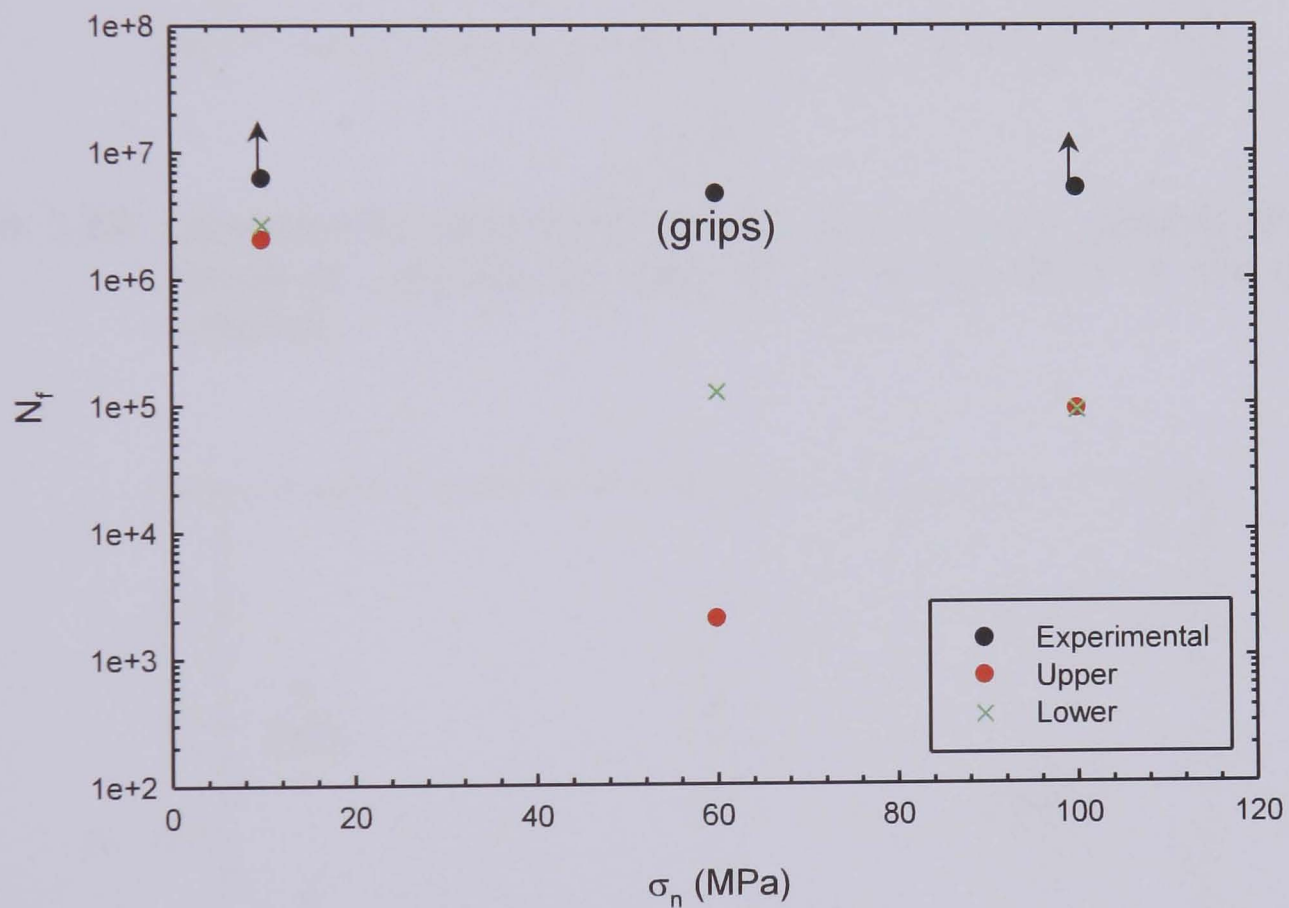


Figure 5.39: Experimental data points of N_f v σ_n and those utilising predicted values of σ_f/σ_n for an axial stress of 70 MPa for the peened condition.

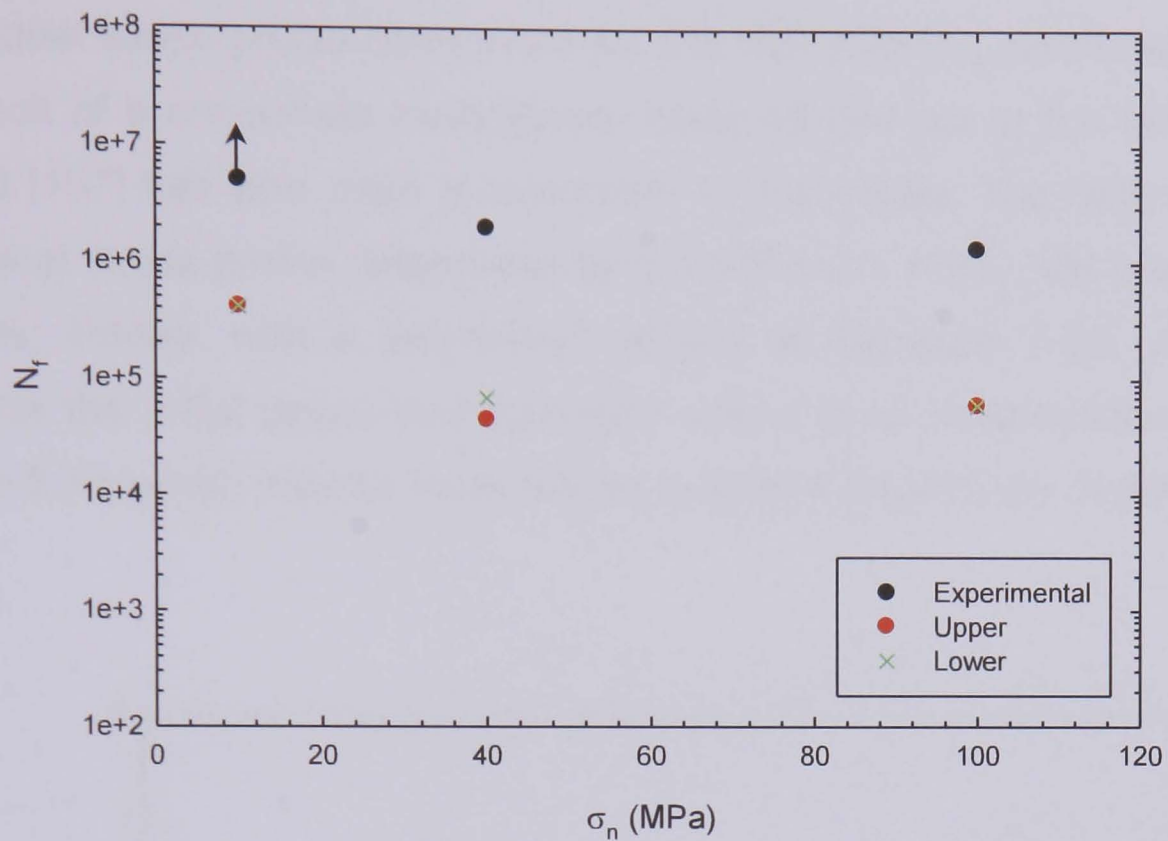


Figure 5.40: Experimental data points of N_f v σ_n and those utilising predicted values of σ_f/σ_n for an axial stress of 100 MPa for the peened condition.

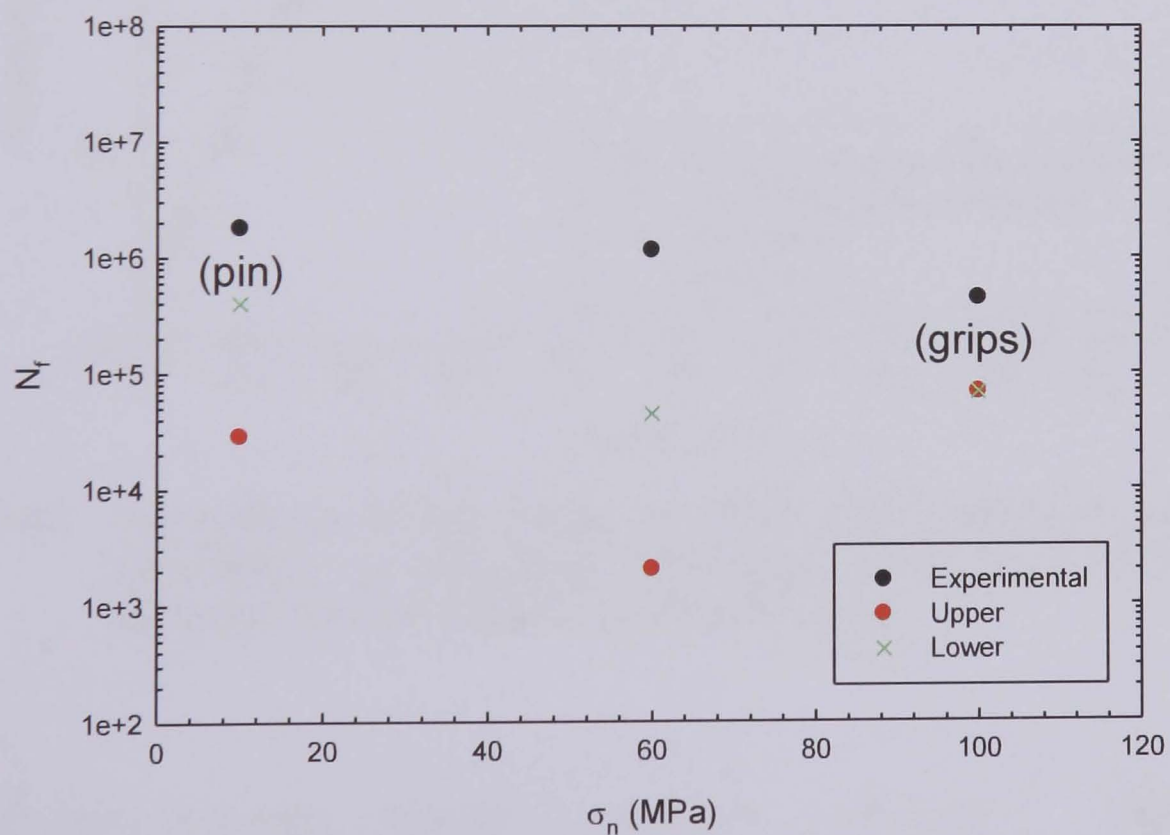


Figure 5.41: Experimental data points of N_f v σ_n and those utilising predicted values of σ_f/σ_n for an axial stress of 125 MPa for the peened condition.

5.3.2.2 Crack growth with residual stresses

The residual stress profile determined for the shot peening parameters utilised as a result of a concurrent investigation being carried out at the University of Sheffield [197] has also been incorporated in this model. The data relating to the residual stress profile determined by Solis-Romero [197], has been fitted in two parts; initially, with a polynomial, shown as Equation 5.15, which best represents the initial decay and thereafter with a linear relationship, shown in Equation 5.16, which may be more readily extended beyond the depth of 1 mm.

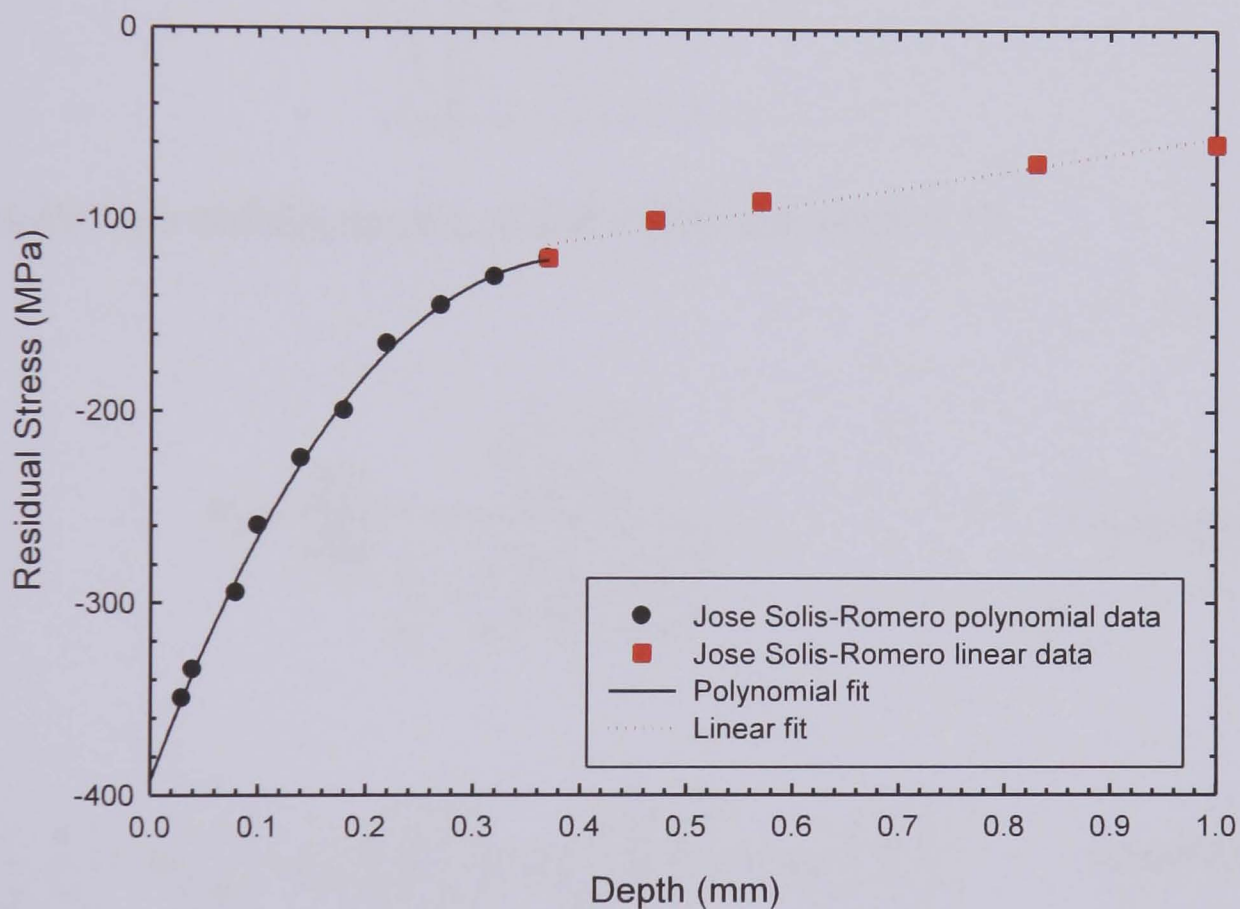


Figure 5.42: The residual stress profile for 2024 T351 optimised shot peening parameters of spherical cast steel shot type S110 at 200% coverage and an angle of incidence of 45°.

$$y = -389.654 + 1370.459x - 979.902x^2 - 4594.914x^3 + 6903.146x^4 \quad \text{Equation 5.15}$$

$$y = 89.385x - 145.922 \quad \text{Equation 5.16}$$

In 1985, Tada et al. [254] published a compendium of stress intensity factors for various loads and geometries including elastic stress solutions for various crack configurations. For the point loaded crack configuration shown in Figure 5.43, the stress intensity factor formula that interpolates the numerical results of Kaya and Erdogan is shown as Equation 5.17, with the Green's function required to solve the inhomogeneous differential equation shown as Equations 5.18 and 5.19, the solutions as Equations 5.20 to 5.22.

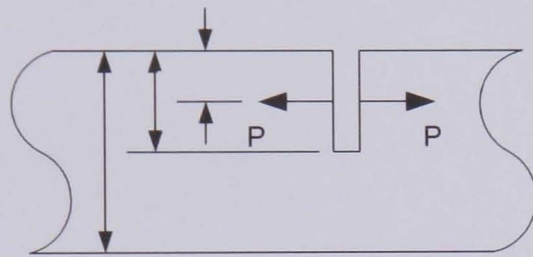


Figure 5.43: The definitions of a , b and c from Equation 5.17.

$$K_I = \frac{2P}{\sqrt{\pi a}} \cdot \frac{G\left(\frac{c}{a}, \frac{a}{b}\right)}{\left(1 - \frac{a}{b}\right)^{\frac{3}{2}} \sqrt{1 - \left(\frac{c}{a}\right)^2}} \quad \text{Equation 5.17}$$

$$G\left(\frac{c}{a}, \frac{a}{b}\right) = g_1\left(\frac{a}{b}\right) + g_2\left(\frac{a}{b}\right)\left(\frac{c}{a}\right) + g_3\left(\frac{a}{b}\right)\left(\frac{c}{a}\right)^2 + g_4\left(\frac{a}{b}\right)\left(\frac{c}{a}\right)^3 \quad \text{Equation 5.18}$$

$$g_1\left(\frac{a}{b}\right) = 0.46 + 3.06\left(\frac{a}{b}\right) + 0.84\left(1 - \frac{a}{b}\right)^5 + 0.66\left(\frac{a}{b}\right)^2\left(1 - \frac{a}{b}\right)^2$$

$$g_2\left(\frac{a}{b}\right) = 3.52\left(\frac{a}{b}\right)^2$$

$$g_3\left(\frac{a}{b}\right) = 6.17 - 28.22\left(\frac{a}{b}\right) + 34.54\left(\frac{a}{b}\right)^2 - 14.39\left(\frac{a}{b}\right)^3 - \left(1 - \frac{a}{b}\right)^{\frac{3}{2}} \\ - 5.88\left(1 - \frac{a}{b}\right)^5 - 2.64\left(\frac{a}{b}\right)^2\left(1 - \frac{a}{b}\right)^2$$

Equation 5.19

$$g_4\left(\frac{a}{b}\right) = -6.63 + 25.16\left(\frac{a}{b}\right) - 31.04\left(\frac{a}{b}\right)^2 + 14.41\left(\frac{a}{b}\right)^3 + 2\left(1 - \frac{a}{b}\right)^{\frac{3}{2}} \\ + 5.04\left(1 - \frac{a}{b}\right)^5 + 1.98\left(\frac{a}{b}\right)^2\left(1 - \frac{a}{b}\right)^2$$

$$K_I = \int_b^a \frac{2\sigma(c)}{\sqrt{\pi a}} \frac{G}{\left(1 - \frac{a}{b}\right)^{\frac{3}{2}} \sqrt{1 - \left(\frac{c}{a}\right)^2}} dc, \quad c = a \sin \theta, \quad dc = a \cos \theta d\theta$$

Equation 5.20

$$K_I = \int_b^a \frac{2\sigma(\theta)}{\sqrt{\pi a}} \cdot \frac{Ga \cos \theta d\theta}{\left(1 - \frac{a}{b}\right)^{\frac{3}{2}} \cos \theta} \cdot a \cos \theta d\theta$$

Equation 5.21

$$K_I = \sigma \cdot \frac{(g_1 + g_2 + g_3 + g_4)}{\left(1 - \frac{a}{b}\right)^{\frac{3}{2}}} \cdot a$$

Equation 5.22

Values of c were determined for values of θ between 0 and $\pi/2$ with corresponding values of P being calculated from Equation 5.15 where $c < 0.44$ and Equation 5.16 where $c > 0.44$.

Values of K_I were thus determined for values of a between 0 mm and 2 mm, from Equation 5.22 with this residual stress profile by means of the Simpson's rule, with a macro written in Microsoft Excel, see Appendix Z and Figure 5.44.

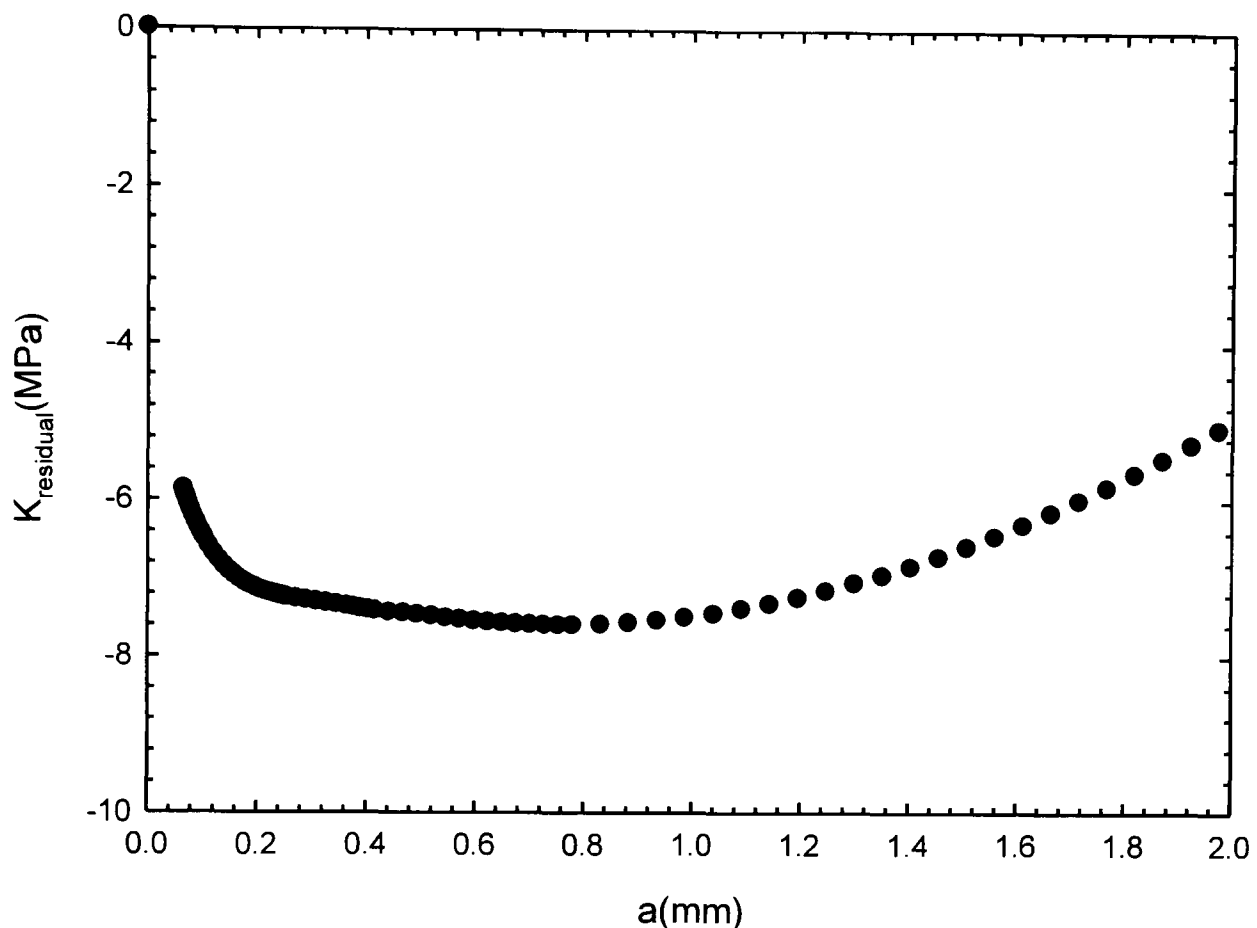


Figure 5.44: The variation of $K_{residual}$ with a .

As the principle of superposition applies in Linear Elastic Fracture Mechanics, this stress intensity factor is then combined with K_I where $K_I + K_{residual} > 0$, to obtain a revised stress intensity factor for mode I.

Figures 5.45, 5.46 and 5.47 show experimental data points for the peened condition, together with the theoretical values of the number of cycles to failure determined for all combinations of axial and normal loading applied as detailed in Chapter 3, friction forces predicted from surface roughness measurements detailed in Chapter 4 and residual stresses detailed in Chapter 3 and incorporated in K_I .

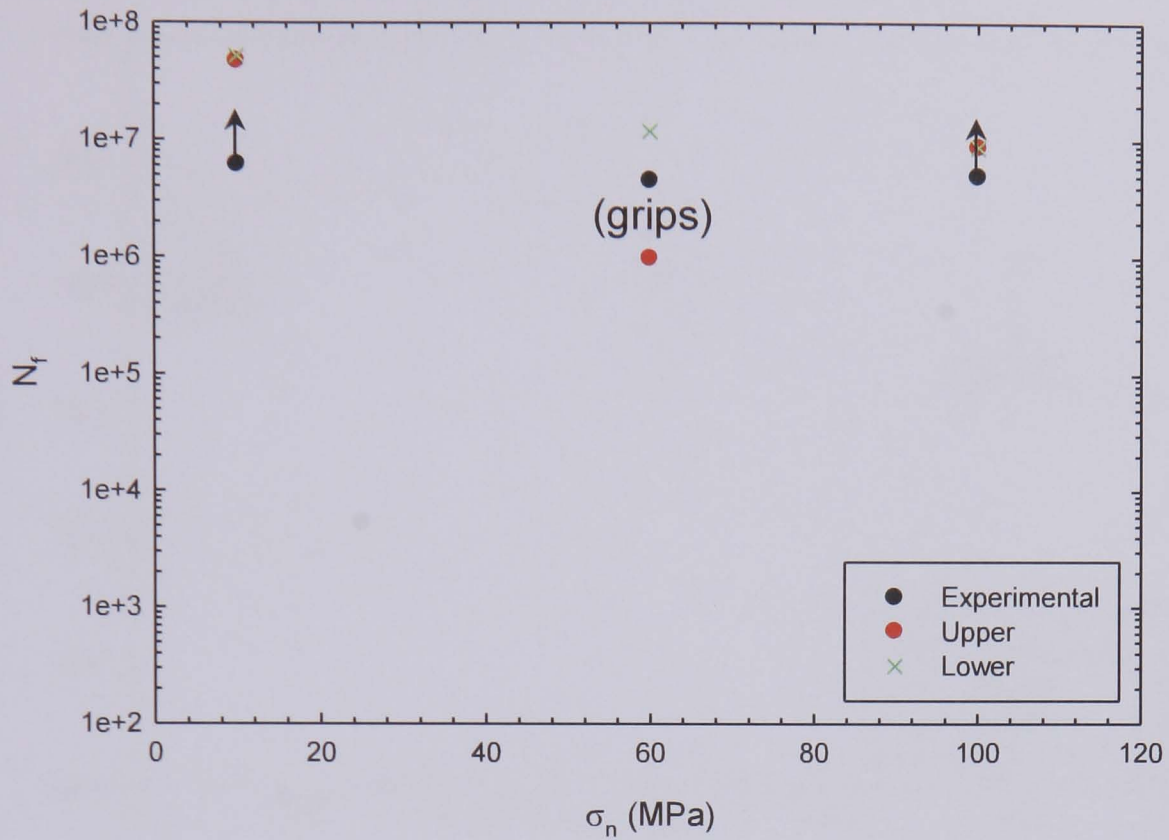


Figure 5.45: Experimental data points of N_f v σ_n and those utilising predicted values of σ_f/σ_n and incorporating residual stresses in K_I for an axial stress of 70 MPa for the peened condition.

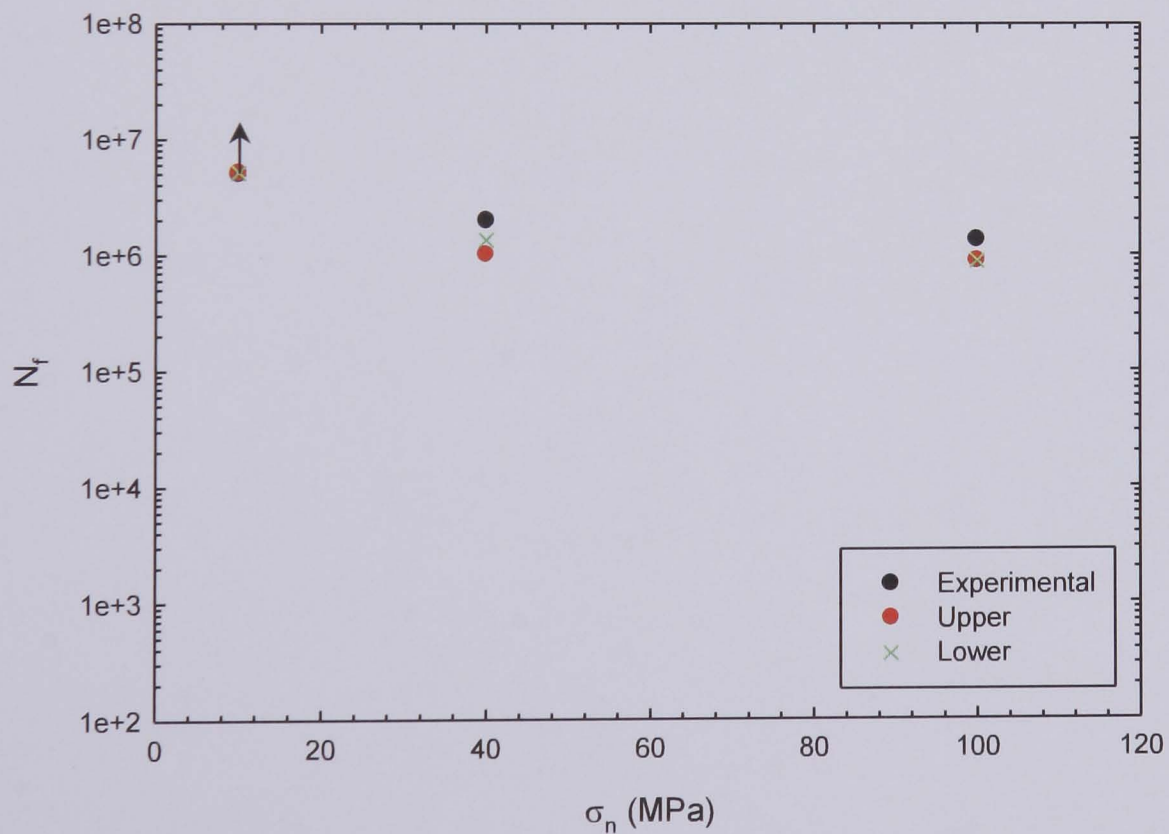


Figure 5.46: Experimental data points of N_f v σ_n and those utilising predicted values of σ_f/σ_n and incorporating residual stresses in K_I for an axial stress of 100 MPa for the peened condition.

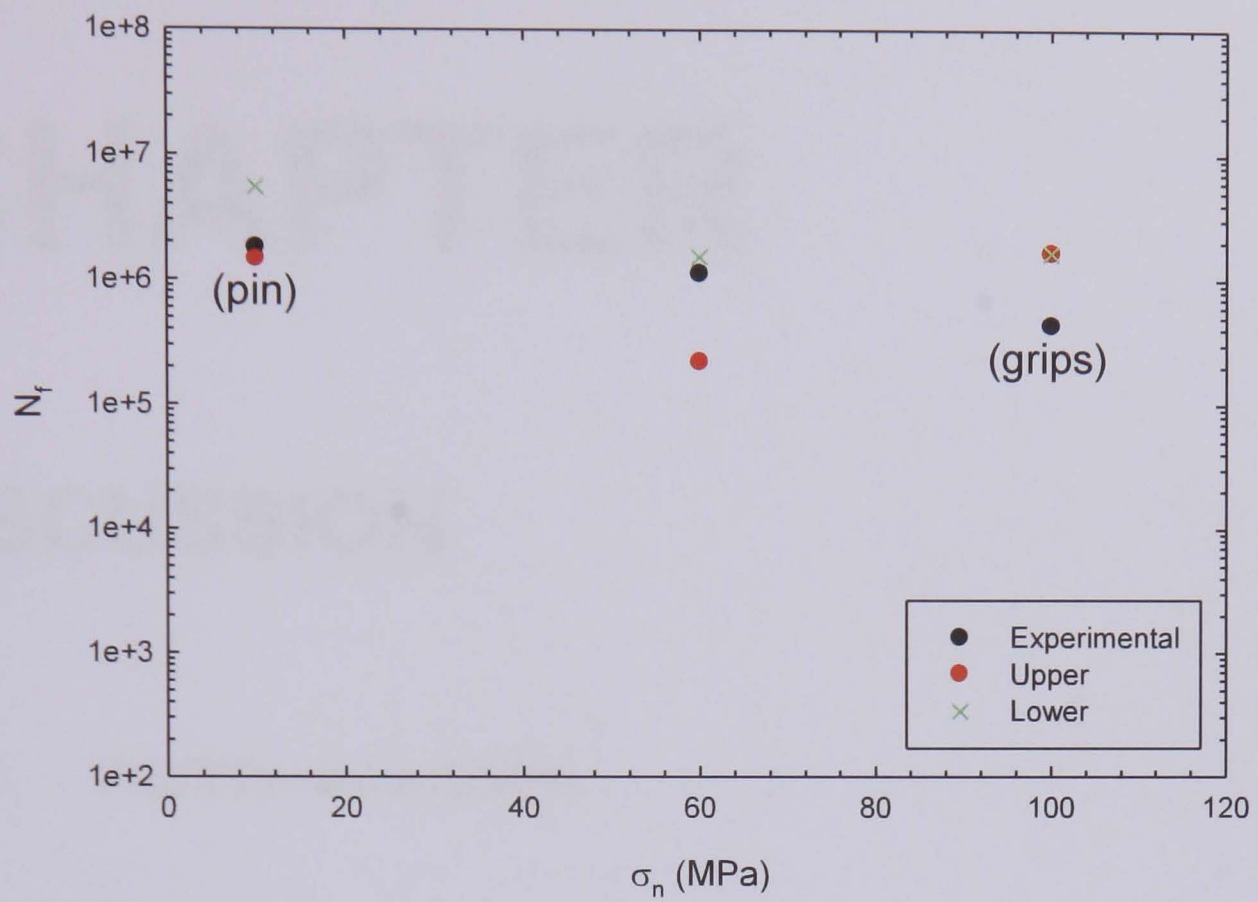


Figure 5.47: Experimental data points of N_f v σ_n and those utilising predicted values of σ_f/σ_n and incorporating residual stresses in K_I for an axial stress of 125 MPa.

CHAPTER

6

DISCUSSION

6.1 FRETTING FATIGUE

6.1.1 Experimental programme

6.1.1.1 Life

Thirty one fretting fatigue tests were completed on aluminium alloy 2024 T351 in flat-on-flat contact with BS S98 steel and aluminium alloy 2024 T351 under a range of six constant normal pressures, in combination with cyclic axial stress amplitudes of 70 MPa, 100 MPa and 125 MPa, with a stress ratio, R , of -1 and a sinusoidal waveform at a frequency of 20 Hz.

The loading conditions for the constant normal pressure tests were selected so that the results could be compared with those previously documented. Using the test results, the fretting fatigue behaviour resulting from both material combinations has been investigated and compared. It has been shown that fretting fatigue life is significantly dependent on the normal load level and in all cases there was a considerable reduction in fatigue strength due to fretting.

These results obtained have been compared with the data reported by Fernando et al. [99] for BS S98 steel in flat-on-flat contact with BS L65 4 % copper aluminium alloy at the same normal pressures and axial stress amplitudes, see Figure 6.1. The behaviour observed was in good agreement with that data previously reported, but shows a difference attributable to the combination of materials used.

The fretting fatigue lives achieved with the application of an aluminium bridge, were greater than those achieved with a steel bridge. This was the case for any given axial stress, but was particularly marked at an axial stress amplitude of 70 MPa. That was not expected, as it was postulated that there would be a greater degree of adhesion occurring between two like materials, which would result in higher friction forces and more surface damage. However, the amplitudes of the friction forces achieved with the application of a steel bridge were greater than those achieved with an aluminium bridge.

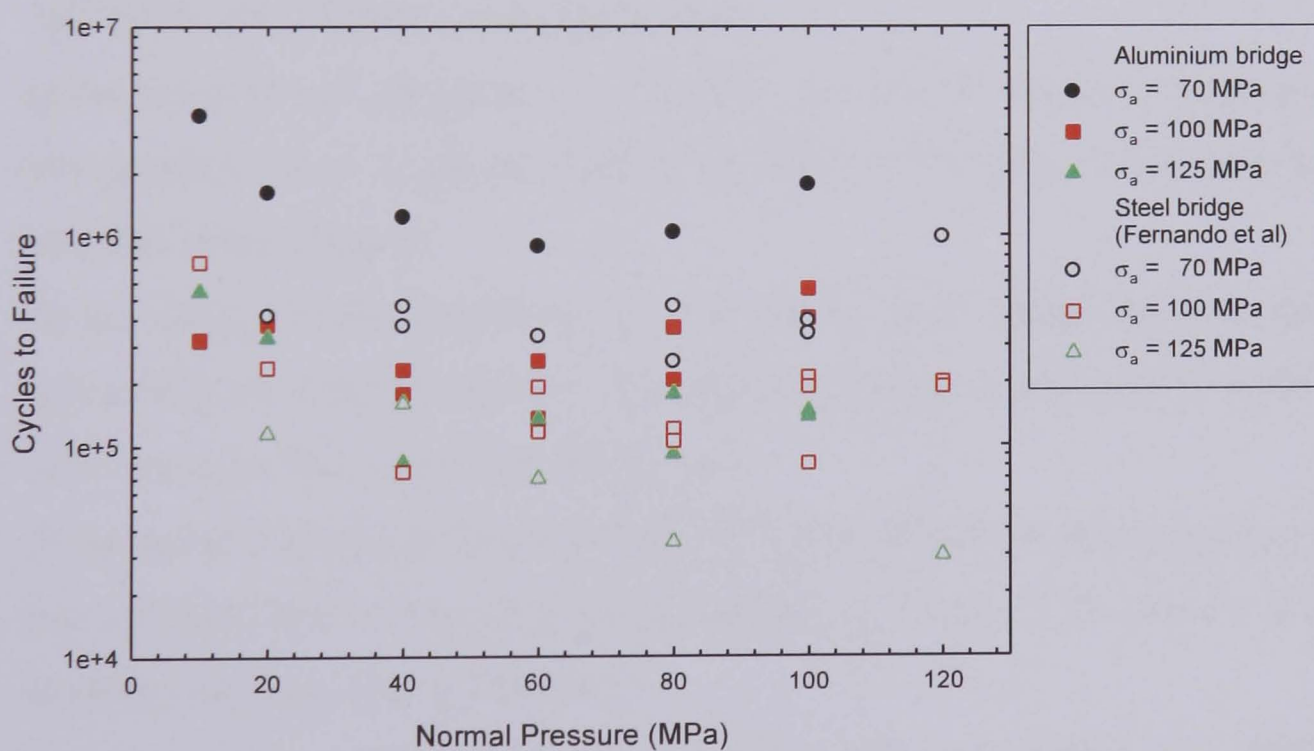


Figure 6.1: A comparison of the experimental results for fretting fatigue tests conducted with a BS S98 steel bridge in contact with BS L65 4 % copper aluminium alloy specimens [99] and an aluminium alloy 2024 T351 bridge in contact with aluminium alloy 2024 T351 specimens subjected to a range of normal pressures and axial stress amplitudes of 70 MPa, 100 MPa and 125 MPa.

Analysis of the results presented in Figure 6.1 indicates that:

- For any given constant normal pressure and axial stress, the fretting fatigue lives are greater with the aluminium bridges than with the steel bridges;
- Fretting fatigue life decreases with increasing axial stress amplitude for any given constant normal pressure with the aluminium bridges and also with the steel bridges;
- For axial stress amplitudes of 70 MPa and 100 MPa for both test conditions and an axial stress amplitude of 125 MPa with the aluminium bridge alone, a characteristic life distribution was achieved, whereby the number of cycles to failure decreases with an increase in normal pressure up to a critical value, whereupon a further increase in normal pressure leads to an increase in life;
- For an axial stress amplitude of 125 MPa for the steel bridges, the number of cycles to failure decreases with an increase in normal pressure, up to 120 MPa, the highest pressure tested;
- At an axial stress amplitude of 70 MPa, the critical normal pressure giving the shortest life is at approximately 60 MPa for both the aluminium bridges and the steel bridges;
- At an axial stress amplitude of 100 MPa, the critical normal pressure giving the shortest life for the aluminium bridges is at 40 MPa and for the steel bridges that point is at 80 MPa;
- At an axial stress amplitude of 125 MPa the critical normal pressure giving the shortest life for the aluminium bridges is at 60 MPa and for the steel bridges that point is at 120 MPa;
- At axial stress amplitudes of 70 MPa and 125 MPa, the difference between the greatest number of cycles to failure and the least number of cycles to failure for the aluminium bridges is greater than that for the steel bridges;

- At an axial stress amplitude of 100 MPa, the difference between the greatest number of cycles to failure and the least number of cycles to failure for the aluminium bridges is smaller than that for the steel bridges.

The reduction in fatigue life due to fretting and the difference in the results achieved by the two combinations of materials used was thought to be due in part to the friction forces involved. Friction force amplitude generally increases with the magnitude of the normal pressure applied, or one half of the applied normal load per bridge foot. Fretting fatigue life generally decreases with the magnitude of the normal pressure applied, up to a critical value.

An increase in normal pressure tends to decrease the coefficient of friction. The highest coefficients of friction were seen at an axial stress amplitude of 125 MPa, decreasing with axial stress amplitude. After an initial decrease, fretting fatigue life generally increases past a critical value of the normal pressure applied. The fretting fatigue life decreases with increasing axial stress amplitude for any given constant normal pressure. Further detail regarding the friction forces can be found in Section 6.1.1.2.

Also, wear scars indicated regions of stress concentration that could be responsible for the fast initiation and propagation of fatigue cracks. Using a Mitutoyo SurfTest, a comparison was made between a wear scar at failure produced by a steel bridge and a wear scar at failure produced by an aluminium bridge for the same combination of normal pressure and axial stress. A sample length of 1.2 mm was maintained in all tests, this being the approximate width of the bridge feet; pre and post travel parameters were set at 0.4 mm and a sample speed of 0.2 mm/s was used in all cases.

Differences in the fretting scars formed due to the two material combinations tested were observed. An example of the surface profile of a scar formed due to the flat-on-flat contact of a BS S98 steel bridge and an aluminium alloy 2024 T351 specimen subjected to a normal pressure of 40 MPa and an axial stress amplitude of 100 MPa is shown in Figure 6.2.

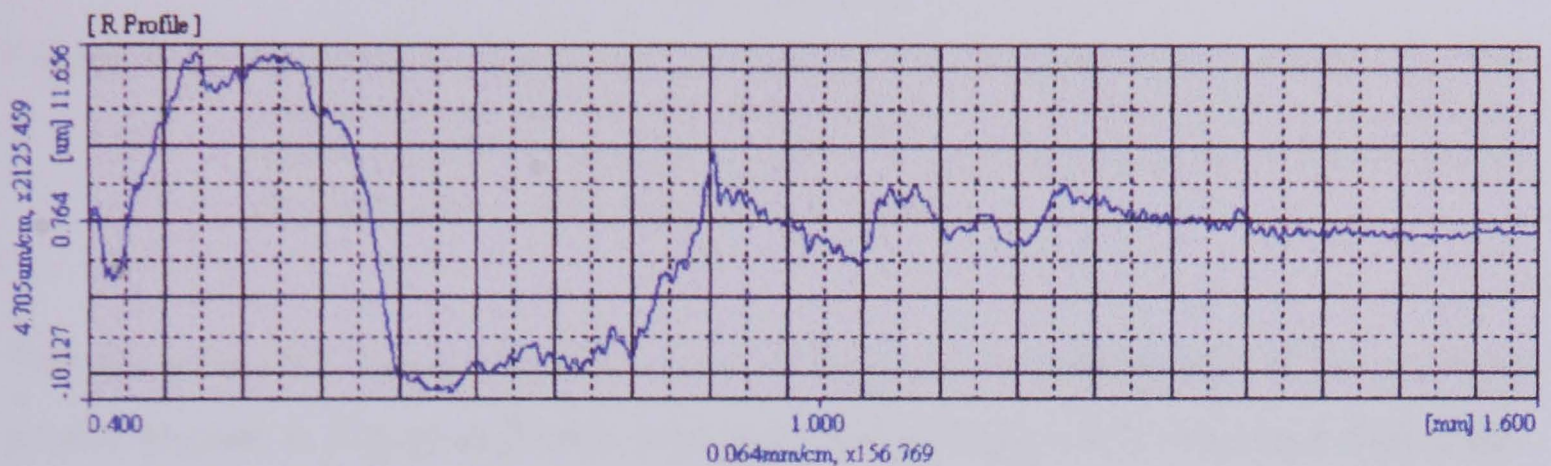


Figure 6.2: A surface roughness profile of the fretting scar created by the contact of a BS S98 steel bridge and an aluminium alloy 2024 T351 specimen under a normal pressure of 40 MPa and an axial stress amplitude of 100 MPa.

The R_a , or centre line average value for this sample was $3.386 \mu\text{m}$. This is the arithmetic mean distance between the roughness peaks and valleys and is the most widely used parameter for measuring surface roughness.

An example of the surface profile of a scar formed due to the flat-on-flat contact of an aluminium alloy 2024 T351 bridge and an aluminium alloy 2024 T351 specimen subjected to a normal pressure of 40 MPa and an axial stress amplitude of 100 MPa is shown in Figure 6.3.

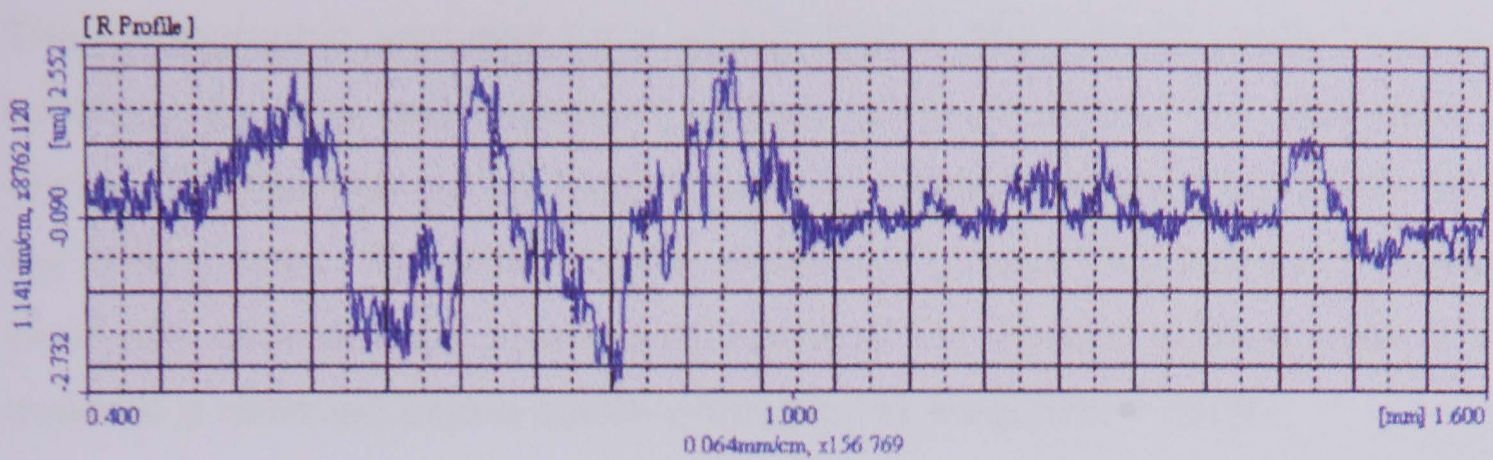


Figure 6.3: A surface roughness profile of the fretting scar created by the contact of an aluminium alloy 2024 T351 bridge and an aluminium alloy 2024 T351 specimen under a normal pressure of 40 MPa and an axial stress amplitude of 100 MPa.

The R_a value for this combination was $0.591 \mu\text{m}$. A comparison of the surface profile shown in Figure 6.2 with that depicted in Figure 6.3 indicates that a BS S98 steel bridge pad indents deeper into an aluminium alloy 2024 T351 specimen than one made from aluminium alloy 2024 T351. The R_a value for the BS S98 steel bridge and aluminium alloy 2024 T351 specimen combination was $2.795 \mu\text{m}$ greater than that of the aluminium alloy 2024 T351 bridge and specimen pair. Further detail regarding the fretting scars for the aluminium-aluminium contact can be found in Section 6.1.1.3.

The reduction in fretting fatigue life due to increasing axial stress and normal pressure is to be expected, see Section 2.2.5.1. However, in this research, fretting fatigue life was found to decrease in relation to an increase in the normal pressure, up to a critical value of 60 MPa for an axial stress amplitude of 70 MPa, 40 MPa for an axial stress amplitude of 100 MPa and 60 MPa for an axial stress amplitude of 125 MPa. Other investigations have reported that it is when the contact pressure is larger than the axial stress amplitude applied that an increase in fatigue life can be achieved [255], [256]. Above this critical value, a further increase in normal pressure tended to increase fretting fatigue life, indicative of a change in the fatigue damage mechanism, despite the fact that more cracks were observed at higher normal loads. This prediction has not been confirmed by the damage model developed here.

The fractographic analyses have shown that at low normal loads there is a tendency for only one dominant surface crack to initiate and propagate to failure, whilst at high normal loads there are multiple crack initiation points along the fretting scars. The latter may be explained by assuming that a high surface wear rate retards crack propagation because the cracked surface layer of the material is removed before cracks propagate to a significant depth.

It has been postulated that the retardation effect produced by crack closure due to a normal load is the reason for the increase in fretting fatigue life above a critical value, at higher normal loads there being a greater degree of crack closure.

Another theory is that the fretting action in the contact region can be regarded as having the same deformation mechanism as low plasticity burnishing, with higher contact loads resulting in higher residual stresses being introduced at the surface in specimens initially free of residual stresses [157].

It is recommended that in the future, a series of constant normal pressure tests, with reducing values of axial stress be conducted, in order to obtain the fatigue limits relating to the six different values of normal pressure undertaken here. This will provide an insight into the fretting behaviour of 2024 T351, by determining how the increase in fretting fatigue life seen above a critical normal pressure varies with the load conditions and if this is the case, what the critical turning point values of normal pressure are for each load condition applied.

By tracing down the fatigue limits, the degree to which the fatigue limits under fretting conditions have dropped, compared to that achieved solely under axial loading can be explored. This information will help in further developing the life prediction model and it will also provide a vital insight into the behaviour of fretting fatigue at low values of normal pressure.

The next step then would be to perform a series of constant normal load tests, with increasing values of axial stress, rising to a maximum of 140 MPa, this being the tension-tension plain fatigue limit of aluminium alloy 2024 T351, at a stress ratio of $R = -1$. These tests will complete the set of σ_n/N curves and aid in developing a full understanding of the influence of fastener clamping forces on fretting fatigue.

As far as the testing is concerned, compared with the original analogue control system, the new Rubicon digital control system has proved to be user friendly. It incorporates a software calibration facility so calibration is straightforward, allows calibration data to be stored, maintains reliable command signals and ensures that the waveforms relating to the horizontal and vertical axes may be synchronised to ensure precise control. However, more effective cooling of the system is required and there is an issue with the amount of data that can be stored in the buffer.

6.1.1.2 Friction

Subsequent analyses were performed to explore some of the potentially influential factors and some data on the friction forces involved were collected. The friction forces for the upper and lower pads were comparable in every case.

By plotting the evolution of the friction forces for every fretting fatigue test, it was shown that the friction forces increase rapidly at the beginning of a test. This is whilst a fretting scar develops. This could be due to the increase in adhesion between clean surfaces that was created by the removal of the initial oxide film.

The friction forces thereafter are thought to arise primarily due to the interlocking of surface asperities. The friction forces at low normal loads may have been insufficient to plastically deform and break these surface asperities, thus higher values of friction coefficients were observed here.

The subsequent decrease in the friction forces may be attributed to fretting wear, with wear debris acting as a solid lubricant before being dispersed.

For an axial stress amplitude of 100 MPa, the friction forces remained steady throughout most of the life of the specimens. Any periodic fluctuations in the friction forces may have been due to the ejection of debris from the contact zone and consequently the occurrence of metal-to-metal contact. This may also have been related to changes in slip behaviour, as the slip displacements can change from one bridge foot to the other due to slight differences in the friction resistance or wear. This could be confirmed in the future by monitoring the displacement of the bridge pads. Recently, measurements of relative slip amplitude taken in situ using a scanning electron microscope have been found to be smaller than those measured using an extensometer as is conventional [257]. The gradual reduction in friction force observed during the later period of life could have been due to the presence of a growing crack.

The results for axial stress amplitudes of 70 MPa and 125 MPa include unreliable readings, apparent due to the negative maxima and the fact that the plots for the top and bottom fretting pads demonstrate the same errors. This is believed to be due to a corruption of the measurement system.

However, by taking a locus of the maximum data points in each case, similar trends to those achieved at an axial stress amplitude of 100 MPa may be observed. Also, the overall values of friction amplitude and friction coefficient calculated fit well in terms of the variation with axial stress amplitude as is shown in Chapter 4.

The reasons for the scatter in the values of friction force seen, particularly that at the higher values of normal pressure and an axial stress amplitude of 70 MPa, are not fully understood.

However, some bridge pads were used for multiple tests and there may have been issues with the geometry of the bridge feet due to grinding, or perhaps there was less deflection with a change in the height of the bridge feet. The roughness measurements do not lend an explanation for this.

Hysteresis loops were used to determine the maximum and minimum friction forces involved, but no account was taken of the shape of these loops and therefore the changes in slip that occurred. The condition of partial slip was observed in the majority of cases.

By calculating the difference between the maximum and minimum friction forces involved, it was shown that friction force amplitude generally increases with the magnitude of the normal pressure applied, or one half of the applied normal pressure per bridge foot. Fretting fatigue life generally decreases with the magnitude of the normal pressure applied, up to a critical value.

An increase in normal pressure also tends to decrease the coefficient of friction; the rate of this decrease is related to the applied axial stress amplitude, being greatest at 125 MPa and decreasing accordingly. The highest coefficients of friction were seen at an axial stress amplitude of 125 MPa, decreasing with axial stress amplitude. After an initial decrease, fretting fatigue life generally increases past a critical value of the normal pressure applied. The fretting fatigue life decreases with increasing axial stress amplitude for any given constant normal pressure.

The results obtained were compared with the data reported by Fernando et al. [99] for a BS S98 steel bridge with a pad span of 16.5 mm, in flat-on-flat contact with BS L65 4 % copper aluminium alloy specimens under the same load conditions, see Figures 6.4, 6.5 and 6.6.

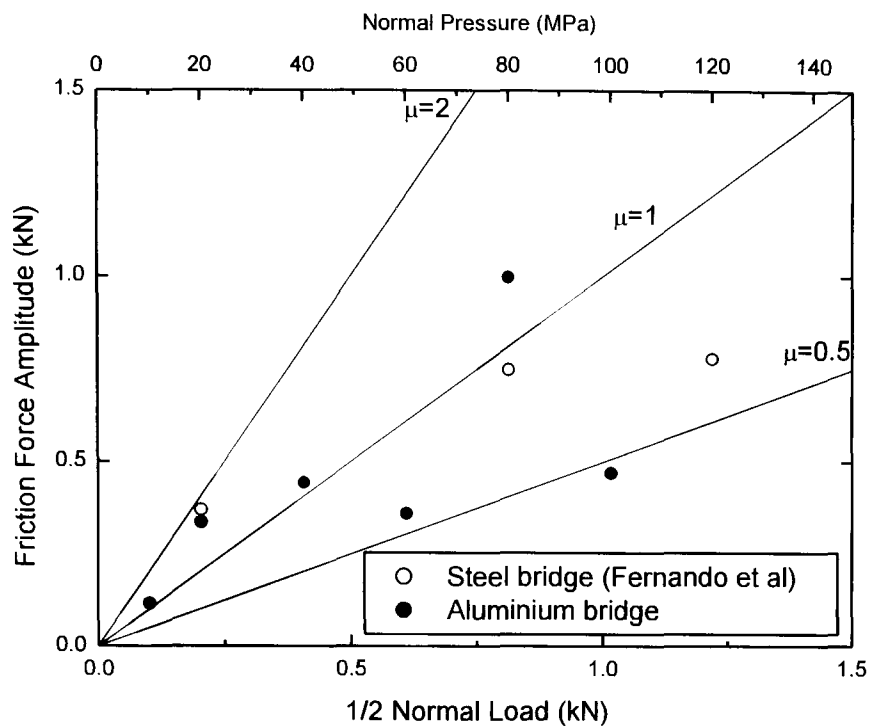


Figure 6.4: A comparison of the friction force amplitudes derived from the maximum and minimum friction forces determined for each test and by Fernando et al. [99] for fretting fatigue tests with a BS S98 steel bridge in contact with aluminium alloy 2024 T351 specimens subjected to an axial stress amplitude of 70 MPa.

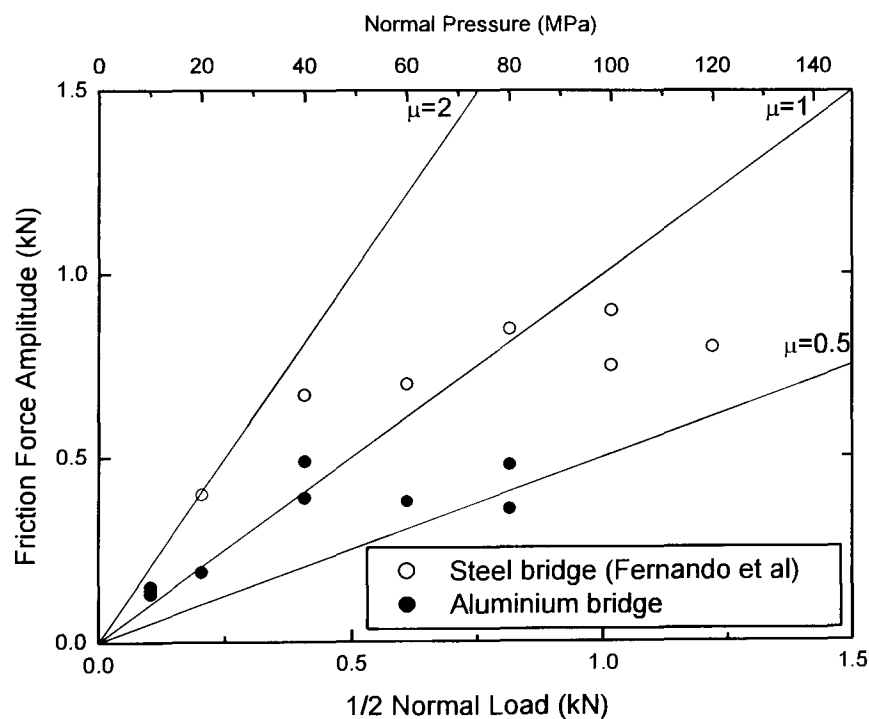


Figure 6.5: A comparison of the friction force amplitudes derived from the maximum and minimum friction forces determined for each test and by Fernando et al. [99] for fretting fatigue tests with a BS S98 steel bridge in contact with aluminium alloy 2024 T351 specimens subjected to an axial stress amplitude of 100 MPa.

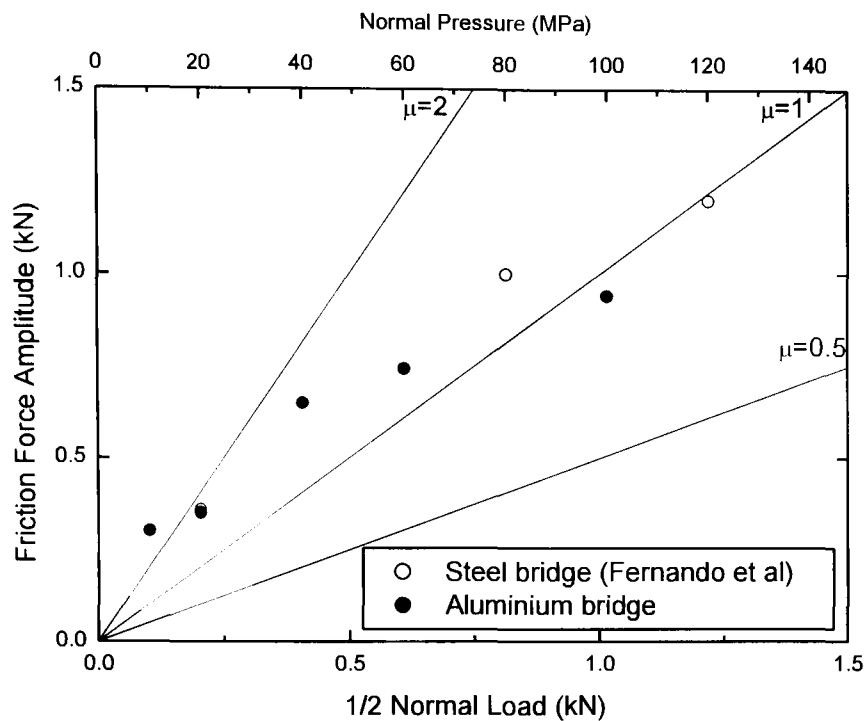


Figure 6.6: A comparison of the friction force amplitudes derived from the maximum and minimum friction forces determined for each test and by Fernando et al. [99] for fretting fatigue tests with a BS S98 steel bridge in contact with aluminium alloy 2024 T351 specimens subjected to an axial stress amplitude of 125 MPa.

Analyses of the results presented in Figures 6.4 to 6.6 indicate that:

- At all axial stress amplitudes the coefficient of friction at low normal pressures is approximately equal to 2 with both the steel bridges and the aluminium bridges;
- Thereafter, the nominal friction coefficients observed were higher with the steel bridges;
- An increase in normal pressure tends to decrease the coefficient of friction with both the steel bridges and the aluminium bridges;
- The amplitudes of the friction forces with the steel bridges are greater than those with the aluminium bridges;

- With both the steel bridge and the aluminium bridges, the amplitude of the friction forces generally increases with the magnitude of the applied normal pressure, although some later reduction in amplitude is observed at high normal pressures with the aluminium bridges and at an axial stress amplitude of 70 MPa and with both the steel bridges and the aluminium bridges at an axial stress amplitude of 100 MPa.

The differences in the friction forces, could contribute to an explanation of the differences observed in the fretting fatigue lives. That is, that the amplitudes of the friction forces with the steel bridges are greater than those with the aluminium bridges and for any given constant normal pressure and axial stress, the fretting fatigue lives are greater with the aluminium bridges than with the steel bridges.

Subsequent examination of the free surfaces using a scanning electron microscope, revealed detail of the considerable wear due to the surface contact. The wear from the aluminium bridges was lower than that from the steel bridges, which may have contributed to the lower friction coefficients of the former.

6.1.1.3 Scar

It was postulated that there is a relationship between friction and fretting damage and that wear scars indicate regions of stress concentration that could be responsible for the fast initiation and propagation of fatigue cracks. This research has aided to the understanding of the characterisation of fretting damage in relation to fatigue life, although much remains to be done and understood.

The development of the fretting scar is a dynamic process, therefore, in order to better understand the evolution of the fretting scar, thirty six unpeened specimens were analysed following a series of interrupted fretting fatigue tests.

These tests were carried out for a tenth, quarter, half and three quarters of the total fretting fatigue lives found at the minimum and maximum normal pressures applied and at that which resulted in the shortest fretting fatigue lives for each axial stress amplitude. A total of 144 profiles were taken for each axial stress, the surface damage was explored and the widths and depths of the wear scars were determined.

Visual differences in the fretting scars formed due to the application of various normal pressures were observed. There tended to be more wear debris apparent at low normal loads, high axial stresses and after a higher number of cycles.

It was discovered, however, that scarring is a continuous process throughout the life of a specimen; the damage does not plateau, despite the fact that the friction does. There was no correlation between the notch peak to valley depth and percentage life for any of the normal pressures applied, and neither was there a correlation between notch width and percentage life. However, the fact that there was significant damage at 10% of life indicates that crack propagation is the dominant failure mechanism.

There was also no discernable effect of the normal pressure on the fretting scar. For an axial stress amplitude of 70 MPa and 125 MPa notch peak to valley depth appeared to decrease with increasing normal pressure, whereas for an axial stress amplitude of 100 MPa notch peak to valley depth decreased with increasing normal pressure and then subsequently increased.

Notch width also increased with increasing normal pressure and then decreased. However, it is debatable whether any of these effects were simply due to scatter in the data. It is acknowledged that no statistical treatment of the data has been made and efforts to find a correlation coefficient should be made.

It is recommended that the mean and standard deviation for each normal pressure be utilised, assuming a Gaussian or normal distribution, and trends of a combination of the two be investigated.

There were a few spurious measurements that were considerably greater than the mean and it is postulated that debris may have become trapped and ploughed into the surface here, or else the edge of a bridge pad. It is also acknowledged that a volume of material above the original surface due to plastic deformation and the adherence of debris may have affected the results and the depths of the profiles may have been underestimated due to the presence of wear debris within the scar. Furthermore, the loss of material and cracking may have been competitive processes, as a loss of material can eliminate small superficial cracks and larger cracks can accommodate imposed displacement, reducing slip amplitude and therefore the formation of debris. The bulk analysis of the profiles by means of a computer program will not have aided the study of each individual wear feature. However, it is a practical method for collating large amounts of data.

Clark and Hoepfner [121] have reported damage up to a depth of 35 μm in aluminium alloy 2024 T3 at a net normal stress of 21 MPa, a maximum net axial stress of 207 MPa and a stress ratio of 0.1. Clark and Hoepfner [121] and Shinde and Hoepfner [122] found no positive correlation between the depth of fretting damage and the fatigue life of a specimen. However, the latter has reported that cracks did form within fretting pits, the deepest pits observed in aluminium alloy 7075 T6 being of the order of 20 μm . Neslen et al. [173] have reported that the average roughness of fretted regions in titanium samples subjected to 2,000 cycles varied from 474 to 600 nm, whilst on samples subjected to 300,000 cycles, it varied from 550 to 1,000 nm. Mutoh et al. [225] have reported that the average depth of surface wear of a steel specimen tested at a stress amplitude of 165 MPa to 10^8 cycles, was almost 60 μm .

The maximum notch peak to valley depth recorded in this research for an unpeened component was 58 μm , at a normal pressure of 10 MPa and an axial stress amplitude of 70 MPa. The maximum notch width recorded was 3.4 mm, at a normal pressure of 60 MPa and an axial stress amplitude of 125 MPa.

However, it has been shown for all load cases, that a fretting site can be compared to a notch that is characterised by the rapid formation of a propagating crack. Indeed, it has been documented that strength reduction factors of between 2 and 5 are quite common [53].

Considerations of the initiation stage could therefore be directed in part towards the fretting scar. The formation of a fretting scar will almost certainly amplify, albeit with a diminishing effect with depth, the applied loads by means of a stress concentration factor K_t , which needs to be quantified. Any notch effect from a scar could be combined with the driving parameter identified in the Finite Element Analyses.

Investigation of the size of scar critical to the initiation of fretting fatigue cracks needs to be established by conducting interrupted fretting fatigue tests at less than 10% of fretting fatigue life.

Furthermore, as multiple crack initiation sites have been observed, the tendency for cracks nucleating from pits in close proximity to one another should be considered. Indeed, Shinde and Hoepfner [122] have postulated potential relationships between the nucleation of fretting cracks and the area damaged by fretting and the location, proximity and topography of the fretting pits. Clark and Hoepfner [121] determined that it is the location of the fretting damage that is the key factor. Fretting damage located near the edge of the fretting pad is more detrimental than damage near the centre of the fretted area.

Multiple crack initiation has been found to occur along the grooves left in machined surfaces [258]. Waterhouse and Taylor [163] have concluded that fretting fatigue cracks originate in the boundary between slip and non slip in the contact region, because of the high stress concentration. But when a crack forms, it relieves the stress concentration at this point and the boundary moves inwards, resulting in the initiation of another crack which propagates more rapidly. The multiple cracks paths imaged using x-ray micro tomography [120] give further credence to the need to consider multiple site damage when estimating life, as most models only incorporate a single critical crack size.

It is not suggested, however, that fretting pits are the sole cause of fretting fatigue crack initiation. Phenomena such as the surface plastic deformation of the contacting surfaces will also need to be examined as a contributory factor towards the crack initiation process, although the proportion of fretting fatigue life spent on short crack propagation is relatively small.

X-ray micro tomography is one method that has recently come to the fore in the study of the microscopic mechanisms of crack propagation and especially short cracks. Recent images have shown that the angle of fretting fatigue crack initiation is strongly influenced by the local microstructure [120].

Initiation may therefore be dominated by a crack permeating a grain boundary, so fretting could be approached as a plain fatigue problem subjected to a localised stress concentration, incorporating asperity contact size, asperity spacing, micro structural dimensions, etc. [259]. Application of a micromechanical model for crack growth at notches such as that devised by Vallellano et al. [260], [261] may also be appropriate.

Clark and Hoepfner [121] and Shinde and Hoepfner [122] have also observed a fretting fatigue damage threshold, upon the removal of the fretting pad and arrest of continued fretting damage.

Work is required to quantify further the circumstances and damage under which this occurs to improve inspection and maintenance techniques. However, it is acknowledged that fretting fatigue significantly reduces the time to initiation and after that initial period, what is happening at the surface is unimportant as the crack is growing away from the surface in any case.

6.1.2 Modelling

In the present study, finite element analyses have contributed towards pinpointing the location of cracks initiated by fretting and to predicting the initial propagation direction of Stage I crack growth, which has been substantiated by investigation of the fracture surfaces. This may be explained by the maximum value of the tangential stress range $\Delta\sigma_{\theta\theta max}$.

The experimental results were then further used in the modelling of fretting fatigue fracture, the fretting fatigue process being dominated by crack growth. Initially, a better estimation of the equivalent stress in the system calculated from the biaxial loading, aided in the understanding of the fact that aluminium alloy 2024 T351 specimens fail under fretting fatigue at axial loads significantly below 140 MPa, the tension-tension plain fatigue limit of aluminium alloy 2024 T351, at a stress ratio of $R = -1$.

The work of Faanes and Fernando [101], for a crack normal to a surface, was further developed to predict fretting fatigue life of unpeened and peened components. A fretting crack was assumed to initiate at the edge of a contact and propagate at an angle of 22.5° , as has been substantiated by this research. Mode I and II stress intensity factors for fretting fatigue cracks devised by Sheikh et al. [102] by means of a finite element procedure, were subsequently derived and incorporated into a Linear Elastic Fracture Mechanics model.

The reported increase in the crack propagation rate of fretting fatigue cracks may be due to the presence of a mode II component. However, it is acknowledged that there is a discrepancy in the fact that although a mode II component has been identified theoretically, one has yet to be demonstrated experimentally. The angled crack could be due to a change in the principal stress field, as under non-proportional loading the directions of the principal stresses rotate, and the ratio between the principal stresses varies. Both the choice of crack angle and coefficient of friction, will affect the principal stress direction and hence mode I crack growth. It is recommended, therefore, that some experimental stress analyses, using Digital Image Correlation for example, be carried out to investigate the real stress field in the contact condition.

Stress intensity factors were used to define the magnitude of the singular stress and displacement fields, local stresses and displacements near the crack tip. Stress Intensity Factors depend on the loading, the crack size, the crack shape, and the geometric boundaries of the specimen. In this analysis a crack angle of 22.5° was assumed. This was justified following observation of the fracture surfaces. The resultant K values are likely to have been too low, as the influence of localised asperity contact was neglected.

The distribution of a normal pressure will be dependent on factors including the geometry of the contact and the material properties of the materials in contact. A uniform distribution of the normal pressure was assumed, due to assumptions made regarding the wear of the contacting surfaces, including the reduction of the regions of high stress concentration at the edges.

Experiments by Sheikh et al. [102], determined that anti-parabolic and triangular load cases resulted in larger values of K . However, Edwards [77] found that the effect of pad load distribution on fretting fatigue life is small and good predictions of life were achieved by Faanes and Fernando [101] assuming a uniform distribution of normal pressure. It was assumed that the friction force varied in phase with the cyclic axial stress, with a stress ratio of -1.

By substituting values of axial pressure, normal pressure and friction coefficient, values of K_I and K_{II} were subsequently calculated for all combinations of axial and normal loading applied and friction force recorded during testing. For mode I, in the tensile region of the load cycle, both the axial and friction components will open a crack, whereas the normal pressure will tend to close a crack. For the compressive region of the load cycle, all three components will enhance crack closure. For mode II, all three components produce negative values of K_{II} .

The influences of friction and normal forces are important, especially during the early part of life when the fretting forces are significant. The effect of the friction component on the values of K_I and K_{II} is apparent, as is shown in Figure 6.7, where a friction ratio of 2 has been specified in all of the K_I and K_{II} friction stress components. The importance of the accuracy of the values of friction force measured is shown in Figure 6.8, the experimental data is included for reference. Figure 6.9 shows the resultant estimations by incorporating values of 2, 1 and 0.5 as the friction ratios with increasing normal pressure, as was the general trend observed, as the coefficient of friction tended to decrease in this manner due to an increasing normal pressure.

Equal slip was assumed and accommodated indirectly due to the fact that the friction forces are measured. Faanes and Fernando [101] concluded that as the components of axial load, normal load and friction force were sufficient to predict fretting fatigue life, then the amplitude of slip affects fretting fatigue primarily through its influence on the friction force in the fretting zone.

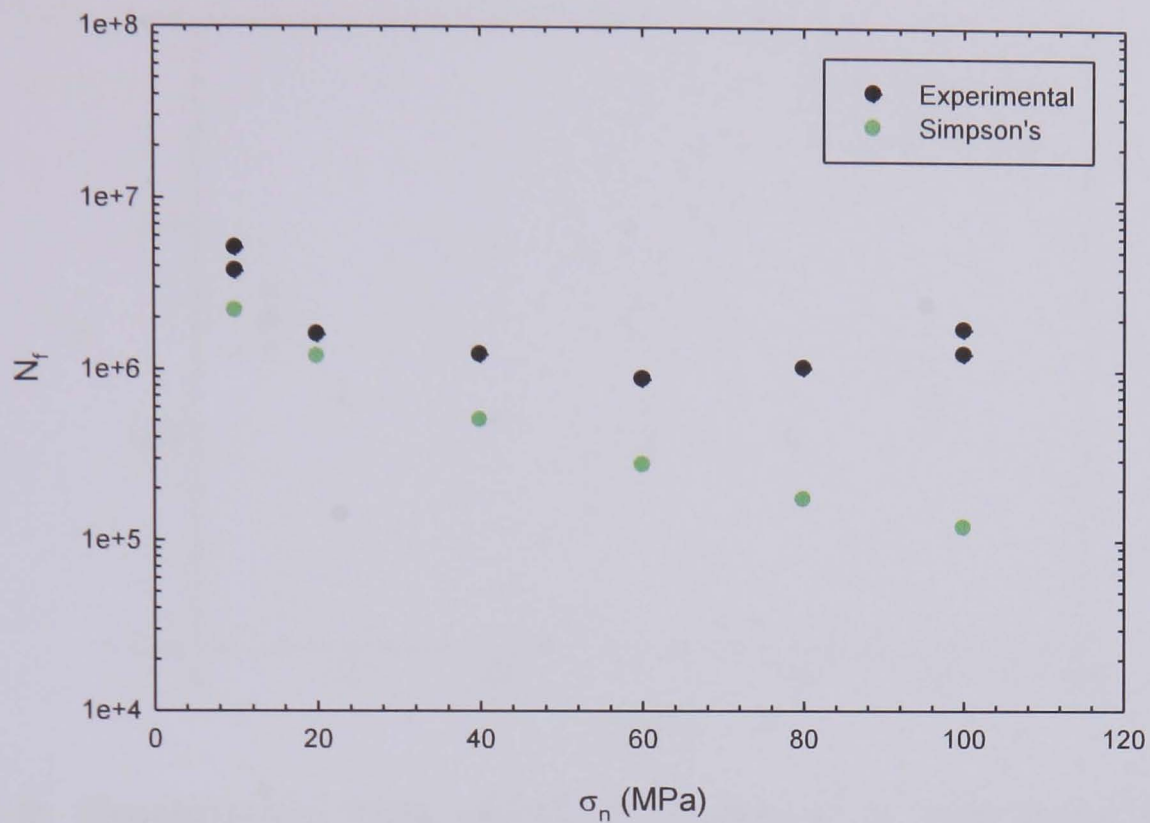


Figure 6.7: Experimental data points of N_f versus σ_n and those determined experimentally using the Simpson's rule incorporating a constant friction ratio of 2, for an axial stress of 70 MPa.

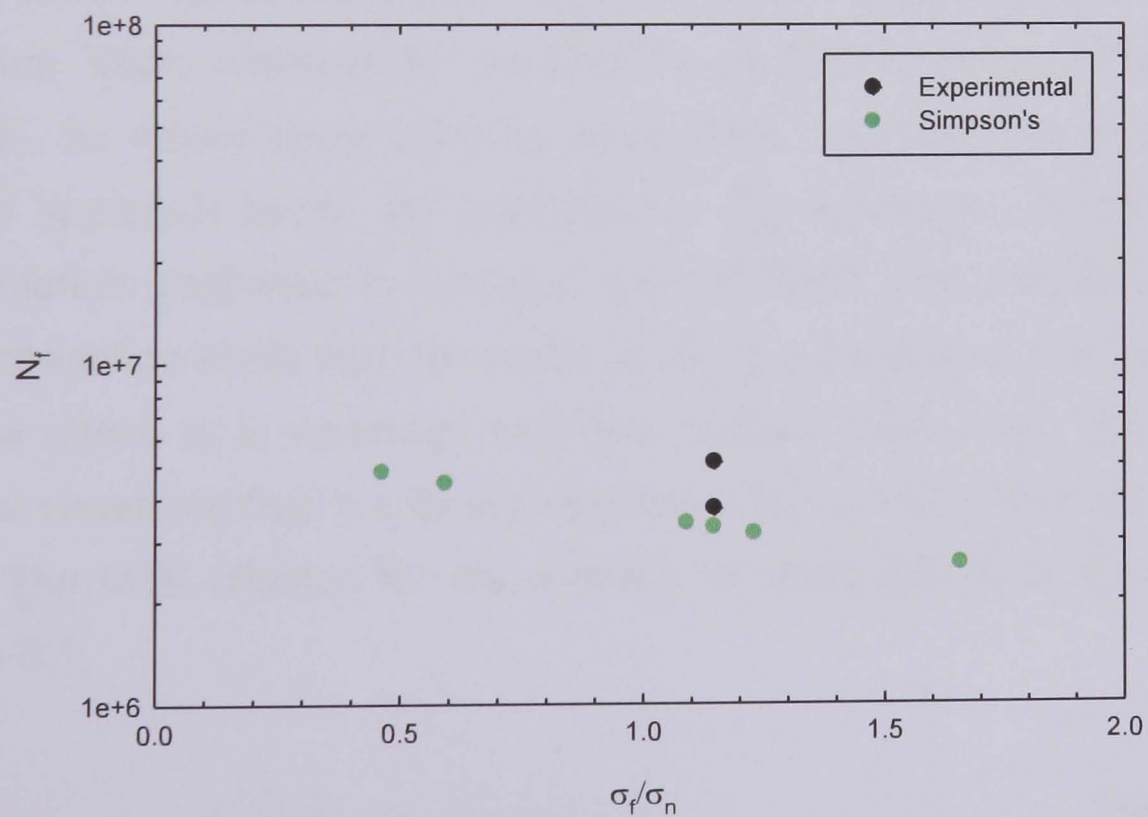


Figure 6.8: Experimental data points of N_f versus the friction ratio and those determined experimentally using the Simpson's rule incorporating a constant normal pressure of 10 MPa, for an axial stress of 70 MPa.

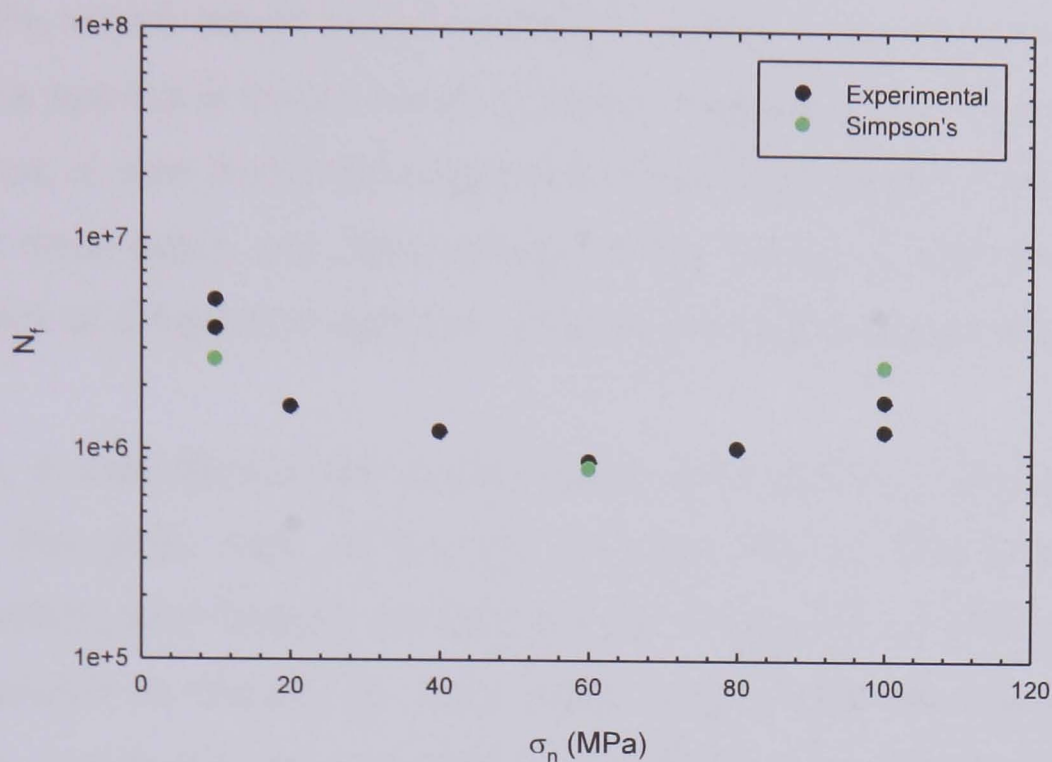


Figure 6.9: Experimental data points of N_f versus σ_n and those determined experimentally using the Simpson's rule incorporating values of 2, 1 and 0.5 as the coefficients of friction, corresponding to increasing normal pressures, for an axial stress of 70 MPa.

ΔK_e was determined based on the addition of Irwin's elastic energy release rate parameters. Many methods for defining the equivalent stress intensity factor range ΔK_e for mixed-mode loadings have been proposed, but no universally accepted approach exists. An alternative is the Maximum Tangential Stress (MTS) criterion, proposed by Erdogan and Sih [262]. This criterion states that crack propagation starts from the crack tip along a radial direction for which the tangential stress is a maximum and that fracture starts when the maximum tangential stress reaches a critical stress equal to the fracture stress in uniaxial tension. The MTS criterion for the direction of crack growth is the solution of Equation 6.1:

$$K_I \sin \theta_0 + K_{II} (3 \cos \theta_0 - 1) = 0 \quad \text{Equation 6.1}$$

However, it has been determined that subsequent values of ΔK_{II} would only differ by 18%, which would be less than the scatter in the experimental results, although this approach would result in smaller values for x , the factor by which the grain size, d , was multiplied to give an initial crack length. Plots of K_e versus a , highlight once again the dependence of the model on the friction ratio, as there is a lack of a logical progression with the normal pressure applied.

Additionally, a_i was fitted to the experimental data. This was determined from a multiple of the grain size, d , thereby incorporating several factors including Stage I cracking and friction, hardening and a measure of fretting damage. It was not possible to discern an initial crack length using the scanning electron microscope, due to the damage done by rubbing of the fracture surfaces near the wear scars. It should be possible to introduce an element of the fretting damage though, by selecting a suitable stress concentration factor calculated from the scar data.

Individual values of a_i were determined for each axial stress applied. The effect of the x factor is highlighted in Figures 6.10, 6.11 and 6.12, where the results calculated with individual values of x are compared with those calculated with a mean value of all three. However, these plots never coincide for all normal pressures applied, primarily due to the scatter in the values of the friction forces measured.

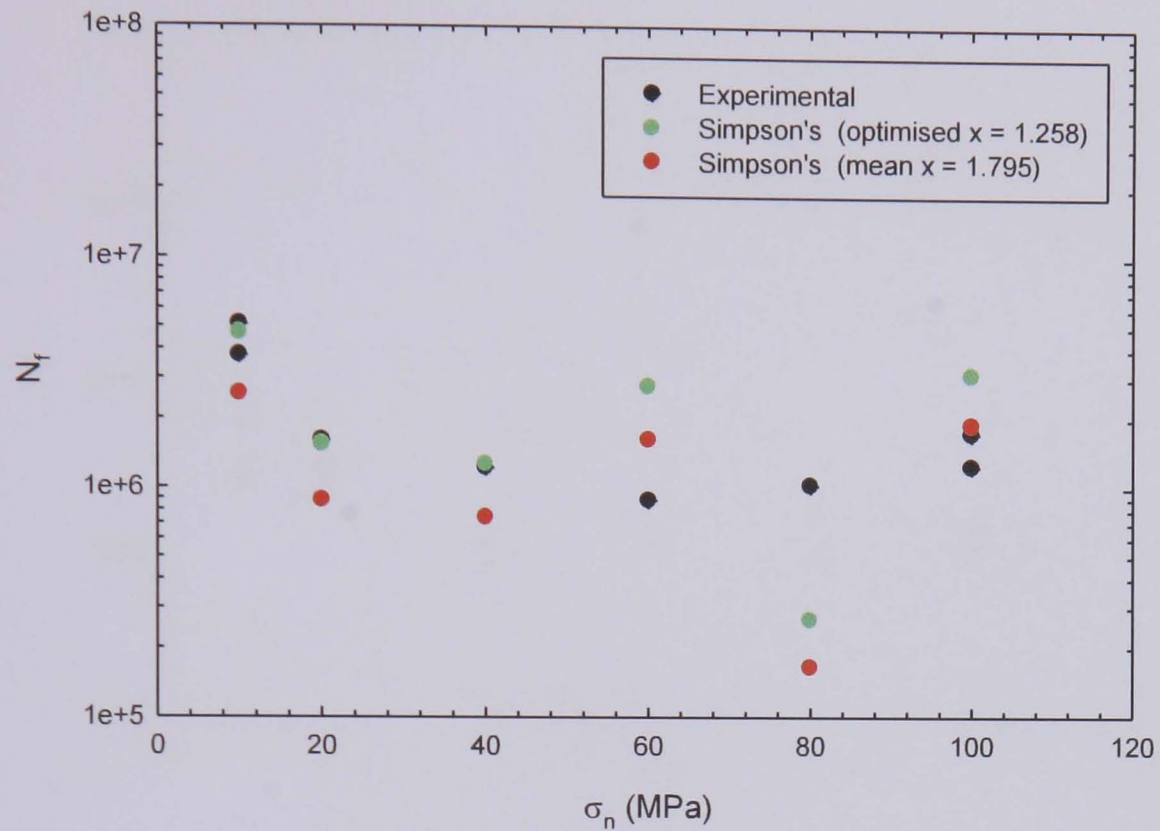


Figure 6.10: A comparison of the theoretical results achieved utilising an optimised value of x for an axial stress amplitude of 70 MPa and a mean value of x determined for all axial stresses applied.

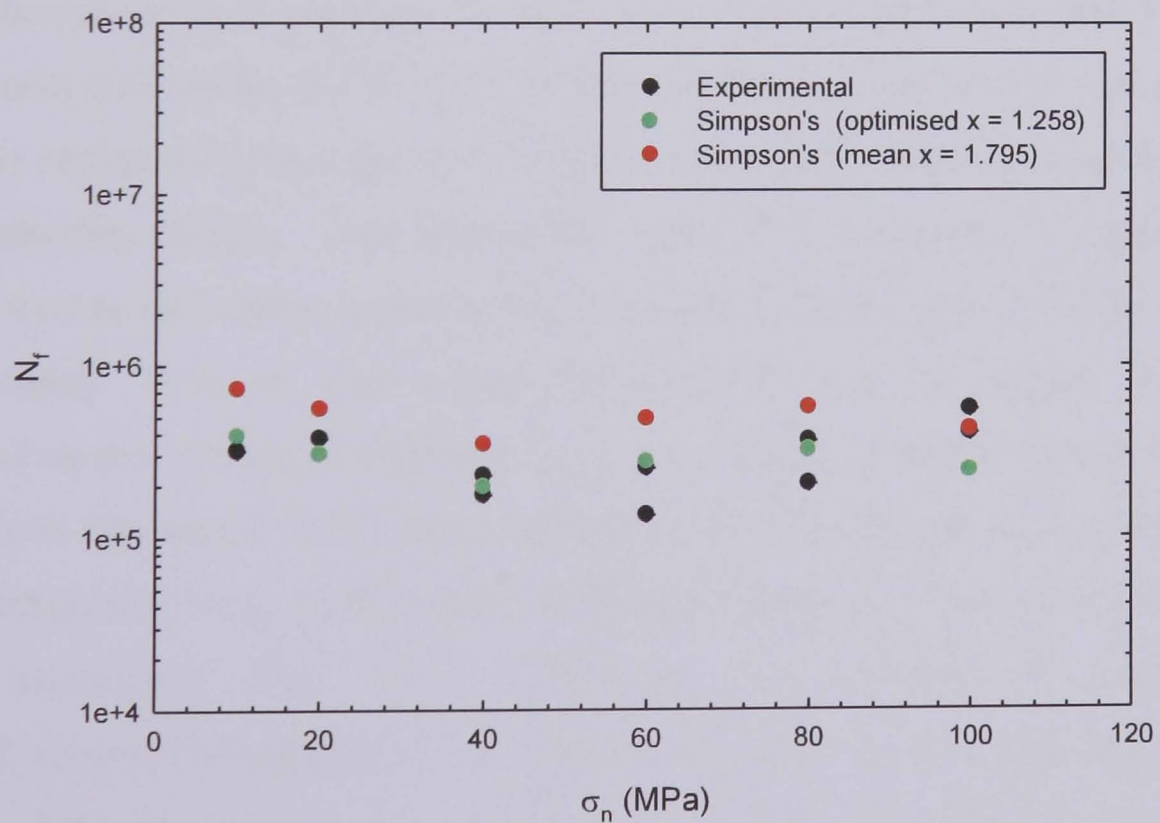


Figure 6.11: A comparison of the theoretical results achieved utilising an optimised value of x for an axial stress amplitude of 100 MPa and a mean value of x determined for all axial stresses applied.

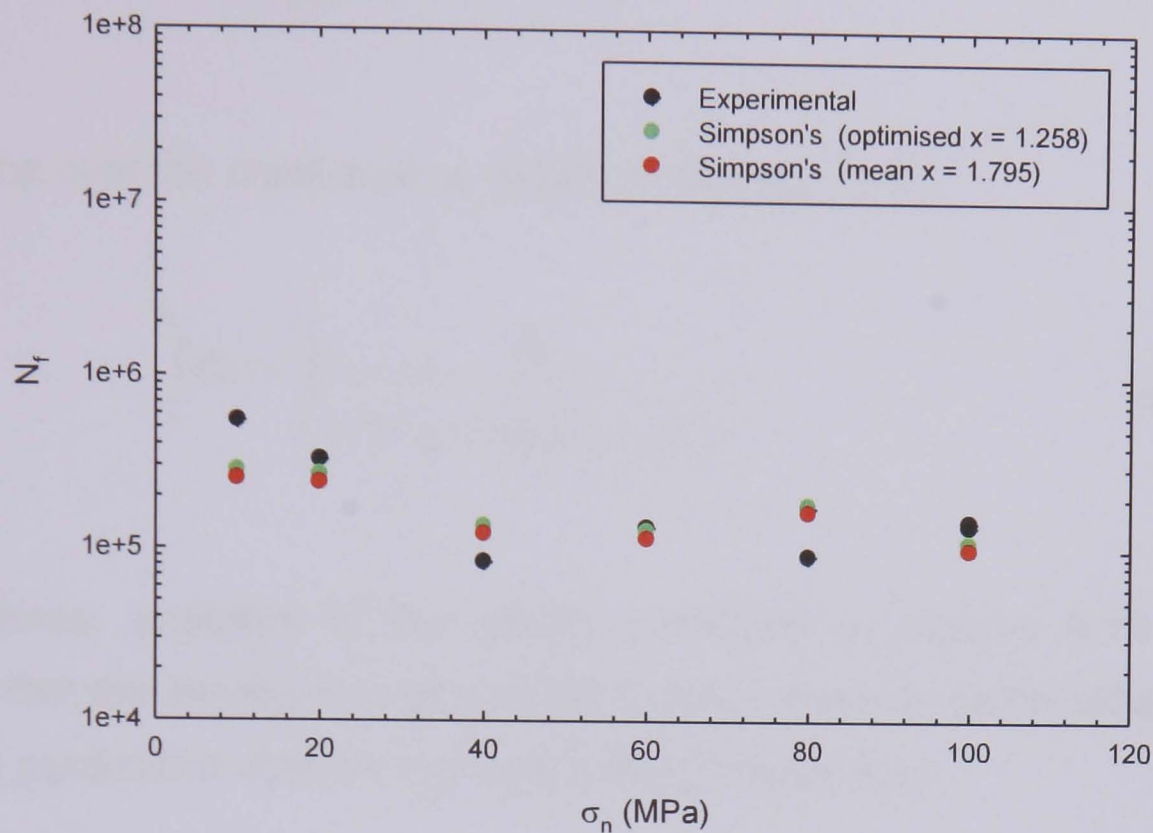


Figure 6.12: A comparison of the theoretical results achieved utilising an optimised value of x for an axial stress amplitude of 125 MPa and a mean value of x determined for all axial stresses applied.

A comparison of the success of this model was made with that devised by Faanes and Fernando [101]. Both models are based on Paris' law and utilise the same material constants, but different methods of determining the relevant stress intensity factors. This being the case, the exponent, n , was taken as 3.25, so that a 10% error in the stress intensity factors would lead to an error of approximately 30% in the crack propagation rate predicted. The model presented in this research contains a K_{II} component and the model devised by Faanes and Fernando [101] takes into account a threshold effect. No threshold was incorporated here, as the tests conducted were not close to the fatigue limit for this aluminium alloy. This model has been modified to incorporate a threshold stress intensity factor to account for the threshold effect, resulting in Equation 6.2, where ΔK_{th} is a material constant, assumed to be fixed and independent of crack length and loading.

$$\frac{da}{dN} = C(\Delta K - \Delta K_{th})^n \quad \text{Equation 6.2}$$

Integrating over the crack size, a , results in Equation 6.3.

$$\int_0^{N_f} dN = \int_{a_i}^{a_f} \frac{da}{(CY^n \Delta \sigma^n (\pi a)^{\frac{n}{2}}) - \Delta K_{th}^{\frac{n}{2}}} \quad \text{Equation 6.3}$$

Nevertheless, analyses of the results presented in Figures 6.13 and 6.14 indicate that the introduction of a mode II stress intensity factor results in more accurate predictions of short and long fretting fatigue lives.

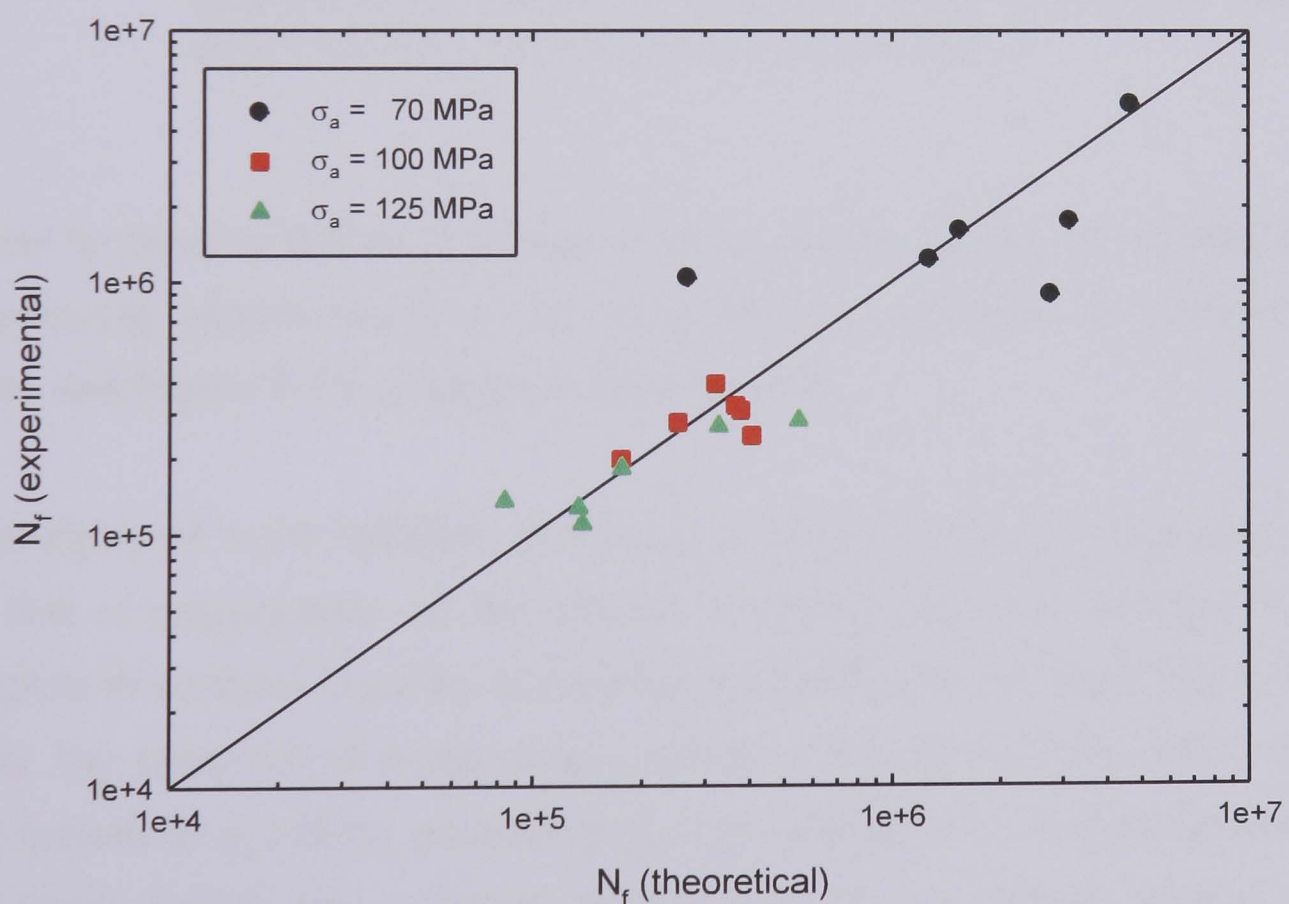


Figure 6.13: A comparison between the fretting fatigue lives obtained experimentally and by means of the life prediction model incorporating mode I and II stress intensity factors.

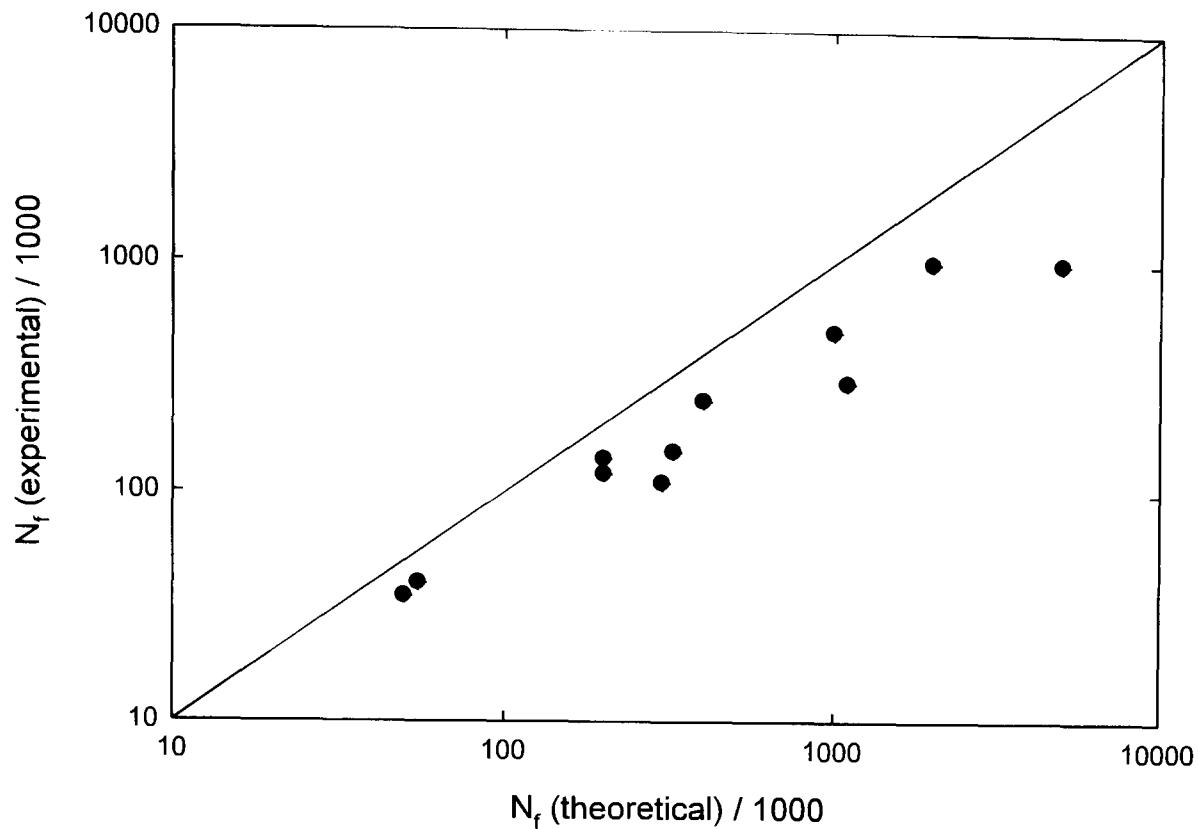


Figure 6.14: A comparison between the fretting fatigue lives obtained experimentally and by means of the life prediction model incorporating mode I intensity factors and a threshold determined by Faanes and Fernando [101].

In order to develop further a complete life prediction model, characterisation of the following stages needs to be completed: a) initiation; b) stage I crack growth, see Figure 6.15; c) stage II crack growth.

The analysis of crack initiation in fretting is known to be far more challenging than that of propagation, as the effects of fretting on crack initiation are less amenable to analysis. Faanes and Fernando [101] acknowledged that in fretting fatigue, the presence of a high stress gradient affects the mechanism of short crack growth in a fretting environment, thus inaccuracies in the description of short crack growth has a lesser influence on the prediction of total fretting fatigue life. Also, the ratio of the number of cycles spent in short crack growth, to the total number of fatigue cycles in life is reduced, hence any discrepancy in the description of short crack growth will have a smaller influence on the total lifetime predicted.

Consideration of short crack behaviour improves fretting fatigue life predictions for long lives. Application of the threshold short crack correction suggested by El Haddad et al. [263] was used. Further work also needs to be completed in order to establish the dominant parameter(s) that control fatigue damage in Stage I and this could be introduced in to a short crack model, such as the Navarro – de los Rios micromechanical model [264].

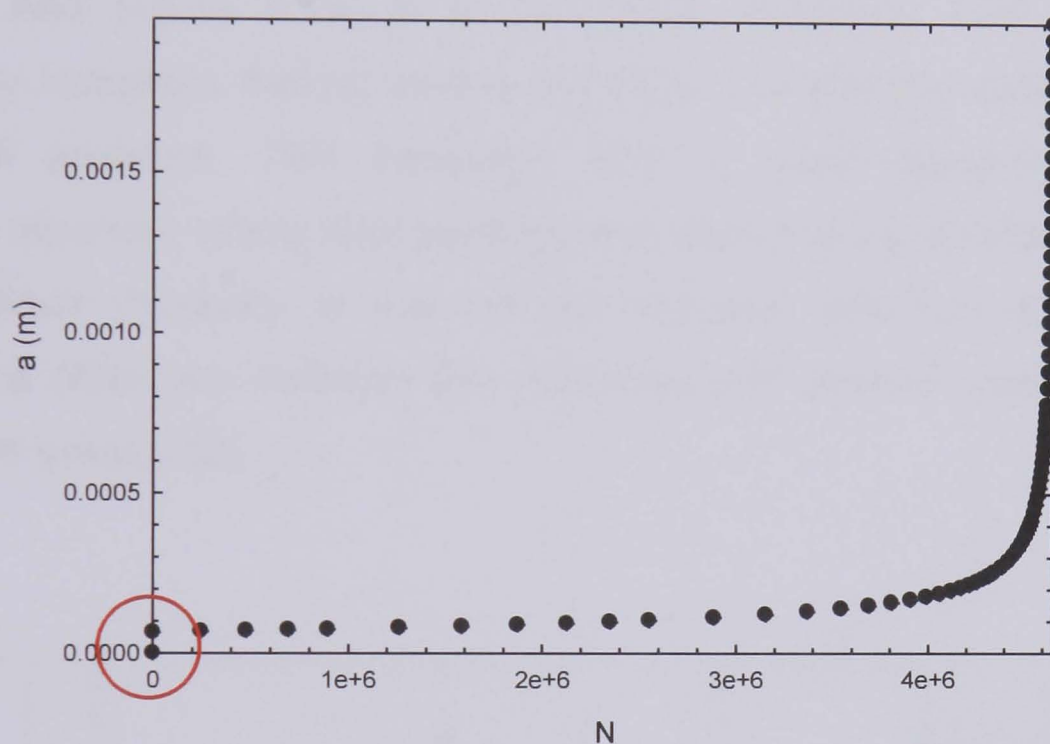


Figure 6.15: The evolution of crack length with the number of cycles applied, highlighting the area of short crack growth.

6.2 SHOT PEENING AND FRETTING FATIGUE

6.2.1 Experimental programme

6.2.1.1 Life

Nine fretting fatigue tests on aluminium alloy 2024 T351 in flat-on-flat contact with peened aluminium alloy 2024 T351 were completed in the constant normal pressure test programme.

Three of these tests were halted when 5×10^6 cycles were reached. Two of these tests resulted in failure, not at the peened test section, but at an unpeened area in the grips and a third was stopped by the failure of one of the steel locating pins. Three tests then ran to completion. Owing to restrictions on time, none of these tests were repeated.

It was still apparent, however, that although there was a considerable reduction in fatigue strength due to fretting, this was less so than with the unpeened condition, see Figure 6.16. It is concluded, therefore, that shot peening significantly increases fretting fatigue durability, but with the same dependency on normal pressure. This behaviour was in good agreement with data previously reported, where shot peening was shown to significantly increase the fretting fatigue durability at low contact stresses, whereas at high contact stresses the difference between the unpeened and peened conditions appears not to be as great [218].

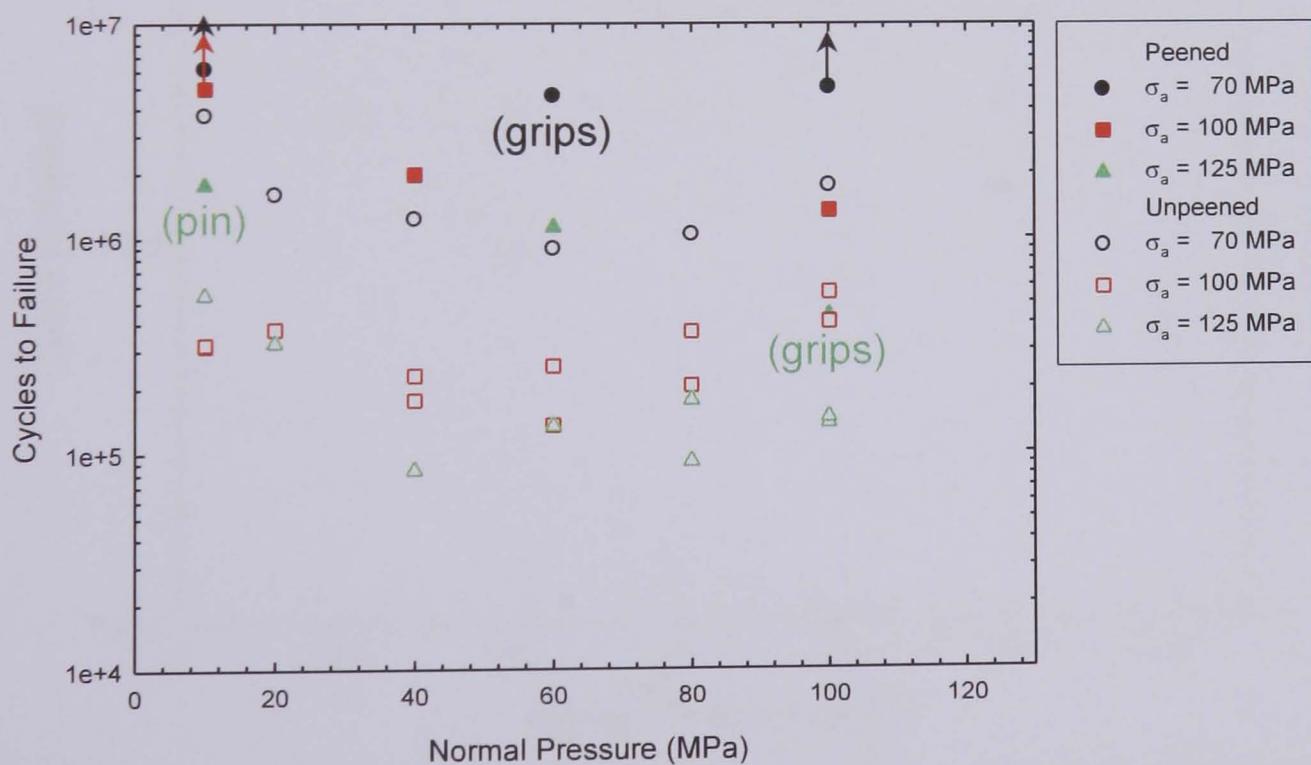


Figure 6.16: A comparison of the number of cycles to failure for fretting fatigue tests conducted with an aluminium alloy 2024 T351 bridge in contact with peened and unpeened aluminium alloy 2024 T351 specimens subjected to a range of normal pressures and axial stress amplitudes of 70 MPa, 100 MPa and 125 MPa.

An analysis of the results presented in Figure 6.16 indicates that:

- The peened condition exhibits a life distribution whereby the number of cycles to failure decreases with an increase in normal pressure;
- Fatigue lives at normal pressures above and below the critical value of the unpeened condition are higher for the peened condition.

The results obtained at an axial stress amplitude of 100 MPa were compared with the data reported by de los Rios et al. [218] for BS S98 steel in flat-on-flat contact with peened BS L65 4 % copper aluminium alloy for similar normal pressures, see Figure 6.17. The behaviour observed was in good agreement with that data previously reported.

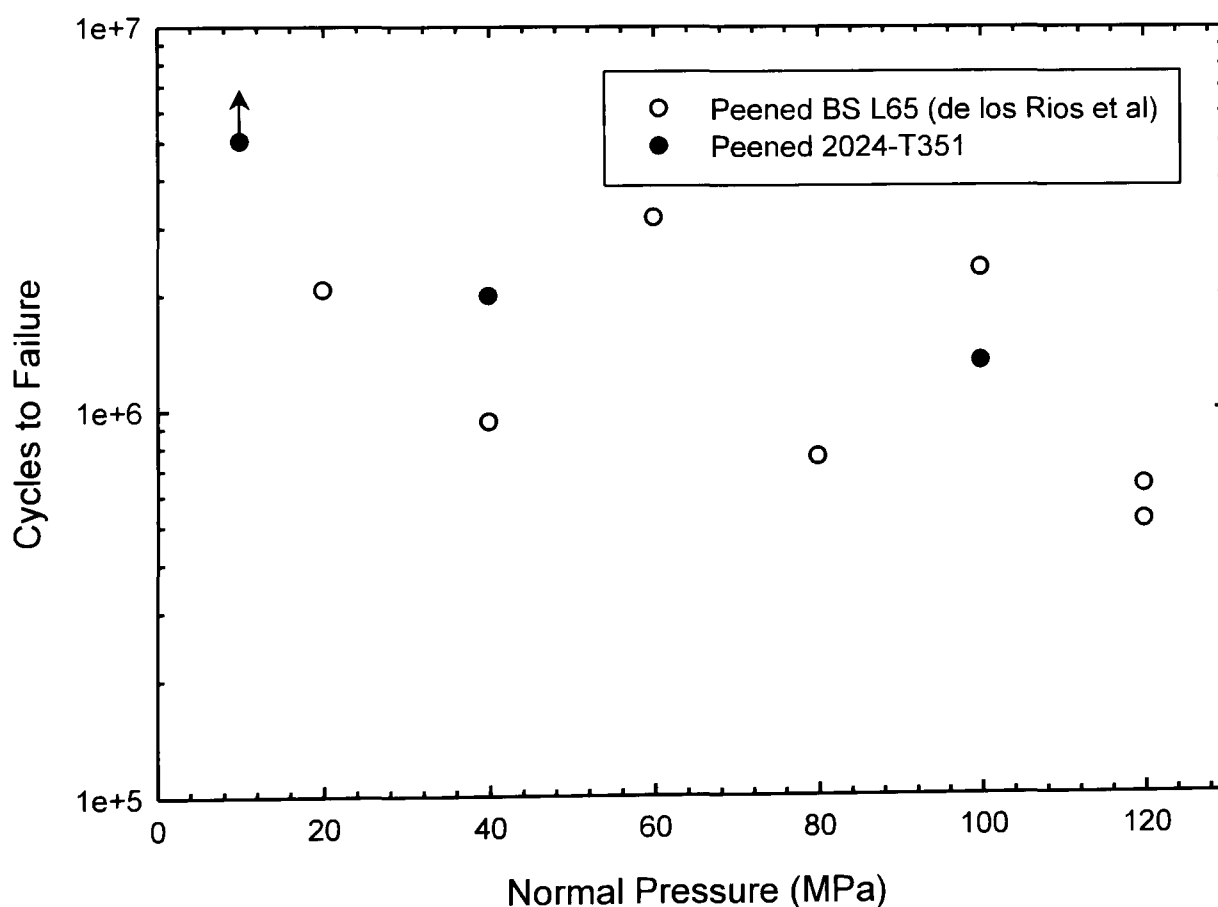


Figure 6.17: A comparison of the number of cycles to failure for fretting fatigue tests conducted with a BS S98 steel bridge [218] and an aluminium alloy 2024 T351 bridge in contact with an aluminium alloy 2024 T351 specimen subjected to an axial stress amplitude of 100 MPa.

An analysis of the results presented in Figure 6.17 indicates that:

- For both the aluminum bridges and the steel bridges, the number of cycles to failure decreases with an increase in normal pressure;
- The fatigue lives at all normal pressures are similar for both the aluminium bridges and the steel bridges.

6.2.1.2 Scar

Surface roughness profiles of a further one hundred and forty four wear scars were obtained following a further thirty six fretting fatigue tests on peened specimens in the scar test programme, in order to quantify the effects of surface condition. Surface damage in terms of notch depth was ultimately found to be greater for the peened condition; surface damage in terms of notch width was found to be greater for the unpeened condition.

The maximum notch peak to valley depth recorded in this research for an peened component was 125 μm for a normal pressure of 10 MPa and an axial stress amplitude of 125 MPa. The maximum notch width recorded was 1.6 mm for a normal pressure of 10 MPa and an axial stress amplitude of 125 MPa.

6.2.2 Modelling

6.2.2.1 Friction

The work of Faanes and Fernando [101] was further developed in predicting the fretting fatigue life of unpeened and peened components using Linear Elastic Fracture Mechanics, by incorporating a model for the friction component.

The relationship between the average friction ratios recorded in the load test programme and the maximum peak to valley depths measured in the surface roughness analyses provided a very simple yet effective, means of predicting the friction ratios, apparent by the subsequent reasonable success of the comparisons with the experimental life data.

However, de los Rios et al. [218] demonstrated that the difference in the friction force values between unpeened and peened specimens is not significant at low to medium normal pressures, but increases thereafter; the dependence of the friction force on the normal pressure applied being similar for both conditions. An alternative, therefore, is shown in Figure 6.18, which demonstrates the effect of incorporating those values of friction coefficient determined in this research for the unpeened condition. The results are improved at the higher normal pressures, when compared with Figure 5.42, but it should be remembered that this form of data is harder to obtain.

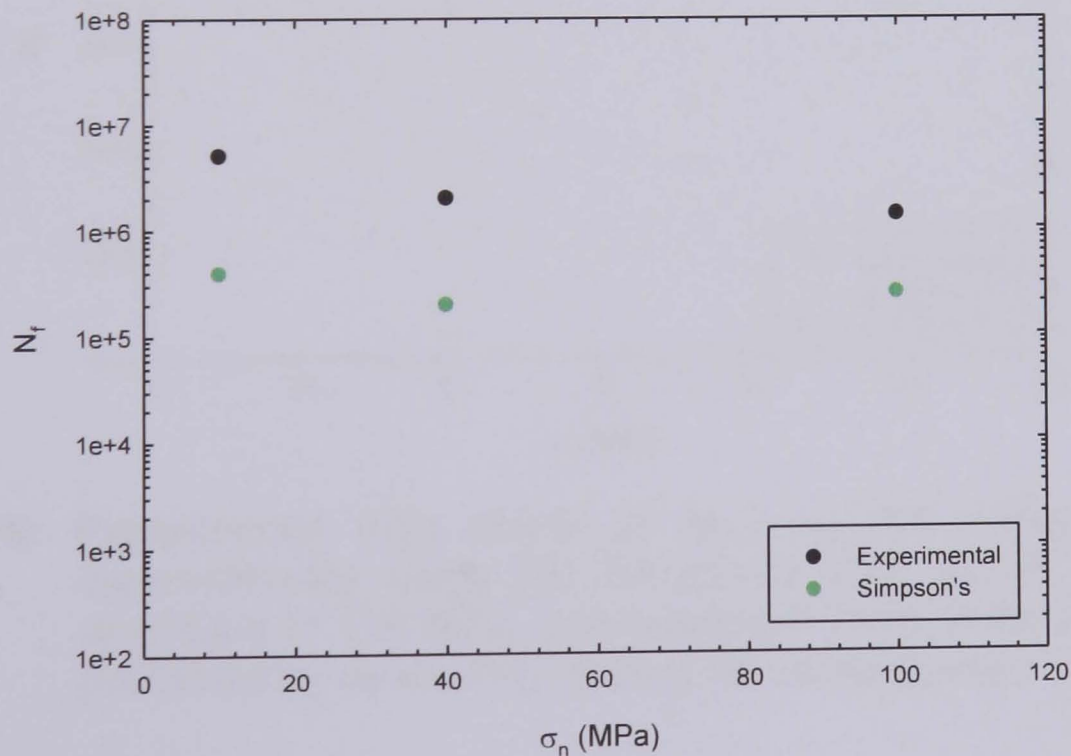


Figure 6.18: Experimental data points of N_f v σ_n and those determined experimentally using the Simpson's rule, for an axial stress amplitude of 100 MPa, incorporating values of friction coefficient determined with the unpeened condition.

Figure 6.19 demonstrates the effect of incorporating those values of friction amplitude for a peened aluminium component published by de los Rios et al. [218] for as peened specimens subjected to an axial stress amplitude of 100 MPa.

However, it should be noted that the surface roughness is different in this case, due to different peening parameters. Also de los Rios et al. [218] utilised a steel bridge pad. It was determined by the few tests conducted in this research, that the amplitudes of the friction forces with the steel bridge are greater than those with the aluminium bridge for any given constant normal pressure and axial stress. The results are very similar to those shown in Figure 6.18.

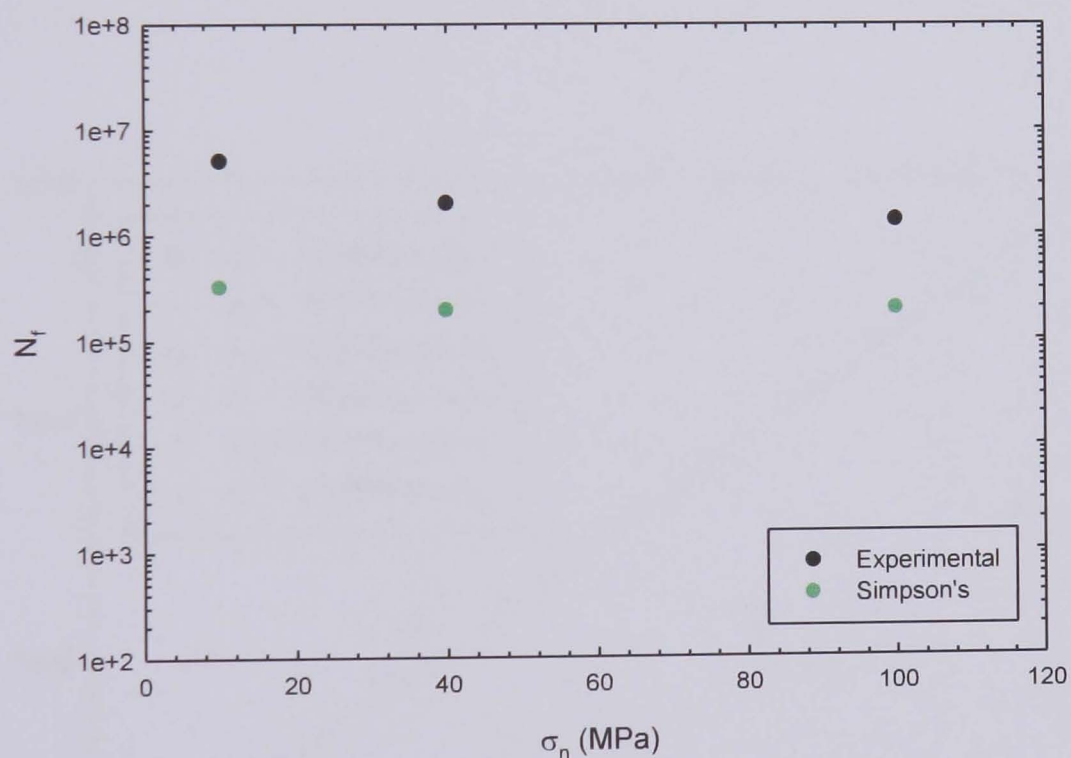


Figure 6.19: Experimental data points of N_f v σ_n and those determined experimentally using the Simpson's rule, for an axial stress amplitude of 100 MPa, incorporating values of friction amplitude published by de los Rios et al. [218] for as peened specimens.

6.2.2.2 Residual stress

Finally, the work of Faanes and Fernando [101] was further developed to predict the fretting fatigue life of shot peened components using Linear Elastic Fracture Mechanics, by incorporating a model for the residual stress component. These results are promising.

Figure 6.20 shows a comparison between the fretting fatigue lives obtained experimentally and by means of the life prediction model, incorporating mode I and mode II stress intensity factors, predicted values for the friction ratio determined from the surface roughness measurements and a residual stress profile. The results are most successful for an axial stress amplitude of 100 MPa and less so for an axial stress amplitude of 70 MPa.

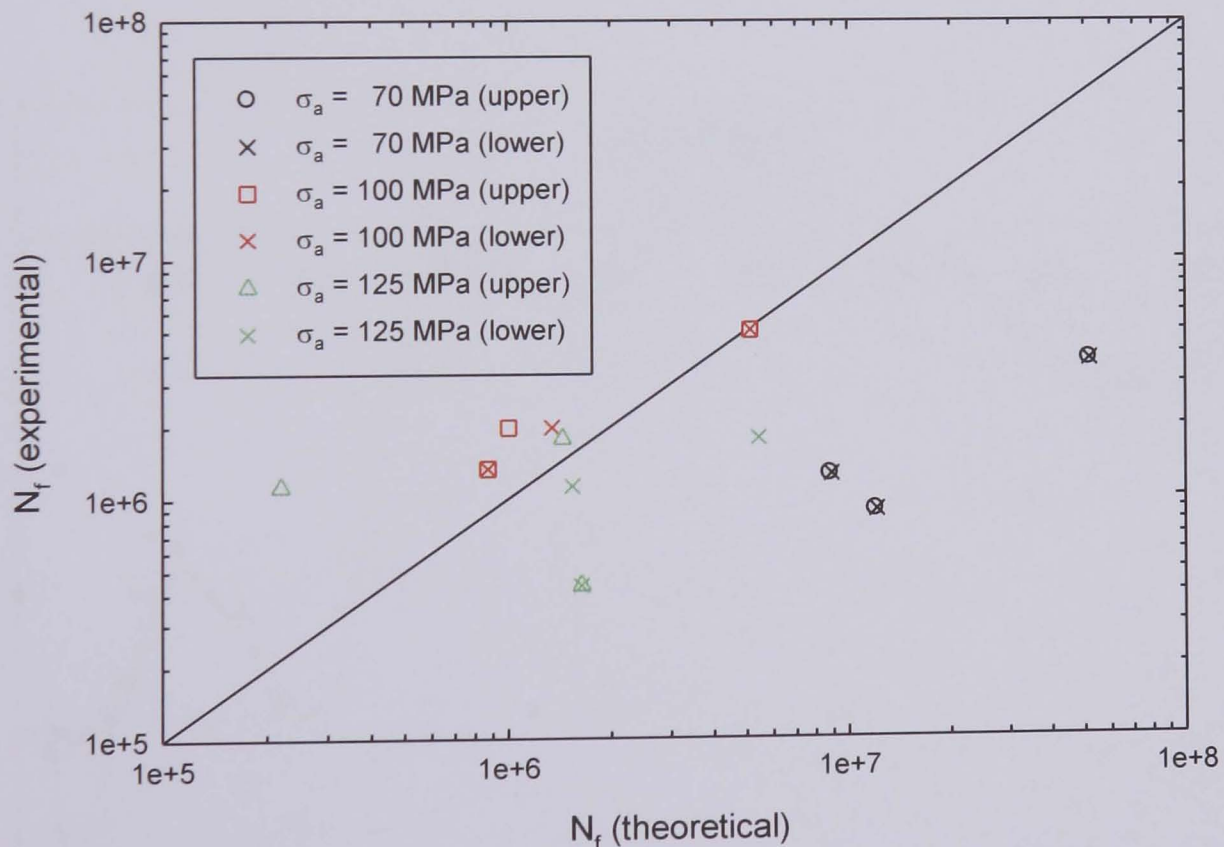


Figure 6.20: A comparison between the fretting fatigue lives obtained experimentally and by means of the life prediction model incorporating mode I and mode II stress intensity factors, predicted values for the friction ratio determined from the surface roughness measurements and a residual stress profile.

There are a number of thoughts concerning the discrepancies in Figure 6.20. Not least, it is assumed that the residual stress profile incorporated is accurate, in terms of the values measured.

Figure 6.21 shows a plot of the residual stress state for aluminium alloy 2024 T351 determined by recent work on residual stresses conducted by Asquith [202], utilising synchrotron x-ray diffraction. This shows that a maximum residual stress of -400 MPa was achieved at a depth of 0.01 mm, rising to a value of -250 MPa at -0.1 mm and tending towards 0 MPa at 0.3 mm.

This is in contrast to those results achieved by Solis-Romero [197], where the maximum residual stress measured was -350 MPa at a depth of 0.03 mm, which rose to a value of -200 MPa at 0.18 mm and which did not reach a value of 0 MPa even after 1 mm. It is these results that were incorporated in this study.

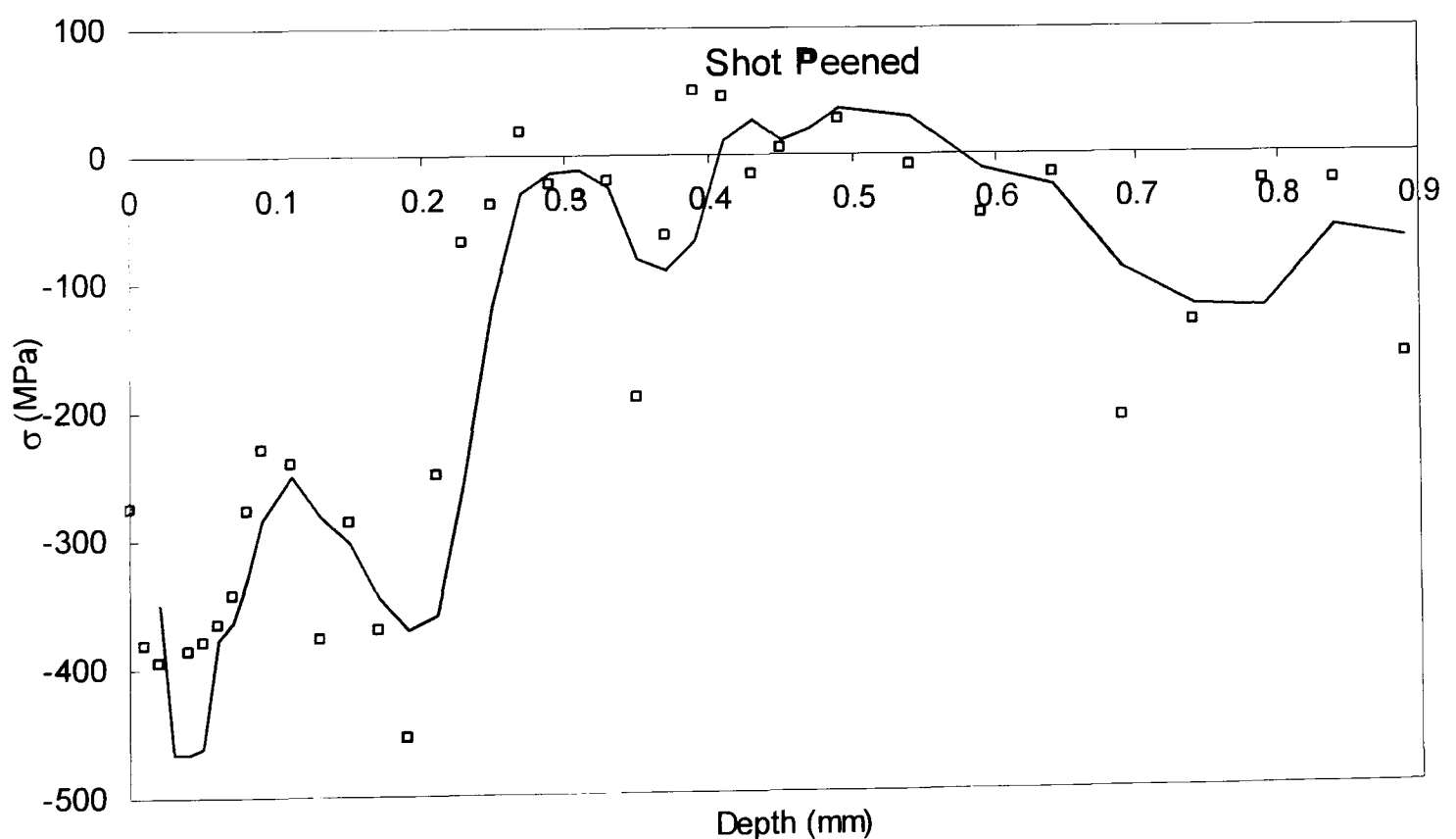


Figure 6.21: The residual stress profile for 2024 T351 optimised shot peening parameters of spherical cast steel shot determined by means of synchrotron x-ray diffraction [202].

However, there are also questions concerning the affect of the fretting phenomena on residual stresses. Studies have shown that there is an evolution of residual stresses in fretting specimens initially free of residual stresses, with an increasing number of cycles. Initially, higher contact loads result in higher residual stresses at the surface, but as the number of fretting fatigue cycles increases, compressive residual stresses increase and then stabilise. The fretting action in the contact region can thus be regarded as having the same deformation mechanism as low plasticity burnishing [157]. What is the effect, therefore, of the various combinations of normal pressures and axial stress amplitudes that are applied here? Also, what is the interaction between the residual stresses induced initially by means of the shot peening process and those that are induced by the fretting process?

There are also questions surrounding the concept of the relaxation of compressive residual stresses. Compressive stresses can be very effective in prolonging fatigue life, so long as they are not reduced significantly by service conditions. For example, their effectiveness can be impaired by: a) exposure to temperatures at which significant stress relaxation can occur, b) fatigue cycling at stress ratios approaching -1, where the residual stress profile tends to fade with an increasing number of cycles, or c) exposure to environments that chemically attack the surface, thereby changing the residual stress pattern [265].

Studies on specimens in which a layer of compressive residual stresses has been introduced prior to testing, have shown that stress relaxation of 20% at less than 10,000 cycles is achieved [156]. However, the lack of the effect of varying the influence of the residual stress profile incorporated in this model is highlighted in Figure 6.22.

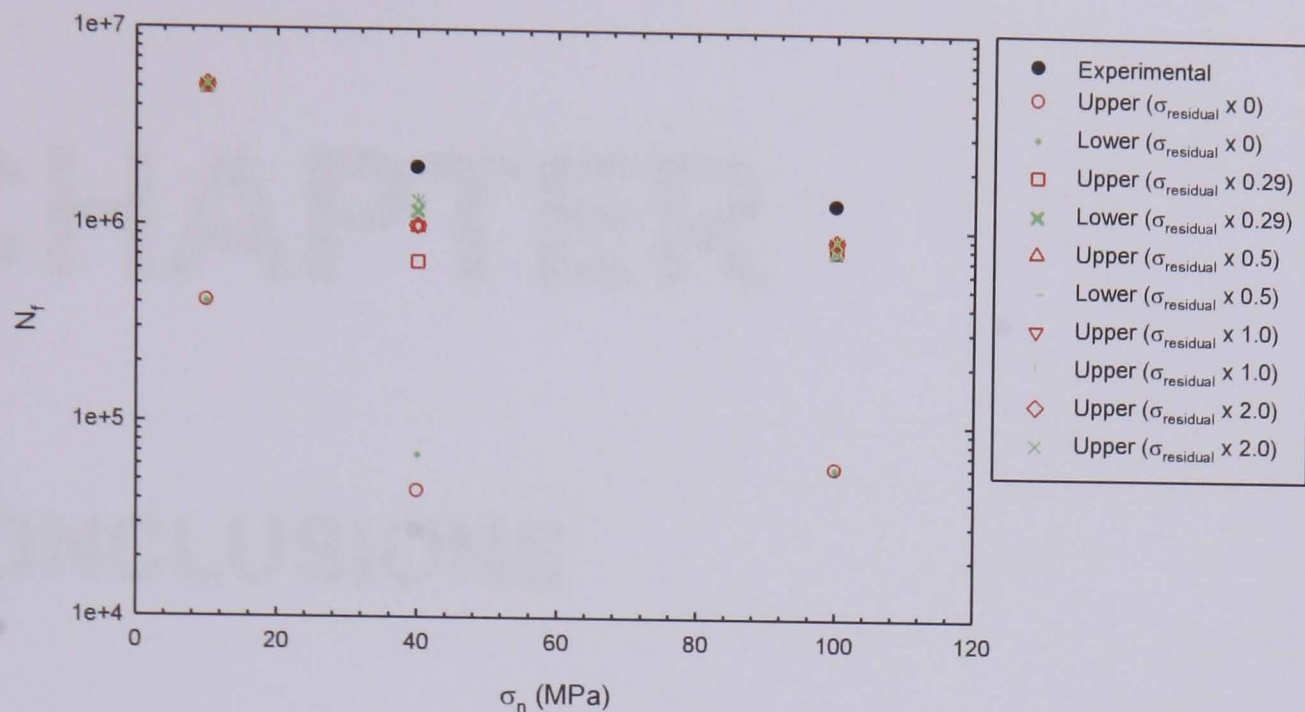


Figure 6.22: The effect of varying the influence of the residual stress profile incorporated in the model by factors of 0.5 and 2.0, for an axial stress amplitude of 100 MPa and incorporating an x factor of 2.446.

The stress intensity due to a residual stress field, $K_{residual}$ was incorporated into the K_I component of the equivalent stress intensity factor, for the condition when the crack is open. $K_{residual}$ had no effect on the mode II component, as a range, ΔK_{II} , was used.

Figure 6.22 shows that there is a non linear relationship between the magnitude of the residual stress integrated and the number of cycles to failure predicted by this model. This suggests that at low residual stress values, residual stress has a significant influence on life, but that when the residual stress values are high, life is dominated by early growth and the ΔK_{II} factor in mode I. If this model holds true, then this could be a useful tool in a strategy for investigating the saturation of shot peening effects in fretting fatigue.

Studies of the effects of shot peening on fretting fatigue incorporating residual stresses have been long been conducted by persons such as Waterhouse [266] and Leadbeater et al. [26], but much remains to be done.

CHAPTER

7

CONCLUSIONS

The primary aim of this research was to investigate fretting fatigue life of aluminium on aluminium in terms of the contact region and the specific case of friction and surface modification, subsequently incorporating the effects of shot peening on fretting fatigue to develop a model based on the mechanics of the fretting fatigue process. The following conclusions may be made regarding the study of shot peening effects on the fretting fatigue process:

1. A Linear Elastic Fracture Mechanics model for lifetime has been developed successfully to predict the fretting fatigue life of shot peened components. This incorporates: load and geometry parameters determined by means of a test programme; the mode I and mode II stress intensity factors for fretting fatigue cracks devised by Sheikh et al. [102] by means of a finite element procedure; a model for the friction component and a model for the residual stress component. This model has been tested against experimental data.
2. Incorporating a mode II stress intensity factor into the model, results in more accurate predictions of short and long fretting fatigue lives for unpeened components, than with a model incorporating a mode I stress intensity factor alone.

3. The relationship between the average friction ratios recorded in the load test programme and the maximum peak to valley depths measured in the surface roughness analyses provided a very simple, yet effective, means of predicting friction ratios. This has been tested against experimental data.
4. Incorporating a residual stress profile into the model, results in reasonable predictions of fretting fatigue lives of peened components. For the residual stress profile chosen here, this effect is most successful for an axial stress amplitude of 100 MPa and less so for an axial stress amplitude of 70 MPa.
5. Varying the influence of the residual stress profile incorporated in this model shows that there is a non linear relationship between the magnitude of the residual stress integrated and the number of cycles to failure predicted. This suggests that at low residual stress values, residual stress has a significant influence on life, but that when the residual stress values are high, life is dominated by early growth and the ΔK_{II} factor in mode I. If this model holds true, then this could be a useful tool in a strategy for investigating the saturation of shot peening effects in fretting fatigue.
6. A finite element model was used for estimating the distribution of stresses over the contact area. A maximum in the tangential stress range, $\Delta\sigma_{xx}$, was found to correspond to the leading edge of the bridge pad, this site being the primary crack initiation location.
7. By studying the variation of $\Delta\sigma_{xx}$ with angular locations below the leading edges of the bridge feet at various depths, it was subsequently possible to identify the early direction of crack growth.
8. In testing, it has been shown that there was a considerable reduction in fatigue strength due to fretting, and that shot peening improves life.

9. Fretting fatigue life, for the unpeened condition, is significantly dependent on the normal pressure applied. Fretting fatigue life decreases with increasing normal pressure up to a critical value. Above this critical value, a further increase in normal pressure tended to increase fretting fatigue life, despite the fact that more cracks were observed at higher normal loads, indicative of a change in the fatigue damage mechanism.
10. Fretting fatigue life decreases with increasing axial stress amplitude for any given constant normal pressure.
11. In this series of tests, the difference in the results achieved by using a steel bridge and an aluminium bridge is thought to be due in part to the friction forces involved. Fretting fatigue life is greater with an aluminium bridge than with a steel bridge and the amplitudes of the friction forces with steel bridges are greater than those with aluminium bridges. The wear from the aluminium bridges was lower than for the steel bridges, which may have contributed to the lower friction coefficients.
12. The friction force increased rapidly at the beginning of each test to reach a stable value for the remainder of the test and then decreased again towards the end. Hysteresis loops showed a distinct micro-slip and macro-slip behaviour in the earlier stages.
13. Friction force amplitude generally increases with the magnitude of the normal pressure applied.
14. An increase in normal pressure tends to decrease the coefficient of friction; the rate of this decrease is related to the applied axial stress amplitude, being greatest at 125 MPa and decreasing accordingly. The highest coefficients of friction were seen at an axial stress amplitude of 125 MPa, decreasing with axial stress amplitude.

15. Visual differences in the fretting scars formed due to the application of various normal pressures were observed. There tended to be more wear debris apparent at low normal loads, high axial stresses and after a larger number of cycles.
16. A fretting site can be compared to a notch, which is characterised by the rapid formation of a propagating crack.
17. There was no correlation between the notch peak to valley depth or width and percentage life for any of the normal pressures applied, except in the unpeened condition for an axial stress amplitude of 70 MPa, where notch peak to valley depth increased continuously with the number of cycles applied. However, the fact that there was significant damage at 10% of life indicates that crack propagation is the dominant failure mechanism for these loading conditions.
18. There was no discernable effect of the normal pressure on the fretting scar in terms of the notch peak to valley depth or width.
19. The maximum notch peak to valley depth recorded in this research for an unpeened component was 58 μm , at a normal pressure of 10 MPa and an axial stress amplitude of 70 MPa. The maximum notch width recorded was 3.4 mm, at a normal pressure of 60 MPa and an axial stress amplitude of 125 MPa.
20. Surface damage in terms of notch depth was ultimately found to be greater for the peened condition; surface damage in terms of notch width was found to be greater for the unpeened condition.

21. The maximum notch peak to valley depth recorded in this research for a peened component was 125 μm for a normal pressure of 10 MPa and an axial stress amplitude of 125 MPa. The maximum notch width recorded was 1.6 mm for a normal pressure of 10 MPa and an axial stress amplitude of 125 MPa.
22. The failure of all test specimens occurred at one of the two leading edges of each bridge pad.
23. The fretting fatigue cracks initiated at angles of greater than 90° to the contact surface and grew at an angle beneath the contact during Stage I, before turning, and continuing their growth perpendicularly to the orientation of the axial stress during Stage II.
24. The initiation of the fretting fatigue cracks was in the terms of a single 3D semi-elliptical crack at low contact pressures. However, at high contact pressures there were multiple crack initiation points.
25. There was evidence of sub surface cracking with the peened condition.

CHAPTER

8

RECOMMENDATIONS

8.1 ADDITIONAL TESTS

It is recommended that in the future, a series of constant normal pressure tests, with reducing values of axial stress be conducted, in order to obtain the fatigue limits relating to the six different values of normal pressure undertaken here.

This will provide an insight into the fretting behaviour of 2024 T351, by determining how the increase in fretting fatigue life seen above a critical normal pressure varies with the load conditions and if this is the case, what the critical turning point values of normal pressure are for each load condition applied.

The degree to which each fatigue limit under fretting conditions drops compared with those achieved solely under axial loading and should be explored. This information will help in further developing the life prediction model and it will also provide a vital insight into the behaviour of fretting fatigue at low values of normal pressure.

The next step would be to perform a series of constant normal load tests, with increasing values of axial stress, rising to a maximum of 140 MPa, this being the tension-tension plain fatigue limit of aluminium alloy 2024 T351, at a stress ratio of $R = -1$. These tests will complete the set of σ_n/N curves and aid in developing a full understanding of the influence of fastener clamping forces on fretting fatigue.

More friction data is required, due to the degree of scatter observed with the unpeened components and the fact that there is no data for the peened condition. Investigation of the size of scar, critical to the initiation of fretting fatigue cracks needs to be established, by conducting interrupted fretting fatigue tests at less than 10% of fretting fatigue life.

The reported increase in the crack propagation rate of fretting fatigue cracks may be due to the presence of a mode II component. It is acknowledged however, that there is a discrepancy in the fact that although a mode II component has been discovered theoretically, one has yet to be determined experimentally.

The angled crack could be due to a change in the principal stress field, as under non-proportional loading the directions of the principal stresses rotate, and the ratio between the principal stresses varies. The choice of crack angle and coefficient of friction, will both affect the principal stress direction and hence mode I crack growth. Therefore it is recommended, that some experimental stress analyses using Digital Image Correlation for example, be carried out to investigate the real stress field in the contact condition. This could include an investigation of whether the increase in fretting fatigue life above a critical value of normal pressure could be due in part to the bridges taking some of the axial load if the friction forces are great enough to transfer load from the specimen.

Further investigation concerning the effect of the fretting phenomena on residual stresses is also required. Studies have shown that there is an evolution of residual stresses in fretting specimens initially free from residual stresses with an increasing number of cycles. Initially, higher contact loads result in higher residual stresses at the surface, but as the number of fretting fatigue cycles increases, compressive residual stresses increase and then stabilise. The fretting action in the contact region can thus be regarded as having the same deformation mechanism as low plasticity burnishing [157].

Therefore the effect of the various combinations of normal pressures and axial stress amplitudes that are applied here needs to be investigated. In addition, the interaction between the residual stresses induced initially by means of the shot peening process and those that are induced by the fretting process should also be studied. This could be undertaken utilising the latest synchrotron technology.

8.2 MODEL IMPROVEMENTS

The analysis of crack initiation in fretting is known to be far more challenging than that of propagation, as the effects of fretting on crack initiation are less amenable to analysis.

It is suggested that a micromechanical notch sensitivity model be incorporated to account for the effect of a fretting scar. The wear element of fretting fatigue may be modelled as a notch. There are two important parameters here: depth and width, which are related to K_t . An approximation of K_t from the geometry of a scar may be feasible using the surface roughness traces, although the localised effects of asperities may be ignored.

Phenomena such as the surface plastic deformation of the contacting surfaces should also be examined as contributory factors towards the crack initiation process; although the proportion of life spent on short crack propagation is relatively small.

Application of the micromechanical model for crack growth at notches devised by Vallellano et al. [260], [261] may be appropriate, as the cracks initiating from a scar are very short. Therefore a microstructural fracture mechanics approach, incorporating both geometrical features and material properties (e.g. grain size) may be appropriate.

Faanes and Fernando [101] acknowledged that in fretting fatigue, the presence of a high stress gradient affects the mechanism of short crack growth in a fretting environment, and so inaccuracies in the description of short crack growth have a smaller influence on the prediction of total fretting fatigue life. In addition, the ratio of the number of cycles spent in short crack growth, to the total number of fatigue cycles in life is reduced and hence any discrepancy in the description of short crack growth will have a less significant influence on the total lifetime predicted.

However, when the application of the threshold short crack correction suggested by El Haddad et al. [263] was incorporated, it was demonstrated that consideration of short crack behaviour improves fretting fatigue life predictions for long lives. Further work also needs to be completed in order to establish the dominant parameter(s) that control fretting fatigue damage in Stage I, a generally microstructurally sensitive process, and this could be introduced in to a short crack model, such as the Navarro – de los Rios micromechanical model [264].

In Stage I, cracks generally propagate along crystallographic planes at a decreasing rate due to the constraint exerted by the grain boundary. However, when the density of the dislocations reaches a level sufficient to ensure that the stress intensity generated is high enough to activate a new dislocation source in a new grain, the constraint effect relaxes and the velocity of the crack increases again. This process recurs until the crack is sufficiently long to produce a near tip stress field capable of readily overcoming the grain boundary barriers [264].

It is assumed that Stage I crack growth terminates when the crack tip stress field is able to initiate plasticity on two successive grains without further growth of the crack [267]. The transition from Stage I, short crack growth, to Stage II, or long crack growth, can be found by means of the Navarro-Rios model [264], observing the decreasing amplitude of oscillations achieved by plotting crack velocity against crack length.

Microstructure is also significant in terms of crack arrest, another region currently ignored. The size and orientation of the grains in a material, as well as the strength of the grain boundaries, are all important factors. This is illustrated by the fact that the density of dislocations ahead of the crack tip will increase leading to a pile-up process against constraining features such as, grain and phase boundaries [264]. The strength of the pile-up increases as the crack approaches the grain boundary, until the stress field ahead of the crack tip is sufficiently high to initiate slip in an adjacent and favourably oriented grain. Based on the above rationale, crack arrest is considered to take place when the crack tip stress field is unable to reach the critical resolved shear stress before the crack reaches the grain boundary and acknowledgement of this phenomenon will also aid in improving the current model.

As multiple crack initiation sites have been observed, the tendency for cracks nucleating from pits in close proximity to one another should be considered. There is the need to consider multiple site damage when estimating life, as most models only incorporate a single critical crack size.

Finally, incorporating a more accurate residual stress profile may lead to more accurate predictions and ultimately, to the development of a theoretical model which will allow the determination of the residual stress distribution to meet specific improvements in fretting fatigue life.

Bibliography

- 1 Clark, P. N.; Jones, K. Huang, J. T. et al, "*Observations from the inspection of an aged fuselage panel,*" *Journal of Aircraft*, 42 : (6), December, 2005, pp. 1403 - 1408.
- 2 www.airdisaster.com/photos/aloha243/7.shtml
- 3 Eden, E. M., Rose, W. N. and Cunningham, F. L., "*Endurance of metals,*" *Proceedings of the Institution of Mechanical Engineers*, 81 : (2), October, 1911, pp. 839 - 974.
- 4 Farris, T. N., Grandt, A. F., Harish, G. and Wang, H. L., "*Analysis of widespread fatigue damage in structural joints,*" 41st International Symposium and Exhibition, Society for the Advancement of Material and Process Engineering, Anaheim, March 1996.
- 5 Iyer, K., Bastias, P. C., Rubin, C. A. and Hahn, G. T., "*Analysis of fatigue and fretting of three-dimensional, single and double rivet-row lap joints,*" *Fatigue in New and Ageing Aircraft, ICAF 97*, (Edited by R. Cook and P. Poole), 1997, Chameleon Press Ltd, London, UK, pp. 855 - 870.
- 6 Elliott, C. B. and Hoepfner, D. W., "*The role of fretting fatigue in aircraft rivet hole cracking,*" *Fatigue in New and Ageing Aircraft, ICAF 97*, (Edited by R. Cook and P. Poole), 1997, Chameleon Press Ltd, London, UK, pp. 883 - 894.
- 7 Birch, P. R., "*A study of fretting fatigue in aircraft components,*" MPhil Thesis, Massachusetts Institute of Technology, USA, 1998.
- 8 Veillette, P., "*Preventing fretting damage becomes increasingly critical as aircraft age,*" *Flight Safety Foundation, Aviation Mechanics Bulletin*, 46 : (6), November - December, 1998, pp. 1 - 11.
- 9 Leen, S. B., Hyde, T. H., Ratsimba, C. H. H., Williams, E. J. and McColl, I. R., "*An investigation of the fatigue and fretting performance of a representative aero-engine spline coupling,*" *Journal of Strain Analysis*, 37 : (6), 2002, pp. 565 - 583.
- 10 Coyle, M. B. and Watson, S. J., "*Fatigue strength of turbine shafts with shrunk-on discs,*" *Proceedings of the Institution of Mechanical Engineers*, 178 : (1), 1963, pp. 147 - 183.

- 11 Maxwell, W. W., Dudley, B. R., Cleary, A. B., Richards, J. and Shaw, J., Proceedings of the Institution of Mechanical Engineers, "*Measures to counter fatigue failure in railway axles,*" 182 : (1), 1967, pp. 89 - 108.
- 12 Hattori, T., "*Fretting fatigue problems in structural design,*" Fretting Fatigue, ESIS 18 (Edited by R. B. Waterhouse and T. C. Lindley), 1994, Mechanical Engineering Publications, London, UK, pp. 437 - 451.
- 13 Brown, S. A. and Merritt, K., "*Fretting corrosion in saline and serum,*" Journal of Biomedical Materials Research, 15, 1981, pp. 479 - 488.
- 14 Zhang, D. K., Ge, S. R. and Qiang, Y. H., "*Research on the fatigue and fracture behavior due to the fretting wear of steel wire in hoisting rope,*" Wear, 255 : (7 - 12), August - September, 2003, pp. 1223 - 1237.
- 15 Hoepfner, D. W., "*Fretting fatigue case studies of engineering components,*" Tribology International, 39 : (10), October, 2006, pp. 1271 - 1276.
- 16 ASM Handbook on Friction, Lubrication and Wear Technology. Volume 18, 1992, pp. 9.
- 17 Waterhouse, R. B., "*Fretting fatigue,*" International Materials Reviews, 37 : (2), February, 1992, pp. 77 - 97.
- 18 Hoepfner, D. W., "*Mechanisms of fretting fatigue,*" Fretting Fatigue, ESIS 18 (Edited by R. B. Waterhouse and T. C. Lindley), 1994, Mechanical Engineering Publications, London, UK, pp. 3 - 19.
- 19 Nowell, D., Dini, D. and Hills, D. A., "*Recent developments in the understanding of fretting fatigue,*" Engineering Fracture Mechanics, 73 : (2), January, 2006, pp. 207 - 222.
- 20 Waterhouse, R. B., "*Fretting Fatigue,*" (Edited by R. B. Waterhouse), Applied Science Publishers, 1981.
- 21 Mutoh, Y., "*Mechanisms of fretting fatigue,*" JSME International Journal, Series A, 38 : (4), October, 1995, pp. 405 - 415.
- 22 Hills, D. A. and Mugadu, A., "*An overview of progress in the study of fretting fatigue,*" Journal of Strain Analysis, Special Issue Paper, 37 : (6), 2002, pp. 591 - 601.
- 23 Gordelier, S. C. and Chivers, T. C., "*A literature review of palliatives for fretting fatigue,*" Wear, 56 : (1), September, 1979, pp. 177 - 190.
- 24 Chivers T. C. and Gordelier, S. C., "*Fretting fatigue palliatives: some comparative experiments,*" Wear, 96 : (2), June, 1984, pp. 153 - 175.

- 25 Beard, J., "*Palliatives for fretting fatigue*," Fretting Fatigue, ESIS 18 (Edited by R. B. Waterhouse and T. C. Lindley), 1994, Mechanical Engineering Publications, London, UK, pp. 419 - 436.
- 26 Leadbeater, G., Noble, B. and Waterhouse, R. B., "*The fatigue of an aluminium alloy produced by fretting on shot peening surfaces*," Proceedings, Sixth International Conference on Fracture, Volume 3, India, 1984, pp. 2125 - 2132.
- 27 Niku-Lari, A., "*Shot-peening*," Proceedings of the First International Conference on Shot-Peening, (Edited by A. Niku-Lari), Pergamon Press, 1981, pp. 1 - 21.
- 28 Bignonnet, A., "*Some observations of the effect of shot peening on fretting fatigue*," Fretting Fatigue, ESIS 18 (Edited by R. B. Waterhouse and T. C. Lindley), 1994, Mechanical Engineering Publications, London, UK, pp. 475 - 482.
- 29 Waterhouse, R. B., Noble, B. and Leadbeater, G., "*The effect of shot-peening on the fretting-fatigue strength of an age-hardened aluminium alloy (2014A) and an austenitic stainless steel (En 58A)*," Journal of Mechanical Working Technology, 8 : (2 - 3), August, 1983, pp. 147 - 153.
- 30 Tomlinson, G. A., "*The rusting of steel surfaces in contact*," Proceedings of the Royal Society of London A: Containing Papers of a Mathematical and Physical Character, 115 : (771), July, 1927, pp. 472 - 483.
- 31 Söderberg, S., Nikoonezhad, S., Salama, K. and Vingsbo, O., "*Accelerated fretting wear testing using ultrasonics*," Ultrasonics, 24 : (6), November, 1986, pp. 348 - 353.
- 32 Kuno, M., Dinsdale, K., Pearson, B. R., Ottewell, B. and Waterhouse, R. B. "*A new fretting wear test apparatus*," Journal of Physics E: Scientific Instruments, 21 : (10), October, 1988, pp. 929 - 931.
- 33 Mohrbacher, H., Celis, J.-P. and Roos, J. R., "*Laboratory testing of displacement and load induced fretting*," Tribology International, 28 : (5), August, 1995, pp. 269 - 278.
- 34 Marui, E., Endo, H., Hasegawa, N. and Mizuno, H., "*Prototype fretting-wear testing machine and some experimental results*," Wear, 214 : (2), February, 1998, pp. 221 - 230.
- 35 Godfrey, D., "*Investigation of fretting corrosion by microscopic observation*," National Advisory Committee for Aeronautics, Technical Note, No. 2039, February, 1950.

- 36 Waterhouse, R. B., "*Fretting corrosion*," Proceedings of the Institution of Mechanical Engineers, 169, 1955, pp. 1157 - 1172.
- 37 Waterhouse, R. B., "*Fretting Corrosion*", 1972, Pergamon Press, Oxford, England.
- 38 Bill, R. C., "*Fretting wear and fretting fatigue - How are they related ?*" Journal of Lubrication Technology, Transactions of the American Society of Mechanical Engineers, 105, 1983, pp. 230 - 238.
- 39 Berthier, Y., Colombie, CH, Vincent, L. and Godet, M., "*Fretting wear mechanisms and their effects on fretting fatigue*," Journal of Tribology, 110 : (3), July, 1988, pp. 517 - 524.
- 40 Waterhouse, R. B., "*Fretting wear*," Wear, 100 : (1 - 3), December, 1984, pp. 107 - 118.
- 41 Mindlin, R. D., "*Compliance of Elastic Bodies in Contact*," Journal of Applied Mechanics, 16, 1949, pp. 259 - 268.
- 42 Johnson, K. L., "*Surface interaction between elastically loaded bodies under tangential forces*," Proceedings of the Royal Society, A, 230, 1955, pp. 531.
- 43 Vingsbo, O. and Soderberg, S., "*On fretting maps*," Wear, 126 : (2), September, 1988, pp. 131 - 147.
- 44 Hills, D. A. and Urriolagoitia Sosa, G., "*Origins of partial slip in fretting – a review of known and potential solutions*," The Journal of Strain Analysis for Engineering Design, 34 : (3), May, 1999, pp. 175 - 181.
- 45 Lindley, T. C., "*Fretting fatigue in engineering alloys*," International Journal of Fatigue, 19 : Supplement No. 1, January, 1997, pp. S39 - S49.
- 46 Waterhouse, R. B., "*Fretting wear*," Proceedings of the International Conference on the Wear of Materials, American Society of Mechanical Engineers, New York, USA, 1981, pp. 17 - 22.
- 47 Yan, P., "*The effect of number of cycles on the critical transition boundary between fretting fatigue and fretting wear*," Wear, 160 : (2), February, 1993, pp. 279 - 289.
- 48 Hurricks, P. L., "*Mechanism of fretting - a review*," Wear, 15 : (6), June, 1970, pp. 389 - 409.
- 49 Sauger, E., Fouvry, S., Ponsonnet, L., Kapsa, Ph., Martin J. M. and Vincent, L., "*Tribologically transformed structure in fretting*," Wear, 245 : (1-2), October, 2000, pp. 39 - 52.

- 50 Sakmann, B. W. and Rightmire, B. G., "*An investigation of fretting corrosion under several conditions of oxidation,*" National Advisory Committee for Aeronautics, Technical Note, No. 1492, June, 1948.
- 51 de Wit, E., Froyen, L. and Celis, J.-P., "*The oxidation reaction during sliding wear influencing the formation of either amorphous or nanocrystalline debris,*" *Wear*, 231 : (1), June, 1999, pp. 116 - 123.
- 52 Wright, K. H. R., "*An investigation of fretting corrosion,*" Proceedings of the Institution of Mechanical Engineers, 1B, 1952, pp. 556 - 571.
- 53 Waterhouse, R. B., "*Effect of material and surface condition on fretting fatigue,*" *Fretting Fatigue*, ESIS 18, (Edited by R. B. Waterhouse and T. C. Lindley), 1994, Mechanical Engineering Publications, London, UK, pp. 339 - 349.
- 54 Zhou, Z. R. and Vincent, L., "*Mixed fretting regime,*" *Wear*, 181 - 183 : (2), March, 1995, pp. 531 - 536.
- 55 Alic, J. A., Hawley, A. L. and Urey, J. M., "*Formation of fretting fatigue cracks in 7075-T7351 aluminium alloy,*" *Wear*, 56 : (2), October, 1979, pp. 351 - 361.
- 56 Zhou, Z. R., Fayeulle, S. and Vincent, L., "*Cracking behaviour of various aluminium-alloys during fretting wear,*" *Wear*, 155 : (2), June, 1992, pp. 317 - 330.
- 57 Berthier, Y., Vincent, L. and Godet, M., "*Fretting fatigue and fretting wear,*" *Tribology International*, 22 : (4), August, 1989, pp. 235 - 242.
- 58 Vincent, L., "*Materials and fretting,*" *Fretting Fatigue*, ESIS 18 (Edited by R. B. Waterhouse and T. C. Lindley), 1994, Mechanical Engineering Publications, London, UK, pp. 323 - 337.
- 59 Bramhall, R., "*Studies in fretting fatigue,*" DPhil Thesis, Oxford University, UK, 1973.
- 60 Magaziner, R., Jin, O. and Mall, S., "*Slip regime explanation of observed size effects in fretting,*" *Wear*, 257 : (1 - 2), July, 2004, pp. 190 - 197.
- 61 Moore, M. A., "*A preliminary investigation of frictional heating during abrasive wear,*" *Wear*, 17 : (1), January, 1971, pp. 51 - 58.
- 62 Reeves, R. K. and Hoepfner, D. W., "*Microstructural and environmental effects on fretting fatigue,*" *Wear*, 47 : (2), April, 1978, pp. 221 - 229.
- 63 Sato, J., Shima, M. and Takeuchi, T., "*Fretting wear in sea water,*" *Wear*, 110 : (3 - 4), August, 1986, pp. 227 - 237.

- 64 Soderberg, S., Bryggman, U. and McCullough, T., "Frequency effects in fretting wear," *Wear*, 110 : (1), July, 1986, pp. 19 - 34.
- 65 Neyman, A. and Olszewski, O., "Research on fretting wear dependence of hardness ratio and friction coefficient of fretted couple," *Wear*, 162 : (Part B), April, 1993, pp. 939 - 943.
- 66 Bailey, J. M. and Godfrey, D., "Coefficient of friction and damage to contact area during the early stages of fretting II – Steel, iron, iron oxide and glass combinations," National Advisory Committee for Aeronautics, Technical Note, No. 3144, April, 1954.
- 67 Iwabuchi, A., "The role of oxide particles in the fretting wear of mild-steel," *Wear*, 151 : (2), December, 1991, pp. 301 - 311.
- 68 Hills, D. A. and Fellows, L. J., "Some observations on contact problems involving fretting in the presence of wear," *Wear*, 231 : (2), July, 1999, pp. 319 - 324.
- 69 Elleuch, K. and Fouvry, S., "Experimental and modelling aspects of abrasive wear of a A357 aluminium alloy under gross slip fretting conditions," *Wear*, 258 : (1-4), January, 2005, pp. 40 - 49.
- 70 Gao, H. S., Gu, H. C. and Zhou, H. J., "Effect of slip amplitude on fretting fatigue," *Wear*, 148 : (1), August, 1991, pp. 15 - 23.
- 71 Schijve, J., "Fatigue of structures and materials – Chapter 15: Fretting Corrosion," Kluwer Academic Publishers, 2001, pp. 378.
- 72 Warlow-Davies, E. J., "Fretting corrosion and fatigue strength: Brief results of preliminary experiments," *Proceedings of the Institution of Mechanical Engineers*, 146, 1941, pp. 32 - 38.
- 73 McDowell, J. R., "Fretting corrosion tendencies of several combinations of materials," Symposium on fretting corrosion, American Society for Testing and Materials, Special Technical Publication, 144, Philadelphia, USA, 1953, pp. 40 - 53.
- 74 Fenner, A. J., Wright, K. H. R. and Mann, J. Y., "Fretting corrosion and its influence on fatigue failure," *Proceedings of the International Conference on Fatigue of Metals*, American Society of Mechanical Engineers, 1956, pp. 386 - 393.
- 75 Fenner, A. J. and Field, J. E., "La fatigue dans les conditions de frottement," *Revue Métallurgique*, 55, 1958, pp. 478 - 485.

- 76 Fenner, A. J. and Field, J. E., "A study of the onset of fatigue damage due to fretting," Transactions of the North East Coast Institute of Engineers and Shipbuilders, 76, 1960, pp. 183 - 228.
- 77 Edwards, P. R., "The application of fracture mechanics to predicting fretting fatigue," Fretting Fatigue, (Edited by R. B. Waterhouse), 1981, Applied Science Publishers Ltd., London, UK, pp. 67 - 97.
- 78 Milestone, W. D., "Fretting and fretting fatigue in metal to metal contacts," Proceedings of the American Institute of Aeronautics and Astronautics, Structural Dynamics and Materials Conference, Denver, USA, 1970, pp. 86.
- 79 Nishioka, K., Nishimura, S. and Hirakawa, K., "Fundamental investigation of fretting fatigue – part 1. On the relative slip amplitude of press-fitted axle assemblies," Bulletin, Japan Society of Mechanical Engineers, 11 : (45), 1968, pp. 437 - 445.
- 80 Nishioka, K. and Hirakawa, K., "Fundamental investigation of fretting fatigue – part 2. Fretting fatigue testing machine and some test results," Bulletin, Japan Society of Mechanical Engineers, 12 : (50), 1969, pp. 180 - 187.
- 81 Nishioka, K. and Hirakawa, K., "Fundamental investigation of fretting fatigue – part 3. Some phenomena and mechanisms of surface cracks," Bulletin, Japan Society of Mechanical Engineers, 12 : (51), 1969, pp. 397 - 407.
- 82 Nishioka, K. and Hirakawa, K., "Fundamental investigation of fretting fatigue – part 4. The effect of mean stress," Bulletin, Japan Society of Mechanical Engineers, 12 : (52), 1969, pp. 408 - 414
- 83 Nishioka, K. and Hirakawa, K., "Fundamental investigation of fretting fatigue – part 5. The effect of relative slip amplitude," Bulletin, Japan Society of Mechanical Engineers, 12 : (52), 1969, pp. 692 - 697.
- 84 Nishioka, K. and Hirakawa, K., "Fundamental investigation of fretting fatigue – part 6. The effect of contact pressure and hardness of materials," Bulletin, Japan Society of Mechanical Engineers, 15 : (80), 1972, pp. 135 - 144.
- 85 Endo, K. and Goto, H., "Initiation and propagation of fretting fatigue cracks," Wear, 38 : (2), July, 1976, pp 311 - 324.
- 86 Johnson, K. L., "Contact Mechanics," 1985, Cambridge University Press, UK.

- 87 Lindley, T. C. and Nix, K. J., "*The role of fretting in the initiation and early growth of fatigue cracks in turbo-generator materials,*" Proceedings, Multiaxial Fatigue, American Society for Testing and Materials, 1985, Philadelphia, USA, pp. 340 - 360.
- 88 Nix, K. J. and Lindley, T. C., "*The application of fracture mechanics to fretting fatigue,*" Fatigue and Fracture of Engineering Materials and Structures, 8 : (2), April, 1985, pp. 143 - 160.
- 89 Nix, K. J. and Lindley, T. C., "*The initiation and propagation of small defects in fretting fatigue,*" Proceedings, Life Assessment of Dynamically Loaded Materials and Structures, Engineering Materials Advisory Services Limited, 1985, UK, pp. 89 - 98.
- 90 Sato, K., Fuji, H. and Kodama, S., "*Crack propagation behaviour in fretting fatigue,*" Wear, 110 : (1), July, 1986, pp. 19 - 34.
- 91 Sato, K., Fuji, H. and Kodama, S., "*Crack propagation behaviour in fretting fatigue of S45C carbon steel,*" Bulletin, Japan Society of Mechanical Engineers, 29, 1986, pp. 3253 - 3258.
- 92 Sato, K., Fuji, H. and Kodama, S., "*Crack propagation behaviour in fretting fatigue of A2024-T3 aluminium alloy,*" Transactions of the Japan Society for Materials Science, Japan, 34 : (384), 1986, pp. 1076 - 1081.
- 93 Sato, K., Fuji, H. and Kodama, S., "*Effects of stress ratio fretting fatigue cycles on the accumulation of fretting fatigue damage to carbon steel S45C,*" Bulletin, Japan Society of Mechanical Engineers, 29, 1986, pp. 2759.
- 94 Nowell, D., Hills, D. A. and O'Connor, J. J., "*An analysis of fretting fatigue, Tribology - friction, lubrication and wear fifty years on,*" 1987, Mechanical Engineering Publications, London, UK, pp. 965 - 973.
- 95 Hills, D. A. and Nowell, D. "*Mechanics of fretting fatigue,*" International Journal of Mechanical Sciences, 29 : (5), 1987, pp. 355 - 365.
- 96 Nowell, D., "*An analysis of fretting fatigue,*" DPhil Thesis, Oxford University, UK, 1988.
- 97 Hattori, T., Nakamura, M., Sakata, H. and Watanabe, T., "*Fretting fatigue analysis using fracture mechanics,*" Japan Society of Mechanical Engineers, International Journal, Series A, 31 : (1), January, 1988, pp. 100 - 107.
- 98 Attia, M. H., "*Fretting fatigue testing: Current practice and future prospects for standardisation,*" American Society for Testing and Materials, 17, 1989, pp. 26 - 31.

- 99 Fernando, U. S., Farrahi, G. H., and Brown, M. W., "*Fretting fatigue crack growth behaviour of BS L65 4 percent copper aluminium alloy under constant normal load*," Fretting Fatigue, ESIS 18, (Edited by R. B. Waterhouse and T. C. Lindley), 1994, Mechanical Engineering Publications, London, pp, 183 - 195.
- 100 Faanes, S. and Fernando, U. S., "*Influence of contact loading on fretting fatigue behaviour*," Fatigue and Fracture of Engineering Materials and Structures, 17 : (8), August, 1994, pp. 939 - 947.
- 101 Faanes, S. and Fernando, U. S., "*Life prediction in fretting fatigue using fracture mechanics*," Fretting Fatigue, ESIS 18, (Edited by R. B. Waterhouse and T. C. Lindley), 1994, Mechanical Engineering Publications, London, UK, pp. 149 - 159.
- 102 Sheikh, M. A., Fernando, U. S., Brown, M. W. and Miller, K. J. M., "*Elastic stress intensity factors for fretting cracks using the finite element method*," Fretting Fatigue, ESIS 18, (Edited by R. B. Waterhouse and T. C. Lindley), 1994, Mechanical Engineering Publications, London, UK, pp. 83 – 101.
- 103 Hoepfner, D. W., Chandrasekaran, V. and Elliott III, C. B., "*Overview*," Fretting Fatigue: Current Technology and Practices, (Edited by D. W. Hoepfner, V. Chandrasekaran and C. B. Elliott III), American Society for Testing and Materials, Special Technical Publication, 1367, 2000, pp. ix - xi.
- 104 Mutoh, Y., Hoepfner, D.W. and Kinyon, S. E., "*Overview*," Fretting Fatigue: Advances in the Basic Understanding and Applications, (Edited by S. E. Kinyon, D.W. Hoepfner and Y. Mutoh), American Society for Testing and Materials, Special Technical Publication, 1425, 2003, pp. ix - x.
- 105 Hills, D., "*Editorial*," Journal of Strain Analysis, 37 : (6), November, 2002, pp. i.
- 106 Giannakopoulos, A. E., Lindley, T. C. and Suresh, S., "*Overview No. 129 – Aspects of equivalence between contact mechanics and fracture mechanics: Theoretical connections and a life-prediction methodology for fretting-fatigue*," Acta Materialia, 46 : (9), May, 1998, pp. 2955 - 2968.
- 107 Ciavarella, M. and Dini, D., "*A refined CLNA model in fretting fatigue using asymptotic characterization of the contact stress fields*," Fatigue And Fracture Of Engineering Materials And Structures, 28 : (12), December, 2005, pp. 1099 - 1112.

- 108 Dini, D. and Hills, D. A., "A consideration of the effects of the slip displacement on fretting fatigue behaviour," *Journal of Strain Analysis for Engineering Design*, 39 : (4), July, 2004, pp. 397 - 407.
- 109 Araujo, J. A. and Nowell, D., "Analysis of pad size effects in fretting fatigue using short crack arrest methodologies," *International Journal of Fatigue*, 21 : (9), October, 1999, pp. 947 - 956.
- 110 Hills, D. A. and Nowell, D., "Mechanics of fretting fatigue," *Solid Mechanics and its Applications*, (Edited by G. M. L. Gladwell), 1994, Kluwer Academic Publishers, The Netherlands, pp. 169 - 174.
- 111 Miller, K. J., "The behaviour of short fatigue cracks and their initiation," *Fatigue and Fracture of Engineering Materials and Structures*, 10 : (1), January, 1987, pp. 75 - 91.
- 112 Hattori, T. and Nakamura, M., "Initiation and propagation behaviour of fretting fatigue cracks," *Proceedings, International Conference on Contact Mechanics*, 1997, pp. 183 - 192.
- 113 Giummarra, C., Bray, G. H. and Duquette, D. J., "Fretting fatigue in 2XXX series aerospace aluminium alloys," *Tribology International*, 39 : (10), October, 2006, pp. 1206 - 1212.
- 114 Nix, K. J. and Lindley, T. C., "The influence of relative slip and contact materials on the fretting fatigue of 3.5% NiCrMoV rotor steel," *Wear*, 125 : (1 - 2), July, 1988, pp. 147 - 162.
- 115 Moobola, R., Nowell D. and Hills, D. A., "Surface roughness and crack initiation in fretting fatigue," *Engineering Against Fatigue*, (Edited by J. H. Beynon, M. W. Brown, R. A. Smith, T. C. Lindley and B. Tomkins), 1999, A. A. Balkema, Rotterdam, Brookfield, pp. 453 - 460.
- 116 Gaul, D. J. and Duquette, D. J., "The effect of fretting and environment on fatigue crack initiation and early propagation in a quenched and tempered 4130 Steel," *Metallurgical Transactions A*, 11 : (9), 1980, pp. 1555 - 1561.
- 117 Spink, G. M., "Fretting fatigue of a 2.5%NiCrMoV low pressure turbine shaft steel – the effect of different contact pad materials and of variable slip amplitude," *Wear*, 136 : (2), 1990, pp. 281 - 297.
- 118 Dobromirski, J. and Smith, I. O., "Metallographic aspects of surface damage, surface temperature and crack initiation in fretting fatigue," *Wear*, 117 : (3), July, 1987, pp. 347 - 357.
- 119 Fellows, L. J., Nowell, D. and Hills, D. A., "On the initiation of fretting fatigue cracks," *Wear*, 205 : (1 - 2), April, 1997, pp. 120 - 129.

- 120 Proudhon, H., Buffire, J.-Y. and Fouvry, S., "*Characterisation of fretting fatigue damage using synchrotron x-ray micro-tomography,*" Tribology International, 39 : (10), October, 2006, pp. 1106 - 1113.
- 121 Clark, P. N. and Hoepfner, D. W., "*Fretting fatigue initial damage state to cracking state: Observations and analysis,*" Fretting Fatigue: Advances in the Basic Understanding and Applications, (Edited by S. E. Kinyon, D. W. Hoepfner and Y. Mutoh), American Society for Testing and Materials, Special Technical Publication, 1425, pp. 44 - 58.
- 122 Shinde, S and Hoepfner, D. W., "*Observations on fretting damage transition to cracking; state of the art and preliminary observations,*" Tribology International, 39 : (10), October, 2006, pp. 1028 - 1035.
- 123 Nishioka, K., Nishimura, S. and Hirakawa, K., "*Fundamental investigation of fretting fatigue – part 1. On the relative slip amplitude of press-fitted axle assemblies,*" Bulletin, Japan Society for Mechanical Engineers, 11 : (45), 1968, pp. 437 - 445.
- 124 Gerdes, C., Bartsch, H. and Härkegård, G., "*Two-dimensional modelling of fretting fatigue,*" Fretting Fatigue, ESIS 18, (Edited by R. B. Waterhouse and T. C. Lindley), 1994, Mechanical Engineering Publications, London, pp. 111 - 124.
- 125 Taylor, D. E. and Waterhouse, R. B., "*Sprayed molybdenum coatings as a protection against fretting fatigue,*" Wear, 20 : (3), July, 1972, pp. 401 - 407.
- 126 Wright, G. P. and O'Conner, J. J., "*Finite-element analysis of alternating axial loading of an elastic plate between two elastic rectangular blocks with finite friction,*" International Journal of Engineering Science," 9 : (6), June, 1971, pp. 555 - 570.
- 127 Rollins, C. T. and Sandorff, P. E., "*Slip front mechanisms in mechanical joints,*" Journal of Aircraft, 1 : (1), August, 1972, pp. 581 - 584.
- 128 Endo, K., "*Practical observation of initiation and propagation of fretting fatigue cracks,*" Fretting Fatigue, (Edited by R. B. Waterhouse), 1981, Applied Science Publications, London, UK.
- 129 Alic, J. A., "*On the early growth of fretting fatigue cracks,*" Wear, 56 : (2), October, 1979, pp. 377 - 389.
- 130 Sato, K., Fujii, H. and Kodama, S., "*Crack propagation behaviour in fretting fatigue,*" Wear, 107 : (3), February, 1986, pp. 245 - 262.
- 131 Forsyth, P. J. E., "*A two-stage process of fatigue crack growth,*" Proceedings of the Crack Propagation Symposium, 1961, pp. 76 - 94.

- 132 Hills, D. A., Nowell, D. and O'Connor, J. J., "*On the mechanics of fretting fatigue*," *Wear*, 125 : (1 - 2), July, 1988, pp. 129 - 146.
- 133 Beard, J., "*An investigation into the mechanisms of fretting fatigue*," PhD Thesis, University of Salford, Manchester, UK, 1982.
- 134 Dobromirski, J. M., "*Variables of fretting process: Are there 50 of them ?*" Standardisation of Fretting Fatigue Test Methods and Equipment, (Edited by Attia and Waterhouse), American Society for Testing and Materials, Special Technical Publication, 1159, November, 1990, pp. 60 - 68.
- 135 Lee, H. and Mall, S., "*Investigation into tangential force and axial stress effects on fretting fatigue behavior*," *Journal of Engineering Materials and Technology*, Transactions of the American Society of Mechanical Engineers, 128 : (2), April, 2006, pp. 202 - 209.
- 136 Iyer, K. and Mall, S., "*Effects of cyclic frequency and contact pressure on fretting fatigue under two-level block loading*," *Fatigue and Fracture of Engineering Materials and Structures*, 23 : (4), April, 2000, pp. 335 - 346.
- 137 Cortez, R., Mall, S. and Calcaterra, J. R., "*Investigation of variable amplitude loading on fretting fatigue behavior of Ti - 6Al - V*," *International Journal of Fatigue*, 21 : (7), August, 1999, pp. 709 - 717.
- 138 Szolwinski, M. P., Matlik, J. F. and Farris, T. N., "*Effects of HCF loading on fretting fatigue crack nucleation*," *International Journal of Fatigue*, 21 : (7), August, 1999, pp. 671 - 677.
- 139 Pomey, J., "*Friction and wear*," National Advisory Committee for Aeronautics, Technical Memorandum, No. 1318, March, 1952.
- 140 Datsyshyn, O. P., Kalakhan, O. S., Kadyra, V. M. and Shchur, R. B., "*Pitting formation under the conditions of fretting fatigue*," *Materials Science*, 40 : (2), April, 2004, pp. 159 - 172.
- 141 Endo, K., Goto, H. and Nakamura, T., "*Fretting fatigue strength of several materials combinations*," *Bulletin, Japan Society of Mechanical Engineers*, 16 : (92), 1973, pp. 143 - 150.
- 142 Dominguez, J., "*Cyclic variations in friction forces and contact stresses during fretting fatigue*," *Wear*, 218 : (1), June, 1998, pp. 43 - 53.
- 143 Wharton, M. H. and Waterhouse, R. B., "*The effect of different contact materials on the fretting fatigue strength of an aluminium alloy*," *Wear*, 26 : (2), November, 1973, pp. 253 - 260.
- 144 Lee, H. and Mall, S., "*Some observations on frictional force during fretting fatigue*," *Tribology Letters*, 17 : (3), October, 2004, pp. 491 - 499.

- 145 Milestone, W. D. and Janeczko, J. T., "*Friction between steel surfaces during fretting*," *Wear*, 18 : (1), July, 1971, pp. 29 - 40.
- 146 Faanes, S., "*Distribution of contact stresses along a worn fretting surface*," *International Journal of Solids and Structures*, 33 : (23), September, 1996, pp. 3477 - 3489.
- 147 Szolwinski, M. P., Harish, G. and Farris, T. N., "*Experimental observation of the effect of contact parameters on fretting fatigue crack nucleation*," *Proceedings of 1995 USAF Structural Integrity Program Conference*, San Antonio, USA, 1995.
- 148 Berthier, Y., Vincent, L. and Godet, M., "*Velocity accommodation in fretting*," *Wear*, 125 : (1 - 2), July, 1988, pp. 25 - 38.
- 149 Okane, M., Satoh, T., Mutoh, Y. and Suzuki, S., "*Effect of relative slip amplitude on fretting fatigue behavior of silicon nitride*," *Japan Society of Mechanical Engineers - International Journal, Series A*, 39 : (1), 1996, pp. 18 - 25.
- 150 Endo, K., Goto, H. and Fukunaga, T., "*Behaviours of frictional force in fretting fatigue*," *Japan Society of Mechanical Engineers - Bulletin*, 17: (108), 1974, pp. 647 - 654.
- 151 Rooke, D. P. and Courtney, T. J., "*The effect of final friction coefficient on fretting fatigue waveforms*," *Fatigue and Fracture of Engineering Materials and Structures*, 12 : (3), March, 1989, pp. 227 - 236.
- 152 Switek, W., "*Fretting fatigue strength of mechanical joints*," *Theoretical and Applied Fracture Mechanics*, 4 : (1), August, 1985, pp. 59 - 63.
- 153 Nakazawa, K., Sumita, M. and Maruyama, N., "*Standardisation of fretting fatigue test methods and equipment*," *Special Technical Publication*, 1159, 1992, American Society for Testing and Materials, Philadelphia, USA.
- 154 Adibnazari, S. and Hoepfner, D. W., "*A fretting fatigue normal pressure threshold concept*," *Wear*, 160 : (1), January, 1993, pp. 33 - 35.
- 155 Fernando, U. S., Brown, M. W., Miller, K. J., Cook, R. and Rayaprolu, D., "*Fretting fatigue behaviour of BS L65 4 percent copper aluminium alloy under variable normal load*," *Fretting Fatigue*, ESIS 18 (Edited by R. B. Waterhouse and T. C. Lindley), 1994, Mechanical Engineering Publications, London, UK, pp. 197 - 209.
- 156 Benrabah, A., Langlade, C. and Vannes, A. B., "*Residual stresses and fretting fatigue*," *Wear*, 224 : (2), February, 1999, pp. 267 - 273.

- 157 Lee, H., Sathish, S. and Mall, S., "*Evolution of residual stress under fretting fatigue,*" *Journal Of Materials Science*, 39 : (23), December, 2004, pp. 7089 - 7092.
- 158 Nowell, D. and Hills, D. A., "*Crack initiation criteria in fretting fatigue,*" *Wear*, 136 : (2), March, 1990, pp. 329 - 343.
- 159 Godet, M., "*The 3rd-body approach - a mechanical view of wear,*" *Wear*, 100: (1-3), March, 1984, pp. 437 - 452.
- 160 Lee, H. and Mall, S., "*Investigation into effects and interaction of various fretting fatigue variables under slip-controlled mode,*" *Tribology International*, 39 : (10), The Fourth International Symposium on Fretting Fatigue, October, 2006, pp. 1213 - 1219.
- 161 Jin, O. and Mall, S., "*Effects of slip on fretting behavior: experiments and analyses,*" *Wear*, 256 : (7-8), April, 2004, pp. 671 - 684.
- 162 Jin, O. and Mall, S., "*Influence of contact configuration on fretting fatigue behaviour of Ti-5Al-4V under independent pad displacement condition,*" *International Journal of Fatigue*, 24 ; (12), December, 2002, pp. 1243 - 1253.
- 163 Waterhouse, R. B. and Taylor, D. E., "*The initiation of fatigue cracks in a 0.7% carbon steel by fretting,*" *Wear*, 17 : (12), February, 1971, pp. 139 - 147.
- 164 Ciavarella, M., "*Indentation by nominally flat or conical indenters with rounded corners,*" *International Journal of Solids and Structures*, 36 : (27), September, 1999, pp. 4149 - 4181.
- 165 Navarro, C., García, M. and Domínguez, J., "*Fretting fatigue in a spherical contact,*" *Journal of Strain Analysis for Engineering Design*, Special Issue Paper, 37 : (6), November, 2002, pp. 469 - 478.
- 166 Iyer, K., "*Peak contact pressure, cyclic stress amplitudes, contact semi-width and slip amplitude: relative effects on fretting fatigue life,*" *International Journal of Fatigue*, 23 : (3), March, 2001, pp. 193 - 206.
- 167 Hills, D. A. and Nowell, D., "*A discussion of: 'Peak contact pressure, cyclic stress amplitudes, contact semi-width and slip amplitude: relative effects on fatigue life' by K. Iyer,*" *International Journal of Fatigue*, 23 : (8), September 2001, pp. 747 - 748.
- 168 Horn, D. R., Waterhouse, R. B. and Pearson, B. R., "*Fretting wear of sintered alumina,*" *Wear*, 113 : (2), December, 1986, pp. 225 - 232.

- 169 Johnson, K. L., "*Energy dissipation at spherical surfaces in contact transmitting oscillating forces,*" *Journal of Mechanical Engineering Science*, 3 : (4), March, 1961, pp. 362 - 368.
- 170 Waterhouse, R. B. and Trowsdale, A. J., "*Residual-stress and surface-roughness in fretting fatigue,*" *Journal of Physics D-Applied Physics*, 25 : (1a), January, 1992, pp. a236 - a239.
- 171 Nowell, D. and Hills, D. A., "*Hertzian contact of ground surfaces,*" *Journal of Tribology-Transactions of the American Society of Mechanical Engineers*, 111 : (1), January, 1989, pp. 175 - 179.
- 172 Proudhon, H., Fouvry, S. and Buffiere, J. Y., "*A fretting crack initiation prediction taking into account the surface roughness and the crack nucleation process volume,*" *International Journal Of Fatigue*, 27 : (5), May, 2005, pp. 569 - 579.
- 173 Neslen, C. L., Mall, S. and Sathish, S., "*Nondestructive characterization of fretting fatigue damage,*" *Journal Of Nondestructive Evaluation*, 23 : (4), December, 2004, pp. 153 - 162.
- 174 Takeuchi, M. and Waterhouse, R. B., "*Environment assisted fatigue,*" (Edited by P. Scott and R. A. Cottis), EGF Publications, London, UK, 1990, pp. 367 - 379.
- 175 Bogdański, S., Olzak, M. and Stupnicki, J., "*Influence of liquid interaction on propagation of rail rolling contact fatigue cracks,*" *Proceedings of the Second Mini Conference on Contact Mechanics and Wear of Rail/Wheel Systems*, (Edited by I. Zobory), Technical University of Budapest, 1996, pp. 134 - 143.
- 176 Lepper, K., James, M., Chashechkina, J. and Rigney, D. A., "*Sliding behaviour of selected aluminium alloys,*" *Wear*, 203-204, 11th International Conference on Wear of Materials, (Edited by D. Rigney and R. C. Bayer), San Diego, USA, March, 1997, pp. 46 - 56.
- 177 Poon, C. and Hoepfner, D. W., "*The effect of environment on the mechanism of fretting fatigue,*" *Wear*, 52 : (1), January, 1979, pp. 175 - 191.
- 178 Goto, H. and Buckley, D. H., "*The influence of water vapour in air on the friction behaviour of pure metals during fretting,*" *Tribology International*, 18 : (4), August, 1985, pp. 237 - 245.
- 179 Stott, F. H., Liu, D. S. and Wood, G. C., "*The structure and mechanism of formation of the 'glaze' oxide layers produced on nickel-based alloys during wear at high temperatures,*" *Corrosion Science*, 13, Part 1 : (6), June, 1973, pp. 449 - 469.

- 180 Iwabuchi, A. Honda, I and Tani, J., "*Tribological properties at temperatures of 293, 77 and 4 K in fretting,*" *Cryogenics*, 29 : (2), February, 1989, pp. 124 - 131.
- 181 Leghorn, G., "*The story of shot peening,*" *Journal American Society Naval Engineering*, 1957, pp. 654.
- 182 Cary, P. E., "*History of shot peening,*" *Proceedings of the First International Conference on Shot Peening*, (Edited by A. Niku-Lari), Pergamon Press, 1981, pp. 23 - 28.
- 183 Kloos, K. H. and Macherauch, E., "*Development of mechanical surface strengthening from the beginning until today,*" *Proceedings of the Third International Conference on Shot Peening*, (Edited by H. Wohlfahrt, R. Kopp and O. Vöhringer), Deutsche Gesellschaft für Metallkunde, 1987, pp. 3 -27.
- 184 Herbert, E. G., "*The workhardening of steel by abrasion,*" *Journal of the Iron and Steel Institute*, 11, 1927, pp. 265.
- 185 German Patent No. 573630, 1929.
- 186 Weibel, E. E., "*The correlation of spring-wire bending and torsion fatigue tests,*" *Transactions of the American Society of Mechanical Engineers*, 57, 1935, pp. 501 - 516.
- 187 Zimmerli, F. P., "*Shot blasting and its effect on fatigue life,*" *Machine Design*, 12, 1940, pp. 62.
- 188 Wiegand, H., *Jahrbuch der deutschen Luftfahrtforschung*, II, 1940, pp. 7.
- 189 Almen, J. O., "*Effects of residual stress on fatigue of metals,*" *Product Engineering*, 14, 1943, pp. 358 - 352.
- 190 Almen, J. O., "*Improving fatigue strength of engine parts,*" *Iron Age*, 151, 1943, pp. 125 - 128.
- 191 Almen, J. O., "*Fatigue failures in common machine parts,*" *Metal Progress*, 43, 1943, pp. 737 - 740.
- 192 Milburn, E. W., *Metallurgical Treatment*, 12, 1945, pp. 259.
- 193 Almen, J. O. and Black, P. H., "*Residual Stresses and fatigue in metals,*" McGraw Hill, USA, 1963.
- 194 Plaster, H. J., "*Technical aspects of shot peening machinery and media,*" *Proceedings of the First International Conference on Shot-Peening*, (Edited by A. Niku-Lari), Pergamon Press, 1981, pp. 83 - 94.

- 195 Johnson, W., *Impact Strength of Materials*, Edward Arnold, England, 1972.
- 196 Tosha, K., *Papers on shot peening published in the world for the last thirteen years*, Proceedings of the Seventh International Conference on Shot-Peening, (Edited by A. Nakonieczny), Institute of Precision Mechanics, 1999, pp. 5 - 10.
- 197 Solis-Romero, J., *Optimisation of the Shot Peening Process in terms of Fatigue Resistance*, PhD Thesis, The University of Sheffield, UK, 2002.
- 198 Wang, R., Xiangbin, L., Tan, Y. and Yan, M., *Investigation on the microstructure in shot-peening surface straining layer of materials*, Proceedings of the First International Conference on Shot-Peening, (Edited by A. Niku-Lari), Pergamon Press, 1981, pp. 185 - 192.
- 199 Natkaniec-Kocanda, D., Kocanda, S. and Miller, K. J., *Influence of shot peening on short crack behaviour in a medium carbon steel*, Fatigue and Fracture of Engineering Materials and Structures, 19 : (7), July, 1996, pp. 911 - 917.
- 200 Clausen, R. and Stangenberg, J., *Roughness of shot-peened surfaces – definition and measurement*, Proceedings of the Seventh International Conference on Shot-Peening, (Edited by A. Nakonieczny), Institute of Precision Mechanics, 1999, pp. 69 - 77.
- 201 Wagner, L. and Luetjering, G., *Influence of shot peening on the fatigue behaviour of titanium alloys*, Proceedings of the First International Conference on Shot-Peening, (Edited by A. Niku-Lari), Pergamon Press, 1981, pp. 435 - 460.
- 202 Asquith, D. T., *Residual stress and fatigue in cold-worked, hard-coated 2024-T351 aluminium alloy*, PhD Thesis, The University of Sheffield, UK, 2007.
- 203 Starker, P., Wohlfahrt, H. and Macherlauch, E., *Subsurface crack initiation during fatigue as a result of residual stresses*, Fatigue of Engineering Materials and Structures, 1, 1979, pp. 319 - 327.
- 204 Hammond, D. A. and Meguid, S. A., *Crack propagation in the presence of shot-peening residual stresses*, Engineering Fracture Mechanics, 37 : (2), 1990, pp. 373 - 387.
- 205 Society of Automotive Engineers, *Manual on Shot Peening*, Third edition, Fatigue Design and Evaluation, Prepared under the direction of the Society of Automotive Engineers Committee, The Society of Automotive Engineers, United States of America, SAE HS-84, 1991, pp. 19 - 20.

- 206 Iida, K., "*Dent and affected layer produced by shot peening*," Proceedings of the Second International Conference on Shot-Peening, (Edited by H. O. Fuchs), 1984, pp. 283 - 292.
- 207 British Aerospace, "*Shot peening for improved fatigue and stress corrosion resistance*," Process Specification, ABP 1-2031, 1997.
- 208 United States Department of Defence, "*Shot peening of metal parts*," MIL-S-13165c, 1989.
- 209 Aston, A. J., "*The need for high quality shot for peening*," Proceedings of the Second International Conference on Impact Treatment Processes, (Edited by S. A. Meguid), Elsevier Applied Science Publishers, 1986, pp. 229 - 236.
- 210 Gillespie, R. D., "*Shot peening media: Its effects on process consistency and resultant improvement in fatigue characteristics*," Proceedings of the Fifth International Conference on Shot-Peening, (Edited by D. Kirk), 1993, pp. 81 - 90.
- 211 Meguid, S. A. and Duxbury, J. K., "*A practical approach to forming and strengthening of metallic components using impact treatment*," Proceedings of the First International Conference on Shot-Peening, (Edited by A. Niku-Lari), Pergamon Press, 1981, pp. 217 - 228.
- 212 Society of Automotive Engineers, Handbook, J2441: Shot-peening 2001.
- 213 Pearson, N. L., "*Effect of shot peening variables on fatigue of aluminium forgings*," Metal Progress, 7, 1981, pp. 33 - 35.
- 214 Simpson, R. S. and Chiasson, G. L., "*A new concept for defining optimum levels of a critical shot peening process variable*," Proceedings of the Second International Conference on Impact Treatment Processes, (Edited by S. A. Meguid), Elsevier Applied Science Publishers, 1986, pp. 101 - 114.
- 215 US Patent No. 2350440, 1942.
- 216 Heywood, R. B., "*Designing against fatigue*," Chapman and Hall Limited, England, 1962, pp. 165.
- 217 Waters, K., American Society for Testing and Materials, Special Technical Publication, 274, 1959, pp. 99 - 111.

- 218 de los Rios, E. R., Brown, M. W., Levers, A., Fernando, U. S. and Orlov, E., "*Effect of shot-peening on the fretting fatigue behaviour of BS L65 aluminium alloy*," Structural Integrity for the Next Millennium, Volume II, (Edited by J. L. Rudd and R. M. Bader), 2001, Electronic Print Imaging Corporation (EPIC), Dayton, USA, pp. 931 - 944.
- 219 Moobola, R., Hills, D. A. and Nowell, D., "*Designing against fretting fatigue: crack self-arrest*," Journal of Strain Analysis for Engineering Design, 33 : (1), January, 1998, pp. 17 - 25.
- 220 Prev y, P. S., "*The uniformity of shot peening induced residual stress*," Residual Stress for Designers & Metallurgists, American Society for Metals, USA, 1981, pp. 151 - 168.
- 221 Von Tein, V. and Seibert, P. E., Proceedings, AGARD, AGARD-CP-161, Session 1, Paper 2, 1974.
- 222 Fouvry, S., Fridrici, V., Langlade, C., Kapsa, P. and Vincent, L., "*Palliatives in fretting: A dynamical approach*," Tribology International, 39 : (10), The Fourth International Symposium on Fretting Fatigue, October, 2006, pp. 1005 – 1015.
- 223 de los Rios, E. R., Walley, A., Milan, M. T. and Hammersley, G., "*Fatigue crack initiation and propagation on shot-peened surfaces in A316 stainless steel*," International Journal of Fatigue, 17 : (7), October, 1995, pp. 493 - 499.
- 224 Gordelier, S. C. and Chivers, T. C., "*Fretting fatigue and contact conditions: A rational explanation of palliative behaviour*," Proceedings of the Institute of Mechanical Engineers, 199 : (C4), 1985, pp. 325 - 337.
- 225 Mutoh, Y., Nishida, T., Kondoh, K. and Satoh, T., "*Effect of surface wear on fretting fatigue strength of shot peened steels*," Engineering Against Fatigue, (Edited by J. H. Beynon, M. W. Brown, R. A. Smith, T. C. Lindley and B. Tomkins), A. A. Balkema, 1999, pp. 633 - 640.
- 226 Watanabe, Y., Hasegawa, N., Endo, H., Marui, E. and Aoki, Y., "*An effect of peening on fretting fatigue*," Shot Peening Present & Future, (Edited by A. Nakonieczny), 1999, Institute of Precision Mechanics, Poland, pp. 127 - 134.
- 227 Harris, W. J., "*The Influence of Fretting on Fatigue, Pt. III*," Advisory Group for Aerospace Research and Development, AGARD Advisory Report, AGARD-AR-45, 1969.
- 228 Kirkpatrick, G. R., "*Fretting fatigue analysis and palliatives*," MPhil Thesis, Massachusetts Institute of Technology, USA, 1999.

- 229 Fernando, U. S., Farrahi, G. H. and Sheikh, M. A., *"An investigation into the fretting fatigue fracture of BS L65 copper aluminium alloy under variable normal loading,"* Progress Report No. 1, SIRIUS, 93764, 1990.
- 230 Metals Handbook®, Tenth edition, Volume 2, Properties and Selection: Nonferrous Alloys and Special-Purpose Materials, Prepared under the direction of the ASM International Handbook Committee, ASM International®, 1990, The Materials Information Society, United States of America, pp. 70 - 73.
- 231 Curtis, S. A., *"The Effects of Shot Peening on Corrosion Fatigue of Aluminium Alloys 2024 T351 and 7150 T651,"* PhD Thesis, The University of Sheffield, UK, 2003.
- 232 Edwards, P. R. and Cook, R., *"Friction force measurements on fretted specimens under constant normal loading,"* RAE Technical Report 78019, 1978.
- 233 Szolwinski, M. P. and Farris, T. N., *"Observation, analysis and prediction of fretting fatigue in 2024 - T351 aluminium alloy,"* Wear, 221 : (1), October, 1998, pp. 24 - 36.
- 234 Fernando, U. S., Farrahi, G. H. and Sheikh, M. A., *"An investigation into the fretting fatigue fracture of BS L65 copper aluminium alloy under variable normal loading,"* Progress Report No. 4, SIRIUS, 93764, 1992.
- 235 Frantziskonis, G. N., Shell, E., Woo, J., Matikas, T. E. and Nicolaou, P. D., *"Wavelet analysis of fretting experimental data,"* Non-destructive Evaluation of Aging Materials and Composites III, (Edited by G. Y. Baaklini, C. A. Lebowitz and E. S. Boltz), SPIE Proceedings Series, 1999, pp. 11 - 27.
- 236 Hull, D., *"Fractography: observing, measuring and interpreting fracture surface topography,"* 1999, Cambridge University Press.
- 237 Leadbeater, G., Kovalevskii, V. V., Noble, B. and Waterhouse, R. B., *"Fractographic investigation of fretting wear and fretting fatigue in aluminium alloys,"* Fatigue of Engineering Materials and Structures, 3, 1981, pp. 237 - 246.
- 238 Dowling, N. E., *"Mean stress effects in stress-life and strain-life fatigue,"* Fatigue 2004.
- 239 Kovalevskii, V. V. and Kozakov, V. A., *"Physics of strength of plasticity of metals and alloys,"* 82, USSR, 1976.
- 240 Faanes, S., *"Inclined cracks in fretting fatigue,"* Engineering Fracture Mechanics, 52 : (1), September, 1995, pp. 71 - 82.

- 241 Rooke, D. P. and Jones, D. A., "*Stress intensity factors in fretting fatigue*," *Journal of Strain Analysis*, 14 : (1), January, 1979 pp. 1 - 6.
- 242 Nix, K. J. and Lindley, T. C., "*The application of fracture mechanics to fretting fatigue*," *Fatigue and Fracture of Engineering Materials and Structures*, 8 : (2), February, 1985, pp. 143 - 160.
- 243 Nicholas, T., Hutson, A., John, R. and Olson, S., "*A fracture mechanics methodology assessment for fretting fatigue*," *International Journal of Fatigue*, 25 : (9 - 11), International Conference on Fatigue Damage of Structural Materials IV, Hyannis, USA, September - November, 2003, pp. 1069 - 1077.
- 244 Conner, B. P., Lindley, T. C. Nicholas, T. and Suresh, S., "*Application of a fracture mechanics based life prediction method for contact fatigue*," *International Journal of Fatigue*, 26 : (5), May, 2004, pp. 511 - 520.
- 245 Attia, M., "*Prediction of fretting fatigue behaviour of metals using a fracture mechanics approach with special consideration to the contact problem*," *Journal of Tribology*, 127 : (4), October, 2005, pp. 685 - 693.
- 246 Giummarra, C. and Brockenbrough, J. R., "*Fretting fatigue analysis using a fracture mechanics based small crack growth prediction method*," *Tribology International*, 39 : (10), The Fourth International Symposium on Fretting Fatigue, October, 2006, pp. 1166 - 1171.
- 247 Chambon, L. and Journet, B., "*Modelling of fretting fatigue in a fracture-mechanics framework*," *Tribology International*, 39 : (10), The Fourth International Symposium on Fretting Fatigue, October, 2006, pp. 1220 - 1226.
- 248 Matterson, R. L. and Roberts. J. G., "*The effect of residual stresses induced by Strain Peening upon Fatigue Strength*," *Internal Stresses and Fatigue of Metals*, (Edited by G. M. Rassweiler and W. L Grube), 1959, Elsevier, New York, USA.
- 249 Berns, H. and Weber, L., "*Influence of residual stresses on crack growth*," *Impact Surface Treatment* (Edited by S. A. Meguid), 1986, Elsevier Applied Science Publishers, London, UK, pp. 31 - 44.
- 250 Hertz, H., *Gesammelte Werke, vol. 1: Schriften Vermischten Inhalts*, 1895, J.A. Barth, Leipzig, Germany.
- 251 Urban, M. R., "*Approximate stresses in 2-D flat elastic contact fretting problems*," *International Journal of Fatigue*, 21 : Supplement, November, 1999, pp. S167 - S172.

- 252 Dubourg, M. C. and Lamacq, V., "*Stage II crack propagation direction under fretting fatigue: A new approach in accordance with experimental observations,*" *Fretting Fatigue: Current Technology and Practices*, ASTM STP 1367, (Edited by D. W. Hoepfner, V. Chandrasekaran and C. B. Elliott), American Society for Testing and Materials, West Conshohocken, USA, 2000.
- 253 Paris, P. and Erdogan, F., "*A critical analysis of crack propagation laws,*" *Journal of Basic Engineering, Transactions of the American Society of Mechanical Engineers*, 85, December, 1963, pp.528 - 534.
- 254 Tada, H., Paris, P. and Irwin, G., "*The Stress Analysis of Cracks Handbook,*" Second Edition, Paris Productions Incorporated, St. Louis, 1985.
- 255 Mutoh, Y., Nishida, T. and Sakamoto, I., "*Effect of relative slip amplitude and contact pressure on fretting fatigue strength,*" *Journal Society of Material Science*, 37 : (417), 1988, pp 65 - 71.
- 256 Nakazawa, K., Samita, M. and Maruyama, N., "*Effect of contact pressure on fretting fatigue of high strength steel and titanium alloy,*" American Society for Testing and Materials, Standardisation of Fretting Fatigue Test Methods and Equipment, 1992.
- 257 Nishida, T., Kondoh, K., Xu, Jin-Quan and Mutoh, Y., "*Observations and analysis of relative slip in fretting fatigue,*" *Fretting Fatigue: Advances in Basic Understanding and Applications, Special Technical Publication*, 1425, (Edited by Y. Mutoh, S. E. Kinyon and D. W. Hoepfner), American Society for Testing and Materials, 2003, pp. 33 - 43.
- 258 Boabaid, J. S., "*Effect of material microstructure, surface topography and residual stresses on fatigue crack initiation in a mechanically prepared surface of Waspaloy,*" PhD Thesis, The University of Sheffield, UK, 1994.
- 259 Araújo, J. A. and Nowell, D., "*The effect of rapidly varying contact stress fields on fretting fatigue,*" *International Journal of Fatigue*, 24 : (7), July, 2002, pp. 763 - 775.
- 260 Vallellano, C. Navarro, A. and Domínguez, J., "*Fatigue crack growth threshold conditions at notches. Part I: theory,*" *Fatigue and Fracture of Engineering of Engineering Materials and Structures*, 23 : (2), February, 2000, pp. 113 - 121.

- 261 Vallellano, C., Navarro A. and Domínguez, J., "*Fatigue crack growth threshold conditions at notches. Part II: generalization and application to experimental results,*" *Fatigue and Fracture of Engineering of Engineering Materials and Structures*, 23 : (2), February, 2000, pp. 123 - 128.
- 262 Erdogan, F. and Sih, G. C., "*On the crack extension in plates under plane loading and transverse shear,*" *Journal of Basic Engineering, Transactions of the American Society of Mechanical Engineers*, 85, December, 1963, pp. 519 - 525.
- 263 El Haddad, M. H., Smith, K. N. and Topper, T. H., "*Fatigue crack propagation of short cracks,*" *Journal of Engineering Materials and Technology, Transactions of the American Society of Mechanical Engineers, Series H*, 101 : (1), January, 1979, pp. 42 - 46
- 264 de los Rios, E. R. and Navarro, A., "*Considerations of grain orientation and work hardening on short-fatigue-crack modelling,*" *Philosophical Magazine*, 61 : (3), March, 1990, pp. 435 - 449.
- 265 Campbell, J. E., "*Shot peening for improved fatigue properties and stress-corrosion resistance,*" Internal Report, Metals And Ceramics Information Center, MCIC-71-02, 1971.
- 266 Waterhouse, R. B., "*Avoidance of fretting fatigue failures,*" *Fretting Fatigue*, Applied Science Publishers, London, UK, 1981, pp. 221 - 240.
- 267 Rodopoulos, C. A. and de los Rios, E. R., "*Theoretical analysis on the behaviour of short fatigue cracks,*" *International Journal of Fatigue*, 24 : (7), July, 2002, pp. 719 - 724.